

Proceedings to the 24th Workshop
**What Comes Beyond the
Standard Models**

Bled, July 5–11, 2021

**[Virtual Workshop]
[July 5.–11. 2021]**

Edited by

Norma Susana Mankoč Borštnik

Holger Bech Nielsen

Dragan Lukman

Astri Kleppe

**The 24th Workshop *What Comes Beyond the Standard Models*,
5.– 11. July 2021, Bled
[Virtual Workshop, 5.–11. July 2021]**

was organized by

Society of Mathematicians, Physicists and Astronomers of Slovenia

and sponsored by

Department of Physics, Faculty of Mathematics and Physics, University of Ljubljana

Society of Mathematicians, Physicists and Astronomers of Slovenia

Beyond Semiconductor (Matjaž Breškvar)

VIA (Virtual Institute of Astroparticle Physics), Paris

MDPI journal "Symmetry", Basel

MDPI journal "Physics", Basel

MDPI journal "Universe", Basel

Scientific Committee

John Ellis, King's College London / CERN

Roman Jackiw, MIT

Masao Ninomiya, Yukawa Institute for Theoretical Physics, Kyoto University

Organizing Committee

Norma Susana Mankoč Borštnik

Holger Bech Nielsen

Maxim Yu. Khlopov

The Members of the Organizing Committee of the International Workshop "What Comes Beyond the Standard Models", Bled, Slovenia, state that the articles published in the Proceedings to the 24th Workshop "What Comes Beyond the Standard Models", Bled, Slovenia are refereed at the Workshop in intense in-depth discussions.

Workshops organized at Bled

- ▷ *What Comes Beyond the Standard Models*
 - (June 29–July 9, 1998), Vol. **0** (1999) No. 1
 - (July 22–31, 1999)
 - (July 17–31, 2000)
 - (July 16–28, 2001), Vol. **2** (2001) No. 2
 - (July 14–25, 2002), Vol. **3** (2002) No. 4
 - (July 18–28, 2003) Vol. **4** (2003) Nos. 2-3
 - (July 19–31, 2004), Vol. **5** (2004) No. 2
 - (July 19–29, 2005) , Vol. **6** (2005) No. 2
 - (September 16–26, 2006), Vol. **7** (2006) No. 2
 - (July 17–27, 2007), Vol. **8** (2007) No. 2
 - (July 15–25, 2008), Vol. **9** (2008) No. 2
 - (July 14–24, 2009), Vol. **10** (2009) No. 2
 - (July 12–22, 2010), Vol. **11** (2010) No. 2
 - (July 11–21, 2011), Vol. **12** (2011) No. 2
 - (July 9–19, 2012), Vol. **13** (2012) No. 2
 - (July 14–21, 2013), Vol. **14** (2013) No. 2
 - (July 20–28, 2014), Vol. **15** (2014) No. 2
 - (July 11–19, 2015), Vol. **16** (2015) No. 2
 - (July 11–19, 2016), Vol. **17** (2016) No. 2
 - (July 9–17, 2017), Vol. **18** (2017) No. 2
 - (June 23–July 1, 2018), Vol. **19** (2018) No. 2
 - (July 6–14, 2019), Vol. **20** (2019) No. 2
 - (July 4–12, 2020), Vol. **21** (2020) No. 1
 - (July 4–12, 2020), Vol. **21** (2020) No. 2
 - (July 1–12, 2021), Vol. **22** (2021) No. 1
- ▷ *Hadrons as Solitons* (July 6–17, 1999)
- ▷ *Few-Quark Problems* (July 8–15, 2000), Vol. **1** (2000) No. 1
- ▷ *Selected Few-Body Problems in Hadronic and Atomic Physics* (July 7–14, 2001), Vol. **2** (2001) No. 1
- ▷ *Quarks and Hadrons* (July 6–13, 2002), Vol. **3** (2002) No. 3
- ▷ *Effective Quark-Quark Interaction* (July 7–14, 2003), Vol. **4** (2003) No. 1
- ▷ *Quark Dynamics* (July 12–19, 2004), Vol. **5** (2004) No. 1
- ▷ *Exciting Hadrons* (July 11–18, 2005), Vol. **6** (2005) No. 1
- ▷ *Progress in Quark Models* (July 10–17, 2006), Vol. **7** (2006) No. 1
- ▷ *Hadron Structure and Lattice QCD* (July 9–16, 2007), Vol. **8** (2007) No. 1
- ▷ *Few-Quark States and the Continuum* (September 15–22, 2008), Vol. **9** (2008) No. 1
- ▷ *Problems in Multi-Quark States* (June 29–July 6, 2009), Vol. **10** (2009) No. 1
- ▷ *Dressing Hadrons* (July 4–11, 2010), Vol. **11** (2010) No. 1
- ▷ *Understanding hadronic spectra* (July 3–10, 2011), Vol. **12** (2011) No. 1
- ▷ *Hadronic Resonances* (July 1–8, 2012), Vol. **13** (2012) No. 1
- ▷ *Looking into Hadrons* (July 7–14, 2013), Vol. **14** (2013) No. 1
- ▷ *Quark Masses and Hadron Spectra* (July 6–13, 2014), Vol. **15** (2014) No. 1
- ▷ *Exploring Hadron Resonances* (July 5–11, 2015), Vol. **16** (2015) No. 1

IV

- ▷ *Quarks, Hadrons, Matter* (July 3–10, 2016), Vol. **17** (2016) No. 1
- ▷ *Advances in Hadronic Resonances* (July 2–9, 2017), Vol. **18** (2017) No. 1
- ▷ *Double-charm Baryons and Dimesons* (June 17–23, 2018), Vol. **19** (2018) No. 1
- ▷ *Electroweak Processes of Hadrons* (July 15–19, 2019), Vol. **20** (2019) No. 1
- ▷
 - *Statistical Mechanics of Complex Systems* (August 27–September 2, 2000)
 - *Studies of Elementary Steps of Radical Reactions in Atmospheric Chemistry* (August 25–28, 2001)

Contents

1 Virtual talks	
<i>A. Addazi, L. Bonora, S. Kabana, E. Kiritsis, R. Mohapatra, Q. Shafi</i>	1
2 Type IIB moduli stabilisation, inflation and waterfall fields	
<i>I. Antoniadis, O. Lacombe, G. K. Leontaris</i>	4
3 New and recent results, and perspectives from DAMA/LIBRA–phase2	
<i>R. Bernabei, P. Belli, A. Bussolotti, V. Caracciolo, R. Cerulli, N. Ferrari, A. Leoncini, V. Merlo, F. Montecchia, F. Cappella, A. d’Angelo, A. Incicchitti, A. Mattei, C.J. Dai, X.H. Ma, X.D. Sheng, Z.P. Ye</i>	20
4 The multicomponent dark matter structure and its possible observed manifestations	
<i>V. Beylin, V. Kuksa, M. Bezuglov, D. Sopin</i>	40
5 Numerical simulation of Bohr-like and Thomson-like dark atoms with nuclei	
<i>T.E. Birkbaev, M. Yu. Khlopov, A.G. Mayorov</i>	53
6 Supersymmetric and Other Novel Features of Hadron Physics from Light-Front Holography	
<i>S. J. Brodsky</i>	66
7 Charge asymmetry of new stable quarks in baryon asymmetrical Universe	
<i>A. Chaudhuri, M. Yu. Khlopov</i>	94
8 Entropy release in Electroweak Phase Transition in 2HDM	
<i>A. Chaudhuri, M. Yu. Khlopov, S. Porey</i>	104
9 Gravitational waves in the modified gravity	
<i>S. Roy Chowdhury, M. Yu. Khlopov</i>	114
10 Representing rational numbers and divergent geometric series by binary graphs	
<i>E. Dmitrieff</i>	123
11 Neutrino masses within a SU(3) family symmetry and a 3+5 scenario	
<i>Albino Hernandez-Galeana</i>	135

12 BSM Cosmology from BSM Physics	
<i>M. Yu. Khlopov</i>	152
13 Statistical analyses of antimatter domains, created by nonhomogeneous baryosynthesis in a baryon asymmetrical Universe	
<i>M. Yu. Khlopov, O. M. Lecian</i>	160
14 Researching of magnetic cutoff for local sources of charged particles in the halo of the Galaxy	
<i>A.O. Kirichenko, A.V. Kravtsova, M.Yu. Khlopov, A.G. Mayorov</i>	170
15 Mass as a dynamical quantity	
<i>M. Land</i>	177
16 New way of second quantization of fermions and bosons	
<i>N.S. Mankoč Borštnik</i>	190
17 The achievements of the <i>spin-charge-family</i> theory so far	
<i>N.S. Mankoč Borštnik</i>	226
18 Novel String Field Theory and Bound State, Projective Line, and sharply 3-transitive group	
<i>H. B. Nielsen, M. Ninomiya</i>	257
19 Atomic Size Dark Matter Pearls, Electron Signal	
<i>H.B. Nielsen, C.D.Froggatt</i>	278
20 Galactic model with a phase transition from dark matter to dark energy	
<i>I. Nikitin</i>	300
21 Ultraviolet divergences in supersymmetric theories regularized by higher derivatives	
<i>K.V. Stepanyantz</i>	332
Virtual Institute of Astroparticle Physics (CosmoVia)	348
22 Challenging BSM physics and cosmology on the online platform of Virtual Institute of Astroparticle physics	
<i>M. Yu. Khlopov</i>	349
Postscriptum	365

1 Preface in English and Slovenian Language

The series of annual workshops on “What Comes Beyond the Standard Models?” started in 1998 with the idea of Norma and Holger for organizing a real workshop, in which participants would spend most of the time in discussions, confronting different approaches and ideas. All this time we have been looking for answers to the question of what the laws of nature are. And we learned a lot. This year in July the 24th workshop took place.

Workshops have always taken place in the picturesque town of Bled by the lake of the same name, surrounded by beautiful mountains and offering pleasant walks and mountaineering. Except for the last two years, 2020 and 2021, when workshop has again taken place in July, but without personal conversations all day and late at night, even between very relaxing walks and mountaineering due to COVID-19 pandemic. We have, however, a very long tradition of videoconferences (cosmovia), enabling discussions and explanations with laboratories all over the world. This enabled us to have these two years a virtual workshop, resembling Bled workshops as much as possible.

In our very open minded, friendly, cooperative, long, tough and demanding discussions several physicists and even some mathematicians have contributed. Most of topics that have been presented and discussed in our Bled workshops deal with the proposals for explaining physics beyond the so far accepted and experimentally confirmed both standard models — in physics of fermion and boson fields and cosmology — in order to understand the origin of assumptions of both standard models and be consequently able to propose new theories, models and to make predictions for future experiments.

Although in all these years most of participants were theoretical physicists, many of them with their own suggestions how to make the next step beyond the accepted models and theories, experts from experimental laboratories were and are very appreciated, helping a lot to understand what do measurements really tell and which kind of predictions can best be tested.

Also in the last two years we tried to keep our habit of (long) presentations (with breaks and continuations over several days), followed by very detailed discussions.

The authors of the articles worked hard and with enthusiasm already before the presentations and as well when preparing the articles for this Proceedings in such a short time.

However, as lectures and especially discussions over the Internet are more exhausting than live, many issues remain open, unresolved, also undefined and undiscussed. And we did not succeed to continue the discussions over the Internet after the workshop, even though we tried, because of several reasons, one of them was that the computer of one of the organizers broke down.

Here are some questions that we have not really discussed yet but have just started discussing:

How efficient are models offering a small next step beyond both standard models, suggesting experiments which could test such a model, to be able to explain all the observations so far, or at least many of them? There are several contributions

with such proposals presented in this Proceedings, most of them trying to explain what does the *dark matter* consist of.

Would the confrontation of these models with string theories, for example, or with the *spin-charge-family* theory, which offers the explanation for all the assumptions of both standard models, offering as well the explanation for several phenomena observed so far, with the *dark matter* and the *matter/antimatter asymmetry* included, the theory is presented in this Proceedings, help to understand our universe better and also to easier propose relevant experiments having correspondingly more chance to be the right next step beyond both standard models?

Combining knowledge, ideas and hard work could increase our opportunities to recognize the real next step beyond the two standard models and to suggest trustable experiments. In particular if experimentalists would be involved in discussions. Experiments are expensive.

Although the *black holes* are experimentally well confirmed objects, the quantum mechanics of *black holes* is not really known. This knowledge is needed for heavy *black holes* as well as if we accept the possibility that the space-time is larger than $(3 + 1)$, as it is in *string theories*, in *Kaluza-Klein theories* and in the *spin-charge-family* theory (with fermions interacting with gravity only) with space-time $(13 + 1)$ or larger (appearing in two contributions in this paper), or might be even infinite (since zero and infinite are easy to be accepted, all other possibilities need the explanation). Do we understand what in this context the *primordial black holes*, discussed in this and last year Proceedings, mean and do they appear before or after the electroweak phase transition? Is in the time of the formation of the *primordial black holes* space-time already $(3 + 1)$? What happens inside the *primordial black holes* and what happens within the very massive experimentally confirmed *black holes*? Can string theories within M-theory help to understand the quantum gravity even in the context that the internal space of fermions and bosons describe the Clifford algebra objects? If Nature does use the Clifford algebra objects to describe internal space of fermions and bosons, what explains the second quantization postulates for fermions and bosons, as explained in one contribution in this proceedings, can the quantum mechanics of *black holes* be easier understood? Would the *novel string* theory, discussed in this proceedings, where noninteracting objects representing strings, are themselves bound states of strings and might explain bound states of objects with the high symmetry, be helpful as well for describing the heavy *black hole* objects? Even under the assumption that the internal space of fermion and gravitational fields are described with the Clifford algebra objects?

It does happen (after having a vision and after a hard work) that a new way of treating quantum mechanics of bound systems, this time the superconformal quantum mechanics and light-front holography used in hadron physics, presented in this proceedings, opens a new understanding of dynamics and symmetries of bound states.

To understand the start and the starting expansion of our universe the knowledge of quantum gravity and the knowledge of the internal space of fermions and bosons is needed.

Some periods and some phenomena in the expansion of our universe can be explained in the context of string theories, as it is the period of the inflation described with one article in this proceedings. When has the inflation taken place and how is it connected with the today non observed extra dimensions?

Do we have besides the ordinary matter also domains of antimatter in our universe? What are properties of the antimatter? Do domains of antimatter contain mostly the *dark matter*? What is the interaction of matter with antimatter on the border of both domains? In the *spin-charge-family* theory the laws and the interactions are the same — for fermions, antifermions and *dark matter*. In several talks these problems were discussed, some of them presented only as a talk on the website on <http://bsm.fmf.uni-lj.si/bled2>

and on Forum of Cosmovia as <https://bit.ly/bled2021bsm> .

Symmetries play the essential role on all levels of physics, on the level of elementary fermion and boson fields, of cosmology and also of matter of all kinds.

In the theories assuming more than $(3 + 1)$ dimensions with fermions which interact with gravity only, like there are the Kaluza-Klein theories, the *spin-charge-family* theory is also of this kind, as well as string theories, the symmetry origins in the Lorentz invariance of spacetime, manifesting also in the internal space of boson and fermion fields. At observable (that is low) energies the Lorentz symmetry of higher dimensions manifests in $(3 + 1)$ spacetime (after breaking the starting symmetry of spacetime) the symmetry of the internal space of fermion and boson fields only, which usually is described by the group theoretical methods.

The symmetries of elementary fermion and boson fields are discussed in several contributions talks of Bled 2021 workshop, manifesting that all these different understanding of symmetries have a strong overlap.

Some talks about symmetries appear in these proceedings, the others can only be found on the follow-up page of the official website of the Workshop:

<http://bsm.fmf.uni-lj.si/bled2021bsm/presentations.html>,

and on the Cosmovia Forum <https://bit.ly/bled2021bsm> .

There are several other topics, discussed in this proceedings, like

i. What is indeed the origin of masses of fermions and gauge fields?

ii. What modes of gravitational waves can be observed?

iii. How far can we interpret experiments correctly if we accept the *standard model* only?

iv. The DAMA/LIBRA experiment, measuring the collisions of the *dark matter* particles with the ordinary matter, reports on the newest results of the annual modulation of data together with the measurements, collected in more than 10 years.

v. Choosing the action for the assumed laws of Nature to predict experiments one must be able to calculate properties of systems accurately enough. One must be able to evaluate the renormalizability, the anomalies, for any proposed theory. The reader can find some answers to these questions in this proceedings.

This year neither the cosmological nor the particle physics experiments offered much new, as also has not happened in the last three years, which would offer new

insight into the elementary fermion and boson fields and also into cosmological events, although a lot of work and effort have been put in.

However, there are more and more cosmological evidences, which require the new step beyond both standard models, the one of the elementary fermion and boson fields and of cosmology. The understanding the universe through the cosmological theories and theories of the elementary fermion and boson fields have, namely, so far never been so dependent on common knowledge and experiments in both fields.

Although cosmopia served the discussions all the time (and we are very glad that we did have in spite of pandemic also the 24th workshop), it was not like previous workshops. Discussions were fiery and sharp, at least during some talks. But this was not our Bled workshop. Effective discussions require the personal presence of the debaters, as well as of the rest of participants, which interrupt the presentations with questions all the time.

And let us add also this year that due to the on line presentations we have students participants, who otherwise would not be able to attend the Bled conference, the travel expenses are too high for them.

The organizers hope that the virus will be defeated at least up to next year, although the data are not supporting our hope. Let our hope be valid for all over the world, especially for the young generation, as well as for the Bled Workshop 2022, so that we will in July next year meet at Bled.

Since, as every year, also this year there has been not enough time to mature the discussions into the written contributions, only two months, authors can not really polish their contributions. Organizers hope that this is well compensated with fresh contents.

The reader can find all the talks and soon also the whole Proceedings on the official website of the Workshop: <http://bsm.fmf.uni-lj.si/bled2021bsm/presentations.html>, and on the Cosmopia Forum <https://bit.ly/bled2021bsm>.

The organizers are thanking Dragan Lukman for his excellent technical support to more than twenty years of Bled workshops, entitled "What comes beyond the standard models", in particular for his excellent work done on proceedings. In July of this year we learned how small the step is between to be and not to be. The member of editors Dragan Lukman, our friend and the man who recognized clearly the essential problems of our planet, is not among us any longer. He left us after this year workshop due to the heart attack. We are missing him very much, also during the preparation of the proceedings, although we copied his way of preparing the proceedings, using his styles. In memory of Dragan, we added a short summary of his work and Astri's song, which says a lot about Dragan.

The organizing committee thanks Astri Kleppe, who offered to take over Dragan's work on the proceedings when our hardship was greatest.

The organizing committee thanks also Ana Bračič and Anamarija Borštnik Bračič who have done the translations of English abstracts to the Slovenian language.

Let us conclude this preface with a heartfelt and warm thank to all the participants, present via videoconference, for their lectures and especially for the very prolific discussions and, nevertheless, an excellent atmosphere. We are very sorry that some of participants could not prepare their talks as contributions to the proceed-

ings.

*Norma Mankoč Borštnik, Holger Bech Nielsen, Maxim Y. Khlopov,
(the Organizing committee)*

*Norma Mankoč Borštnik, Holger Bech Nielsen, Dragan Lukman, Astri Kleppe
(the Editors)*

*Ana Bračič, Anamarija Bračič Borštnik
(the translators into Slovenian)*

Ljubljana, December 2021

2 Predgovor (Preface in Slovenian Language)

Vsakoletne delavnice z naslovom „Kako preseči oba standardna modela, kozmološkega in elektrošibkega“ (“What Comes Beyond the Standard Models?”) sta postavila leta 1998 Norma in Holger z namenom, da bi udeleženci v izčrpnih diskusijah kritično soočali različne ideje in teorije. V vsem tem času smo iskali odgovore na vprašanje kakšni so zakoni narave. In se veliko naučili.

To leto je stekla 24. delavnica.

Delavnice domujejo v Plemljevi hiši na Bledu ob slikovitem jezeru, kjer prijetni sprehodi in pohodi na čudovite gore, ki kipijo nad mestom, ponujajo priložnosti in vzpodbudo za diskusije. Tako je bilo vse do zadnjih dveh let.

Tudi zadnji dve leti, v letu 2020 in 2021, sta bili delavnici v juliju, vendar nam je tokrat covid-19 onemogočil srečanje v Plemljevi hiši. Tudi diskutirali nismo med hojo okoli jezera ali med hribolazenjem. Vendar nam je dolgoletna iskušnja s “cosmovio” — videopovezavami z laboratoriji po svetu — omogočila, da je tudi letos stekla Blejska delavnica, tokrat prek interneta.

K našim zelo odprtim, prijateljskim, dolgim in zahtevnim diskusijam, polnim iskrivega sodelovanja, je prispevalo veliko fizikov in celo nekaj matematikov. V večini predavanj in razprav so udeleženci poskusili razumeti in pojasniti predpostavke obeh standardnih modelov, elektrošibkega in barvnega v fiziki osnovnih delcev in polj ter kozmološkega, predpostavke in napovedi obeh modelov pa vskladiti z meritvami in opazovanji, da bi poiskali model, ki preseže oba standardna modela, kar bi omogočilo zanesljivejšo napovedi za nove poskuse.

Čeprav je večina udeležencev teoretičnih fizikov, mnogi z lastnimi idejami kako narediti naslednji korak onkraj sprejetih modelov in teorij, so še posebej dobrodošli predstavniki eksperimentalnih laboratorijev, ki nam pomagajo v odprtih diskusijah razjasniti resnično sporočilo meritev in nam pomagajo razumeti kakšne napovedi so potrebne, da jih lahko s poskusi dovolj zanesljivo preverijo.

Tudi v zadnjih dveh letih smo poskušali ohraniti navado, da so bile predstavitve dolge, ker so jih udeleženci prekinjali z vprašanji, da bi bili privzetki in predpostavke jasni. Predavanja so se zato po dveh urah prekinila in se nadaljevala naslednje dni.

Avtorji prispevkov so trdo in z navdušenjem delali, da so pripravili predavanja, in da so v tako kratkem času pripravili članke za ta zbornik.

Ker pa so predavanja preko interneta bolj naporna kot v predavanja v živo, so mnoga vprašanja ostala odprta, nerazjasnena, tudi nedefinirana in nerešena.

Ni nam uspelo nadaljevati pogovorov preko interneta po končani delavnici, četudi smo poskušali. Razlogi so bili različni, med njimi sesutje računalnika ene(ga) od organizatorjev.

Med vprašanji, ki smo jih odprli, pa o njih nismo uspeli zares razpravljati, so:

Kako učinkoviti so lahko modeli, ki ponudijo majhen naslednji korak glede na oba standardna modela, da bi nato predlagali izvedbo poskusov, ki naj povedo ali so taki modeli v skladu z naravo, pri iskanju odgovorov na vsa odprta vprašanja, ali vsaj na del odprtih vprašanj? Kar nekaj prispevkov v tem zborniku, ki poskušajo pojasniti, iz česa utegne biti temna snov, je te vrste.

Ali bi bilo smiselno in bi zmogli primerjati te predloge, denimo, s teorijami strun ali s teorijo *spinov, nabojev, družin*, ki že odgovori na odprta vprašanja obeh standardnih modelov in ponudi tudi napovedi, ki jih je potrebno preveriti, za temno snov in tudi za druga kozmološka opažanja.

Združevanje znanja, idej in vložene delo bi lahko povečalo možnosti, da prepoznamo, kaj je pravi naslednji korak, ki prinaša odgovore na odprta vprašanja v fiziki osnovnih fermionskih in bozonskih polj in kozmologiji ter bi pomagalo predlagati zaupanja vredne poskuse, ki bodo domneve potrdili, posebej, če bi pri diskusijah tvorno sodelovali tudi experimentalci. Experimenti so dragi.

Čeprav so *črne luknje* eksperimentalno potrjeni objekti, kvantna mehanika *črnih lukenj* v resnici ni znana. Vendar je to znanje potrebno, če sprejmemo možnost, da je prostor-čas več kot $(3 + 1)$ -razsežen, kot to domnevajo *teorije strun* in *Kaluza-Kleinove teorije*, da je njegova razsežnost morda celo $(13 + 1)$ ali več, kot domneva teorija *spin-charge-family* (s fermioni, ki interagirajo samo z gravitacijsko silo, z dvema prispevkoma v tem zborniku), ali kot domneva tudi *teorija strun*, ali pa je lahko neskončen, saj je nič in neskončno enostavno sprejeti, vse druge možnosti potrebujejo pojasnila. Kako v tem kontekstu razumeti primordiale *črne luknje*? Ali se pojavijo po elektrošibkem faznem prehodu? Ali nastanejo že prej? Ali tedaj prostor-čas že učinkuje kot $(3 + 1)$ -razsežen? In kaj se dogaja znotraj teh primordialnih *črnih lukenj*? Kaj pa se dogaja znotraj zelo masivnih *črnih lukenj*? Ali lahko teorije strun v kontekstu M-teorije pomagajo razumeti kvantno gravitacijo tudi, če notranji prostor fermionov in bozonov določa Cliffordova algebra?

Ali bi teorija, imenovana *nova teorja strun*, poročilo je najti v tem zborniku, s strunami iz inertnih objektov, ki so dejansko strune vezane v struno z veliko stopnjo simetrije, bila sprejemljiva tudi, če bi notranje stopnje fermionov in bozonov določali Cliffordovi objekti? Bi bile take strune koristne tudi za razumevanje kvantne mehanike zelo masivnih *črnih lukenj*?

Zgodi se, da nov način obravnavanja kvantne mehanike vezanih sistemov, kakršen je uporaba superkonformne kvantne mehanike in holografije "light-front" v hadronski fiziki, omogoči nov pogled in novo razumevanje dinamike in simetrij vezanih stanj. Poročilo o tem prinaša zbornik.

Za razumevanje nastanka in začetne širitve našega vesolja sta kvantna gravitacija in poznavanje notranjega prostora fermionov in bozonov potrebno orodje. Vsaj nekatera obdobja širitve, obdobje inflacije denimo, je mogoče razložiti v kontekstu teorije strun, o čemer poriča en prispevek.

Ali imamo v našem vesolju poleg običajne snovi tudi domene antisnovi? Je anti-snov pretežno iz *temne snovi*? Kakšne so interakcije snovi s *temno snovjo*? O tem diskutirajo avtorji nekaterih prispevkov v tem zborniku. Teorija *spina, nabojev in družin* gradi na predpostavki, da so zakoni gibanja enotni — za snov, za antisnov in za temno snov.

Simetrije igrajo bistveno vlogo na vseh ravneh fizike: v kozmologiji, v fiziki osnovnih fermionskih in bozonskih polj, tudi v fiziki vseh vrst snovi.

V teorijah, ki predpostavijo da ima prostor več kot $(3 + 1)$ razsežnost, in da interagirajo fermioni samo z gravitacijskimi bozoni — take so Kaluza-Kleinove teorije, tudi teorija *spina-nabojev-družin*, pa tudi teorije strun — je izvor simetrije v

Lorentzovi invariantnosti prostor-časa, ki vključuje tudi notranji prostor fermionov in bozonov. Pri opaženih (nizkih) energijah (po zlomitvi začetne simetrije) določa lastnosti prostora z razsežnostimi $d > (3 + 1)$ notranji prostor fermionskih in bozonskih polj, kar opazimo v $d = (3 + 1)$ -razsežnem prostor-času kot simetrije, ki jih lahko opišemo tudi z metodami teorije grup.

Simetrije osnovnih fermionskih in bozonskih polj so obravnavane v nekaj prispevkih. Koliko skupnega imajo različni pristopi pa bi bilo potrebno in koristno raziskati.

Naj omenimo še nekatere druge teme, k jih prispevki v zborniku obravnavajo:

- i. Kaj je pravi vzrok, da imajo fermioni in nekatera bozonska polja maso?
- ii. Kako dolgo še lahko pravilno interpretiramo rezultate poskusov z uporabo samo *standardnega modela*?
- iii. Experiment DAMA/LIBRA prinša poročilo o zadnjih rezultatih meritev letne modulacije trkov delcev temne snovi z običajno snovjo v njihovih merilnih aparat-urah, povzema pa tudi vse dolgoletne meritve.
- iv. Ko izberemo model, moramo v modelu znati primerjati rezultate meritev dovolj natančno. Moramo vedeti ali je teorija renormalizabilna, ali ima anomalije, in kako se računov lotiti. Tudi na taka vprašanja poskuša odgovoriti eden od prispevkov. Tako kot v preteklih treh letih tudi to leto niso eksperimenti v kozmologiji in fiziki osnovnih fermionskih in bozonskih polj ponudili rezultatov, ki bi omogočili nov vpogled v fiziko osnovnih delcev in polj, čeprav je bilo vanje vložena veliko truda.

Vse več je tudi kozmoloških meritev, za katere se zdi, da jih *standardni model* osnovnih fermionskih in bozonskih polj ne more pojasniti in vse bolj kozmološke meritve in opažanja ter experimentalne meritve v fiziki osnovnih fermionskih in bozonskih polj določajo iskanje teorije, ki lahko pojasni vse predpostavke *standardnega modela*, pa tudi vsa nova kozmološka opažanja in vse nove meritve ter predlaga prave experimente.

Četudi je cosmovia poskrbela, da so diskusije tekle ves čas, tako kot je bilo na vseh delavnicah doslej, blejskih diskusij v živo diskusije po internetu niso mogle nadomestiti. Diskusije so bile ognjevite in ostre, vsaj pri nekaterih predavanjih, vendar potrebujejo učinkovite diskusije osebno prisotnost diskutantov in poslušalcev, ki z vprašanji poskrbijo, da je debata razumljiva vsem. Tudi študentom internet ne more nadomestiti dobrega učitelja.

Organizatorji upamo, da bo vsaj do naslednjega leta virus premagan, četudi ta trenutek naše upanje ni podprto s statističnimi podatki. Naj naše upanje velja za ves svet, za mlado generacijo pa še posebej, pa tudi za Blejsko delavnico 2022, da bo stekla v živo na Bledu.

Ker je vsako leto le malo časa od delavnice do zaključka redakcije, manj kot dva meseca, avtorji ne morejo dovolj skrbno pripraviti svojih prispevkov, vendar upamo, da to nadomesti svežina prispevkov.

Bralec najde zapise vseh predavanj in kmalu tudi letošnji zbornik na uradnem naslovu Delavnice na medmrežju:

<http://bsm.fmf.uni-lj.si/bled2021bsm/presentations.html>,

in na Cosmovia Forum <https://bit.ly/bled2021bsm>.

Zahvaljujemo se Draganu Lukmanu za odlično tehnično podporo več kot dva-
setletnim blejskim delavnicam z naslovom "Kako preseči oba standardna modela",

ter za tehnično pripravo zbornikov. Letos smo izvedeli, kako majhen je korak med biti in ne biti. Član uredniškega odbora Dragan Lukman, naš prijatelj in človek, ki je jasno prepoznaval probleme naše družbe, ni več med nami. Zapustil nas je kmalu za tem, ko se je končala letošnja Blejska delavnica. Imel je srčni napad. Pogrešamo ga, še posebej zdaj med pripravo zbornika, čeprav nam je zapustil tehnično znanje priprave zbornika..

Draganu v spomin smo dodali kratek povzetek njegovega dela ter Astrino pesem, ki veliko pove o Draganu.

Organizacijski odbor se zahvaljuje Astri Kleppe, ki se je ponudila, da prevzame Draganovo delo na zborniku, ko je bila naša stiska največja.

Zahvaljujemo se tudi Ani Bračič in Anamariji Borštnik Bračič za prevode angleškega teksta v slovenščino.

Naj zaključimo ta predgovor s pristrčno in toplo zahvalo vsem udeležencem, prisotnim preko videokonference, za njihova predavanja in še posebno za zelo plodne diskusije in kljub vsemu odlično vzdušje.

Zelo nam je žal, da nekateri udeleženci niso utegnili pripraviti poleg predavamj tudi zapis teh predavanj v obliki prispevkov.

*Norma Mankoč Borštnik, Holger Bech Nielsen, Maxim Y. Khlopov,
(Organizacijski odbor)*

*Norma Mankoč Borštnik, Holger Bech Nielsen, Dragan Lukman, Astri Kleppe
(uredniki)*

*Ana Bračič, Anamarija Bračič Borštnik
(prevodi v slovenščino)*

Ljubljana, grudna (decembra) 2021



1 Virtual talks

A. Addazi, L. Bonora, S. Kabana, E. Kiritsis, R. Mohapatra, Q. Shafi

<http://bsm.fmf.uni-lj.si/bled2021bsm/presentations.html>

<https://bit.ly/bled2021bsm>

1.1 Virtual talks

Because of the pandemic, the Bled Workshop has now been virtual for the two last years, 2020 and 2021.

Not all the talks come as articles in this year's Proceedings, but all the talks can be found

on the official website of the Workshop and on the Cosmovia forum:

<http://bsm.fmf.uni-lj.si/bled2021bsm/presentations.html>

<https://bit.ly/bled2021bsm>. Some of the talks are only available online, namely:

A. Addazi: The multicomponent dark matter structure and its possible observed manifestations.

L. Bonora: HS Yang-Mills-like models:

I review the attempt to construct massless gauge field theories in Minkowski spacetime that go under the name of HS-YM. I present their actions and their symmetries. I motivate their gravitational interpretation. In particular I show how to recover the local Lorentz invariance, which is absent in the original formulation of the theories. Then I propose a perturbative quantization in the so-called frozen momentum frame. I discuss physical and unphysical modes and show how to deal with them. Finally I uncover the gauge symmetry hidden under such unphysical modes. This requires a nonlocal reformulation of the theory, which is, however, characterized by an augmented degree of symmetry.

Povzetek: Avtor pregledno poroča o teorijah z imenom HS-YM, ki v prostoru Minkovskega obravnavajo brezmasna umeritvena polja. Predstavi privzete akcije in simetrije ter njihovo gravitacijsko interpretacijo. Pokaže, kako obnoviti lokalno Lorentzovo invariantnost, ki je v prvotni formulaciji teorij ni. Predlaga kvantizacijo v teoriji motenj v tako imenovanem okviru zamrznjene gibalne količine. Predstavi fizikalne (opazljive) in nefizikalne dele polj in predlaga, kako z njimi ravnati. Razkrije umeritveno simetrijo, skrito v nefizikalnih delih polj, ki pa jo je

opaziti v okviru nelokalne reformulacije teorij z večjo stopnjo simetrije.

S. Kabana: Sexaquarks, the unexpected Dark Matter candidate: Sexaquarks are a hypothetical low mass, small radius uuddss dibaryon which has been proposed recently and especially as a candidate for Dark Matter. The low mass region below 2 GeV escapes upper limits set from experiments which have searched for the uuddss dibaryon and did not find it. Depending on its mass, such state may be absolutely stable or almost stable with decay rate of the order of the lifetime of the Universe therefore making it a possible Dark Matter candidate. Even though not everyone agrees its possible cosmological implications as DM candidate cannot be excluded and it has been recently searched in the BaBar experiment. We use a model which has very successfully described hadron and nuclei production in nucleus-nucleus collisions at the LHC in order to estimate the thermal production rate of Sexaquarks with characteristics such as discussed previously rendering them DM candidates. We show results on a study of the variation of the Sexaquark production rates with mass, radius and temperature and chemical potentials assumed and their ratio to hadrons and nuclei and discuss the interdependences and their consequences. These estimates are important for future experimental searches and enrich theoretical estimates in the multi-quark sector.

Povzetek: Šest-kvarki so hipotetični dibarioni uuddss z majhno maso, velikostnega reda 2GeV in majhnim polmerom. Zato jih je težko izmeriti. Ker je njihov razpadni čas zelo dolg, vsaj tolikšen kot je starost našega vesolja, se zde primerni kandidati za *temno snov* (DM). Četudi jih doslej še niso našli, iskali so jih tudi v eksperimentu BaBar, ostajajo kandidati za *temno snov*, vsj izključiti jih ni mogoče. Avtorji prispevka uporabijo model, ki uspešno opiše nastanek hadronov in jeder pri trkih dveh jeder v velikem hadronskem trkalniku (LHC). Študirajo verjetnost za tvorbo šest-kvarkov v odvisnosti od mase, radija, temperature nastanka in izbire kemičnega potenciala in jo primerjajo z verjetnostjo za nastanek hadronov in jeder. Rezultati ne le bogatijo teoretično vedenje o možnih vezanih stanjih večjega števila kvarkov, ampak ponudijo možnosti za nove experimente.

E. Kiritsis: Coleman de Luccia transitions, and their implications for Quantum Field Theories in De Sitter space.

R. Mohapatra: The Next Symmetry of Nature:

B-L as a gauge generator of electroweak interactions were proposed forty years ago. The discovery of neutrino mass has made pursuing its phenomenological and experimental implications more interesting. In this talk I focus on a minimal model of gauged B-L symmetry and show how the Higgs field that breaks this symmetry can provide a candidate for dark matter which very weakly coupled to matter. I also present how such a version of B-L can be tested in ongoing LHC experiments. I then discuss possible grand unification of the weakly coupled B-L

in an $SO(10)$ in five dimensions and its test in the proton decay experiment.

Reference: R. N. Mohapatra and N. Okada, *Phys.Rev. D* **101** 11, 115022 (2020)

Povzetek: Simetrija B-L in ustrezno umeritveno polje sta bila predlagana kot pojasnilo nastanka elektrošibkega polja že pred štiridesetimi leti. Po odkritju, da imajo tudi nevtrini maso, se je zanimanje za to polje in za morebitne napovedi v zvezi z njim znova obudilo. Avtor predstavi minimalni model simetrije B-L in pokaže, kako lahko Higgsovo polje, ki poruši to simetrijo, zagotovi kandidata za temno snov, ki je zelo šibko povezana z običajno snovjo. Predstavi, kako je mogoče polje B-L opaziti pri poskusih na LHC. Predlaga tudi veliko poenotenje polja B-L, ki je šibko povezano z $SO(10)$ v petih dimenzijah in prispevek poenotenja v poskusu, ki meri razpad protona.

Q. Shafi: Quest for Unification:

Grand Unified Theories (GUTs) provide a compelling framework for unifying the strong, weak and electromagnetic interactions. I will review gauge and Yukawa unification, dark matter, proton decay, topological defects and inflation in supersymmetric and non-supersymmetric GUTs. Some implications of merging grand unification and the weak gravity conjecture are briefly discussed.

Povzetek: Velike poenotene teorije (GUT) ponujajo okvir za poenotenje močnih, šibkih in elektromagnetnih interakcij. Avtor pregledno predstavi poenotenje umeritvenih polj in Yukawinih sklopitev, temno snov, protonski razpad, topološke okvare in inflacijo v supersimetričnih in nesupersimetričnih teorijah poenotenja. Na kratko obravnava tudi nekatere posledice, ko velikemu poenotenju pridruži tudi šibko gravitacijsko polje.



2 Type IIB moduli stabilisation, inflation and waterfall fields

I. Antoniadis^{1**}

email:antoniad@lpthe.jussieu.fr

O. Lacombe^{1,2}

email:osmin@lpthe.jussieu.fr

G. K. Leontaris³

email: leonta@uoi.gr

¹Laboratoire de Physique Théorique et Hautes Énergies, Sorbonne Université, CNRS, 4 place Jussieu, 75005 Paris, France

²Center for Gravitational Physics, Yukawa Institute for Theoretical Physics, Kyoto University, Kyoto 606-8502, Japan

³Physics Department, University of Ioannina, Ioannina 45110, Greece

Abstract. We present a string realisation of the hybrid inflationary scenario within type IIB effective string theory constructions and a geometric configuration of intersecting D7 branes. A metastable de Sitter minimum is ensured by perturbative logarithmic corrections and D-term contributions from abelian factors associated with the D7 branes. The inflaton is identified with the internal volume modulus whereas possible waterfall fields correspond to excitations of open strings attached to the magnetised D7 branes. Incorporating contributions of these fields in the scalar potential, inflation stops and the metastable vacuum settles to a minimum with the observed tuneable value of the cosmological constant.

Povzetek: Avtorji predstaviijo hibridni model inflacije vesolja. Uporabijo efektivno teorijo strun vrste IIB z branami D7. Poiščejo logaritmične popravke, ki hkrati s prispevki člana D za "brane" D7 zagotovijo metastabilni de Sitterjev minimum. Notranji volumnski modul določa napihovanje vesolja, "polja slapov" pa so določena z vzbujenimi stanji odprtih strun, ki so pritrjena na magnetizirane brane D7. Inflacijo vesolja ustavijo, ko vgradijo ta polja v skalarno polje, ki minimum poveže s kozmološko konstanto.

2.1 Introduction

At present, String Theory formulated in ten or eleven dimensions appears to be the only promising candidate for a consistent quantum theory of the four known fundamental forces and their interactions. Compactification of the higher dimensional theory to four spacetime dimensions entails an immense number of string vacua dubbed as the string landscape. Numerous Effective Quantum Field Theories, on the other hand, have been built to describe the low energy physics and make cosmological predictions. Amongst the most important features such a

** Presenter

theory should possess, is a positive tiny cosmological constant $\Lambda \approx 10^{-120} M_{\text{Planck}}^4$ in order to account for the dark energy suggested by cosmological observations. The simplest way to realise the dark energy scenario is to introduce a scalar field ϕ with a potential $V(\phi)$, which displays a minimum value equal to the cosmological constant $V_{\text{min}}(\phi_0) = \Lambda$, at some suitable point ϕ_0 . There is a significant ongoing debate, however, on whether the string landscape contains any de Sitter vacua which comply with the prediction of positive Λ . Recent Swampland conjectures [1], in particular, suggest that the first and second derivatives of $V(\phi)$ must satisfy the inequalities $|\nabla V|/V \geq c$ or $\min(\nabla_i \nabla_j V) \leq -c'$ (in Planck units) where c, c' are positive constants of order one. If these inequalities are true, some apparently consistent (anomaly free) theories in four dimensions do not have an ultra-violet completion and cannot be derived from string theory. In other words, they belong to the Swampland¹. Putting it differently, starting from a successful Effective Field Theory weakly coupled to gravity which describes adequately the known physics phenomena, we cannot always embed it in the string theory landscape.

The above considerations have far reaching consequences both in cosmology and particle physics [5]. Here, we mention a few implications on otherwise very successful cosmological scenarios. For example, it is rather obvious that the Swampland criteria summarised in the aforementioned inequalities contradict the assumption that the cosmological constant can account for the dark energy of the universe. Furthermore, slow roll inflation is inconsistent with these criteria. Instead, there are suggestions [5] that quintessence models where the cosmological constant varies over time satisfy current observational constraints. If this scenario prevails, the present acceleration phase eventually will terminate whereas the expansion of the universe will come to an end in the distant future.

The ensuing years since their formulation, Swampland conjectures have faced increased scrutiny. Most of the criticism focused on the assumed heuristic arguments, and the neglected role of string quantum corrections. Indeed, the latter are anticipated to be essential for the final form of the effective scalar potential in the resulting field theory model after compactification. This presentation will focus on investigations of de Sitter vacua and the realisation of inflation in type IIB superstring theory. These investigations will take place assuming a geometric configuration of intersecting D-brane stacks with magnetic fluxes [6]. At the same time, we will consider the effects of a new four-dimensional Einstein-Hilbert term (localised in the internal space) which is generated from higher derivative terms in the ten-dimensional string effective action [7,8]. This set up induces logarithmic corrections to the scalar potential via loop effects [9]. Minimisation of the whole scalar potential of the theory fixes the internal volume Kähler modulus, \mathcal{V} , whereas the ratios of the worldvolumes along the three D7-brane stacks are fixed by virtue of D-term contributions and their parameters depending on the quantised magnetic fluxes. In addition, slow-roll inflation can be realised considering the (canonically normalised) inflaton field to be proportional to the logarithm of the internal volume \mathcal{V} . Furthermore, the open string spectrum associated with the D7 brane stacks plays a significant role. One can fix magnetic fluxes and brane separations so that charged open string states have positive squared-masses, except

¹ For reviews and further references see [2–4]

for one of them which becomes tachyonic when \mathcal{V} becomes less than some critical value. It turns out that this state can be identified with a waterfall field which can be used to stop the inflationary phase and deepen the vacuum. A generalisation of this scenario with several waterfall fields shows that the model can accommodate the present dark energy.

2.2 Type IIB moduli stabilisation

We briefly introduce the basic geometric set up and the moduli field content. We consider a six-dimensional compactification on a Calabi-Yau (CY) threefold within a type IIB framework in the presence of quantised 3-form fluxes. Deformations of the compactification correspond to massless scalars which do not acquire tree-level potential and do not affect the four-dimensional action. Such scalars are the dilaton field Φ , the Kähler moduli \mathcal{T}_i , the complex structure (CS) ones z_a , moduli corresponding to brane deformations and so on. We further introduce a two index antisymmetric tensor denoted with $B_{\mu\nu}$ (the Kalb-Ramond field) and the p -form potentials C_p , $p = 0, 2, 4$. The C_0 potential and the dilaton field, define the usual axion-dilaton combination $S = C_0 + i e^{-\Phi} \rightarrow C_0 + \frac{i}{g_s}$ where g_s is the string coupling. At the effective theory level, there are two basic ingredients: the superpotential of the moduli fields and the Kähler potential.

To construct the superpotential one introduces p -form field strengths $F_p = d C_{p-1}$, $H_3 := d B_2$ and defines $\mathbf{G}_3 := F_3 - S H_3$. In terms of these, the fluxed induced superpotential \mathcal{W}_0 is given, at the classical level, by the well-known formula [10]:

$$\mathcal{W}_0 = \int \mathbf{G}_3 \wedge \Omega(z_a), \quad (2.1)$$

where $\Omega(z_a)$ is a holomorphic 3-form. It turns out that the perturbative superpotential \mathcal{W}_0 is a holomorphic function which depends on the axion-dilaton modulus S , and the CS moduli z_a . Imposing the supersymmetric conditions, the moduli z_a, S can be stabilised. On the contrary, the Kähler moduli, do not participate in the perturbative superpotential and thus remain completely undetermined at this stage.

The second ingredient is the Kähler potential which depends logarithmically on the various moduli fields through the expression:

$$\mathcal{K}_0 = -2 \ln(\mathcal{V}) - \ln(-i \int \Omega \wedge \bar{\Omega}), \quad (2.2)$$

where \mathcal{V} is the volume of the 6d internal CY manifold \mathcal{X}_6 , in string units. The effective potential is computed from (2.2) using the standard supergravity formula

$$V_{\text{eff}} = e^{\mathcal{K}} \left(\sum_{I,J} \mathcal{D}_I \mathcal{W}_0 \mathcal{K}^{I\bar{J}} \mathcal{D}_{\bar{J}} \mathcal{W}_0 - 3 |\mathcal{W}_0|^2 \right), \quad (2.3)$$

where $\mathcal{D}_I = \partial_I + \mathcal{K}_I$ is the Kähler covariant derivative. At the classical level this potential vanishes identically due to its no-scale structure, and appropriate

supersymmetric (flatness) conditions for the dilaton and the CS moduli. It is thus impossible to stabilise the Kähler moduli at this level. These moduli can be stabilised when quantum corrections breaking the no-scale structure of the Kähler potential are included.

Several ways to fix this problem have appeared over the last two decades. A first approach [11, 12] was based on the inclusion of non-perturbative superpotential terms of the form $\mathcal{W}_{np} \sim \sum_i A_i e^{-\alpha_i \mathcal{T}_i}$. The coefficients A_i may depend on the complex structure moduli, and the exponential factors on the Kähler ones \mathcal{T}_i . The parameters α_i may arise from gaugino condensation on D-brane stacks and for the $SU(N)$ case, they are of the form $\frac{2\pi}{N}$. The above ingredients can stabilise the Kähler fields, however the potential acquires an anti-de Sitter (AdS) vacuum [11]. A possible solution to this problem [12] is to uplift the vacuum by taking into account contributions from $\overline{D3}$ branes. There are two issues regarding this solution. Firstly, in order to obtain an AdS minimum the coefficients \mathcal{W}_0 , A_i and α_i require unnatural fine-tuning. Secondly, these contributions rely on non-perturbative effects which cannot be controlled at the full string level. Some improvements of the original models, however, have appeared using nilpotent chiral multiplets [13], which lead to a new mechanism for uplifting the vacua in the string landscape [14]. A different way to stabilise the moduli is based on Large Volume Scenario (LVS) [15]. This proposal takes advantage of the leading α' corrections to the Kähler potential (together with the non-perturbative contributions) which ensure an AdS solution in the Large Volume Limit but avoid tuning \mathcal{W}_0 in (2.1) at extremely small values. Uplift to a de Sitter (dS) vacuum can be realised through D-terms.

Perturbative moduli-dependent corrections in weakly coupled string theory, on the other hand, are fully controllable and therefore more reliable. However, not all types of corrections are suitable for moduli stabilisation. Ordinary perturbative expansions, either in α' or in powers of the weak string coupling g_s , fail to generating a (meta)stable dS minimum in a controllable way. This is the well-known Dine-Seiberg problem which we now describe in brief. When perturbative moduli-dependent quantum corrections are included in the Kähler potential they induce contributions to the scalar potential, $V(\tau_i)$ where τ_i are the imaginary parts of the Kähler moduli \mathcal{T}_i and are associated with the internal volume. The validity of perturbation theory implies that such corrections should vanish for $\tau_i \rightarrow \infty$ implying also the vanishing of the scalar potential $V(\tau_i)_{\tau \rightarrow \infty} \rightarrow 0$. If the zero at infinity is reached from negative values, then, for non-contrived scalar potentials $V(\tau_i)$, this implies an AdS minimum which is not acceptable. Thus, the vanishing of the potential at infinity should be approached from positive values. Again, for reasonable $V(\tau_i)$, this implies that there should be somewhere a maximum before a dS minimum is formed. These three shapes are plotted in figure 2.1. The potential on the right-hand side exhibits **local** minimum and maximum and its shape suggests that there should be **two** competing terms of different functional dependence on τ . While previously considered perturbative corrections do not share this property at large volumes, a possible exception known from field theory are logarithmic corrections similar to those in the Coleman-Weinberg mechanism [16].

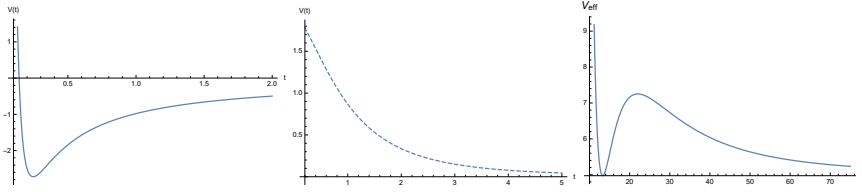


Fig. 2.1: Left figure: Vanishing of $V(\tau)$ from 0^- happens for potentials with an AdS minimum. Middle: Large τ behaviour of $V(\tau)$ with power law correction $\sim \frac{1}{\tau^n}$. The potential on the right-hand side exhibits **local** minimum and maximum.

The above observation shows the way to overcome the difficulties in superstring constructions. We recall that string theory has a rich structure including non-perturbative objects such as D-branes which open up possibilities to construct realistic cosmological models. Another ingredient, of particular interest in the present study, comes from high order curvature terms in the ten dimensional effective action. These elements are sufficient to generate loop corrections which induce new contributions to the Kähler potential \mathcal{K} , break its no scale invariance and stabilise the moduli. We will describe in short how perturbative logarithmic corrections are generated with the above constituents.

The low-energy expansion of the type IIB superstring action contains fourth order terms in the Riemann curvature, R^4 , which do not receive any perturbative corrections beyond one loop [7, 17, 18]. Upon compactification to our four dimensional spacetime M_4 , these one-loop corrections induce a novel Einstein-Hilbert (EH) term $\mathcal{R}_{(4)}$. Its coefficient is proportional to the Euler characteristic χ , defined on \mathcal{X}_6 by

$$\chi = \frac{3}{4\pi^3} \int_{\mathcal{X}_6} R \wedge R \wedge R.$$

Observing that χ contains three powers of R , we deduce that the effective EH term $\mathcal{R}_{(4)}$ (originating from R^4) is only possible in four dimensions. Furthermore, such an EH term can be viewed as a vertex localised at certain points in the six-dimensional bulk where χ acquires non-zero values, emitting closed strings (gravitons). We thus study the case of three-graviton scattering involving two massless gravitons and a Kaluza-Klein (KK) excitation propagating towards a D7-brane stack. The sum over the KK modes corresponds to a propagation that takes place in a two-dimensional bulk space transverse to the D7 stack, see Figure 1.2. Consequently, this process yields logarithmic contributions breaking the no-scale invariance of the Kähler potential [6, 9]. Taking these logarithmic contributions into account the final effective action (obtained in the T^6/Z_N orbifold limit) contains [9]

$$S \ni \frac{1}{(2\pi)^3} \int_{M_4 \times \mathcal{X}_6} e^{-2\Phi} \mathcal{R}_{(10)} + \frac{4\zeta(2)\chi}{(2\pi)^3} \int_{M_4} \left(1 - \sum_{k=1,2,3} e^{2\Phi} T_k \log \frac{R_{\perp}^k}{w} \right) \mathcal{R}_{(4)}. \quad (2.4)$$

Here, T_k is the brane tension of the k -th stack, R_{\perp}^k the size of the two-dimensional space transverse to the D7-stack and w an ‘effective’ localisation width of the

graviton vertex, given by $w = \ell_s/\sqrt{N}$ with $\ell_s = \sqrt{\alpha'}$ the fundamental string length [8].

From the correction terms (2.4) in the 4d reduced action we can readily extract the corresponding induced terms in the Kähler potential. For simplicity we assume the same tension for all three brane stacks, so that $T_k \equiv T = e^{-\Phi} T_0$, and for each Kähler modulus \mathcal{T}_k we denote $\tau_k = \text{Im}\mathcal{T}_k$. For D7-brane stacks with orthogonal co-volumes, the internal volume is simply $\mathcal{V} = \sqrt{\tau_1\tau_2\tau_3}$, and the the Kähler potential takes the form

$$\mathcal{K} = -2 \ln(\sqrt{\tau_1\tau_2\tau_3} + \xi + \gamma \ln(\tau_1\tau_2\tau_3)) \equiv -2 \ln(\mathcal{V} + \xi + \gamma \ln \mathcal{V}) . \quad (2.5)$$

Computations for the orbifold and smooth CY cases show that the parameters ξ and γ are given by [8, 9]

$$\gamma \equiv -\frac{1}{2} g_s T_0 \xi , \quad \text{with } \xi = -\frac{\chi}{4} \times \begin{cases} \frac{\pi^2}{3} g_s^2 & \text{for orbifolds} \\ \zeta(3) & \text{for smooth CY} \end{cases} , \quad (2.6)$$

In (2.6) tree-level contributions for the orbifold case have not been included, since the $\zeta(3)\chi$ correction to the EH term vanishes [7, 8]. The identity $\zeta(2) = \frac{\pi^2}{8}$ has also been used in the orbifold action (2.4).

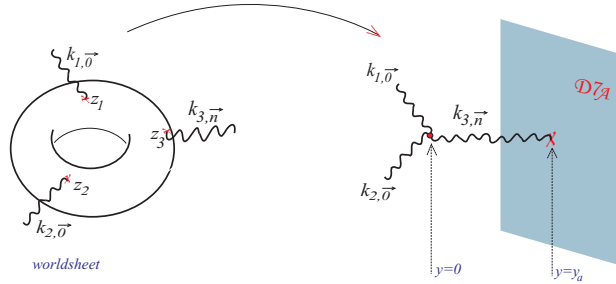


Fig. 2.2: Non-zero contribution from 1-loop; 3-graviton scattering amplitude of 2 massless gravitons and 1 KK mode corresponding to a closed string propagation in 2-dimensions towards a D7 brane.

2.3 Inflationary phase

From (2.3) we can readily compute the F-part of the scalar potential V_F . To this end, we assume that all complex structure moduli are stabilised and the fluxed induced superpotential \mathcal{W}_0 can be taken as a constant, while for convenience we introduce the new parameter $\mu = e^{\frac{\xi}{2\gamma}}$. The exact expression for V_F can thus be written as

$$V_F = \frac{3\gamma\mathcal{W}_0^2}{\kappa^4} \frac{2(\gamma + 2\mathcal{V}) + (4\gamma - \mathcal{V}) \ln(\mu\mathcal{V})}{(\mathcal{V} + 2\gamma \ln(\mu\mathcal{V}))^2 (6\gamma^2 + \mathcal{V}^2 + 8\gamma\mathcal{V} + \gamma(4\gamma - \mathcal{V}) \ln(\mu\mathcal{V}))} , \quad (2.7)$$

where $\kappa = \sqrt{8\pi G_N}$ is the reduced Planck length. In the large volume limit, V_F takes the simplified form

$$V_F = \frac{3\mathcal{W}_0^2}{2\kappa^4\mathcal{V}^3} (\xi + 2\gamma(\ln \mathcal{V} - 4)) + \dots \quad (2.8)$$

By virtue of the logarithmic term the potential (2.8) acquires a global minimum, although this is an anti-de Sitter vacuum. Yet, a D-part contribution to the scalar potential comes from the existence of universal $U(1)$ factors associated with the three D7-brane stacks. In the large world-volume limit this contribution takes the form

$$V_D = \frac{d_1}{\kappa^4\tau_1^3} + \frac{d_2}{\kappa^4\tau_2^3} + \frac{d_3}{\kappa^4\tau_3^3} + \dots \quad (2.9)$$

where the d_i for $i = 1, 2, 3$ are model-dependent constants related to $U(1)$ Fayet-Iliopoulos (FI) terms.

For the subsequent discussion it is useful to replace the dependence of the potential on Kähler moduli with the canonically normalised fields. We identify them with a logarithmic function of the volume and two perpendicular directions defined in terms of τ_i ratios. We also recall that we consider a simple setup with ‘‘orthogonal’’ D7-brane stacks, such that $\mathcal{V} = \sqrt{\tau_1\tau_2\tau_3}$. The new basis then reads:

$$\phi = \sqrt{\frac{2}{3}} \ln(\mathcal{V}), \quad (2.10)$$

$$u = \frac{1}{2} \log\left(\frac{\tau_1}{\tau_2}\right), \quad (2.11)$$

$$v = \frac{\sqrt{3}}{6} \log\left(\frac{\tau_1\tau_2}{\tau_3\tau_3}\right). \quad (2.12)$$

In terms of these, the total scalar potential $V_{\text{eff}} = V_F + V_D$ in the large volume limit is

$$V_{\text{eff}} \approx \frac{3\mathcal{W}_0^2}{2\kappa^4} e^{-3\sqrt{\frac{2}{3}}\phi} \left(\gamma(\sqrt{6}\phi - 4) + \xi \right) + \frac{e^{-\sqrt{6}\phi}}{\kappa^4} \left(d_1 e^{-\sqrt{3}v-3u} + d_2 e^{-\sqrt{3}v+3u} + d_3 e^{2\sqrt{3}v} \right). \quad (2.13)$$

In the inflationary scenario that we will discuss shortly, the field ϕ defined in 2.10 will play the role of the inflaton. In order to examine its evolution during the inflation era, we need first to stabilise the three moduli $u, v, \mathcal{V} = e^{\sqrt{\frac{2}{3}}\phi}$ and derive the constraints in order to ensure a dS vacuum. We first minimise V_{eff} with respect to the two transverse fields u, v , and find their values at the minimum:

$$u_0 = \frac{1}{6} \ln\left(\frac{d_1}{d_2}\right), \quad v_0 = \frac{1}{6\sqrt{3}} \ln\left(\frac{d_1 d_2}{d_3^2}\right). \quad (2.14)$$

Substituting back into (2.13) we obtain the simple expression

$$V(\phi) \simeq -\frac{C}{\kappa^4} e^{-3\sqrt{\frac{2}{3}}\phi} \left(\sqrt{\frac{3}{2}}\phi - 4 + q + \frac{3}{2}\sigma e^{\sqrt{\frac{2}{3}}\phi} \right), \quad (2.15)$$

where we have defined

$$C \equiv -3\mathcal{W}_0^2\gamma > 0, \quad d \equiv 3(d_1 d_2 d_3)^{\frac{1}{3}}, \quad q \equiv \frac{\xi}{2\gamma}, \quad \sigma \equiv \frac{2d}{9\mathcal{W}_0^2\gamma}. \quad (2.16)$$

A few comments are in order. First, in order to ensure a dS vacuum, the parameter γ must be negative, hence the coefficient C is positive. Moreover, the parameter d , related to the D-term part of the potential, is always positive. Furthermore, increasing of the value of the parameter q shifts the local extrema towards larger volumes. Finally, σ is the only free parameter of the model. It acquires negative values, hence the total coefficient of the last term is positive and is expected to uplift the minimum of the potential to positive values.

To study inflation and compute the slow-roll parameters we need to determine the extrema of the potential with respect to the inflaton field ϕ [19]. Thus we take the first and second derivatives of the potential with respect to ϕ and obtain

$$V'(\phi) = 3\sqrt{\frac{3}{2}} \frac{C}{\kappa^4} e^{-3\sqrt{\frac{3}{2}}\phi} \left(\sqrt{\frac{3}{2}}\phi + q - \frac{13}{3} + \sigma e^{\sqrt{\frac{3}{2}}\phi} \right), \quad (2.17)$$

$$V''(\phi) = -\frac{27}{2} \frac{C}{\kappa^4} e^{-3\sqrt{\frac{3}{2}}\phi} \left(\sqrt{\frac{3}{2}}\phi + q - \frac{14}{3} + \frac{2}{3}\sigma e^{\sqrt{\frac{3}{2}}\phi} \right). \quad (2.18)$$

Requiring the vanishing of the first derivative, $V'(\phi) = 0$, we obtain two solutions which are expressed in terms of the two branches W_0 and W_{-1} of the Lambert W function (product logarithm):

$$\phi_- = -\sqrt{\frac{2}{3}} \left(q - \frac{13}{3} + W_0(-e^{-x-1}) \right), \quad (2.19)$$

$$\phi_+ = -\sqrt{\frac{2}{3}} \left(q - \frac{13}{3} + W_{-1}(-e^{-x-1}) \right). \quad (2.20)$$

The new parameter x introduced in the above solutions is defined by

$$x \equiv q - \frac{16}{3} - \log(-\sigma) \quad \leftrightarrow \quad \sigma = -e^{q - \frac{16}{3} - x}. \quad (2.21)$$

while ϕ_- is the local minimum and ϕ_+ the local maximum. Large volumes can be achieved at weak coupling for $q < 0$, implying a negative Euler number $\chi < 0$, see 2.6 and 2.16.

Notably, most of the important quantities are expressed through simple analytical forms in terms of x . For example, the slow-roll parameter η depends only on x through the Lambert W function:

$$\eta(\phi_{-/+}) = \frac{V''(\phi_{-/+})}{V(\phi_{-/+})} = -9 \frac{1 + W_{0/-1}(-e^{-x-1})}{\frac{2}{3} + W_{0/-1}(-e^{-x-1})}. \quad (2.22)$$

Similarly, the distance between the two extrema is

$$\phi_+ - \phi_- = \sqrt{\frac{2}{3}} [W_0(-e^{-x-1}) - W_{-1}(-e^{-x-1})] > 0. \quad (2.23)$$

The parameter x thus clearly plays a significant role. For the critical value $x_c \simeq 0.072132$ the potential at the minimum vanishes, $V(\phi_-) = 0$, which corresponds to a Minkowski minimum. Below this critical value, in the region $0 < x < x_c$, the potential acquires a dS vacuum whereas for $x > x_c$ it displays an AdS minimum. For $x < 0$ the two branches of the Lambert function join and the potential loses its local extrema. The potential for the three regimes described above is depicted in 2.3.

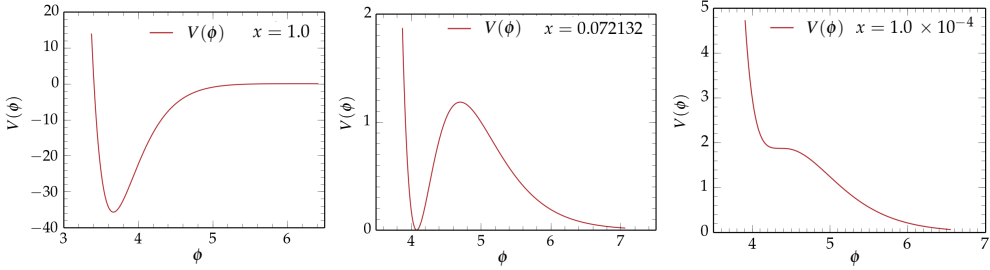


Fig. 2.3: Scalar potential $V(\phi)$ for different values of x giving an AdS, Minkowski or dS vacuum.

Having determined the region of the parameter x which is consistent with dS minima, we are now ready to study cosmological implications and in particular inflationary observables. We first find that some well-known inflationary scenarios such as slow-roll inflation hilltop, cannot be realised in our restricted model. We can easily adjust the value of the slow-roll parameter η (which depends only on x) by varying $x \in (0, x_c)$, so that inflation starts near the maximum, and the modes exit horizon with the required value of the spectral index. It is found, however, that the slow-roll parameters ϵ, η remain much less than unity all the way down the slope, hence inflation does not stop, and as a result an unacceptably large number of e-folds is generated.

As we describe below, in order to study more general inflationary scenarios, we will scan the x parameter space. For each value of x , we can solve the evolution equation for the Hubble parameter and derive the relevant parameters to study the eventual inflationary stage. Before entering the details of such a procedure, we thus recall a few basic equations regarding the evolution of the expansion of the Universe and the inflationary epoch assuming a single scalar field ϕ in the standard Friedmann-Lemaître-Robertson-Walker (FLRW) background. The Friedmann equations for an expanding Universe are

$$3H^2 = \frac{1}{2}\dot{\phi}^2 + \kappa^2 V(\phi), \quad (2.24)$$

$$2\dot{H} = -\dot{\phi}^2, \quad (2.25)$$

where, as usual $H(t) = \frac{\dot{a}}{a}$, represents the Hubble parameter. The equation of motion for the scalar field reads

$$\ddot{\phi} + 3H\dot{\phi} + \kappa^2 V'(\phi) = 0. \quad (2.26)$$

Changing variable $\dot{H} = \frac{dH}{d\phi}\dot{\phi}$, equation (2.25) yields

$$\frac{dH}{d\phi} = H'(\phi) = -\frac{1}{2}\dot{\phi}. \quad (2.27)$$

Using (2.24) and expressing $\dot{\phi}$ as a function of H and V , we obtain the Hubble parameter evolution equation:

$$H'(\phi) = \mp \frac{1}{\sqrt{2}} \sqrt{3H^2(\phi) - \kappa^2 V(\phi)}. \quad (2.28)$$

The exact forms of the slow-roll parameters η , ϵ are [20]

$$\eta(\phi) = 2 \frac{H''(\phi)}{H(\phi)}, \quad \epsilon(\phi) = -\frac{\dot{H}}{H^2} = 2 \left(\frac{H'(\phi)}{H(\phi)} \right)^2, \quad (2.29)$$

while in the slow-roll limit they acquire the usual forms $\eta(\phi) \approx \frac{V''(\phi)}{V(\phi)}$, and $\epsilon(\phi) \approx \frac{1}{2} \left(\frac{V'(\phi)}{V(\phi)} \right)^2$. From the first expression of ϵ in (2.29), we obtain

$$\frac{\ddot{a}}{aH^2} = 1 - \epsilon, \quad (2.30)$$

so that $\epsilon < 1$ is the natural criterium characterising inflation, a phase with $\ddot{a} > 0$. Finally, the number of e-folds N is given by

$$N = \int_t^{t_{\text{end}}} H dt = \frac{1}{\sqrt{2}} \int_{\phi_{\text{end}}}^{\phi} \frac{d\phi}{\sqrt{\epsilon}}. \quad (2.31)$$

As mentioned above, one can investigate inflationary possibilities through a scan of the χ parameter in the following way. The value of χ determines the shape of the inflaton scalar potential $V(\phi)$, which enters the evolution equation (2.28) for the Hubble parameter. For a given value of χ , solving this equation thus allows to compute the slow-roll parameters and number of e-folds, through 2.29 and 2.31, and study the inflationary phase.

The above scan gave rise to a novel scenario where most of the e-folds are obtained near the minimum. In this scenario, the inflaton starts rolling down from a point close to the maximum towards the minimum of its potential with zero initial speed. If $\eta(\phi_+) < -0.02$, because at the inflection point the second derivative $V''(\phi)$ changes sign, the inflaton will pass through the point where $\eta(\phi_*) = -0.02$ before it crosses the inflection point. We can then choose the parameter χ so that 60 e-folds are obtained from this point to minimum. Thus, in order to reproduce the observational data, the initial position of the inflaton has to be higher than the inflection point, where η is negative, so that $\eta = -0.02$ is taken at the horizon exit. In order to realise this scenario, we have solved numerically the evolution equation (2.28) for various values of χ , starting near the maximum with vanishing initial speed for the inflaton. The required number of e-folds, $N_* \simeq 60$ are achieved for $\chi \simeq 3.3 \cdot 10^{-4}$ while the two extrema of the potential are found at $\phi_- = 4.334$ and $\phi_+ = 4.376$. The e-folds are computed from the horizon exit $\phi_* \simeq 4.354$

at which $\eta(\phi_*) = -0.02$, down to the minimum ϕ_- . Is it worth observing that the corresponding inflaton field displacement $\Delta\phi \simeq 0.02$, is much less than one in Planck units. Hence it corresponds to small field inflation, and as such is compatible with the validity of the effective field theory. Finally, this model predicts an inflation scale $H_* \simeq 5 \times 10^{12}$ GeV and a ratio of tensor to scalar perturbations $r \simeq 4 \times 10^{-4}$.

2.4 Waterfall fields and hybrid inflation

Up to this point, we have explained how in the simple geometric set up of three D7-brane stacks we can ensure Kähler moduli stabilisation in a dS vacuum and investigated the conditions to realise inflation. We found that logarithmic radiative corrections and brane magnetisations generate a scalar potential with a very shallow dS minimum, which can realise inflation with the required 60 e-folds collected near the minimum (as opposed -for example- to the case of hilltop scenario). However, the tight constraints imposed by the various requirements entail a metastable minimum with a cosmological constant much larger than the one observed today. A detailed consideration shows that this false vacuum of the so-obtained scalar potential is suggestive for a solution through hybrid inflation [21] where a waterfall field ends the inflation phase and settles to a lower (true) vacuum with the anticipated value of the cosmological constant. Such a waterfall field is realised by a scalar field with effective mass depending on the value of the inflaton. If this field becomes tachyonic under a certain critical value for the inflaton, it generates the waterfall direction of the scalar potential.

Within the present geometric configuration, potential waterfall field candidates are the various states associated with the excitations of open strings with endpoints attached to D7 brane stacks. The scalar components of these states may receive supersymmetric positive square masses from brane separation or Wilson lines, and non-supersymmetric contributions due to the presence of the worldvolume magnetic fields generating the D-terms required for moduli stabilisation.

In the following, we briefly describe how these fields contribute to the materialisation of this scenario in the context of a $\mathbb{Z}_2 \times \mathbb{Z}_2$ orbifold. We assume a factorised 6-torus into three 2-tori $T^6 = T^2 \times T^2 \times T^2$ spanning the internal dimensions (45), (67) and (89) respectively. The model under consideration consists of three D7 brane stacks, which we denote with $D7_1, D7_2$ and $D7_3$. Each of them spans four internal dimensions and is localised in the remaining two. This setup can be considered as dual to the configuration of the D9 and D5 branes as in the toroidal orbifold model described in the literature [22, 23]. This is shown schematically in the following table where we impose T-duality along (45) dimensions.

	(45)	(67)	(89)			(45)	(67)	(89)
D7 ₁	·	×	×		D9 ₁	×	×	×
D7 ₂	×	×	·		D5 ₂	·	×	·
D7 ₃	×	·	×		D5 ₃	·	·	×

We use a cross \times to represent the D7 world-volume spanning the corresponding torus, and a dot \cdot to indicate the transverse directions where the D7 brane is localised.

As motivated above, we can introduce magnetic fields $H_a^{(i)}$, on the a -th stack $D7_a$ and in the i -th torus T_i^2 . They are subject to the Dirac quantization condition $m_a^{(i)} \int H_a^{(i)} = 2\pi n_a^{(i)}$, leading to the magnetic field quantisation $2\pi H_a^{(i)} \mathcal{A}_i = k_a^{(i)}$, where $4\pi^2 \mathcal{A}_i$ is the T_i^2 area. Here $m_a^{(i)}$, $n_a^{(i)}$ are the winding numbers and the flux quanta and we defined the ratio $k_a^{(i)} = n_a^{(i)}/m_a^{(i)} \in \mathbb{Q}$. The magnetic fields modify the world-sheet action by introducing boundary terms [24,25] and shift the modes of the charged oscillators by

$$\zeta_a^{(i)} = \frac{1}{\pi} \text{Arctan}(2\pi\alpha' q_a H_a^{(i)}). \quad (2.32)$$

where $q_a = \pm 1, 0$ are the $U(1)$ charges of the open string endpoints.

The mass spectrum can be extracted, either from the field theory mass formula or from vacuum amplitudes, and one sees that when magnetic fields are introduced into the D7-brane configuration, tachyonic states may appear in the spectrum [25,26]. In general, one can eliminate them by introducing appropriate brane separations or Wilson lines.

To be concrete, we consider magnetic fields on each D7 stack, denoted by a circled cross \otimes as the following table.

	(45)	(67)	(89)
D7 ₁	\cdot	\otimes	\times
D7 ₂	\times	\cdot	\otimes
D7 ₃	\otimes	\times	\cdot

Three different kinds of states appear. The first two describe strings with both endpoints on the “same” stack $D7_i$ - $D7_i$ which are either neutral (attached to the same brane, hence with opposite endpoints charges) or doubly charged (stretching between the brane and its orientifold image). The last ones are mixed states $D7_i$ - $D7_j$, with $i \neq j$. Due to the presence of magnetic fields, the massless states of the original orbifold model are modified. The masses of the $D7_i$ - $D7_i$ doubly charged states read $\alpha' m^2 = -2|\zeta_i^{(j)}|^2$ whereas those of the $D7_i$ - $D7_j$ states are of the form $(|\zeta_2^{(3)}| - |\zeta_1^{(2)}|)$, $(|\zeta_1^{(2)}| - |\zeta_3^{(1)}|)$ and $(|\zeta_3^{(1)}| - |\zeta_2^{(3)}|)$.

Observing the above mass formulae, it can be deduced that tachyonic states indeed appear in the spectrum [25,26]. The only way to eliminate all three potential tachyons along the D7-brane intersections ($D7_i$ - $D7_j$ mixed states) is to choose $|\zeta_1^{(2)}| = |\zeta_2^{(3)}| = |\zeta_3^{(1)}|$. On the other hand, in order to uplift the tachyons on the $D7_i$ - $D7_i$ sectors, we can introduce distance separations between branes and their images in the direction orthogonal to their worldvolume, or Wilson lines i.e. constant background gauge fields on unmagnetised worldvolume tori. In the Table below we present a configuration keeping only one potential tachyonic state that can play the role of the waterfall field:²

² The following definitions are introduced: the discrete Wilson lines in the dual lattice are expressed as $A_k = a_{kx} \mathbf{R}_k^{*x} + a_{ky} \mathbf{R}_k^{*y}$, with $a_{kx}, a_{ky} \in \mathbb{Q}$. The $D7_k$ brane position x_k

$$\begin{array}{c|ccc} & (45) & (67) & (89) \\ \hline D7_1 & \cdot & \otimes & \times \\ D7_2 & \times & \cdot & \otimes \\ D7_3 & \otimes & \times & \cdot \end{array} \quad \longrightarrow \quad \begin{array}{c|ccc} & (45) & (67) & (89) \\ \hline D7_1 & \cdot & \otimes & \times_{\mathcal{A}_1} \\ D7_2 & \times & \cdot_{\pm x_2} & \otimes \\ D7_3 & \otimes & \times_{\mathcal{A}_3} & \cdot \end{array}$$

We introduce discrete Wilson lines along the third torus T_3^2 for the $D7_1$ stack and along the second torus T_2^2 for the $D7_3$ stack, while we separate the $D7_2$ stack from its orientifold image in its transverse directions. Next, we denote the \mathcal{A}_i tori areas ($i = 1, 2, 3$) as power fractions of the total volume $\mathcal{A}_i \equiv \alpha' r_i \mathcal{V}^{1/3}$, with $r_1 r_2 r_3 = 1$ and U_i the corresponding complex structure moduli. Then, the masses for the doubly charged states in the three brane stacks are found to be [19]

$$\alpha' m_{11}^2 \approx -\frac{2|k_1^{(2)}|}{\pi r_2 \mathcal{V}^{1/3}} + \frac{a_1^2}{r_3 \mathcal{V}^{1/3}}, \quad (2.33)$$

$$\alpha' m_{22}^2 \approx -\frac{2|k_2^{(3)}|}{\pi r_3 \mathcal{V}^{1/3}} + y_2 r_2 \mathcal{V}^{1/3}, \quad (2.34)$$

$$\alpha' m_{33}^2 \approx -\frac{2|k_3^{(1)}|}{\pi r_1 \mathcal{V}^{1/3}} + \frac{a_3^2}{r_2 \mathcal{V}^{1/3}}, \quad (2.35)$$

where a_1 , a_3 and y_2 are functions of the complex structure moduli U_i defined in 2. By choosing appropriately a_1 , a_3 with respect to the values of the magnetic fluxes $|k_1^{(2)}|$ and $|k_3^{(1)}|$, one can eliminate the $D7_1$ - $D7_1$ and $D7_3$ - $D7_3$ tachyons. For $a_i = 1/2$, typical for \mathbb{Z}_2 orbifolds, this requires flux numbers smaller than wrapping numbers. On the other hand, the $D7_2$ - $D7_2$ state becomes tachyonic at and below a critical value of the volume that can be chosen to be in the vicinity of the minimum of the potential, as required for the waterfall field, denoted by φ_- in the following.

We turn now to the scalar potential. The magnetic fields contribute through a D-term of the form

$$\begin{aligned} V_D &= \sum_a \frac{g_{U(1)_a}^2}{2} \left(\xi_a + \sum_n q_a^n |\varphi_a^n|^2 \right)^2 + \dots \\ &= \sum_{a=1,3} \frac{g_{U(1)_a}^2}{2} \xi_a^2 + \frac{g_{U(1)_2}^2}{2} (\xi_2 + 2|\varphi_+|^2 - 2|\varphi_-|^2 + \dots)^2 + \dots, \end{aligned} \quad (2.36)$$

where in the second line contributions only from the tachyonic field and its charge conjugate are taken into account.

We have also explained that the tachyonic scalar, coming from strings stretching between the $D7_2$ brane stack and its image, may receive a positive mass contribution due to the brane position. In the effective field theory, this contribution is described by a trilinear superpotential obtained by an appropriate $N = 1$ truncation of an $N = 4$ supersymmetric theory. The physical mass for the canonically normalised fields can be computed from the physical Yukawa couplings, derived from the

as $x_k \equiv x_k^x \mathbf{R}_{kx} + x_k^y \mathbf{R}_{ky}$ with $x_k^x, x_k^y \in \mathbb{Q}$, while $\mathbf{R}_{ik} \cdot \mathbf{R}_i^{\alpha l} = \delta_k^l$. For later use, we also define $y_k(U) = \frac{4|x_k^x - iUx_k^y|^2}{\text{Re}(U)}$ and $a_k(U) = \frac{|a_{ky} + iUa_{kx}|^2}{\text{Re}(U)}$.

supergravity action, and can be expressed as [27] $\mathcal{W}_{\text{tach}} = Y_{ijk} \varphi_i \varphi_j \varphi_k$, where Y_{ijk} are Yukawa coefficients expressed in terms of the Kähler metrics of related matter fields. Their volume dependence can be worked out and the final form of the coupling is

$$\mathcal{W}_{\text{tach}} = g_s^{1/2} \kappa^3 \sqrt{\frac{\mathcal{A}_2}{\alpha' \mathcal{V}}} \varphi_2 \varphi_+ \varphi_-, \quad (2.37)$$

which induces a scalar potential F-part of the form $V_F \ni m_{x_2}^2 (|\varphi_+|^2 + |\varphi_-|^2)$ with $m_{x_2}^2 = y_2 (g_s^2 / \kappa^2 \mathcal{V}) \mathcal{A}_2 / \alpha'$. In addition to this mass-squared terms, the F-term scalar potential also contains quartic terms. They can be worked out and the leading term in the scalar potential for the tachyonic scalar is found to be of the form $V_F \ni \kappa^2 m_{x_2}^2 |\varphi_-|^4$.

The effective scalar potential includes the D-term and F-term contributions and its final form is achieved after the minimisation procedure whose details can be found in [19]. Neglecting, in particular, the massive φ_+ field, the scalar potential receives the simplified form

$$V(\mathcal{V}, \varphi_-) = \frac{C}{\kappa^4} \left(-\frac{\ln \mathcal{V} - 4 + q}{\mathcal{V}^3} - \frac{3\sigma}{2\mathcal{V}^2} \right) + \frac{1}{2} m_Y^2(\mathcal{V}) |\varphi_-|^2 + \frac{\lambda(\mathcal{V})}{4} |\varphi_-|^4, \quad (2.38)$$

where the explicit forms of the volume dependent mass m_Y^2 and quartic coupling λ are given in terms of integers representing magnetic fluxes [19] and other string parameters. The final dependence of $V(\mathcal{V}, \varphi_-)$ on the two fields has been written in the form of the hybrid scenario [21] scalar potential. In this form it is even clearer that the role of the waterfall field is played by the scalar field φ_- associated with the state stretching between the D7₂ brane and its orientifold image. Its mass squared m_Y^2 depends on the internal volume \mathcal{V} , directly related to the inflaton, and turns negative when the internal volume acquires a critical value. A waterfall direction is thus generated, as in the hybrid scenario. This mechanism leads to a new lower minimum. It has been found [19] that when only a single tachyon is involved, the amount of reduction falls short to explain the observed value of dark energy of our Universe. This situation can be remedied within our model by introducing more tachyons, coming from the two other D7-brane stacks and from a fourth magnetised stack, parallel to one of the initial stacks. These additional tachyons contribute negatively to the scalar potential and are sufficient to achieve the present value of the cosmological constant. Apart from (or instead of) these contributions, one should of course expect new physics at low energies, leading to other phase transitions that affect the scalar potential. Hence, the precise tuning of the vacuum energy within our high energy model should be regarded as a proof of principle.

2.5 Conclusions

In this presentation we have discussed aspects of perturbative corrections in the weak string coupling regime and large volume compactifications within the framework of type IIB string theory. We have considered a geometric configuration of intersecting D7-brane stacks and investigated the role of logarithmic corrections

which are present by virtue of local tadpoles induced by localised gravity kinetic terms. Such terms are generated from the dimensional reduction of the R^4 terms in the effective ten dimensional action and arise only in four spacetime dimensions. We have shown that in this string theory context, metastable de Sitter vacua can be ensured together with Kähler moduli stabilisation.

Subsequently, we have examined the possibility of realising the mechanism of cosmological inflation. We have shown that the inflationary scenario can be naturally implemented when the internal volume modulus is considered to be the inflaton field. The effective scalar potential contains only a single free parameter, whose value is fixed in order to meet the inflationary conditions and in particular the requirement of 60 e-folds which, in our construction, are collected near the minimum, while the horizon exit occurs near the infection point. These requirements, however, lead to a very shallow potential with its minimum much larger than the known value of the cosmological constant.

To resolve this discrepancy, we have suggested that a string version of the hybrid inflationary scenario could be realised where possible waterfall fields could be identified with some of the charged string states stretching between the branes and their orientifold images. In the effective theory, the (volumed dependent) masses squared of such excitations consist of positive contributions from brane separations and possible negative ones when worldvolume magnetic fields are turned on. With suitable conditions on various quantities such as magnetic fluxes and geometric characteristics, tachyonic states may appear. For illustrative purposes, we have presented a simple scenario where a tachyonic field arises, with its mass squared turning negative as soon as the internal volume acquires a critical value. This is exactly what is required for a waterfall field. More specifically, in the effective field theory, states of the kind described above induce specific contributions to the F- and D-terms of the effective potential. When these contributions are included in the total scalar potential [19], the tachyonic field can indeed play the role of the waterfall field, providing in this way an explicit string realisation of the hybrid inflationary scenario. Finally, we have discussed the role of multiple tachyonic fields in order to obtain the present value of the cosmological constant. Remarkably, the present construction offers an explicit counter-example to de Sitter Swampland conjecture.

References

1. C. Vafa, *The String landscape and the swampland*, hep-th/0509212.
2. E. Palti, *The Swampland: Introduction and Review*, *Fortsch. Phys.* **67** (2019) 1900037, [1903.06239].
3. C. Vafa, *Cosmic Predictions from the String Swampland*, *APS Physics* **12** (2019) 115.
4. M. van Beest, J. Calderón-Infante, D. Mirfendereski and I. Valenzuela, *Lectures on the Swampland Program in String Compactifications*, 2102.01111.
5. P. Agrawal, G. Obied, P. J. Steinhardt and C. Vafa, *On the Cosmological Implications of the String Swampland*, *Phys. Lett. B* **784** (2018) 271–276, [1806.09718].
6. I. Antoniadis, Y. Chen and G. K. Leontaris, *Perturbative moduli stabilisation in type IIB/F-theory framework*, *Eur. Phys. J. C* **78** (2018) 766, [1803.08941].

7. I. Antoniadis, S. Ferrara, R. Minasian and K. S. Narain, *R**4 couplings in M and type II theories on Calabi-Yau spaces*, *Nucl. Phys. B* **507** (1997) 571–588, [hep-th/9707013].
8. I. Antoniadis, R. Minasian and P. Vanhove, *Noncompact Calabi-Yau manifolds and localized gravity*, *Nucl. Phys. B* **648** (2003) 69–93, [hep-th/0209030].
9. I. Antoniadis, Y. Chen and G. K. Leontaris, *Logarithmic loop corrections, moduli stabilisation and de Sitter vacua in string theory*, *JHEP* **01** (2020) 149, [1909.10525].
10. S. Gukov, C. Vafa and E. Witten, *CFT's from Calabi-Yau four folds*, *Nucl. Phys. B* **584** (2000) 69–108, [hep-th/9906070].
11. J. P. Derendinger, L. E. Ibanez and H. P. Nilles, *On the Low-Energy $d = 4$, $N=1$ Supergravity Theory Extracted from the $d = 10$, $N=1$ Superstring*, *Phys. Lett. B* **155** (1985) 65–70.
12. S. Kachru, R. Kallosh, A. D. Linde and S. P. Trivedi, *De Sitter vacua in string theory*, *Phys. Rev. D* **68** (2003) 046005, [hep-th/0301240].
13. I. Antoniadis, E. Dudas, S. Ferrara and A. Sagnotti, *The Volkov–Akulov–Starobinsky supergravity*, *Phys. Lett. B* **733** (2014) 32–35, [1403.3269].
14. S. Ferrara, R. Kallosh and A. Linde, *Cosmology with Nilpotent Superfields*, *JHEP* **10** (2014) 143, [1408.4096].
15. J. P. Conlon, F. Quevedo and K. Suruliz, *Large-volume flux compactifications: Moduli spectrum and D3/D7 soft supersymmetry breaking*, *JHEP* **08** (2005) 007, [hep-th/0505076].
16. S. R. Coleman and E. J. Weinberg, *Radiative Corrections as the Origin of Spontaneous Symmetry Breaking*, *Phys. Rev. D* **7** (1973) 1888–1910.
17. M. T. Grisaru, A. E. M. van de Ven and D. Zanon, *Four Loop beta Function for the $N=1$ and $N=2$ Supersymmetric Nonlinear Sigma Model in Two-Dimensions*, *Phys. Lett. B* **173** (1986) 423–428.
18. M. B. Green and P. Vanhove, *D instantons, strings and M theory*, *Phys. Lett. B* **408** (1997) 122–134, [hep-th/9704145].
19. I. Antoniadis, O. Lacombe and G. K. Leontaris, *Hybrid inflation and waterfall field in string theory from D7-branes*, 2109.03243.
20. A. R. Liddle and D. H. Lyth, *Cosmological inflation and large scale structure*. 2000.
21. A. D. Linde, *Hybrid inflation*, *Phys. Rev. D* **49** (1994) 748–754, [astro-ph/9307002].
22. M. Larosa and G. Pradisi, *Magnetized four-dimensional $Z(2) \times Z(2)$ orientifolds*, *Nucl. Phys. B* **667** (2003) 261–309, [hep-th/0305224].
23. G. Aldazabal, A. Font, L. E. Ibanez and G. Violero, *$D = 4$, $N=1$, type IIB orientifolds*, *Nucl. Phys. B* **536** (1998) 29–68, [hep-th/9804026].
24. A. Abouelsaood, C. G. Callan, Jr., C. R. Nappi and S. A. Yost, *Open Strings in Background Gauge Fields*, *Nucl. Phys. B* **280** (1987) 599–624.
25. C. Bachas, *A Way to break supersymmetry*, hep-th/9503030.
26. C. Angelantonj, I. Antoniadis, E. Dudas and A. Sagnotti, *Type I strings on magnetized orbifolds and brane transmutation*, *Phys. Lett. B* **489** (2000) 223–232, [hep-th/0007090].
27. V. Kaplunovsky and J. Louis, *Model independent analysis of soft terms in effective supergravity and in string theory*, *Phys. Lett. B* **306** (1993) 269–275, [hep-th/9303040].



3 New and recent results, and perspectives from DAMA/LIBRA–phase2

R. Bernabei, P. Belli, A. Bussolotti, V. Caracciolo, R. Cerulli, N. Ferrari, A. Leoncini, V. Merlo, F. Montecchia^{***1,2}

F. Cappella, A. d'Angelo, A. Incicchitti, A. Mattei^{3,4}

C.J. Dai, X.H. Ma, X.D. Sheng, Z.P. Ye^{†5}

¹ Dip. di Fisica, Università di Roma Tor Vergata, Rome, Italy

² INFN, sez. Roma Tor Vergata, Rome, Italy

³ Dip. di Fisica, Università di Roma La Sapienza, Rome, Italy

⁴ INFN, sez. Roma, Rome, Italy

⁵ Key Laboratory of Particle Astrophysics IHEP, Chinese Academy of Sciences, Beijing, PR China

Abstract. Here the results obtained by analysing other two annual cycles of DAMA/LIBRA–phase2 are presented and the long-standing model-independent annual modulation effect measured by DAMA deep underground at the Gran Sasso National Laboratory (LNGS) of the I.N.F.N. with different experimental configurations is summarized. In particular, profiting from a second generation high quantum efficiency photomultipliers and new electronics, the DAMA/LIBRA–phase2 apparatus ($\simeq 250$ kg highly radio-pure NaI(Tl)) has allowed the reaching of lower software energy threshold. Including the results of the two new annual cycles, the total exposure of DAMA/LIBRA–phase2 over 8 annual cycles is $1.53 \text{ ton} \times \text{yr}$. The evidence of a signal that meets all the requirements of the model independent Dark Matter (DM) annual modulation signature is further confirmed: 11.8σ C.L. in the energy region (1–6) keV. In the energy region between 2 and 6 keV, where data are also available from DAMA/NaI and DAMA/LIBRA–phase1, the achieved C.L. for the full exposure ($2.86 \text{ ton} \times \text{yr}$) is 13.7σ ; the modulation amplitude of the *single-hit* scintillation events is: $(0.01014 \pm 0.00074) \text{ cpd/kg/keV}$, the measured phase is (142.4 ± 4.2) days and the measured period is $(0.99834 \pm 0.00067) \text{ yr}$, values all well in agreement with those expected for DM particles. No systematics or side reaction able to mimic the exploited DM signature (i.e. to account for the whole measured modulation amplitude and to simultaneously satisfy all the requirements of the signature) has been found or suggested by anyone throughout some decades thus far.

Povzetek: Avtorji predstavijo rezultate zadnjih in vseh dosedanjih meritev na eksperimentu DAMA/LIBRA, ki meri letno modulacijo sipanja delcev, za katere zdaj že z veliko gotovostjo menijo, da so lahko samo delci *temne snovi*. Nacionalni laboratorij Gran Sasso (LNGS) I.N.F.N. se nahaja globoko pod zemljo. V teh letih so uporabili različne konfiguracije in vsebnosti merilcev ter poskrbeli za njihovo čistost in učinkovitost. V poskusu

^{***} F. Montecchia also Dip. di Ing. Civile e Informatica, Università di Roma Tor Vergata, Rome, Italy

[†] Z.P. Ye also University of Jinggangshan, Jiangxi, China

DAMA/LIBRA-phase2 ($\simeq 250$ kg visoko radijsko čistega NaI(Tl)) uporabljajo drugo generacijov fotopomnoževalk z visoko kvantno učinkovitostjo in najsodobnejšo elektroniko, kar jim je omogočilo, da so znižali energijski prag, do katerega so meritve še zanesljive. Rezultati novih meritev letne modulacije trkov delcev *temne snovi* z delci v merilni aparaturi, ki so neodvisne od modela, potrjujejo stare meritve *temne snovi* ($1.53 \text{ ton} \times \text{leto}$) z $11,8 \sigma$ C.L.(stopnja zanesljivosti) v energijskem območju (1–6) KeV. V energijskem območju med (2 - 6) KeV, kjer so podatki zbrani že s poskusoma DAMA/NaI in DAMA/LIBRA-phase1, pa je C.L. (stopnja zanesljivosti) za polno izpostavljenost ($2,86 \text{ ton} \times \text{leto}$) enaka $13,7 \sigma$. Amplituda modulacije scintilacijskih dogodkov *single-hit* je: ($0,01014 \pm 0,00074$) cpd/kg/keV, izmerjena faza je ($142,4 \pm 4,2$) dni in izmerjeno obdobje je ($0,99834 \pm 0,00067$) na leto. Vse te meritve so v skladu s predpostavko, da so izmerjene dogotke povzročili delci *temne snovi*. Noben drug dogodek, v zadnjih desetletjih so jih predlali kar nekaj, ni v skladu z izmerjenimi rezultati.

3.1 Introduction

The DAMA/LIBRA [1–23] experiment, as well as the pioneer DAMA/NaI [24–51], has the main aim to investigate the presence of DM particles in the galactic halo by exploiting the DM annual modulation signature (originally suggested in Ref. [52, 53]). In particular, the developed highly radio-pure NaI(Tl) target-detectors [1,6,9,54] ensure sensitivity to a wide range of DM candidates, interaction types and astrophysical scenarios (see e.g. Refs. [2, 14, 16–18, 25–32, 35–42], and in literature).

The investigated process is the DM annual modulation signature and related properties; as a consequence of the Earth’s revolution around the Sun, which is moving in the Galaxy with respect to the Local Standard of Rest towards the star Vega near the constellation of Hercules, the Earth should be crossed by a larger flux of DM particles around $\simeq 2$ June and by a smaller one around $\simeq 2$ December (in the first case the Earth orbital velocity is summed to that of the solar system with respect to the Galaxy, while in the other one the two velocities are subtracted). Thus, this DM annual modulation signature is due to the Earth motion with respect to the DM particles constituting the Galactic Dark Halo.

The DM annual modulation signature is very distinctive since the effect induced by DM particles must simultaneously satisfy all the following requirements: the rate must contain a component modulated according to a cosine function (1) with one year period (2) and a phase that peaks roughly $\simeq 2$ June (3); this modulation must only be found in a well-defined low energy range, where DM particle induced events can be present (4); it must apply only to those events in which just one detector of many actually “fires” (*single-hit* events), since the DM particle multi-interaction probability is negligible (5); the modulation amplitude in the region of maximal sensitivity must be $\lesssim 7\%$ of the constant part of the signal for usually adopted halo distributions (6), but it can be larger in case of some proposed scenarios such as e.g. those in Ref. [55–59] (even up to $\simeq 30\%$). Thus this signature has many peculiarities and, in addition, it allows to test a wide range of parameters in many possible astrophysical, nuclear and particle physics scenarios. This DM signature might be mimicked only by systematic effects or side reactions able

to account for the whole observed modulation amplitude and to simultaneously satisfy all the requirements given above.

The description of the DAMA/LIBRA set-up and the adopted procedures during the phase1 and phase2 and other related arguments have been discussed in details e.g. in Refs. [1–6, 19–21, 23]. The radio-purity and details are discussed e.g. in Refs. [1–5, 54] and references therein. The adopted procedures provide sensitivity to large and low mass DM candidates inducing nuclear recoils and/or electromagnetic signals. The data of the former DAMA/NaI setup and, later, those of the DAMA/LIBRA–phase1 have already given (with high confidence level) positive evidence for the presence of a signal that satisfies all the requirements of the exploited DM annual modulation signature [2–5, 35, 36]. In particular, at the end of 2010 all the photomultipliers (PMTs) were replaced by a second generation PMTs Hamamatsu R6233MOD, with higher quantum efficiency (Q.E.) and with lower background with respect to those used in phase1, allowing the achievement of the software energy threshold at 1 keV as well as the improvement of some detector's features such as energy resolution and acceptance efficiency near software energy threshold [6]. The adopted procedure for noise rejection near software energy threshold and the acceptance windows are the same unchanged along all the DAMA/LIBRA–phase2 data taking, throughout the months and the annual cycles. The typical behaviour of the overall efficiency for *single-hit* events as a function of the energy is also shown in Ref. [6]; the percentage variations of the efficiency follow a gaussian distribution with $\sigma = 0.3\%$ and do not show any modulation with period and phase as expected for the DM signal (for a partial data release see Ref. [21]). At the end of 2012 new preamplifiers and special developed trigger modules were installed and the apparatus was equipped with more compact electronic modules [60]. In particular, the sensitive part of DAMA/LIBRA–phase2 set-up is made of 25 highly radio-pure NaI(Tl) crystal scintillators (5-rows by 5-columns matrix) having 9.70 kg mass each one; quantitative analyses of residual contaminants are given in Ref. [1]. In each detector two 10 cm long UV light guides (made of Suprasil B quartz) act also as optical windows on the two end faces of the crystal, and are coupled to two low background PMTs working in coincidence at single photoelectron level. The detectors are housed in a sealed low-radioactive copper box installed in the center of a low-radioactive Cu/Pb/Cd-foils/polyethylene/paraffin shield; moreover, about 1 m concrete (made from the Gran Sasso rock material) almost fully surrounds (mostly outside the barrack) this passive shield, acting as a further neutron moderator. The shield is decoupled from the ground by a metallic structure mounted above a concrete basement; a neoprene layer separates the concrete basement and the floor of the laboratory. The space between this basement and the metallic structure is filled by paraffin for several tens cm in height. A threefold-level sealing system prevents the detectors from contact with the environmental air of the underground laboratory and continuously maintains them in HP (high-purity) Nitrogen atmosphere. The whole installation is under air conditioning to ensure a suitable and stable working temperature. The huge heat capacity of the multi-tons passive shield ($\approx 10^6$ cal/ $^{\circ}$ C) guarantees further relevant stability of the detectors' operating temperature. In particular, two independent systems of air conditioning are available for

redundancy: one cooled by water refrigerated by a dedicated chiller and the other operating with cooling gas. A hardware/software monitoring system provides data on the operating conditions. In particular, several probes are read out and the results are stored with the production data. Moreover, self-controlled computer based processes automatically monitor several parameters, including those from DAQ, and manage the alarms system. All these procedures, already experienced during DAMA/LIBRA-phase1 [1–5], allow us to control and to maintain the running conditions stable at a level better than 1% also in DAMA/LIBRA-phase2 (see e.g. Ref. [21,23]).

During phase2 the light response of the detectors typically ranges from 6 to 10 photoelectrons/keV, depending on the detector. Energy calibration with X-rays/ γ sources are regularly carried out in the same running condition down to few keV (for details see e.g. Ref. [1]); in particular, double coincidences due to internal X-rays from ^{40}K (which is at ppt levels in the crystals) provide (when summing the data over long periods) a calibration point at 3.2 keV close to the software energy threshold. The DAQ system records both *single-hit* events (where just one of the detectors fires) and *multiple-hit* events (where more than one detector fires) up to the MeV region despite the optimization is performed for the lowest energy.

3.2 Eight DAMA/LIBRA-phase2 annual cycles

Table 3.1 summarizes the details of the DAMA/LIBRA-phase2 annual cycles including the last two released ones. The first cycle was dedicated to commissioning and optimizations towards the achievement of the 1 keV software energy threshold [6]. On the other hand that cycle having: i) no data before/near Dec. 2, 2010 (the expected minimum of the DM signal); ii) data sets with some set-up modifications; iii) $(\alpha - \beta^2) = 0.355$ well different from 0.5 (i.e. the detectors were not being operational evenly throughout the year), cannot be used for the annual modulation studies; however, it has been used for other purposes [6,13]. Thus (see Table 3.1) the considered annual cycles of DAMA/LIBRA-phase2 are eight for an exposure of 1.53 ton \times yr. The cumulative exposure, when considering also the former DAMA/NaI and DAMA/LIBRA-phase1, is 2.86 ton \times yr.

The total number of events collected for the energy calibrations during the eight annual cycles of DAMA/LIBRA-phase2 is about 1.6×10^8 , while about 1.7×10^5 events/keV have been collected for the evaluation of the acceptance window efficiency for noise rejection near the software energy threshold [1,6]. Finally, the duty cycle of the experiment is high, ranging between 76% and 86%: the routine calibrations and the data collection for the acceptance windows efficiency mainly affect it.

3.2.1 The annual modulation of the residual rate

In Fig. 3.1 the time behaviours of the experimental residual rates of the *single-hit* scintillation events in the (1–3), and (1–6) keV energy intervals are shown

Table 3.1: Details about the annual cycles of DAMA/LIBRA–phase2. The mean value of the squared cosine is $\alpha = \langle \cos^2 \omega(t - t_0) \rangle$ and the mean value of the cosine is $\beta = \langle \cos \omega(t - t_0) \rangle$ (the averages are taken over the live time of the data taking and $t_0 = 152.5$ day, i.e. June 2nd); thus, the variance of the cosine, $(\alpha - \beta^2)$, is $\simeq 0.5$ for a detector being operational evenly throughout the year.

DAMA/LIBRA–phase2 annual cycle	Period	Mass (kg)	Exposure (kg×day)	$(\alpha - \beta^2)$
1	Dec. 23, 2010 – Sept. 9, 2011	commissioning of phase2		
2	Nov. 2, 2011 – Sept. 11, 2012	242.5	62917	0.519
3	Oct. 8, 2012 – Sept. 2, 2013	242.5	60586	0.534
4	Sept. 8, 2013 – Sept. 1, 2014	242.5	73792	0.479
5	Sept. 1, 2014 – Sept. 9, 2015	242.5	71180	0.486
6	Sept. 10, 2015 – Aug. 24, 2016	242.5	67527	0.522
7	Sept. 7, 2016 – Sept. 25, 2017	242.5	75135	0.480
8	Sept. 25, 2017 – Aug. 20, 2018	242.5	68759	0.557
9	Aug. 24, 2018 – Oct. 3, 2019	242.5	77213	0.446
DAMA/LIBRA–phase2 Nov. 2, 2011 – Oct. 3, 2019		557109 kg×day $\simeq 1.53$ ton×yr		0.501
DAMA/NaI + DAMA/LIBRA–phase1 + DAMA/LIBRA–phase2:			2.86 ton×yr	

for DAMA/LIBRA–phase2. The residual rates are calculated from the measured rate of the *single-hit* events after subtracting the constant part, as described in Refs. [2–5,35,36]. The null modulation hypothesis is rejected at very high C.L. by χ^2 test: $\chi^2 = 176$ and 202, respectively, over 69 d.o.f. ($P = 2.6 \times 10^{-11}$, and $P = 5.6 \times 10^{-15}$, respectively). The residuals of the DAMA/NaI data (0.29 ton × yr) are given in Ref. [2,5,35,36], while those of DAMA/LIBRA–phase1 (1.04 ton × yr) in Ref. [2–5].

The former DAMA/LIBRA–phase1 and the new DAMA/LIBRA–phase2 residual rates of the *single-hit* scintillation events are reported in Fig. 3.2. The energy interval is from 2 keV, the software energy threshold of DAMA/LIBRA –phase1, up to 6 keV. The null modulation hypothesis is rejected at very high C.L. by χ^2 test: $\chi^2/\text{d.o.f.} = 240/119$, corresponding to P-value = 3.5×10^{-10} .

The *single-hit* residual rates of the DAMA/LIBRA–phase2 (Fig. 3.1) have been fitted with the function: $A \cos \omega(t - t_0)$, considering a period $T = \frac{2\pi}{\omega} = 1$ yr and a phase $t_0 = 152.5$ day (June 2nd) as expected by the DM annual modulation signature; this can be repeated for the only case of (2–6) keV energy interval when including also the former DAMA/NaI and DAMA/LIBRA–phase1 data. The goodness of the fits is well supported by the χ^2 test; for example, $\chi^2/\text{d.o.f.} = 81.6/68, 66.2/68, 130/155$ are obtained for the (1–3) keV and (1–6) keV cases of DAMA/LIBRA–phase2, and for the (2–6) keV case of DAMA/NaI, DAMA/LIBRA–phase1 and DAMA/LIBRA–phase2, respectively. The results of the best fits in the different cases are summarized in Table 3.2. In Table 3.2 also the cases when the period and the phase are kept free in the fitting procedure are shown. The period and the phase are well compatible with expectations for a DM annual modulation signal. In particular, the phase is consistent with about June 2nd and is fully consistent with the value independently determined by Maximum Likelihood analysis (see later). For com-

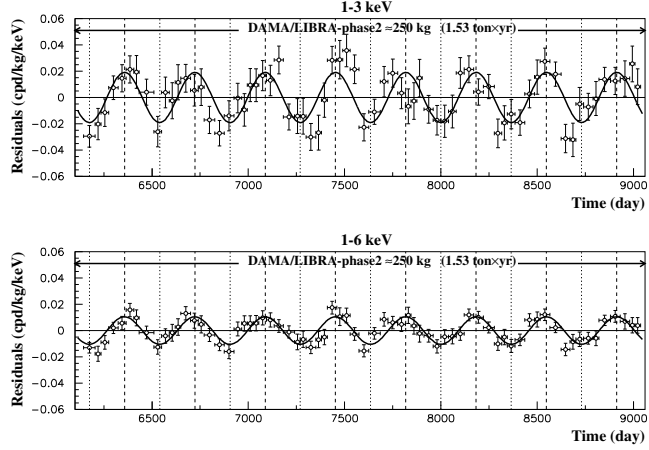


Fig. 3.1: Experimental residual rate of the *single-hit* scintillation events measured by DAMA/LIBRA-phase2 over eight annual cycles in the (1–3), and (1–6) keV energy intervals as a function of the time. The time scale is maintained the same of the previous DAMA papers for consistency. The data points present the experimental errors as vertical bars and the associated time bin width as horizontal bars. The superimposed curves are the cosinusoidal functional forms $A \cos \omega(t - t_0)$ with a period $T = \frac{2\pi}{\omega} = 1$ yr, a phase $t_0 = 152.5$ day (June 2nd) and modulation amplitudes, A , equal to the central values obtained by best fit on the data points of the entire DAMA/LIBRA-phase2. The dashed vertical lines correspond to the maximum expected for the DM signal (June 2nd), while the dotted vertical lines correspond to the minimum.

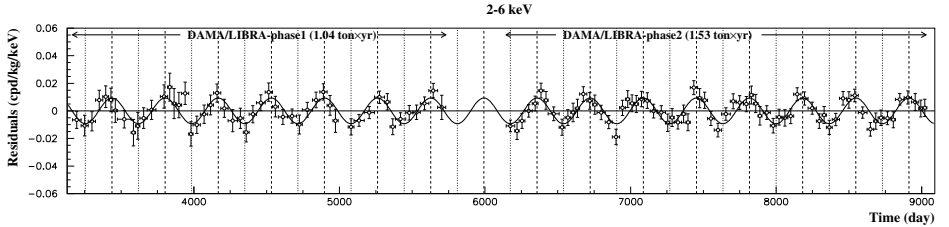


Fig. 3.2: Experimental residual rate of the *single-hit* scintillation events measured by DAMA/LIBRA-phase1 and DAMA/LIBRA-phase2 in the (2–6) keV energy intervals as a function of the time. The superimposed curve is the cosinusoidal functional forms $A \cos \omega(t - t_0)$ with a period $T = \frac{2\pi}{\omega} = 1$ yr, a phase $t_0 = 152.5$ day (June 2nd) and modulation amplitude, A , equal to the central value obtained by best fit on the data points of DAMA/LIBRA-phase1 and DAMA/LIBRA-phase2. For details see Fig. 3.1.

pletteness, we recall that a slight energy dependence of the phase could be expected (see e.g. Refs. [38, 58, 59, 61–63]), providing intriguing information on the nature of Dark Matter candidate and related aspects.

Table 3.2: Modulation amplitude, A , obtained by fitting the *single-hit* residual rate of DAMA/LIBRA–phase2, as reported in Fig. 3.1, and also including the residual rates of the former DAMA/NaI and DAMA/LIBRA–phase1. It was obtained by fitting the data with the formula: $A \cos \omega(t - t_0)$. The period $T = \frac{2\pi}{\omega}$ and the phase t_0 are kept fixed at 1 yr and at 152.5 day (June 2nd), respectively, as expected by the DM annual modulation signature, and alternatively kept free. The results are well compatible with expectations for a signal in the DM annual modulation signature.

	A (cpd/kg/keV)	$T = \frac{2\pi}{\omega}$ (yr)	t_0 (days)	C.L.
DAMA/LIBRA–phase2:				
1-3 keV	(0.0191 ± 0.0020)	1.0	152.5	9.7σ
1-6 keV	(0.01048 ± 0.00090)	1.0	152.5	11.6σ
2-6 keV	(0.00933 ± 0.00094)	1.0	152.5	9.9σ
1-3 keV	(0.0191 ± 0.0020)	(0.99952 ± 0.00080)	149.6 ± 5.9	9.6σ
1-6 keV	(0.01058 ± 0.00090)	(0.99882 ± 0.00065)	144.5 ± 5.1	11.8σ
2-6 keV	(0.00954 ± 0.00076)	(0.99836 ± 0.00075)	141.1 ± 5.9	12.6σ
DAMA/LIBRA–phase1 + phase2:				
2-6 keV	(0.00941 ± 0.00076)	1.0	152.5	12.4σ
2-6 keV	(0.00959 ± 0.00076)	(0.99835 ± 0.00069)	142.0 ± 4.5	12.6σ
DAMA/NaI + DAMA/LIBRA–phase1 + phase2:				
2-6 keV	(0.00996 ± 0.00074)	1.0	152.5	13.4σ
2-6 keV	(0.01014 ± 0.00074)	(0.99834 ± 0.00067)	142.4 ± 4.2	13.7σ

3.2.2 Absence of background modulation

Since the background in the lowest energy region is essentially due to “Compton” electrons, X-rays and/or Auger electrons, muon induced events, etc., which are strictly correlated with the events in the higher energy region of the spectrum, if a modulation detected in the lowest energy region were due to a modulation of the background (rather than to a signal), an equal or larger modulation in the higher energy regions should be present. Thus, as done in previous data releases, absence of any significant background modulation in the energy spectrum for energy regions not of interest for DM. has also been verified in the present one. In particular, the measured rate integrated above 90 keV, R_{90} , as a function of the time has been analysed. Fig. 3.3 shows the distribution of the percentage variations of R_{90} with respect to the mean values for all the detectors in DAMA/LIBRA–phase2. It shows a cumulative gaussian behaviour with $\sigma \simeq 1\%$, well accounted for by the statistical spread provided by the used sampling time. Moreover, fitting the time behaviour of R_{90} including a term with phase and period as for DM particles, a modulation amplitude $A_{R_{90}}$ compatible with zero has been found for all the annual cycles (see Table 3.3). This also excludes the presence of any background modulation in the whole energy spectrum at a level much lower than the effect found in the lowest energy region for the *single-hit* scintillation events. In fact, otherwise – considering the R_{90} mean values – a modulation amplitude of order of tens cpd/kg would be present for each annual cycle, that is $\simeq 100 \sigma$ far away from the measured values.

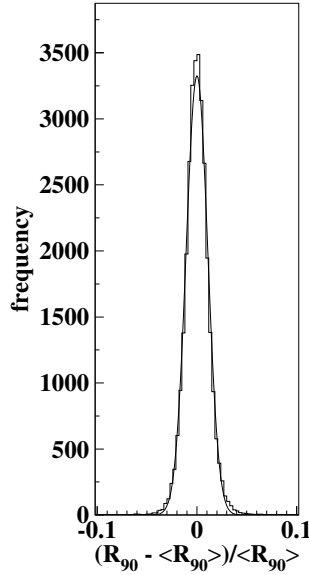


Fig. 3.3: Distribution of the percentage variations of R_{90} with respect to the mean values for all the detectors in the DAMA/LIBRA-phase2 (histogram); the superimposed curve is a gaussian fit.

Table 3.3: Modulation amplitudes, $A_{R_{90}}$, obtained by fitting the time behaviour of R_{90} in DAMA/LIBRA-phase2, including a term with a cosine function having phase and period as expected for a DM signal. The obtained amplitudes are compatible with zero, and incompatible ($\simeq 100 \sigma$) with modulation amplitudes of tens cpd/kg. Modulation amplitudes, $A_{(6-14)}$, obtained by fitting the time behaviour of the residual rates of the *single-hit* scintillation events in the (6–14) keV energy interval. In the fit the phase and the period are at the values expected for a DM signal. The obtained amplitudes are compatible with zero.

DAMA/LIBRA-phase2 annual cycle	$A_{R_{90}}$ (cpd/kg)	$A_{(6-14)}$ (cpd/kg/keV)
2	(0.12 ± 0.14)	(0.0032 ± 0.0017)
3	$-(0.08 \pm 0.14)$	(0.0016 ± 0.0017)
4	(0.07 ± 0.15)	(0.0024 ± 0.0015)
5	$-(0.05 \pm 0.14)$	$-(0.0004 \pm 0.0015)$
6	(0.03 ± 0.13)	(0.0001 ± 0.0015)
7	$-(0.09 \pm 0.14)$	(0.0015 ± 0.0014)
8	$-(0.18 \pm 0.13)$	$-(0.0005 \pm 0.0013)$
9	(0.08 ± 0.14)	$-(0.0003 \pm 0.0014)$

Similar results are obtained when comparing the *single-hit* residuals in the (1–6) keV with those in other energy intervals; for example Fig. 3.4 shows the *single-hit* residuals in the (1–6) keV and in the (10–20) keV energy regions, for the 8 annual cycles of DAMA/LIBRA–phase2 as if they were collected in a single annual cycle (i.e. binning in the variable time from the January 1st of each annual cycle).

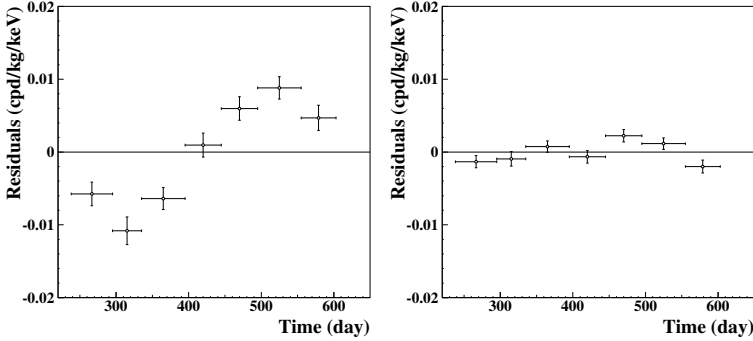


Fig. 3.4: Experimental *single-hit* residuals in the (1–6) keV and in the (10–20) keV energy regions for DAMA/LIBRA–phase2 as if they were collected in a single annual cycle (i.e. binning in the variable time from the January 1st of each annual cycle). The data points present the experimental errors as vertical bars and the associated time bin width as horizontal bars. The initial time of the figures is taken at August 7th. A clear modulation satisfying all the peculiarities of the DM annual modulation signature is present in the lowest energy interval with $A=(0.00956 \pm 0.00090)$ cpd/kg/keV, while it is absent just above: $A=(0.0007 \pm 0.0005)$ cpd/kg/keV.

Moreover, Table 3.3 shows the modulation amplitudes obtained by fitting the time behaviour of the residual rates of the *single-hit* scintillation events in the (6–14) keV energy interval for the DAMA/LIBRA–phase2 annual cycles. In the fit the phase and the period are at the values expected for a DM signal. The obtained amplitudes are compatible with zero.

A further relevant investigation on DAMA/LIBRA–phase2 data has been performed by applying the same hardware and software procedures, used to acquire and to analyse the *single-hit* residual rate, to the *multiple-hit* one. Since the probability that a DM particle interacts in more than one detector is negligible, a DM signal can be present just in the *single-hit* residual rate. Thus, the comparison of the results of the *single-hit* events with those of the *multiple-hit* ones corresponds to compare the cases of DM particles beam-on and beam-off. This procedure also allows an additional test of the background behaviour in the same energy interval where the positive effect is observed.

In particular, in Fig. 3.5 the residual rates of the *single-hit* scintillation events collected during 8 annual cycles of DAMA/LIBRA–phase2 are reported, as collected in a single cycle, together with the residual rates of the *multiple-hit* events, in

the considered energy intervals. While, as already observed, a clear modulation, satisfying all the peculiarities of the DM annual modulation signature, is present in the *single-hit* events, the fitted modulation amplitude for the *multiple-hit* residual rate is well compatible with zero: (0.00030 ± 0.00032) cpd/kg/keV in the (1–6) keV energy region. Thus, again evidence of annual modulation with proper features as required by the DM annual modulation signature is present in the *single-hit* residuals (events class to which the DM particle induced events belong), while it is absent in the *multiple-hit* residual rate (event class to which only background events belong). Similar results were also obtained for the two last annual cycles of DAMA/NaI [36] and for DAMA/LIBRA-phase1 [2–5]. Since the same identical hardware and the same identical software procedures have been used to analyse the two classes of events, the obtained result offers an additional strong support for the presence of a DM particle component in the galactic halo.

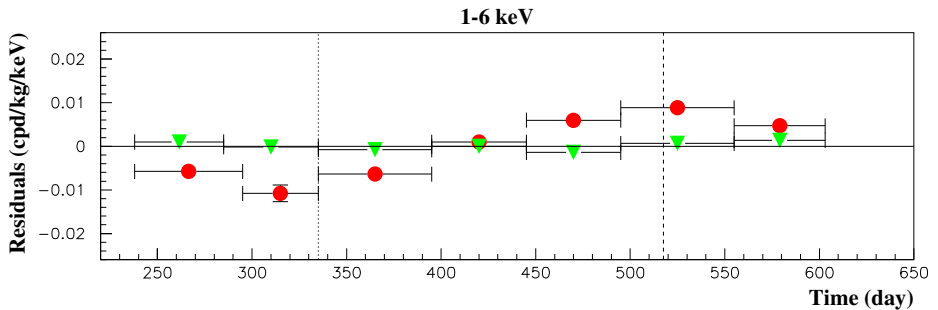


Fig. 3.5: Experimental residual rates of DAMA/LIBRA-phase2 *single-hit* events (filled red on-line circles), class of events to which DM events belong, and for *multiple-hit* events (filled green on-line triangles), class of events to which DM events do not belong. They have been obtained by considering for each class of events the data as collected in a single annual cycle and by using in both cases the same identical hardware and the same identical software procedures. The initial time of the figure is taken on August 7th. The experimental points present the errors as vertical bars and the associated time bin width as horizontal bars. Analogous results were obtained for DAMA/NaI (two last annual cycles) and DAMA/LIBRA-phase1 [2–5,36].

In conclusion, no background process able to mimic the DM annual modulation signature (that is, able to simultaneously satisfy all the peculiarities of the signature and to account for the measured modulation amplitude) has been found or suggested by anyone throughout some decades thus far (see also discussions e.g. in Ref. [1–5,7,8,19–21,23,34–36]).

3.3 The analysis in frequency

In order to perform the Fourier analysis of the data of DAMA/LIBRA-phase1 and of the present 8 annual cycles of phase2 in a wider region of considered frequency, the *single-hit* events have been grouped in 1 day bins. Due to the low statistics in

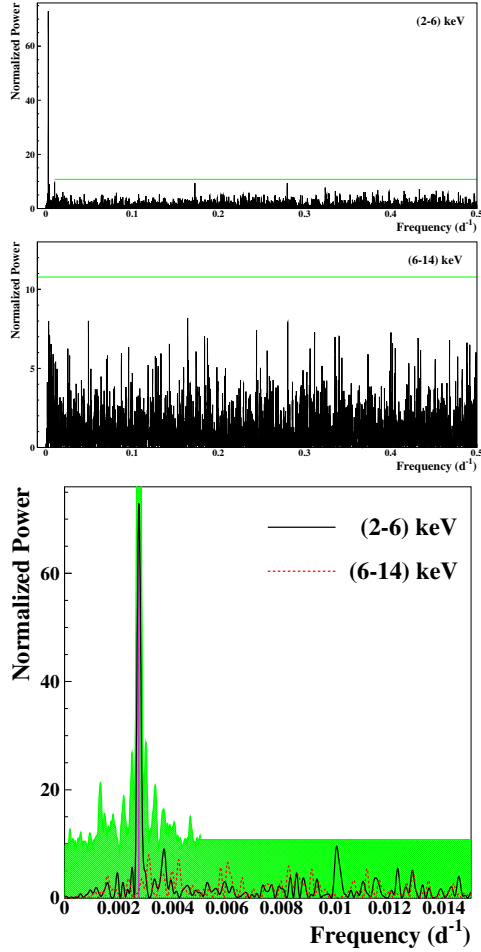


Fig. 3.6: Power spectra of the time sequence of the measured *single-hit* events for DAMA/LIBRA–phase1 and DAMA/LIBRA–phase2 grouped in 1 day bins. From top to bottom: spectra up to the Nyquist frequency for (2–6) keV and (6–14) keV energy intervals and their zoom around the 1 y^{-1} peak, for (2–6) keV (solid line) and (6–14) keV (dotted line) energy intervals. The main mode present at the lowest energy interval corresponds to a frequency of $2.74 \times 10^{-3} \text{ d}^{-1}$ (vertical line, purple on-line). It corresponds to a period of $\simeq 1$ year. A similar peak is not present in the (6–14) keV energy interval. The shaded (green on-line) area in the bottom figure – calculated by Monte Carlo procedure – represents the 90% C.L. region where all the peaks are expected to fall for the (2–6) keV energy interval. In the frequency range far from the signal for the (2–6) keV energy region and for the whole (6–14) keV spectrum, the upper limit of the shaded region (90% C.L.) can be calculated to be 10.8 (continuous lines, green on-line).

each time bin, a procedure detailed in Ref. [64] has been applied. Fig. 3.6 shows the whole power spectra up to the Nyquist frequency and the zoomed ones: a clear peak corresponding to a period of 1 year is evident for the lowest energy interval, while the same analysis in the (6–14) keV energy region shows only aliasing peaks, instead. Neither other structure at different frequencies has been observed. To derive the significance of the peaks present in the periodogram, one can remind that the periodogram ordinate, z , at each frequency follows a simple exponential distribution e^{-z} in case of null hypothesis or white noise [65].

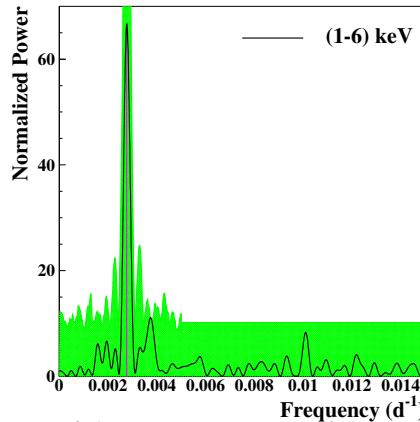


Fig. 3.7: Power spectrum of the time sequence of the measured *single-hit* events in the (1–6) keV energy interval for DAMA/LIBRA-phase2 grouped in 1 day bin. The main mode present at the lowest energy interval corresponds to a frequency of $2.77 \times 10^{-3} \text{ d}^{-1}$ (vertical line, purple on-line). It corresponds to a period of $\simeq 1$ year. The shaded (green on-line) area – calculated by Monte Carlo procedure – represents the 90% C.L. region where all the peaks are expected to fall for the (1–6) keV energy interval.

Thus, if M independent frequencies are scanned, the probability to obtain values larger than z is: $P(> z) = 1 - (1 - e^{-z})^M$. In general M depends on the number of sampled frequencies, the number of data points N , and their detailed spacing. It turns out that $M \simeq N$ when the data points are approximately equally spaced and when the sampled frequencies cover the frequency range from 0 to the Nyquist one [66, 67]. In the present case, the number of data points used to obtain the spectra in Fig. 3.6 is $N = 5047$ (days measured over the 5479 days of the 15 DAMA/LIBRA-phase1 and phase2 annual cycles) and the full frequencies region up to Nyquist one has been scanned. Thus, assuming $M = N$, the significance levels $P = 0.10, 0.05$ and 0.01 , correspond to peaks with heights larger than $z = 10.8, 11.5$ and 13.1 , respectively, in the spectra of Fig 3.6. In the case below 6 keV, a signal is present; thus, to properly evaluate the C.L. the signal must be included. This has been done by a dedicated Monte Carlo procedure where a large number of similar experiments has been simulated. The 90% C.L. region (shaded, green on-line) where all the peaks are expected to fall for the (2–6) keV energy interval is

reported in Fig 3.6. Several peaks, satellite of the one year period frequency, are present.

Moreover, for each annual cycle of DAMA/LIBRA–phase1 and phase2, the annual baseline counting rates have been calculated for the (2–6) keV energy interval. Their power spectrum in the frequency range $0.00013 - 0.0019 \text{ d}^{-1}$ (corresponding to a period range 1.4–21.1 year) has been calculated according to Ref. [5]. No statistically-significant peak is present at frequencies lower than 1 y^{-1} . This implies that no evidence for a long term modulation in the counting rate is present.

Finally, the case of the (1–6) keV energy interval of the DAMA/LIBRA–phase2 data is reported in Fig. 3.7. As previously the only significant peak is the one corresponding to one year period. No other peak is statistically significant being below the shaded (green on-line) area obtained by Monte Carlo procedure.

In conclusion, apart from the peak corresponding to a 1 year period, no other peak is statistically significant either in the low and high energy regions.

3.4 The modulation amplitudes by the maximum likelihood approach

The annual modulation present at low energy can also be pointed out by depicting the energy dependence of the modulation amplitude, $S_m(E)$, obtained by maximum likelihood method considering fixed period and phase: $T = 1 \text{ yr}$ and $t_0 = 152.5 \text{ day}$. For this purpose the likelihood function of the *single-hit* experimental data in the k –th energy bin is defined as: $L_k = \prod_{ij} e^{-\mu_{ijk}} \frac{N_{ijk}^{\mu_{ijk}}}{N_{ijk}!}$, where N_{ijk} is the number of events collected in the i –th time interval (hereafter 1 day), by the j –th detector and in the k –th energy bin. N_{ijk} follows a Poisson’s distribution with expectation value $\mu_{ijk} = [b_{jk} + S_i(E_k)] M_j \Delta t_i \Delta E \epsilon_{jk}$. The b_{jk} are the background contributions, M_j is the mass of the j –th detector, Δt_i is the detector running time during the i –th time interval, ΔE is the chosen energy bin, ϵ_{jk} is the overall efficiency. The signal can be written as:

$$S_i(E) = S_0(E) + S_m(E) \cdot \cos \omega(t_i - t_0),$$

where $S_0(E)$ is the constant part of the signal and $S_m(E)$ is the modulation amplitude. The usual procedure is to minimize the function $y_k = -2 \ln(L_k) - \text{const}$ for each energy bin; the free parameters of the fit are the $(b_{jk} + S_0)$ contributions and the S_m parameter.

The modulation amplitudes for the whole data sets: DAMA/NaI, DAMA /LIBRA–phase1 and DAMA/LIBRA–phase2 (total exposure $2.86 \text{ ton} \times \text{yr}$) are plotted in Fig. 3.8; the data below 2 keV refer only to the DAMA/LIBRA–phase2 exposure ($1.53 \text{ ton} \times \text{yr}$). It can be inferred that positive signal is present in the (1–6) keV energy interval, while S_m values compatible with zero are present just above. All this confirms the previous analyses. The test of the hypothesis that the S_m values in the (6–14) keV energy interval have random fluctuations around zero yields $\chi^2/\text{d.o.f.}$ equal to $20.3/16$ (P-value = 21%).

For the case of (6–20) keV energy interval $\chi^2/\text{d.o.f.} = 42.2/28$ (P-value = 4%). The obtained χ^2 value is rather large due mainly to two data points, whose centroids

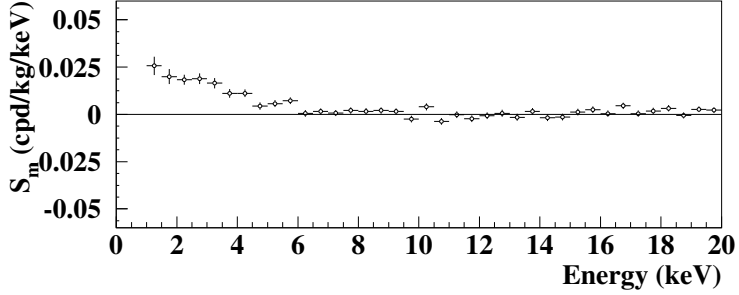


Fig. 3.8: Modulation amplitudes, S_m , for the whole data sets: DAMA/NaI, DAMA/LIBRA-phase1 and DAMA/LIBRA-phase2 (total exposure 2.86 ton \times yr) above 2 keV; below 2 keV only the DAMA/LIBRA-phase2 exposure (1.53 ton \times yr) is available and used. The energy bin ΔE is 0.5 keV. A clear modulation is present in the lowest energy region, while S_m values compatible with zero are present just above. In fact, the S_m values in the (6–20) keV energy interval have random fluctuations around zero with $\chi^2/\text{d.o.f.}$ equal to 42.2/28 (P-value is 4%).

are at 16.75 and 18.25 keV, far away from the (1–6) keV energy interval. The P-values obtained by excluding only the first and either the points are 14% and 23%.

This method also allows the extraction of the S_m values for each detector. In particular, the modulation amplitudes S_m integrated in the range (2–6) keV for each of the 25 detectors for the DAMA/LIBRA-phase1 and DAMA/LIBRA-phase2 periods can be produced. They have random fluctuations around the weighted averaged value confirmed by the χ^2 analysis. Thus, the hypothesis that the signal is well distributed over all the 25 detectors is accepted.

As previously done for the other data releases [2–5, 19–21, 23], the S_m values for each detector for each annual cycle and for each energy bin have been obtained. The S_m are expected to follow a normal distribution in absence of any systematic effects. Therefore, the variable $x = \frac{S_m - \langle S_m \rangle}{\sigma}$ has been considered to verify that the S_m are statistically well distributed in the 16 energy bins ($\Delta E = 0.25$ keV) in the (2–6) keV energy interval of the seven DAMA/LIBRA-phase1 annual cycles and in the 20 energy bins in the (1–6) keV energy interval of the eight DAMA/LIBRA-phase2 annual cycles and in each detector. Here, σ are the errors associated to S_m and $\langle S_m \rangle$ are the mean values of the S_m averaged over the detectors and the annual cycles for each considered energy bin.

Defining $\chi^2 = \Sigma x^2$, where the sum is extended over all the 272 (192 for the 16th detector [4]) x values, $\chi^2/\text{d.o.f.}$ values ranging from 0.8 to 2.0 are obtained, depending on the detector.

The mean value of the 25 $\chi^2/\text{d.o.f.}$ is 1.092, slightly larger than 1. Although this can be still ascribed to statistical fluctuations, let us ascribe it to a possible systematics. In this case, one would derive an additional error to the modulation amplitude measured below 6 keV: $\leq 2.4 \times 10^{-4}$ cpd/kg/keV, if combining quadratically the

errors, or $\leq 3.6 \times 10^{-5}$ cpd/kg/keV, if linearly combining them. This possible additional error: $\leq 2.4\%$ or $\leq 0.4\%$, respectively, on the DAMA/LIBRA-phase1 and DAMA /LIBRA-phase2 modulation amplitudes is an upper limit of possible systematic effects coming from the detector to detector differences.

Among further additional tests, the analysis of the modulation amplitudes as a function of the energy separately for the nine inner detectors and the remaining external ones has been carried out for DAMA/LIBRA-phase1 and DAMA/LIBRA-phase2, as already done for the other data sets [2–5, 19–21, 23]. The obtained values are fully in agreement; in fact, the hypothesis that the two sets of modulation amplitudes belong to same distribution has been verified by χ^2 test, obtaining e.g.: $\chi^2/\text{d.o.f.} = 1.9/6$ and $36.1/38$ for the energy intervals (1–4) and (1–20) keV, respectively ($\Delta E = 0.5$ keV). This shows that the effect is also well shared between inner and outer detectors.

Moreover, to test the hypothesis that the amplitudes, singularly calculated for each annual cycle of DAMA/LIBRA-phase1 and DAMA/LIBRA-phase2, are compatible and normally fluctuating around their mean values, the χ^2 test has been performed together with another independent statistical test: the *run test* (see e.g. Ref. [69]), which verifies the hypothesis that the positive (above the mean value) and negative (under the mean value) data points are randomly distributed. Both tests accept at 95% C.L. the hypothesis that the modulation amplitudes are normally fluctuating around the best fit values.

3.5 Investigation of the annual modulation phase

Finally, let us release the assumption of the phase value at $t_0 = 152.5$ day in the procedure to evaluate the modulation amplitudes, writing the signal as:

$$\begin{aligned} S_i(E) &= S_0(E) + S_m(E) \cos \omega(t_i - t_0) + Z_m(E) \sin \omega(t_i - t_0) \\ &= S_0(E) + Y_m(E) \cos \omega(t_i - t^*). \end{aligned} \quad (3.1)$$

For signals induced by DM particles one should expect: i) $Z_m \sim 0$ (because of the orthogonality between the cosine and the sine functions); ii) $S_m \simeq Y_m$; iii) $t^* \simeq t_0 = 152.5$ day. In fact, these conditions hold for most of the dark halo models; however, as mentioned above, slight differences can be expected in case of possible contributions from non-thermalized DM components (see e.g. Refs. [38, 58, 59, 61–63]).

Considering cumulatively the data of DAMA/NaI, DAMA/LIBRA-phase1 and DAMA/LIBRA-phase2 the obtained 2σ contours in the plane (S_m, Z_m) for the (2–6) keV and (6–14) keV energy intervals are shown in Fig. 3.9–*left* while the obtained 2σ contours in the plane (Y_m, t^*) are depicted in Fig. 3.9–*right*. Moreover, Fig. 3.9 also shows only for DAMA/LIBRA-phase2 the 2σ contours in the (1–6) keV energy interval.

The best fit values in the considered cases (1σ errors) for S_m versus Z_m and Y_m versus t^* are reported in Table 3.4.

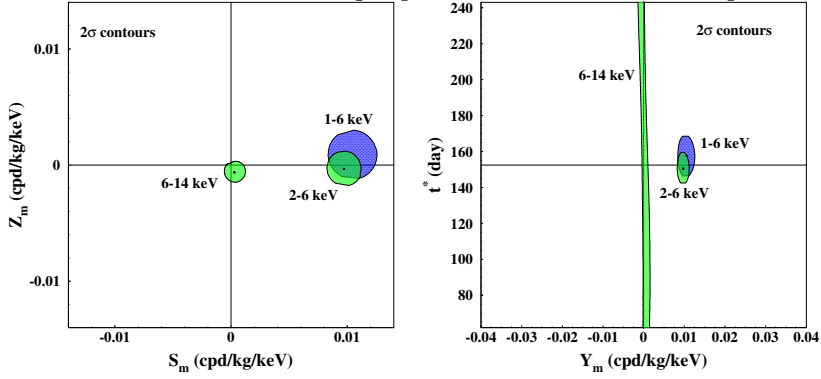


Fig. 3.9: 2σ contours in the plane (S_m, Z_m) (left) and in the plane (Y_m, t^*) (right) for: i) DAMA/NaI, DAMA/LIBRA-phase1 and DAMA/LIBRA-phase2 in the (2–6) keV and (6–14) keV energy intervals (light areas, green on-line); ii) only DAMA/LIBRA-phase2 in the (1–6) keV energy interval (dark areas, blue on-line). The contours have been obtained by the maximum likelihood method. A modulation amplitude is present in the lower energy intervals and the phase agrees with that expected for DM induced signals.

Table 3.4: Best fit values (1σ errors) for S_m versus Z_m and Y_m versus t^* , considering: i) DAMA/NaI, DAMA/LIBRA-phase1 and DAMA/LIBRA-phase2 in the (2–6) keV and (6–14) keV energy intervals; ii) only DAMA/LIBRA-phase2 in the (1–6) keV energy interval. See also Fig. 3.9.

E (keV)	S_m (cpd/kg/keV)	Z_m (cpd/kg/keV)	Y_m (cpd/kg/keV)	t^* (day)
DAMA/NaI+DAMA/LIBRA-phase1+DAMA/LIBRA-phase2:				
2–6	(0.0097 ± 0.0007)	$-(0.0003 \pm 0.0007)$	(0.0097 ± 0.0007)	(150.5 ± 4.0)
6–14	(0.0003 ± 0.0005)	$-(0.0006 \pm 0.0005)$	(0.0007 ± 0.0010)	undefined
DAMA/LIBRA-phase2:				
1–6	(0.0104 ± 0.0007)	(0.0002 ± 0.0007)	(0.0104 ± 0.0007)	(153.5 ± 4.0)

Finally, the Z_m values as function of the energy have also been determined by using the same procedure and setting S_m in eq. (3.1) to zero. The Z_m values as a function of the energy for DAMA/NaI, DAMA/LIBRA-phase1, and DAMA/LIBRA-phase2 data sets are expected to be zero. The χ^2 test applied to the data supports the hypothesis that the Z_m values are simply fluctuating around zero; in fact, in the (1–20) keV energy region the $\chi^2/\text{d.o.f.}$ is equal to $40.6/38$ corresponding to a $P\text{-value} = 36\%$.

The energy behaviors of Y_m and of phase t^* are also produced for the cumulative exposure of DAMA/NaI, DAMA/LIBRA-phase1, and DAMA/LIBRA-phase2; as in the previous analyses, an annual modulation effect is present in the lower energy intervals and the phase agrees with that expected for DM induced signals. No modulation is present above 6 keV and the phase is undetermined.

3.6 Perspectives

To further increase the experimental sensitivity of DAMA/LIBRA and to disentangle some of the many possible astrophysical, nuclear and particle physics scenarios in the investigation on the DM candidate particle(s), an increase of the exposure ($M \times t_{\text{running}}$, i.e. t_{running} in our case at fixed M) in the lowest energy bin and a further decreasing of the software energy threshold are needed. This is pursued by running DAMA/LIBRA–phase2 and upgrading the experimental set-up to lower the software energy threshold below 1 keV with high acceptance efficiency.

Firstly, particular efforts for lowering the software energy threshold have been done in the already-acquired data of DAMA/LIBRA–phase2 by using the same technique as before with dedicated studies on the efficiency. As consequence, a new data point has been added in the modulation amplitude as function of energy down to 0.75 keV, see Fig. 3.10. A modulation is also present below 1 keV, from 0.75 keV. This preliminary result confirms the necessity to lower the software energy threshold by a hardware upgrade and an improved statistics in the first energy bin.

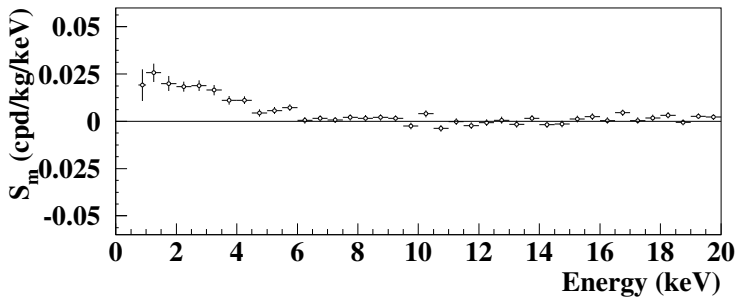


Fig. 3.10: As Fig. 3.8; the new data point below 1 keV, with software energy threshold at 0.75 keV, shows that an annual modulation is also present below 1 keV. This preliminary result confirms the necessity to lower the software energy threshold by a hardware upgrade and to improve the experimental error on the first energy bin.

This dedicated hardware upgrade of DAMA/LIBRA–phase2 is underway. It consists in equipping all the PMTs with miniaturized low background new concept preamplifiers and HV dividers mounted on the same socket, and related improvements of the electronic chain, mainly the use of higher vertical resolution 14-bit digitizers.

3.7 Conclusions

DAMA/LIBRA–phase2 confirms a peculiar annual modulation of the *single-hit* scintillation events in the (1–6) keV energy region satisfying all the many requirements of the DM annual modulation signature; the cumulative exposure by the

former DAMA/NaI, DAMA/LIBRA-phase1 and DAMA/LIBRA-phase2 is $2.86 \text{ ton} \times \text{yr}$.

As required by the exploited DM annual modulation signature: 1) the *single-hit* events show a clear cosine-like modulation as expected for the DM signal; 2) the measured period is well compatible with the 1 yr period as expected for the DM signal; 3) the measured phase is compatible with the roughly $\simeq 152.5$ days expected for the DM signal; 4) the modulation is present only in the low energy (1–6) keV interval and not in other higher energy regions, consistently with expectation for the DM signal; 5) the modulation is present only in the *single-hit* events, while it is absent in the *multiple-hit* ones as expected for the DM signal; 6) the measured modulation amplitude in NaI(Tl) target of the *single-hit* scintillation events in the (2–6) keV energy interval, for which data are also available by DAMA/NaI and DAMA/LIBRA-phase1, is: $(0.01014 \pm 0.00074) \text{ cpd/kg/keV}$ ($13.7 \sigma \text{ C.L.}$).

No systematic or side processes able to mimic the signature, i.e. able to simultaneously satisfy all the many peculiarities of the signature and to account for the whole measured modulation amplitude, has been found or suggested by anyone throughout some decades thus far (for details see e.g. Ref. [1–5, 7, 8, 19–23, 35, 36]). In particular, arguments related to any possible role of some natural periodical phenomena have been discussed and quantitatively demonstrated to be unable to mimic the signature (see references; e.g. Refs. [7, 8]). Thus, on the basis of the exploited signature, the model independent DAMA results give evidence at $13.7\sigma \text{ C.L.}$ (over 22 independent annual cycles and in various experimental configurations) for the presence of DM particles in the galactic halo.

The DAMA model independent evidence is compatible with a wide set of astrophysical, nuclear and particle physics scenarios for high and low mass candidates inducing nuclear recoil and/or electromagnetic radiation, as also shown in various literature. Moreover, both the negative results and all the possible positive hints, achieved so-far in the field, can be compatible with the DAMA model independent DM annual modulation results in many scenarios considering also the existing experimental and theoretical uncertainties; the same holds for indirect approaches. For a discussion see e.g. Ref. [5] and references therein.

The present new data released determine the modulation parameters with increasing precision and will allow us to disentangle with larger C.L. among different DM candidates, DM models and astrophysical, nuclear and particle physics scenarios. Finally, we stress that to efficiently disentangle among at least some of the many possible candidates and scenarios an increase of exposure in the new lowest energy bin and the decrease of the software energy threshold below the present 1 keV is important. The experiment is collecting data and the hardware efforts towards the lowering of the software energy threshold is in progress; a preliminary result below 1 keV is given.

References

1. R. Bernabei et al., Nucl. Instr. and Meth. A **592**, 297 (2008).
2. R. Bernabei et al., Eur. Phys. J. C **56**, 333 (2008).
3. R. Bernabei et al., Eur. Phys. J. C **67**, 39 (2010).

4. R. Bernabei et al., *Eur. Phys. J. C* **73**, 2648 (2013).
5. R. Bernabei et al., *Int. J. of Mod. Phys. A* **28**, 1330022 (2013).
6. R. Bernabei et al., *J. of Instr.* **7**, P03009 (2012).
7. R. Bernabei et al., *Eur. Phys. J. C* **72**, 2064 (2012).
8. R. Bernabei et al., *Eur. Phys. J. C* **74**, 3196 (2014).
9. DAMA coll., issue dedicated to DAMA, *Int. J. of Mod. Phys. A* **31** (2016) and refs therein.
10. R. Bernabei et al., *Eur. Phys. J. C* **74**, 2827 (2014).
11. R. Bernabei et al., *Eur. Phys. J. C* **62**, 327 (2009).
12. R. Bernabei et al., *Eur. Phys. J. C* **72**, 1920 (2012).
13. R. Bernabei et al., *Eur. Phys. J. A* **49**, 64 (2013).
14. R. Bernabei et al., *Eur. Phys. J. C* **75**, 239 (2015).
15. P. Belli et al., *Phys. Rev. D* **84**, 055014 (2011).
16. A. Addazi et al., *Eur. Phys. J. C* **75**, 400 (2015).
17. R. Bernabei et al., *Int. J. of Mod. Phys. A* **31**, 1642009 (2016).
18. R. Cerulli et al., *Eur. Phys. J. C* **77**, 83 (2017).
19. R. Bernabei et al., *Universe* **4**, 116 (2018).
20. R. Bernabei et al., *Nucl. Phys. At. Energy* **19**, 307 (2018).
21. R. Bernabei, *Bled Workshops in Physics* **19** n. 2, 27 (2018).
22. R. Bernabei et al., *Nucl. Phys. At. Energy* **20(4)**, 317 (2019).
23. R. Bernabei et al., *Prog. Part. Nucl. Phys.* **114**, 103810 (2020).
24. P. Belli, R. Bernabei, C. Bacci, A. Incicchitti, R. Marcovaldi, D. Prosperi, DAMA proposal to INFN Scientific Committee II, April 24th 1990.
25. R. Bernabei et al., *Phys. Lett. B* **389**, 757 (1996).
26. R. Bernabei et al., *Phys. Lett. B* **424**, 195 (1998).
27. R. Bernabei et al., *Phys. Lett. B* **450**, 448 (1999).
28. P. Belli et al., *Phys. Rev. D* **61**, 023512 (2000).
29. R. Bernabei et al., *Phys. Lett. B* **480**, 23 (2000).
30. R. Bernabei et al., *Phys. Lett. B* **509**, 197 (2001).
31. R. Bernabei et al., *Eur. Phys. J. C* **23**, 61 (2002).
32. P. Belli et al., *Phys. Rev. D* **66**, 043503 (2002)
33. R. Bernabei et al., *Il Nuovo Cim. A* **112**, 545 (1999).
34. R. Bernabei et al., *Eur. Phys. J. C* **18**, 283 (2000).
35. R. Bernabei et al., *La Rivista del Nuovo Cimento* **26** n.1, 1-73 (2003), and refs. therein.
36. R. Bernabei et al., *Int. J. Mod. Phys. D* **13**, 2127 (2004) and refs. therein.
37. R. Bernabei et al., *Int. J. Mod. Phys. A* **21**, 1445 (2006).
38. R. Bernabei et al., *Eur. Phys. J. C* **47**, 263 (2006).
39. R. Bernabei et al., *Int. J. Mod. Phys. A* **22**, 3155 (2007).
40. R. Bernabei et al., *Eur. Phys. J. C* **53**, 205 (2008).
41. R. Bernabei et al., *Phys. Rev. D* **77**, 023506 (2008).
42. R. Bernabei et al., *Mod. Phys. Lett. A* **23**, 2125 (2008).
43. R. Bernabei et al., *Phys. Lett. B* **408**, 439 (1997).
44. P. Belli et al., *Phys. Lett. B* **460**, 236 (1999).
45. R. Bernabei et al., *Phys. Rev. Lett.* **83**, 4918 (1999).
46. P. Belli et al., *Phys. Rev. C* **60**, 065501 (1999).
47. R. Bernabei et al., *Il Nuovo Cimento A* **112**, 1541 (1999).
48. R. Bernabei et al., *Phys. Lett. B* **515**, 6 (2001).
49. F. Cappella et al., *Eur. Phys. J.-direct C* **14**, 1 (2002).
50. R. Bernabei et al., *Eur. Phys. J. A* **23**, 7 (2005).
51. R. Bernabei et al., *Eur. Phys. J. A* **24**, 51 (2005).
52. K.A. Drukier et al., *Phys. Rev. D* **33**, 3495 (1986).

53. K. Freese et al., *Phys. Rev. D* **37**, 3388 (1988).
54. R. Bernabei and A. Incicchitti, *Int. J. Mod. Phys. A* **32**, 1743007 (2017).
55. D. Smith and N. Weiner, *Phys. Rev. D* **64**, 043502 (2001).
56. D. Tucker-Smith and N. Weiner, *Phys. Rev. D* **72**, 063509 (2005).
57. D. P. Finkbeiner et al, *Phys. Rev. D* **80**, 115008 (2009).
58. K. Freese et al., *Phys. Rev. D* **71**, 043516 (2005).
59. K. Freese et al., *Phys. Rev. Lett.* **92**, 111301 (2004).
60. P. Belli et al., *Int. J. of Mod. Phys. A* **31**, 1642005 (2016).
61. P. Gondolo et al., *New Astron. Rev.* **49**, 193 (2005).
62. G. Gelmini and P. Gondolo, *Phys. Rev. D* **64**, 023504 (2001).
63. F.S. Ling, P. Sikivie and S. Wick, *Phys. Rev. D* **70**, 123503 (2004).
64. G. Ranucci and M. Rovere, *Phys. Rev. D* **75**, 013010 (2007).
65. J.D. Scargle, *Astrophys. J.* **263**, 835 (1982).
66. W.H. Press et al., *Numerical recipes in Fortran 77: the art of scientific computing*, Cambridge University Press, Cambridge, England 1992, section 13.8.
67. J.H. Horne and S.L. Baliunas, *Astrophys. J.* **302**, 757 (1986).
68. R. Bernabei et al., *Bled Workshop in Physics* **15**, no. 2, 19 (2014).
69. W.T. Eadie et al., *Statistical methods in experimental physics*, ed. American Elsevier Pub. (1971).



4 The multicomponent dark matter structure and its possible observed manifestations

V. Beylin¹

email: vitbeylin@gmail.com

V. Kuksa¹

M. Bezuglov²

email: Bezuglov.ma@phystech.edu

D. Sopin¹

email: sopindo@mail.ru

¹Southern Federal University, Russia, Institute of Physics, Russia

²Laboratory of Theoretical Physics, JINR, Dubna, Russia

Abstract. In the framework of hypercolor extension of the Standard Model having vector-like hyperquarks and two stable dark matter candidates originated from different hypercurrents, we consider some effects which result from reactions with participation of the dark matter components. Namely, there are decays of charged hyperpions into leptons and neutral component, annihilation and transitions of heavy dark matter candidates into the light ones. In the last case, low energy photon radiation from intermediate charged states is possible. This type of the dark matter luminescence is analyzed in more detail.

Povzetek: Avtorji uporabijo model, ki kvarkom in leptonom *standardnega modela* doda nove vektorske "hiper kvarke" in dva kandidata za temno snov. Študirajo razpade nabityh hiperpionov na nabite leptone in nevtrine, anihilacijo in prehode masivnih kandidatov temne snovi v manj masivne. Pri tem se lahko pojavi fotonsko sevanje nizkih energij, ki ga podrobneje analizirajo

PACS: 12.60 - i, 96.50.S-,95.35.+d.

4.1 Introduction

Experimental evidence of symmetry breaking mechanism in the Standard Model (SM) and the existence of Higgs bosons with the properties predicted have even worsened, in some sense, the situation in high-energy physics. From this time the SM has acquired the features of a complete and closed theory, without being such. This obviously means that the SM is only a kind of limit of a more general theory that should give solutions of open problems of the SM. Unfortunately, the inspiring idea of supersymmetry (SuSy) does not manifest itself in experiments at a scale of ~ 1 TeV, which reduces the potential of the theory, although it does not completely close it. Then, the search for ideas to solve the SM problems leads to analysis of the extension options for the SM. A lot of variants of the generalization

and extension of the SM have been discussed in literature, in particular, those that offer different ways of explaining the structure and properties of dark matter (DM). At the moment, the DM existence is a firmly established fact, which is confirmed by many astrophysical observations. About a quarter of the universe mass is the DM and it plays a crucial role in the evolution of galaxies. Despite the fact that the existence of this substance has been known for an almost a century, and that it literally surrounds us, we still do not have the faintest idea what it is. All that we have is a set of hypothetical essences for its explanation, they are neutralinos from SuSy, axions, sterile neutrinos, inert Higgses, primordial black holes, manifestations of modified dynamics and last but not list WIMPs. The most popular option is considered to be the WIMPs and they will be discussed in this work. It should be added that all efforts to catch the DM particles directly do not successful up to now, and indirect methods to see some and measure any signals of processes with the DM participation become much more important [1–7].

Multicomponent models of the DM have become the object of attention and study mainly in recent decade [8, 9] because, on the one hand, various variants of the SM extension were proposed suggesting some possible types of the DM carriers. On the other hand, there are unexplained astrophysical phenomena that can be better interpreted and explained within the framework of a multicomponent DM scenario. These phenomena are, in particular, monochromatic photon signals of unknown origin from Galaxy center with energies up to tens of GeV [10, 11] and some features of spectra of cosmic leptons (positron excess, for instance) [13, 31]. In accordance with these two aspects, it is possible to divide the proposed DM variants into some two classes. In the first one, a multicomponent DM is resulted from a specific symmetry, which extends and generalizes the SM group of symmetry and consequently introduces some additional degrees of freedom providing stability for the part of them. What manifestations and specific effects can be induced by these new particles - it depends on the properties of the model symmetry and interactions. But the second type of scenarios introduces new Dark Matter candidates aiming the explanation of the observed physical phenomena, for example, the positron fraction excess in cosmic-ray spectra (leptophilic models [14, 15]) or to interpret photon signals (gamma emission from Galactic center region) as the result of annihilation of DM particles. Certainly, to stabilize new objects the initial SM symmetry should be also modified, for instance, using discrete symmetries. Namely, imposing a Z_N symmetry (it can result from spontaneously broken $U(1)$) provides simultaneously an existence of several stable scalar fields as the DM candidates [16].

As another example, the renormalizable extension of the SM by a scalar, pseudoscalar and a singlet fermion fields is considered where the DM has a fermion and a scalar components [17, 18]. It allows to explain photon signal with energy in a keV region by the light scalar decay, and 130-GeV photons emerging, for example, as a consequence of heavy fermions annihilation. Another approach to introduce and use a two-component Dark Matter is to add a neutral Majorana fermion and a neutral scalar singlet interacting with the SM fields through the Higgs portal. Fermion, however, interacts at the tree level as Yukawa particle.

And again, in various regions for the mass of the scalar, the photon signal can be interpreted as result of the scalars annihilation [19].

As the most obvious case, some co-existence of axions with neutralino or wino [20, 21] allows to keep the SuSy scale near 1 TeV (however, it is difficult to provide the necessary value of the DM relic density). There also suggested also an interesting way to use Exceptional Supersymmetric Standard Model (E6SSM) [22], where two DM components arise from the set of Higgs superfields due to discrete symmetries again.

The DM candidates can be built from any suitable "matter" - additional scalars, fermions, even strongly interacted objects, Higgses portal, dark atoms, the DM can be presented by elementary particles or some compound states. In any case, these DM candidates should be neutral and stable, and channels and steps of their production in direct experiments at colliders together with their indirect manifestations in astrophysics phenomena or observed by space telescopes and at ground observatories (IceCube, LHAASO etc.) are analyzed carefully in a lot of papers [23–27, 29–31] and also in [32, 33, 35–44]. Certainly, all possible scenarios consider two aspects of the DM physics: theoretical validity and self-consistency of the model, and (qualitative and quantitative) description of the observed specific effects.

An existence of several DM components substantially increases the number of reactions with the DM participation and allows to predict some interesting channels of its manifestations. The most important for such predictions is the structure of the DM sector in the model and features of the dark matter interactions with the SM particles and between the DM components. To clarify this possibility, we consider hypercolor model with additional heavy fermions (hyperquarks) in confinement, which can produce a set of composite states, hyperhadrons, in the framework of σ -model at some high scale [45–48] in an analogy with low-energy quark-meson theory. So, in the model a number of pseudo-Nambu-Goldstone (pNG) particles emerges, they acquire masses after the chiral symmetry breaking. There arise fifteen pNG states (and their chiral partners) which are connected with corresponding H-quark currents. The model includes almost standard Higgs boson which is (slightly) mixed with scalar σ - meson.

Specifically, the model contains several neutral stable particles they can be interpreted as the DM candidates. In more detail, these states and their main characteristics will be presented in Section 2. Section 3 will be devoted to analysis of some new effect induced by the complex structure of the DM sector - radiation of photons in transitions of one of the DM component into another one. In Conclusion we discuss some possible application of this effect.

4.2 Hyperquark scenario: features of the dark matter sector

The SM content and possibilities can be extended by introducing a new fermion sector in confinement using, for example, an extra gauge symmetry $SU(2)_{tc}$. Besides, an additional $SU(2)_w$ symmetry should be to ensure electroweak interaction of new fermions (H-quarks) with the SM fields. Then, the hypercolor model in its minimal form contains only one doublet (with zero hypercharge) of heavy

Dirac H-quarks doublet and keeps the standard Higgs boson. It, however, will mix with scalar $\tilde{\sigma}$ -meson generated by extra singlet scalar field, which is necessary for a spontaneous symmetry breaking. As a result, the new fields can acquire masses. Note, the mixing between scalars should be small to ensure the stability of precisely measured SM parameters (in other words, oblique corrections of Peskin Tackeuchi should be sufficiently small).

In an analogy with the low-energy hadron QCD-based theory, H-quarks should form H-hadrons, which can be described in the H- σ -model with an effective Lagrangian. So, there arises (due to global SO(4) symmetry breaking) a set of pseudo-Nambu-Goldstone (pNG) states: a triplet of pseudoscalar H-pions and one neutral H-baryon along with its antiparticle. More exactly, H-baryon is a diquark state having an additive conserved quantum number, H-pions possess a multiplicative conserving quantum number [48,49]. Importantly, neutral states, $\tilde{\pi}^0$ and B^0 , \bar{B}^0 , are stable. Consequently, they can be interpreted as the DM candidates with equal masses at the tree level.

Because we are mostly interested to analyze the stable candidates properties, we do not consider heavier unstable H-hadrons and H-mesons (see, however, study of their mass spectrum at lattice [50,51] in the same gauge Sp(4) theory). Then, we need to know tree-level masses of lowest states (H-pions and H-baryon), mass of H-sigma and its v.e.v.; all of them are supposed to be $O(\text{TeV})$. The angle of mixing, θ , between H-sigma and the Higgs boson, as it dictates by Peskin - Tackeuchi parameters for the model, should be such that $\sin \theta \lesssim 0.1$.

There were calculated both the mass splitting between neutral and charged states in H-pion triplet (induced by electroweak loops only) and between the lowest states of different origin (H-pions and H-baryons). In the last case, the mass splitting depends on some renormalization scale because of different H-quark currents generating these H-states, so, the mass splitting can be as much as tens of GeV. Electroweak mass splitting in H-pions triplet is well known and it is ≈ 160 GeV. So, in this minimal scenario there are three stable particles possibly constituting dark matter: neutral stable H-baryon along with its antiparticle (we will consider them as the one component) and the lightest neutral H-pion.

To estimate their masses, there was used known way of analysis of the dark matter density evolution to its modern value. Namely, there were written down five equations for each DM component taking into account charged H-pions that are decayed eventually into neutral one, i.e. so-called, co-annihilation processes were also considered for H-baryons and H-pions. Numerical solution of the system of equations demonstrates that the correct value of the DM abundant corresponds to some areas in the parameter plane-of H-pions and H-sigma masses. Despite of the DM candidates masses estimation (approximately, they are in the region $0.8 - 1.2$ TeV), it was found that in all permitted areas of parameters B^0 -baryons dominate in the DM density [52]. The reason of this asymmetry for the DM components contributions into the total density follows from asymmetry of their interactions with the SM matter: H-pions have EW channels, but H-baryons do not participate in tree level EW interactions, they use (pseudo)scalar exchanges through Higgs boson and/or $\tilde{\sigma}$ -meson instead. It is an important consequence

of different origin for these DM components providing slower burnout of B^0 component in comparison with H-pion component.

Remind, both DM components were considered initially as having equal masses, mass splitting in the H-pion triplet is defined only EW loops and it is small. However, one-loop mass splitting between $\tilde{\pi}^0$ and B^0 can be as high as 10 – 15 GeV depending on $\tilde{\sigma}$ - meson mass and value of renormalization parameter, μ . Again, it is due to the different structures of H- quark currents with which these components are associated. Corresponding mass splittings are demonstrated in Fig.1a,b. Note, mass of $\tilde{\sigma}$ - meson is near the value which is dictated by relation $m_{\tilde{\sigma}}^2 \approx 3 \cdot m_{\tilde{\pi}}^2$ resulted from zero H – $\tilde{\sigma}$ mixing.

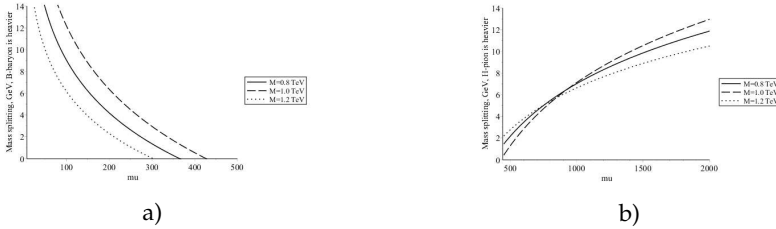


Fig. 4.1: Mass splitting between DM components in dependence on renormalization scale: a) B^0 is heavier; b) $\tilde{\pi}^0$ is heavier.

For nonzero mass splitting between the components, there occur an interesting process of the heavier DM component transformations into the lighter one. It can result to some effects, which are specific for suitable scenarios of multicomponent DM. Here, we will consider the case when B^0 is heavier than $\tilde{\pi}^0$, it is that the scenario when the tree level process of annihilation of heavy $B^0 B^0$ pair into H-pions can be accompanied with some final state radiation (FSR).

4.3 Transitions between DM components and an effect of luminescence

To discuss possible γ -radiation in the transitions between dark matter components, we firstly analyzed the ratio of cross section of $B^0 B^0$ pair annihilation into H-pions (see diagrams in Fig.2a) to the total cross section of $B^0 B^0$ pair annihilation into all possible SM final states.

Denoting this ratio as α , we consider its values in the $\tilde{\pi} - \tilde{\sigma}$ plane for various sets of model parameters: scale of renormalization (it also determines the mass splitting between B^0 and $\tilde{\pi}$ states), mixing angle, and the vacuum shift for a heavy scalar field. Some regions of α values are shown in Fig.3; in all cases it is possible to find an areas where α parameter is sufficiently large, $\alpha \geq 10$. Fortunately, in these regions H-pions and B^0 -H-baryons masses are ~ 1 TeV, as it also follows from kinetics of the DM burn out. Thus, it is possible to fix a suitable interval of the DM components and the sigma meson masses, at which the $B\tilde{B}$ -pair transition into charged unstable H-pions dominates.

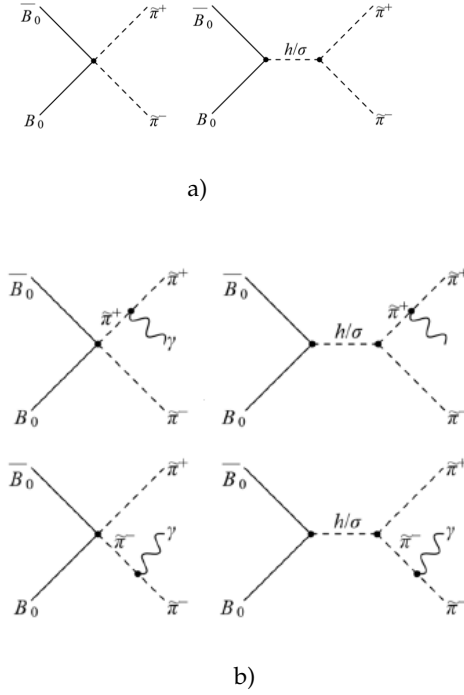


Fig. 4.2: Diagrams for B^0 annihilation into H-pions: a) without FSR, b) with FSR.

Effect of FCR occurs just in the reaction $B^0 B^0 \rightarrow \tilde{\pi}^+ \tilde{\pi}^- + \gamma$ (see diagrams in Fig. 2b) with subsequent decays of charged H-pions, $\tilde{\pi}^+ \rightarrow \tilde{\pi}^0 + \nu_l$. These charged states decay through strong and EW channels producing neutral stable $\tilde{\pi}^0$ and pair of lepton plus (anti)neutrino; corresponding widths [48] are:

$$\begin{aligned} \Gamma(\tilde{\pi}^\pm \rightarrow \tilde{\pi}^0 \pi^\pm) &= 6 \cdot 10^{-17} \text{ GeV}, \quad \tau_\pi = 1.1 \cdot 10^{-8} \text{ s}, \quad c\tau_\pi \approx 330 \text{ cm}; \\ \Gamma(\tilde{\pi}^\pm \rightarrow \tilde{\pi}^0 l^\pm \nu_l) &= 3 \cdot 10^{-15} \text{ GeV}, \quad \tau_l = 2.2 \cdot 10^{-10} \text{ s}, \quad c\tau_l \approx 6.6 \text{ cm}. \end{aligned} \quad (4.1)$$

Now, for the differential cross section we get the following expression:

$$\begin{aligned} \frac{d\sigma(B^0 B^0 \rightarrow \tilde{\pi}^+ \tilde{\pi}^- \gamma)}{dE_\gamma} &= \frac{4\alpha_e \sigma(B^0 B^0 \rightarrow \tilde{\pi}^+ \tilde{\pi}^-)}{\pi M_B E_\gamma \sqrt{M_B^2 - m_\pi^2}}. \quad (4.2) \\ &\left(-2\sqrt{M_B(M_B - E_\gamma)} \sqrt{M_B(M_B - E_\gamma) - m_\pi^2} + \right. \\ &\left. (2M_B(E_\gamma - M_B) + m_\pi^2) \log\left[\frac{2\sqrt{M_B(M_B - E_\gamma)}}{\sqrt{M_B(M_B - E_\gamma)} + \sqrt{M_B(M_B - E_\gamma) - m_\pi^2}} - 1 \right] \right). \end{aligned}$$

So, possibility of radiation from (unstable) charged components (of H-pion triplet) is a specifics of the SM extensions with a complex structure resulting to the

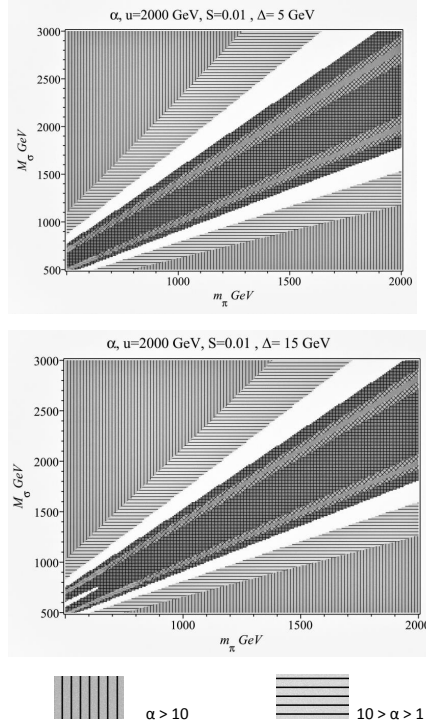


Fig. 4.3: Ratio of the $B^0 B^0$ annihilation cross sections, notations of important regions for parameter α are depicted.

multi-component DM. If there are suitable channels of interaction, heavier DM component can transform into the light one, but for the FSR (or virtual internal bremsstrahlung) an occurrence of this transition should have an intermediate stage with some charged states. Here is exactly the same case.

Cross sections for different values of the DM component masses, mixing angle, mass of $\tilde{\sigma}$ -meson and scale of H-symmetry breaking are presented in Fig.5 and 6. Here are shown also total cross sections demonstrating an obvious s-channel resonance near $M_{\tilde{\sigma}}$ in Fig. 7. .

With an integration of the differential cross section from energies $\sim (0.1 - 0.2) \text{ GeV}$ up to $2 \cdot \Delta_m$, we have found the total cross section, its values are shown in Fig.5 in dependence on $M_{\tilde{\sigma}}$ for various mass splittings and masses of B^0 . Obviously, there are some features of the effect considered. First, the resonance structure is manifested at $M_{\tilde{\sigma}}$ due to s-channel contributions, and the total cross section is practically independent on $\tilde{\sigma}$ - meson mass when its value is $\geq (2.0 - 2.5) \text{ TeV}$. We also estimate total flux of photons using σ_{tot} values between 10^{-28} and $10^{-26} \text{ cm}^3/\text{s}$ and the Navarro-Frank-White profile for the dark matter density, $\rho_{\text{NFW}}(l, \theta, \phi)$. We used also known astrophysical J-factor for the Galaxy center, namely, we take the angular resolution $\sim 1^\circ$ and the value of $J \approx 10^{-21}$.

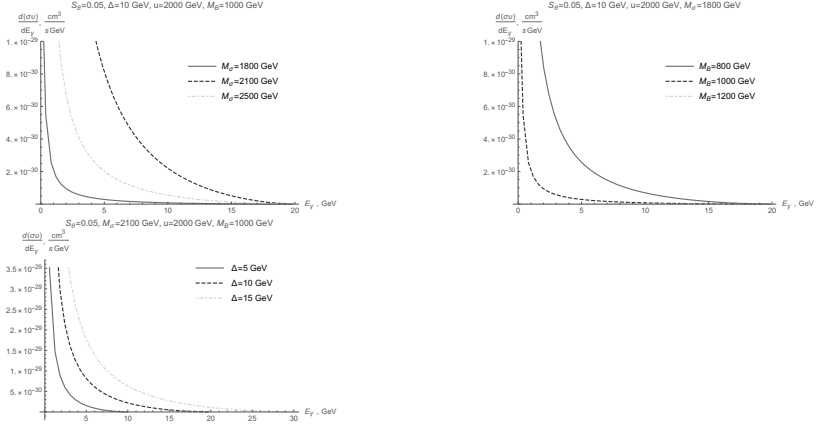


Fig. 4.4: Differential cross sections for $B^0 B^0 \rightarrow \tilde{\pi}^+ \tilde{\pi}^- \gamma$ process for various model parameters.



Fig. 4.5: Total cross section for the process if transition between the DM components with FSR, values of parameters are depicted in figures.

Then, the values of total gamma-flux of low-energy photons produced by transitions between the dark matter components near Galaxy center are the following:

$$\Phi(E_\gamma) \approx (0.9 - 1.5) \cdot (10^{-14} - 10^{-12}) \text{ cm}^{-2} \text{ s}^{-1}. \quad (4.3)$$

However, J-factor for the Galaxy center can increase up to an order or two if the parameter γ in NFW profile changes from 1 to 1.4 to simulate the DM spike in the DM distribution near the GC. Then, the flux also increases up to two orders.

In this minimal scenario the mass splitting is much lower than the DM masses, so, there arises diffuse photons with energies in a narrow limited area. Certainly, these photons are only an admixture for (monochromatic) radiation from the DM annihilation into photon pairs. This luminescence of the DM is, however, too small to explain the whole excess of GeV photons from GC.

Note also that scenarios with a complex DM sector structure should be analyzed carefully in the case of $\Delta_m \sim M_{\text{DM}}$: the DM candidates can be freezed out at different temperatures, so, they can be produced at different stages and contribute separately to features of evolution processes.

Of course, the possible effect of small photonic flux from regions with the increased DM density is specific because it does not lead to the resorption of dense DM clumps. Total mass and the particle number density does not change practically

in this process. Indeed, there takes places also an "ordinary" annihilation of DM components into two photons or into pairs of SM particles with subsequent photon emission from final or intermediate bosons, leptons and quarks. However, monochromatic photons with energies of the order of the DM masses are separated by an energy gap in the full spectrum of emitted photons.

Unfortunately, a large background is produced by diffuse FSR from the SM particles; the total gamma flux can be noticeably larger than the indicated effect. So, analysis of the photons spectrum at GeV energies is a difficult task.

Indeed, detection and selection of a (nearly constant) photonic component with energies of the order of (1 – 10) GeV can indicate the presence of some structure in the DM mass spectrum, or the possibility of transitions between excited levels in the spectrum of states, as it can occur in the hadronic DM scenario [53].

This specific radiation also should be collimated with a some (small) angular aperture if it comes from some "point sources" – GC, dwarf galaxies, subhaloes or other types of DM regions with high density. If the DM clump not very far (~ 0.1 pc) from our space telescopes, the low-energy limited flux of photons can be seen and recognized.

Note, an inverse case when the neutral H-pions are heavier also should be considered, however, annihilation into the (lighter) B^0 -components with radiation of photons is difficult to ensure in this case - diffuse photons production takes place mostly due to VIB from H-pions and/or H-quarks loops and corresponding cross section should be smaller.

4.4 Conclusion

As some additional considerations, it should be noted that stable DM candidates can be produced from H-quark-gluon plasma at early stages at large temperatures. Besides, due to high scale of H-vacuum condensates, H-hadronization should occur before the QCD hadronization, so the photons from transitions between various H-states can contribute significantly to total density of radiation. This process can maintain the plasma temperature as a kind of delay mechanism that prevents cooling during expansion, in accordance with the Le Chatelier principle. This type of annihilation induced by transition between the DM components, is interesting also from the point of view of the DM accumulation inside massive objects – red giants, white dwarfs and the possible dark stars at early stage. In this case, photons, leptons, and neutrinos generated during the transition between components will heat up the interior of the gravitationally coupled system more slowly than the annihilation of DM into SM particles would do (this reaction, of course, also takes place, but with a noticeably smaller cross section for some model parameter values). In the case, the dark star life time in the relatively "cold" state should increase.

Moreover, if such reactions dominate, the gravitating mass of the object also will changes slowly. Energies of the photons emitted from such objects will be distributed over significantly different regions separated by a gap of the order of the DM mass. Such an analysis would be reasonable for (early) dark stars with long lifetimes. Their thermonuclear heating is actually replaced by an energy

release during the annihilation of DM particles. The discussed effect shows that the presence of a specific complex structure of DM states can be important for the dark stars study. Namely, the luminosity of dark stars can be provided also by low-energy component which is induced by transitions between the DM objects within the stars.

Thus, it was considered the scenario in which one DM component can be effectively transform into another through intermediate stage of charged H-pions production and decay. Certainly, it is possible an annihilation of $B^0\bar{B}^0$ pair into standard quarks and gauge bosons (via scalar exchanges or loops), but it turned out that there is a region of parameters where the cross section for annihilation into hyperpions dominates. Note, the lifetime of charged H-pions is larger than the lifetime of gauge bosons. So, the emission of photons from intermediate charged states, in principle, could be observed. The (small) flux of photons is proportional to the squared DM density, so the most interesting should be to study intensity of such radiation from the GC (from where an increased flux of low-energy photons is observed) or from probable DM clumps. Note also, the DM number density in these processes does not change, intermediate charged H-pions produce neutral stable H-pions together with the low-energy secondaries such as leptons and neutrinos. Apart from the low-energy characteristic radiation with small flux, the effect obviously leads to the burn out of heavier DM component transforming it to another one. This process, however, is very slow, since the DM concentration is low. Both DM components are practically in equilibrium, so that a small change in their concentrations is hardly noticeable.

It would be interesting to analyze another scenarios of the SM extensions with a complex structure of DM sector and rich phenomenology to study possible observed manifestations of multicomponent dark matter using multi-messenger approach for the analysis of possible signals.

Acknowledgements

The work was supported by grant of the Russian Science Foundation (Project No-18-12-00213-P)

References

1. J.L. Feng: Dark Matter Candidates from Particle Physics and Methods of Detection, *Ann. Rev. Astron. Astrophys.* **48**, 495 (2010).
2. L. Roszkowski, E.M. Sessolo, S. Trojanowski: WIMP dark matter candidates and searches — current status and future prospects, *Rept. Prog. Phys.* **81**, 066201 (2018) [arXiv:1707.06277].
3. M. Cirelli: Dark Matter Indirect searches: phenomenological and theoretical aspects. *J. Phys.: Conf. Series* **447**, 012006 (2013).
4. M.Y. Khlopov: Introduction to the special issue on indirect dark matter searches, *Int. J. Mod. Phys. A.* **29**, 1443002 (2014).
5. J.M. Gaskins: A review of indirect searches for particle dark matter, *Contemp. Phys.* **57**, 496 (2016) [arXiv:1604.00014].

6. G. Arcadi, M. Dutra, P. Ghosh, M. Lindner, Y. Mambrini, M. Pierre, D. Profumo, F.S. Queiroz: The waning of the WIMP? A review of models, searches, and constraints, *Eur.Phys. J. C* **78**, 203 (2018) [arXiv:1703.07364].
7. K.M. Belotsky, E.A. Esipova, A.Kh. Kamaletdinov, E.S. Shlepkina, M.L. Soloviyov: Indirect effects of dark matter, *IJMPD* **28**, 1941011 (2019).
8. M. Khlopov: Physical arguments, favouring multicomponent dark matter. In: *Dark matter in cosmology, clocks and tests of fundamental laws*. Eds.B.Guiderdoni et al. Editions Frontiers, 1995. PP. 133-138.
9. M. Aoki, M. Duerr, J. Kubo, H. Takano: Multicomponent dark matter systems and their observation prospects, *Phys. Rev. D* **86**, 076015 (2012).
10. M. Di Mauro: Characteristics of the Galactic Center excess measured with 11 years of Fermi-LAT data, *Phys. Rev. D* **103**, 063029 (2021).
11. HESS collaboration: Search for γ -Ray Line Signals from Dark Matter Annihilations in the Inner Galactic Halo from 10 Years of Observations with HESS, *Phys. Rev. Lett.* **120** 201101 (2018) [arXiv:1805.05741].
12. M. Ackermann et al. (Fermi-LAT Collaboration): Measurement of separate cosmic-ray electron and positron spectra with the Fermi Large Area Telescope, *Phys. Rev. Lett.* **108**, 011103 (2012) [arXiv:1109.0521].
13. M. Aguilar et al. (AMS Collaboration): Towards Understanding the Origin of Cosmic-Ray Positrons, *Phys. Rev. Lett.* **122**, 041102 (2019).
14. K.M. Zurek: Multi-Component Dark Matter, *Phys. Rev. D* **79**, 115002 (2009) [arXiv:0811.4429].
15. C.-Q. Geng, Da Huang, C. Lai: Multi-component dark matter, *IJMPA* **30**, 28 (2015).
16. C.E. Yaguna, O. Zapata: Multi-component scalar dark matter from a ZN symmetry: a systematic analysis, *JHEP* **109**, 3 (2020).
17. A. Biswas, D. Majumdar, A. Sil, P. Bhattacharjee: Two Component Dark Matter: A Possible Explanation of 130 GeV γ -Ray Line from the Galactic Centre, *JCAP* **12**, 049 (2013) [arXiv:1301.3668].
18. A. Dutta Banik, M. Pandey, D. Majumdar, A. Biswas: Two component WIMP-FIMP dark matter model with singlet fermion, scalar and pseudo scalar, *Eur. Phys. J. C* **77**, 657 (2017) [arXiv:1612.08621].
19. S. Bhattacharya, A. Drozd, B. Grzadkowski, J. Wudka: Two-Component Dark Matter, *JHEP* **10**, 158 (2013) [arXiv:1309.2986].
20. H. Baer, A. Lessa, W. Sreethawong: Coupled Boltzmann calculation of mixed axion/neutralino cold dark matter production in the early universe, *JCAP* **1201** 036 (2012) [arXiv:1110.2491].
21. K. J. Bae, H. Baer, A. Lessa, H. Serce, Mixed axion-wino dark matter, *Front.in Phys.* **3**, 49 (2015) [arXiv:1502.07198].
22. S. Khalil, S. Moretti, D. Rojas-Ciofalo, H. Waltari: Multi-component Dark Matter in a Simplified E6SSM Model, *Phys. Rev. D* **102**, 075039 (2020).
23. S. Bhattacharya, P. Ghosh, N. Sahu: Multiparticle Dark Matter with Scalars, Fermions and signatures at LHC, *JHEP* **02**, 059 (2019) [arXiv:1809.07474].
24. S. Bhattacharya, P. Poullose, P. Ghosh: Multiparticle Interacting Scalar Dark Matter in the light of updated LUX data, *JCAP* **04**, 043 (2017) [arXiv:1607.08461].
25. G. Arcadi, C. Gross, O. Lebedev, Y. Mambrini, S. Pokorski, T. Toma: Multicomponent Dark Matter from Gauge Symmetry, *JHEP* **12**, 081 (2016) [arXiv:1611.00365].
26. D. Borah, A. Dasgupta, U.K. Dey, S. Patra, G. Tomar, Multi-component Fermionic Dark Matter and IceCube PeV scale Neutrinos in Left-Right Model with Gauge Unification: *JHEP* **09**, 005 (2017) [arXiv:1704.04138].
27. A. Ahmed, M. Duch, B. Grzadkowski, M. Iglicki: Multi-Component Dark Matter: the vector and fermion case, *Eur. Phys. J. C* **78**, 905 (2018) [arXiv:1710.01853].

28. S. Chakraborti, P. Poullose: Interplay of Scalar and Fermionic Components in a Multi-component Dark Matter Scenario, *Eur. Phys. J. C* **79**, 420 (2019) [arXiv:1808.01979].
29. D. Borah, R. Roshan, A. Sil: Minimal two-component scalar doublet dark matter with radiative neutrino mass, *Phys. Rev. D* **100**, 055027 (2019) [arXiv:1904.04837].
30. G. Palacio, A. Rivera, A. Betancura: Inert doublet as multicomponent dark matter: *Nucl. Phys. B* **962**, 115276 (2021).
31. S. Bhattacharya, P. Ghosh, A.K. Saha, A. Sil: Two component dark matter with inert Higgs doublet: neutrino mass, high scale validity and collider searches, *JHEP* **03**, 090 (2020) [arXiv:1905.12583].
32. C.H. Nam, D.V. Loi, L.X. Thuy, P.V. Dong: Multi-component dark matter in noncommutative B-L gauge theory, *JHEP* **29**, 12 (2020).
33. N. Bernal, D. Restrepo, C. Yaguna, O. Zapata: Two-component dark matter and a massless neutrino in a new B-L model, *Phys. Rev. D* **99**, 015038 (2019) [arXiv:1808.03352].
34. S. Esch, M. Klasen, C.E. Yaguna: A minimal model for two-component dark matter, *JHEP* **09**, 108 (2014) [arXiv:1406.0617].
35. L. Bian, T. Li, J. Shu and X.-C. Wang: Two component dark matter with multi-Higgs portals, *JHEP* **03**, 126 (2015) [arXiv:1412.5443].
36. A. DiFranzo, G. Mohlabeng: Multi-component Dark Matter through a Radiative Higgs Portal, *JHEP* **01**, 080 (2017) [arXiv:1610.07606].
37. S. Bhattacharya, P. Ghosh, T.N. Maity, T.S. Ray: Mitigating Direct Detection Bounds in Non-minimal Higgs Portal Scalar Dark Matter Models, *JHEP* **10**, 088 (2017) [arXiv:1706.04699].
38. S. Chakraborti, A. Dutta Banik, R. Islam: Probing Multicomponent Extension of Inert Doublet Model with a Vector Dark Matter, *Eur. Phys. J. C* **79**, 662 (2019) [arXiv:1810.05595].
39. A. Poulin, S. Godfrey: Multi-component dark matter from a hidden gauged SU(3), *Phys. Rev. D* **99**, 076008 (2019).
40. J. Heeck, H. Zhang: Exotic Charges, Multicomponent Dark Matter and Light Sterile Neutrinos, *JHEP* **05**, 164 (2013) [arXiv:1211.0538].
41. A. Ahmed, M. Duch, B. Grzadkowski, M. Iglikli: Multi-component dark matter: the vector and fermion case. *Eur. Phys. J.C* **78**, 905 (2018).
42. V. Beylin, V. Kuksa: Possibility of hadronic dark matter. *IJMPD* **28**, 1941001 (2019).
43. J.R. Cudell, M. Khlopov: Dark atoms with nuclear shell: A status review, *IJMPD* **24**, 1545007 (2015).
44. V. Beylin, M. Khlopov, V. Kuksa, N. Volchanskiy: Hadronic and Hadron-Like Physics of Dark Matter. *Symmetry* **11**, 587 (2019).
45. C.Kilic, T. Okui, R. Sundrum: Vector-like Confinement at the LHC. *JHEP* **18**, 18 (2010).
46. O. Antipin, M. Redi, A. Strumia: Dynamical generation of the weak and Dark Matter scales from strong interactions. *JHEP*. **157**, 157 (2015).
47. R. Pasechnik, V. Beylin, V. Kuksa, G. Vereshkov: Chiral-symmetric technicolor with standard model Higgs boson. *Phys. Rev. D* **88**, 075009 (2013).
48. V. Beylin, M. Bezuglov, V. Kuksa, N. Volchanskiy: An analysis of a minimal vector-like extension of the Standard Model. *Adv. High Energy Phys.* **2017**, 1765340 (2017).
49. Y. Bai, R.J. Hill: Weakly interacting stable hidden sector pions. *Phys. Rev. D* **82**, 111701 (2010).
50. E. Bennett, D.K.i Hong, J.-W. Lee, C.-J. David Lin, B. Lucini, M. Mesiti, M. Piai, J. Rantaharju, D. Vadacchino: Sp(4) gauge theories on the lattice: Quenched fundamental and antisymmetric fermions. *Phys. Rev. D* **101**, 074516 (2020).
51. A. Maas, F. Zierler, Strong isospin breaking in Sp(4) gauge theory. arXiv.org (hep-lat) [2109.14377].

52. V. Beylin, M. Bezuglov, V. Kuksa, E. Tretiakov, A. Yagozinskaya, A.: On the scattering of a high-energy cosmic ray electrons off the dark matter. *Int.J.of Mod. Phys. A* **6**(7), 34 (2019).
53. V. Kuksa, V. Beylin: Hyperfine Splitting of Excited States of New Heavy Hadrons and Low-Energy Interaction of Hadronic Dark Matter with Photons, Nucleons, and Leptons. *Universe* **6**, 6 (2020).



5 Numerical simulation of Bohr-like and Thomson-like dark atoms with nuclei

T.E. Bikbaev¹
M.Yu. Khlopov^{1,2,3}
e-mail: khlopov@apc.univ-paris.fr
A.G. Mayorov

¹ National Research Nuclear University MEPhI, 115409 Moscow, Russia

² Institute of Physics, Southern Federal University, Russia, Stachki 194 Rostov on Don 344090, Russia

³ Université de Paris, CNRS, Astroparticule et Cosmologie, France; F-75013 Paris, France

Abstract. The puzzles of direct dark matter searches can be solved in the scenario of dark atoms, which bind hypothetical, stable, lepton-like particles with charge $-2n$, where n is any natural number, with n nuclei of primordial helium. Avoid experimental discovery because they form with primary helium neutral atom-like states OHe (X – helium), called “dark” atoms. The proposed solution to this problem involves rigorous proof of the existence of a low-energy bound state in the dark atom interaction with nuclei. It implies self-consistent account for nuclear attraction and Coulomb repulsion in such an interaction. We approach the solution of this problem by numerical modeling to reveal the essence of the processes of dark atom interaction with nuclei. We start with the classical three-body problem, to which the effects of quantum physics are added. The numerical model of the dark atom interaction was developed for O^{--} having a charge of -2 , bound with He in Bohr-like OHe dark atom and for $-2n$ charged X bound with n α -particle nucleus in the Thomson-like atom XHe . The development of our approach should lead to the solution of the puzzles of direct dark matter searches in the framework of dark atom hypothesis.

Povzetek: Rezulate neposrednih meritev temne snovi je mogoče razložiti s temnimi atomi, ki povežejo hipotetične, stabilne, leptonu podobne delce z nabojem $-2n$, n je poljubno naravno število, z n jedri helija v nevtralne atome, ki jih avtorji imenujejo “temni atomi” OHe . Z numeričnim modeliranjem skupka treh teles in z upoštevanjem kvantnih popravkov iščejo dokaz, da so vezana stanja takih “temnih atomov” mogoča in so stabilna. Začeli so s študijem “temnega atoma” O^{--} , z nabojem -2 , ki se poveže s helijevim jedrom v OHe , zdaj študirajo tudi kompleksnejše “temne atome”.

PACS: 02.60.-x; 02.70.-c; 12.60.-i; 36.10.-k; 98.80.-k

5.1 “Dark” atoms XHe

If dark matter consists of particles, then they are predicted beyond the Standard Model. In particular, it is assumed that stable, electrically charged particles can exist [1–3]. Stable negatively charged particles can only have a charge of -2 – we

will denote them by O^{--} (in the general case $-2n$, where n is any natural number, we will denote them by X) [4]. In this paper, we investigate a composite dark matter scenario [5–7].

Hypothetical stable $O^{--}(X)$ particles avoid experimental discovery because they form neutral atom-like states OHe (X -helium) with primordial helium called "dark" atoms [8]. Since all these models also predict the corresponding $+2n$ charged antiparticles, the cosmological scenario should provide a mechanism for their suppression, which, naturally, can take place in the charge-asymmetric case, corresponding to an excess of $-2n$ charged particles [1]. The electric charge of the excess of these particles is compensated by the corresponding excess of positively charged baryons. So the electroneutrality of the Universe is preserved. Hence, positively charged antiparticles can effectively annihilate in the early universe. There are various models predicting such stable $-2n$ charged particles [9–11].

A "dark" atom is a system consisting of $-2n$ charged particles (in the case $n = 1$, this is O^{--}), bound by the Coulomb force with n ${}^4\text{He}$ nuclei. The structure of bound state depends on the value of $a \approx Z_\alpha Z_o \alpha \Lambda m_p R_{n\text{He}}$ parameter, where α is fine structure constant, Z_o and Z_α are the charge numbers of particle X and n nuclei of He , respectively, m_p is the proton mass, Λ is the mass number of n -nucleus He , and $R_{n\text{He}}$ is the radius of the corresponding nucleus.

For $0 < a < 2$, the bound state looks like a Bohr atom with a negatively charged particle in the core and a nucleus moving in a Bohr orbit. For $2 < a < \infty$, the bound states look like Thomson's atoms, in which the body of the nucleus vibrates around a heavy negatively charged particle.

In model of X -helium, X behaves like a lepton or as a specific cluster of heavy quarks of new families with suppressed hadron interaction [12]. And the experimental lower limit on the mass of multiple charged stable particles is about 1TeV [13].

The main problem with $X\text{He}$ atoms is their strong interaction with matter. This is because X -helium has an unshielded nuclear attraction to the nuclei of matter. This, in turn, can lead to the destruction of a bound system of dark matter atoms and the formation of anomalous isotopes. To avoid the problem of overproduction of anomalous isotopes, it is necessary that the effective potential between $X\text{He}$ and the nucleus of matter has a barrier preventing the fusion of He and/or X with the nucleus. In this paper, we construct a numerical model of such an interaction, to carry out calculations and calculate the interaction potential.

5.2 Improvement of description of the interaction of a "dark" atom in Bohr's model with the nucleus of matter by adding the Stark effect.

For $0 < a < 2$, the bound state of a dark atom looks like a Bohr atom. That is, dark atoms are $O\text{He}$ atoms with $Z_\alpha = 2$ and $Z_o = -2$. The process of constructing a numerical model of the interaction of $O\text{He}$ with the nucleus and the results of this interaction are given in article [14]. In this section, we have improved this numerical model by adding the Stark effect to it.

We fix the He rotation orbit in the OHe atom, which excludes the possibility of its polarization and we observe the Coulomb repulsion. On the other hand, the Stark effect should take place in the external electric field of a target nucleus, which leads to polarization of OHe. In our semiclassical numerical model, this can be taken into account by including the interaction dipole moment δ caused by the Stark effect. Thus, by manually including δ , we calculated the Stark force, which is obtained from the potential and is specified using the same dipole moment. δ appears due to the action of the nuclear force and the Coulomb force on the He nucleus and also the Coulomb force on O^{--} , from here you can get the expression for δ :

$$\delta(\vec{r}) = \frac{Z_\alpha E(\vec{r})}{Z_o \rho} + \frac{|\vec{F}_{i\alpha}^N|}{e\rho Z_o}, \quad (5.1)$$

where E is the strength of the external electric field, $\rho = \frac{Z_\alpha e}{R_b^3}$ is the charge density of the He nucleus, where R_b is the Bohr radius of He rotation in "dark" OHe atoms and $|\vec{F}_{i\alpha}^N|$ is nuclear interaction of the Saxon-Woods type, between the He nucleus and the target nucleus [14].

The Stark potential is calculated as follows: $U_{St} = eZ_\alpha E\delta$. And the Stark force, respectively: $\vec{F}_{St} = -\text{grad } U_{St}$.

Bearing in mind the problem of interpreting the results of the DAMA/NaI experiment on the direct search for dark matter atoms, we concentrate our calculations on the case when the target nucleus is Na [7]. Therefore, in all subsequent pictures, the target nucleus should be understood as the nucleus Na.

Based on the data obtained, the program builds the trajectories of the α -particle and the O^{--} particle (see Figures 1 and 2). In Figures 1 and 2, showing the result of the program, the black circle shows the location of the target nucleus, the blue dots and the red dotted line show the trajectories of α -particles and O^{--} particles in the XY plane, respectively.

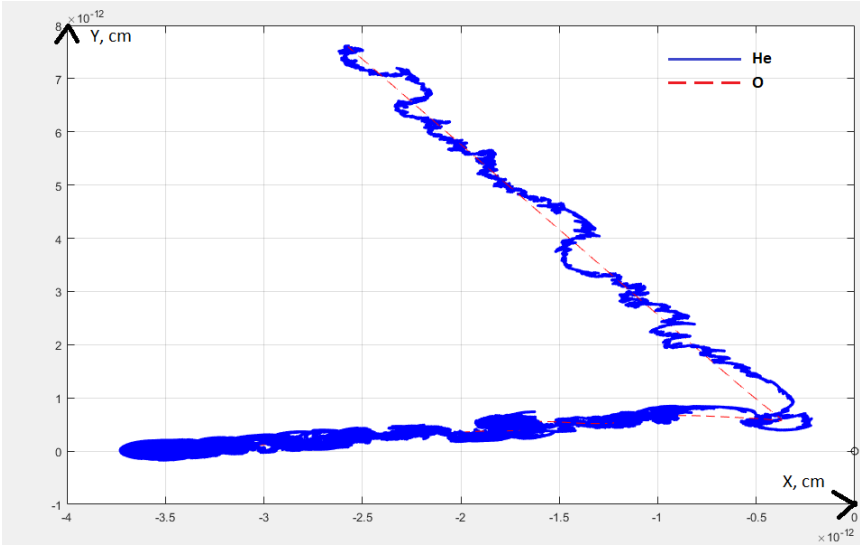
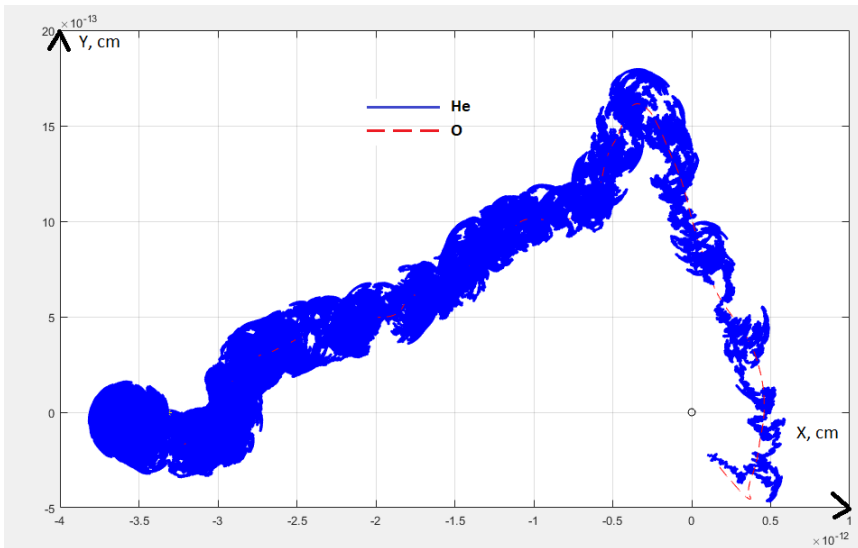
For the corresponding trajectories of the α -particle, it is possible to construct the total interaction potential between He and the target nucleus depending on the distance between He and the target nucleus (see Figures 3 and 4).

In Figure 1, a dark atom OHe was scattered by a target nucleus of matter. This also follows from Figure 3, where you can see the Coulomb barrier preventing the particles of a dark atom from entering the nucleus.

In Figure 2, approximately at coordinates $(0, 1; -2, 5)$, the trajectories of the particles are interrupted, because the dark atom is destroyed and falls into the target nucleus. This is confirmed in Figure 4, where one can see the predominance of the nuclear potential over the Coulomb potential at distances close to the target nucleus.

The results of the interaction can be quite varied, which requires a detailed study by collecting statistics of trajectories with varying the initial values of the system and the parameters of the target nucleus.

The approach of the Bohr atom model has some drawbacks, for example, in our numerical model, the Coulomb force between helium and O^{--} is not explicitly specified, but the He rotation orbit in the OHe atom is manually fixed, which

Fig. 5.1: Trajectories of α -particle and O^{--} particleFig. 5.2: Trajectories of α -particle and O^{--} particle

excludes the possibility of its polarization. And when considering Thomson's model of the atom, this problem can be solved, since with this approach helium is not a point charge stochastically moving in a fixed Bohr orbit, but is a charged ball inside which the particle O^{--} can oscillate. Moreover, the case of -2 charged particles is only a special case, since the particles we are considering can have a charge $-2n$ and form with n nuclei ${}^4\text{He}$ "dark" atoms X -helium, which by

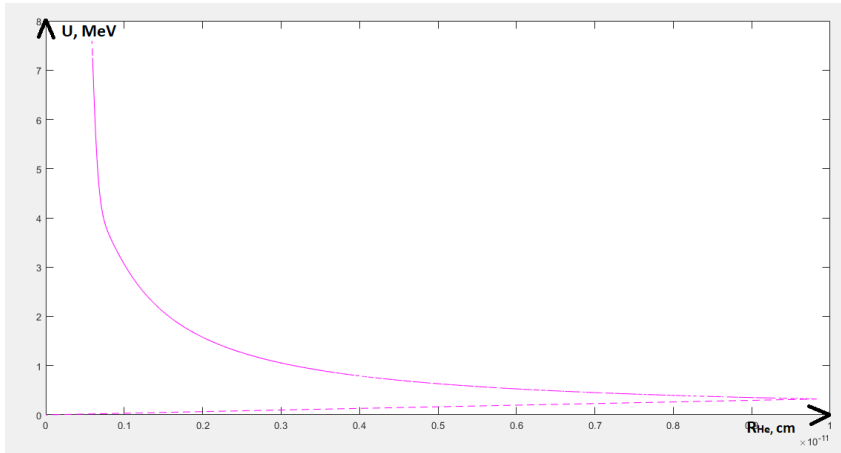


Fig. 5.3: Total potential of interaction between He and target nucleus

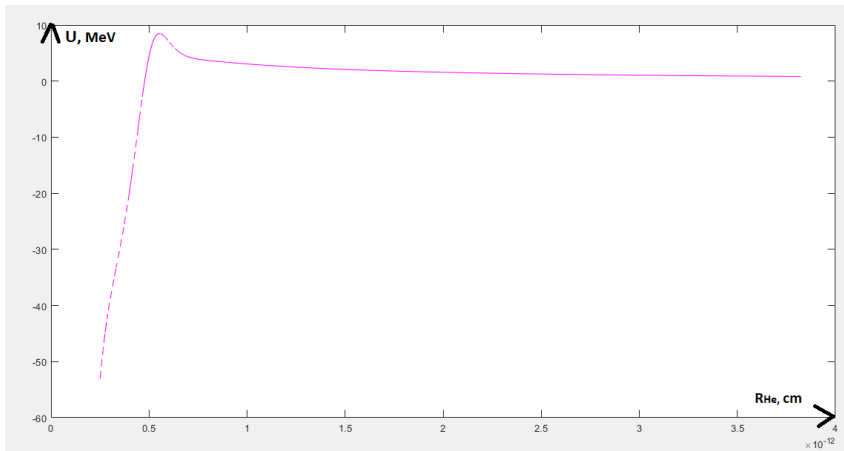


Fig. 5.4: Total potential of interaction between He and target nucleus

themselves, starting from $n = 2$, are Thomson atoms. With all this, the Stark effect, when considering the Thomson atom, should arise by itself automatically. It should be clarified that in the following sections we simulated a dark XHe atom and its interaction with a target nucleus, and in all the figures the case of a Thomson atom at $n = 1$ was considered. That is, we considered the OHe atom in the Thomson approximation. But since OHe is a special case of XHe, and our model successfully describes the general case, we left the designation XHe in all the following sections.

5.3 Numerical simulation of the interaction of Thomson's "dark" atom with the nucleus.

5.3.1 Modeling X – helium

The "dark" atom of X – helium is the bound state of an n – α -particle (n – helium) nucleus and the particle X with charge $-2n$. We place the spherical coordinate system at the center of the n – helium nucleus, which is a charged ball. Inside which, in the center, there is a point particle X. When external forces begin to act, the distance between the center of n – helium and X becomes nonzero and the particle X begins to oscillate inside the nHe nucleus (in reality, nHe is much lighter than X, therefore it is a nuclear a drop that fluctuates around X).

The force of the Coulomb interaction between n – helium and X is given by the following formula:

$$\vec{F}_{XHe}(R_{XHe}) = \begin{cases} -\frac{4e^2n^2}{R_{XHe}^3}\vec{R}_{XHe} & \text{for } R_{XHe} > R_{He}, \\ -\frac{4e^2n^2}{R_{He}^3}\vec{R}_{XHe} & \text{for } R_{XHe} < R_{He}, \end{cases} \quad (5.2)$$

where $|\vec{R}_{XHe}|$ is the distance between X and the center of the nHe nucleus, and R_{He} is the radius of the n – helium nucleus.

The scheme of numerical simulation of the dynamical system XHe:

1) Initial coordinates $X R_{0X} = 0$ and its initial speed, which we set equal to the thermal speed in the medium, $V_{0X} = \left(\frac{3kT}{M_{nuc}}\right)^{1/2}$, where M_{nuc} is the mass of the target nucleus, T is the temperature (we take 25 degrees Celsius), and k is the Boltzmann constant.

2) Consider state of the system at next moment of time, taken on the time interval dt. The i-th value of increment of components of radius vector X is determined, dr_i :

$$dr_i = V_{iX} dt. \quad (5.3)$$

3) The i + 1 value of the components of the radius vector X is calculated, r_{i+1} :

$$r_{i+1} = r_i + dr_i. \quad (5.4)$$

4) In each iteration, the program calculates the force acting on X, \vec{F}_{iXHe} . Using which the increment of the momentum $d\vec{P}_i$ of the particle X is determined:

$$d\vec{P}_i = \vec{F}_{iXHe} dt. \quad (5.5)$$

5) Using the increment of the momentum $d\vec{P}_i$, the increment of the particle velocity X, $d\vec{V}_{iX}$, is calculated, for the subsequent finding of the new velocity used in the next iteration:

$$d\vec{V}_{iX} = \frac{d\vec{P}_i}{m_X}. \quad (5.6)$$

Using the obtained data, it is possible to plot the dependence of modulus of the radius vector of particle X on time (see Figure 5). In Figure 5 one can observe the oscillation of the particle X inside the nucleus nHe with a period approximately equal to $2 \cdot 10^{-20}$ second. They appear because the Coulomb force between the nucleus nHe and X tends to return X to the center of the nucleus and to neutralize the external disturbance given to the particle X. $R_{XHe} < 1$ fm, which indicates the stability of the X – helium system.

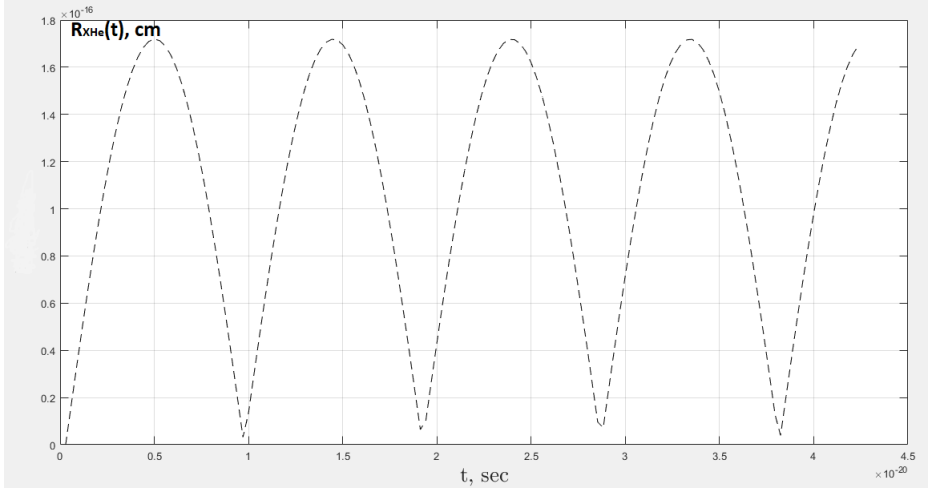


Fig. 5.5: Dependence of modulus of radius vector of particle X on time t

5.3.2 Interaction in the XHe –nucleus system

The coordinate system XHe – is the core, in which the interaction of XHe with the target nucleus will be simulated, similar to the coordinate system OHe – the core described in the 3.2 paragraph of article [14]. The difference is that the distance between X and nHe is no longer strictly fixed and is not equal to the Bohr radius. Thus, the radius vector nHe, r_{He} , and X, r , are determined independently, and the distance between X and nHe, r_{XHe} , is determined as follows:

$$\vec{r}_{XHe} = \vec{r}_\alpha - \vec{r} \quad (5.7)$$

In our Thomson approximation, helium is a charged droplet, but when considering the coulomb force and the nuclear force between He and the target nucleus, non-point of helium has not yet been taken into account and this will have to be done in the future.

Therefore, the Coulomb and nuclear forces acting between the particles of a dark atom and the target nucleus in the XHe –nucleus system are similar to the forces described in paragraphs 3.3 and 3.4 of article [14]. To these forces are added two additional forces, equal in magnitude, but opposite in sign. This is the Coulomb

force between X and nHe (see formula 2). The force acting on nHe is denoted by $\vec{F}_{i\alpha}^{XHe}$. And the force acting on X is denoted by $\vec{F}_{iX}^{XHe} = -\vec{F}_{i\alpha}^{XHe}$.

The total force acting on the particle X, \vec{F}_{iSum}^X , is calculated as follows:

$$\vec{F}_{iSum}^X = \vec{F}_{iZO}^e + \vec{F}_{iX}^{XHe}. \quad (5.8)$$

The total force acting on nHe, $\vec{F}_{i\alpha}$, is:

$$\vec{F}_{i\alpha} = \vec{F}_{i\alpha}^e + \vec{F}_{i\alpha}^N + \vec{F}_{i\alpha}^{XHe}. \quad (5.9)$$

Let us construct a numerical scheme for calculating these forces depending on the distance between objects.

1) We use the following initial conditions: initial coordinates X and nHe, $\vec{r}_0 = \vec{r}_{0\alpha}$, and their initial velocities, which we set equal to the thermal speed in the medium,

$$V_{X_0} = V_{\alpha_0} = \left(\frac{3kT}{M_{nuc}} \right)^{1/2}.$$

2) Consider the state of the system at the next moment in time, taken on the time interval dt. The i-th value of the impulse increment nHe, $d\vec{P}_{i\alpha}$, and X, $d\vec{P}_i$, is determined:

$$d\vec{P}_{i\alpha} = \vec{F}_{i\alpha} dt, \quad (5.10)$$

$$d\vec{P}_i = \vec{F}_{iSum}^X dt. \quad (5.11)$$

3) Using the increment $d\vec{P}_{i\alpha}$ and $d\vec{P}_i$, $i + 1$ values of the velocities of the nucleus nHe and X, $\vec{V}_{\alpha_{i+1}}$ and $\vec{V}_{X_{i+1}}$:

$$\vec{V}_{\alpha_{i+1}} = \vec{V}_{\alpha_i} + \frac{d\vec{P}_{i\alpha}}{m_{He}}, \quad (5.12)$$

$$\vec{V}_{X_{i+1}} = \vec{V}_{X_i} + \frac{d\vec{P}_i}{m_X}. \quad (5.13)$$

4) Calculate the $i + 1$ value of the radius vector X and nHe:

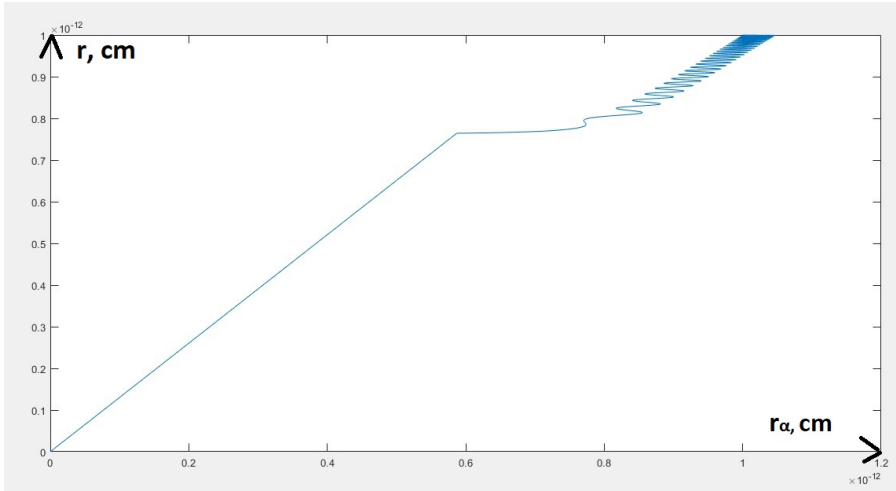
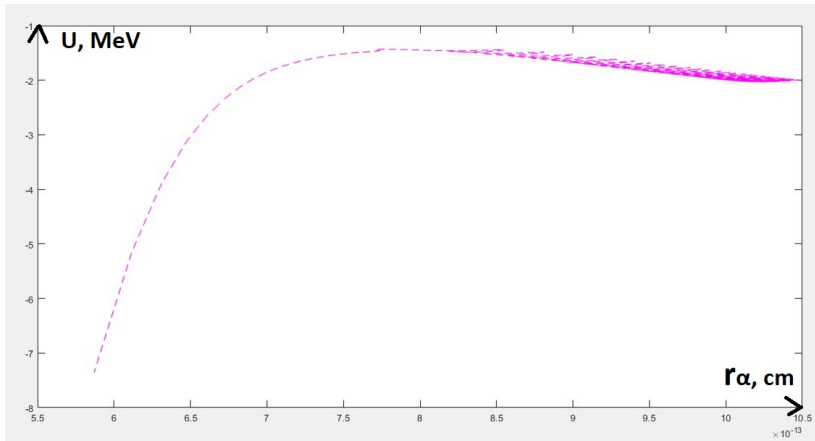
$$\vec{r}_{i+1} = \vec{r}_i + \vec{V}_{\alpha_{i+1}} dt, \quad (5.14)$$

$$\vec{r}_{\alpha_{i+1}} = \vec{r}_{\alpha_i} + \vec{V}_{X_{i+1}} dt, \quad (5.15)$$

5) In each cycle, program calculates total force acting on X particle, \vec{F}_{iSum}^X , and the total force acting on nHe, $\vec{F}_{i\alpha}$.

The dependence of the radius of the particle vector X on the radius of the vector of the n-helium nucleus see Figure 6 and the total potential of nHe interaction with the target nucleus depending on r_α see Figure 7.

It can be seen from the figures that the XHe system moves towards the target nucleus as a bound system. The radius vector of the X particle is always less than the radius of the He vector at the same time, that is, the X particle is slightly closer to the target nucleus than helium (see Figure 6). Therefore, we see the polarization

Fig. 5.6: Dependence of r on r_α Fig. 5.7: Dependence of the total potential of $n\text{He}$ interaction with the target nucleus on r_α

of the "dark" atom. But at a sufficiently close distance from the target nucleus, the nuclear force becomes strong enough to overcome the Coulomb repulsion of $n\text{He}$ by the target nucleus and n -helium, pushing forward, penetrates the nucleus, which is clearly seen in Figure 7.

After that, we supplemented the Coulomb force acting between $n\text{He}$ and the nucleus, and the Coulomb force acting between X and the nucleus, similarly to formula 2, i.e. added a condition so that its form would change upon penetration of $n\text{He}$ and X particles into the target nucleus.

The main task of our modeling is to reconstruct the total potential of interaction between $n\text{He}$ and the target nucleus.

From the analysis of trajectories, two characteristic cases can be distinguished. With a zero impact parameter, the XHe atom flies through the target nucleus, then comes back and flies in the opposite direction (see Figures 8).

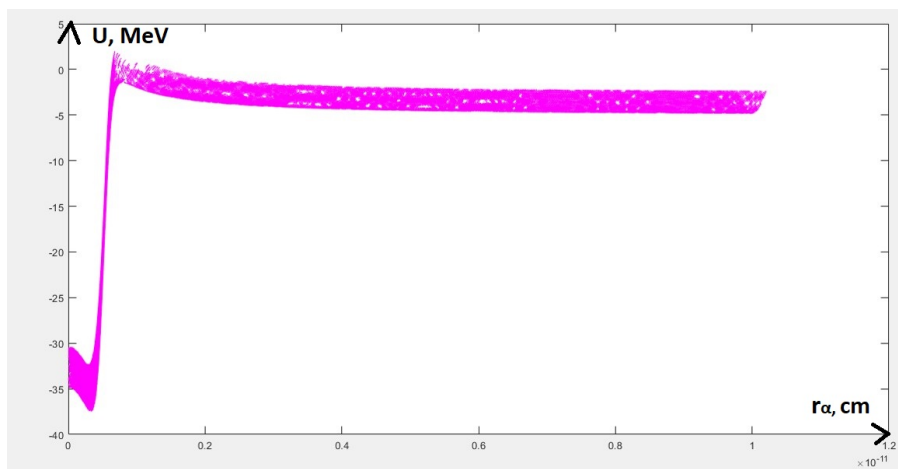


Fig. 5.8: Dependence of the total potential of nHe interaction with the target nucleus on r_α

It is assumed that the interaction of slow X–helium atoms with nuclei can lead to their low-energy binding. Thus, the low-energy bound state of the XHe–nucleus must be an oscillating three-body system. And we see that with a nonzero impact parameter, the XHe atom hits the target nucleus, and a certain oscillatory system of three bodies is formed (this can be seen in Figures 9 and 10).

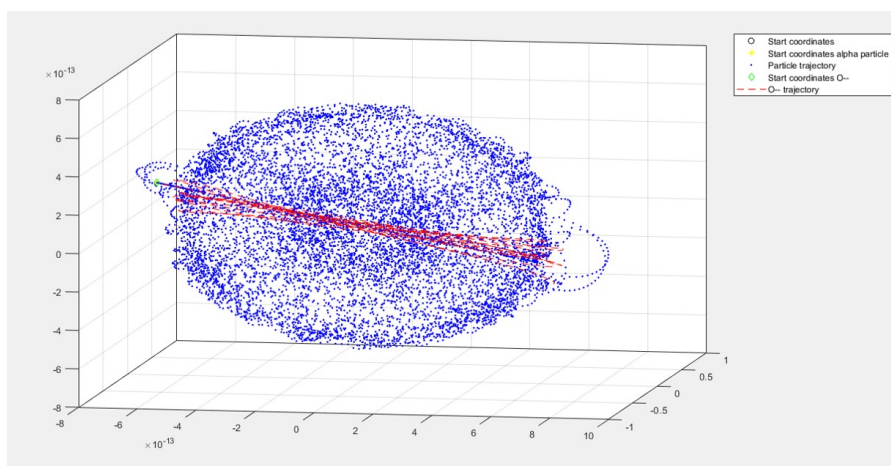


Fig. 5.9: Trajectories of nHe and particle X

In Figure 9, the black circle shows the target nucleus, the yellow asterisk and the green rhombus are the initial locations of nHe and the X particle, respectively, the blue dots and the red dotted line show the trajectories of nHe and the X particle, respectively.

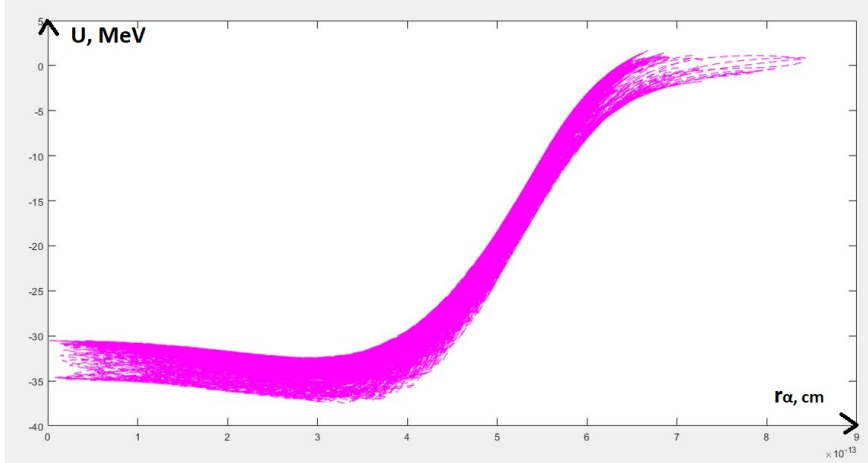


Fig. 5.10: Dependence of the total potential of nHe interaction with the target nucleus on r_α

When analyzing the trajectories, it turned out that the variation in the mass of X does not affect the result in any way. There is a dependence on the aiming parameter and the initial speed of the system. But for any of their values, the cloud of particle coordinates is inside the target nucleus. This is probably reasonable, since the zero balance of forces for helium can only be achieved in the region where the nuclear and Coulomb forces from the nucleus are balanced. But the nuclear force is small outside of it. Thus, the Coulomb polarization of XHe occurs up to the nuclear boundary, and nuclear polarization becomes possible only inside it.

5.4 Conclusions

The paper investigates the hypothesis of composite dark matter, in which hypothetical stable particles with a charge of $-2n$ form neutral atom-like states XHe with primary helium nuclei. X-helium will interact with the nuclei of ordinary matter. The nuclear interaction of dark atoms with matter is a key problem in the composite dark matter scenario. Solving this problem and correctly describing this interaction will reveal the role of dark atoms in primary nucleosynthesis, stellar processes, and will also explain the conflicting results of experiments on the direct search for dark matter due to the peculiarities of the interaction of “dark” atoms with the substance of underground detectors [15].

The XHe hypothesis cannot work unless a repulsive interaction occurs at some distance between XHe and the nucleus, and the solution of this problem is vital for

the further existence of the XHe atomic model of dark matter [16]. Therefore, we were faced with the task of constructing a numerical model of the interaction of XHe with a target nucleus. Such a numerical model is constructed in this work in the form of a Thomson model of the atom, as an attempt to avoid the disadvantages found in Bohr's model. Our model describes a system of three charged particles interacting with each other by means of Coulomb and nuclear forces.

When simulating in the Thomson atom approximation, the following effects were observed: with a zero impact parameter, the XHe atom flies through the target nucleus, then returns and flies in the opposite direction; with a nonzero impact parameter, the XHe atom hits the target nucleus, and a kind of vibrational system of three bodies, this is what is expected to be seen in the formation of a low-energy bound state in the interaction of slow X –helium atoms with the nuclei of matter. However, the disadvantage of this is that particle oscillations occur inside the target nucleus. Thus, in the current version of the numerical model, nHe can easily penetrate into the target nucleus and the elastic collisions of nuclei do not arise. In the approach of the Bohr atom, the opposite was true [14]. Therefore, in the future it should be taken into account that nuclear matter is incompressible and opaque. In other words, we need to figure out how to take into account the real properties of nuclear matter.

Acknowledgements

The work by TB, MK and AM has been supported by the grant of the Russian Science Foundation (Project No-18-12-00213-P).

References

1. M. Khlopov: Fundamental particle structure in the cosmological dark matter, *International Journal of Modern Physics A*, **28**, 1330042 (2013)
2. G. Bertone, D. Hooper, J. Silk: Particle dark matter: evidence, candidates and constraints, *Physics Reports* **405**, 279 – 390 (2005)
3. P. Scott: Searches for Particle Dark Matter: An Introduction, (2011), e-Print: arXiv:1110.2757.
4. O. V. Bulekov, M.Yu.Khlopov, A. S. Romaniouk, Yu. S. Smirnov: Search for Double Charged Particles as Direct Test for Dark Atom Constituents, *Bled Workshops in Physics* **18**, 11-24 (2017)
5. M. Yu. Khlopov, C. Kouvaris: Composite dark matter from a model with composite Higgsboson, *Phys. Rev.* **78**, 065040 (2008)
6. D. Fargion, M. Yu. Khlopov: Tera-leptons' shadows over Sinister Universe, *Gravitation Cosmol.* **19**, 219 (2013)
7. M. Yu. Khlopov, A. G. Mayorov, and E. Yu. Soldatov: Towards nuclear physics of OHe darkmatter, *Bled Workshops Phys.* **12**, 94 (2011)
8. M. Y. Khlopov: Conspiracy of BSM physics and cosmology, *Bled Workshops in Physics*, V.20 PP.21-35 (2019), e-Print: arXiv: 1911.03294.
9. K. M. Belotsky, M. Y. Khlopov, K. I. Shibaev: Composite Dark Matter and its Charged Constituents, *Grav.Cosmol.*, V.12 PP.93-99, (2006), arXiv:astro-ph/0604518

10. M. Y. Khlopov, C. A. Stephan, D. Fargion: Dark matter with invisible light from heavy double charged leptons of almost-commutative geometry?, *Classical and Quantum Gravity* **23**, 7305–7354 (2006)
11. M. Y. Khlopov, C. Kouvaris: Strong interactive massive particles from a strong coupled theory, *Physical Review D* **77**, PP. 065002 (2008)
12. M. Y. Khlopov: Composite dark matter from 4th generation, *JETP Letters* **83**, 1–4 (2006)
13. V. Beylin, M. Khlopov, V. Kuksa, N. Volchanskiy: New physics of strong interaction and Dark Universe, *Universe* **6**, 196 (2020)
14. T. E. Bikbaev, M. Yu. Khlopov, A. G. Mayorov: Numerical simulation of dark atom interaction with nuclei, *Bled Workshops in Physics* **21**, 105–117 (2020)
15. R. Bernabei: Dark matter investigation by DAMA in Gran Sasso, *International Journal of Modern Physics A* **28**, 1330022 (2013)
16. M. Yu. Khlopov: 10 years of dark atoms of composite dark matter, *Bled Workshops Physics* **16**, 71–77 (2015)
17. J. R. Cudell, M. Y. Khlopov, Q. Wallemacq: The nuclear physics of OHe, *Bled Workshops Physics* **13**, 10–27 (2012)



6 Supersymmetric and Other Novel Features of Hadron Physics from Light-Front Holography

S. J. Brodsky

e-mail: sjbth@slac.stanford.edu

SLAC National Accelerator Laboratory, Stanford University

Abstract. I survey recent developments in hadron physics which follow from the application of superconformal quantum mechanics and light-front holography. This includes new insights into the physics of color confinement, chiral symmetry, the spectroscopy and dynamics of hadrons, as well as surprising supersymmetric relations between the masses of mesons, baryons, and tetraquarks. I also will discuss some novel features of QCD – such as color transparency, hidden color, and asymmetric intrinsic heavy-quark phenomena. The elimination of renormalization scale ambiguities and the modification of QCD sum rules due to diffractive phenomena are also briefly reviewed.

Povzetek: Avtor študira uporabnost superkonformne kvantne mehanike in holografije na svetlobnem stožcu na primeru novih spoznanj v hadronski fiziki. Poroča o novem, drugačnem razumevanju kvantne barvne kromodinamike, ročnosti (kiralnosti), spektroskopskih lastnosti in dinamike hadronov. Nov pristop mu pokaže presenetljive supersimetrične relacije med masami mezonov, barionov in tetrakvarkov, razkrije mu nove lastnosti kvantne kromodinamike, kot so transparentnost barv, skrita barva in asimetrične lastnosti težkih kvarkov. Na kratko poroča o nedorečenosti renormalizacijske sheme v barvni kromodinamiki ter o spremembi vsotnih pravil zaradi difrakcijskih pojavov.

QCD, Light-Front, Holography, Intrinsic Charm, Color Transparency, Supersymmetry, Principle of Maximum Conformality

6.1 Color Confinement and Light-Front Holography

A key problem in hadron physics is to obtain a first approximation to QCD which can accurately predict not only the spectroscopy of hadrons, but also the light-front wave functions which underly their properties and dynamics. Guy de Téramond, Guenter Dosch, and I [1] have shown that a mass gap and a fundamental color confinement scale can be derived from light-front holography – the duality between five-dimensional anti-de Sitter (AdS) space physical 3+1 spacetime using light-front time. The combination of superconformal quantum mechanics [2, 3], light-front quantization [4] and the holographic embedding on a higher dimensional gravity theory [5] (gauge/gravity correspondence) has led to new analytic insights into the structure of hadrons and their dynamics [1, 6–10]. This new approach to nonperturbative QCD dynamics, *holographic light-front QCD*,

has led to effective semi-classical relativistic bound-state equations for arbitrary spin [11], and it incorporates fundamental properties which are not apparent from the QCD Lagrangian, such as the emergence of a universal hadron mass scale, the prediction of a massless pion in the chiral limit, and remarkable connections between the spectroscopy of mesons, baryons and tetraquarks across the full hadron spectrum [12–15]. See Fig. 6.5.

The light-front equation for mesons of arbitrary spin J can be derived [11] from the holographic mapping of the “soft-wall” modification [35] of AdS_5 space with the specific dilaton profile $e^{+\kappa^2 z^2}$, where one identifies the fifth dimension coordinate z with the light-front coordinate ζ , where $\zeta^2 = b_\perp^2 \chi(1 - \chi)$. As emphasized by Maldacena [5], a key feature of five-dimensional AdS_5 space is that it provides a geometrical representation of the conformal group. Moreover AdS_5 is holographically dual to 3+1 spacetime where the time coordinate is light-front time $\tau = t + z/c$. The resulting light-front potential has the unique form of a harmonic oscillator $\kappa^4 \zeta^2$ in the light-front invariant variable ζ . The result is a frame-independent relativistic equation of motion for $q\bar{q}$ bound states – a “Light-Front Schrödinger Equation” [6], analogous to the nonrelativistic radial Schrödinger equation in quantum mechanics. This bound state equation incorporates color confinement and other essential spectroscopic and dynamical features of hadron physics, including a massless pion for zero quark mass and linear Regge trajectories with the same slope in both the radial quantum number n and the internal orbital angular momentum L . The derivation of the confining Light-Front Schrödinger Equation is outlined in Fig. 6.1.

The predictions for hadron spectroscopy and dynamics [7, 8, 12] include effective QCD light-front equations for both mesons and baryons based on the generalized supercharges of superconformal algebra [3]. The supercharges connect the baryon and meson spectra and their Regge trajectories to each other in a remarkable manner: each meson has internal angular momentum one unit higher than its superpartner baryon: $L_M = L_B + 1$. See Fig. 6.7. Only one mass parameter κ appears; it sets the confinement and the hadron mass scale in the chiral limit, as well as the length scale which underlies hadron structure. Light-Front Holography in fact not only predicts meson and baryon spectroscopy successfully, but also hadron dynamics: light-front wave functions, vector meson electroproduction, distribution amplitudes, form factors, and valence structure functions. The holographic duality connecting LF physics in 3+1 physical space-time with AdS space in 5 dimensions is illustrated in Fig. 6.6. The dilaton $e^{\kappa z^2}$ modification of the metric of AdS space leads to a color-confining potential in the LF Schrödinger equation.

The combination of light-front dynamics, its holographic mapping to AdS_5 space, and the de Alfaro-Fubini-Furlan (dAFF) procedure [2] provides new insight into the physics underlying color confinement, the nonperturbative QCD coupling, and the QCD mass scale. A comprehensive review is given in Ref. [9]. The $q\bar{q}$ mesons and their valence LF wave functions are the eigensolutions of a frame-independent bound state equation, the Light-Front Schrödinger Equation. The mesonic $q\bar{q}$ bound-state eigenvalues for massless quarks have the simple Regge

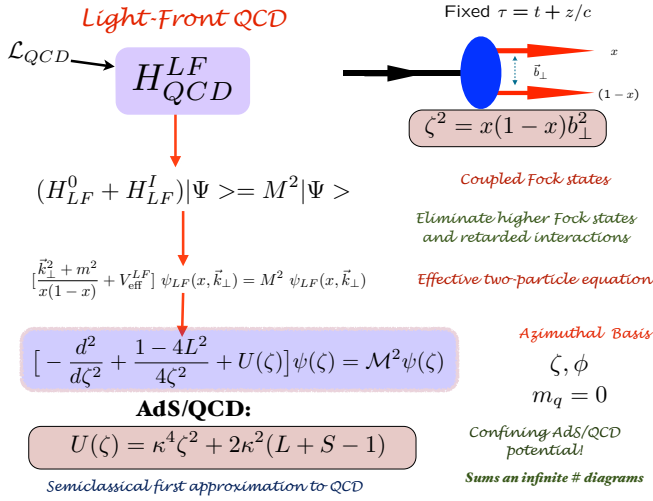


Fig. 6.1: Derivation of the Effective Light-Front Schrödinger Equation from QCD. As in QED, one reduces the LF Heisenberg equation $H_{LF}|\Psi\rangle = M^2|\Psi\rangle$ to an effective two-body eigenvalue equation for $q\bar{q}$ mesons by systematically eliminating higher Fock states. One utilizes the LF radial variable ζ , where $\zeta^2 = x(1-x)b_\perp^2$ is conjugate to the $q\bar{q}$ LF kinetic energy $\frac{k_\perp^2}{x(1-x)}$ for $m_q = 0$. This allows the reduction of the dynamics to a single-variable bound-state equation acting on the valence $q\bar{q}$ Fock state. The confining potential $U(\zeta)$, including its spin- J dependence, is derived from the soft-wall AdS/QCD model with the dilaton $e^{+\kappa^2 z^2}$, where z is the fifth coordinate of AdS₅ holographically dual to ζ . See Ref. [1]. The resulting light-front harmonic oscillator confinement potential $\kappa^4 \zeta^2$ for light quarks is equivalent to a linear confining potential for heavy quarks in the instant form [16].

form $M^2(n, L, S) = 4\kappa^2(n + L + S/2)$. The equation predicts that the pion eigenstate $n = L = S = 0$ is massless at zero quark mass.

6.2 Light-Front Holography QCD and Supersymmetric Features of Hadron Physics

One of the most remarkable feature of hadron spectroscopy is that, to a very good approximation, mesons and baryons are observed to lie on almost identical Regge trajectories: $M_M^2 = 2\kappa^2(n + L_M)$ for mesons with light quarks and $M_B^2 = 2\kappa^2(n + L_B + 1)$ for baryons with light quarks. The slopes $\lambda = \kappa^2$ in $M_H^2(n, L)$ are identical for both mesons and baryons in both the principal number n and orbital angular momentum L . (The index n can be interpreted as the number of nodes in the resulting two-body wave function.) The universality of the slopes of Regge trajectories across the hadronic spectrum is shown in Fig. 6.3. An example

Prediction from AdS/QCD: Meson LFWF

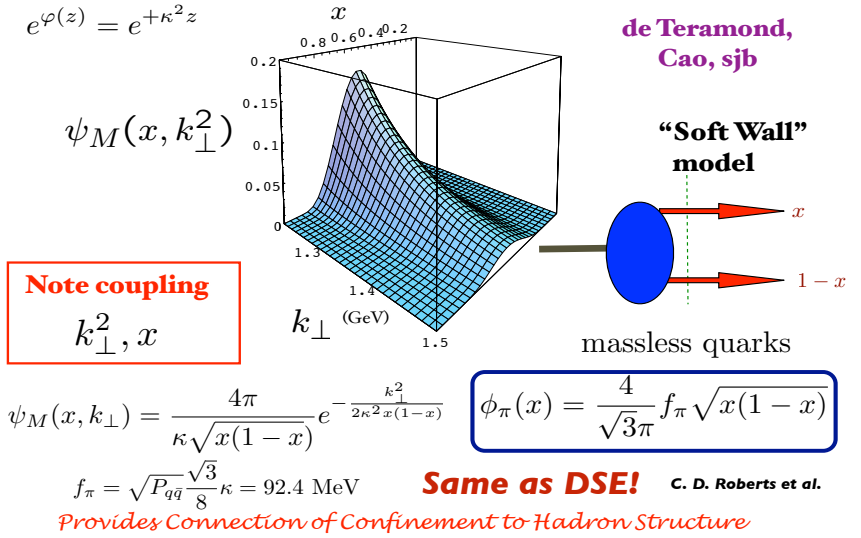


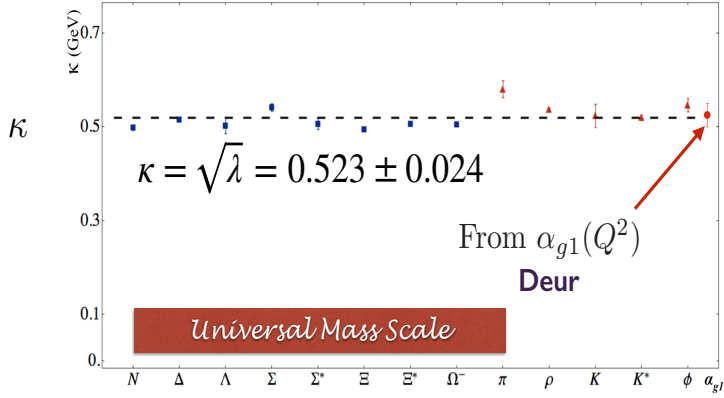
Fig. 6.2: The LF wave function of the pion predicted by LF holography. The results are consistent with analyses based on the Dyson-Schwinger equation.

comparing the pion and proton trajectories is shown in Fig. 6.4. This degeneracy between the Regge slopes of the two-body mesons and three-body baryons provides compelling evidence that two of the three quarks in the baryon valence Fock state pair up as diquark clusters. Then L_M represents the orbital and angular momentum between the 3_C quark and $\bar{3}_C$ antiquark for mesons, and L_B represents the orbital angular momentum between the 3_C quark and a $\bar{3}_C$ spin-0 [qq] or spin-1 (qq) diquark in baryons. The identical $3_C - \bar{3}_C$ color-confining interaction appears for mesons and baryon. The index n can be interpreted as the number of nodes in the resulting two-body wave function.

The unified spectroscopy of hadronic bosons and fermions point to an underlying *supersymmetry* between mesons and baryons in QCD. In fact, the supersymmetric Light Front Holographic approach to QCD not only provides a unified spectroscopy of mesons and baryons, but it also predicts the existence and spectroscopy of tetraquarks: the mass degeneracy of mesons and baryons with their tetraquark partners, bound states of 3_C diquarks and $\bar{3}_C$ anti-diquarks. The meson-baryon-tetraquark 4-plet predicted by the LF supersymmetric approach is illustrated in Fig. 5. The baryon has two entries in the 4-plet, analogous to the upper and lower spinor components of a Dirac spinor. For example, the proton |[ud]u) with $J^z = +1/2$ has equal probability to be a bound state of a scalar [ud] diquark and a u quark with $S^z = +1/2, L^z = 0$ or the u quark with nonzero orbital angular momentum $S^z = -1/2, L^z = +1$. The spin-flip matrix element of the electromagnetic current between these two states gives the proton’s Pauli form factor in the light-front formalism [17].

$$\lambda = \kappa^2$$

$$m_u = m_d = 46 \text{ MeV}, m_s = 357 \text{ MeV}$$



**Fit to the slope of Regge trajectories,
including radial excitations**

**Same Regge Slope for Meson, Baryons:
Supersymmetric feature of hadron physics**

Fig. 6.3: The slopes of the measured meson and baryon Regge trajectories.

The holographic theory incorporates the dependence on the total quark spin, $S = 0$ for the π Regge trajectory, and $S = 1$ for the ρ trajectory, as given by the additional term $2\kappa^2 S$, where $S = 0, 1$, in the LF Hamiltonian. This leads, for example to the correct prediction for the $\pi - \rho$ mass gap: $M_\rho^2 - M_\pi^2 = 2\kappa^2$. In order to describe the quark spin-spin interaction, which distinguishes for example the nucleons from Δ particles, one includes an identical term, $2\kappa^2 S$, with $S = 0, 1$ in the LF baryon Hamiltonian which maintains hadronic supersymmetry. The prediction for the mass spectrum of mesons, baryons and tetraquarks is given by [18]

$$M_{M\perp}^2 = 4\kappa^2(n + L_M) + 2\kappa^2 S, \tag{6.1}$$

$$M_{B\perp}^2 = 4\kappa^2(n + L_B + 1) + 2\kappa^2 S, \tag{6.2}$$

$$M_{T\perp}^2 = 4\kappa^2(n + L_T + 1) + 2\kappa^2 S, \tag{6.3}$$

with the same slope $\lambda = \kappa^2$ in L and n , the radial quantum number. The Regge spectra of the pseudoscalar $S = 0$ and vector $S = 1$ mesons are then predicted correctly, with equal slope in the principal quantum number n and the internal orbital angular momentum. The nonperturbative pion distribution amplitude $\phi_\pi(x) \propto f_\pi \sqrt{x(1-x)}$ predicted by LF holography is consistent with the Belle data for the photon-to-pion transition form factor [19]. The prediction for the LF wave function $\psi_\rho(x, k_\perp)$ of the ρ meson gives excellent predictions for the observed

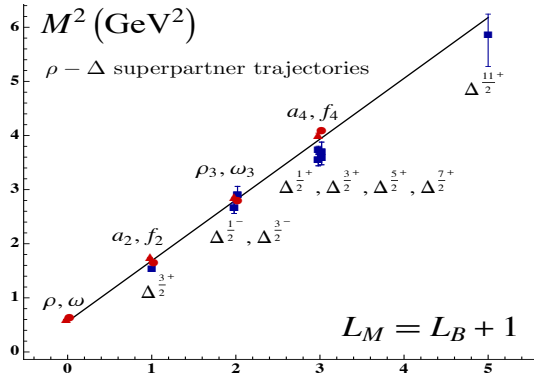
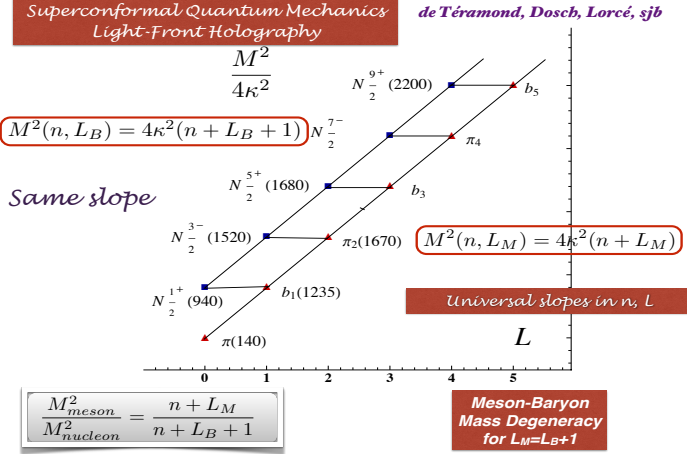


Fig. 6.4: Examples of supersymmetric meson and baryon Regge trajectories. Comparison of the pion and proton trajectories and the comparison of the ρ/ω meson Regge trajectory with the $J = 3/2$ Δ baryon trajectory. The degeneracy of the meson and baryon trajectories if one identifies a meson with internal orbital angular momentum L_M with its superpartner baryon with $L_M = L_B + 1$ using superconformal algebra. See Refs. [7, 8].

features of diffractive ρ electroproduction $\gamma^* p \rightarrow \rho p'$ [20]. The prediction for the valence LF wave function of the pion is shown in Fig. 6.2.

These predictions for the meson, baryon and tetraquark spectroscopy are specific to zero mass quarks. In a recent paper [21], we have shown that the breaking of chiral symmetry in holographic light-front QCD from nonzero quark masses is encoded in the longitudinal dynamics, independent of ζ . The results for $M^2 = M_{\perp}^2 + M_L^2$, where M_L^2 is the longitudinal contribution from the nonzero quark mass, retains the zero-mass chiral property of the pion predicted by the superconformal algebraic structure which governs its transverse dynamics. The mass scale in the longitudinal light-front Hamiltonian determines the confinement strength in this

direction; It is also responsible for most of the light meson ground state mass, consistent with the standard Gell-Mann-Oakes-Renner constraint. Longitudinal confinement and the breaking of chiral symmetry are found to be different manifestations of the same underlying dynamics that appears in the 't Hooft large- N_C QCD(1 + 1) model. One also obtains spherical symmetry of the 3-dimensional confinement potential in the nonrelativistic limit. For related work, see Refs. [22–25].

Superconformal Algebra

2X2 Hadronic Multiplets

Bosons, Fermions with Equal Mass!

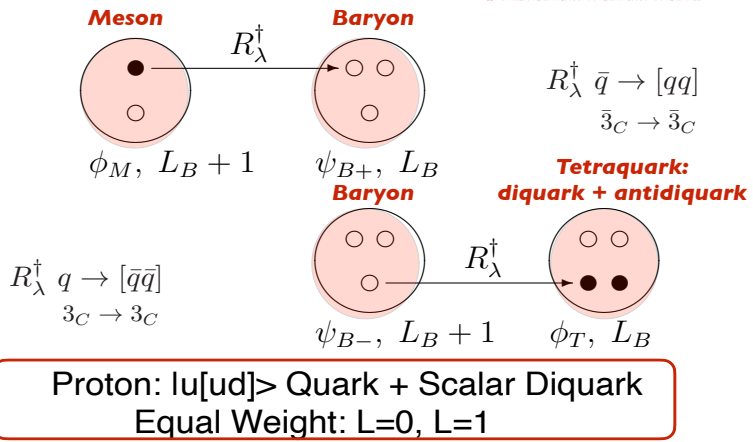


Fig. 6.5: The supersymmetric meson-baryon-tetraquark 4-plet. The operator R_λ^\dagger transforms an antiquark $\bar{3}_C$ into a diquark $\bar{3}_C$.

Phenomenological extensions of the holographic QCD approach have also led to nontrivial connections between the dynamics of form factors and polarized and unpolarized quark distributions with pre-QCD nonperturbative approaches such as Regge theory and the Veneziano model [26–28]. As discussed in the next section, it also predicts the analytic behavior of the QCD coupling $\alpha_s(Q^2)$ in the nonperturbative domain [29,30].

The LF Schrödinger Equations for baryons and mesons derived from superconformal algebra are shown in Fig. 6.7. The comparison between the meson and baryon masses of the ρ/ω Regge trajectory with the spin-3/2 Δ trajectory is shown in Fig. 6.7. Superconformal algebra predicts the meson and baryon masses are identical if one identifies a meson with internal orbital angular momentum L_M with its superpartner baryon with $L_B = L_M - 1$. Notice that the twist $\tau = 2 + L_M = 3 + L_B$ of the interpolating operators for the meson and baryon superpartners are the same. Superconformal algebra also predicts that the LFWFs of the superpartners are

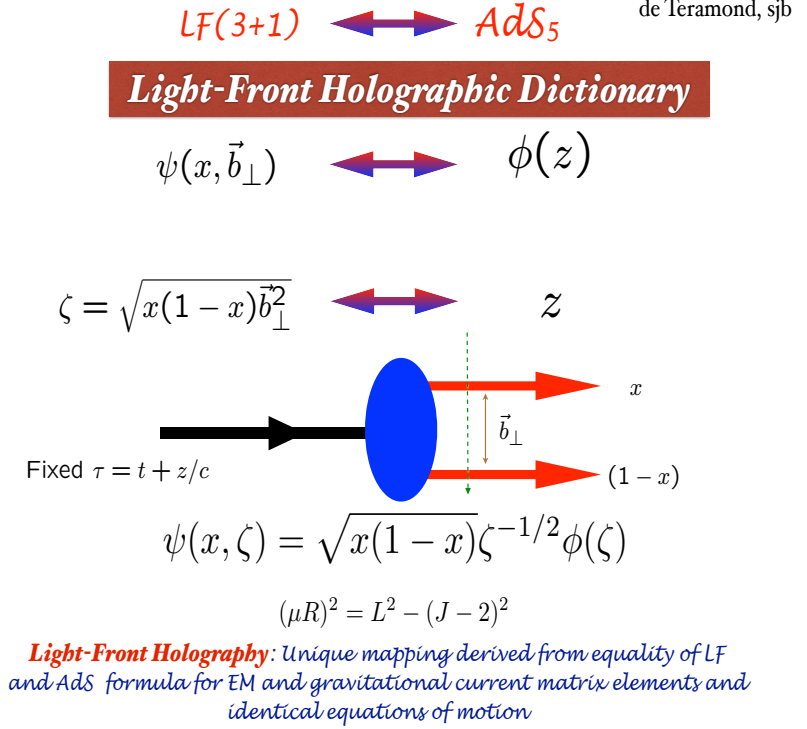


Fig. 6.6: The holographic duality connecting LF physics in 3+1 physical space-time with AdS space in 5 dimensions. The coordinate z in the fifth dimension of AdS space is holographically dual to the LF radial variable ζ where $\zeta^2 = b_\perp^2 x(1-x)$.

identical, and thus they have identical dynamics, such their elastic and transition form factors. These features can be tested for spacelike form factors at JLab12. The extension of light-front QCD to superconformal algebra has leads to a specific mass degeneracy between mesons, baryons and tetraquarks [7,8,18] underlying the $SU(3)_C$ representation properties, since a diquark cluster has the same color-triplet representation as an antiquark, namely $\bar{3} \in 3 \times 3$. The meson wave function ϕ_M , the upper and lower components of the baryon wave function, $\phi_{B\pm}$, and the tetraquark wave function, ϕ_T , can be arranged as a supersymmetric 4-plet matrix [18,32]

$$|\Phi\rangle = \begin{pmatrix} \phi_M^{(L+1)} & \phi_{B-}^{(L+1)} \\ \phi_{B+}^{(L)} & \phi_T^{(L)} \end{pmatrix}, \quad (6.4)$$

with $H^{LF}|\Phi\rangle = M^2|\Phi\rangle$ and $L_M = L_B + 1$, $L_T = L_B$. The constraints from superconformal structure uniquely determine the form of the effective transverse confining potential for mesons, nucleons and tetraquarks [7,8,18], and lead to the remarkable relations $L_M = L_B + 1$, $L_T = L_B$. The superconformal algebra also predicts the universality of Regge slopes with a unique scale $\lambda = \kappa^2$ for all hadron families.

LF Holography**Baryon Equation**

$$\left(-\partial_\zeta^2 + \kappa^4 \zeta^2 + 2\kappa^2(L_B + 1) + \frac{4L_B^2 - 1}{4\zeta^2}\right)\psi_J^+ = M^2\psi_J^+ \quad \mathbf{G}_{22}$$

$$\left(-\partial_\zeta^2 + \kappa^4 \zeta^2 + 2\kappa^2 L_B + \frac{4(L_B + 1)^2 - 1}{4\zeta^2}\right)\psi_J^- = M^2\psi_J^- \quad \mathbf{G}_{11}$$

$$M^2(n, L_B) = 4\kappa^2(n + L_B + 1)$$

S=1/2, P=+**Meson Equation***both chiralities*

$$\left(-\partial_\zeta^2 + \kappa^4 \zeta^2 + 2\kappa^2(J - 1) + \frac{4L_M^2 - 1}{4\zeta^2}\right)\phi_J = M^2\phi_J \quad \mathbf{G}_{11}$$

$$M^2(n, L_M) = 4\kappa^2(n + L_M)$$

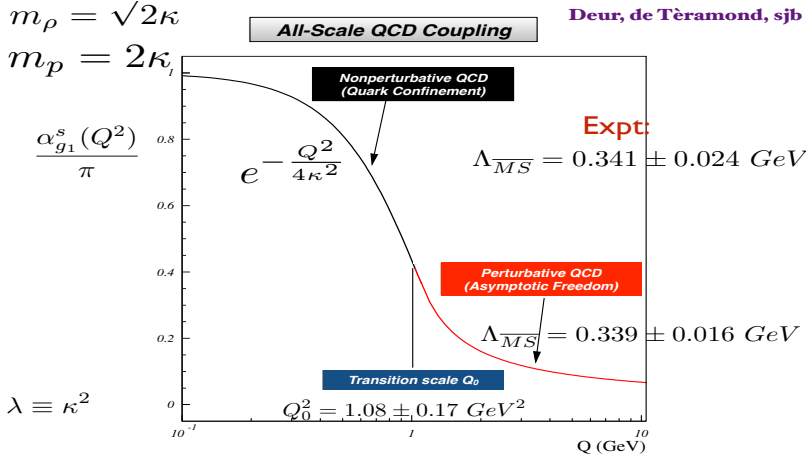
*Same κ !***S=0, I=1 Meson is superpartner of S=1/2, I=1 Baryon****Meson-Baryon Degeneracy for $L_M=L_B+1$**

Fig. 6.7: The LF Schrödinger equations for baryons and mesons for zero quark mass derived from the Pauli 2×2 matrix representation of superconformal algebra. The ψ^\pm are the baryon quark-diquark LFWFs where the quark spin $S_q^z = \pm 1/2$ is parallel or antiparallel to the baryon spin $J^z = \pm 1/2$. The meson and baryon equations are identical if one identifies a meson with internal orbital angular momentum L_M with its superpartner baryon with $L_B = L_M - 1$. See Refs. [7, 8, 12].

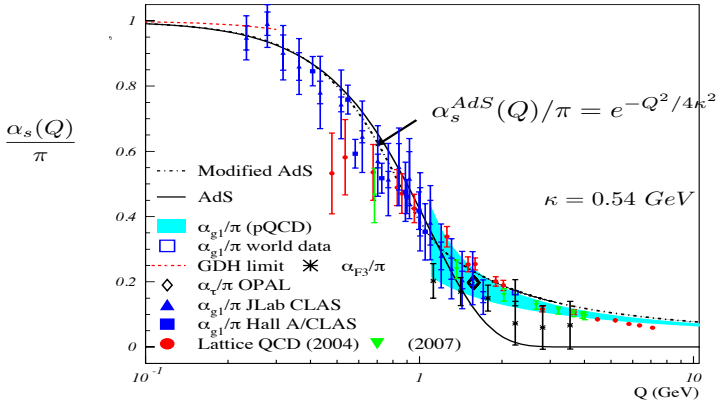
6.3 The QCD Coupling at all Scales

The QCD running coupling can be defined [33] at all momentum scales from any perturbatively calculable observable, such as the coupling $\alpha_{g_1}^s(Q^2)$ which is defined from measurements of the Bjorken sum rule. At high momentum transfer, such “effective charges” satisfy asymptotic freedom, obey the usual pQCD renormalization group equations, and can be related to each other without scale ambiguity by commensurate scale relations [34]. The dilaton $e^{+\kappa^2 z^2}$ soft-wall modification [35] of the AdS₅ metric, together with LF holography, predicts the functional behavior in the small Q^2 domain [29]: $\alpha_{g_1}^s(Q^2) = \pi e^{-Q^2/4\kappa^2}$. Measurements of $\alpha_{g_1}^s(Q^2)$ are remarkably consistent with this predicted Gaussian form. We have also shown how the parameter κ , which determines the mass scale of hadrons in the chiral limit, can be connected to the mass scale Λ_s controlling the evolution of the perturbative QCD coupling [29–31]. This connection can be done for any choice of renormalization scheme, including the $\overline{\text{MS}}$ scheme, as seen in Fig. 6.8. The relation between scales is obtained by matching at a scale Q_0^2 the nonperturbative behavior of the effective QCD coupling, as determined from light-front holography, to the perturbative QCD coupling with asymptotic

freedom. The result of this perturbative/nonperturbative matching is an effective QCD coupling which is defined at all momenta.



Running Coupling from Light-Front Holography and AdS/QCD
Analytic, defined at all scales, IR Fixed Point



AdS/QCD dilaton captures the higher twist corrections to effective charges for $Q < 1 \text{ GeV}$

$e^\varphi = e + \kappa^2 z^2$

Deur, de Tèramond, sjb

Fig. 6.8: (A). Prediction from LF Holography for the QCD running Coupling $\alpha_{g1}^s(Q^2)$. The magnitude and derivative of the perturbative and nonperturbative coupling are matched at the scale Q_0 . This matching connects the perturbative scale $\Lambda_{\overline{MS}}$ to the nonperturbative scale κ which underlies the hadron mass scale. (B). Comparison of the predicted nonperturbative coupling with measurements of the effective charge $\alpha_{g1}^s(Q^2)$ defined from the Bjorken sum rule. See Ref. [31].

6.4 Light-Front Wave Functions and QCD

Measurements of hadron structure – such as the structure functions determined by deep inelastic lepton-proton scattering (DIS) – are analogous to a flash photograph: one observes the hadron at fixed $\tau = t + z/c$ along a light-front, not at a given instant of time t . The underlying physics follows from the the light-front wave functions (LFWFs) $\psi_n(x_i, \vec{k}_{\perp i}, \lambda_i)$ with $x_i = \frac{k_i^+}{p^+} = \frac{k_i^0 + k_i^z}{p^0 + p^z}$, $\sum_i^n x_i = 1$, $\sum_i^n \vec{k}_{\perp i} = \vec{0}_{\perp}$ and spin projections λ_i . The LFWFs are the Fock state projections of the eigenstates of the QCD LF invariant Hamiltonian $H_{LF}|\Psi\rangle = M^2|\Psi\rangle$ [36], where the LF Hamiltonian is the light-front time evolution operator defined directly from the QCD Lagrangian. One can avoid ghosts and longitudinal gluonic degrees of freedom by choosing to work in the light-cone gauge $A^+ = 0$. The LFWFs are boost invariant; i.e., they are independent of the hadron's momentum $P^+ = P^0 + P^z$, \vec{P}_{\perp} . This contrasts with the wave functions defined at a fixed time t – the Lorentz boost of an instant-form wave function is much more complicated than a Melosh transform [37] – even the number of Fock constituents changes under a boost. Current matrix elements such as form factors are simple overlaps of the initial-state and final-state LFWFs, as given by the Drell-Yan-West formula [17, 38, 39]. There is no analogous formula for the instant form, since one must take into account the coupling of the external current to connected vacuum-induced currents. Observables such as structure functions, transverse momentum distributions, and distribution amplitudes are defined from the hadronic LFWFs. The distribution amplitudes $\phi_H(x_i, Q)$ are given by the valence LFWF integrated over transverse momentum $k_{\perp}^2 < Q^2$.

Since they are frame-independent, the structure functions measured in DIS are the same whether they are measured in an electron-proton collider or in a fixed-target experiment where the proton is at rest. There is no concept of length contraction of the hadron or nucleus at a collider – no collisions of “pancakes” – since the observations of the collisions of the composite hadrons are made at fixed τ , not at fixed time. The dynamics of a hadron in the LF formalism is not dependent on the observer's Lorentz frame. Hadron form factors are matrix elements of the noninteracting electromagnetic current j^μ of the hadron, as in the interaction picture of quantum mechanics. One chooses the frame where the virtual photon 4-momentum q^μ has $q^+ = 0$, $\vec{q}_{\perp}^2 = Q^2 = -q^2$ and $q^- P^+ = q \cdot p$. One can also choose to evaluate matrix elements of $j^+ = j^0 + j^z$ which eliminates matrix elements between Fock states with and extra $q\bar{q}$ pair.

The frame-independent LF Heisenberg equation $H_{LF}^{QCD}|\psi_H\rangle = M_H^2|\psi_H\rangle$ can be solved numerically by matrix diagonalization of the LF Hamiltonian in LF Fock space using “Discretized Light-Cone Quantization” (DLCQ) [40], where anti-periodic boundary conditions in x^- render the k^+ momenta discrete as well as limiting the size of the Fock basis. In fact, one can easily solve 1+1 quantum field theories such as QCD(1 + 1) [41] for any number of colors, flavors, and quark masses. Unlike lattice gauge theory, the nonperturbative DLCQ analysis is in Minkowski space, it is frame-independent, and it is free of fermion-doubling problems. A new method for solving nonperturbative QCD “Basis Light-Front Quantization” (BLFQ) [42, 43], uses the eigensolutions of a color-confining approx-

imation to QCD (such as LF holography) as the basis functions, rather than the plane-wave basis used in DLCQ. The LFWFs can also be determined from covariant Bethe-Salpeter wave function by integrating over k^- [44]. In fact, advanced quantum computers are now being used to obtain the DLCQ and BLFQ solutions. Factorization theorems as well as the DGLAP and ERBL evolution equations for structure functions and distribution amplitudes, respectively, can be derived using the light-front Hamiltonian formalism [45]. In the case of an electron-ion collider, one can represent the cross section for $e - p$ collisions as a convolution of the hadron and virtual photon structure functions times the subprocess cross-section in analogy to hadron-hadron collisions. This description of $\gamma^* p \rightarrow X$ reactions gives new insights into electroproduction physics such as the dynamics of heavy quark-pair production, where intrinsic heavy quarks play an important role [46]. In the case of $ep \rightarrow e'X$, one can consider the collisions of the confining QCD flux tube appearing between the q and \bar{q} of the virtual photon with the flux tube between the quark and diquark of the proton. Since the $q\bar{q}$ plane is aligned with the scattered electron's plane, the resulting "ridge" of hadronic multiplicity produced from the $\gamma^* p$ collision will also be aligned with the scattering plane of the scattered electron. The virtual photon's flux tube will also depend on the photon virtuality Q^2 , as well as the flavor of the produced pair arising from $\gamma^* \rightarrow q\bar{q}$. The resulting dynamics [47] is a natural extension of the flux-tube collision description of the ridge produced in $p - p$ collisions [48].

6.5 Other Features of Light-Front QCD

There are a number of advantages if one uses LF Hamiltonian methods for perturbative QCD calculations. The LF formalism is frame-independent and causal. If one chooses LF gauge $A^+ = 0$ the gluons have only transverse polarization and no ghosts. If one chooses the frame $q^+ = 0$ the current does not create pairs. Unlike instant form, where one must sum over $n!$ frame-dependent amplitudes, only the τ -ordered diagrams where every line has positive $k^+ = k^0 + k^z$ can contribute [49]. The number of nonzero amplitudes is also greatly reduced by noting that the total angular momentum projection $J^z = \sum_i^{n-1} L_i^z + \sum_i^n S_i^z$ and the total P^+ are conserved at each vertex. In addition, in a renormalizable theory the change in orbital angular momentum is limited to $\Delta L^z = 0, \pm 1$ at each vertex. The calculation of a subgraph of any order in pQCD only needs to be done once; the result can be stored in a "history" file, since in light-front perturbation theory, the numerator algebra is independent of the process; the denominator changes, but only by a simple shift of the initial P^- . Loop integrations are three-dimensional: $\int d^2\vec{k}_\perp \int_0^1 dx$. Renormalization can be done using the "alternate denominator" method which defines the required subtraction counter-terms [50].

The LF vacuum in LF Hamiltonian theory is defined as the eigenstate of H_{LF} with lowest invariant mass. Since propagation of particles with negative k^+ does not appear, there are no loop amplitudes appearing in the LF vacuum – it is thus trivial up to possible $k^+ = 0$ "zero" modes. The usual quark and gluon QCD vacuum condensates of the instant form are replaced by physical effects, such as the running quark mass and the physics contained within the hadronic LFWFs in

the hadronic domain. This is referred to as “in-hadron” condensates [51–53]. In the case of the Higgs theory, the traditional Higgs vacuum expectation value (VEV) is replaced by a zero mode, analogous to a classical Stark or Zeeman field. [54] This approach contrasts with the traditional view of the vacuum based on the instant form.

The instant-form vacuum, the lowest energy eigenstate of the instant-form Hamiltonian, is defined at one instant of time over all space; it is thus acausal and frame-dependent. It is usually argued that the QCD contribution to the cosmological constant – dark energy – is 10^{45} times larger than observed, and in the case of the Higgs theory, the Higgs VEV is argued to be 10^{54} larger than observed [55], estimates based on the loop diagrams of the acausal frame-dependent instant-form vacuum. However, the universe is observed within the causal horizon, not at a single instant of time. In contrast, the light-front vacuum provides a viable description of the visible universe [53]. Thus, in agreement with Einstein’s theory of general relativity, quantum effects do not contribute to the cosmological constant. In the case of the Higgs theory, the Higgs zero mode has no energy density, so again it gives no contribution to the cosmological constant. However, it is possible that if one solves the Higgs theory in a curved universe, the zero mode will be replaced with a field of nonzero curvature which could give a nonzero contribution.

6.6 Gluon matter distribution in the proton and pion from extended holographic light-front QCD

The holographic light-front QCD framework provides a unified nonperturbative description of the hadron mass spectrum, form factors and quark distributions. In a recent article [56] we have extended our previous description of quark distributions [27, 28] in LF holographic QCD to predict the gluonic distributions of both the proton and pion from the coupling of the metric fluctuations induced by the spin-two Pomeron with the energy momentum tensor in anti-de Sitter space, together with constraints imposed by the Veneziano model without additional free parameters. The gluonic and quark distributions are shown to have significantly different effective QCD mass scales. The comparison of our predictions with the gluon gravitational form factor computed from Euclidean lattice gauge theory and the gluon distribution in the proton and pion from global analyses also give very good results.

6.7 Intrinsic Heavy Quarks

Quantum Chromodynamics (QCD), the underlying theory of strong interactions, with quarks and gluons as the fundamental degrees of freedom, predicts that the heavy quarks in the nucleon-sea to have both perturbative “extrinsic” and nonperturbative “intrinsic” origins. The extrinsic sea arises from gluon splitting which is triggered by a probe in the reaction. It can be calculated order-by-order in perturbation theory. In contrast, the intrinsic sea is encoded in the nonperturbative wave functions of the nucleon eigenstate.

The existence of nonperturbative intrinsic charm (IC) was originally proposed in the BHPS model [57] and developed further in subsequent papers [58–60]. The intrinsic contribution to the heavy quark distributions of hadrons at high x corresponds to Fock states such as $|\text{uud}Q\bar{Q}\rangle$ where the heavy quark pair is multiply connected to two or more valence quarks of the proton, in distinction to the higher order corrections to DGLAP evolution. The LF wave function is maximal at minimal off-shellness; i.e., when the constituents all have the same rapidity y_i , and thus $x_i \propto \sqrt{(m_i^2 + k_{\perp i}^2)}$. Here $x = \frac{k^+}{p^+} = \frac{k_0^+ + k_3^+}{p_0^+ + p_3^+}$ is the frame-independent light-front momentum fraction carried by the heavy quark in a hadron with momentum P^μ . In the case of deep inelastic lepton-proton scattering, the LF momentum fraction variable x in the proton structure functions can be identified with the Bjorken variable $x = \frac{Q^2}{2p \cdot q}$. These heavy quark contributions to the nucleon's PDF thus peak at large x_{bj} and thus have important implication for LHC and EIC collider phenomenology, including Higgs and heavy hadron production at high x_F [61]. It also opens up new opportunities to study heavy quark phenomena in fixed target experiments such as the proposed AFTER [62] fixed target facility at CERN. Other applications are presented in Refs. [63–65]. The existence of intrinsic heavy quarks also illuminates fundamental aspects of nonperturbative QCD.

In Light-Front Hamiltonian theory, the intrinsic heavy quarks of the proton are associated with non-valence Fock states, such as $|\text{uud}Q\bar{Q}\rangle$ in the hadronic eigenstate of the LF Hamiltonian; this implies that the heavy quarks are multi-connected to the valence quarks. The probability for the heavy-quark Fock states scales as $1/m_Q^2$ in non-Abelian QCD. Since the LF wave function is maximal at minimum off-shell invariant mass; i.e., at equal rapidity, the intrinsic heavy quarks carry large momentum fraction x_Q . A key characteristic is different momentum and spin distributions for the intrinsic Q and \bar{Q} in the nucleon; for example the charm-anticharm asymmetry, since the comoving quarks are sensitive to the global quantum numbers of the nucleon [62]. Furthermore, since all of the intrinsic quarks in the $|\text{uud}Q\bar{Q}\rangle$ Fock state have similar rapidities as the valence quarks, they can re-interact, leading to significant Q vs \bar{Q} asymmetries. The concept of intrinsic heavy quarks was also proposed in the context of meson-baryon fluctuation models [66,67], where intrinsic charm was identified with two-body state $\bar{D}^0(u\bar{c})\Lambda_c^+(udc)$ in the proton. This identification predicts large asymmetries in the charm versus anti-charm momentum and spin distributions, Since these heavy quark distributions depend on the correlations determined by the valence quark distributions, they are referred to as *intrinsic* contributions to the hadron's fundamental structure. A specific analysis of the intrinsic charm content of the deuteron is given in Ref. [68]. In contrast, the contribution to the heavy quark PDFs arising from gluon splitting are symmetric in Q vs \bar{Q} . The contributions generated by DGLAP evolution at low x can be considered as *extrinsic* contributions since they only depend on the gluon distribution. The gluon splitting contribution to the heavy-quark degrees of freedom is perturbatively calculable using DGLAP evolution. To first approximation, the perturbative extrinsic heavy quark distribution falls as $(1-x)$ times the gluon distribution and is limited to low x_{bj} . Thus, unlike the conventional $\log m_Q^2$ dependence of the low x extrinsic gluon-splitting contributions, the probabilities

for the intrinsic heavy quark Fock states at high x scale as $\frac{1}{m_Q^2}$ in non-Abelian QCD, and the relative probability of intrinsic bottom to charm is of order $\frac{m_c^2}{m_b^2} \sim \frac{1}{10}$. In contrast, the probability for a higher Fock state containing heavy leptons in a QED atom scales as $\frac{1}{m_l^4}$, corresponding to the twist-8 Euler-Heisenberg light-by-light self-energy insertion. Detailed derivations based on the OPE have been given in Ref. [58,60].

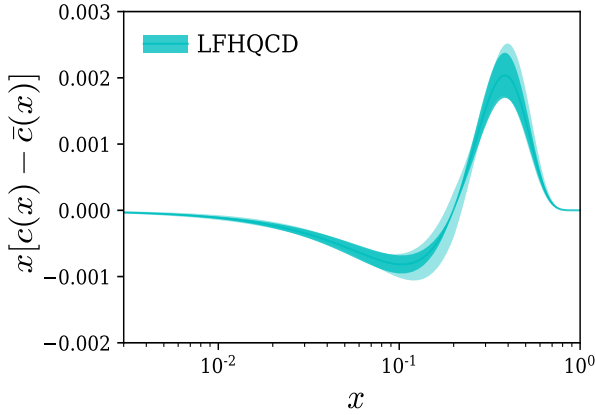


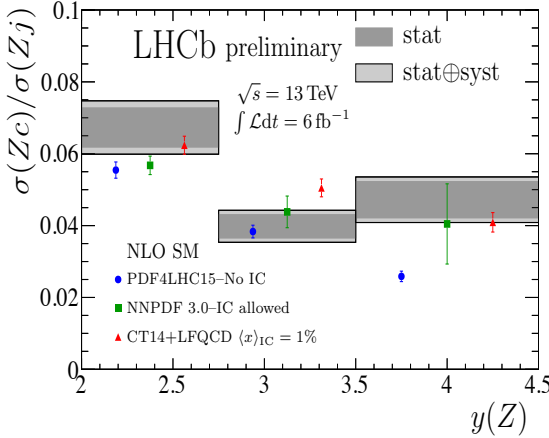
Fig. 6.9: The difference of charm and anticharm structure functions $x[c(x) - \bar{c}(x)]$ obtained from the LFHQCD formalism using the lattice QCD input of charm electromagnetic form factors $G_{E,M}^c(Q^2)$. The outer cyan band indicates an estimate of systematic uncertainty in the $x[c(x) - \bar{c}(x)]$ distribution obtained from a variation of the hadron scale κ_c by 5%. From Ref. [69].

In an important recent development [69], the difference of the charm and anticharm quark distributions in the proton, $\Delta c(x) = c(x) - \bar{c}(x)$, has been computed from first principles in QCD using lattice gauge theory. A key theoretical tool is the computation of the charm and anticharm quark contribution to the electromagnetic form factor of the proton which would vanish if $c(x) = \bar{c}(x)$. The exclusive-inclusive connection, together with the LFHQCD formalism, predicts the asymmetry of structure functions $c(x) - \bar{c}(x)$ which is also odd under charm-anticharm interchange. The predicted $c(x) - \bar{c}(x)$ distribution is large and nonzero at large $x \sim 0.4$, consistent with the expectations of intrinsic charm. See Fig. 6.9. The $c(x)$ vs. $\bar{c}(x)$ asymmetry can also be understood physically by identifying the $|uudc\bar{c}\rangle$ Fock state with the $|\Lambda_{u,d,c} D_{u,\bar{c}}\rangle$ off-shell excitation of the proton. A related application of lattice gauge theory to the nonperturbative strange-quark sea from lattice QCD is given in Ref. [70].

There have been many phenomenological calculations involving the existence of a non-zero IC component which can explain anomalies in the experimental data and to predict its novel signatures of IC in upcoming experiments [62]. A recent measurement by LHCb is shown in Fig. 10. The observed spectrum exhibits a

Z + c: results

LHCb-PAPER-2021-029



- ▶ Clear enhancement in highest- y bin
- ▶ Consistent with expected effect from $|uud\bar{c}\bar{c}\rangle$ component predicted by LFQCD
- ▶ Inconsistent with No-IC theory at ~ 3 standard deviations
- ▶ Global PDF analysis required to determine true significance

Fig. 6.10: The charm distribution in the proton determined from LHCb measurements of Z bosons produced in association with charm at forward rapidity [71].

sizable enhancement at forward Z rapidities, consistent with the effect expected if the proton contains the $|uud\bar{c}\bar{c}\rangle$ Fock state predicted by LFQCD. [71]

Thus QCD predicts two separate and distinct contributions to the heavy quark distributions $q(x, Q^2)$ of the nucleons at low and high x . Here $x = \frac{k^+}{P^+} = \frac{k^0 + k^3}{P^0 + P^3}$ is the frame-independent light-front momentum fraction carried by the heavy quark in a hadron with momentum P^μ . In the case of deep inelastic lepton-proton scattering, the LF momentum fraction variable x in the proton structure functions can be identified with the Bjorken variable $x = \frac{Q^2}{2p \cdot q}$. At small x , heavy-quark pairs are dominantly produced via the standard gluon-splitting subprocess $g \rightarrow Q\bar{Q}$.

6.8 Color Transparency [72]

One of the most striking properties of QCD phenomenology is “color transparency” [73], the reduced absorption of a hadron as it propagates through nuclear matter, if it is produced at high transverse momentum in a hard exclusive process, such as elastic lepton-proton scattering. The nuclear absorption reflects the size of the color dipole moment of the propagating hadron; i.e., the separation between its colored constituents.

The key quantity which measures the transverse size of a scattered hadron in a given Fock state is [72] $a_\perp = \sum_{i=1}^{n-1} x_i b_{\perp i}$. The LF QCD formula for form factors

can then be written compactly in impact space as

$$F(Q^2) = \int_0^1 dx d^2 a_{\perp} e^{i\vec{q}_{\perp} \cdot \vec{a}_{\perp}} q(x, a_{\perp}), \tag{6.5}$$

and thus $\langle a_{\perp}^2(Q^2) \rangle = -4 \frac{\frac{d}{dQ^2} F(Q^2)}{F(Q^2)}$ measures the slope of the hadron factor. We can use LF holography to show that $\langle a_{\perp}^2(Q^2) \rangle_{\tau} = 4 \frac{\tau-1}{Q^2}$ for a Fock state of twist τ at large Q^2 ; thus, as expected, the hadronic size decreases with increasing momentum transfer Q^2 , and that the size of the hadron increases with its twist τ .

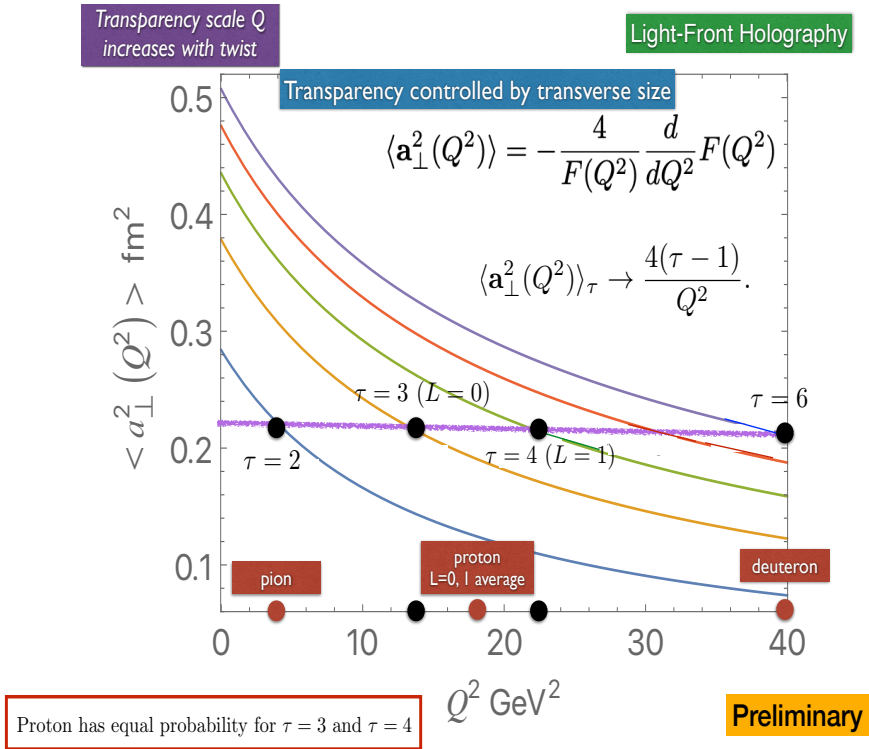


Fig. 6.11: Predictions from LF holography for the effective transverse size of hadrons.

A key prediction is that the size of a_{\perp} is smaller for mesons ($\tau = 2$) than for baryons with $\tau = 3, 4$, corresponding to the quark-diquark Fock states with $L = 0$ and $L = 1$ respectively. In fact, the proton is predicted to have “two-stage” color transparency $Q^2 > 14 \text{ GeV}^2$ for the $|[ud]u\rangle$ twist-3 Fock state with orbital angular momentum $L = 0$ and $Q^2 > 16 \text{ GeV}^2$ for the later onset of CT for its $L = 1$ twist-4 component. See fig. 6.11 Note that LF holography predicts equal quark probability for the $L = 0$ and $L = 1$ Fock states. Color transparency is thus predicted to occur at a significantly higher Q^2 for baryons ($Q^2 > 14 \text{ GeV}^2$), than for mesons

($Q^2 > 4 \text{ GeV}^2$). This is consistent with a recent test of color transparency at JLab which has confirmed color transparency for the π and ρ [74]; however, the measurements in this experiment are limited to values below the range of Q^2 where proton color transparency is predicted to occur.

Color transparency fundamental prediction of QCD

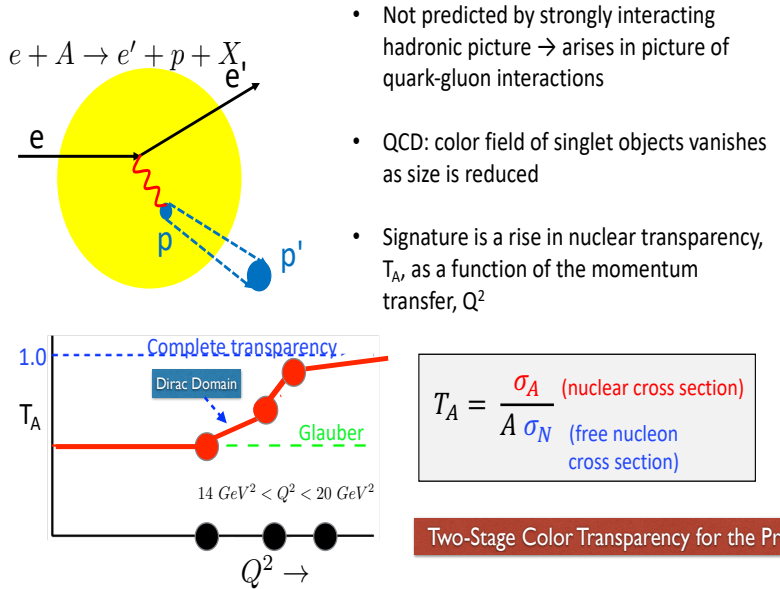


Fig. 6.12: Two-stage color transparency and transmission probability of the proton in a nuclear medium from LF Holography.

Remarkably, color transparency for the production of an intact deuteron nucleus in $eA \rightarrow d + X_{(A-2)}$ quasi-exclusive reactions should be observed at $Q^2 > 50 \text{ GeV}^2$. This can be tested in $ed \rightarrow ed$ elastic scattering in a nuclear background. It has been speculated [75] that the “Feynman mechanism”, where the behavior of the struck quark at $x \sim 1$ in the proton LFWF plays a key role for hard exclusive hadronic processes does not predict color transparency. However, LF wave functions are functions of the invariant mass $\sum_i \frac{\vec{k}_{\perp i}^2 + m_i^2}{x_i}$ so that their behavior at large k_{\perp} and large x are correlated. Thus color transparency occurs for scattering amplitudes involving both the large transverse momentum and large x domains. The three-dimensional LF spatial symmetry of LFWFs also leads to the exclusive-inclusive connection, relating the counting rules for the behavior of form factors at large Q^2 and structure functions at $x_{bj} \rightarrow 1$.

6.9 Removing Renormalization Scale Ambiguities

It has become conventional to simply guess the renormalization scale and choose an arbitrary range of uncertainty when making perturbative QCD (pQCD) predictions. However, this *ad hoc* assignment of the renormalization scale and the estimate of the size of the resulting uncertainty leads to anomalous renormalization scheme-and-scale dependences. In fact, relations between physical observables must be independent of the theorist's choice of the renormalization scheme, and the renormalization scale in any given scheme at any given order of pQCD is not ambiguous. The *Principle of Maximum Conformality* (PMC) [76], which generalizes the conventional Gell-Mann-Low method for scale-setting in perturbative QED to non-Abelian QCD, provides a rigorous method for achieving unambiguous scheme-independent, fixed-order predictions for observables consistent with the principles of the renormalization group. The renormalization scale of the running coupling depends dynamically on the virtuality of the underlying quark and gluon subprocess and thus the specific kinematics of each event.

The key problem in making precise perturbative QCD predictions is the uncertainty in determining the renormalization scale μ of the running coupling $\alpha_s(\mu^2)$. The purpose of the running coupling in any gauge theory is to sum all terms involving the β function; in fact, when the renormalization scale is set properly, all non-conformal $\beta \neq 0$ terms in a perturbative expansion arising from renormalization are summed into the running coupling. The remaining terms in the perturbative series are then identical to that of a conformal theory; i.e., the corresponding theory with $\beta = 0$.

The renormalization scale in the PMC is fixed such that all β nonconformal terms are eliminated from the perturbative series and are resummed into the running coupling; this procedure results in a convergent, scheme-independent conformal series without factorial renormalon divergences. The resulting scale-fixed predictions for physical observables using the PMC are also *independent of the choice of renormalization scheme* – a key requirement of renormalization group invariance. The PMC predictions are also independent of the choice of the *initial* renormalization scale μ_0 . The PMC thus sums all of the non-conformal terms associated with the QCD β function, thus providing a rigorous method for eliminating renormalization scale ambiguities in quantum field theory. Other important properties of the PMC are that the resulting series are free of renormalon resummation problems, and the predictions agree with QED scale-setting in the Abelian limit. The PMC is also the theoretical principle underlying the BLM procedure, commensurate scale relations between observables, and the scale-setting method used in lattice gauge theory. The number of active flavors n_f in the QCD β function is also correctly determined. We have also showed that a single global PMC scale, valid at leading order, can be derived from basic properties of the perturbative QCD cross section. We have given a detailed comparison of these PMC approaches by comparing their predictions for three important quantities R_{e+e} , R_τ and $\Gamma_{H \rightarrow b\bar{b}}$ up to four-loop pQCD corrections [76]. The numerical results show that the single-scale PMCs method, which involves a somewhat simpler analysis, can serve as a reliable substitute for the full multi-scale PMCm method, and that it leads to more precise

pQCD predictions with less residual scale dependence. The PMC thus greatly improves the reliability and precision of QCD predictions at the LHC and other colliders [76]. As we have demonstrated, the PMC also has the potential to greatly increase the sensitivity of experiments at the LHC to new physics beyond the Standard Model.

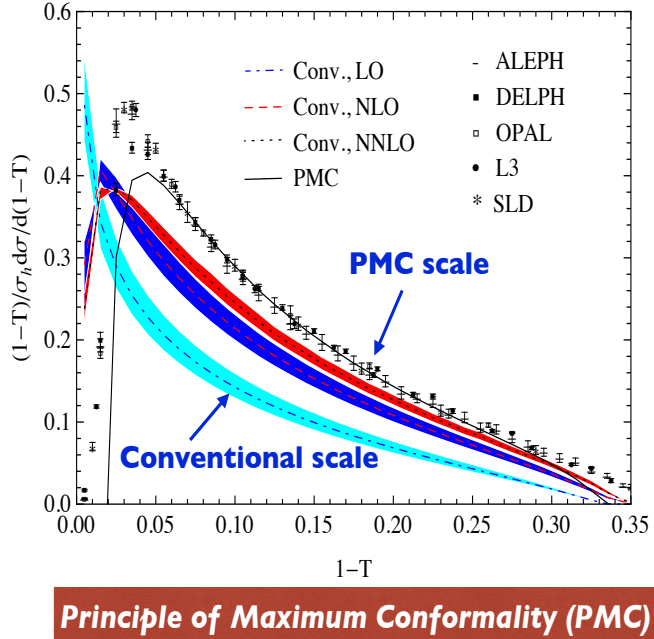


Fig. 6.13: Comparison of predictions for the thrust distribution for jet production in e^+e^- annihilation, using the PMC to set the pQCD renormalization scale vs. conventional methods.

An essential property of renormalizable $SU(N)/U(1)$ gauge theories, is “Intrinsic Conformality,” [77]. It underlies the scale invariance of physical observables and can be used to resolve the conventional renormalization scale ambiguity *at every order* in pQCD. This reflects the underlying conformal properties displayed by pQCD at NNLO, eliminates the scheme dependence of pQCD predictions and is consistent with the general properties of the PMC. We have also introduced a new method [77] to identify the conformal and β terms which can be applied either to numerical or to theoretical calculations and in some cases allows infinite resummation of the pQCD series, The implementation of the PMC_∞ can significantly improve the precision of pQCD predictions; its implementation in multi-loop analysis also simplifies the calculation of higher orders corrections in a

general renormalizable gauge theory. This method has also been used to improve the NLO pQCD prediction for $t\bar{t}$ pair production and other processes at the LHC, where subtle aspects of the renormalization scale of the three-gluon vertex and multi gluon amplitudes, as well as large radiative corrections to heavy quarks at threshold play a crucial role. The large discrepancy of pQCD predictions with the forward-backward asymmetry measured at the Tevatron is significantly reduced from 3σ to approximately 1σ . The PMC has also been used to precisely determine the QCD running coupling constant $\alpha_s(Q^2)$ over a wide range of Q^2 from event shapes for electron-positron annihilation measured at a single energy \sqrt{s} [78]. The PMC method has also been applied to a spectrum of LHC processes including Higgs production, jet shape variables, and final states containing a high p_T photon plus heavy quark jets, all of which, sharpen the precision of the Standard Model predictions.

6.10 Is the Momentum Sum Rule Valid for Nuclear Structure Functions?

Sum rules for deep inelastic lepton-hadron scattering processes are analyzed using the operator product expansion of the forward virtual Compton amplitude, assuming it depends in the limit $Q^2 \rightarrow \infty$ on matrix elements of local operators such as the energy-momentum tensor. The moments of the structure function and other distributions can then be evaluated as overlaps of the target hadron's light-front wave function, as in the Drell-Yan-West formulae for hadronic form factors [17,79–81]. The real phase of the resulting DIS amplitude and its OPE matrix elements reflects the real phase of the stable target hadron's wave function. The "handbag" approximation to deeply virtual Compton scattering also defines the "static" contribution [82,83] to the measured parton distribution functions (PDF), transverse momentum distributions, etc. The resulting momentum, spin and other sum rules reflect the properties of the hadron's light-front wave function. However, final-state interactions which occur *after* the lepton scatters on the quark, can give non-trivial contributions to deep inelastic scattering processes at leading twist and thus survive at high Q^2 and high $W^2 = (q+p)^2$. For example, the pseudo-T-odd Sivers effect [84] is directly sensitive to the rescattering of the struck quark. Similarly, diffractive deep inelastic scattering involves the exchange of a gluon after the quark has been struck by the lepton [85]. In each case the corresponding DVCS amplitude is not given by the handbag diagram since interactions between the two currents are essential. These "lensing" corrections survive when both W^2 and Q^2 are large since the vector gluon couplings grow with energy. Part of the phase can be associated with a Wilson line as an augmented LFWF [86] which do not affect the moments.

The cross section for deep inelastic lepton-proton scattering $\ell p \rightarrow \ell' p' X$ includes a diffractive deep inelastic (DDIS) contribution in which the proton remains intact with a large longitudinal momentum fraction $x_F > 0.9$ greater than 0.9 and small transverse momentum. The DDIS events, which can be identified with Pomeron exchange in the t-channel, account for approximately 10% of all of the DIS events. Diffractive DIS contributes at leading-twist (Bjorken scaling) and is the essential

component of the two-step amplitude which causes shadowing and antishadowing of the nuclear PDF [87–90]. It is important to analyze whether the momentum and other sum rules derived from the OPE expansion in terms of local operators remain valid when these dynamical rescattering corrections to the nuclear PDF are included. The OPE is derived assuming that the LF time separation between the virtual photons in the forward virtual Compton amplitude $\gamma^*A \rightarrow \gamma^*A$ scales as $1/Q^2$. However, the propagation of the vector system V produced by the diffractive DIS interaction on the front face and its inelastic interaction with the nucleons in the nuclear interior $V + N_b \rightarrow X$ are characterized by a longer LF time which scales as $1/W^2$. Thus the leading-twist multi-nucleon processes that produce shadowing and antishadowing in a nucleus are evidently not present in the $Q^2 \rightarrow \infty$ OPE analysis.

Thus, when one measures DIS, one automatically includes the leading-twist Bjorken-scaling DDIS events as a contribution to the DIS cross section, whether or not the final-state proton is explicitly detected. In such events, the missing momentum fraction in the DDIS events could be misidentified with the light-front momentum fraction carried by sea quarks or gluons in the proton's Fock structure. The underlying QCD Pomeron-exchange amplitude which produces the DDIS events thus does not obey the operator product expansion nor satisfy momentum sum rules – the quark and gluon distributions measured in DIS experiments will be misidentified, unless the measurements explicitly exclude the DDIS events [88,91]. The Glauber propagation of the vector system V produced by the diffractive DIS interaction on the nuclear front face and its subsequent inelastic interaction with the nucleons in the nuclear interior $V + N_b \rightarrow X$ occurs after the lepton interacts with the struck quark. Because of the rescattering dynamics, the DDIS amplitude acquires a complex phase from Pomeron and Regge exchange; thus final-state rescattering corrections lead to nontrivial “dynamical” contributions to the measured PDFs; i.e., they involve the physics aspects of the scattering process itself [92]. The $I = 1$ Reggeon contribution to diffractive DIS on the front-face nucleon leads to flavor-dependent antishadowing [89,93]. This could explain why the NuTeV charged current measurement $\mu A \rightarrow \nu X$ scattering does not appear to show antishadowing in contrast to deep inelastic electron nucleus scattering [90]. Again, the corresponding DVCS amplitude is not given by the handbag diagram since interactions between the two currents are essential to explain the physical phenomena.

It should be emphasized that shadowing in deep inelastic lepton scattering on a nucleus involves nucleons at or near the front surface; i.e., the nucleons facing the incoming lepton beam. This geometrical orientation is not built into the frame-independent nuclear LFWFs used to evaluate the matrix elements of local currents. Thus the dynamical phenomena of leading-twist shadowing and antishadowing appear to invalidate the sum rules for nuclear PDFs. The same complications occur in the leading-twist analysis of deeply virtual Compton scattering $\gamma^*A \rightarrow \gamma^*A$ on a nuclear target.

6.11 Summary

Light-Front Hamiltonian theory provides a causal, frame-independent, ghost-free nonperturbative formalism for analyzing gauge theories such as QCD. Remarkably, LF theory in 3+1 physical space-time is holographically dual to five-dimensional AdS space, if one identifies the LF radial variable ζ with the fifth coordinate z of AdS₅. If the metric of the conformal AdS₅ theory is modified by a dilaton of the form $e^{+\kappa^2 z^2}$, one obtains an analytically-solvable Lorentz-invariant color-confining LF Schrödinger equations for hadron physics. The parameter κ of the dilaton becomes the fundamental mass scale of QCD, underlying the color-confining potential of the LF Hamiltonian and the running coupling $\alpha_s(Q^2)$ in the nonperturbative domain. When one introduces super-conformal algebra, the result is “Holographic LF QCD” which not only predicts a unified Regge-spectroscopy of mesons, baryons, and tetraquarks, arranged as supersymmetric 4-plets, but also the hadronic LF wavefunctions which underly form factors, structure functions, and other dynamical phenomena. In each case, the quarks and antiquarks cluster in hadrons as 3_C diquarks, so that mesons, baryons and tetraquarks all obey a two-body $3_C - \bar{3}_C$ LF bound-state equation. Thus tetraquarks are compact hadrons, as fundamental as mesons and baryons. “Holographic LF QCD” also leads to novel phenomena such as the color transparency of hadrons produced in hard-exclusive reactions traversing a nuclear medium and asymmetric intrinsic heavy-quark distributions $Q(x) \neq \bar{Q}(x)$, appearing at high x in the non-valence higher Fock states of hadrons.

Acknowledgements

Contribution to the Proceedings of the 24th Workshop, “What Comes Beyond the Standard Models”, Bled, July 3. – 11., 2021. I am grateful to all of my collaborators, especially Guy de Téramond, Hans Guenter Dosch, Cedric Lorcé, Maria Nielsen, Tianbo Liu, Sabbir Sufian, and Alexandre Deur, for their collaboration on light-front holography and its implications. This work is supported by the Department of Energy, Contract DE-AC02-76SF00515. SLAC-PUB-17634

References

1. S. J. Brodsky, G. F. de Téramond and H. G. Dosch, “Threefold complementary approach to holographic QCD,” <http://www.sciencedirect.com/science/article/pii/S0370269313010198>, Phys. Lett. B **729**, 3 (2014) [arXiv:1302.4105 [hep-th]].
2. V. de Alfaro, S. Fubini and G. Furlan, “Conformal invariance in quantum mechanics,” Nuovo Cim. A **34**, 569 (1976).
3. S. Fubini and E. Rabinovici, “Superconformal quantum mechanics,” Nucl. Phys. B **245**, 17 (1984).
4. P. A. M. Dirac, “Forms of relativistic dynamics,” Rev. Mod. Phys. **21**, 392 (1949).
5. J. M. Maldacena, “The large-N limit of superconformal field theories and supergravity,” Int. J. Theor. Phys. **38**, 1113 (1999) [arXiv:hep-th/9711200].

6. G. F. de Téramond and S. J. Brodsky, "Light-front holography: A first approximation to QCD," *Phys. Rev. Lett.* **102**, 081601 (2009) [arXiv:0809.4899 [hep-ph]].
7. G. F. de Téramond, H. G. Dosch and S. J. Brodsky, "Baryon spectrum from superconformal quantum mechanics and its light-front holographic embedding," *Phys. Rev. D* **91**, 045040 (2015) [arXiv:1411.5243 [hep-ph]].
8. H. G. Dosch, G. F. de Téramond and S. J. Brodsky, "Superconformal baryon-meson symmetry and light-front holographic QCD," *Phys. Rev. D* **91**, 085016 (2015) [arXiv:1501.00959 [hep-th]].
9. S. J. Brodsky, G. F. de Téramond, H. G. Dosch and J. Erlich, "Light-front holographic QCD and emerging confinement," *Phys. Rept.* **584**, 1-105 (2015) [arXiv:1407.8131 [hep-ph]].
10. S. J. Brodsky, G. F. de Téramond and H. G. Dosch, "Light-front holography and supersymmetric conformal algebra: A novel approach to hadron spectroscopy, structure, and dynamics," [arXiv:2004.07756 [hep-ph]].
11. G. F. de Téramond, H. G. Dosch and S. J. Brodsky, "Kinematical and dynamical aspects of higher-spin bound-state equations in holographic QCD," *Phys. Rev. D* **87**, 075005 (2013) [arXiv:1301.1651 [hep-ph]].
12. H. G. Dosch, G. F. de Téramond and S. J. Brodsky, "Supersymmetry across the light and heavy-light hadronic spectrum," *Phys. Rev. D* **92**, 074010 (2015) [arXiv:1504.05112 [hep-ph]].
13. H. G. Dosch, G. F. de Téramond and S. J. Brodsky, "Supersymmetry across the light and heavy-light hadronic spectrum II," *Phys. Rev. D* **95**, 034016 (2017)
14. M. Nielsen and S. J. Brodsky, "Hadronic superpartners from a superconformal and supersymmetric algebra," *Phys. Rev. D* **97**, 114001 (2018)
15. M. Nielsen, S. J. Brodsky, G. F. de Téramond, H. G. Dosch, F. S. Navarra and L. Zou, "Supersymmetry in the double-heavy hadronic spectrum," *Phys. Rev. D* **98**, 034002 (2018) [arXiv:1805.11567 [hep-ph]].
16. A. P. Trawiński, S. D. Głazek, S. J. Brodsky, G. F. de Téramond and H. G. Dosch, "Effective confining potentials for QCD," *Phys. Rev. D* **90**, 074017 (2014) [arXiv:1403.5651 [hep-ph]].
17. S. J. Brodsky and S. D. Drell, "The Anomalous Magnetic Moment and Limits on Fermion Substructure," *Phys. Rev. D* **22**, 2236 (1980) doi:10.1103/PhysRevD.22.2236
18. S. J. Brodsky, G. F. de Téramond, H. G. Dosch and C. Lorcé, "Universal effective hadron dynamics from superconformal algebra," *Phys. Lett. B* **759**, 171 (2016) [arXiv:1604.06746 [hep-ph]].
19. S. J. Brodsky, F. G. Cao and G. F. de Téramond, "Meson Transition Form Factors in Light-Front Holographic QCD," *Phys. Rev. D* **84**, 075012 (2011) doi:10.1103/PhysRevD.84.075012 [arXiv:1105.3999 [hep-ph]].
20. J. R. Forshaw and R. Sandapen, "An AdS/QCD holographic wave function for the rho meson and diffractive rho meson electroproduction," *Phys. Rev. Lett.* **109**, 081601 (2012) doi:10.1103/PhysRevLett.109.081601 [arXiv:1203.6088 [hep-ph]].
21. G. F. de Téramond and S. J. Brodsky, "Longitudinal dynamics and chiral symmetry breaking in holographic light-front QCD," [arXiv:2103.10950 [hep-ph]].
22. Y. Li and J. P. Vary, "Light-front holography with chiral symmetry breaking," [arXiv:2103.09993 [hep-ph]].
23. M. Ahmady, H. Dahiya, S. Kaur, C. Mondal, R. Sandapen and N. Sharma, "Extending light-front holographic QCD using the 't Hooft Equation," *Phys. Lett. B* **823**, 136754 (2021) [arXiv:2105.01018 [hep-ph]].
24. M. Ahmady, S. Kaur, S. L. MacKay, C. Mondal and R. Sandapen, "Hadron spectroscopy using the light-front holographic Schrödinger equation and the 't Hooft equation,"

- Phys. Rev. D **104**, 074013 (2021) doi:10.1103/PhysRevD.104.074013 [arXiv:2108.03482 [hep-ph]].
25. C. M. Weller and G. A. Miller, "Confinement in Two-Dimensional QCD and the Infinitely Long Pion," [arXiv:2111.03194 [hep-ph]].
 26. R. S. Sufian, G. F. de T eramond, S. J. Brodsky, A. Deur and H. G. Dosch, Analysis of nucleon electromagnetic form factors from light-front holographic QCD: The spacelike region, Phys. Rev. D **95**, 014011 (2017) [arXiv:1609.06688 [hep-ph]].
 27. G. F. de T eramond, T. Liu, R. S. Sufian, H. G. Dosch, S. J. Brodsky and A. Deur, "Universality of generalized parton distributions in light-front holographic QCD," Phys. Rev. Lett. **120**, 182001 (2018) [arXiv:1801.09154 [hep-ph]].
 28. T. Liu, R. S. Sufian, G. F. de T eramond, H. G. Dosch, S. J. Brodsky and A. Deur, Unified description of polarized and unpolarized quark distributions in the proton, Phys. Rev. Lett. **124**, 082003 (2020) [arXiv:1909.13818 [hep-ph]].
 29. S. J. Brodsky, G. F. de T eramond and A. Deur, "Nonperturbative QCD coupling and its β function from light-front holography," Phys. Rev. D **81**, 096010 (2010) [arXiv:1002.3948 [hep-ph]].
 30. A. Deur, S. J. Brodsky and G. F. de T eramond, "Connecting the hadron mass scale to the fundamental mass scale of quantum chromodynamics," Phys. Lett. B **750**, 528 (2015) [arXiv:1409.5488 [hep-ph]].
 31. S. J. Brodsky, G. F. de T eramond, A. Deur and H. G. Dosch, "The Light-Front Schr odinger Equation and the Determination of the Perturbative QCD Scale from Color Confinement: A First Approximation to QCD," Few Body Syst. **56**, no.6-9, 621-632 (2015) doi:10.1007/s00601-015-0964-1 [arXiv:1410.0425 [hep-ph]].
A. Deur, S. J. Brodsky and G. F. de T eramond, " On the interface between perturbative and nonperturbative QCD," Phys. Lett. B **757**, 275 (2016) [arXiv:1601.06568 [hep-ph]].
 32. L. Zou and H. G. Dosch, "A very practical guide to light front holographic QCD" [arXiv:1801.00607 [hep-ph]].
 33. G. Grunberg, "Renormalization Group Improved Perturbative QCD," Phys. Lett. B **95**, 70 (1980) [erratum: Phys. Lett. B **110**, 501 (1982)] doi:10.1016/0370-2693(80)90402-5
 34. S. J. Brodsky and H. J. Lu, "Commensurate scale relations in quantum chromodynamics," Phys. Rev. D **51**, 3652-3668 (1995) doi:10.1103/PhysRevD.51.3652 [arXiv:hep-ph/9405218 [hep-ph]].
 35. A. Karch, E. Katz, D. T. Son and M. A. Stephanov, Linear confinement and AdS/QCD, Phys. Rev. D **74**, 015005 (2006) [arXiv:hep-ph/0602229].
 36. S. J. Brodsky, H. C. Pauli and S. S. Pinsky, " Quantum chromodynamics and other field theories on the light cone," Phys. Rept. **301**, 299 (1998) [arXiv:hep-ph/9705477].
 37. S. J. Brodsky and J. R. Primack, "The Electromagnetic Interactions of Composite Systems," Annals Phys. **52**, 315-365 (1969) doi:10.1016/0003-4916(69)90264-4
 38. S. D. Drell and T. M. Yan, "Connection of Elastic Electromagnetic Nucleon Form-Factors at Large Q^2 and Deep Inelastic Structure Functions Near Threshold," Phys. Rev. Lett. **24**, 181-185 (1970) doi:10.1103/PhysRevLett.24.181
 39. G. B. West, "Phenomenological model for the electromagnetic structure of the proton," Phys. Rev. Lett. **24**, 1206-1209 (1970) doi:10.1103/PhysRevLett.24.1206
 40. H. C. Pauli and S. J. Brodsky, "Solving Field Theory in One Space One Time Dimension," Phys. Rev. D **32**, 1993 (1985) doi:10.1103/PhysRevD.32.1993
 41. K. Hornbostel, S. J. Brodsky and H. C. Pauli, "Light cone quantized QCD in (1+1)-Dimensions," Phys. Rev. D **41**, 3814 (1990).
 42. J. P. Vary, H. Honkanen, J. Li, P. Maris, S. J. Brodsky, A. Harindranath, G. F. de T eramond, P. Sternberg, E. G. Ng and C. Yang, "Hamiltonian light-front field theory in a basis function approach," Phys. Rev. C **81**, 035205 (2010) [arXiv:0905.1411 [nucl-th]].

43. J. P. Vary, X. Zhao, A. Ilderton, H. Honkanen, P. Maris and S. J. Brodsky, "Applications of Basis Light-Front Quantization to QED," Nucl. Phys. B Proc. Suppl. **251-252**, 10-15 (2014) doi:10.1016/j.nuclphysbps.2014.04.002 [arXiv:1406.1838 [nucl-th]].
44. S. J. Brodsky, A. L. Deshpande, H. Gao, R. D. McKeown, C. A. Meyer, Z. E. Meiziani, R. G. Milner, J. Qiu, D. G. Richards and C. D. Roberts, "QCD and Hadron Physics," [arXiv:1502.05728 [hep-ph]].
45. G. P. Lepage and S. J. Brodsky, "Exclusive Processes in Perturbative Quantum Chromodynamics," Phys. Rev. D **22**, 2157 (1980) doi:10.1103/PhysRevD.22.2157
46. S. J. Brodsky and S. Gardner, "Comment on New Limits on Intrinsic Charm in the Nucleon from Global Analysis of Parton Distributions." Phys. Rev. Lett. **116**, no.1, 019101 (2016) doi:10.1103/PhysRevLett.116.019101 [arXiv:1504.00969 [hep-ph]].
47. S. J. Brodsky, "Novel QCD Phenomena at the LHC: The Ridge, Digluon-Initiated Subprocesses, Direct Reactions, Non-Universal Antishadowing, and Forward Higgs Production," Nucl. Part. Phys. Proc. **258-259**, 23-30 (2015) doi:10.1016/j.nuclphysbps.2015.01.007 [arXiv:1410.0404 [hep-ph]].
48. J. D. Bjorken, S. J. Brodsky and A. Scharff Goldhaber, "Possible multiparticle ridge-like correlations in very high multiplicity proton-proton collisions," Phys. Lett. B **726**, 344-346 (2013) doi:10.1016/j.physletb.2013.08.066 [arXiv:1308.1435 [hep-ph]].
49. C. Cruz-Santiago, P. Kotko and A. M. Staśto, "Scattering amplitudes in the light-front formalism," Brodsky:1973kb Prog. Part. Nucl. Phys. **85**, 82-131 (2015) doi:10.1016/j.pnpnp.2015.07.002
50. S. J. Brodsky, R. Roskies and R. Suaya, "Quantum Electrodynamics and Renormalization Theory in the Infinite Momentum Frame," Phys. Rev. D **8**, 4574 (1973) doi:10.1103/PhysRevD.8.4574
51. A. Casher and L. Susskind, "Chiral magnetism (or magnetohydrochironics)," Phys. Rev. D **9**, 436-460 (1974) doi:10.1103/PhysRevD.9.436
52. S. J. Brodsky and R. Shrock, "Condensates in Quantum Chromodynamics and the Cosmological Constant," Proc. Nat. Acad. Sci. **108**, 45-50 (2011) doi:10.1073/pnas.1010113107 [arXiv:0905.1151 [hep-th]].
53. S. J. Brodsky, C. D. Roberts, R. Shrock and P. C. Tandy, "Essence of the vacuum quark condensate," Phys. Rev. C **82**, 022201 (2010) doi:10.1103/PhysRevC.82.022201 [arXiv:1005.4610 [nucl-th]].
54. P. P. Srivastava and S. J. Brodsky, "A Unitary and Renormalizable Theory of the Standard Model in Ghost Free Light Cone Gauge," Phys. Rev. D **66**, 045019 (2002) doi:10.1103/PhysRevD.66.045019 [arXiv:hep-ph/0202141 [hep-ph]].
55. A. Zee, "Dark energy and the cosmological constant paradox," Mod. Phys. Lett. A **23**, 1336-1345 (2008) doi:10.1142/S0217732308027709
56. G. F. de Téramond, H. G. Dosch, T. Liu, R. S. Sufian, S. J. Brodsky and A. Deur, "Gluon matter distribution in the proton and pion from extended holographic light-front QCD," [arXiv:2107.01231 [hep-ph]].
57. S. J. Brodsky, P. Hoyer, C. Peterson and N. Sakai, "The Intrinsic Charm of the Proton," Phys. Lett. B **93**, 451-455 (1980) doi:10.1016/0370-2693(80)90364-0
58. S. J. Brodsky, J. C. Collins, S. D. Ellis, J. F. Gunion and A. H. Mueller, "Intrinsic Chevrolets at the SSC," DOE/ER/40048-21 P4.
59. B. W. Harris, J. Smith and R. Vogt, "Reanalysis of the EMC charm production data with extrinsic and intrinsic charm at NLO," Nucl. Phys. B **461**, 181-196 (1996) doi:10.1016/0550-3213(95)00652-4 [arXiv:hep-ph/9508403 [hep-ph]].
60. M. Franz, M. V. Polyakov and K. Goeke, "Heavy quark mass expansion and intrinsic charm in light hadrons," Phys. Rev. D **62**, 074024 (2000) doi:10.1103/PhysRevD.62.074024 [arXiv:hep-ph/0002240 [hep-ph]].

61. C. Royon, "Forward physics using proton tagging at the LHC," AIP Conf. Proc. **1654**, no.1, 040004 (2015) doi:10.1063/1.4915969
62. S. J. Brodsky, A. Kusina, F. Lyonnet, I. Schienbein, H. Spiesberger and R. Vogt, "A review of the intrinsic heavy quark content of the nucleon," Adv. High Energy Phys. **2015**, 231547 (2015) doi:10.1155/2015/231547 [arXiv:1504.06287 [hep-ph]].
63. S. J. Brodsky, G. I. Lykasov, A. V. Lipatov and J. Smiesko, "Novel Heavy-Quark Physics Phenomena," Prog. Part. Nucl. Phys. **114**, 103802 (2020) doi:10.1016/j.pnnp.2020.103802 [arXiv:2006.09443 [hep-ph]].
64. V. A. Bednyakov, S. J. Brodsky, A. V. Lipatov, G. I. Lykasov, M. A. Malyshev, J. Smiesko and S. Tokar, "Constraints on the intrinsic charm content of the proton from recent ATLAS data," Eur. Phys. J. C **79**, no.2, 92 (2019) doi:10.1140/epjc/s10052-019-6605-y [arXiv:1712.09096 [hep-ph]].
65. S. J. Brodsky, V. A. Bednyakov, G. I. Lykasov, J. Smiesko and S. Tokar, "The Physics of Heavy Quark Distributions in Hadrons: Collider Tests," Prog. Part. Nucl. Phys. **93**, 108-142 (2017) doi:10.1016/j.pnnp.2016.12.001 [arXiv:1612.01351 [hep-ph]].
66. J. Pumplin, "Light-cone models for intrinsic charm and bottom," Phys. Rev. D **73**, 114015 (2006) doi:10.1103/PhysRevD.73.114015 [arXiv:hep-ph/0508184 [hep-ph]].
67. F. S. Navarra, M. Nielsen, C. A. A. Nunes and M. Teixeira, "On the intrinsic charm component of the nucleon," Phys. Rev. D **54**, 842-846 (1996) doi:10.1103/PhysRevD.54.842 [arXiv:hep-ph/9504388 [hep-ph]].
68. S. J. Brodsky, K. Y. J. Chiu, J. P. Lansberg and N. Yamanaka, "The gluon and charm content of the deuteron," Phys. Lett. B **783**, 287-293 (2018) doi:10.1016/j.physletb.2018.06.070 [arXiv:1805.03173 [hep-ph]].
69. R. S. Sufian, T. Liu, A. Alexandru, S. J. Brodsky, G. F. de Téramond, H. G. Dosch, T. Draper, K. F. Liu and Y. B. Yang, "Constraints on charm-anticharm asymmetry in the nucleon from lattice QCD," Phys. Lett. B **808**, 135633 (2020) doi:10.1016/j.physletb.2020.135633 [arXiv:2003.01078 [hep-lat]].
70. R. S. Sufian, T. Liu, G. F. de Téramond, H. G. Dosch, S. J. Brodsky, A. Deur, M. T. Islam and B. Q. Ma, "Nonperturbative strange-quark sea from lattice QCD, light-front holography, and meson-baryon fluctuation models," Phys. Rev. D **98**, no.11, 114004 (2018) doi:10.1103/PhysRevD.98.114004 [arXiv:1809.04975 [hep-ph]].
71. R. Aaij *et al.* [LHCb], "Study of Z bosons produced in association with charm in the forward region," [arXiv:2109.08084 [hep-ex]].
72. This section is based on a collaboration with G. de Téramond. (to be published).
73. S. J. Brodsky and A. H. Mueller, "Using Nuclei to Probe Hadronization in QCD," Phys. Lett. B **206**, 685-690 (1988) doi:10.1016/0370-2693(88)90719-8
74. D. Bhetuwal *et al.* [Hall C], "Ruling out Color Transparency in Quasi-elastic $^{12}\text{C}(e,e'p)$ up to Q^2 of $14.2 (\text{GeV}/c)^2$," Phys. Rev. Lett. **126**, no.8, 082301 (2021) doi:10.1103/PhysRevLett.126.082301 [arXiv:2011.00703 [nucl-ex]].
75. O. Caplow-Munro and G. A. Miller, "Color transparency and the proton form factor: Evidence for the Feynman mechanism," Phys. Rev. C **104**, no.1, L012201 (2021) doi:10.1103/PhysRevC.104.L012201 [arXiv:2104.11168 [nucl-th]].
76. S. J. Brodsky and L. Di Giustino, "Setting the Renormalization Scale in QCD: The Principle of Maximum Conformality," Phys. Rev. D **86**, 085026 (2012) doi:10.1103/PhysRevD.86.085026 [arXiv:1107.0338 [hep-ph]].
77. L. Di Giustino, S. J. Brodsky, S. Q. Wang and X. G. Wu, "Infinite-order scale-setting using the principle of maximum conformality: A remarkably efficient method for eliminating renormalization scale ambiguities for perturbative QCD," Phys. Rev. D **102**, no.1, 014015 (2020) doi:10.1103/PhysRevD.102.014015 [arXiv:2002.01789 [hep-ph]].
78. S. Q. Wang, S. J. Brodsky, X. G. Wu, J. M. Shen and L. Di Giustino, "Novel method for the precise determination of the QCD running coupling from event shape dis-

- tributions in electron-positron annihilation," *Phys. Rev. D* **100**, no.9, 094010 (2019) doi:10.1103/PhysRevD.100.094010 [arXiv:1908.00060 [hep-ph]].
79. S. Liuti, A. Rajan, A. Courtoy, G. R. Goldstein and J. O. Gonzalez Hernandez, "Partonic Picture of GTMDs," *Int. J. Mod. Phys. Conf. Ser.* **25**, 1460009 (2014) doi:10.1142/S201019451460009X [arXiv:1309.7029 [hep-ph]].
80. C. Mondal and D. Chakrabarti, "Generalized parton distributions and transverse densities in a light-front quark-diquark model for the nucleons," *Eur. Phys. J. C* **75**, no.6, 261 (2015) doi:10.1140/epjc/s10052-015-3486-6 [arXiv:1501.05489 [hep-ph]].
81. C. Lorce, B. Pasquini and M. Vanderhaeghen, "Unified framework for generalized and transverse-momentum dependent parton distributions within a 3Q light-cone picture of the nucleon," *JHEP* **05**, 041 (2011) doi:10.1007/JHEP05(2011)041 [arXiv:1102.4704 [hep-ph]].
82. S. J. Brodsky, "Dynamic versus Static Structure Functions and Novel Diffractive Effects in QCD," *AIP Conf. Proc.* **1105**, no.1, 315-322 (2009) doi:10.1063/1.3122202 [arXiv:0811.0875 [hep-ph]].
83. S. J. Brodsky, "Dynamic versus Static Hadronic Structure Functions," *Nucl. Phys. A* **827**, 327C-332C (2009) doi:10.1016/j.nuclphysa.2009.05.068 [arXiv:0901.0781 [hep-ph]].
84. S. J. Brodsky, D. S. Hwang and I. Schmidt, "Final state interactions and single spin asymmetries in semi-inclusive deep inelastic scattering," *Phys. Lett. B* **530**, 99-107 (2002) doi:10.1016/S0370-2693(02)01320-5 [arXiv:hep-ph/0201296 [hep-ph]].
85. S. J. Brodsky, P. Hoyer, N. Marchal, S. Peigne and F. Sannino, "Structure functions are not parton probabilities," *Phys. Rev. D* **65**, 114025 (2002) doi:10.1103/PhysRevD.65.114025 [arXiv:hep-ph/0104291 [hep-ph]].
86. S. J. Brodsky, B. Pasquini, B. W. Xiao and F. Yuan, "Phases of Augmented Hadronic Light-Front Wave Functions," *Phys. Lett. B* **687**, 327-330 (2010) doi:10.1016/j.physletb.2010.03.049 [arXiv:1001.1163 [hep-ph]].
87. S. J. Brodsky, V. E. Lyubovitskij and I. Schmidt, "The Diffractive Contribution to Deep Inelastic Lepton-Proton Scattering: Implications for QCD Momentum Sum Rules and Parton Distributions," [arXiv:2105.01435 [hep-ph]].
88. S. J. Brodsky, V. E. Lyubovitskij and I. Schmidt, "Novel Corrections to the Momentum Sum Rule for Nuclear Structure Functions," [arXiv:2110.13682 [hep-ph]].
89. S. J. Brodsky, I. Schmidt and J. J. Yang, "Nuclear antishadowing in neutrino deep inelastic scattering," *Phys. Rev. D* **70**, 116003 (2004) doi:10.1103/PhysRevD.70.116003 [arXiv:hep-ph/0409279 [hep-ph]].
90. I. Schienbein, J. Y. Yu, C. Keppel, J. G. Morfin, F. Olness and J. F. Owens, "Nuclear parton distribution functions from neutrino deep inelastic scattering," *Phys. Rev. D* **77**, 054013 (2008) doi:10.1103/PhysRevD.77.054013 [arXiv:0710.4897 [hep-ph]].
91. S. J. Brodsky, I. Schmidt and S. Liuti, "Is the Momentum Sum Rule Valid for Nuclear Structure Functions?," [arXiv:1908.06317 [hep-ph]].
92. S. J. Brodsky, D. S. Hwang, Y. V. Kovchegov, I. Schmidt and M. D. Sievert, "Single-Spin Asymmetries in Semi-inclusive Deep Inelastic Scattering and Drell-Yan Processes," *Phys. Rev. D* **88**, no.1, 014032 (2013) doi:10.1103/PhysRevD.88.014032 [arXiv:1304.5237 [hep-ph]].
93. S. J. Brodsky and H. J. Lu, "Shadowing and Antishadowing of Nuclear Structure Functions," *Phys. Rev. Lett.* **64**, 1342 (1990) doi:10.1103/PhysRevLett.64.1342



7 Charge asymmetry of new stable quarks in baryon asymmetrical Universe

A. Chaudhuri¹

email: arnabchaudhuri.7@gmail.com

M. Yu. Khlopov²

email: khlopov@apc.in2p3.f

¹ Department of Physics and Astronomy, Novosibirsk State University, Russia

² Institute of Physics, Southern Federal University, Russia; Université de Paris, CNRS, Astroparticule et Cosmologie, France; and National Research Nuclear University "MEPHI", Russia

Abstract. Effects of electroweak phase transition (EWPT) in balance between baryon excess and the excess of stable quarks of new generation is studied. With the conservation of SU(2) symmetry and other quantum numbers, it makes possible sphaleron transitions between baryons, leptons and new of leptons and quarks. A definite relationship between the excess relative to baryon asymmetry is established. In passing by we also show the small, yet negligible dilution in the pre-existing dark matter density due the sphaleron transition.

Povzetek: Avtorji privzamejo model, ki dopušča poleg doslej izmerjenih kvarkov in leptonov tudi novo družino kvarkov in leptonov. V tem modelu študirajo v elektrošibkem prehodu ravnovesje med presežkom barionov pretežno prve družine kvarkov in leptonov in med barioni privzete družine kvarkov. V območju, ko se še ohranjajo vsa kvantna števila sistema, študirajo učinke prehoda sfalerona med kvarki in leptoni standardnega modela in kvarki in leptoni privzete družine ter vpliv prehoda na gostoto temne snovi. Opazijo majno, skoraj zanemarljivo, razredčitev njene gostote.

7.1 Introduction

The matter-antimatter asymmetry, otherwise known as the baryon asymmetry of the universe (BAU) has been the focus of physicists for many a decade [1–3]. Various models have been developed to answer the question, ranging from the grand unified theory (GUT) to electroweak phase transition (EWPT). Irrespective of the mechanisms, the preexisting asymmetry is diluted by the baryon number violating mechanisms in the electroweak theory. This is due to the violation of the baryon and lepton number and the non-trivial topological structure of the Yang–Mills theory.

The possibility to convert baryons into anti-leptons and the reverse exists in electroweak theory. The difference between the baryon and lepton numbers ($B - L$) is conserved, even though individually, the quantum numbers are violated. Hence, it is important to know about the transition rates of such processes.

Sphalerons are generally associated with saddle points [4], and is interpreted as the peak energy configuration, thus the transitions between vacua are associated with a violation of Baryon (and lepton) number. EWPT can be of first order, second order or a smooth crossover. Within the framework of the SM, it is a smooth crossover. However, BSM physics can lead to any of the three. The order of the phase transition can affect the outcome of the process. Entropy production and, in return, the dilution of preexisting frozen out species and baryon asymmetry can be some of them. Although baryon excess can be created at the time of electroweak symmetry breaking, it is preserved during the first order phase transition. In the second order, sphalerons can wipe out the total asymmetry created, but in first order, only the asymmetry created in the unbroken phase is wiped out.

A recent overview of physics beyond the standard model and its cosmological signatures can be found in [20], where it was shown that from the lack of supersymmetric particles at the LHC and from the positive results of the directly searched Weakly Interacting Massive Particles (WIMPs), the list of dark matter candidates can be strongly extended. The model of dark atoms of dark matter deserves special attention in this list, in light of its possibility to propose a nontrivial solution for the puzzles of direct dark matter searches, explaining the positive results of the DAMA/LIBRA experiment by the annual modulation of the low energy binding of dark atoms with sodium nuclei, which can be elusive in other experiments for direct WIMP searches.

In this approach, dark atoms represent a specific form of asymmetric, strongly interacting dark matter, being an atom-like state of stable -2 (or $-2n$) charged particles of a new origin bounded by a Coulomb interaction with (correspondingly, n) nuclei of primordial helium (see [17] for recent review and references). This explanation implies the development of a correct quantum mechanical description of the dark atom interaction with nuclei, which is now under way [19].

Even though there are several models predicting ± 2 ($\pm 2n$)-charged stable species, [8–11, 11–15, 15–18], in this work we restrict our self to the 4th generation family as an extension to the standard model (SM) and proceed to study the electroweak phase transition (EWPT). The simplest charge-neutral model is considered here; also, we consider that EWPT is of the second order. In passing by, we show the dilution of pre-existing frozen out dark matter density in the presence of the 4th generation.

The paper is organized as follows: In the next section, we talk about the 4th generation family, defining a definite relationship between the value and sign of the 4th generation family excess, relative to the baryon asymmetry, which is due to the electroweak phase transition and possible sphaleron production being established. This is followed by the calculation of the dilution factor of pre-existing dark matter density, followed by a general conclusion.

7.2 A brief review of 4th generation

The fourth generation is of theoretical interest in the context of sphaleron transition, electroweak symmetry breaking and large CP violating processes in the 4×4 CKM matrix, which may play a crucial role in understanding the baryon asymmetry in

the universe. Thus, there are significant ongoing efforts to search for the fourth generation. In this work, we consider the stable 4th generation, which is basically constrained by contributions of virtual 4th generation particles in the Higgs boson decay rates, in the precision tests of standard model parameters, as well as by the LHC searches for R-hadrons, which mimic stable 4th generation stable hadrons. These constraints can still leave some room for the existence of such a family and an explanation of the puzzles of direct dark matter searches by dark atoms formed with primordial helium by $(\bar{U}\bar{U}\bar{U})$ antiquark clusters.

Due to the excess of \bar{U} , only -2 charge or neutral 4th generation species are present in the universe. Indeed, stable antiquarks can form a $(\bar{U}\bar{U}\bar{U})$ cluster and a small fraction of neutral $\bar{U}u$ with ordinary u -quark. In principle, $(\bar{U}\bar{U}\bar{u})$ baryon should also be stable, but in a baryon asymmetrical universe, its interaction with ordinary baryons leads to its destruction in two $\bar{U}u$ mesons. ${}^4\text{He}$, formed during the Big Bang nucleosynthesis, completely screens Q^{--} charged hadrons in composite [${}^4\text{He}Q^{--}$] "atoms". If this 4th family follows from string phenomenology, we have new charge (F) associated with 4th family fermions. Principally, F should be the only conserved quantity but to keep matters simple, an analogy with WTC model is made and we assume two numbers: FB (for 4th quark) and L' (for 4th neutrino). Detailed calculations of WTC were made in [8, 14] and most of the terminology were kept the same as the above mentioned papers.

As the universe expanded and the temperature decreased and the quantum number violating processes ceased to exist, the relation among the particles emerging from the process (SM + 4th generation) followed the following expression:

$$3(\mu_{u_L} + \mu_{d_L}) + \mu + \mu_{U_L} + \mu_{D_L} + \mu_{L'} = 0. \quad (7.1)$$

here, μ is the chemical potential of all the SM particles, $\mu_{L'}$ is the chemical potential of the new species leptons and μ_{u_L} and μ_{d_L} are that of the 4th generation quarks; see [14]. The number densities follow, respectively, for bosons and fermions:

$$n = g_* T^3 \frac{\mu}{T} f\left(\frac{m}{T}\right), \quad (7.2)$$

and

$$n = g_* T^3 \frac{\mu}{T} g\left(\frac{m}{T}\right), \quad (7.3)$$

where f and g are hyperbolic mathematical functions and g_* is the effective degrees of freedom, which are given by the following:

$$f(z) = \frac{1}{4\pi^2} \int_0^\infty x^2 \cosh^{-2} \left(\frac{1}{2} \sqrt{z^2 + x^2} \right) dx, \quad (7.4)$$

and

$$g(z) = \frac{1}{4\pi^2} \int_0^\infty x^2 \sinh^{-2} \left(\frac{1}{2} \sqrt{z^2 + x^2} \right) dx. \quad (7.5)$$

The number density of baryons follows the following expression:

$$B = \frac{n_B - n_{\bar{B}}}{gT^2/6}. \quad (7.6)$$

As the main point of interest is the ratio of baryon excess to the excess of the stable 4th generation, the normalization cancels out, without loss of generality.

Let us define a parameter σ , which, respectively, for fermions and bosons are given by the following:

$$\sigma = 6f \frac{m}{T_c}, \quad (7.7)$$

and

$$\sigma = 6g \frac{m}{T_c}. \quad (7.8)$$

T_c is the transition temperature and is given by the following:

$$T_c = \frac{2M_W(T_c)}{\alpha_W \ln(M_{pl}/T_c)} B\left(\frac{\lambda}{\alpha_W}\right). \quad (7.9)$$

In the above equation, M_W is the mass of W-boson, M_{pl} is the Planck mass and λ is the self-coupling. The function B is derived from experiment and takes the value from 1.5 to 2.7.

The new generation charge is calculated to be the following:

$$FB = \frac{2}{3}(\sigma_{u_L} \mu_{u_L} + \sigma_{u_L} \mu_{D_L} + \sigma_{D_L} \mu_{D_L}), \quad (7.10)$$

where FB corresponds to the anti-U (\bar{U}) excess. For detailed calculations, please see [14].

The SM baryonic and leptonic quantum numbers are expressed as the following:

$$B = [(2 + \sigma_t)(\mu_{uL} + \mu_{uR}) + 3(\mu_{dL} + \mu_{dR})] \quad (7.11)$$

and

$$L = 4\mu + 6\mu_W \quad (7.12)$$

where in Equation (7.11), the factor 3 of down-type quarks is the number of families. For the 4th generation lepton family, the quantum number is given by the following:

$$L' = 2(\sigma_{\nu'} + \sigma_{u_L})\mu_{\nu'L} + 2\sigma_{u_L}\mu_W + (\sigma_{\nu'} - \sigma_{u_L})\mu_0 \quad (7.13)$$

where ν' is the new family of neutrinos originating from the extension of SM, and μ_0 is the chemical potential from the Higgs sector in SM.

Due to the presence of a single Higgs particle, the phase transition is of the second order. The ratio of the number densities of the 4th generation to the baryons is determined by the following:

$$\frac{\Omega_{FB}}{\Omega_B} = \frac{3}{2} \frac{FB}{B} \frac{m_{FB}}{m_p}. \quad (7.14)$$

The electrical neutrality and negligibly small chemical potential of the Higgs sector is the result of the second order phase transition. The ratio of the number density of the 4th generation to the baryon number density can be expressed as a function

of the ratio of the original and new quantum numbers. In the limiting case of the second order EWPT, we obtain the following:

$$-\frac{FB}{B} = \frac{\sigma_{u_L}}{3(18 + \sigma_{\nu'})} \left[(17 + \sigma_{\nu'}) + \frac{(21 + \sigma_{\nu'}) L}{3} \frac{L}{B} + \frac{29 + 5\sigma_{\nu'} L'}{3} \frac{L'}{B} \right]. \quad (7.15)$$

In the following Figure 7.1, the predicted relationship between the frozen out excess of \bar{U} -antiquarks and baryon asymmetry is shown as a function of U-quark mass m . The minimal mass m can be determined from the R-hadrons search at the LHC as 1 TeV. The predicted contribution of dark atoms, in which $(\bar{U}\bar{U}\bar{U})$ are bound with primordial helium nuclei, can explain the observed dark matter density at $m \sim 3.5$ TeV, which is compatible with the above mentioned experimental lower limit.

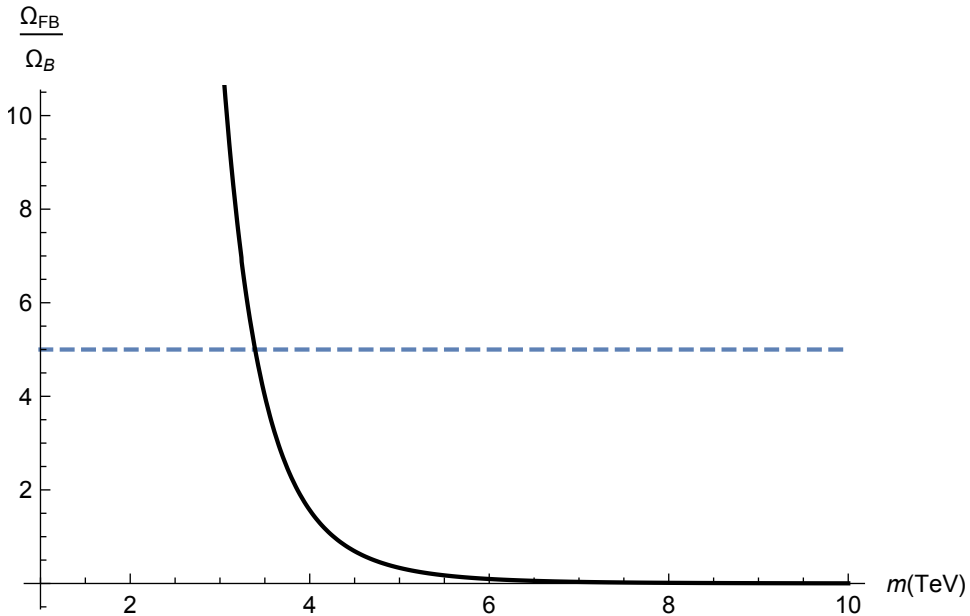


Fig. 7.1: The ratio of dark matter and baryon densities as a function of the U-quark mass (m). This ratio is frozen out at the critical temperature of the assumed second order EWPT $T = T_c = 179$ GeV. At the U-quark mass $m \approx 3.5$ TeV, the predicted density of dark atoms, formed by $(\bar{U}\bar{U}\bar{U})$ bound with primordial helium nuclei, can explain the observed dark matter density.

Hence, we establish a relationship between the baryon excess and the excess of \bar{U} for the second order EWPT.

7.3 Dilution of Pre-Existing Dark Matter Density

The thermodynamic quantity, entropy density, is a conserved quantity in the initial stage of universe expansion, especially when the primeval plasma is in

thermal equilibrium with a negligible chemical potential. As soon as the universe enters into the state of thermal non-equilibrium, i.e., when $\Gamma > H$, where Γ is the reaction rate and H is the Hubble parameter, the conservation law breaks down, and entropy starts pouring into the plasma; this can dilute the pre-existing baryon asymmetry and dark matter density.

There are many instances of entropy production, such as primordial black hole evaporation [21], electroweak phase transition within the standard model and the two Higgs doublet model [3, 6, 11]. Apart from these, the freeze out of dark matter density might lead to entropy production, which in turn, can dilute the pre-existing dark matter density.

The Lagrangian theory consists of the Lagrangian of the standard model (SM) and the interaction terms of the 4th generation fermionic family. It is given by the following:

$$\mathcal{L} = \mathcal{L}_{SM} + \mathcal{L}_{4^{th}}, \quad (7.16)$$

where \mathcal{L}_{SM} is given by the following:

$$\mathcal{L}_{SM} = \frac{1}{2} g^{\mu\nu} \partial_\mu \phi \partial_\nu \phi - U_\phi(\phi) + \sum_j i \left[g^{\mu\nu} \partial_\mu \chi_j^\dagger \partial_\nu \chi_j - U_j(\chi_j) \right]. \quad (7.17)$$

The CP violating potential of the theory is as follows:

$$U_\phi(\phi) = \frac{\lambda}{4} (\phi^2 - \eta^2)^2 + \frac{T^2 \phi^2}{2} \sum_j h_j \left(\frac{m_j(T)}{T} \right). \quad (7.18)$$

here, $\lambda = 0.13$ is the quartic coupling constant and η is the vacuum expectation values, which is ~ 246 GeV in the SM. T is the plasma temperature and $m_j(T)$ is the mass of the χ_j -particle at temperature T ; see [25].

To calculate the dilution factor, it is necessary to compute the energy and the pressure density of the plasma, using the energy-momentum tensor. Following the detailed calculation in [6] and assuming that the universe was flat in the early epoch with the metric $g_{\mu\nu} = (+, -, -, -)$, we have the following:

$$\rho + \mathcal{P} = \dot{\phi}^2 + \frac{4}{3} \frac{\pi^2 g_*}{30} T^4. \quad (7.19)$$

In order to proceed with the calculation of the dilution factor, the EWPT transition temperature needs to be calculated first. The transition temperature is derived using the following expression:

$$V(\phi = 0, T = T_c) = V(\phi = \eta, T = T_c). \quad (7.20)$$

here, η is the vacuum expectation value and T_c is the transition temperature. In Equation (7.20), substituting the values of the standard model particles and the minimal allowed masses of the 4th generation particle, which can be estimated from the R-hadrons search at the LHC as 1 TeV, T_c is found to be ~ 179 GeV. With a range of allowed values, one can obtain a range of T_c s and study the nature of the EWPT and other related properties, but that is beyond the scope of the current

paper. With proper data and tools, this analysis will certainly be made in the near future.

The last term in Equation (7.19) arises from the Yukawa interaction between fermions. The Higgs field starts to oscillate around the minimum, which appears during the phase transition. Particle production from this oscillating field causes damping. The characteristic time of decay is equal to the decay width of the Higgs bosons. If it is large in comparison to the expansion, and thus the universe cooling rate, then we may assume that the Higgs bosons essentially live in the minimum of the potential. This was clearly discussed in [11].

To calculate the entropy production, it is necessary to solve the evolution equation for energy density conservation as follows:

$$\dot{\rho} = -3H(\rho + P). \quad (7.21)$$

In Figure 8.1, both the dilution of the pre-existing dark matter (blue line) and the entropy production in the presence of 4th generation lepton family (black line) are shown. It is clear that since the sphaleron transition is of the second order, the net dilution and entropy production ($\sim 18\%$) are somewhat low compared to the scenarios of the first order. Again, the presence of a single Higgs field makes the phase transition of the second order.

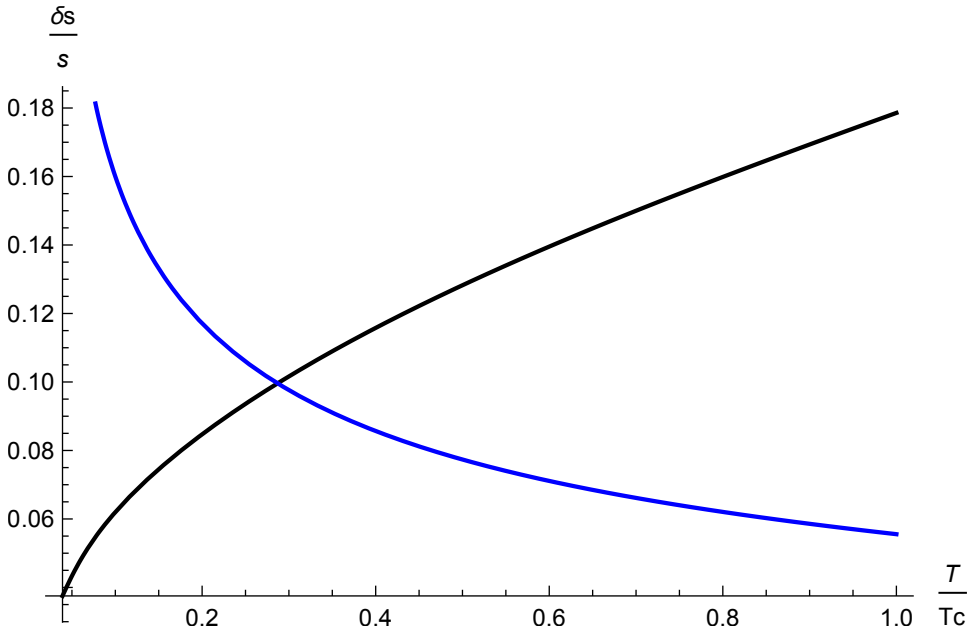


Fig. 7.2: Entropy production (black line) and the dilution of pre-existing dark matter (blue line) in the presence of 4th generation fermions are presented.

7.4 Conclusions

In the present paper, we have deduced a definite relationship between the value and sign of the 4th generation family excess and baryon asymmetry due to the sphaleron effects frozen out at the electroweak phase transition, as is clear from Equation (7.15) and Figure 7.1.

At the transition temperature, $T_c = 179$ GeV and the mass of the stable U-quark of the new family $m \approx 3.5$ TeV, the predicted density of the dark atoms can explain the observed cosmological dark matter density. This value and experimental constraints on the contribution of new electroweakly interacting fermions appeal to the involvement of additional Higgs bosons, whose existence can influence the value of T_c and, correspondingly, the determination of the mass of the U-quark, for which dark atoms explain the dark matter density. Being beyond the scope of the present work, such a self-consistent analysis of the models with new stable quarks, accompanied by an extended Higgs sector, can open up a new specific direction of studies of BSM physics.

The search for new physics and dark matter has been an ongoing area of research for decades. Even though there are many multi-Higgs models, there are few multi-charged models present. The theory of the 4th generation can serve to leap toward new physics in the framework of heterotic string phenomenology. As seen from the work, just like the standard model, we can link the stable quarks of the new generation particles with the baryon asymmetry theoretically. The existence of new stable quarks with the SM electroweak charges can follow from other unifying schemes (in the approach [11, 15] in particular); the important conclusion of our work is that balancing baryon asymmetry with sphaleron transitions can provide an excess of \bar{U} antiquarks, forming a $(\bar{U}\bar{U}\bar{U})$ 'core' of dark atoms in which it is bound by a Coulomb force with primordial helium. The possibility of dark atoms extends the list of possible dark matter candidates, predicted in such models. To make new quarks with electroweak charges compatible with the data on the Higgs boson decay rates, their coupling to the SM Higgs boson should be suppressed, and they should acquire their mass from coupling to other Higgs bosons [26]. It would imply the accomplishment of models with new stable generations with SM electroweak charges by multi-Higgs models, opening up a probe of studying the Higgs and electroweak symmetry breaking sectors in a rigorous manner.

Dark matter candidates in the form of bounded dark atom can emerge from this model, due to the excess of \bar{U} within the primordial He nuclei. We have considered only the lightest and most stable particles and also took into account only the second order phase transition. The dilution of pre-existing dark matter density was calculated; in the present scenarios, the dark matter density was reduced by $\sim 18\%$.

Acknowledgements

The work of A.C. is funded by RSF Grant 19-42-02004. The research by M.K. was supported by the Ministry of Science and Higher Education of the Russian

Federation under Project "Fundamental problems of cosmic rays and dark matter", No. 0723-2020-0040.

References

1. Dolgov, A.D.; Zeldovich, Y.B. Cosmology and elementary particles. *Rev. Mod. Phys.* **1981**, *53*, 1, doi:10.1103/RevModPhys.53.1.
2. Cohen, A.G.; Kaplan, D.B.; Nelson, A.E. Progress in Electroweak Baryogenesis. *Ann. Rev. Nucl. Part. Sci.* **1993**, *43*, 27–70, doi:10.1146/annurev.ns.43.120193.000331.
3. Cohen, A.G.; Kaplan, D.B.; Nelson, A.E. Diffusion enhances spontaneous electroweak baryogenesis. *Phys. Lett. B* **1994**, *336*, 41–47, doi:10.1016/0370-2693(94)00935-X.
4. Klinkhamer, F.R.; Manton, N.S. A saddle-point solution in the Weinberg-Salam theory. *Phys. Rev. D* **1984**, *30*, 2212–2220.
5. Khlopov, M.Y. What comes after the Standard Model? *Prog. Part. Nucl. Phys.* **2021**, *116*, 103824, doi:10.1016/j.pnpnp.2020.103824
6. Beylin, V.; Khlopov, M.; Kuksa, V.; Volchaanskiy, N. New physics of strong interaction and Dark Universe. *Universe* **2020**, *6*, 196.
7. Bikbaev, T.E.; Khlopov, M.Y.; Mayorov, A.G. Numerical simulation of dark atom interaction with nuclei. *Bled Work. Phys.* **2020**, *21*, 105–117.
8. Khlopov, M.Y.; Kouvaris, C. Strong interactive massive particles from a strong coupled theory. *Phys. Rev. D* **2008**, *77*, 065002, doi:10.1103/PhysRevD.77.065002.
9. Sannino, F.; Tuominen, K. Orientifold theory dynamics and symmetry breaking. *Phys. Rev. D* **2005**, *71*, 051901, doi:10.1103/PhysRevD.71.051901.
10. Hong, D.K.; Hsu, S.D.H.; Sannino, F. Composite Higgs from higher representations. *Phys. Lett. B* **2004**, *597*, 89, doi:10.1016/j.physletb.2004.07.007.
11. Dietrich, D.D.; Sannino, F.; Tuominen, K. Light composite Higgs boson from higher representations versus electroweak precision measurements: predictions for CERN LHC. *Phys. Rev. D* **2005**, *72*, 055001, doi:10.1103/PhysRevD.72.055001.
12. Dietrich, D.D.; Sannino, F.; Tuominen, K. Light composite Higgs and precision electroweak measurements on the Z resonance: An update. *Phys. Rev. D* **2006**, *73*, 037701, doi:10.1103/PhysRevD.73.037701.
13. Gudnason, S.B.; Kouvaris, C.; Sannino, F. Towards working technicolor: Effective theories and dark matter. *Phys. Rev. D* **2006**, *73*, 115003, doi:10.1103/PhysRevD.73.115003.
14. Gudnason, S.B.; Kouvaris, C.; Sannino, F. Dark matter from new technicolor theories. *Phys. Rev. D* **2006**, *74*, 095008, doi:10.1103/PhysRevD.74.095008.
15. Belotsky, K.M.; Khlopov, M.Y.; Shibaev, K.I. Stable quarks of the 4th family? In *Physics of Quarks: New Research; Horizons in World Physics*
16. Khlopov, M.Y. Composite dark matter from the fourth generation. *JETP Lett.* **2006**, *83*, 1, doi:10.1134/S0021364006010012 .
17. Belotsky, K.M.; Khlopov, M.Y.; Shibaev, K.I. Stable matter of 4th generation: Hidden in the Universe and close to detection? *arXiv* **2006**, arXiv:astro-ph/0602261.
18. Belotsky, K.M.; Khlopov, M.Y.; Shibaev, K.I. Composite Dark Matter and its Charged Constituents. *Gravit. Cosmol.* **2006**, *12*, 1–7, doi:10.1134/S0202289312020028.
19. Mankoc-Borstnik, N. Unification of spins and charges in Grassmann space? *Mod. Phys. Lett.* **1995**, *10*, 587–596.
20. Mankoc-Borstnik, N.S. The spin-charge-family theory is explaining the origin of families, of the Higgs and the Yukawa couplings. *J. Mod. Phys.* **2013**, *4*, 823.
21. Chaudhuri, A.; Dolgov, A. PBH evaporation, baryon asymmetry and dark matter. *arXiv* **2020**, arXiv:2001.11219.

22. Chaudhuri, A.; Dolgov, A. Electroweak phase transition and entropy release in the early universe. *JCAP* **2018**, *2018*, 032, doi:10.1088/1475-7516/2018/01/032.
23. Chaudhuri, A.; Khlopov, M.Y. Entropy production due to electroweak phase transition in the framework of two Higgs doublet model. *Physics* **2021**, *3*, 275–289, doi:10.3390/physics3020020.
24. Chaudhuri, A.; Khlopov, M.Y.; Porey, S. Effects of 2HDM in electroweak phase transition. *Galaxies* **2021**, *9*, 45, doi:10.3390/galaxies9020045.
25. Melo, I. Higgs potential and fundamental physics. *Eur. J. Phys.* **2017**, *38*, 065404, doi:10.1088/1361-6404/aa8c3d.
26. Khlopov, M.Y.; Shibaev, R.M. Probes for 4th generation constituents of dark atoms in Higgs boson studies at the LHC. *Adv. High Energy Phys.* **2014**, *2014*, 406458.



8 Entropy release in Electroweak Phase Transition in 2HDM

A. Chaudhuri¹

email: arnabchaudhuri.7@gmail.com

M. Yu. Khlopov²

email: khlopov@apc.in2p3.fr

S. Porey¹

email: shiladityamailbox@gmail.com

¹Department of Physics and Astronomy, Novosibirsk State University, Russia

²Institute of Physics, Southern Federal University, Russia; Université de Paris, CNRS, Astroparticule et Cosmologie, France; and National Research Nuclear University "MEPHI", Russia

Abstract. Electroweak phase transition in the simplest extension of the standard model namely two Higgs doublet model and entropy production within this framework is studied. We have considered several benchmark points which were called using BSMPT, a C++ package, within the limit of $v_{\text{ev}}/T_{\text{C}} > 0.2$ are studied, and corresponding entropy productions are shown in this paper.

Povzetek: Povzetek: Avtorji obravnavajo povečanje entropije pri elektrošibkem faznem prehodu v modelu, ki razširi standardni model z dvema Higgsovima skalarjema. Prispevek prinaša rezultate teh računov za več referenčnih točk, ki so jih poiskali z uporabo BSMPT, paketa C++, znotraj meje $v_{\text{ev}}/T_{\text{C}} > 0.2$.

8.1 Introduction

For a successful explanation about the origin of excess baryons over antibaryons in the universe through electroweak baryogenesis (EWBG), a strong first-order electroweak phase transition (EWPT) in the early universe is necessary. Cosmic EWPT happened when the hot universe cooled down enough in the primeval time so that the potential of the Higgs field got and settled at a non-zero minimum and in consequence, the symmetry of the theory $SU(2)_{\text{L}} \times U(1)_{\text{Y}}$ broke to $U(1)_{\text{em}}$. At the time of first-order EWPT, bubbles of the broken phase originate and baryon-antibaryon asymmetry generates outside the wall of the bubbles of the broken phase. However, after the discovery of the standard model (SM) Higgs boson, it is widely known that EWPT in SM with a single Higgs field is just a smooth cross-over. Therefore, for a successful EWBG, a theory of EWPT in beyond SM (BSM) is needed [1].

On the other side, $\sim 26.5\%$ of the total energy density of the universe is contributed by the dark matter (DM) whose mysterious nature has not been unveiled till now. Although, primordial black holes and MACHOs which are considered as one of the viable baryonic DM candidates, it is now clear that they are unable to contribute completely to the DM energy density of the universe. There are theories about multicharged extension of the standard model like dark atoms which can be viable dark matter candidates, [2]. But there are no experimental evidences as of now.

Not only about the baryogenesis, but there is also no irrefutable theory in SM about nonbaryonic DM particle which can successfully explain all the observations. Similar to the above mentioned facts, there are many limitations of the SM. Thus scientists are desperately searching for experimental evidence of BSM. For them the recent result from Fermilab about $g_\mu - 2$ for muon may be a ray of hope. g_μ is the gyromagnetic ratio of muon which is defined as the ratio of magnetic moment to the angular moment of muon and whose value is 2 from tree-level calculation. If we define $a_\mu = (g_\mu - 2)/2$, then higher order loop corrections from SM gives $a_\mu = 116,591,810(43) \times 10^{-11}$ where the value measured from Fermilab is $16,592,061(41) \times 10^{-11}$ which differs from SM at 3.3σ level [3]. This contradiction is actually buttressed the previously claimed result from the E821 experiment at Brookhaven National Lab (BNL). There are numerous explanation for this anomalous result including the existence of BSM.

Among all the BSM theories, the two Higgs doublet model (2HDM) is one of the most popular theories which not only exhibits strong first-order EWPT for the proper choice of parameter space but also provides the minimal phenomenological description of some effects of the supersymmetric model predicting two Higgs boson doublet. In addition to that, this model can produce dark matter particles [4] and gives a satisfactory explanation for the g_μ anomaly of muon [5] if the parameter space is properly chosen.

At or around the epoch of EWPT the energy density of the universe was dominated by relativistic species with negligible chemical potential. In addition to that, the universe was almost always in thermal equilibrium except some special epochs. Thus entropy density per comoving volume of the relativistic plasma was conserved. However, EWPT is a strongly thermally non-equilibrium process and thus there is a possibility that entropy might have been generated during this cosmic process.

In this work, we explored the increase in entropy during the epoch of EWPT in the real type-I 2HDM framework. We have shown that entropy density per comoving volume increases if EWPT happens as a first-order phase transition in 2HDM model.

The article is arranged as follows: In the next section the Lagrangian of the model along with the results are given. A generic conclusion follows and in the appendix the detailed potential is mentioned.

8.2 Lagrangian density of the model

The Lagrangian density of EWPT theory in real type-I 2HDM is given by

$$\mathcal{L} = \mathcal{L}_{\text{gauge,kin}} + \mathcal{L}_f + \mathcal{L}_{\text{Yuk}} + \mathcal{L}_{\text{Higgs}} - V(\Phi_1, \Phi_2, T) \quad (8.1)$$

where $\mathcal{L}_{\text{gauge,kin}}$, \mathcal{L}_f and \mathcal{L}_{Yuk} are the kinetic energy term of gauge bosons (W_α and B_α with $\alpha = 0, 1, 2, 3$), kinetic energy of fermions and Yukawa interaction term of fermions with Higgs bosons. These terms are defined in [6,7] and also discussed in Appendix A. Throughout this article, all the Greek indices used in super or sub-script run from 0 to 3 and Latin indices from 1 to 3 if not mentioned otherwise. $\mathcal{L}_{\text{Higgs}}$ incorporates the kinetic term of the Higgs field and their interaction with the gauge bosons. Thus

$$\mathcal{L}_{\text{Higgs}} = \{(\partial^\mu + i\mathcal{W}^\mu)\Phi_a\}^\dagger \{(\partial_\mu + i\mathcal{W}_\mu)\Phi_a\} \quad (8.2)$$

where $a = 1, 2$ for two Higgs field, $i = \sqrt{-1}$, $i\mathcal{W}^\mu \equiv +igT^k W^{k\mu} + ig'YB^\mu$, and g and g' are coupling constants, T^i is the generator of $SU(2)_L$ (left-Chiral), which is also a form of Pauli matrices, and Y is the hyper-charge generator of the $U(1)$. The total CP-conserving potential for our 2HDM model considered is

$$V(\Phi_1, \Phi_2, T) = V_{\text{tree}}(\Phi_1, \Phi_2) + V_{\text{CW}}(\Phi_1, \Phi_2) + V_T(T) + V_{\text{daisy}}(T) \quad (8.3)$$

The tree-level potential can be written as

$$\begin{aligned} V_{\text{tree}}(\Phi_1, \Phi_2) = & m_{11}^2 \Phi_1^\dagger \Phi_1 + m_{22}^2 \Phi_2^\dagger \Phi_2 - \left[m_{12}^2 \Phi_1^\dagger \Phi_2 + m_{12}^* \Phi_2^\dagger \Phi_1 \right] + \frac{1}{2} \lambda_1 (\Phi_1^\dagger \Phi_1)^2 \\ & + \frac{1}{2} \lambda_2 (\Phi_2^\dagger \Phi_2)^2 + \lambda_3 (\Phi_1^\dagger \Phi_1) (\Phi_2^\dagger \Phi_2) + \lambda_4 (\Phi_1^\dagger \Phi_2) (\Phi_2^\dagger \Phi_1) \\ & + \left[\frac{1}{2} \lambda_5 (\Phi_1^\dagger \Phi_2)^2 + \frac{1}{2} \lambda_5^* (\Phi_2^\dagger \Phi_1)^2 \right]. \end{aligned} \quad (8.4)$$

m_{12}^2 , m_{11}^2 , and m_{22}^2 can be estimated from the following formula

$$m_{12}^2 = 100^2 \text{ GeV}^2 \quad (8.5)$$

$$m_{11}^2 = \frac{1}{4v_1} (-2\lambda_1 v_1^3 + 4m_{12}^2 v_2 - 2\lambda_3 v_1 v_2^2 - 2\lambda_4 v_1 v_2^2 - \lambda_5 v_1 v_2^2 - v_1 v_2^2 \lambda_5) \quad (8.6)$$

$$m_{22}^2 = \frac{1}{4v_2} (4m_{12}^2 v_1 - 2\lambda_3 v_1^2 v_2 - 2\lambda_4 v_1^2 v_2 - \lambda_5 v_1^2 v_2 - 2\lambda_2 v_2^3 - v_1^2 v_2 \lambda_5) \quad (8.7)$$

The value of m_{12}^2 can alter for different parameter space. These formulas are valid since λ_5 is real and $\lambda_6 = \lambda_7 = 0$. The λ_{1-5} can be calculated from the parameter

space as

$$l_1 = \frac{m_H^2 \cos^2 \alpha + m_h^2 \sin^2 \alpha - m_{12}^2 \tan \beta}{v^2 \cos^2 \beta}, \quad (8.8)$$

$$l_2 = \frac{m_H^2 \sin^2 \alpha + m_h^2 \cos^2 \alpha - m_{12}^2 \tan \beta^{-1}}{v^2 \sin^2 \beta}, \quad (8.9)$$

$$l_3 = \frac{(m_H^2 - m_h^2) \sin \alpha \cos \alpha + 2m_{H\pm}^2 \cos \beta \sin \beta - m_{12}^2}{v^2 \sin \beta \cos \beta}, \quad (8.10)$$

$$l_4 = \frac{(m_\lambda^2 - 2m_{H\pm}^2) \sin \beta \cos \beta + m_{12}^2}{v^2 \sin \beta \cos \beta}, \quad (8.11)$$

$$l_5 = \frac{m_{12}^2 - m_\lambda^2 \sin \beta \cos \beta}{v^2 \sin \beta \cos \beta}. \quad (8.12)$$

where v is the standard model expectation value, $v^2 = v_1^2 + v_2^2$, $\tan \beta = v_2/v_1$ and $\cos(\beta - \alpha) \rightarrow 0$ leads to SM result. The details about the parameter space of m_H , m_h , $m_{H\pm}$ can be found in the recent works [8–10].

The Coleman–Weinberg correction to the potential -

$$V_{\text{CW}}(v_1 + v_2) = \sum_j \frac{n_j}{64\pi^2} (-1)^{2s_j} m_j^4(v_1, v_2) \left[\log \left(\frac{m_j^2(v_1, v_2)}{\mu^2} \right) - c_j \right] \quad (8.13)$$

The values of n_j , s_j , c_j and different mass-values $m_j^2(v_1, v_2)$ are mention in Appendix B and $\mu = 246$ GeV.

Temperature correction of potential and its series expansion in Landau gauge are

$$V_T = \frac{T^4}{2\pi^2} \left(\sum_{j=\text{bosons}} n_j J_B \left[\frac{m_j^2(v_1, v_2)}{T^2} \right] + \sum_{j=\text{fermions}} n_j J_F \left[\frac{m_j^2(v_1, v_2)}{T^2} \right] \right) \quad (8.14)$$

$$T^4 J_B \left[\frac{m^2}{T} \right] = -\frac{\pi^4 T^4}{45} + \frac{\pi^2}{12} T^2 m^2 - \frac{\pi}{6} T (m^2)^{3/2} - \frac{1}{32} m^4 \ln \frac{m^2}{a_b T^2} + \dots \quad (8.15)$$

$$T^4 J_F \left[\frac{m^2}{T} \right] = \frac{7\pi^4 T^4}{360} - \frac{\pi^2}{24} T^2 m^2 - \frac{1}{32} m^4 \ln \frac{m^2}{a_f T^2} + \dots, \quad (8.16)$$

where $a_b = 16a_f = 16\pi^2 \exp(3/2 - 2\gamma_E)$ with γ_E being the Euler-Mascheroni constant.

The daisy term is defined as

$$V_{\text{daisy}}(T) = -\frac{T}{12\pi} \sum_{i=1} \left[(M_i^2(v_1, v_2, T))^{3/2} - (m_i^2(v_1, v_2))^{3/2} \right] \quad (8.17)$$

Details about the $M_i^2(v_1, v_2, T)$ term can be found in [12, 13]. Actually, we will see later that all these terms will be taken care of the software package we have used for this work.

At sufficiently high temperature, the total potential of eq.(8.3) has only one minimum at $\langle \Phi_1 \rangle = \langle \Phi_2 \rangle = 0$ and there is no symmetry breaking. The critical temperature (T_c) is defined as the temperature at which if the temperature drops down,

the total potential gets a second minimum at $(\Phi_{a,\min}) \equiv \{(\langle\Phi_1\rangle = v_1, \langle\Phi_2\rangle = v_2)\}$. For simplicity, we are assuming in this work that both of the Higgs field Φ_1 and Φ_2 get the second minimum at the same temperature T_c at the same time. Thus

$$V(\Phi_1 = 0, \Phi_2 = 0, T_c) = V(\Phi_1 = v_1, \Phi_2 = v_2, T_c). \quad (8.18)$$

As soon as the Higgs potential gets a non-zero minimum, the other relativistic particles start to gain mass and become non-relativistic. The reaction rate among them and also with photon becomes comparable with the Hubble parameter and thus decouples from relativistic plasma. The mass of the particle and coupling constant determine the decoupling temperature. For instance, top quark decouples earlier than electron or other quarks.

Now, at the time of EWPT the universe can be assumed as perfectly homogeneous and isotropic and thus we can neglect the spatial partial derivatives of the Higgs fields. Therefore, when the Higgs fields start to oscillate around their minima $(\Phi_{a,\min})$ then energy density ρ and pressure P are

$$\rho = \dot{\Phi}_{a,\min}^2 + V_{\text{tot}}(\Phi_1, \Phi_2, T) + \frac{g_* \pi^2}{30} T^4. \quad (8.19)$$

$$P = \dot{\Phi}_{a,\min}^2 - V_{\text{tot}}(\Phi_1, \Phi_2, T) + \frac{1}{3} \frac{g_* \pi^2}{30} T^4 \quad (8.20)$$

The last terms in eq.(8.19) and eq.(8.20) arise from the Yukawa interaction between fermions and Higgs bosons and from the energy density of the fermions, the gauge bosons, and the interaction between the Higgs and gauge bosons. g_* depends on the effective number of particles present in the relativistic soup at or near the EWPT. It's value in our model is greater than the value in SM.

Since the oscillation of Φ_a around $\Phi_{a,\min}$ is small compared to Hubble expansion, we can neglect the time derivative of $\dot{\Phi}_{a,\min}$ [11] for simplicity in this work.

Again, entropy density per comoving volume is defined as

$$s = \frac{\rho + P}{T} a^3 \quad (8.21)$$

which is conserved for relativistic species with negligible chemical potential. From eq.(8.19) and eq.(8.20) we get

$$\rho + P = 2\dot{\Phi}_{a,\min}^2 + \frac{4}{3} \frac{g_* \pi^2}{30} T^4 \quad (8.22)$$

As discussed earlier, g_* will change with the decoupling process and thus s for relativistic plasma will increase for our considered scenario. Then the increase in entropy can be calculated using conservation of energy momentum tensor

$$\dot{\rho} = -3H(\rho + P) \quad (8.23)$$

To solve eq.(8.23), we have used BSMPT [13,14], a C++ package to calculate the vacuum expectation value (VEV) of the total potential, value of the total potential at VEV for different temperatures including T_c . We have chosen the parameter in such a way so that $\text{VEV}/T_c > 0.02$. We have considered five sets of benchmark values and the corresponding figures are shown in Fig. 8.1

Table 8.1: 2HDM Benchmark points for entropy production

	m_h [GeV]	m_H [GeV]	m_{H^\pm} [GeV]	m_A [GeV]	$\tan \beta$	$\cos(\beta - \alpha)$	$m_{1/2}^2$ GeV ²	λ_1	λ_2	λ_3	λ_4	λ_5	T_c	v_{ev}/T_c	$\delta s/s[\%]$
BM 1	125	500	500	500	2	0	10^5	0.258	0.258	0.258	0	0	161.36	1.4	57
BM 2	"	"	485	500	2	0.00	10^5	0.258	.258	-0.23	0.49	0	153.27	1.25	53
BM 3	"	"	485	485	2	0.07	10^5	1.28	0.002	0.21	0.244	0.244	168.61	1.7	59
BM 4	"	485	485	485	10	0.1	23,289.6	3.9	0.22	3.9	0	0	230.18	1.86	70
BM 5	"	90	200	300	10	0	801.98	0.258	0.258	1.31	0.3	-1.35	135.38	1.06	37

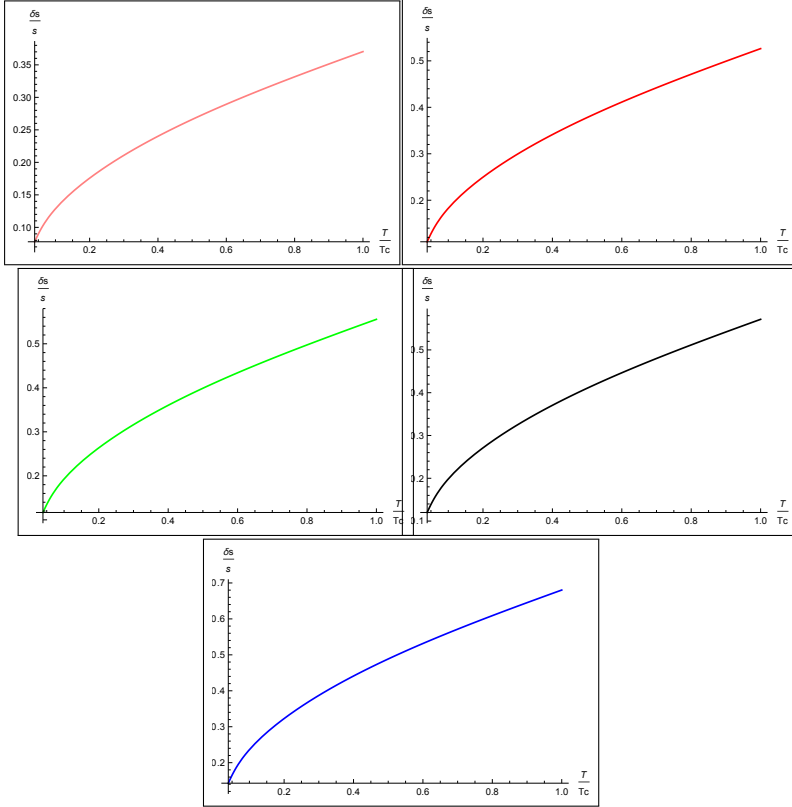


Fig. 8.1: The figures show the entropy production for five different benchmark (BM) points: Pink line (BM 5, $T_c = 135.38$ GeV and $\delta s/s = 37\%$), Red line (BM 2, $T_c = 153.27$ GeV and $\delta s/s = 53\%$), Green line (BM 1, $T_c = 161.36$ GeV and $\delta s/s = 30\%$), Black line (BM 3, $T_c = 168.61$ GeV and $\delta s/s = 59\%$), and Blue line (BM 4 $T_c = 230.18$ GeV and $\delta s/s = 70\%$).

8.3 Conclusion

As seen from Fig.8.1, the entropy productions for some benchmark points are shown here. A proper difference can be noticed from the standard model scenario. As seen in [11], the entropy released is around 13% and in the present scenario, we see that the production is considerably higher. This is because first-order phase transition as seen in 2HDM can release more entropy compared to smooth

crossover or second-order in the case of the standard model. The massive scalar particles in 2HDM contribute considerably to this production as well.

Acknowledgements

The work of S.P. and A.C. is funded by RSF Grant 19-42-02004. The research by M.K. was supported by the Ministry of Science and Higher Education of the Russian Federation under Project "Fundamental problems of cosmic rays and dark matter", No. 0723-2020-0040.

References

1. D. E. Morrissey and M. J. Ramsey-Musolf, *New J. Phys.* **14** (2012), 125003 doi:10.1088/1367-2630/14/12/125003 [arXiv:1206.2942 [hep-ph]].
2. A. Chaudhuri and M. Yu. Khlopov, *Universe* **7**, (2021) 8, 275 doi:10.3390/universe7080275 [arXiv:2106.11646 [hep-ph]].
3. B. Abi *et al.* [Muon $g-2$], *Phys. Rev. Lett.* **126** (2021) no.14, 141801 doi:10.1103/PhysRevLett.126.141801 [arXiv:2104.03281 [hep-ex]].
4. L. Wang and X. F. Han, *Phys. Lett. B* **739** (2014), 416-420 doi:10.1016/j.physletb.2014.11.016 [arXiv:1406.3598 [hep-ph]].
5. L. Wang and X. F. Han, *JHEP* **05** (2015), 039 doi:10.1007/JHEP05(2015)039 [arXiv:1412.4874 [hep-ph]].
6. A. Chaudhuri and M. Y. Khlopov, *MDPI Physics* **3** (2021) no.2, 275-289 doi:10.3390/physics3020020 [arXiv:2103.03477 [hep-ph]].
7. A. Chaudhuri, M. Y. Khlopov and S. Porey, *Galaxies* **9** (2021) no.2, 45 doi:10.3390/galaxies9020045 [arXiv:2105.10728 [hep-ph]].
8. O. Eberhardt, A. P. Martínez and A. Pich, *JHEP* **05** (2021), 005 doi:10.1007/JHEP05(2021)005 [arXiv:2012.09200 [hep-ph]].
9. S. Karmakar, *Springer Proc. Phys.* **248** (2020), 193-198 doi:10.1007/978-981-15-6292-1_23
10. G. C. Dorsch, S. J. Huber, K. Mimasu and J. M. No, *Phys. Rev. D* **93** (2016) no.11, 115033 doi:10.1103/PhysRevD.93.115033 [arXiv:1601.04545 [hep-ph]].
11. A. Chaudhuri and A. Dolgov, *JCAP* **01** (2018), 032 doi:10.1088/1475-7516/2018/01/032 [arXiv:1711.01801 [hep-ph]].
12. J. Bernon, L. Bian and Y. Jiang, *JHEP* **05** (2018), 151 doi:10.1007/JHEP05(2018)151 [arXiv:1712.08430 [hep-ph]].
13. P. Basler and M. Mühlleitner, *Comput. Phys. Commun.* **237** (2019), 62-85 doi:10.1016/j.cpc.2018.11.006
14. P. Basler, M. Mühlleitner and J. Müller, *Comput. Phys. Commun.* **269** (2021), 108124 doi:10.1016/j.cpc.2021.108124 [arXiv:2007.01725 [hep-ph]].
15. P. Basler, M. Krause, M. Mühlleitner, J. Wittbrodt and A. Wlotzka, *JHEP* **02** (2017), 121 doi:10.1007/JHEP02(2017)121 [arXiv:1612.04086 [hep-ph]].

Appendix A

The kinetic energy term of gauge bosons, kinetic energy of fermions and Yukawa interaction term of fermions with Higgs bosons are

$$\mathcal{L}_f = \sum_{\Psi=Q,L,u,d,l} i (\bar{\Psi}_L \not{D} \Psi_L + \bar{\Psi}_R \not{D} \Psi_R) \quad (8.24)$$

$$\mathcal{L}_{\text{Yuk}} = - [y_e \bar{e}_R \Phi_a^\dagger L_L + y_e^* \bar{L}_L \Phi_a^\dagger e_R + \dots] \quad (8.25)$$

$$\mathcal{L}_{\text{gauge,kin}} = -\frac{1}{4} G_{\mu\nu}^j G^{j\mu\nu} - \frac{1}{4} F_{\mu\nu}^B F^{B\mu\nu} \quad (8.26)$$

where Ψ is the fermionic field, subscript L (R) is for the left (right) chiral field. The sum in eq.(8.25) is also over quarks. y_e is the complex constant and

$$G_{\mu\nu}^j = \partial_\mu W_\nu^j - \partial_\nu W_\mu^j - g \epsilon^{jkl} W_\mu^k W_\nu^l \quad (8.27)$$

$$F_{\mu\nu}^B = \partial_\mu B_\nu - \partial_\nu B_\mu \quad (8.28)$$

$$\not{D} \Psi_{L,R}^{(j)} \equiv \gamma^\mu (\partial_\mu + ig W_\mu + ig' Y_{L,R} B_\mu) \Psi_{L,R}^{(j)} \quad (8.29)$$

8.4 Appendix B: Masses of new Scalars

$$c_i = \begin{cases} \frac{5}{6}, & (i = W^\pm, Z, \gamma) \\ \frac{3}{2}, & \text{otherwise} \end{cases} \quad (8.30)$$

Bosons	n_i	s_i	$m(v)^2$	
h	1	1	eigenvalues of 8.42	Higgs
H	1	1	eigenvalues of 8.42	Higgs
A	1	1	eigenvalues of 8.42	Higgs
G^0	1	1	eigenvalues of 8.42	Goldstone
H^\pm	2	1	Eq.8.34	Charged Higgs
G^\pm	2	1	Eq.8.35	Charged Goldstone
Z_L	1	1	Eq.8.32	Higgs
Z_T	2	2	Eq.8.32	Higgs
W_L	2	1	Eq.8.31	Higgs
W_T	4	2	Eq.8.31	Higgs
γ_L	1	2	Eq.8.33	
γ_T	2	2	Eq.8.33	

$$m_W^2 = \frac{g^2}{4} v^2. \quad (8.31)$$

$$m_Z^2 = \frac{g^2 + g'^2}{4} v^2. \quad (8.32)$$

$$m_\gamma^2 = 0. \quad (8.33)$$

$$\bar{m}_{H^\pm}^2 = \frac{1}{2} (\mathcal{M}_{11}^C + \mathcal{M}_{22}^C) + \frac{1}{2} \sqrt{4 \left((\mathcal{M}_{12}^C)^2 + (\mathcal{M}_{13}^C)^2 \right) + (\mathcal{M}_{11}^C - \mathcal{M}_{22}^C)^2} \quad (8.34)$$

$$\bar{m}_{G^\pm}^2 = \frac{1}{2} (\mathcal{M}_{11}^C + \mathcal{M}_{22}^C) - \frac{1}{2} \sqrt{4 \left((\mathcal{M}_{12}^C)^2 + (\mathcal{M}_{13}^C)^2 \right) + (\mathcal{M}_{11}^C - \mathcal{M}_{22}^C)^2} \quad (8.35)$$

where

$$c_1 = \frac{1}{48} (12\lambda_1 + 8\lambda_3 + 4\lambda_4 + 3(3g^2 + g'^2)) \quad (8.36)$$

$$c_2 = \frac{1}{48} \left(12\lambda_2 + 8\lambda_3 + 4\lambda_4 + 3(3g^2 + g'^2) + \frac{24}{v_2^2} m_t^2(T=0) \right) + \frac{1}{2v_2^2} m_b^2(T=0) \quad (8.37)$$

where $m_t(T=0) = 172.5\text{Gev}$ and $m_b(T=0) = 4.92\text{GeV}$. For our case ($v_3 = 0$),

$$\mathcal{M}_{11}^C = m_{11}^2 + \lambda_1 \frac{v_1^2}{2} + \lambda_3 \frac{v_2^2}{2} \quad (8.38)$$

$$\mathcal{M}_{22}^C = m_{22}^2 + \lambda_2 \frac{v_2^2}{2} + \lambda_3 \frac{v_1^2}{2} \quad (8.39)$$

$$\mathcal{M}_{12}^C = \frac{v_1 v_2}{2} (\lambda_4 + \lambda_5) - m_{12}^2 \quad (8.40)$$

$$\mathcal{M}_{13}^C = 0 \quad (8.41)$$

Masses of h , H and A are the eigen values of the matrix

$$\bar{\mathcal{M}}^N = (\mathcal{M}^N) \quad (8.42)$$

For our case ($v_3 = 0$),

$$\mathcal{M}_{11}^N = m_{11}^2 + \frac{3\lambda_1}{2} v_1^2 + \frac{\lambda_3 + \lambda_4}{2} v_2^2 + \frac{1}{2} \lambda_5 v_2^2 \quad (8.43)$$

$$\mathcal{M}_{22}^N = m_{11}^2 + \frac{\lambda_1}{2} v_1^2 + \frac{\lambda_3 + \lambda_4}{2} v_2^2 - \frac{1}{2} \lambda_5 v_2^2 \quad (8.44)$$

$$\mathcal{M}_{33}^N = m_{22}^2 + \frac{3\lambda_2}{2} v_2^2 + \frac{1}{2} (\lambda_3 + \lambda_4 + \lambda_5) v_1^2 \quad (8.45)$$

$$\mathcal{M}_{44}^N = m_{22}^2 + \frac{\lambda_2}{2} v_2^2 + \frac{1}{2} (\lambda_3 + \lambda_4 - \lambda_5) v_1^2 \quad (8.46)$$

$$\mathcal{M}_{12}^N = 0 \quad (8.47)$$

$$\mathcal{M}_{13}^N = -m_{12}^2 + (\lambda_3 + \lambda_4 + \lambda_5) v_1 v_2 \quad (8.48)$$

$$\mathcal{M}_{14}^N = 0 \quad (8.49)$$

$$\mathcal{M}_{23}^N = 0 \quad (8.50)$$

$$\mathcal{M}_{24}^N = -m_{12}^2 + \lambda_5 v_1 v_2 \quad (8.51)$$

$$\mathcal{M}_{34}^N = 0 \quad (8.52)$$

Table 8.2: Field dependent mass of all fermions

Fermions	n_i	s_i	$m_f(T=0)$	
e	4	$\frac{1}{2}$	$\frac{y_e}{\sqrt{2}}v_k$	lepton
μ	4	$\frac{1}{2}$	$\frac{y_\mu}{\sqrt{2}}v_k$	lepton
τ	4	$\frac{1}{2}$	$\frac{y_\tau}{\sqrt{2}}v_k$	lepton
u	12	$\frac{1}{2}$	$\frac{y_u}{\sqrt{2}}v_k$	quark
c	12	$\frac{1}{2}$	$\frac{y_c}{\sqrt{2}}v_k$	quark
t	12	$\frac{1}{2}$	$\frac{y_t}{\sqrt{2}}v_k$	quark
d	12	$\frac{1}{2}$	$\frac{y_d}{\sqrt{2}}v_k$	quark
s	12	$\frac{1}{2}$	$\frac{y_s}{\sqrt{2}}v_k$	quark
b	12	$\frac{1}{2}$	$\frac{y_b}{\sqrt{2}}v_k$	quark



9 Gravitational waves in the modified gravity

S. Roy Chowdhury¹

email : roic@sfedu.ru

M. Khlopov^{1,2}

email : khlopov@apc.in2p3.fr

¹Research Institute of Physics, Southern Federal University, Russia

²Université de Paris, CNRS, Astroparticule et Cosmologie, France; F-75013 Paris, France, and Center for Cosmoaprticle Physics Cosmion, National ResearchNuclear University “MEPHI”, 31 Kashirskoe Chaussee, 115409 Moscow, Russia

Abstract. We have taken a modified version of the Einstein Hilbert action, $f(R, T^\phi)$ gravity under consideration, where T^ϕ is the energy-momentum tensor trace for the scalar field under consideration. The structural behaviour of the scalar field considered varies with the form of the potential. The number of polarization modes of gravitational waves in modified theories has been studied extensively for the corresponding fields. There are two additional scalar modes, in addition to the usual two transverse-traceless tensor modes found in general relativity: a massive longitudinal mode and a massless transverse mode (the breathing mode).

Povzetek: V spremenjeni razli'v cici Einstein-Hilbertove akcije, $f(R, T^\phi)$, gravitacije, kjer je T^ϕ sled tenzorja energije in gibalne količine za obravnavano skalarno polje, študirajo pojav gravitacijskih valov.

Število polarizacij gravitacijskih valov v različicah teorije za izbrana skalarna polja je bilo doslej dobro raziskano.

Poleg običajnih dveh transverzalnih tenzorskih polarizacij gravitacijskih valov, ki jih predvidi splošna teorija relativnosti, obstajata še dva dodatna skalarna načina, ki ju avtorja opazita, ko spreminjata obliko skalarnega potenciala: masivni vzdolžni način in brezmasni prečni (dihalni) način.

9.1 Introduction

The FLRW metric is an exact solution to Einstein's equations, achieved under the implication of space homogeneity and isotropy. It has been well recognized for satisfactorily explaining several other observational evidence about our Universe, including the distribution of large-scale galaxies and the near-uniformity of the CMB temperature [1]. The FLRW metric [2] underpins the existing accepted cosmological model, which is quite good at likely fitting continued application data sets and trying to explain measured cosmic acceleration. The fact that the cosmological space-time metric differs from the FLRW metric would have massive consequences for inflation theory as well as fundamental physics.

Alternative explanations of gravity have long been considered to prevent a few of the contradictions in conventional cosmology [3, 4]. A potential substitute is the $f(R, T)$ gravity, created recently by Harko et al. [5]. The latest identification of gravitational waves (GWs) by the Advanced LIGO group has opened up a massive door to analyse the Universe. [6–8]. Apart from directly detecting GWs with LIGO/VIRGO interferometers, one could use the informal identification of GWs by assessing the substantial reduction of the orbital period of stellar binary configuration. Detecting nano-Hertz GWs with a pulsar timing array includes timing various millisecond pulsars, which seem to be extremely stable celestial clocks, according to Jenet [9]. This connection is effected by the angular distance (θ) between both the two pulsars, as well as the polarization of GW and graviton mass, according to $C(\theta)$ [10].

The range of the GW, including its polarization modes, is based on the theories. In the radiative domain, the polarization and dispersion of GWs in vacuum are two critical features of GWs that distinguish between the authenticity of gravity theories. GWs can also have up to six conceivable polarization states in substitute metric theories, four more than GR permits.

Hou et al. [11] carried out a detailed analysis of the polarization mode for the Horndeski theory. Using GWs polarization, Alves et al. [12] investigated the $f(R)$ framework. In $f(R)$ gravity metric methodology, the model, including other $f(R)$ theoretical models, confirms the effectiveness of scalar degrees of freedom. There is a scalar mode of polarization of GWs exists in theory. This polarization mode appears in two different states: a massive longitudinal mode and a transverse massless breathing mode with non-vanishing trace [13]. Capozziello and Laurentis [14] find the palatini formalism, conformal transformations and find the new polarization states for gravitational radiation for the higher order of extended gravity ($f(R) = R + \alpha R^2$) Later on, Alves et al. [15] studied for $f(R, T)$ and $f(R, T^\phi)$ theoretical models, .

In this article, we studied the polarization modes based on the potential, which is a function of the scalar field under the framework of modified gravity $f(R, T^\phi)$ for the vacuum system. In Sec. 9.2 we developed the basic formalism of the modified gravity. The scalar field structure and equation of motion is developed in Sec. 9.3. Polarization modes using Newman-Penrose (NP) formalism is analyzed Sec. 9.4. And in Sec. 9.5 we conclude the results.

9.2 Basic formalism of the modified gravity

In the context of modified gravity [5], for the vacuumed system, the total action including the scalar field can be introduced in the following manner,

$$S = \int d^4x \sqrt{-g} [f(R, T^\phi) + \mathcal{L}(\phi, \partial_\mu \phi)], \quad (9.1)$$

where R stands for the Ricci scalar, while T^ϕ is the trace of the scalar field's energy-momentum tensor.

The field's action, with g as the metric's determinant and signature $(-, +, +, +)$. We use geometric units with the formula $G = c = 1$.

Following that, we considered $\mathcal{L}(\phi, \partial_\mu \phi) = \mathcal{L}_\phi$. Here \mathcal{L}_ϕ is the standard Lagrangian density for a real scalar field (ϕ), as follow [16],

$$\mathcal{L}_\phi = \frac{1}{2} \nabla_\alpha \phi \nabla^\alpha \phi - V(\phi). \quad (9.2)$$

A self-interacting potential is represented by $V(\phi)$. In this theory, matter fields have a relatively limited coupling to gravity and no coupling to the scalar field. The stress-energy tensor can define as

$$T_{\mu\nu}^\phi = -\frac{2}{\sqrt{-g}} \frac{\delta(\sqrt{-g}\mathcal{L})}{\delta g^{\mu\nu}}. \quad (9.3)$$

We assumed that the Lagrangian density L is free of its derivatives and is only conditional on the metric tensor modules $g^{\mu\nu}$.

Therefore, the energy-momentum tensor of the scalar field is

$$T_{\mu\nu}^\phi = \frac{1}{2} g_{\mu\nu} \nabla_\alpha \phi \nabla^\alpha \phi - g_{\mu\nu} V(\phi) - \nabla_\mu \phi \nabla_\nu \phi, \quad (9.4)$$

and the corresponding trace is given by

$$T^\phi = \nabla_\alpha \phi \nabla^\alpha \phi - 4V(\phi). \quad (9.5)$$

The generalized form of the Einstein field equation in vacuum in the involvement of scalar field is obtained by varying the gravitational field's action S concerning the metric tensor components, $g_{\mu\nu}$, and then on integration as follow,

$$f_R R_{\mu\nu} - \frac{f}{2} g_{\mu\nu} = \frac{1}{2} T_{\mu\nu}^\phi + f_T T_{\mu\nu}^\phi - f_T g_{\mu\nu} \mathcal{L}_\phi \quad (9.6)$$

Here, $f_R = f_R(R, T^\phi)$ and $f_T = f_T(R, T^\phi)$ denotes $\partial f(R, T^\phi)/\partial R$ and $\partial f(R, T^\phi)/\partial T^\phi$, respectively.

We assume that the modified gravity function $f(R, T^\phi)$ is given by $f(R, T^\phi) = R + \beta T^\phi$, β is an arbitrary constant. The field equation immediately takes the following form,

$$G_{\mu\nu} = \frac{1}{2} [T_{\mu\nu}^\phi + g_{\mu\nu} \beta T^\phi - 2\beta \nabla_\mu \phi \nabla_\nu \phi]. \quad (9.7)$$

9.3 Scalar Field

On contraction and simplification, the Eq. (9.6) the Ricci scalar of can be obtained as follows,

$$R = -\frac{1}{2} [4\beta T^\phi + T^\phi - 2\beta \nabla_\mu \phi \nabla^\mu \phi] \quad (9.8)$$

The equation of motion for the scalar field can be found from the covariant divergence of the field Eq. (9.7) as follows,

$$(1 + 2\beta) \square \phi + (1 + 4\beta) \left(\frac{\partial V}{\partial \phi} \right) = 0. \quad (9.9)$$

Since we are considering the vacuum system, we consider the potential in the following form,

$$V(\phi) = \frac{1}{2}\mu^2\phi^2 + \frac{1}{4}\lambda\phi^4, \quad (9.10)$$

where, μ and λ are real constants.

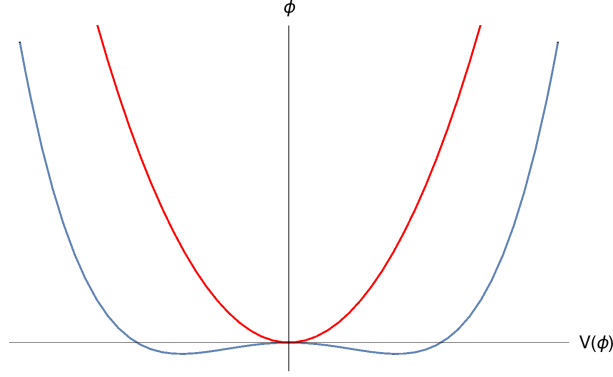


Fig. 9.1: variation of the potential $V(\phi)$ with scalar variable ϕ . Red curve shows the variation for $\mu^2 > 0$, and Blue curve shows the variation for $\mu^2 < 0$.

We limited ourselves to first-order terms in ϕ . The third term of Eq. (9.9) disappear as a result of this estimation. V is being expanded around the non-null minimum value V_0 . $\eta = \phi - \phi_0$ can be used to expand the field. Following identical approach as before, we encounter it with such assumptions and first-order restrictions,

$$\square\phi + \left(\frac{1+4\beta}{1+2\beta}\right)\left(\frac{\partial V}{\partial\phi}\right) = 0. \quad (9.11)$$

The field equations in the linear region has been investigated and leads to the solution in the following form,

$$\phi(x) = \phi' + \phi_1 \exp(iq_\rho x^\rho), \quad (9.12)$$

Solution of the scalar field corresponds to the above equation can be written as in Eq. (9.12) with,

$$\phi' = \phi_0 - \left(\frac{\mu^2 + \lambda\phi_0^2}{\mu^2 + 3\lambda\phi_0^2}\right)\phi_0, \quad (9.13)$$

and

$$q_\mu q^\mu = (\mu^2 + 3\lambda\phi_0^2)\left(\frac{1+4\beta}{1+2\beta}\right). \quad (9.14)$$

The variation of the effective mass (m_ϕ) with the coupling constant is shown in the Fig. 20.2. The restricted range is for $-0.50 \leq \beta \leq -0.25$, from Eq. (9.14).

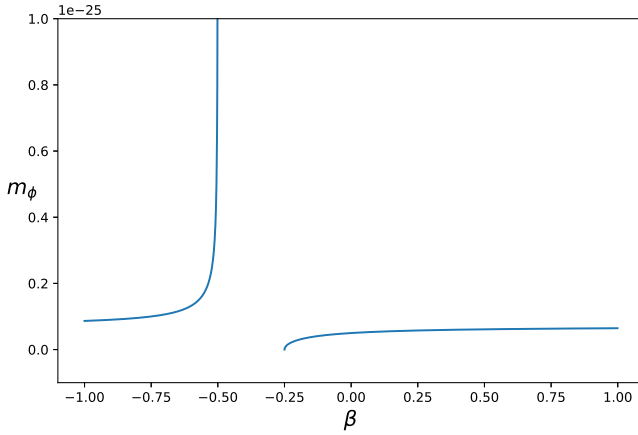


Fig. 9.2: variation of the mass function m_ϕ with coupling constant β .

Corresponding energy of the system can be written as

$$E = \pm \left[q^2 + (\mu^2 + 3\lambda\phi_0^2) \left(\frac{1+4\beta}{1+2\beta} \right) \right]^{1/2} \quad (9.15)$$

The first-order minimally coupled scalar field exposes an effective cosmological constant, as follows:

$$\Lambda = \frac{V_0}{2} (4\beta + 1). \quad (9.16)$$

With λ being a positive constant, the potential in Eq. (9.10) could be categorized into two situations: (i) $\mu^2 > 0$, and (ii) $\mu^2 < 0$. This is what the universe needs to be stable. While the minimum scalar field for $\mu^2 < 0$ is non-zero, the effective cosmological constant is non-zero. The cosmological constant that is effective is

$$\Lambda = -\frac{1}{2} \left[\beta \left(\frac{\mu^4}{\lambda} \right) + \frac{\mu^4}{4\lambda} \right]. \quad (9.17)$$

The steady minimum of the scalar field is zero for $\mu^2 > 0$, which causes the effective cosmological constant (Λ) to be zero.

9.4 Polarization modes of the modified gravity

Newman-Penrose formalism

The Newman-Penrose (NP) [17, 18] method is used to find additional polarization modes; further information is available in the references [19, 20]. Tetrads are a combination of standardized linearly independent vectors (e_t, e_x, e_y, e_z) that could be used to describe the NP quantities that correlate to all of the six polarization

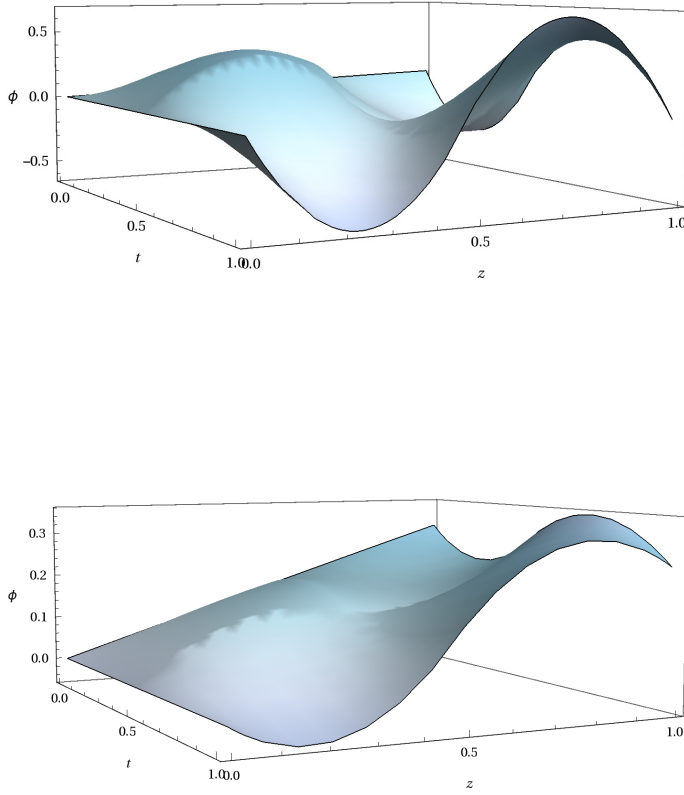


Fig. 9.3: Propagation for the perturbation of vacuum scalar field. Upper panel shows the variation for $\mu^2 < 0$, and lower panel shows the variation for $\mu^2 > 0$. Considered $\beta = 0.5$.

modes of GWs at any spatial position. The NP tetrads k, l, m, \bar{m} . can be used to recognize these vectors. The actual null vectors are as follows:

$$k = \frac{1}{\sqrt{2}}(e_t + e_z), \quad l = \frac{1}{\sqrt{2}}(e_t - e_z), \quad (9.18)$$

And the other two complex null vector are,

$$m = \frac{1}{\sqrt{2}}(e_x + ie_y), \quad \bar{m} = \frac{1}{\sqrt{2}}(e_x - ie_y). \quad (9.19)$$

$-k.l = m.\bar{m} = 1, \quad E_\alpha = (k, l, m, \bar{m}).$

While all other dot product vanishes.

In the NP notation, the indefinable components of the Riemann tensor $R_{\lambda\mu\kappa\nu}$ are defined by ten components of the Wey tensor (Ψ 's), nine components of the traceless Ricci tensor (Φ 's), and a curvature scalar (Λ). They are reduced to six by some symmetrical and differential properties: Ψ_2, Ψ_3, Ψ_4 and Φ_{22} are real and Ψ_3 and Ψ_4 are complex. These NP variables are associated with the following components of the Riemann tensor in the null tetrad basis:

$$\begin{aligned}\Psi_2 &= -\frac{1}{6}R_{lklk} \sim \text{longitudinal scalar mode,} \\ \Psi_3 &= -\frac{1}{2}R_{lkl\bar{m}} \sim \text{vector-x \& vector-y modes,} \\ \Psi_4 &= -R_{l\bar{m}l\bar{m}} \sim +, \times \text{ tensorial mode,} \\ \Phi_{22} &= -R_{lm\bar{l}\bar{m}} \sim \text{breathing scalar mode.}\end{aligned}\quad (9.20)$$

The additional nonzero NP variables are $\Phi_{11} = 3\Psi_2/2$, $\Phi_{12} = \Phi_{21} = \Psi_3$ and $\Lambda = \Psi_2/2$, respectively. All of them can be defined base on the variables in Eq. (9.20).

The group $E(2)$, the group of the Lorentz group for massless particles, can be used to classify these four NP variables Ψ_2, Ψ_3, Ψ_4 , and Φ_{22} based on their transformation properties. Only Ψ_2 is invariant, and the amplitudes of the four NP variables are not observer-independent, according to these transformations. The absence (zero amplitude) of some of the four NP variables, on the other hand, is not dependent on the observer.

The following relations for the Ricci tensor and the Ricci scalar hold:

$$\begin{aligned}R_{lklk} &= R_{lk}, \\ R_{lklm} &= R_{lm}, \\ R_{lkl\bar{m}} &= R_{l\bar{m}}, \\ R_{l\bar{m}l\bar{m}} &= \frac{1}{2}R_{ll}, \\ R &= -2R_{lklk} = 2R_{lk}.\end{aligned}\quad (9.21)$$

Following Eq. (9.6), the Ricci tensor can be written as,

$$R_{\mu\nu} = \frac{1}{2\alpha}[\alpha R g_{\mu\nu} + g_{\mu\nu} f(T^\Phi) + T_{\mu\nu}^\Phi - 2f_T \nabla_\mu \phi \nabla^\mu \phi] \quad (9.22)$$

Using Eq. (9.20) and Eq. (9.21), one finds the following Ricci tensors:

$$R_{lklk} \neq 0, R_{lm\bar{l}\bar{m}} \neq 0, R_{lklm} = R_{lkl\bar{m}} = 0.$$

From the above relation and Eq. (9.20), one finds the following NP quantities:

$$\Psi_2 \neq 0; \Psi_3 = 0; \Psi_4 \neq 0, \text{ and } \Phi_{22} \neq 0$$

Thus we get four polarization modes for the GW: $+, \times$ tensorial mode, breathing scalar mode and longitudinal scalar mode.

9.5 Conclusion

The theoretical foundations of modified gravity, a new approach intended to address and find solutions to the shortcomings and discrepancies of GR, are outlined in this report. These issues primarily manifest themselves at infrared and ultraviolet ranges, i.e., cosmological and astrophysical scales on the one hand and quantum scales on the other.

The stability analysis of the scalar field varies depending on the circumstances of potential, and we have taken into account the spontaneous symmetry breaking analogous potential for our structure. The scalar field's behaviour varies identification and characterization of the critical parameter (μ^2). The stable minimum value of the scalar field for $\mu^2 > 0$ is zero, resulting in a zero effective cosmological constant (Λ). For $\mu^2 < 0$, the minimum scalar field would be non-zero, and the effective cosmological constant is non-zero as well. The variation of potential is shown in Fig. 20.3. The $\mu^2 > 0$ variation is shown in red, whereas in blue coloured, the interpretation of $\mu^2 < 0$ is shown.

The scalar field Lagrangian is taken in conjunction may emerge a new set of Friedmann equations. Due to a mathematical constraint, the effective mass has a finite discontinuity. It is found for the range $-0.50 \leq \beta \leq -0.25$ effective mass is discontinuous. The variation is shown in Fig. 20.2.

The post-Minkowskian constraint of modified gravity, the problem of gravitational radiation, also deserves careful consideration. When the gravitational action is just not Hilbert–Einstein, new polarizations emerge: in general, massive, massless, and ghost modes must be considered, whereas, in GR, only massless modes and two polarizations are present. This result necessitates a rethinking of GW physics. If GWs have nontensorial polarization modes, as mentioned, an analyzed signal, such as a stochastic cosmological background of GWs, would be an integration of each of these modes.

In Einstein's General Relativity, the plus and cross modes of polarization are quite common. The plus mode is depicted by $P_+ = R_{txtx} + R_{tyty}$, the cross mode by $P_\times = R_{txty}$, the vector-x mode by $P_{xz} = R_{txtz}$, the vector-y mode by $P_{yz} = R_{tytz}$, and the longitudinal mode by $P_l = R_{tztz}$, and the transverse breathing mode by $P_b = R_{txtx} + R_{tyty}$. For the form of potential $V(\phi) = \frac{1}{2}\mu^2\phi^2 + \frac{1}{4}\lambda\phi^4$, in the frame of modified gravity $f(R, T^\phi) = R + \beta T^\phi$, we obtain four polarization modes of GWs exists: +, \times tensorial mode, breathing scalar mode and longitudinal scalar mode, respectively.

Acknowledgements

The southern federal university supported the work of SRC (SFedU) (grant no. P-VnGr/21-05-IF). SRC is also thankful to Ranjini Mondol of IISc, Bangalore, for the fruitful discussion to improve the manuscript.

References

1. Planck Collaboration and P. A. R. Ade et al., *A & A* **594**, A13 (2016).

2. S. Cao et al., *Scie. Reports* **94**, 11608 (2019).
3. T. Clifton, P. G. Ferreira, A. Padilla, and C. Skordis, *Phys. Reports* **513**, 1 (2012).
4. T. Padmanabhan, *Phys. Reports* **380**, 235 (2003).
5. T. Harko, F. S. N. Lobo, S. Nojiri, and S. D. Odintsov, *Phys. Rev. D* **84**, 024020 (2011).
6. B. P. Abbott et al. (LIGO Scientific Collaboration and Virgo Collaboration), *Phys. Rev. Lett.* **116**, 061102 (2016).
7. B. P. Abbott et al. (LIGO Scientific Collaboration and Virgo Collaboration), *Phys. Rev. Lett.* **119**, 161101 (2017).
8. B. P. Abbott et al. (LIGO Scientific Collaboration and Virgo Collaboration), *Astrophys. J. L* **848**, L12 (2017).
9. F. A. Jenet, G. B. Hobbs, K. J. Lee, and R. N. Manchester, *Astrophys. J.* **625**, L123 (2005).
10. K. J. Lee, F. A. Jenet, and R. H. Price, *Astrophys. J.* **685**, 1304 (2008).
11. Y. Hou, S. Gong and Y. Liu, *Eur. Phys. J. C* **78**, 378 (2018).
12. M. Alves, O. Miranda, and J. de Araujo, *Phys. Lett. B* **679**, 401 (2009).
13. D. J. Gogoi and U. DevGoswami, *Eur. Phys. J. C* **80**, 1101 (2020).
14. S. Capozziello, M. De Laurentis, *Physics Reports* **509**, 167 (2011).
15. M. E. S. Alves, P. H. R. S. Moraes, J. C. N. de Araujo, and M. Malheiro, *Phys. Rev. D* **94**, 024032 (2016).
16. P. H. R. S. Moraes and J. R. L. Santos, *Eur. Phys. J. C* **76**, 60 (2016).
17. E. Newman and R. Penrose, *J. Math. Phys.* **3**, 566 (1962).
18. E. Newman and R. Penrose, *J. Math. Phys.* **4**, 998 (1963).
19. D. M. Eardley, D. L. Lee, and A. P. Lightman, *Phys. Rev. D* **8**, 3308 (1973).
20. D. M. Eardley et al., *Phys. Rev. Lett.* **30**, 884 (1973).



10 Representing rational numbers and divergent geometric series by binary graphs

E. Dmitrieff

email: elia@quantumgravityresearch.org, elia@linden.institute

Irkutsk State University

Abstract. We consider digital (mostly binary) representations of rational numbers as explicit finite graphs, meaning digits as nodes, and expressing their positioning with directed edges. Following the symmetries of graphs, we found out that some divergent geometric series also can be represented this way as finite graphs. They manifest arithmetical properties that allow us to map them onto the set of negative fractions with odd denominators. Their values appear the same with results of sum formula $S = \frac{1}{1-b}$ continued to the range of common rates b exceeding 1. We suppose that these series in fact converge when they are expressed declarative as graphs, while the divergence is connected to the character of the sum operator, that can be in some cases avoided.

Povzetek: Avtor predstavi racionalna (večinoma binarna) racionalna števila kot končne grafe, kjer ševilke določajo vozle in robovi usmerjenost. Ugotovi, da lahko nekatere divergentne vrste predstavi s končnimi grafi s simetrijo, ki omogočajo preslikavo na množico negativnih ulomkov z lihimi imenovalci. Njihove vsote so izrazljive z enačbo $S = \frac{1}{1-b}$, ko b preseže vrednost 1. Avtor domneva, da te vrste, predstavljene z grafi, dejansko konvergirajo, divergentnost pa poveže z načinom iskanja vsote vrste, čemur se je v nekaterih primerih mogoče izogniti.

10.1 Overview of numeric representations and graphs

Representation of integer and rational numbers by sequences of digits is the common way to visualize, express and manipulate them. Real numbers in practical applications are usually approximated by rationals, that also assumes using their digital representations.

The way the numbers being written is following some rules. They establish relationships between digits that can be, in principle, expressed explicitly. We review here the rules of writing numbers focusing on expressing them in the declarative style, as graphs.

10.1.1 Digital representation of a number

The number a is mapped to the ordered sequence of digits a_i , usually written as a string from left to right. Digits are elements of a finite set isomorphic to \mathbb{Z}_b , where b is called the base of the representation.

By default, the base $b = 10$ and the digit set is $\{0, 1, \dots, 9\}$.

It is assumed that the represented number can be calculated as a sum of base's powers with digits' numeric values as factors:

$$a = \dots a_n a_{n-1} a_{n-2} a_{n-3} \dots a_1 a_0 . a_{-1} a_{-2} \dots = \sum_{i=-\infty}^{\infty} a_i b^i. \quad (10.1)$$

To mark the place of digit a_0 that corresponds to the 0^{th} power of the base, the *point* or comma symbol is used. The point can be omitted. In this case, it is implicitly assumed after the last written digit, so the number expressed this way is an integer.

10.1.2 Calculability of representations

Note that the sum with infinite starting index can *not* be calculated directly since the starting digit in the position $-\infty$ is unreachable.

However, in most practical cases, the leading, or trailing digits, or both are all zeroes, so they are omitted. The remaining finite number of 'significant' digits are usually written. This sum $\sum_n^m a_i b^i$ can be calculated following (10.1), producing the represented rational number. The infinite sum with the most significant digit but without the less significant one also can be calculated iterating from the m^{th} power down:

$$\sum_{i=-\infty}^m a_i b^i = \sum_{i=-m}^{\infty} a_{-i} b^{-i} = \lim_{n \rightarrow \infty} \sum_{i=-m}^n a_{-i} b^{-i} = a. \quad (10.2)$$

It converges to the represented number, that is in this case real. The calculation can be stopped when the desired precision is reached.

On another hand, the sum having no most significant digit

$$\sum_{i=n}^{\infty} a_i b^i = \lim_{m \rightarrow \infty} \sum_{i=n}^m a_i b^i = \infty \quad (10.3)$$

is not limited from above and diverges. In most cases it is treated as having no meaning, but in some applications it is possible to re-normalize some infinities, obtaining finite results by using special tricks.

10.1.3 Splitting into integer and fractional parts

There is other way to make the sum (10.1) calculable, that has the advantage of symmetry. Namely, the sequence of digits is splitted in two parts by the point. The left part, starting with 0^{th} power, is integer, and the right part, starting with -1^{th} power, is fractional:

$$a = \sum_{i=-\infty}^{\infty} a_i b^i = \sum_{i=0}^{\infty} a_i b^i + \sum_{i=1}^{\infty} a_{-i} b^{-i}. \quad (10.4)$$

Both parts are sequences of digits starting at the point. The calculations can be performed recurrently with the same initial power b^0 that is 1, and with the same

algorithm. It includes finding current power of b , multiplying it to the current digit's value and accumulating the sum.

The difference is just in the b power modification on each iteration, that is the post-multiplication by b for integer, and the pre-division by b for fraction part.

Note that there is exactly one bit of information that is required to determine whether the part is integer or fractional.

Also note that the integer parts sequences should have leading zeros on the left to avoid divergence, while the fractional part may end with either trailing zeroes or *nines* (for binary numbers, *ones*) since both converge.

10.1.4 Non-equivalence of numbers and their representations

The tradition of representing numbers in the form of digital symbol chains has become so well established, that it is sometimes perceived as the only conceivable or natural way of expressing a particular number. In practice, in the mind digital strings often actually replace original numbers that they represent.

However, there are some differences between them:

- The map of numbers to digital sequences is not bijective. Leading zeroes for integers, and also trailing zeroes for finite rationals, can be freely added or eliminated without affecting the represented value. Being omitted in writing, they appear back when they are needed to perform a digit-wise calculations.
- It is known that in decimal representations ($b = 10$) the least significant digit, that resides just before the trailing zeroes, can be decreased by one together with replacing of all these zeroes with nines, for instance:

$$5.3840000 \dots = 5.3839999 \dots \quad (10.5)$$

It can be proved by taking the limit of the sum in (10.1).

So, the integers, and also fractional rational numbers with denominators of 10^n , $n \in \mathbb{N}$ can be decimal-represented in two different ways. Zeroes (that are omitted) are preferred to nines for convenience reasons.

Representations with other bases also have this effect. In case of base=2 trailing zeros and ones are the only possible cases of repeating digits.

- The negative numbers have no representations in the sense noted above. It is obvious because all the factors are non-negative. Instead, conventional representations of positive numbers are used, preceded by the extra (*non-digital*) minus sign, for instance “ -0.155 ”. This sign has a meaning of subtraction operation $0 - a$, that should be applied to this positive number to make it negative.

This problem becomes serious in digital computers, that have native digits 0 and 1 but do not have any native minus sign.

Luckily this problem has been gracefully solved by implementing the so-called two's complement encoding [1], that involves leading *ones* that is the binary equivalent of *leading nines*.

In our opinion, this solution is not just a useful trick but it sheds some light on the mathematical nature of numbers.

10.1.5 Loops in rational numbers representations

Unlike the irrationals, rational numbers with denominators other than 10^n are represented by infinite sequences of digits (that are finite-periodic). These sequences are conventionally written using some extra non-digital symbols, for instance $2\frac{1}{7} = 2.1428571428\dots = 2.\overline{142857} = 2.(142857)$. In vague writing, and also often in calculators and computers they are implicitly rounded or truncated without any notice to the nearest finite decimal number, that sometimes may cause computational errors.

These additional parenthesis or lines applied to help keeping the representations finite and writable. Without them the loops and infinite chains would not be writable on paper or in computer memory.

So these representations are either non-writable infinite sequences, or they are not pure sequences of digits if they are decorated by extra non-digital symbols to make them finite.

10.1.6 Graphs

Graphs are mathematical objects that correspond to the common-sense concept of entities interconnected to each other by some relations.

The graph is a set of nodes, and the nodes can be explicitly related to each others by edges. Both nodes and edges can be weighted, i.e. carry some additional information.

Generally, graph may consist of one or more connectivity components, nodes of which are *connected* to each other through some path of edges (may be, through intermediate nodes), but nodes from different components have no such connection. We consider here the special, limited kind of graphs that have all the edges directed (weighted with one bit of information about direction), and all the nodes also weighted with one binary digit.

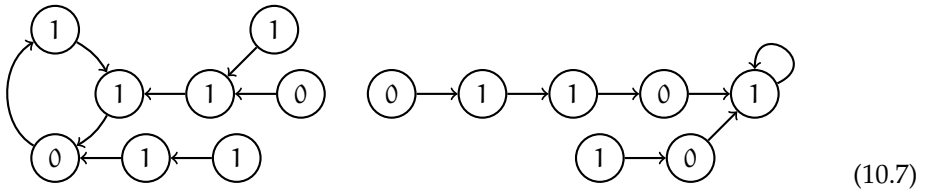
Such a graph we call a *binary graph* [3].

In order to represent numbers, we restrict the freedom of graphs a little more, by requirement that each node has one and only one outgoing edge, meaning that when standing on the particular node, the next node is always known.

The edge must end on some node. When it ends on the same node, it is the shortest loop:

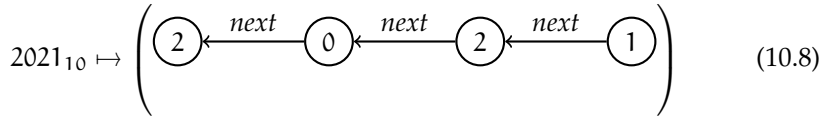


With this restriction, the graph has well-known structure [2]. Each connectivity component has the only loop with trees on its nodes. The loop can be of one node and the tree can have a form of the linear sequence.



10.2 Converting numbers into graphs

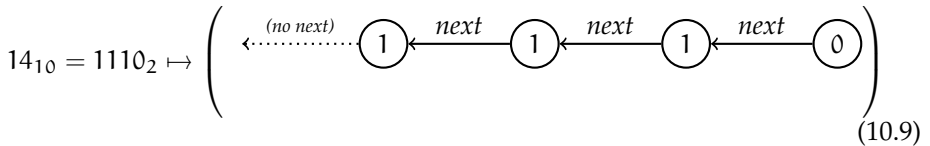
We see that number representations in form of strings of digits have the structure similar to linear graphs. The digits corresponding to nodes are followed by (related to) other digits:



Here we convert numbers of several kinds into graphs.

In this paper, we consider only *binary* graphs as representations of numbers, so the rules for the conversion are the following:

- the base $b = 2$, so the digits are bits with values in the set $\mathbb{Z}_2 = \{0, 1\}$,
- all graph nodes are weighted, and the weight is always one explicit bit - either 0 or 1.
- the implicit connections between digits in the sequence are expressed explicitly by directed edges,
- edges follow the symmetrical calculation scheme of (10.4), starting from the *point* towards the positions of higher powers by magnitude.



As noted before, each node is equipped with an outgoing edge.

This requirement fixes the possible structure of graph connectivity component that now can contain a forest of one or more directed trees or sequences, terminated by one loop.

To satisfy the requirement, the last node of the graph (10.9) should also be terminated by a loop that represent trailing zeroes. The loop can be the minimal, containing one zero node.

10.2.1 Positive integers

To build the binary-graph representation of a positive integer number, we simply treat the bits of the binary representation as nodes, and explicitly apply the

edges between them, in the order of the bits in the string. The leading zeros are represented by one additional self-cycled zero-bit:

$$14_{10} = (0)1110_2 \mapsto \begin{array}{c} \textcircled{0} \leftarrow \textcircled{1} \leftarrow \textcircled{1} \leftarrow \textcircled{1} \leftarrow \textcircled{0} \\ \uparrow \\ \textcircled{0} \end{array} \quad (10.10)$$

We can see that any linear binary graph with the zero terminating loop of one node corresponds to the binary representation of an integer number.

It is not strong bijection since one could 'unwind' one or more zeroes from the loop into the linear part without affecting the numeric value.

$$\begin{array}{c} \textcircled{0} \leftarrow \\ \uparrow \\ \textcircled{0} \end{array} \sim \begin{array}{c} \textcircled{0} \leftarrow \textcircled{0} \leftarrow \\ \uparrow \\ \textcircled{0} \end{array} \quad (10.11)$$

10.2.2 Positive binary fractions

There is the mirror symmetry between finite integers and fractional parts of the representation. Since that they are linear, the difference is only in the the *Next* operation. According to this symmetry, the graphs corresponding to integers also can be mapped to positive binary fractions, $0 \leq a < 1$, with the denominator 2^n . We re-write the graph (10.10) from left to right, as fractions are usually written, to show this correspondence:

$$\frac{7}{16}_{10} = .0111(0)_2 \mapsto \begin{array}{c} \textcircled{0} \rightarrow \textcircled{1} \rightarrow \textcircled{1} \rightarrow \textcircled{1} \rightarrow \textcircled{0} \\ \uparrow \\ \textcircled{0} \end{array} \quad (10.12)$$

10.2.3 Negative integers

According to the *two's complement* encoding consideration, negative integers can be represented by performing the subtraction of their magnitude from zero (ignoring the carry bit). The leading zeroes turns into the leading ones. The same result is achieved by inversion of all the bits and incrementing by one.

This representations is focused on the arithmetic: the addition and subtraction are performed the same way as with positive numbers, so they can be mixed in expressions and computations. For instance, adding 1 to -1 gives 0:

$$-1 + 1 = (1). + (0)1. = \dots 1111. + \dots 0001. = [\text{carrybit}] \dots 0000. = 0 \quad (10.13)$$

The carry bit gets "lost in the infinity". In the graph form there is no infinity and after two bit additions the calculation ends and the carry bit is discarded.

Subtracting positive numbers from the binary representations of 0 or -1, we always get representations with leading ones, or graphs with the looped one.

Thus, negative integers can be mapped to linear binary graphs terminated with the loop of node 1.

$$-14_{10} = (1)0010_{2} \mapsto \begin{array}{c} \text{loop} \\ \circlearrowleft \\ \text{1} \leftarrow \text{0} \leftarrow \text{0} \leftarrow \text{1} \leftarrow \text{0} \end{array} \quad (10.14)$$

10.2.4 Reflected negative integers are again the positive binary fractions

Making the same reflection as with positive integers (that is, in fact, just rewriting from left to right) we do not get representations of negative fractions. Instead, we get another representations of positive binary fractions, this time with trailing 1s. To get the same value, two bits are inverted: the bit in the loop, zero to one, and the last bit before loop - one to zero.

$$\frac{7}{16}_{10} = .0110(1)_{2} \mapsto \begin{array}{c} \text{loop} \\ \circlearrowright \\ \text{0} \rightarrow \text{1} \rightarrow \text{1} \rightarrow \text{0} \rightarrow \text{1} \end{array} \quad (10.15)$$

10.2.5 Non-binary fractions

In case the loop consist of two or more nodes, the corresponding binary fraction is periodic, so it maps to geometric series that converges to some fraction with the denominator that is not the power of 2:

$$\begin{array}{c} \text{0} \rightarrow \text{1} \rightarrow \text{1} \rightarrow \text{0} \rightarrow \text{1} \\ \text{loop} \end{array} \mapsto .011(01)_{2} = \frac{3}{8} + \frac{1}{8} \sum_{i=1}^{\infty} \frac{1}{4^i} = \frac{5}{12} \quad (10.16)$$

$$\begin{array}{c} \text{0} \rightarrow \text{1} \rightarrow \text{1} \rightarrow \text{1} \\ \text{loop} \end{array} \mapsto .01(101)_{2} = \frac{1}{4} + \frac{1}{4} \sum_{i=1}^{\infty} \frac{5}{8^i} = \frac{3}{7} \quad (10.17)$$

Each loop of N nodes gives fractions with the denominator $2^N - 1$. Probably there always exists such N that $2^N - 1$ has an arbitrary divisor d, to ensure that each rational fraction $0 \leq a < 1$ can be represented by the finite binary graph. If the fraction has even denominator, the representation must be shifted right according with the power of two in the denominator.

10.2.6 Irrational numbers

Irrational numbers in their digital representations have infinite tail of non-repeating digits on the right side. Corresponding binary graphs would also be infinite, having no loops. We did not focus on them since we interested namely in closed forms. To be practically usable, they may be rounded up into finite graphs (representing rational fractions) by switching the end of some node's outgoing edge, instead of the next node, to some previous one or to self, forming a loop. So the rounding has here the literal meaning of closure the sequence into the circle.

The length of this loop determines denominator of the rational number, as noted above (10.2.5). Taking in account the local quasi-periodicity of digits, one can choose optimal place and loop length for rounding, getting rational approximations with the size and precision balanced.

For instance, the binary representation of

$$\pi \approx 11.00100\ 10000\ 11111\ 10110\ 10101\ 00010\ 00100\ 00101\ 10100\dots \quad (10.18)$$

can be cut in any place and looped back. Doing so after the 3rd position and looping back to the 1st one, we exploit the repeating sequence (001) $\mapsto \frac{1}{7}$. Here 1 is the value represented by 001 and $7 = 2^3 - 1$ follows from the length of the loop. The corresponding rational value is $3 + \frac{1}{7} = 3.(142857)$.

Looping to self in the 7th position we get the finite binary fraction with trailing zeros: $11.001001(0) = 3 + \frac{9}{64} = \frac{201}{64} = 3.140625$.

The repeating 1s starting from the 11th position allow to get

$$11.0010010000(1) = 3 + \frac{144}{1024} + \frac{1}{1024}, \text{ or} \quad (10.19)$$

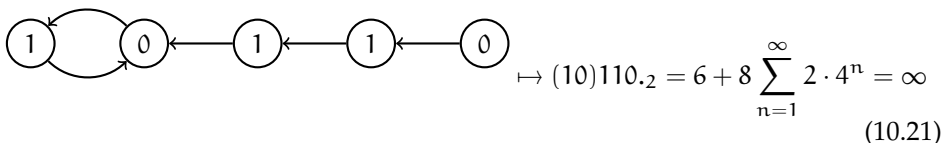
$$11.0010010001(0) = 3 + \frac{145}{1024} = 3.1416015625. \quad (10.20)$$

By cutting the tail in the 20th position, where the pattern 01 repeats three times, and rounding 2 nodes back, we get the loop (01) $\mapsto \frac{1}{3}$ and the result is $3 + \frac{74235}{54288} + \frac{1}{2^{20}} \frac{1}{3} \approx 3.1415923$.

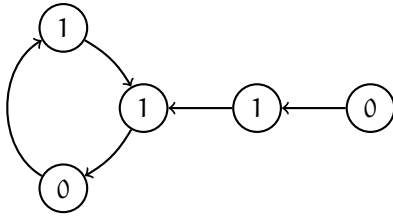
10.2.7 Reflections of non-binary fractions

We consider here the reflections of graphs (10.17) corresponding to the fractions. Rewritten right to left, they map to infinite geometric series that now have the common ratio $b = 2$ instead of $\frac{1}{2}$. These series are divergent, but representing binary graphs are still finite. They terminate with the loop that contains different bits (Thus, the minimal length of the loop is 2 because loops 11 and 00 can be replaced by 1 and 0, respectively).

Consider the following examples:



Here $6 = 0 \cdot 2^0 + 1 \cdot 2^1 + 1 \cdot 2^2$ comes from the linear part of the graph, $8 = 2^3$ arises because the loop begins in the 3rd place (shift by one position to the left is multiplication by 2), 2 is the value of bits 1 and 0 in the loop and the 4 in the power base is used because the loop size is 2 and each iteration is shifted left for two positions, so that is the multiplication by 4.



$$\mapsto (101)10.2 = 2 + 4 \sum_{n=1}^{\infty} 5 \cdot 8^n = \infty \quad (10.22)$$

Again, 2 is linear part, the loop is shifted left twice, so the factor before sum is $2^2 = 4$, the loop "101" is 5 and the loop length of three digits shifts this 5 three times left on each iteration.

We can see that despite of the divergence of the series, that comes from the loop, and the formal infinite sum as the result, the graphs of such a form keep their individuality. The set of such graphs is as rich as set of rationals in the segment $(0; 1]$.

10.2.8 Arithmetic of divergent series in the graph form

Consider two "divergent" graphs of the kind 10.2.7:

$$A = \begin{array}{c} \text{1} \quad \text{0} \\ \curvearrowright \quad \curvearrowleft \\ \text{0} \quad \text{1} \end{array} \quad \mapsto (10). = \dots 10101010. = \sum_{n=0}^{\infty} (2 \cdot 4^n) = \infty \quad (10.23)$$

and

$$B = \begin{array}{c} \text{0} \quad \text{1} \\ \curvearrowright \quad \curvearrowleft \\ \text{1} \quad \text{0} \end{array} \quad \mapsto (01). = \dots 01010101. = \sum_{n=0}^{\infty} 4^n = \infty \quad (10.24)$$

They are the same (consisting of the loop of 1 and 0 only), excepting that the starting *point* points to different nodes.

Binary representation of A can be produced from B by shifting left once, so

$$A = 2B. \quad (10.25)$$

They can be added with the usual way. Since there is no carry, the result is obvious:

$$A + B \mapsto (10). + (01). = (11). = (1). = \dots 1111. \mapsto -1. \quad (10.26)$$

In the binary representation it is an infinite sequence of leading ones, that is mapped to -1 (10.2.3).

Combining with (10.25) we get $A \mapsto -\frac{2}{3}, B \mapsto -\frac{1}{3}$

The same result we get when applying the formula of convergent geometric series sum, $S = 1/(1 - q)$:

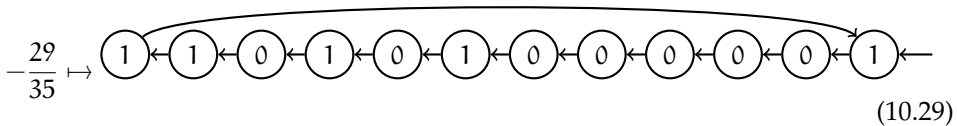
$$B = \sum_{n=0}^{\infty} 4^n = \frac{1}{1-4} = -\frac{1}{3}. \tag{10.27}$$

Addition of graphs representing negative numbers can be more complicated in case of different loop lengths. It corresponds to the addition of fractions with different denominators.

To perform this addition, one must first turn the denominators into the form $2^N - 1$, that would be its multiple. Then both operands are denormalized by explicit repetition of their loops, making them equal-sized. Maximal length of loop is the product of lengths of the operands' loops:

$$\begin{aligned} -\frac{2}{5} - \frac{3}{7} &= -\frac{6}{15} - \frac{3}{7} \mapsto (0110). + (011). \\ &= (011001100110). + (011011011011). = \\ &= (110101000001). \mapsto -\frac{3393}{4095} = -\frac{29}{35}. \end{aligned} \tag{10.28}$$

In this example 4-loop and 3-loop, repeated 3 and 4 times, become 12-loops, that corresponds to denominator $2^{12} - 1 = 4095$. Adding 12-loops node-by-node with carrying, we get the result in the form of 12-loop.



In the case of carry in the loop, that occurs to the *pointed* node, it must be avoided by unwinding turns of the chain:

$$\begin{aligned} -\frac{4}{5} - \frac{6}{7} &= -\frac{12}{15} - \frac{6}{7} \mapsto (1100). + (110). \\ &= (110011001100). + (110110110110). = \\ &= (101010000011)101010000010. = \\ &= (110101000001)0. \mapsto -1\frac{23}{35}. \end{aligned} \tag{10.30}$$

The carry bit that goes from the "most significant" bit of the loops sum, is added to the "least significant" bit of it, again. This process is not repeated since there are zeroes inside, stopping the carry.

But the carry bit must not be added to the first instance of the loop, that follows the point. To avoid it, one turn is unwinded, and in it the zero in the first position is kept.

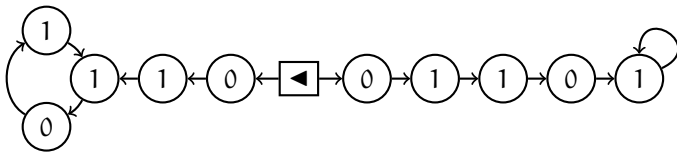
We can see that there is no need to unwind the whole turn, so eleven nodes can be winded back to the loop.

This avoiding of addition of carry bit is in fact the same operation as subtraction of one, and it is reflected in the result.

10.3 Discussion

From examples above we can see that negative rational numbers, which can be represented by the single-component graphs having non-trivial loop, are not limited by range $-1 < a < 0$ but can contain both integer and fractional parts. However, the negative numbers with denominators containing 2 as a divisor, are not representable by graphs of the kind considered, since the common denominator $2^N - 1$ is odd.

It is not strict limit. The rational numbers having both integer and fractional part are also non-representable by just one of them. So the negative numbers with 2 in denominators can be effectively represented by shifting digits from the left, "integer" part, to the right, "fractional" one. The right shift is the operation of division by 2, so all the powers of 2 can be excluded from the left part this way. The general form of the graph representing a number seems to be two symmetric components discussed above, together with special non-digital node explicitly representing the point. This node has *two* outgoing edges instead of usual one, but no explicit bits weighting the node:



(10.31)

The symmetry is broken by one implicit bit of information encoded by the point. This bit determines, along which edge the power of base must rise, i.e. which outgoing edge points to the left, "integer" component, and which points to the "fractional", right. Note that in most cases there is no extra information carried by the point, since in the absence of point the starting nodes of both components can be determined by the absence of incoming edges.

10.4 Summary and Conclusion

We found out that at least some finite binary graphs with non-trivial loop can be mapped to the set of negative rational numbers.

These graphs allow some arithmetic on them that is similar to usual arithmetic of the integers.

Another result is that some divergent geometric series can be represented by finite binary graphs.

As a combination, we have the way to obtain finite and meaningful numeric values for some divergent series instead of useless infinities. The key point here is avoiding repetitive carries between nodes.

This result may meet its application as a method of renormalization of infinities that arise in some models in the theoretical physics.

Some other graphs also have quasi-numerical meaning and this feature can be studied more systematically. For instance, the *pointless* loops and non-linear trees can be mapped to multi-valued objects such as colors in chromodynamics [3] or rational matrix eigenvalues.

References

1. D.E.Knuth, "The Art of Computer Programming: Seminumerical algorithms", Addison-Wesley, Reading - Massachusetts (1997).
2. Arnold, V. I. "Topology and statistics of arithmetic and algebraic formulae." (2003).
3. E.G. Dmitrieff: Experience in modeling properties of fundamental particles using binary codes, in: N.S. Mankoč Borštnik, H.B.F. Nielsen, D. Lukman: Proceedings to the 19th Workshop 'What Comes Beyond the Standard Models', Bled, 11. - 19. July 2016.



11 Neutrino masses within a SU(3) family symmetry and a 3+5 scenario

Albino Hernandez-Galeana
e-mail: ahernandez@ipn.mx

Departamento de Física, ESFM - Instituto Politécnico Nacional, U. P. "Adolfo López Mateos". C. P. 07738, Ciudad de México, México

Abstract. Within a broken local vector-like SU(3) family symmetry, we address the problem of quark masses and mixing in a framework with five sterile neutrinos.

Heavy fermions, top and bottom quarks and tau lepton become massive at tree level from see-saw mechanisms implemented by the introduction of a new set of SU(2)_L weak singlets vector-like fermions U, D, E, N, with N a neutral lepton. The fermion content also include three right handed neutrinos. Therefore, in this scenario light quarks and leptons, including active neutrinos, become massive from radiative loop corrections mediated by the massive SU(3) gauge bosons.

We correct the number of neutrino free parameters, update numerical results and report the non-unitary $(U_{PMNS})_{4 \times 8}$ lepton mixing matrix.

Povzetek: Avtor obravnava mase in mešalno matriko kvarkov v modelu z lokalno družinsko simetrijo SU(3) ter ustreznimi umeritvenimi polji, katerih simetrijo zlomi, doda pa še pet sterilnih nevtrinov. Fermioni z veliko maso, to so kvarki top in bottom ter lepton tau, pridobijo maso že na drevesnem nivoju s pomočjo mehanizma "see-saw, ki sledi, ko avtor privzame še niz šibkih singletnih vektorskih fermionov U, D, E, N s simetrijo SU(2)_L, kjer je N nevtralni lepton. Doda tudi tri desnorodne nevtrine. V tem modelu poskrbijo za maso lahkih kvarkov in leptonov masivna umeritvena polja družinske simetrije SU(3) v popravkih višjih redov. Avtor pokaže nove rezultate za mase kvarkov in leptonov, za mešalno matriko kvarkov, pa tudi za neunitarno mešalno matriko leptonov $(U_{PMNS})_{4 \times 8}$.

11.1 Introduction

The origin of the hierarchy of fermion masses and mixing continues to be one of the most important open problems in particle physics. In this report we address the problem of generating neutrino masses and mixing within the framework of a broken SU(3) gauged family symmetry model [1,2].

This framework introduce a hierarchical mass generation mechanism in which light fermions become massive from radiative corrections, mediated by the massive gauge bosons associated to the SU(3) family symmetry that is spontaneously broken, while the masses of the top and bottom quarks as well as for the tau lepton, are generated at tree level from "Dirac See-saw" mechanisms implemented by the introduction of a new set of SU(2)_L weak singlets U, D, E and N vector-like

fermions, with N a neutral lepton. In addition this BSM introduce three right handed neutrinos in order to cancel anomalies. Therefore, we have a scenario with five "Standard Model"(SM) singlet "sterile neutrinos" and three active L-handed neutrinos, that is a 3+5 scenario.

Previous theories addressing the problem of quark and lepton masses and mixing with spontaneously broken $SU(3)$ gauge symmetry of generations include the ones with chiral $SU(3)$ family symmetry [3]- [6], as well as other $SU(3)$ family symmetry proposals [7]- [10]

Neutrinos are one of the most exciting areas of research. Cosmology and Short Baseline Oscillation experiments hint the possible existence of light sterile neutrinos. For recent studies of neutrino masses, including sterile neutrinos, see for instance [11]- [14]

11.2 $SU(3)$ family symmetry model

The model is based on the gauge symmetry

$$G \equiv SU(3) \otimes SU(3)_C \otimes SU(2)_L \otimes U(1)_Y \quad (11.1)$$

where $SU(3)$ is a completely vector-like and universal gauged family symmetry. That is, the corresponding gauge bosons couple equally to Left and Right Handed ordinary Quarks and Leptons, with g_H , g_s , g and g' the corresponding coupling constants. The content of fermions assumes the standard model quarks and leptons:

$$\Psi_q^o = (3, 3, 2, \frac{1}{3})_L \quad , \quad \Psi_l^o = (3, 1, 2, -1)_L \quad (11.2)$$

$$\Psi_u^o = (3, 3, 1, \frac{4}{3})_R \quad , \quad \Psi_d^o = (3, 3, 1, -\frac{2}{3})_R \quad , \quad \Psi_e^o = (3, 1, 1, -2)_R \quad (11.3)$$

where the last entry is the hypercharge Y , with the electric charge defined by $Q = T_{3L} + \frac{1}{2}Y$.

The model includes two types of extra fermions: Right Handed Neutrinos: $\Psi_{\nu_R}^o = (3, 1, 1, 0)_R$, introduced to cancel anomalies [7], and a new family of $SU(2)_L$ weak singlet vector-like fermions: Vector like quarks $U_L^o, U_R^o = (1, 3, 1, \frac{4}{3})$ and $D_L^o, D_R^o = (1, 3, 1, -\frac{2}{3})$, Vector Like electrons: $E_L^o, E_R^o = (1, 1, 1, -2)$, and New Sterile Neutrinos: $N_L^o, N_R^o = (1, 1, 1, 0)$.

The particle content and gauge symmetry assignments are summarized in Table 11.1. *Notice that all $SU(3)$ non-singlet fields transform as the fundamental representation under the $SU(3)$ symmetry.*

11.3 $SU(3)$ family symmetry breaking

$SU(3)$ family symmetry is broken spontaneously by heavy SM singlet scalars $\eta_1 = (3, 1, 1, 0)$ and $\eta_2 = (3, 1, 1, 0)$ in the fundamental representation of $SU(3)$, with the "Vacuum Expectation Values" (VEV's):

	SU(3)	SU(3) _C	SU(2) _L	U(1) _Y
$\Psi_{\text{d}}^{\text{o}}$	3	3	2	$\frac{1}{3}$
$\Psi_{\text{uR}}^{\text{o}}$	3	3	1	$\frac{4}{3}$
$\Psi_{\text{dR}}^{\text{o}}$	3	3	1	$-\frac{2}{3}$
$\Psi_{\text{l}}^{\text{o}}$	3	1	2	-1
$\Psi_{\text{eR}}^{\text{o}}$	3	1	1	-2
$\Psi_{\text{vR}}^{\text{o}}$	3	1	1	0
$U_{\text{L,R}}^{\text{o}}$	1	3	1	$\frac{4}{3}$
$D_{\text{L,R}}^{\text{o}}$	1	3	1	$-\frac{2}{3}$
$E_{\text{L,R}}^{\text{o}}$	1	1	1	-2
$N_{\text{L,R}}^{\text{o}}$	1	1	1	0
Φ^{u}	3	1	2	-1
Φ^{d}	3	1	2	+1
η_1, η_2	3	1	1	0

Table 11.1: Particle content and charges under the gauge symmetry

$$\langle \eta_1 \rangle^{\text{T}} = (\Lambda_1, 0, 0) \quad , \quad \langle \eta_2 \rangle^{\text{T}} = (0, \Lambda_2, 0) . \quad (11.4)$$

It is worth to mention that these two scalars in the fundamental representation is the minimal set of scalars to break down completely the SU(3) family symmetry.

The interaction of the SU(3) gauge bosons to the SM massless fermions is

$$i\mathcal{L}_{\text{int,SU(3)}} = g_{\text{H}} (f_1^{\text{o}}, f_2^{\text{o}}, f_3^{\text{o}}) \gamma_{\mu} \begin{pmatrix} \frac{Z_1^{\mu}}{2} + \frac{Z_2^{\mu}}{2\sqrt{3}} & \frac{Y_1^{+\mu}}{\sqrt{2}} & \frac{Y_2^{+\mu}}{\sqrt{2}} \\ \frac{Y_1^{-\mu}}{\sqrt{2}} & -\frac{Z_2^{\mu}}{\sqrt{3}} & \frac{Y_3^{+\mu}}{\sqrt{2}} \\ \frac{Y_2^{-\mu}}{\sqrt{2}} & \frac{Y_3^{-\mu}}{\sqrt{2}} & -\frac{Z_1^{\mu}}{2} + \frac{Z_2^{\mu}}{2\sqrt{3}} \end{pmatrix} \begin{pmatrix} f_1^{\text{o}} \\ f_2^{\text{o}} \\ f_3^{\text{o}} \end{pmatrix} \quad (11.5)$$

where g_{H} is the SU(3) coupling constant, Z_1, Z_2 and $Y_j^{\pm} = \frac{Y_j^1 \mp iY_j^2}{\sqrt{2}}$, $j = 1, 2, 3$ are the eight gauge bosons.

Thus, the contribution to the horizontal gauge boson masses from the VEV's of Eq.(11.4) read

- $\langle \eta_1 \rangle$: $\frac{g_{\text{H}}^2 \Lambda_1^2}{2} (Y_1^+ Y_1^- + Y_2^+ Y_2^-) + \frac{g_{\text{H}}^2 \Lambda_1^2}{4} (Z_1^2 + \frac{Z_2^2}{3} + 2Z_1 \frac{Z_2}{\sqrt{3}})$
- $\langle \eta_2 \rangle$: $\frac{g_{\text{H}}^2 \Lambda_2^2}{2} (Y_1^+ Y_1^- + Y_3^+ Y_3^-) + g_{\text{H}}^2 \Lambda_2^2 \frac{Z_2^2}{3}$

The "Spontaneous Symmetry Breaking" (SSB) of SU(3) occurs in two stages

$$\text{SU(3)} \times G_{\text{SM}} \xrightarrow{\langle \eta_2 \rangle} \text{SU(2)} \times G_{\text{SM}} \xrightarrow{\langle \eta_1 \rangle} G_{\text{SM}} \quad (11.6)$$

FCNC ?

Notice that the hierarchy of scales $\Lambda_2 > \Lambda_1$ yield an "approximate SU(2) global symmetry" in the spectrum of SU(2) gauge boson masses of order $g_{\text{H}} \Lambda_1$.

Therefore, neglecting tiny contributions from electroweak symmetry breaking, the gauge boson masses read

$$(M_1^2 + M_2^2) Y_1^+ Y_1^- + M_1^2 Y_2^+ Y_2^- + M_2^2 Y_3^+ Y_3^- + \frac{1}{2} M_1^2 Z_1^2 + \frac{1}{2} \frac{M_1^2 + 4M_2^2}{3} Z_2^2 + \frac{1}{2} (M_1^2) \frac{2}{\sqrt{3}} Z_1 Z_2 \quad (11.7)$$

$$M_1^2 = \frac{g_H^2 \Lambda_1^2}{2}, \quad M_2^2 = \frac{g_H^2 \Lambda_2^2}{2} \quad (11.8)$$

	Z ₁	Z ₂
Z ₁	M ₁ ²	$\frac{M_1^2}{\sqrt{3}}$
Z ₂	$\frac{M_1^2}{\sqrt{3}}$	$\frac{M_1^2 + 4M_2^2}{3}$

Table 11.2: Z₁ – Z₂ mixing mass matrix

Diagonalization of the Z₁ – Z₂ squared mass matrix yield the eigenvalues

$$M_-^2 = \frac{2}{3} \left(M_1^2 + M_2^2 - \sqrt{(M_2^2 - M_1^2)^2 + M_1^2 M_2^2} \right) \quad (11.9)$$

$$M_+^2 = \frac{2}{3} \left(M_1^2 + M_2^2 + \sqrt{(M_2^2 - M_1^2)^2 + M_1^2 M_2^2} \right) \quad (11.10)$$

and finally

$$(M_1^2 + M_2^2) Y_1^+ Y_1^- + M_1^2 Y_2^+ Y_2^- + M_2^2 Y_3^+ Y_3^- + M_-^2 \frac{Z_-^2}{2} + M_+^2 \frac{Z_+^2}{2}, \quad (11.11)$$

where

$$\begin{pmatrix} Z_1 \\ Z_2 \end{pmatrix} = \begin{pmatrix} \cos \phi & \sin \phi \\ -\sin \phi & \cos \phi \end{pmatrix} \begin{pmatrix} Z_- \\ Z_+ \end{pmatrix} \quad (11.12)$$

$$\cos \phi \sin \phi = \frac{\sqrt{3}}{4} \frac{M_1^2}{\sqrt{M_1^4 + M_2^2(M_2^2 - M_1^2)}} \quad (11.13)$$

11.4 Electroweak symmetry breaking

The ‘‘Electroweak Symmetry Breaking’’ (EWSB) is achieved by the Higgs fields Φ_i^u and Φ_i^d , which transform simultaneously as triplets under SU(3) and as Higgs doublets with hypercharges -1 and $+1$ under the SM, respectively, explicitly:

$$\Phi^u = \begin{pmatrix} \begin{pmatrix} (\phi^o)^u \\ (\phi^-)_1 \end{pmatrix} \\ \begin{pmatrix} (\phi^o)^u \\ (\phi^-)_2 \end{pmatrix} \\ \begin{pmatrix} (\phi^o)^u \\ (\phi^-)_3 \end{pmatrix} \end{pmatrix}, \quad \Phi^d = \begin{pmatrix} \begin{pmatrix} (\phi^+)^d \\ (\phi^o)_1 \end{pmatrix} \\ \begin{pmatrix} (\phi^+)^d \\ (\phi^o)_2 \end{pmatrix} \\ \begin{pmatrix} (\phi^+)^d \\ (\phi^o)_3 \end{pmatrix} \end{pmatrix}$$

with the VEV's

$$\langle \Phi^u \rangle = \begin{pmatrix} \frac{1}{\sqrt{2}} \begin{pmatrix} v_{u1} \\ 0 \end{pmatrix} \\ \frac{1}{\sqrt{2}} \begin{pmatrix} v_{u2} \\ 0 \end{pmatrix} \\ \frac{1}{\sqrt{2}} \begin{pmatrix} v_{u3} \\ 0 \end{pmatrix} \end{pmatrix}, \quad \langle \Phi^d \rangle = \begin{pmatrix} \frac{1}{\sqrt{2}} \begin{pmatrix} 0 \\ v_{d1} \end{pmatrix} \\ \frac{1}{\sqrt{2}} \begin{pmatrix} 0 \\ v_{d2} \end{pmatrix} \\ \frac{1}{\sqrt{2}} \begin{pmatrix} 0 \\ v_{d3} \end{pmatrix} \end{pmatrix}$$

The contributions from $\langle \Phi^u \rangle$ and $\langle \Phi^d \rangle$ generate the W and Z_o SM gauge boson masses

$$\frac{g^2}{4} (v_u^2 + v_d^2) W^+ W^- + \frac{(g^2 + g'^2)}{8} (v_u^2 + v_d^2) Z_o^2 \quad (11.14)$$

+ tiny contribution to the SU(3) gauge boson masses and mixing with Z_o ,

$v_u^2 = v_{1u}^2 + v_{2u}^2 + v_{3u}^2$, $v_d^2 = v_{1d}^2 + v_{2d}^2 + v_{3d}^2$. So, if $M_W \equiv \frac{1}{2} g v$, we may write $v = \sqrt{v_u^2 + v_d^2} \approx 246$ GeV.

11.5 Fermion masses

11.5.1 Dirac see-saw mechanisms

The gauge symmetry $G \equiv SU(3) \times G_{SM}$, the fermion content, and the transformation of the scalar fields, all together, avoid Yukawa couplings between SM fermions. The allowed Yukawa couplings involve terms between the SM fermions and the corresponding vector-like fermions U, D, E and N :

The scalars and fermion content allow the gauge invariant Yukawa couplings for quarks and charged leptons

$$H_u \overline{\psi}_q^o \Phi^u U_R^o + h_{\eta_1}^u \overline{\psi}_{uR}^o \eta_1 U_L^o + h_{\eta_2}^u \overline{\psi}_{uR}^o \eta_2 U_L^o + M_U \overline{U}_L^o U_R^o + \text{h.c}$$

$$H_d \overline{\psi}_q^o \Phi^d D_R^o + h_{\eta_1}^d \overline{\psi}_{dR}^o \eta_1 D_L^o + h_{\eta_2}^d \overline{\psi}_{dR}^o \eta_2 D_L^o + M_D \overline{D}_L^o D_R^o + \text{h.c}$$

$$H_e \overline{\psi}_l^o \Phi^d E_R^o + h_{\eta_1}^e \overline{\psi}_{eR}^o \eta_1 E_L^o + h_{\eta_2}^e \overline{\psi}_{eR}^o \eta_2 E_L^o + M_E \overline{E}_L^o E_R^o + \text{h.c}$$

M_U, M_D, M_E are free mass parameters and $H_u, H_d, H_e, h_{\eta_1}^f, h_{\eta_2}^f, f = u, d, e$ are coupling constants. When the involved scalar fields acquire VEV's, we get for charged leptons in the gauge basis $\psi_{L,R}^o = (e^o, \mu^o, \tau^o, E^o)_{L,R}$, the mass terms $\overline{\psi}_L^o \mathcal{M}^o \psi_R^o + \text{h.c}$, where

$$\mathcal{M}^o = \begin{pmatrix} 0 & 0 & 0 & H_e v_{d1} \\ 0 & 0 & 0 & H_e v_{d2} \\ 0 & 0 & 0 & H_e v_{d3} \\ h_1^e \Lambda_1 & h_2^e \Lambda_2 & 0 & M_E \end{pmatrix} \quad (11.15)$$

It is worth to notice that completed analogous tree level mass matrices are obtained for u and d quarks

\mathcal{M}^o is diagonalized by applying a biunitary transformation $\psi_{L,R}^o = V_{L,R}^o \chi_{L,R}$.

$$V_L^{oT} \mathcal{M}^o V_R^o = \text{Diag}(0, 0, -\lambda_3, \lambda_4) \quad (11.16)$$

$$V_L^{oT} \mathcal{M}^o \mathcal{M}^{oT} V_L^o = V_R^{oT} \mathcal{M}^{oT} \mathcal{M}^o V_R^o = \text{Diag}(0, 0, \lambda_3^2, \lambda_4^2), \quad (11.17)$$

where λ_3 and λ_4 are the nonzero eigenvalues, λ_4 being the fourth heavy fermion mass, and λ_3 of the order of the top, bottom and tau mass for u, d and e fermions, respectively. We see from Eqs.(11.16,11.17) that from tree level there exist two massless eigenvalues associated to the light fermions:

11.6 Neutrino masses

Now we describe the procedure to generate neutrino masses

11.6.1 Tree level Dirac neutrino masses

With the fields of particles introduced in the model, we may write the Dirac type gauge invariant Yukawa couplings

$$h_D \overline{\Psi}_l^o \Phi^u N_R^o + h_1 \overline{\Psi}_\nu^o \eta_1 N_L^o + h_2 \overline{\Psi}_\nu^o \eta_2 N_L^o + h_3 \overline{\Psi}_\nu^o \eta_3 N_L^o + M_D \overline{N}_L^o N_R^o + \text{h.c} \quad (11.18)$$

h_D, h_1, h_2 and h_3 are Yukawa couplings, and M_D a Dirac type, invariant neutrino mass for the sterile neutrinos $N_{L,R}^o$. After electroweak symmetry breaking, we obtain in the interaction basis $\Psi_{\nu L,R}^{oT} = (\nu_e^o, \nu_\mu^o, \nu_\tau^o, N^o)_{L,R}$, the mass terms

$$h_D [v_1 \bar{\nu}_{eL}^o + v_2 \bar{\nu}_{\mu L}^o + v_3 \bar{\nu}_{\tau L}^o] N_R^o + [h_1 \Lambda_1 \bar{\nu}_{eR}^o + h_2 \Lambda_2 \bar{\nu}_{\mu R}^o + h_3 \Lambda_3 \bar{\nu}_{\tau R}^o] N_L^o + M_D \bar{N}_L^o N_R^o + h.c. \quad (11.19)$$

11.6.2 Tree level Majorana masses:

Since $N_{L,R}^o$, Table 1, are sterile neutrinos, we may also write left and right handed Majorana type couplings

$$h_L \bar{\Psi}_L^o \Phi^u (N_L^o)^c + m_L \bar{N}_L^o (N_L^o)^c + h.c \quad (11.20)$$

and

$$h_{1R} \bar{\Psi}_\nu^o \eta_1 (N_R^o)^c + h_{2R} \bar{\Psi}_\nu^o \eta_2 (N_R^o)^c + h_{3R} \bar{\Psi}_\nu^o \eta_3 (N_R^o)^c + m_R \bar{N}_R^o (N_R^o)^c + h.c, \quad (11.21)$$

respectively. After spontaneous symmetry breaking, we also get the left handed and right handed Majorana mass terms

$$h_L [v_1 \bar{\nu}_{eL}^o + v_2 \bar{\nu}_{\mu L}^o + v_3 \bar{\nu}_{\tau L}^o] (N_L^o)^c + m_L \bar{N}_L^o (N_L^o)^c + h.c., \quad (11.22)$$

$$+ [h_{1R} \Lambda_1 \bar{\nu}_{eR}^o + h_{2R} \Lambda_2 \bar{\nu}_{\mu R}^o + h_{3R} \Lambda_3 \bar{\nu}_{\tau R}^o] (N_R^o)^c + m_R \bar{N}_R^o (N_R^o)^c + h.c. \quad (11.23)$$

Thus, in the basis $\Psi_\nu^{oT} = (\nu_{eL}^o, \nu_{\mu L}^o, \nu_{\tau L}^o, N_L^o, (\nu_{eR}^o)^c, (\nu_{\mu R}^o)^c, (\nu_{\tau R}^o)^c, (N_R^o)^c)$, the Generic 8×8 tree level Majorana mass matrix for neutrinos \mathcal{M}_ν^o , from Table 11.3, $\bar{\Psi}_\nu^o \mathcal{M}_\nu^o (\Psi_\nu^o)^c$, read

$$\mathcal{M}_\nu^o = \begin{pmatrix} 0 & 0 & 0 & \alpha_1 & 0 & 0 & 0 & a_1 \\ 0 & 0 & 0 & \alpha_2 & 0 & 0 & 0 & a_2 \\ 0 & 0 & 0 & \alpha_3 & 0 & 0 & 0 & a_3 \\ \alpha_1 & \alpha_2 & \alpha_3 & m_L & b_1 & b_2 & 0 & m_D \\ 0 & 0 & 0 & b_1 & 0 & 0 & 0 & \beta_1 \\ 0 & 0 & 0 & b_2 & 0 & 0 & 0 & \beta_2 \\ 0 & 0 & 0 & 0 & 0 & 0 & 0 & 0 \\ a_1 & a_2 & a_3 & m_D & \beta_1 & \beta_2 & 0 & m_R \end{pmatrix} \quad (11.24)$$

Diagonalization of $\mathcal{M}_\nu^{(o)}$, Eq.(11.24), yields four zero eigenvalues:

$$U_\nu^{oT} \mathcal{M}_\nu^o U_\nu^o = \text{Diagonal}(0, 0, 0, 0, m_5^o, m_6^o, m_7^o, m_8^o) \quad (11.25)$$

	$(\nu_{eL}^o)^c$	$(\nu_{\mu L}^o)^c$	$(\nu_{\tau L}^o)^c$	$(N_L^o)^c$	ν_{eR}^o	$\nu_{\mu R}^o$	$\nu_{\tau R}^o$	N_R^o
$\overline{\nu_{eL}^o}$	0	0	0	$h_L v_1$	0	0	0	$h_D v_1$
$\overline{\nu_{\mu L}^o}$	0	0	0	$h_L v_2$	0	0	0	$h_D v_2$
$\overline{\nu_{\tau L}^o}$	0	0	0	$h_L v_3$	0	0	0	$h_D v_3$
$\overline{N_L^o}$	$h_L v_1$	$h_L v_2$	$h_L v_3$	m_L	$h_1 \Lambda_1$	$h_2 \Lambda_2$	0	M_D
$(\overline{\nu_{eR}^o})^c$	0	0	0	$h_1 \Lambda_1$	0	0	0	$h_{1R} \Lambda_1$
$(\overline{\nu_{\mu R}^o})^c$	0	0	0	$h_2 \Lambda_2$	0	0	0	$h_{2R} \Lambda_2$
$(\overline{\nu_{\tau R}^o})^c$	0	0	0	0	0	0	0	0
$(\overline{N_R^o})^c$	$h_D v_1$	$h_D v_2$	$h_D v_3$	M_D	$h_{1R} \Lambda_1$	$h_{2R} \Lambda_2$	0	m_R

Table 11.3: Tree Level Majorana masses

11.7 One loop neutrino masses:

11.7.1 One loop Dirac Neutrino masses

After the breakdown of the electroweak symmetry, neutrinos may get tiny Dirac mass terms from the generic one loop diagram in Fig. 1, The internal fermion line in this diagram represent the tree level see-saw mechanisms, Eqs.(11.18-11.23). The vertices read from the SU(3) family symmetry interaction Lagrangian

$$i\mathcal{L}_{\text{int}} = \frac{g_H}{2} (\bar{\nu}_e^o \gamma_\mu \nu_e^o - \bar{\nu}_\tau^o \gamma_\mu \nu_\tau^o) Z_1^\mu + \frac{g_H}{2\sqrt{3}} (\bar{\nu}_e^o \gamma_\mu \nu_e^o - 2\bar{\nu}_\mu^o \gamma_\mu \nu_\mu^o + \bar{\nu}_\tau^o \gamma_\mu \nu_\tau^o) Z_2^\mu \\ + \frac{g_H}{\sqrt{2}} (\bar{\nu}_e^o \gamma_\mu \nu_\mu^o Y_1^+ + \bar{\nu}_e^o \gamma_\mu \nu_\tau^o Y_2^+ + \bar{\nu}_\mu^o \gamma_\mu \nu_\tau^o Y_3^+ + \text{h.c.}) \quad (11.26)$$

The contribution from these diagrams may be written as

$$c_Y \frac{\alpha_H}{\pi} m_\nu(M_Y)_{ij} \quad , \quad \alpha_H = \frac{g_H^2}{4\pi} \quad , \quad (11.27)$$

$$m_\nu(M_Y)_{ij} \equiv \sum_{k=5,6,7,8} m_k^o \mathcal{U}_{\nu ik}^o \mathcal{U}_{\nu jk}^o f(M_Y, m_k^o) \quad , \quad (11.28)$$

$$f(M_Y, m_k^o) = \frac{M_Y^2}{M_Y^2 - m_k^o{}^2} \ln \frac{M_Y^2}{m_k^o{}^2} \approx \ln \frac{M_Y^2}{m_k^o{}^2} \quad , \quad M_Y^2 \gg m_k^o{}^2 \quad \text{valid for neutrinos.}$$

11.7.2 One loop L-handed and R-handed Majorana masses

Neutrinos also obtain one loop corrections to L-handed and R-handed Majorana masses from the diagrams of Fig. 2 and Fig. 3, respectively. A similar procedure as for Dirac Neutrino masses, leads to the one loop Majorana mass terms

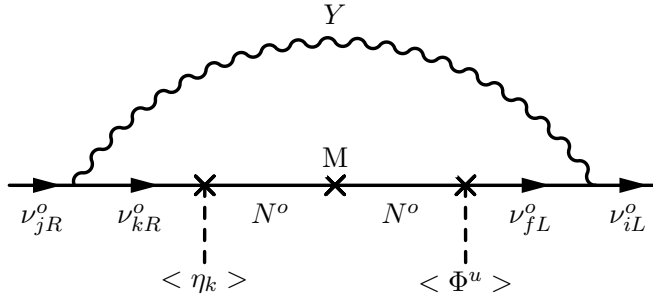


Fig. 11.1: Generic one loop diagram contribution to the Dirac mass term $m_{ij} \bar{\nu}_{iL}^o \nu_{jR}^o$. $M = M_D, m_L, m_R$

	ν_{eR}^o	$\nu_{\mu R}^o$	$\nu_{\tau R}^o$	N_R^o
$\bar{\nu}_{eL}^o$	$D_{\nu 15}$	$D_{\nu 16}$	0	0
$\bar{\nu}_{\mu L}^o$	$D_{\nu 25}$	$D_{\nu 26}$	0	0
$\bar{\nu}_{\tau L}^o$	$D_{\nu 35}$	$D_{\nu 36}$	$D_{\nu 37}$	0
\bar{N}_L^o	0	0	0	0

Table 11.4: One loop Dirac mass terms $\frac{\alpha_H}{\pi} D_{\nu ij} \bar{\nu}_{iL}^o \nu_{jR}^o$

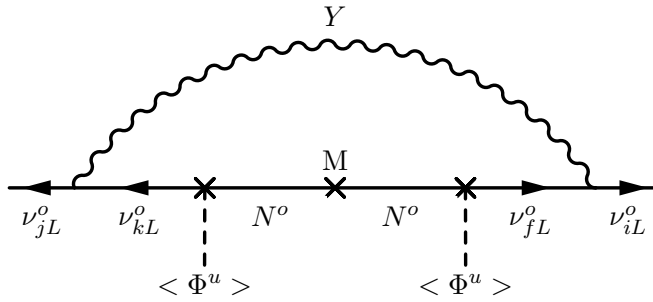


Fig. 11.2: Generic one loop diagram contribution to the L-handed Majorana mass term $m_{ij} \bar{\nu}_{iL}^o (\nu_{jL}^o)^T$. $M = M_D, m_L, m_R$

Thus, in the Ψ_ν^o basis, the one loop contribution for neutrinos read

	ν_{eL}^o	$\nu_{\mu L}^o$	$\nu_{\tau L}^o$	N_L^o
ν_{eL}^o	$L_{\nu 11}$	$L_{\nu 12}$	$L_{\nu 13}$	0
$\nu_{\mu L}^o$	$L_{\nu 12}$	$L_{\nu 22}$	$L_{\nu 23}$	0
$\nu_{\tau L}^o$	$L_{\nu 13}$	$L_{\nu 23}$	$L_{\nu 33}$	0
N_L^o	0	0	0	0

Table 11.5: One loop L-handed Majorana mass terms $\frac{\alpha_H}{\pi} L_{\nu ij} \tilde{\nu}_{iL}^o (\nu_{jL}^o)^T$

	ν_{eR}^o	$\nu_{\mu R}^o$	$\nu_{\tau R}^o$	N_R^o
ν_{eR}^o	$R_{\nu 55}$	$R_{\nu 56}$	0	0
$\nu_{\mu R}^o$	$R_{\nu 56}$	$R_{\nu 66}$	0	0
$\nu_{\tau R}^o$	0	0	0	0
N_R^o	0	0	0	0

Table 11.6: One loop R-handed Majorana mass terms $\frac{\alpha_H}{\pi} R_{\nu ij} \tilde{\nu}_{iR}^o (\nu_{jR}^o)^T$

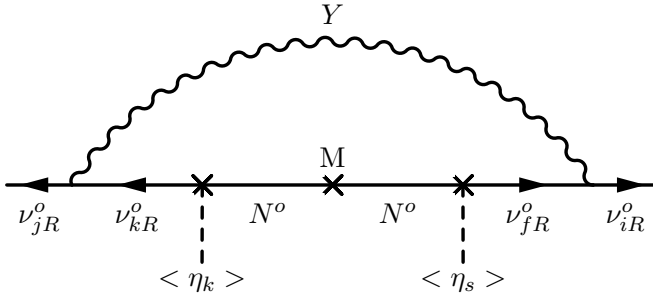


Fig. 11.3: Generic one loop diagram contribution to the R-handed Majorana mass term $m_{ij} \tilde{\nu}_{iR}^o (\nu_{jR}^o)^T$. $M = M_D, m_L, m_R$

$$\mathcal{M}_{1\nu}^o = \begin{pmatrix} L_{\nu 11} & L_{\nu 12} & L_{\nu 13} & 0 & D_{\nu 15} & D_{\nu 16} & 0 & 0 \\ L_{\nu 12} & L_{\nu 22} & L_{\nu 23} & 0 & D_{\nu 25} & D_{\nu 26} & 0 & 0 \\ L_{\nu 13} & L_{\nu 23} & L_{\nu 33} & 0 & D_{\nu 35} & D_{\nu 36} & D_{\nu 37} & 0 \\ 0 & 0 & 0 & 0 & 0 & 0 & 0 & 0 \\ D_{\nu 15} & D_{\nu 25} & D_{\nu 35} & 0 & R_{\nu 55} & R_{\nu 56} & 0 & 0 \\ D_{\nu 16} & D_{\nu 26} & D_{\nu 36} & 0 & R_{\nu 56} & R_{\nu 66} & 0 & 0 \\ 0 & 0 & D_{\nu 37} & 0 & 0 & 0 & 0 & 0 \\ 0 & 0 & 0 & 0 & 0 & 0 & 0 & 0 \end{pmatrix} \frac{\alpha_H}{\pi}, \quad (11.29)$$

where, after using the relationships coming from the zero entries of \mathcal{M}_ν° , eq.(11.24);

$$\mathcal{M}_\nu^\circ = \mathcal{U}_\nu^\circ \text{Diagonal}(0, 0, 0, 0, m_5^\circ, m_6^\circ, m_7^\circ, m_8^\circ) \mathcal{U}_\nu^{\circ T}, \quad (11.30)$$

and in the limit $M_\nu^2 \gg m_k^{\circ 2}$, we may write:

$$L_{\nu ij} = \frac{1}{3} F_{ij}, \quad i, j = 1, 2, 3$$

$$D_{\nu 15} = \frac{1}{3} F_{15} + \frac{1}{2} F_{26}, \quad D_{\nu 16} = -\frac{1}{6} F_{16},$$

$$D_{\nu 25} = -\frac{1}{6} F_{25}, \quad D_{\nu 26} = \frac{1}{3} F_{26} + \frac{1}{2} F_{15},$$

$$D_{\nu 35} = -\frac{1}{6} F_{35}, \quad D_{\nu 36} = -\frac{1}{6} F_{36}, \quad D_{\nu 37} = \frac{1}{2}(F_{15} + F_{26})$$

$$R_{\nu 55} = \frac{1}{3} F_{55}, \quad R_{\nu 56} = \frac{1}{3} F_{56}, \quad R_{\nu 66} = \frac{1}{3} F_{66}$$

where

$$F_{ij} = \mathcal{U}_{\nu i5}^\circ \mathcal{U}_{\nu j5}^\circ \ln \frac{m_8^{\circ 2}}{m_5^{\circ 2}} + \mathcal{U}_{\nu i6}^\circ \mathcal{U}_{\nu j6}^\circ \ln \frac{m_8^{\circ 2}}{m_6^{\circ 2}} + \mathcal{U}_{\nu i7}^\circ \mathcal{U}_{\nu j7}^\circ \ln \frac{m_8^{\circ 2}}{m_7^{\circ 2}} \quad (11.31)$$

11.7.3 Neutrino mass matrix up to one loop

Finally, we obtain the Majorana mass matrix for neutrinos up to one loop

$$\mathcal{M}_\nu = \mathcal{U}_\nu^{\circ T} \mathcal{M}_{1\nu}^\circ \mathcal{U}_\nu^\circ + \text{Diag}(0, 0, 0, 0, m_5^\circ, m_6^\circ, m_7^\circ, m_8^\circ), \quad (11.32)$$

11.7.4 $(V_{CKM})_{4 \times 4}$ and $(V_{PMNS})_{4 \times 8}$ mixing matrices

Within this scenario, the transformation from massless to physical mass fermion eigenfields for quarks and charged leptons is

$$\psi_L^\circ = V_L^\circ V_L^{(1)} \Psi_L \quad \text{and} \quad \psi_R^\circ = V_R^\circ V_R^{(1)} \Psi_R,$$

and for neutrinos $\Psi_\nu^\circ = \mathcal{U}_\nu^\circ \mathcal{U}_\nu^1 \Psi_\nu$;

$$\mathcal{U}_\nu^{1T} \mathcal{M}_\nu \mathcal{U}_\nu^1 = \text{Diagonal}(\lambda_1, \lambda_2, \lambda_3, \lambda_4, \lambda_5, \lambda_6, \lambda_7, \lambda_8) \quad (11.33)$$

Recall now that vector like fermions, Table 1, are $SU(2)_L$ weak singlets, and hence, they do not couple to W boson in the interaction basis. So, the coupling of L-handed up and down quarks; $f_{uL}^{\circ T} = (u^\circ, c^\circ, t^\circ)_L$ and $f_{dL}^{\circ T} = (d^\circ, s^\circ, b^\circ)_L$, to the W charged gauge boson is

$$\begin{aligned} & \frac{g}{\sqrt{2}} \bar{f}_{uL}^\circ \gamma_\mu f_{dL}^\circ W^{+\mu} \\ &= \frac{g}{\sqrt{2}} \bar{\Psi}_{uL} [(V_{uL}^\circ V_{uL}^{(1)})_{3 \times 4}]^T (V_{dL}^\circ V_{dL}^{(1)})_{3 \times 4} \gamma_\mu \Psi_{dL} W^{+\mu}, \quad (11.34) \end{aligned}$$

with g the $SU(2)_L$ gauge coupling. Hence, the non-unitary V_{CKM} of dimension 4×4 is identified as

$$(V_{CKM})_{4 \times 4} = [(V_{uL}^o V_{uL}^{(1)})_{3 \times 4}]^T (V_{dL}^o V_{dL}^{(1)})_{3 \times 4} \quad (11.35)$$

$$[V_{uL}^o V_{uL}^{(1)}]_{3 \times 4} = (V_{uL}^o)_{3 \times 4} (V_{uL}^{(1)})_{4 \times 4}, \quad [V_{dL}^o V_{dL}^{(1)}]_{3 \times 4} = (V_{dL}^o)_{3 \times 4} (V_{dL}^{(1)})_{4 \times 4}$$

Similar analysis of the coupling between active L-handed neutrinos and L-handed charged leptons to W boson, leads to the lepton mixing matrix

$$(U_{PMNS})_{4 \times 8} = [(V_{eL}^o V_{eL}^{(1)})_{3 \times 4}]^T (U_\nu^o U_\nu^1)_{3 \times 8} \quad (11.36)$$

$$[V_{eL}^o V_{eL}^{(1)}]_{3 \times 4} = (V_{eL}^o)_{3 \times 4} (V_{eL}^{(1)})_{4 \times 4}, \quad (U_\nu^o U_\nu^1)_{3 \times 8} = (U_\nu^o)_{3 \times 8} (U_\nu^1)_{8 \times 8}$$

11.8 Numerical results for Neutrino masses and mixing in a 3+5 scenario

We report here numerical results for lepton masses and mixing, at the M_Z scale [15]

The input values for the horizontal boson masses, Eq.(8), and the coupling constant of the $SU(3)$ family symmetry are:

$$M_1 = 5.3 \times 10^3 \text{ TeV}, \quad M_2 = 3.3 \times 10^5 \text{ TeV}, \quad \frac{\alpha_H}{\pi} = 0.05, \quad (11.37)$$

$$\Lambda_1 = 3352.7 \text{ TeV}, \quad \Lambda_2 = 10^3 \Lambda_1, \quad g_H = 2.23561$$

Horizontal gauge bosons from the $SU(3)$ family symmetry introduce flavor changing couplings, and in particular mediate $\Delta F = 2$ processes at tree level. The above high scales and heavy boson masses provide the proper suppression of $K^o - \bar{K}^o$ and $D^o - \bar{D}^o$ meson mixing from the tree level exchange diagrams mediated by the $SU(3)$ horizontal gauge bosons.

11.8.1 Charged leptons:

Tree level:

$$\mathcal{M}_e^o = \begin{pmatrix} 0 & 0 & 0 & 2670.25 \\ 0 & 0 & 0 & 11902.6 \\ 0 & 0 & 0 & 16264.7 \\ 1.21882 \times 10^{10} & -2.32202 \times 10^9 & 0 & 6.07835 \times 10^{10} \end{pmatrix} \text{ MeV},$$

up to one loop corrections:

$$\mathcal{M}_e = \begin{pmatrix} 0 & -19.9797 & -83.226 & -16.9884 \\ 0.6408 & 71.9782 & 293.027 & 59.814 \\ -0.8544 & 168.853 & -1712.54 & 480.432 \\ -2.74 \times 10^{-7} & 0.000054 & 0.000755 & 6.20 \times 10^{10} \end{pmatrix} \text{MeV}$$

the charged lepton masses

$$(m_e, m_\mu, m_\tau, M_E) = (0.486031, 102.717, 1746.17, 6.20 \times 10^{10}) \text{MeV}$$

Mixing matrix:

$$V_{eL} = V_{eL}^o V_{eL}^{(1)}:$$

$$\begin{pmatrix} 0.986458 & 0.0744614 & -0.146138 & 4.30921 \times 10^{-8} \\ 0.00276675 & -0.898433 & -0.439101 & 1.93334 \times 10^{-7} \\ -0.163991 & 0.43275 & -0.886473 & 2.62497 \times 10^{-7} \\ 0 & 5.68933 \times 10^{-8} & 3.23887 \times 10^{-7} & 1 \end{pmatrix}$$

11.8.2 Neutrino masses and Lepton (U_{PMNS}) $_{4 \times 8}$ mixing:

Tree level \mathcal{M}_ν^0 , eq.(11.24): in eV

$$\begin{pmatrix} 0 & 0 & 0 & 975.261 & 0 & 0 & 0 & 13.2472 \\ 0 & 0 & 0 & 4601.39 & 0 & 0 & 0 & 62.502 \\ 0 & 0 & 0 & 5663.49 & 0 & 0 & 0 & 76.9286 \\ 975.261 & 4601.39 & 5663.49 & 800. & 1404. & 2188.33 & 0 & 22500. \\ 0 & 0 & 0 & 1404. & 0 & 0 & 0 & 2.73 \times 10^7 \\ 0 & 0 & 0 & 2188.33 & 0 & 0 & 0 & 1.24382 \times 10^7 \\ 0 & 0 & 0 & 0 & 0 & 0 & 0 & 0 \\ 13.2472 & 62.502 & 76.9286 & 22500. & 2.73 \times 10^7 & 1.24382 \times 10^7 & 0 & 1.81238 \times 10^9 \end{pmatrix}$$

$\mathcal{M}_{1\nu}^0$, eq.(11.29): in eV

$$\begin{pmatrix} -0.57491 & -2.71249 & -3.33859 & 0 & -0.755918 & 0.148816 & 0 & 0 \\ -2.71249 & -12.7979 & -15.7519 & 0 & -3.18585 & 0.62145 & 0 & 0 \\ -3.33859 & -15.7519 & -19.3877 & 0 & -3.9212 & 0.864196 & -0.0806809 & 0 \\ 0 & 0 & 0 & 0 & 0 & 0 & 0 & 0 \\ -0.755918 & -3.18585 & -3.9212 & 0 & -284546. & -129640. & 0 & 0 \\ 0.148816 & 0.62145 & 0.864196 & 0 & -129640. & -59065.7 & 0 & 0 \\ 0 & 0 & -0.0806809 & 0 & 0 & 0 & 0 & 0 \\ 0 & 0 & 0 & 0 & 0 & 0 & 0 & 0 \end{pmatrix}$$

\mathcal{M}_ν , eq.(11.32): in eV

$$\begin{pmatrix} 0 & 0 & 0 & -0.0470918 & 0.00670865 & 0.00603167 & 0.0648786 & -0.00107364 \\ 0 & 0 & 0.0515474 & 0.0490276 & -0.00671814 & -0.00655172 & 0.0368801 & -0.00061029 \\ 0 & 0.0515474 & 0 & -0.0116693 & -0.0442476 & -0.0419316 & 3.5622 \times 10^{-6} & -3.4263 \times 10^{-9} \\ -0.0470918 & 0.0490276 & -0.0116693 & -3.45879 & -6.3112 & -5.99272 & 2.35948 & -0.0390377 \\ 0.00670865 & -0.00671814 & -0.0442476 & -6.3112 & -7121.58 & -12.9471 & -873.148 & 14.4492 \\ 0.00603167 & -0.00655172 & -0.0419316 & -5.99272 & -12.9471 & 7892.83 & 897.758 & -14.8564 \\ 0.0648786 & 0.0368801 & 3.5622 \times 10^{-6} & 2.35948 & -873.148 & 897.758 & -839967. & 5684.58 \\ -0.00107364 & -0.00061029 & -3.4263 \times 10^{-9} & -0.0390377 & 14.4492 & -14.8564 & 5684.58 & 1.8128 \times 10^9 \end{pmatrix}$$

Neutrino masses:

$$(m_1 = 0.000645302, m_2 = 0.0510146, m_3 = 0.0517498, m_4 = 3.45909,$$

$$m_5 = 7120.68, m_6 = 7893.8, m_7 = 839969, m_8 = 1.81288 \times 10^9) \text{ eV}$$

Squared neutrino mass differences:

$$m_2^2 - m_1^2 = 2.602 \times 10^{-3} \text{ eV}^2$$

$$m_3^2 - m_2^2 = 7.555 \times 10^{-5} \text{ eV}^2$$

$$m_4^2 - m_1^2 = 11.965 \text{ eV}^2$$

Neutrino mixing: $\mathcal{U}_\nu = \mathcal{U}_\nu^0 \mathcal{U}_\nu^1$

$$\left(\begin{array}{cccc} 0.97728 & 0.123928 & -0.106511 & -0.035932 \\ -0.211124 & 0.529448 & -0.536153 & -0.103884 \\ -0.000103928 & -0.448468 & 0.452078 & -0.1536 \\ -0.0000170002 & 9.508 \times 10^{-6} & -0.0000155169 & -0.00116041 \\ -0.00557906 & 0.00505439 & -0.00311974 & -0.407139 \\ 0.0122451 & -0.0110938 & 0.00684744 & 0.893615 \\ 0.0129939 & -0.709263 & -0.704815 & -0.00358262 \\ 1.45741 \times 10^{-9} & 6.46089 \times 10^{-10} & -1.15813 \times 10^{-10} & 9.37014 \times 10^{-9} \\ & 0.0945439 & -0.0893912 & 3.50955 \times 10^{-6} & 7.30727 \times 10^{-9} \\ & 0.446074 & -0.421754 & 0.000016186 & 3.44794 \times 10^{-8} \\ & 0.549035 & -0.519105 & 0.000019873 & 4.24383 \times 10^{-8} \\ & -0.687182 & -0.726481 & -0.0021559 & 0.0000124295 \\ & -0.0576333 & 0.0524664 & 0.909874 & 0.015054 \\ & 0.122879 & -0.11889 & 0.41455 & 0.00685878 \\ & 6.22084 \times 10^{-6} & 5.30567 \times 10^{-6} & 0 & 0 \\ & 0.0000333177 & 0.0000346837 & -0.0165428 & 0.999863 \end{array} \right)$$

 $(\mathcal{U}_{\text{PMNS}})_{4 \times 8}$ lepton mixing matrix :

$$\left(\begin{array}{cccc}
 0.963479 & 0.19726 & -0.180688 & -0.0105438 \\
 0.262405 & -0.660521 & 0.669404 & 0.0241869 \\
 -0.0500208 & 0.146962 & -0.149764 & 0.187029 \\
 1.26831 \times 10^{-9} & -1.00207 \times 10^{-8} & 1.04226 \times 10^{-8} & -6.19523 \times 10^{-8} \\
 & 0.00446092 & -0.00421887 & 2.47814 \times 10^{-7} & 3.442 \times 10^{-10} \\
 & -0.156133 & 0.147619 & -5.68064 \times 10^{-6} & -1.20681 \times 10^{-8} \\
 & -0.696392 & 0.658429 & -0.000025237 & -5.38282 \times 10^{-8} \\
 & 2.34435 \times 10^{-7} & -2.21655 \times 10^{-7} & 0 & 0
 \end{array} \right)$$

11.9 Conclusions

We have reported an updated numerical analysis for neutrino masses and mixing in a 3+5 scenario, within a local SU(3) Family symmetry model, which combines tree level "Dirac see-saw" mechanisms and radiative corrections to implement a successful hierarchical spectrum, for charged fermion masses and mixing.

The mass of the active SM neutrinos and a sterile neutrino with mass of a few eV's come out from the application of the see-saw approximation.

We update numerical results for neutrinos and report the non-unitary $(U_{\text{PMNS}})_{4 \times 8}$ lepton mixing matrix.

11.10 Acknowledgements

It is my pleasure to thank the organizers N.S. Mankoc-Borstnik, H.B. Nielsen, M. Y. Khlopov, and all participants for this year stimulating Virtual Bled Workshop 2021. This work was partially supported by the "Instituto Politécnico Nacional", Grant from COFAA.

References

1. A. Hernandez-Galeana, Rev. Mex. Fis. **Vol. 50(5)**, (2004) 522. hep-ph/0406315.
2. A. Hernandez-Galeana, Bled Workshops in Physics, (ISSN:1580-4992), **Vol. 17, No. 2**, (2016) Pag. 36; arXiv:1612.07388[hep-ph]; **Vol. 16, No. 2**, (2015) Pag. 47; arXiv:1602.08212[hep-ph]; **Vol. 15, No. 2**, (2014) Pag. 93; arXiv:1412.6708[hep-ph]; **Vol. 14, No. 2**, (2013) Pag. 82; arXiv:1312.3403[hep-ph]; **Vol. 13, No. 2**, (2012) Pag. 28; arXiv:1212.4571[hep-ph]; **Vol. 12, No. 2**, (2011) Pag. 41; arXiv:1111.7286[hep-ph]; **Vol. 11, No. 2**, (2010) Pag. 60; arXiv:1012.0224[hep-ph]; Bled Workshops in Physics, **Vol. 10, No. 2**, (2009) Pag. 67; arXiv:0912.4532[hep-ph];
3. Z. Berezhiani and M. Yu.Khlopov: Theory of broken gauge symmetry of families, Sov.J.Nucl.Phys. **51**, 739 (1990).
4. Z. Berezhiani and M. Yu.Khlopov: Physical and astrophysical consequences of family symmetry breaking, Sov.J.Nucl.Phys. **51**, 935 (1990).

5. J.L. Chkareuli, C.D. Froggatt, and H.B. Nielsen, Nucl. Phys. B **626**, 307 (2002).
6. Z.G. Berezhiani: The weak mixing angles in gauge models with horizontal symmetry: A new approach to quark and lepton masses, Phys. Lett. B **129**, 99 (1983).
7. T. Yanagida, Phys. Rev. D **20**, 2986 (1979).
8. T. Appelquist, Y. Bai and M. Piai: SU(3) Family Gauge Symmetry and the Axion, Phys. Rev. D **75**, 073005 (2007).
9. T. Appelquist, Y. Bai and M. Piai: Neutrinos and SU(3) family gauge symmetry, Phys. Rev. D **74**, 076001 (2006).
10. T. Appelquist, Y. Bai and M. Piai: Quark mass ratios and mixing angles from SU(3) family gauge symmetry, Phys. Lett. B **637**, 245 (2006).
11. G.H. Collin, C.A. Argüelles, J.M. Conrad, and M.H. Shaevitz, Phys. Rev. Lett. **117**, 221801 (2016).
12. M.C. Gonzalez-Garcia, Michele Maltoni, Jordi Salvado, and Thomas Schwetz, arXiv:1209.3023[hep-ph].
13. Ivan Esteban, M.C. Gonzalez-Garcia, Alvaro Hernandez-Cabezudo, Michele Maltoni, and Thomas Schwetz, arXiv:1811.05487[hep-ph].
14. Suman Bharti, Ushak Rahaman, and S. Uma Sankar, arXiv:2001.08676[hep-ph].
15. Zhi-zhong Xing, He Zhang and Shun Zhou, Phys. Rev. D **86**, 013013 (2012).



12 BSM Cosmology from BSM Physics

M. Yu. Khlopov

e-mail: khlopov@apc.univ-paris7.fr

Virtual Institute of Astroparticle physics, Université de Paris, CNRS, Astroparticule et Cosmologie, F-75013 Paris, France; Center for Cosmoparticle physics “Cosmion”, National Research Nuclear University MEPhI, 115409 Moscow, Russia, and Research Institute of Physics, Southern Federal University, Stachki 194, Rostov on Don 344090, Russia

Abstract. Now Standard Λ CDM cosmology is based on physics Beyond the Standard Model (BSM), which in turn needs cosmological probes for its study. This vicious circle of problems can be resolved by methods of cosmoparticle physics, in which cosmological messengers of new physics provide sensitive model dependent probes for BSM physics. Such messengers, which are inevitably present in any BSM basis for now Standard cosmology, lead to deviations from the Standard cosmological paradigm. We give brief review of some possible cosmological features and messengers of BSM physics, which include balancing of baryon asymmetry and dark matter by sphaleron transitions, hadronic dark matter and exotic cosmic ray components, a solution for puzzles of direct dark matter searches in dark atom model, antimatter in baryon asymmetrical Universe as sensitive probe for models of inflation and baryosynthesis and its possible probe in AMS02 experiment, PBH and GW messengers of BSM models and phase transitions in early Universe. These aspects are discussed in the general framework of methods of cosmoparticle physics.

Povzetek: Kozmologija CDM temelji na fiziki, ki standardni model razširi (BSM), vendar so zato potrebne metode, primerne za opazovanje novih fenomenov, ki jih nove teorije ponujajo. Avtor ponudi kratek pregled nekaterih kozmoloških modelov, ki razširijo standardni model in napovedujejo uravnoteženje barionske asimetrije in temne snovi s prehodi sfaleronov, hadronsko temno snov in eksotične komponente kozmičnih žarkov. Ponuja tudi razlago za dosedanje neujemanje rezultatov različnih poskusov, ki merijo sipanje delcev temne snovi na merilnih aparaturah, razlago za morebitni obstoj antisnovi v barionskem asimetričnem vesolju, ki utegne biti občutljiva sonda za preizkušanje modelov za inflacijo vesolja in bariosinteze ter možna sonda v eksperimentu AMS02, PBH in GW ter za fazne prehode v zgodnjem vesolju.

12.1 Introduction

The now Standard model of elementary particles appeals to its extension for recovery of its internal problems and/or embedding in the framework of unified description of the fundamental natural forces (see [23] for recent review). Such extensions are unavoidable in the fundamental physical basis for now Standard cosmological scenario, involving inflation, baryosynthesis and dark matter/energy [2, 3, 3–5, 8, 9, 20]. Probes for the BSM physics, underlying now standard cosmology, inevitably imply methods of cosmoparticle physics of cross disciplinary study of

physical, astrophysical and cosmological signatures of new physics [3,8]. Here we discuss some development of these methods presented at the XXIV Bled Workshop "What comes beyond the Standard models?" with special emphasis on the cosmological messengers of new physics, which can find positive evidence in the experimental data and thus acquire the meaning of signatures for the corresponding BSM models, specifying their classes and ranges of parameters.

If confirmed, such cosmological signatures should find explanation together with the basic elements of the modern cosmology. Therefore, the approach, which pretends on the unified description of Nature [11, 15] should not only reproduce the Standard model of elementary particles and propose BSM features, which provide realistic description of inflation, baryosynthesis and dark matter, but should be in possession to confront possible signatures of new physics, which can go beyond the standard cosmological paradigm.

Cosmological messengers of new physics can help to remove conspiracy of BSM physics, related with absence of its experimental evidence at the LHC, as well as conspiracy of BSM cosmology, reflected in concordance of the data of precision cosmology with now standard Λ CDM cosmological scenario [12]. Multimessenger cosmological probes can provide effective tool to study new physics at very high energy scale [13, 14]. Signatures for new physics play especially important role in these studies. They can strongly reduce the possible class of BSM models and provide determination of their parameters with high precision.

We consider such possible signatures in the direct searches of dark matter (Section 12.2.1), in gravitational wave signals from coalescence of massive black holes and searches for antinuclear component of cosmic rays (Section 12.3). We specify open questions in their confrontation with the corresponding messengers of BSM physics. We discuss in the conclusive Section 12.4 there signatures and their significance in the context of cosmoparticle physics of BSM physics and cosmology.

12.2 Signatures of dark matter physics

12.2.1 Dark atom signature in direct dark matter searches

The highly significant positive result of underground direct dark matter search in DAMA/NaI and DAMA/LIBRA experiments [15] can hardly be explained in the framework of the Standard cosmological paradigm of Weakly Interacting Massive Particles (WIMP), taking into account negative results of direct WIMP searches by other groups (see [23] for review and references). Though these apparently contradicting results may be somehow explained by difference of experimental strategy and still admit WIMP interpretation, their non-WIMP interpretation seems much more probable, making the positive results of DAMA group the signature for dark atom nature of cosmological dark matter [14, 16, 17, 23].

The idea that dark matter can be formed by stable particles with negative even charge $-2n$ bound in dark atoms with n primordial helium nuclei can qualitatively explain negative results of direct WIMP searches based on the search for nuclear recoil from WIMP interaction [14, 16, 23]. Dark atom interaction with matter is determined by its nuclear interacting helium shell, so that cosmic dark atoms

slow down in terrestrial matter and cannot cause significant recoil in underground experiments. However, in the matter of underground detector dark atoms can form low energy (few keV) bound states with nuclei of detector. The energy release in such binding possess annual modulation due to adjustment of local concentration of dark atoms to the incoming cosmic flux and can lead to the signal, detected in DAMA experiment.

Dark atoms represent strongly interacting asymmetric dark matter, since the corresponding models assume excess of $-2n$ charged particles over their $+2n$ antiparticles. Such excess can naturally be related with baryon asymmetry, if multiple charged particles possess electroweak charges and participate in electroweak sphaleron transitions. It is shown in [18] that the excess of $-2n$ charged particles in model of Walking Technicolor (WTC) and \bar{U} antiquarks (with the charge $-2/3$ of new stable generation can be balanced with baryon asymmetry and explain the observed dark matter density by dark atoms. The open question is whether such balance, which should also take place in the case stable 5th generation in the approach [11], can lead to the sufficient excess of \bar{u}_5 antiquarks to implement the idea of dark atoms in this case.

Pending on the value of $-2n$ charge, multiple charged constituents of dark atoms form either Bohr-like OHe atoms, binding -2 charged particles with primordial helium nucleus, or Thomson-like XHe atoms for $n > 1$. In the first case, double charged particles may be either composite, being formed by chromo-Coulomb binding in cluster $\bar{U}\bar{U}\bar{U}$ of stable antiquarks \bar{U} with charge $-2/3$, or -2 stable technileptons or technibaryons. Heavy quark clusters have strongly suppressed interaction with nucleons, while techniparticles behave as leptons. It leads to rather peculiar properties of dark atom - they have a heavy lepton or lepton-like core and nuclear interacting helium shell, which determines their interaction with baryonic matter.

Though interaction of dark atoms with nuclei are determined by their helium shell and thus don't involve parameters of new physics, the problem needs development of special methods for its solution. The approach of [19], assumed continuous extension of a classical three body problem to realistic quantum-mechanical description, taking into account finite size of interacting nuclei and helium shell, in order to reach self-consistent account for Coulomb repulsion and nuclear attraction, which can lead to creation of a shallow potential well with low energy bound state in dark atom - nucleus interaction. The development of this approach is presented in [20] for both Bohr-like and Thomson-like atoms. However, it becomes clear that probably the correct quantum-mechanical description should start from very beginning from quantum-mechanical nature of dark atom and numerical solutions for Schrodinger equation for dark-atom -nucleus quantum system. Development of self-consistent quantum-mechanical model of dark-atom interaction with nuclei and will make possible interpretation of the results [15] in terms of signature of dark atoms.

12.2.2 Multimessenger probes for decaying dark matter

Development of large scale experimental facilities like IceCube, HAWC, AUGER and LHAASO provides multimessenger astronomical probes for cosmological

messengers of superhigh energy physics [21]. The complex of LHAASO can provide unique measurement of ultra high energy photons, being in some cases most sensitive probe for existence of messengers of new physics at ultra-high energy scales. Superheavy decaying dark matter may be one of such messengers. Its decay products may contain ultrahigh energy neutrinos, photons, charged leptons and quarks. Sensitivity of LHAASO for the measurement of dark matter decay time

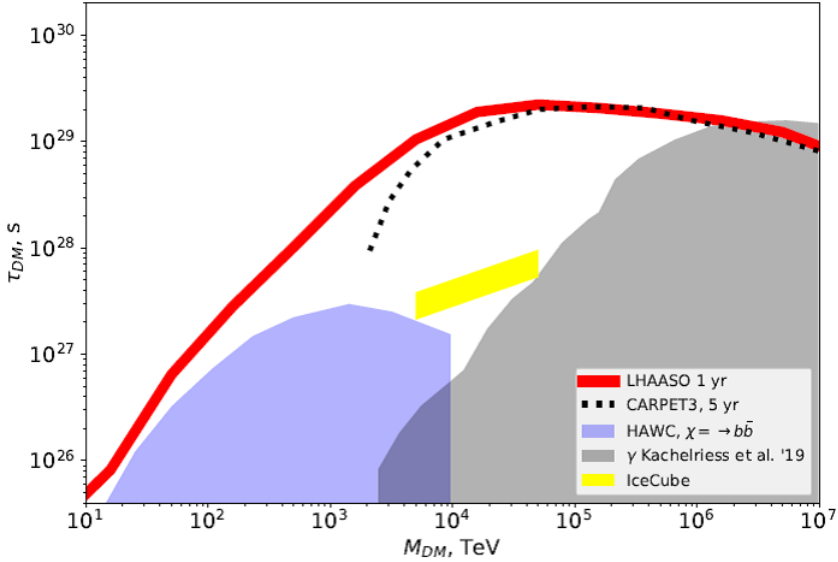


Fig. 12.1: Multimessenger probes for decaying supermassive dark matter particles

for DM decaying to quarks is demonstrated on Fig. 22.9, taken from [22]. Yellow band shows the range of decay times for which DM decays give sizable contribution to the IceCube neutrino signal [23]. Blue and gray shaded regions show the existing bounds imposed by HAWC [24] and ultra-high-energy cosmic ray experiments [25], and dashed curves are from the HAWC search of the DM decay signal in the Fermi Bubble regions [26]. It makes possible to confront multimessenger cosmological probes with the data of multimessenger astronomy.

12.3 Signatures for strong primordial inhomogeneities

12.3.1 Massive PBHs

Strong inhomogeneity of early Universe can lead to formation of primordial black holes (PBH). Such inhomogeneity may result from BSM physics at superhigh energy scales and thus even absence of positive evidence of PBH existence can provide important tool to probe allowed parameters of new physics at these scales [21, 27]. Formed within the cosmological horizon, which was small in the early Universe, it can seem that PBHs should have mass much smaller, than Solar

mass M_{\odot} . However, the mechanisms of PBH formation can provide formation of PBHs with stellar mass, and even larger than stellar up to the seeds for Active Galactic nuclei (AGN) [28–30].

LIGO/VIRGO detected gravitational wave signal from coalescence of black holes with masses exceeding the limit of pair instability ($50M_{\odot}$). Therefore black holes of such mass cannot be formed in the evolution of first stars. It has put forward the question on their primordial origin [31,32] and may be considered as signature for BSM physics, underlying formation of such massive PBHs.

In the approach [28] massive PBHs are formed in the collapse of closed walls originated from succession of phase transitions of breaking of U(1) symmetry and their mass is determined by the scale f of spontaneous symmetry breaking at the inflationary stage and scale Λ of successive explicit symmetry breaking. Therefore confirmation of primordial origin of massive PBHs would strongly narrow the choice of models of very early Universe and its underlying physics.

12.3.2 Cosmic antinuclei as probe for matter origin

Baryon asymmetry of the Universe reflects absence of macroscopic antimatter in the amount comparable with baryonic matter within the observed Universe. Its origin is related with the mechanism of baryosynthesis, in which baryon excess is created in very early Universe. However, inhomogeneous baryosynthesis can lead not only to change of the value of baryon excess in different regions of space, but in the extreme case can change sign of this excess, giving rise to antimatter, produced in the same process, in which the baryonic matter was created [3,9,11,13,17,33]. Antimatter domains should be sufficiently large to survive in matter surrounding and it implies also effect of inflation in addition to nonhomogeneous baryosynthesis. It means that the prediction of macroscopic antimatter, surviving to the present time, involves rather specific combination of necessary conditions and correspondingly specific choice of BSM model parameters.

The choice of BSM model parameters determines the forms of macroscopic antimatter in our Galaxy. Antimatter domain can evolve in the way, similar to the baryonic matter and form antimatter globular cluster in our Galaxy [3,39]. The antibaryon density may be much higher, than the baryonic density and then specific ultra-dense antibaryon stars can be formed [12]. In any case, the predicted fraction of antihelium nuclei in cosmic rays from astrophysical sources is far below the sensitivity of AMS02 experiment, making positive results of cosmic antihelium signature of macroscopic antihelium in our Galaxy.

The possibility of confirmation of first indications to the antihelium events in AMS02 makes necessary to study in more details evolution of antibaryon domains in baryon asymmetrical universe [42,43] in the context of models of inhomogeneous baryosynthesis. It makes necessary to study expected composition and spectrum of cosmic antinuclei from antimatter globular cluster [44], as well as to consider more general question on propagation in galactic magnetic fields of antinuclei from local source in galactic halo [45]

12.4 Conclusions

There are some hints to new phenomena in the observational data [46–48]. The deviations from the standard cosmological model may be related with the modified gravity [49, 50], leading beyond the Standard model of all the four fundamental interactions. Then one can expect additional types of polarization of gravitational waves [51]. Such hints are not at such high significance level as the results of DAMA experiments [15], but they can strongly extend the list of multimessenger probes of BSM physics.

Constraints on such exotic phenomena, as PBHs or antimatter in baryon asymmetrical Universe exclude rather narrow ranges of BSM model parameters. Signatures for such phenomena make these ranges preferential, strongly reducing the class of BSM models and fixing their parameters with high precision. In the context of cosmoparticle physics, studying fundamental relationship of macro- and micro- worlds signatures for cosmological messengers of BSM physics acquires the meaning of precision measurement of parameters of fundamental structure of microworld with astronomical accuracy.

Acknowledgements

The work was supported by grant of Russian Science Foundation (Project No-18-12-00213-P).

References

1. M.Khlopov: What comes after the Standard model? *Progress in Particle and Nuclear Physics*, **116**, 103824 (2021).
2. A.D. Linde: *Particle Physics and Inflationary Cosmology*, Harwood, Chur, 1990.
3. E.W. Kolb and M.S. Turner: *The Early Universe*, Addison-Wesley, Boston, MA, USA, 1990.
4. D.S. Gorbunov and V.A. Rubakov: *Introduction to the Theory of the Early Universe Hot Big Bang Theory. Cosmological Perturbations and Inflationary Theory*, World Scientific, Singapore, 2011.
5. D.S. Gorbunov and V.A. Rubakov: *Introduction to the Theory of the Early Universe Hot Big Bang Theory*, World Scientific, Singapore, 2011.
6. M.Y. Khlopov: *Cosmoparticle Physics*, World Scientific, Singapore, 1999.
7. M.Y. Khlopov: *Fundamentals of Cosmoparticle Physics*, CISP-Springer, Cambridge, UK: 2012.
8. M. Khlopov: Cosmological Reflection of Particle Symmetry, *Symmetry* **8**, 81 (2016).
9. M. Khlopov: Fundamental particle structure in the cosmological dark matter, *Int. J. Mod. Phys. A* **28**, 1330042 (2013).
10. N. Mankoc-Borstnik: Unification of spins and charges in Grassmann space? *Mod. Phys. Lett. A* **10**, 587-596 (1995).
11. N. Mankoc-Borstnik: Achievements of spin-charge family theory so far. *Bled Workshops in Physics*. **22**, 202-232 (2021), This issue
12. M.Yu. Khlopov: Removing the conspiracy of BSM physics and BSM cosmology, *Int. J. Mod. Phys. D* **28**, 1941012 (2019).
13. M.Khlopov: Multi-messenger cosmology of new physics. *Journal of Physics: Conference Series* (2020), arXiv:2010.14581.

14. M.Khlopov: Multimessenger Probes for New Physics in Light of A. Sakharov's Legacy in Cosmoparticle Physics. *Universe* **7**, 222 (2021). <https://doi.org/10.3390/universe7070222>
15. R.Bernabei, et al: New and recent results, and perspectives from DAMA/LIBRA-phase2. *Bled Workshops in Physics*. **22**, 32-51 (2021), This issue.
16. M. Y. Khlopov: Composite dark matter from 4th generation, *JETP Letters* **83**, 1–4 (2006).
17. V. Beylin, M. Khlopov, V. Kuksa, N. Volchaanskiy: New physics of strong interaction and Dark Universe, *Universe* **6**, 196 (2020).
18. A.Chaudhuri, M.Khlopov. Balancing asymmetric dark matter with baryon asymmetry and dilution of frozen dark matter by sphaleron transition. *Universe* **7**, 275 (2021) <https://doi.org/10.3390/universe7080275>. arXiv:2106.11646
19. T.E. Bikkbaev, M.Yu. Khlopov, A.G. Mayorov: Numerical simulation of dark atom interaction with nuclei, *Bled Workshops in Physics*, **21**, 105-117 (2020), arXiv:2011.01362 [hep-ph].
20. T.E.Bikkbaev, M.Yu.Khlopov and A.G. Mayorov: Numerical simulation of Bohr-like and Thomson-like dark atoms with nuclei. *Bled Workshops in Physics*. **22**, 65-77 (2021), arXiv:2111.09042. This issue
21. S.V. Ketov, M.Yu. Khlopov: Cosmological Probes of Supersymmetric Field Theory Models at Superhigh Energy Scales, *Symmetry* **11**, 511 (2019).
22. A.Addazi, et al: Dark Matter Searches for heavy Dark Matter with LHAASO. *PoS(ICRC2021)*, **395**, 574 (2021).
23. A. Neronov, M Kachelrieß, and DV Semikoz: Multimessenger gamma-ray counterpart of the IceCube neutrino signal. *Phys. Rev. D*, **98**(2):023004, (2018). doi:10.1103/PhysRevD.98.023004.
24. A. U. Abeysekara et al. A search for dark matter in the Galactic halo with HAWC JCAP, **1802**(02):049, 2018. arXiv:1710.10288, doi:10.1088/1475-7516/2018/02/049.
25. M. Kachelrieß, O. E. Kalashev, and M. Yu. Kuznetsov: Heavy decaying dark matter and IceCube high energy neutrinos *Phys. Rev., D* **98**(8):083016, (2018). doi:10.1103/PhysRevD.98.083016.
26. A. Neronov and D. Semikoz: LHAASO sensitivity for diffuse gamma-ray signals from the Galaxy. *Phys. Rev. D* **102**, 043025 (2020)
27. M.Yu. Khlopov: Primordial black holes, *Res. Astron. Astrophys.***10**, 495 (2010).
28. S.G. Rubin, A.S. Sakharov, M.Y. Khlopov: Formation of primordial galactic nuclei at phase transitions in the early Universe, *JETP* **92**, 921 (2001).
29. K.M. Belotsky, V.I. Dokuchaev, Y.N. Eroshenko, E.A. Esipova, M.Y. Khlopov, L.A. Khromykh, A.A. Kirillov, V.V. Nikulin, S.G. Rubin, I.V. Svadkovsky: Clusters of primordial black holes, *Eur. Phys. J. C* **79**, 246 (2019).
30. A.D. Dolgov: Massive primordial black holes in contemporary and young universe (old predictions and new data) *Int.J.Mod.Phys. A* **33**, 1844029 (2018).
31. The LIGO Scientific Collaboration; the Virgo Collaboration; R. Abbott *et al*: GW190521: A Binary Black Hole Merger with a Total Mass of $150 M_{\odot}$, *Phys. Rev. Lett.* **125**, 101102 (2020)
32. The LIGO Scientific Collaboration; the Virgo Collaboration; R. Abbott *et al*: Properties and astrophysical implications of the $150 M_{\text{sun}}$ binary black hole merger GW190521, *Astrophys J. Lett.* **900**, L13 (2020)
33. V.M. Chechetkin, M.Yu. Khlopov, M.G. Sapozhnikov, Y.B. Zeldovich: Astrophysical aspects of antiproton interaction with He (Antimatter in the Universe), *Phys. Lett. B* **118**, 329 (1982).
34. A.D. Dolgov: Matter and antimatter in the universe, *Nucl. Phys. Proc. Suppl.* **113**, 40 (2002)

35. A. Dolgov, J. Silk: Baryon isocurvature fluctuations at small scales and baryonic dark matter, *Phys. Rev. D* **47**, 4244 (1993).
36. A.D. Dolgov, M. Kawasaki, N. Kevlishvili: Inhomogeneous baryogenesis, cosmic antimatter, and dark matter, *Nucl. Phys. B* **807**, 229 (2009).
37. M.Y. Khlopov, S.G. Rubin, A.S. Sakharov: Possible origin of antimatter regions in the baryon dominated Universe, *Phys. Rev. D* **62**, 083505 (2000).
38. K.M. Belotsky, Y.A. Golubkov, M.Y. Khlopov, R.V. Konoplich, A.S. Sakharov: Antihelium flux as a signature for antimatter globular cluster in our Galaxy, *Phys. Atom. Nucl.* **63**, 233 (2000).
39. M.Yu. Khlopov: An antimatter globular cluster in our Galaxy - a probe for the origin of the matter, *Gravitation and Cosmology*, **4**, 69-72 (1998).
40. S.I. Blinnikov, A.D. Dolgov, K.A. Postnov: Antimatter and antistars in the universe and in the Galaxy, *Phys. Rev. D* **92**, 023516 (2015).
41. V. Poulin, P. Salati, I. Cholis, M. Kamionkowski, J. Silk: Where do the AMS-02 antihelium events come from? *Phys. Rev. D* **99**, 023016 (2019).
42. M.Yu.Khlopov, O.M.Lecian: Analyses of Specific Aspects of the Evolution of Antimatter Glubular Clusters Domains. *Astronomy Reports*, **65**, 967–972 (2021) DOI: 10.1134/S106377292110019X
43. M.Khlopov, O.M.Lecian: Statistical analyses of antimatter domains, created by non-homogeneous baryosynthesis in a baryon asymmetrical Universe. *Bled Workshops in Physics*, **22** (2021), arXiv:2111.14114 This issue
44. M.Yu. Khlopov, A.O. Kirichenko, A.G. Mayorov: Anihelium flux from antimatter globular cluster, *Bled Workshops in Physics*, **21**, 118-127 (2020), arXiv:2011.06973 [astro-ph.HE].
45. A.O.Kirichenko, A.V.Kravtsova, M.Yu.Khlopov and A.G. Mayorov Researching of magnetic cutoff for local sources of charged particles in the halo of the Galaxy. *Bled Workshops in Physics*, **22** (2021), arXiv:2112.00361. This issue
46. Z. Arzoumanian *et al* [NANOGrav Collaboration]: The NANOGrav 12.5-year Data Set: Search For An Isotropic Stochastic Gravitational-Wave Background, *Astrophys. J. Lett.* **905**, L34 (2020).
47. S. Vagnozzi: New physics in light of the H_0 tension: An alternative view, *Phys. Rev. D* **102**, 023518 (2020).
48. S.A. Levshakov, M.G. Kozlov, I.I. Agafonova: Constraints on the electron-to-proton mass ratio variation at the epoch of reionization, *Mon.Not.Roy.Astr. Soc.* **498**,3624–3632 (2020).
49. P. Kroupa, M. Haslbauer, I. Banik, S.T. Nagesh, J. Pflamm-Altenburg: Constraints on the star formation histories of galaxies in the Local Cosmological Volume, *Mon. Not. Roy. Astr. Soc.* **497**, 37 (2020)
50. K.-H. Chae, F. Lelli, H. Desmond, S.S. McGaugh, P. Li, J.M. Schombert: Testing the Strong Equivalence Principle: Detection of the External Field Effect in Rotationally Supported Galaxies, *Astrophys. J.* **904** (2020) arXiv:2009.11525.
51. S. Roy Chowdhury, M.Yu. Khlopov: Gravitational waves in the modified gravity. *Bled Workshops in Physics*, **22**, 127-135 (2021), arXiv:2111.07704. This issue



13 Statistical analyses of antimatter domains, created by nonhomogeneous baryosynthesis in a baryon asymmetrical Universe

M. Yu. Khlopov¹

email: khlopov@apc.in2p3.fr

O.M. Lecian²

email: orchideamaria.lecian@uniroma1.it

¹Institute of Physics, Southern Federal University, Russia; National Research Nuclear University "MEPHI", 115409 Moscow, Russia, and Université de Paris, CNRS, Astroparticule et Cosmologie, France;

²Sapienza University of Rome, Faculty of Medicine and Pharmacy, V.le Regina Elena, 324- 00185 Rome, Italy

Abstract. Within the framework of scenarios of nonhomogeneous baryosynthesis, the formation of macroscopic antimatter domains is predicted in a matter-antimatter asymmetrical Universe. The properties of antimatter within the domains are outlined; the matter-antimatter boundary interactions are studied. The correlation functions for two astrophysical objects are calculated. The theoretical expression in the limiting process of the two-points correlation function of an astrophysical object and an antibaryon is derived.

Povzetek: Avtorja uporabita model nehomogene barionsinteze za nesimetrično vesolje. Študirata nastanek domen antisnovi, lastnosti antisnovi v domenah ter interakcijo med snovjo in antisnovjo na mejah domen. Izračunala sta korelacijske funkcije dveh astrofizikalnih objektov v nehomogenem vesolju. Prikazeta teoretične relacije za limitne procese dvotočkovnih korelacijskih funkcij astrofizikalnega objekta in antibariona.

Keywords: General Relativity, Dark matter.

13.1 Introduction

The origin of the baryon asymmetry of the Universe is explained in the now Standard cosmology by the mechanism of baryosynthesis. If baryon excess generation is nonhomogeneous, the appearance of domains with antibaryon excess can be predicted in baryon asymmetrical Universe.

In such non-trivial baryosynthesis frameworks, we study evolution of antimatter domains according to their dependence on the size and antimatter densities within them.

The boundary conditions for antimatter domains are determined through the interaction with the surrounding baryonic medium.

Within the analysis, new classifications for antibaryon domains, which can evolve in antimatter globular clusters, are in order.

Differences must be discussed within the relativistic framework chosen, the nucleosynthesis processes, the description of the surrounding matter medium, the confrontation with the experimental data within the observational framework. The space-time-evolution of antimatter domains and the correlation functions are described within the nucleon-antinucleon boundary interactions.

The manuscript is organized as follows.

We consider formation of antibaryon domains in the spontaneous CP-symmetry-breaking scenario (Section 13.2) and in the model of spontaneous baryosynthesis. Evolution of such domains is determined by nucleon-antinucleon interaction at the boundaries of antimatter domains.

We deduce correlation functions for the celestial objects, predicted in these scenarios.

Them manuscript is organized as follows.

In Section 13.2, the symmetry-breaking scenario have been recalled.

In Section 13.3, the cosmological implications have been studied.

In Section 13.4, the spontaneous baryosynthesis process has been analyzed.

I Section 13.5, different antimatter spacetime distributions have been presented.

In Section 13.6, antimatter interactions have been studied.

Is Section 13.7, nucleon-antinucleon interactions have been codified.

In Section 13.8, correlation function for celestial objects have been analytically calculated.

Is Section 13.9, brief outlook and perspectives have been outlined.

Concluding remarks end the paper.

13.2 Symmetry-breaking scenario

The symmetry-breaking scenarios have been stusied in [1]- [5].

The spontaneous CP violation is described [1] after the Lagrangean potential density

$$\begin{aligned}
 V(\phi_1, \phi_2, \chi) = & -\mu_1^2(\phi_1^\dagger \phi_1 + \phi_2^\dagger \phi_2) + \lambda_1[(\phi_1^\dagger \phi_1)^2 + (\phi_2^\dagger \phi_2)^2] + 2\lambda_3(\phi_1^\dagger \\
 & \phi_1)(\phi_2^\dagger \phi_2)(\phi_1^\dagger \phi_2) + 2\lambda_4(\phi_1^\dagger \phi_2)(\phi_2^\dagger \phi_1) + \lambda_5[(\phi_1^\dagger \phi_2)^2 + \text{h.c.}] + \\
 & \lambda_6(\phi_1^\dagger \phi_1 + \phi_2^\dagger \phi_2)(\phi_1^\dagger \phi_2 + \phi_2^\dagger \phi_1) - \mu_2^2 \chi^\dagger \chi + \delta(\chi^\dagger \\
 & \chi)^2 + 2\alpha(\chi^\dagger \chi)(\phi_1^\dagger \phi_1 + \phi_2^\dagger \phi_2) + 2\beta[(\phi_1^\dagger \chi)(\chi^\dagger \phi_1) + (\phi_2^\dagger \chi)(\chi^\dagger \phi_2)].
 \end{aligned}
 \tag{13.1}$$

As a result, an effective low-energy electroweak $SU(2) \otimes U(1)$ theory is achieved, allowing for a GUT spontaneous CP violation. The formation of vacuum structures separated from the rest of the matter universe by domain walls follows. The size of the domains is calculated to grow with the evolution of the Universe. The behavior is calculated not to affect the evolution of the Universe if the volume energy $\rho(\tilde{V})$ density of the walls for

$$\rho(\tilde{V}) \sim \sigma_\phi^2 T^4 / \tilde{\hbar},$$

with \tilde{h} value of the scalar coupling constant.

In Eq. (13.1), for the three effective scalar fields, the CP violation is achieved with complex vev's and vacuum domain structures appear with opposite CP violation sign: walls are predicted to be massive, and the size of walls is predicted to grow [1].

A CP-invariant Lagrangian density can be assumed of the form [2]

$$L = (\partial\phi)^2 - \lambda^2(\phi^2 - \chi^2)^2 + \bar{\psi}(i\partial - m - ig\gamma_5\phi)\psi \quad (13.2)$$

in which the vacuum is characterized by the values $\langle \phi \rangle = \sigma\eta$, with $\sigma = \pm 1$.

The rotation $\psi \rightarrow e^{i\alpha\gamma_5}\psi$, with $\tan 2\alpha = -g\sigma\eta/m$

induces the appearance in the Lagrangian density of two terms with opposite CP symmetry. The sign of the phase depends on σ , with $\lambda \leq 1$, for which $1 \leq \eta$.

For the Lagrangian density [6]

$$L = (\partial\chi)^2 - \frac{1}{2}m_\chi^2\chi^2 - 4\sigma\lambda_2\chi\eta^3 - \lambda^2\chi^4 + \bar{\psi}(i\hat{\partial} - M - i\frac{gm}{M}\gamma_5\chi - \frac{g^2\sigma\eta}{M}\chi)\psi. \quad (13.3)$$

a CP violation can be achieved after the substitution $\phi = \chi + \sigma\eta$.

For the Lagrangian potential

$$V(\chi) = -m_\chi^2\chi^2 + \lambda_\chi(\chi^*\chi)^2 + V_0, \quad (13.4)$$

with $\chi = \frac{f}{\sqrt{2}}e^{i\frac{\alpha}{f}}$, a U(1) symmetry breaking is achieved, with $\theta = \alpha/f$.

The domain wall problem can be solved after the Kuzmin-Shaposhnikov-Tkachev mechanism.

13.3 Implications in cosmology

Several phenomena can be looked for following the described mechanisms.

The research for antinuclei in cosmic rays is analyzed as a possible outcome of the model.

The research for annihilation products constitutes a further verification procedure for the theoretical framework.

In particular, annihilation at rest on Relativistic background is to be studied.

The annihilation of small-scale domains is a further investigation theme. It can be achieved within the *thin-boundary approximation*.

Moreover, at different times, the *diffusion of the baryon charge* is determined after different processes.

13.4 Spontaneous baryosynthesis

A spontaneous baryosynthesis allowing for the possibility of sufficiently large domains through proper combination of effects of inflation and baryosynthesis is described after the choice of fields

$\chi \equiv \frac{f}{\sqrt{2}} e^\theta$, for which the variance reads

$$\langle \delta\theta \rangle = \frac{H^3 t}{4\pi^2 f^2}. \tag{13.5}$$

as in [7], [8], [9], [10], [11]. This way, the **probability for the existence of antimatter particles** is set.

The number of objects $\tilde{N}(t) - \tilde{N}(t_0)$ is calculated as

$$\tilde{N}(t) - \tilde{N}(t_0) \equiv \int_{t_0}^{t_i} P(\chi) \ln \chi d\chi(t), \tag{13.6}$$

with $P(\chi)$ including variance.

The evaluation of the number of antibaryons is performed after the use of the quantity \tilde{H} , i.e. the Hubble-radius function, and after the definition of *effective quantities* Δf_{eff} , i.e. the effective (time-dependent) phase function, and

$$f_{eff} = f \sqrt{1 + \frac{g_{\phi\chi} M_{Pl}}{12\pi\lambda} (N_c - N)}, \tag{13.7}$$

i.e. the effective phase, with N the e-foldings at inflation.

The following consequences are extracted.

If the density is so low that nucleosynthesis is not possible, low density antimatter domains contain only antiprotons (and positrons).

High density antimatter domains contain antiprotons and antihelium.

Heavy elements can appear in stellar nucleosynthesis, or in the high-density antimatter domains.

Strong non-homogeneity in antibaryons might imply (probably as a necessary condition) strong non-homogeneity for baryons, and produce some exotic results in nucleosynthesis.

13.5 Spacetime antimatter statistical distributions

It is possible to specify the standard deviation for the field χ for different spacetime antimatter statistical distributions.

13.5.1 Binomial spacetime antimatter distribution

In the hypothesis antibaryons are described as following a binomial [12] statistical spacetime distribution, the number of antibaryons \tilde{N} contained in an antimatter domain reads

$$\tilde{N}(k) - \tilde{N}_0(k) \simeq \sum_k \frac{1}{(k!)(1-k)!} \frac{\chi_{t_a}}{\chi_{t_0}} \frac{2}{\Delta f_{eff}(t; t_a, t_i, t_0)} \left(\frac{(-2)}{4\pi^2} \cdot \left[\ln \frac{L_u e^{H_c(t_c-t_0)} - e^{H_0 t_0}}{l} \right] \right)^k (t)^{k-3} \tag{13.8}$$

which is described after the effective quantities f_{eff} and those defined after the Hubble function H .

13.5.2 Poisson space-time antimatter statistical distribution

In the hypothesis antibaryons are described as following a Poisson statistical space-time distribution, the number of antibaryons \tilde{N} contained in an antimatter domain reads

$$\tilde{N}(k) - \tilde{N}_0(k)(\Delta t) \simeq \sum_n \sum_k \frac{k^n e^k}{n!} \frac{\chi_{t_a}}{\chi_{t_0}} \frac{2}{\Delta f_{eff}(t; t_a, t_i, t_0)} \cdot \left(\frac{(-2)}{4\pi^2} \left[\ln \frac{L_u e^{H_c(t_c - t_0)} - e^{H_0 t_0}}{l} \right] \right)^k (t)^{k-3}, \quad (13.9)$$

which is described after the effective quantities f_{eff} and those defined after the Hubble function H .

13.5.3 Bernoulli spacetime antimatter distribution

In the hypothesis antibaryons are described as following a Bernoulli statistical spacetime distribution, the number of antibaryons \tilde{N} contained in an antimatter domain reads

$$\tilde{N}(k) - \tilde{N}_0(k) \simeq \frac{1}{(k!)(1-k)!} \frac{\chi_{t_a}}{\chi_{t_0}} \frac{2}{\Delta f_{eff}(t; t_a, t_i, t_0)} \left(\frac{(-2)}{4\pi^2} \cdot \left[\ln \frac{L_u e^{H_c(t_c - t_0)} - e^{H_0 t_0}}{l} \right] \right)^k (t)^{k-3} \quad (13.10)$$

which is described after the effective quantities f_{eff} and those defined after the Hubble function H .

13.6 Antimatter domains and antibaryons interactions

At the *radiation-dominated era*

within the cosmological evolution, the dominant contribution to the total energy is due to photons.

In the case of *low density antimatter domains*, the contribution of the density of antibaryons $\rho_{\bar{B}}$ is smaller than the contribution due to the radiation ρ_{γ} even at the matter-dominated stage.

In a FRW Universe, within its thermal history, for $T < 100\text{keV}$, only photons as a dominant components are considered.

At the *matter-dominated era and following*

within a *non-homogeneous* scenario, $\rho_{DM} > \rho_B$, with $\rho \equiv \rho(x)$.

The creation of high density antibaryon domains can be accompanied by similar increase in baryon density in the surrounding medium. Therefore outside high density antimatter domain baryonic density may be also higher than DM density $\rho_B(x) > \rho_{DM}(x)$.

In the case of *low density antimatter domains*:

the total density is such that $\rho_{\bar{B}} + \rho_{\gamma}$, and $\rho_{\bar{B}} < \rho_{\gamma}$, with $\rho_{dm} > \rho_B$

13.7 Nucleon-antinucleon interaction studies

Within the framework of the studies of nucleons-antinucleons interaction, several schematizations are possible.

In the case of *proton-antiproton annihilation probability*, the *limiting process* and the *theoretical formulation* can be studied.

Let $P(\bar{p})$ be the probability of existence of one antiproton of mass m_p , with m_p being the proton mass, in the spherical shell of section r_I , of (antimatter)-density ρ_I , delimiting the antimatter domain, in which the interaction takes place $P(\bar{p}) \equiv 3Nm_p/(r_I\rho_I)$. This way, the interaction probability reads

$$\tilde{P}_i \equiv \tilde{P}_{\bar{p} \rightarrow (d.c.i)}$$

i.e. it constitutes the probability of antiproton \bar{p} interaction with a proton p in a chosen i annihilation channel a.c., possibly also depending on the chemical potential.

Let Δt be the time interval considered, under the most general hypotheses (most stringent constraint), $\Delta t \pm \delta t$, $\Delta t \simeq t_U \simeq 4 \cdot 10^{17} s$, with t_U age of the universe, δt to be set according to the particular phenomena considered. This way $\bar{P}_{\bar{p},i}(t, \Delta t)$. i.e. the probability of antiproton interaction, i.e. antiproton-proton annihilation (density), reads

$$\bar{P}_{\bar{p},i} \simeq \frac{1}{\Delta t} P_{\bar{p}} \tilde{P}_i \tag{13.11}$$

As a second study, the

nucleon-antinucleon interaction (annihilation) probabilities are evaluated after the antinucleus \bar{M} interaction probability $\bar{P}_{\bar{M},j}(t, \Delta t)$ through the annihilation channel(s) k as

$$\bar{P}_{\bar{M},k}(t, \Delta t) \simeq \frac{1}{\Delta t} P_{\bar{A}} \tilde{P}_{\bar{A},k}. \tag{13.12}$$

In these examples, all the probabilities are normalized as $[t^{-1}]$.

The studies of nucleons-antinucleons interactions are to be further specified for non-trivial Relativistic scenarios *such as perturbed FRW with the thermal history of the Universe, i.e., also, according to the Standard Cosmological Principle*.

The non-trivial Relativistic scenarios are schematized as at large scales asymptotically isotropic and homogeneous.

Further specifications can be in order in the case of non-trivial nucleosynthesis, possibilities of surrounding media, antibaryon-baryon annihilation. In the latter case, the most stringent constraint follows after \bar{P} evaluated for present times in the description of reducing density in the limiting process of a low-density antimatter domain.

13.7.1 An example

In the example of low-density antimatter domains, non-interacting antiprotons are described, boundary interactions are taken onto account, and interaction with

surrounding medium can be considered.

In particular, low-density antimatter domains can be surrounded by low-density matter regions.

13.8 Correlation functions

Two-point correlation functions \tilde{C}_2 for two antimatter domains α_1 and α_2 of size $> 10^3 M_\odot$ each can be within the present framework analytically calculated.

More in detail, on (homogeneous, isotropic) Minkowski-flat background, and under the hypothesis antimatter densities $\rho \equiv \tilde{N}/V$ following a Poisson space-time statistical distribution.

The two-point correlation function \tilde{C}_2 is defined as

$$d\tilde{C}_2(\alpha_1, \alpha_2) \equiv \rho^2(1 + \xi(|\vec{r}_{\alpha_1\alpha_2}|))dV_1dV_2 \quad (13.13)$$

where

$$\xi(|\vec{r}_{\alpha_1\alpha_2}|) \equiv |\vec{r}_{\alpha_1\alpha_2}| \quad (13.14)$$

defines the estimator, and $\vec{r}_{\alpha_1\alpha_2}$ the distance of the two antimatter domains.

Given two antimatter domains α_1 and α_2 of volume $V_{\alpha_1} \equiv \frac{4}{3}\pi r_1^3$, separated of a distance $|\vec{r}_{\alpha_1\alpha_2}|$ *the correlation function is analytically integrated as*

$$\tilde{C}_2(\alpha_1, \alpha_2) = 2\pi\tilde{n}(n, k; \Delta f_{eff}, \tilde{H}; \Delta t) |\vec{r}_{\alpha_1\alpha_2}| \left(\frac{1}{r_2} + \frac{1}{r_1} \right) \tilde{H}_c^{2k} t^{4k-4} \quad (13.15)$$

evaluated at the present time t , with \tilde{H}_c the effective Hubble-radius function.

13.8.1 An example: the two-point correlation functions for an antimatter domain and another object

It is possible to consider the *limiting example* of the correlation function between an antimatter domain α_1 and an antibaryon α_3 . The *Davis-Peebles estimator* for the macroscopic objects described in terms of density distribution and temperature distribution reads

$$\xi_{l,l'} \equiv \frac{\tilde{N}_{bin}}{\tilde{N}} \frac{D_l(|\vec{r}|)}{D_{l'}(|\vec{r}|)} - 1, \quad (13.16)$$

with \tilde{N} number of antibaryons in a low-density antimatter domain, where the antimatter is assumed to be distributed according to a Poisson space-time statistical distribution, and \tilde{N}_{bin} the number of antibaryons in a low-density antimatter domain where the antimatter is distributed according to a binomial space-time statistical distribution,

the quantity $D_l(|\vec{r}|)$ indicates the number of pairs of low-density appropriate-mass antimatter domains within the geodesics (coordinate) interval distance $[r - \frac{dr}{2}, r + \frac{dr}{2}]$, the quantity $D_{l'}(|\vec{r}|)$ indicates the number of pairs of objects between an antimatter domain and

an (*Poisson-distributed*) antibaryon on the coordinate geodesics. For the Davis-Peebles estimator

$$\xi_{l,l'} \equiv \frac{\tilde{n}_{\text{bin}}(n, k; \Delta f_{\text{eff}}, \tilde{H}; \Delta t) D_l(|\vec{r}|)}{\tilde{n}(n, k; \Delta f_{\text{eff}}, \tilde{H}; \Delta t) D_l'(|\vec{r}|)} - 1 \quad (13.17)$$

within the use of statistical estimators, the time dependence $\tilde{H}_c^{2k} t^{4k-4}$ is suppressed, and the *time dependence* is expressed after the ratio $\frac{\tilde{n}_{\text{bin}}(n, k; \Delta f_{\text{eff}}, \tilde{H}; \Delta t)}{\tilde{n}(n, k; \Delta f_{\text{eff}}, \tilde{H}; \Delta t)}$, i.e. on the different statistical antimatter space-time distributions and on their dependence on the \tilde{H} Hubble-radius function, and on the Δf_{eff} effective (time-dependent) phase function.

13.8.2 Hamilton estimator

The Hamilton estimator

$\tilde{\xi}_{l,l'}$ takes into account the difference in distances among the Binomial distribution and the Poisson distribution.

13.9 Outlook and perspectives

In the case antimatter domains are described to be separated in a small angular distance, the Rubin-Limber correlation functions [13], [14] for small angles can be used.

An analysis of the metric requiring a time evaluation after the time of the surface of last scattering can be analyzed also for different metrics, as in [15]

13.10 Concluding remarks

Prediction of macroscopic antimatter in baryon asymmetrical Universe is based on rather specific choice of parameters of baryosynthesis. To make antimatter domains sufficiently large to survive in the baryon matter surrounding a nontrivial combination of baryosynthesis and inflation are needed. It may look like we study a highly improbable and very exotic case. However, on the other hand, positive evidence for existence of macroscopic antimatter in our Galaxy, which may appear in the searches of cosmic antinuclei in AMS02 [22] would strongly favor models, predicting antimatter domains in baryon asymmetric Universe, and would make possible to select the narrow classes of models of inflation and baryosynthesis, as well as to specify their parameters with high precision [20]. In view of this possibility we started to develop in the present work statistical analysis of possible space distribution of antimatter domains with the account for their evolution.

Confrontation of the predicted distribution of antimatter domains with the observational data would be important for multimessenger test of the models of nonhomogeneous baryosynthesis. The observable signatures of this distribution is the important direction of our future studies. In particular, the most probable forms of the evolved antimatter in our Galaxy should be clarified in this analysis.

It should be noted that the mechanisms of generation of antibaryon excess in baryon asymmetrical Universe may be accompanied by formation of domain walls at the border of antimatter domains. If these closed walls start to dominate, before they enter the horizon, the corresponding domains, surrounded by walls would become closed worlds, separating from our Universe. This open question is another challenge for our future analysis

Acknowledgements

The work by MK has been supported by the grant of the Russian Science Foundation (Project No-18-12-00213-P).

References

1. V.A. Kuzmin, M.E. Shaposhnikov, I.I. Tkachev, Matter-antimatter domains in the Universe: a solution of the vacuum walls problem, *Phys. Lett.* **B 105**, 1 (1981).
2. Ya.B. Zeldovich, L.B. Okun, L.Yu. Kobzarev, Cosmological Consequences of a Spontaneous Breakdown of a Discrete Symmetry, *Zh. Eksp. Teor. Fiz.* **40**, 1 (1974).
3. V.M. Chechetkin, M.G. Sapozhnikov, M.Yu. Khlopov, Ya.B. Zeldovich, Astrophysical aspects of antiproton interaction with ^4He (antimatter in the universe) *Phys. Lett.* **B 118**, 329 (1982).
4. V.M. Chechetkin, M.G. Sapozhnikov, M.Yu. Khlopov, Antiproton interactions with light elements as a test of GUT cosmology, *Riv. N. Cim.* **5**, 1 (1982).
5. V.A. Kuzmin, I.I. Tkachev, M.E. Shaposhnikov, Are There Domains of Antimatter in the Universe?, *Zh. Eksp. Teor. Fiz. Lett.* **33**, 557 (1981).
6. M.Yu. Khlopov, S.G. Rubin, A.S. Sakharov, Possible origin of antimatter regions in the baryon dominated universe, *Phys. Rev.* **D 62**, 083505 (2000)-
7. M.Yu. Khlopov, S.G. Rubin, A.S. Sakharov, Possible origin of antimatter regions in the baryon dominated universe, *Phys. Rev.* **D 62**, 083505 (2000).
8. M.Yu. Khlopov, S.G. Rubin, A.S. Sakharov, Antimatter regions in the baryon dominated universe, 14th Rencontres de Blois on Matter- Anti-matter Asymmetry [hep-ph/0210012].
9. A.D. Dolgov et al., Baryogenesis During Reheating in Natural Inflation and Comments on Spontaneous Baryogenesis, *Phys. Rev.* **D 56**, 6155 (1997).
10. A.G. Cohen and D.B. Kaplan, Thermodynamic generation of the baryon asymmetry, *Phys. Lett.* **B 199** (1987) 251.
11. A.G. Cohen and D.B. Kaplan, Spontaneous baryogenesis, *Nucl. Phys.* **B 308** (1988) 913.
12. J. Bernoulli, *Ars Conjectandi, Opus Posthumum. Accedit Tractatus de Seriebus infinitis, et Epistola Gallice scripta de ludo Pilae rectorialis; Impensis Thurnisiorum, Fratrum, Basel* (1713).
13. V.C. Rubin, Fluctuations in the space distribution of galaxies, *Proc. Natl. Acad. Sci. USA* **40**, 541 (1954).
14. D.N. Limber, The Analysis of Counts of the Extragalactic Nebulae in Terms of a Fluctuating Density Field. II., *Astrophys. J.* **119**, 655 (1954).
15. A. Pontzen, A. Challinor, Linearization of homogeneous, nearly-isotropic cosmological models, *Class. Quant. Grav.* **28**, 185007 (2011), Eq. (52).
16. A.D. Dolgov: Matter and antimatter in the universe, *Nucl. Phys. Proc. Suppl.* **113**, 40 (2002).

17. A. Dolgov, J. Silk: Baryon isocurvature fluctuations at small scales and baryonic dark matter, *Phys. Rev. D* **47**, 4244 (1993).
18. A.D. Dolgov, M. Kawasaki, N. Kevlishvili: Inhomogeneous baryogenesis, cosmic anti-matter, and dark matter, *Nucl. Phys. B* **807**, 229 (2009).
19. V. Poulin, P. Salati, I. Cholis, M. Kamionkowski, J. Silk: Where do the AMS-02 anti-helium events come from? *Phys. Rev. D* **99**, 023016 (2019).
20. M.Y. Khlopov. What comes after the Standard Model? *Prog. Part. Nucl. Phys.* **116**, 103824, (2021).



14 Researching of magnetic cutoff for local sources of charged particles in the halo of the Galaxy

A.O. Kirichenko²

e-mail: aokirichenko@yandex.ru

A.V. Kravtsova²

M.Yu. Khlopov^{1,2,3}

A.G. Mayorov²

¹ Institute of Physics, Southern Federal University, Russia

² National Research Nuclear University MEPhI, 115409 Moscow, Russia

³ Université de Paris, CNRS, Astroparticule et Cosmologie, F-75013 Paris, France

Abstract. Models of highly inhomogeneous baryosynthesis of the baryonic asymmetric Universe allow for the existence of macroscopic domains of antimatter, which could evolve in a globular cluster of antimatter stars in our Galaxy. We assume the symmetry of the evolution of a globular cluster of stars and antistars based on the symmetry of the properties of matter and antimatter. Such object can be a source of a fraction of antihelium nuclei in galactic cosmic rays. It makes possible to predict the expected fluxes of cosmic antinuclei with use of known properties of matter star globular clusters. We have estimated the lower cutoff energy for the penetration of antinuclei from the antimatter globular cluster, situated in halo, into the galactic disk based on the simulation of particle motion in the large-scale structure of magnetic fields in the Galaxy. We have estimated the magnitude of the magnetic cutoff for the globular cluster M4.

Povzetek: V modelih, ki predpostavijo zelo nehomogeno barosintezo asimetričnega vesolja, se lahko pojavijo makroskopske domene antisnovi. V naši galaksiji bi domena antisnovi lahko nastala v kroglasti kopici zvezd iz antisnovi in bi bila izvor antihelijevih jeder v galaktičnih kozmičnih žarkih. Avtorji prilagodijo spremembo simetrije rastoče kroglaste kopice zvezd in antizvezd tako, da se lastnosti ujemajo s poznanimi lastnostmi snovi. Od tod napovedo tok kozmičnih antijeder. S simulacijo gibanja delcev v magnetnih poljih v naši galaksiji ocenijo mejno energijo, pri kateri še lahko antijedra iz kroglaste kopice antisnovi, ki se nahaja v haloju galaksije, prodrejo v galaktični disk. Ti rezultati so namenjeni iskanju kozmičnega antihelija v poskusu AMS02.

14.1 Introduction

Today, our knowledge of the chemical composition of galactic cosmic rays is being enhanced by precision experiments such as PAMELA [1], BESS [2] and AMS-02 [3] in near-Earth orbit. Along with common components such as protons or helium nuclei, there is no doubt about the presence of antiprotons in the cosmic ray flux, and a search for heavier anti-nuclei is also underway.

For the first time experimentally antinuclei were discovered at accelerators, which contributed to the development of theoretical models suggesting the existence of antimatter in the Universe and, in particular, in our Galaxy [4]. According to them, antimatter is usually classified into three groups:

- Relic or primary.
- Secondary.
- From exotic sources.

There is a classical mechanism of particle production, and antiparticles, as we understand it, are born as a secondary component (for example, positrons, antiprotons, antideuterons or antihelium [5]). But nevertheless, modern models of cosmic ray generation suggest their formation and acceleration after supernova explosions in termination shocks [6] and when propagating in the interstellar medium, the fraction of various components in cosmic rays changes as a result of nuclear reactions with interstellar gas [5].

In addition, secondary particles or antiparticles are born that are initially absent from the sources, for example, positrons, antiprotons, antideuterons or antihelium. Also, the creation of galactic antiprotons as a result of annihilation or decay of massive hypothetical dark matter particles or during the evaporation of primordial black holes is not excluded [7]. In this case, the calculated fluxes can exceed the flux of the secondary component.

Antideuterons can be formed in the same mechanisms, but with a lesser probability, they have not yet been detected in cosmic rays [5].

Antihelium was not found either: in the case of its secondary origin, the calculated ratio of the fluxes of antihelium and helium nuclei is small and does not exceed $\sim 10^{12} - 10^{14}$ [5]. Detection of antinuclei above this value would indicate the existence of primordial antimatter, preserved from the moment of the Big Bang [8,9]. The creation of 4 antinucleons at once with a relatively small relative momentum in processes in exotic sources is unlikely.

Today, primary antimatter could exist in the form of antimatter domains, which are not excluded in models of inhomogeneous baryosynthesis, taking the form of clusters of anti-stars or antigalaxies [10].

14.2 Globular cluster of antistars

Based on the symmetry of matter and antimatter [4], it is possible to indicate the expected parameters of a globular cluster of antistars. That is, a globular cluster will have the same set of properties as an ordinary cluster of ordinary stars. This approach assumes similar initial conditions and similar evolution of antimatter and matter. One should note that the mechanisms of nonhomogeneous baryosynthesis may lead to difference in the conditions within antimatter domain and in ordinary baryonic matter. In particular, the approach [11, 12] predicts much higher antibaryon density in antimatter domains, than in surrounding baryonic matter, what leads to prediction of ultra dense antibaryonic objects in the Galaxy and their specific effects [12]. Here we follow the approach of [13], which assumes similar conditions in antimatter domains as in the surrounding matter,

and elaborate the prediction of antihelium flux from antistars accessible to the AMS02 experiment [3], which follows from this similarity.

A globular cluster of stars is a group of stars that gather in the shape of a sphere and orbit around the core of the Galaxy. The stars turn out to be gravitationally bound, which, in fact, is the reason for such a shape of these clusters. Globular clusters are localized far from most other objects in the Galaxy - in the halo. They are much denser than open clusters, and they are also older and contain more stars. In the Milky Way, the number of globular clusters about 150.

The birth regions of such clusters are the dense interstellar medium. However, no star formation is currently observed in globular clusters. All dust and gas have long been "blown out" from the clusters. This confirms the opinion that globular clusters are the oldest objects in the Galaxy [14]. Orbiting the outskirts of the galaxy, globular clusters take several hundred million years to complete one orbit. At the center of the cluster, the highest density is achieved - on the order of 100-1000 stars/pc³. For comparison, the density of stars near the Sun is 0.14 stars/pc³. Globular clusters have a low metallicity due to the fact that they are composed of first generation stars. Which once again confirms the opinion that globular clusters are old clusters [15]

14.3 Cosmic antihelium propagation in interstellar medium

After generation and acceleration in the source, cosmic ray particles enter the interstellar medium, where they change their original trajectory, "entangled" in the magnetic fields of the Galaxy and can leave it.

The propagation of cosmic rays in the modern view is of a diffusion nature. The GCR confinement time before leaving the Galaxy is inversely proportional to the diffusion coefficient, i.e. decreases with increasing energy. For particles with energies of 1–2 GeV, it is $\sim 4 \cdot 10^7$ years. During this time, they manage to fill the halo of the Galaxy and, although the substance in the Galaxy is generally very rarefied, they also pass through a thickness of matter of about 10 g/cm². For high-energy particles, the distance traveled sharply decreases and, for example, at an energy of 10 TeV is 0.1-0.4 g/cm², and the lifetime is $\sim 10^6$ years [5, 16].

At present, attempts are being made to calculate the fluxes of galactic CRs. Solving this problem requires knowledge of the structure and size of the Galaxy, the location and power of the sources, the location of the Solar System, and the properties of the interstellar medium. CR propagation in the Galaxy is seriously determined by the structure of magnetic fields. The regular field lines lie in the galactic plane and approximately run along the spiral arms. The average amplitude of the field strength is $(2-3) \cdot 10^{-6}$ G. The magnetic field also exists in the halo, but its structure is not exactly known. It should be noted that currently there is a numerical implementation of the leaky box model in the form of a set of GALPROP programs.

GALPROP is a numerical solver of the diffusion equation taking into account a detailed description of the distributions of the interstellar gas and the galactic magnetic field [5].

The approach used in this work differs from the work of the GALPROP software package, and instead of solving the transport equation, individual particles are traced in interstellar space and we also take into account the parameters of the interstellar medium and the structure of magnetic field.

14.4 Boris - Bunemann tracing method

Now there are various software packages that perform tracing of particles in electromagnetic fields [17]. In 1970 Boris [18] proposed a convenient way to solve the equations of motion of particles in electromagnetic fields, this method is now widely known as the Boris method. De facto, it is the standard for modeling particle motion in plasma.

The method solves the classical equation of motion in an electromagnetic field specified by vectors \vec{E} and \vec{B} (vectors of electric and magnetic fields, respectively). Further, the electric field is eliminated by redefining the variables and the equation is reduced to describing only the rotational motion in the magnetic field. Then Bunemann introduces some additions to Boris's algorithm that increase the accuracy of the method. Today, there is an implementation of the method with the inclusion of relativistic corrections [19].

14.4.1 Using of method

To make the method convenient to use, a software package was created that allows you to transfer all the necessary parameters to the function for calculating the trajectory of the environment. Below is a list of them.

- Particle initial coordinates and directional distribution.
- Particle type and energy.
- Configuration of magnetic and electric fields.
- Characteristics of temporal and spatial steps for numerical solution.
- Conditions for saving trajectories, interrupting the tracing algorithm.

It is also important to note that for the development of the software package, it is possible to determine the interstellar medium for calculating the absorption of cosmic rays, and a program for calculating such interactions.

14.4.2 Helium antinucleus tracing

The following initial conditions were chosen for tracing helium antinuclei:

- The initial coordinates correspond to the globular cluster M4 with the position (-5.9, -0.3, 0.6) kpc in the galactic coordinate system [17].
- The angular distribution of particles at the point of birth is isotropic.
- The energy of particles varied from 10 GeV to 10 TeV.
- The structure of regular component of magnetic field of the Galaxy is taken from publication [18].

14.5 Results

Figure 1 shows examples of trajectories of helium antinuclei launched towards the plane of the galactic disk with different energies. Particles with an energy of

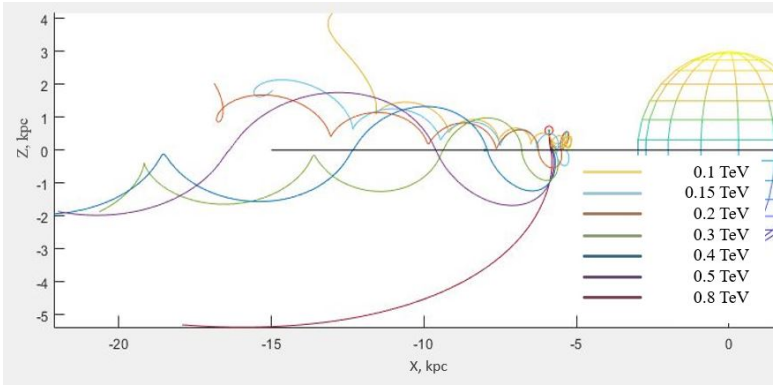


Fig. 14.1: Helium trajectories in regular galactic magnetic field. The plane of the galactic disk is shown in black.

100 GeV did not penetrate into the plane of the disk, deflected and flew away into intergalactic space. Particles of higher energy penetrated into the galactic disk and at an energy close to 1 TeV they had the opportunity to leave it.

In Fig. 2, the line connecting the points with errors shows the fraction of antihelium that fell into the galactic disk 300 pc thick, depending on the particle energy.

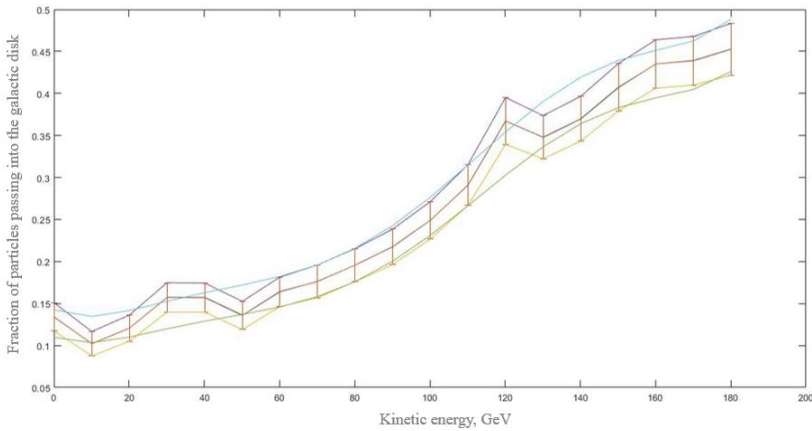


Fig. 14.2: The dependence of the fraction of particles penetrated into the disk on the particle energy

The obtained dependence was smoothed taking into account the error and the energies were determined at which the smoothed curves intersect the 0.25 level,

i.e. width at half-height of the graph (with increasing energy, the graph tends to a value of ~ 0.5 , which corresponds to the geometric factor of the disk plane from the point with the coordinates of the M4 cluster). The obtained energy – magnetic cutoff energy is 100 ± 10 GeV. This means that the flux of helium antinuclei from the hypothetically globular cluster of antistars M4 will be largely suppressed at energies less than ~ 100 GeV, but will not be completely suppressed.

14.6 Conclusion

Helium antinuclei were traced with [24] from the M4 cluster, hypothetically consisting of antistars, to the plane of the galactic disk. The characteristic energy of magnetic cutoff is determined, below which it is difficult for particles to penetrate into the disk. Predictions of antihelium flux would strongly depend on the interference of the initial spectrum, which is expected to be falling down with energy and magnetic cutoff, which reduces the lower energy part of the spectrum in galactic disk. The result will be used to interpret the experimental data on antinuclear fluxes obtained by the PAMELA and AMS-02 in near-earth orbit.

The preliminary indications to possible detection of antihelium events in AMS02 experiment, which cannot be explained as secondaries from astrophysical sources [22], if confirmed, would become serious evidence for existence of forms of primordial antimatter in our Galaxy. It will favor Beyond the Standard Model (BSM) physics, which can support creation and survival of antimatter domains in baryon asymmetrical Universe, and provide a sensitive probe for parameters of the corresponding models [23]. Whatever is the actual form of antimatter objects in our Galaxy, propagation of antinuclei from these sources would inevitably involve their diffusion in galactic magnetic fields, studied in the present paper.

Acknowledgements

The work by AK and AM has been supported by the grant of the Russian Science Foundation (Project No-18-12-00213-P).

References

1. O. Adriani, G. Barbarino: Ten years of PAMELA in space, *Rivista del Nuovo Cimento* **10**, 473-522 (2017).
2. K. Abe et al.: Search for Antihelium with the BESS-Polar Spectrometer, *Phys. Rev. Lett.* **108**, 131301 (2012).
3. K.M. Belotsky, Y.A. Golubkov, M.Y. Khlopov, R.V. Konoplich, A.S. Sakharov: Antihelium flux as a signature for antimatter globular cluster in our Galaxy, *Phys. Atom. Nucl.* **63**, 233 (2000).
4. L. Boyle, K. Finn and N. Turok: CPT-Symmetric Universe, *Phys. Rev. Lett.* **121**(25), 251301 (2018).
5. A.W. Strong, I.V. Moskalenko: Propagation of cosmic-ray nucleons in the Galaxy, *The Astrophysical Journal* **509**, 212-228 (1998)

6. N. Tomassetti, A. Oliva: Secondary antinuclei from supernova remnants and background for dark matter searches, 35th International Cosmic Ray Conference - ICRC2017 **301**, 271, 2017.).
7. F.W. Stecker, A.J. Tylka: The cosmic-ray antiproton spectrum from dark matter annihilation and its astrophysical implications: a new look, *Astrophysical Journal* **336** L51 (1989), doi: 10.1086/185359 .
8. M.Y. Khlopov: *Fundamentals of Cosmoparticle Physics* CISP-Springer, Cambridge, UK, (2012).
9. A.D. Dolgov: Matter and antimatter in the universe, *Nucl. Phys. Proc. Suppl.* **113**, 40 (2002).
10. M.Yu. Khlopov: An antimatter globular cluster in our Galaxy - a probe for the origin of the matter, *Gravitation and Cosmology*, **4**, 69-72 (1998).
11. A.D. Dolgov, M. Kawasaki, N. Kevlishvili: Inhomogeneous baryogenesis, cosmic antimatter, and dark matter, *Nucl. Phys. B* **807**, 229 (2009).
12. S.I. Blinnikov, A.D. Dolgov, K.A. Postnov: Antimatter and antistars in the universe and in the Galaxy, *Phys. Rev. D* **92**, 023516 (2015). doi:10.1103/PhysRevD.92.023516.
13. M.Y. Khlopov, S.G. Rubin, A.S. Sakharov: Possible origin of antimatter regions in the baryon dominated Universe, *Phys. Rev. D* **62**, 083505 (2000).
Place, Year.
14. M. Paul: *Star Clusters. Encyclopedia of Astronomy and Astrophysics*, CRC Press, Boca Raton, 2014.
15. J.S. Kalirai, H.B. Richer: Star clusters as laboratories for stellar and dynamical evolution, *Royal society publishing* **368**, 755-782 (2010).
16. A.W. Strong, I.V. Moskalenko: Secondary antiprotons and propagation of cosmic rays in the galaxy and heliosphere, *The Astrophysical Journal* **564**, 280-296 (2001).
17. Yuting Ng, et. al.: Introduction to motion of charged particles in Earth's magnetosphere, (2013) URL: <https://www.s.u-tokyo.ac.jp/en/utrip/archive/2013/pdf/06NgYuting.pdf>
18. J.P. Boris: The acceleration calculation from a scalar potential, *Plasma Physics Laboratory, Princeton University, MATT-152*, (1970) URL: <https://www.osti.gov/biblio/4168374>
19. S. Zenitani, T. Umeda: On the Boris solver in particle-in-cell simulation, *Physics of Plasmas* **25**, 112110 (2018).
20. <http://gclusters.altervista.org>
21. C.J. Nixon, T.O. Hands: The origin of the structure of large-scale magnetic fields in disc galaxies, *Notices of the Royal Astronomical Society* **3** **477**, 3539–3551 (2018).
22. V. Poulin, P. Salati, I. Cholis, M. Kamionkowski, J. Silk: Where do the AMS-02 anti-helium events come from?, *Phys. Rev. D* **99**, 023016 (2019).
23. M. Khlopov: What comes after the Standard model? *Progress in Particle and Nuclear Physics* **116**, 103824 (2021)
24. V. Golubkov, A. Mayorov: Software for Numerical Calculations of Particle Trajectories in the Earth's Magnetosphere and Its Use in Processing PAMELA Experimental Data, *Bull.Russ.Acad.Sci.Phys.* **85**, 383-385 (2021).



15 Mass as a dynamical quantity

M. Land

email: martin@hac.ac.il

Hadassah College Jerusalem

Abstract. The Standard Model (SM) ascribes the observed mass of elementary particles to an effective interaction between basis states defined without mass terms and a scalar potential associated with the Higgs boson.

In the relativistic field theory that underlies the SM, mass itself, understood as the Lorentz-invariant squared 4-momentum of a particle or field, is fixed *a priori*, imposing a constraint on possible momentum states.

Stueckelberg introduced an alternative approach, positing antiparticles as particles evolving backward in time, thus relaxing the mass shell constraint for individual particles.

Further work by Piron and Horwitz established a covariant Hamiltonian mechanics on an unconstrained 8D phase space, leading to a gauge field theory that mediates the exchange of mass between particles, while the total mass of particles and fields remains conserved. In a recently developed extension of general relativity, consistent with this approach, the spacetime metric evolves in a manner that permits the exchange of mass across spacetime through the gravitational field.

Mechanisms that restrict mass exchange between particles have also been identified.

Nevertheless, mass exchange remains possible under certain circumstances and may have phenomenological implications in particle physics and cosmology.

Povzetek Standardni model pripiše maso osnovnih delcev interakciji delcev s skalarnim poljem — Higgsovim bozonom. V kvantni teoriji polja, na kateri standardni model gradi, je masa določena s kvadratom Lorentzove invariantne gibalne količine delca ali polja, kar omeji njuno gibalno količino.

Stueckelbergov privzetek, da so antidelci delci, ki potujejo v času nazaj, omejitev masne lupine za posamezne delce odstrani.

Delo Pirona in Horwita uveljavi kovariantno Hamiltonovo mehaniko na neomejenem 8D faznem prostoru, kar vodi do teorije umeritvenega polja, ki posreduje izmenjavo mase med delci in polji, medtem ko se skupna masa delcev in polj ohrani.

V nedavno razviti razširitvi splošne teorije relativnosti, ki je skladna z omenjenim pristopom, se metrika prostora-časa razvija na način, ki dovoljuje izmenjavo mase preko gravitacijskega polja pod določenimi pogoji. Avtor študira fenomenološke posledice te omejitve v fiziki delcev in kozmologiji.

15.1 Introduction

The Standard Model (SM) of elementary particles is a locally gauge invariant relativistic quantum field theory with particular choices for the basis states and

the gauge group. While efforts to move beyond the SM usually begin by generalizing the algebraic structure of the gauge fields, other work has focused on the underlying framework of relativistic dynamics. In this paper, we present such an approach pioneered by Stueckelberg in 1941 in his work on antiparticles. In this approach, particle mass is treated as a dynamical quantity, leading to gauge theories in which fields and particles may exchange mass, just as they exchange energy-momentum. We review the resulting classical and quantum electrodynamics, indicating mechanisms that maintain particle masses at their familiar on-shell values. Recent work on general relativity and gravitation is also outlined.

The notion of an elementary particle characterized by a fixed mass can be traced back to the 1897 discovery by Thomson [1] that cathode rays are composed of discrete bodies with a fixed charge-to-mass ratio, and the 1909 Millikan-Fletcher [2] oil-drop experiment indicating a minimum electron charge. Today, the measured mass uncertainty of an electron is on the order of $\Delta m \simeq 10^{-8}$ [3] and so it is conventional to write single-electron equations of the type

$$m \frac{du^\mu}{d\tau} = eF^{\mu\nu}u_\nu \quad (i\partial - e\mathcal{A} - m) \psi = 0 \quad (15.1)$$

for fixed m and metric signature

$$\eta_{\mu\nu} = (-, +, +, +) . \quad (15.2)$$

The fixed mass shell $p^\mu p_\mu = -m^2 c^2$ is expressed in scattering by writing

$$d^4 p \delta(p^\mu p_\mu + m^2 c^2) = \frac{d^3 \mathbf{p}}{2\sqrt{\mathbf{p}^2 + m^2 c^2}} \quad (15.3)$$

for the momentum space measure. This picture is, of course, complicated by the SM, which defines a Lagrangian containing no mass terms for elementary states, finding effective mass terms through interaction with the symmetry-broken Higgs boson. Intriguingly, the effective masses of the composite nucleons p and n are sharper ($\Delta m \sim 10^{-10}$) than the masses of their constituent u and d quarks ($\Delta m \sim 25\%$) [3]. The assumption of fixed masses is associated with a number of issues in physics, including flavor oscillations, the problem of time, and missing mass/energy in cosmology [4].

15.2 The Stueckelberg-Horwitz-Piron (SHP) framework

A different approach was proposed by Stueckelberg [5] in his work on antiparticles. Pair creation and annihilation are described in QED by the Feynman diagram in Figure 1a, showing an intermediate electron state propagating backward in time with $E < 0$, but observed as a positron with $E > 0$ propagating forward in time. In the quantum picture, the electron jumps from forward timelike propagation to backward timelike propagation, remaining on its mass shell throughout.

But Stueckelberg proposed this model of pair processes in *classical* electrodynamics, for a continuously evolving spacetime trajectory $x^\mu(\tau)$ as shown in Figure 1b. In such a curve, $\dot{x}^0(\tau) = dx^0/d\tau$ must vanish for some τ , and so $\dot{x}^\mu(\tau)$ must cross the spacelike region twice.

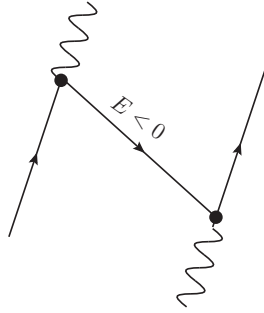


Figure 1a

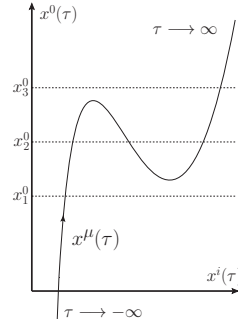


Figure 1b

Stueckelberg observed that $\dot{x}^2(\tau) = \dot{x}^\mu \dot{x}_\mu$ is a dynamical quantity for this trajectory, and so all eight components of $x^\mu(\tau)$ and $\dot{x}^\mu(\tau)$ must be independent. Moreover, since \dot{x}^2 changes sign, the evolution cannot be parameterized by the proper time of the motion $ds = \sqrt{-\dot{x}^2} d\tau$. The evolution parameter τ must be external to the spacetime manifold, much as Newtonian time t is external to space.

Horwitz and Piron [6] were led to a similar model when constructing a covariant canonical mechanics with non-trivial interactions. Writing a classical Lagrangian system on 8D unconstrained phase space

$$L = \frac{1}{2} M \dot{x}^\mu \dot{x}_\mu + e \dot{x}^\mu A_\mu(x) - V \quad \frac{d}{d\tau} \frac{\partial L}{\partial \dot{x}_\mu} - \frac{\partial L}{\partial x_\mu} = 0 \quad (15.4)$$

one obtains the generalized Lorentz force

$$M (\ddot{x}^\mu + \Gamma_{\nu\rho}^\mu \dot{x}^\nu \dot{x}^\rho) = e F^{\mu\nu} \dot{x}_\nu - \partial^\mu V \quad (15.5)$$

with field strength and conjugate momentum

$$F^{\mu\nu} = \partial^\mu A^\nu - \partial^\nu A^\mu \quad p_\mu = \frac{\partial L}{\partial \dot{x}^\mu} = M \dot{x}_\mu + e A_\mu(x) . \quad (15.6)$$

Transforming to the manifestly covariant Hamiltonian mechanics

$$K = \dot{x}^\mu p_\mu - L = \frac{1}{2M} (p^\mu - e A^\mu)(p_\mu - e A_\mu) + V \quad (15.7)$$

leads to the classical and quantum equations of motion

$$\dot{x}^\mu = \frac{\partial K}{\partial p_\mu} \quad \dot{p}^\mu = -\frac{\partial K}{\partial x_\mu} \quad i \partial_\tau \psi(x, \tau) = K \psi(x, \tau) . \quad (15.8)$$

Generalizing the classical central force problem as

$$V(x_1, x_2) = V(\rho) \quad \rho = \sqrt{(x_1 - x_2)^2 - (t_1 - t_2)^2} \quad (15.9)$$

Horwitz and Arshansky [7] obtained solutions for relativistic scattering and bound states, Horwitz and Land studied radiative transitions, selection rules, perturbation theory, Zeeman and Stark effects, and bound state decay [8], and Horwitz demonstrated entanglement and interference in time [9].

The physical picture [10] that emerges from Stueckelberg's unconstrained mechanics can be summarized as an upgrade of nonrelativistic classical and quantum mechanics in which Galilean symmetry is replaced with Poincaré symmetry:

$$\left. \begin{array}{l} \text{Newtonian time } t \\ + \\ \text{Unconstrained } \left\{ x^i, \frac{dx^j}{dt} \right\} \\ + \\ \text{Scalar Hamiltonian } H \end{array} \right\} \longrightarrow \left\{ \begin{array}{l} \text{External time } \tau \\ + \\ \text{Unconstrained } \left\{ x^\mu, \frac{dx^\nu}{d\tau} \right\} \\ + \\ \text{Scalar Hamiltonian } K \end{array} \right.$$

This covariant canonical mechanics inherits many methods and insights of Newtonian mechanics, so for example, from the Poisson bracket

$$\{F, G\} = \frac{\partial F}{\partial x^\mu} \frac{\partial G}{\partial p_\mu} - \frac{\partial G}{\partial x^\mu} \frac{\partial F}{\partial p_\mu} \quad \frac{dF}{d\tau} = \{F, K\} + \frac{\partial F}{\partial \tau} \quad (15.10)$$

it follows that

$$\frac{\partial H}{\partial t} = 0 \Rightarrow \text{conserved energy} \quad \longrightarrow \quad \frac{\partial K}{\partial \tau} = 0 \Rightarrow \text{conserved mass}$$

which for a free particle can be seen from

$$K = \frac{1}{2M} p^\mu p_\mu \quad \longrightarrow \quad \dot{x}^\mu = \frac{p^\mu}{M}, \quad \dot{p}^\mu = 0 \quad \longrightarrow \quad \dot{x}^2 = \text{constant}. \quad (15.11)$$

As discussed by Horwitz, Arshansky, and Elitzur [11], this framework formalizes a distinction between two aspects of time: the time t is one of four spacetime coordinates x^μ characterizing the location of a single event, while the time τ represents the chronological order of multiple events. The physical spacetime event $x^\mu(\tau)$ is understood as an irreversible occurrence **at** time τ so that for $\tau_2 > \tau_1$, event $x^\mu(\tau_2)$ occurs **after** $x^\mu(\tau_1)$ and **cannot change** it. This changes the significance of a closed timelike curve, resolving the grandfather paradox. The proverbial traveler revisiting at $\tau_3 > \tau_2$ the spacetime locations $x^\mu(\tau)$ of his grandfather's trajectory as it evolved from τ_1 to $\tau_2 > \tau_1$, may add events $x^\mu(\tau_3)$ but cannot alter that life trajectory as it has irreversibly occurred. More generally, the 4D block universe $\mathcal{M}(\tau)$ occurs at τ , evolving to the infinitesimally close the 4D block universe $\mathcal{M}(\tau + d\tau)$ under motion generated by the Hamiltonian K . Because K is a Lorentz scalar and τ is external, we expect no conflict with general diffeomorphism invariance.

15.3 Classical Off-Shell Electrodynamics

The origin of the scalar potential V in (15.4) can be understood by requiring invariance under τ -dependent gauge transformations [12], leading to a theory with five gauge fields, $A_\mu(x) \rightarrow a_\mu(x, \tau)$ and $a_5(x, \tau)$. The maximal gauge freedom of the classical action [13]

$$\int d\tau L \longrightarrow \int d\tau \left[L + \frac{d}{d\tau} \Lambda(x, \tau) \right] = \int d\tau [L + \dot{x}^\mu \partial_\mu \Lambda + \partial_\tau \Lambda] \quad (15.12)$$

suggests a coupling with a pure gauge field with components $\partial_\mu \Lambda$ and $\partial_\tau \Lambda$. Introducing the notation

$$\mu, \nu = 0, 1, 2, 3 \quad \text{and} \quad \alpha, \beta = 0, 1, 2, 3, 5 \quad (15.13)$$

and writing $x^5 = c_5 \tau$ in analogy to $x^0 = ct$, we rewrite the classical interaction as

$$\frac{e}{c} \dot{x}^\mu A_\mu(x) - V(x) \longrightarrow \frac{e}{c} \dot{x}^\mu a_\mu(x, \tau) + \frac{e}{c} \dot{x}^5 a_5(x, \tau) = \frac{e}{c} \dot{x}^\alpha a_\alpha(x, \tau) \quad (15.14)$$

now invariant under 5D gauge transformations $a_\alpha \rightarrow a_\alpha + \partial_\alpha \Lambda(x, \tau)$. The Lagrangian

$$L = \frac{1}{2} M \dot{x}^\mu \dot{x}_\mu + \frac{e}{c} \dot{x}^\alpha a_\alpha(x, \tau) \quad (15.15)$$

admits the conserved 5-current

$$j^\alpha(x, \tau) = c \dot{x}^\alpha \delta^4(x - X(\tau)) \quad \partial_\alpha j^\alpha = \partial_\mu j^\mu + \partial_5 j^5 = 0 \quad (15.16)$$

which can be related to the Maxwell current by observing that under appropriate boundary conditions

$$J^\mu(x) = \int d\tau j^\mu(x, \tau) \longrightarrow \partial_\mu J^\mu = 0. \quad (15.17)$$

This integral is called concatenation, understood as the sum of contributions $g(x, \tau)$ to $G(x)$ along the worldline, under $g(x, \pm\infty) = 0$. The interaction (15.14) appears to be 5D symmetric, but this symmetry is broken to vector and scalar representations of $O(3,1)$, because $\dot{x}^5 = c_5 \ll c$ is a constant and not a dynamical quantity. The Lorentz force [14] found from the Euler-Lagrange equations are

$$M \ddot{x}_\mu = \frac{e}{c} \dot{x}^\beta f_{\mu\beta} = \frac{e}{c} (\dot{x}^\nu f_{\mu\nu} - c_5 f_{5\mu}) \quad (15.18)$$

$$\frac{d}{d\tau} \left(-\frac{1}{2} M \dot{x}^\mu \dot{x}_\mu \right) = c_5 \frac{e}{c} \dot{x}^\mu f_{5\mu} \quad (15.19)$$

with 5D field strength

$$f_{\alpha\beta} = \partial_\alpha a_\beta - \partial_\beta a_\alpha \quad \alpha, \beta = 0, 1, 2, 3, 5. \quad (15.20)$$

From (15.19) we see that $\varepsilon^\mu(x, \tau) = f^{5\mu}(x, \tau) = \partial^5 a^\mu - \partial^\mu a^5$ induces mass exchange. The field $f_{\mu\nu}(x, \tau)$ becomes the Maxwell field $F_{\mu\nu}(x)$ under concatenation, decoupling from $f^{5\mu}$.

Expanding the interaction term

$$\dot{X}^\alpha a_\alpha \longrightarrow \int d^4x \dot{X}^\alpha(\tau) \delta^4(x - X(\tau)) a_\alpha(x, \tau) \quad (15.21)$$

we define the sharp current, a delta function on 4D spacetime,

$$j^\alpha(x, \tau) = c \dot{X}^\alpha(\tau) \delta^4(x - X(\tau)) \quad (15.22)$$

which by (15.17) recovers the standard Maxwell current

$$J^\mu(x) = c \int d\tau \dot{X}^\mu(\tau) \delta^4(x - X(\tau)) . \quad (15.23)$$

To complete the electromagnetic action, we introduce a kinetic term for the electromagnetic field

$$S_{\text{em}} \int d^4x d\tau \left\{ 10 \frac{e}{c^2} j^\alpha(x, \tau) a_\alpha(x, \tau) - \int \frac{ds}{\lambda} \frac{1}{4c} [f^{\alpha\beta}(x, \tau) \Phi(\tau - s) f_{\alpha\beta}(x, s)] \right\} \quad (15.24)$$

where the interaction kernel

$$\Phi(\tau) = \delta(\tau) - (\xi\lambda)^2 \delta''(\tau) \quad \xi = \frac{1}{2} \left[1 + \left(\frac{c_5}{c} \right)^2 \right] \quad (15.25)$$

smooths the sharp current (15.22). The constant λ has dimensions of time and serves as a correlation length along the worldline. The scalars $j^\alpha a_\alpha$ and $f^{\alpha\beta} f_{\alpha\beta}$ suggest a 5D symmetry containing $O(3,1)$, either $O(4,1)$ or $O(3,2)$. Although any higher symmetry is broken by $\dot{x}^5 = \text{constant}$ and by the $\delta''(\tau)$ term in $\Phi(\tau)$, it is convenient to introduce a formal 5D metric

$$g_{\alpha\beta} \xrightarrow{\text{flat}} \eta_{\alpha\beta} = \text{diag}(-1, 1, 1, 1, \sigma) \quad \eta_{55} = \sigma = \pm 1 \quad (15.26)$$

for raising the 5-index in $f^{\alpha\beta}$. Since $f^{\alpha\beta} f_{\alpha\beta} = f^{\mu\nu} f_{\mu\nu} + 2\eta^{55} f_5^\mu f_{5\mu}$ we may regard $\sigma = \eta^{55}$ as simply the relative sign of the vector-vector kinetic term, with no geometric significance. The interaction kernel is invertible as

$$\varphi(\tau) = \lambda \Phi^{-1}(\tau) = \lambda \int \frac{d\kappa}{2\pi} \frac{e^{-i\kappa\tau}}{1 + (\xi\lambda\kappa)^2} = \frac{1}{2\xi} e^{-|\tau|/\xi\lambda} \quad (15.27)$$

$$\int \frac{ds}{\lambda} \varphi(\tau - s) \Phi(s) = \delta(\tau) \quad \int \frac{d\tau}{\lambda} \varphi(\tau) = 1 \quad (15.28)$$

so that variation of the electromagnetic action with respect to $a_\alpha(x, \tau)$ provides the field equations

$$\partial_\beta f^{\alpha\beta}(x, \tau) = \frac{e}{c} \int ds \varphi(\tau - s) j^\alpha(x, s) = \frac{e}{c} j_\varphi^\alpha(x, \tau) \quad (15.29)$$

$$\partial_\alpha f_{\beta\gamma} + \partial_\gamma f_{\alpha\beta} + \partial_\beta f_{\gamma\alpha} = 0 \quad (\text{identically}) \quad (15.30)$$

with source current $j_\varphi^\alpha(x, \tau)$ smoothed along the worldline by convolution of $j^\alpha(x, \tau)$ with the inverse interaction kernel φ . These are known as pre-Maxwell equations, and when written in 4+1 (spacetime + τ) components

$$\begin{aligned} \partial_\nu f^{\mu\nu} - \frac{1}{c_5} \frac{\partial}{\partial\tau} f^{5\mu} &= \frac{e}{c} j_\varphi^\mu & \partial_\mu f^{5\mu} &= \frac{e}{c} j_\varphi^5 \\ \partial_\mu f_{\nu\rho} + \partial_\nu f_{\rho\mu} + \partial_\rho f_{\mu\nu} &= 0 & \partial_\nu f_{5\mu} - \partial_\mu f_{5\nu} + \frac{1}{c_5} \frac{\partial}{\partial\tau} f_{\mu\nu} &= 0 \end{aligned} \quad (15.31)$$

are comparable to Maxwell's equations in 3+1 (space + time) components where $f_{5\mu}$ plays the role of the electric field sourced by j_Φ^5 in Gauss's law, and $f^{\mu\nu}$ is a magnetic field induced by "curl" and τ dependence of $f_{5\mu}$. Writing

$$f_\Phi^{\alpha\beta}(x, \tau) = \int \frac{ds}{\lambda} \Phi(\tau - s) f^{\alpha\beta}(x, s) \quad (15.32)$$

translation invariance of the action leads to the Noether symmetry

$$\partial_\alpha T_\Phi^{\alpha\beta} = -\frac{e}{c^2} f^{\beta\alpha};_\alpha \quad T_\Phi^{\alpha\beta} = \frac{1}{c} \left(f_\Phi^{\alpha\gamma} f_\gamma^\beta - \frac{1}{4} g^{\alpha\beta} f_\Phi^{\delta\gamma} f_{\delta\gamma} \right) \quad (15.33)$$

where $T_\Phi^{\mu\nu}$ is the energy-momentum tensor, and the terms $T_\Phi^{5\alpha}$ represent mass density in the field and the flow of mass into spacetime. Inserting the current (15.22) into (15.33) and using the second Lorentz force equation (15.19), we find

$$\frac{d}{d\tau} \left(\int d^4x T^{5\mu} + M\dot{x}^\mu \right) = 0 \quad \frac{d}{d\tau} \left(\int d^4x T^{55} - \sigma \frac{1}{2} M\dot{x}^2 \right) = 0 \quad (15.34)$$

demonstrating that the total energy-momentum and mass of the particle and field are conserved [14]. As was seen for the current, concatenation of the pre-Maxwell equations leads to the Maxwell equations

$$\left. \begin{array}{l} \partial_\beta f^{\alpha\beta}(x, \tau) = \frac{e}{c} j_\Phi^\alpha(x, \tau) \\ \partial_{[\alpha} f_{\beta\gamma]} = 0 \end{array} \right\} \xrightarrow{\int \frac{d\tau}{\lambda}} \left\{ \begin{array}{l} \partial_\nu F^{\mu\nu}(x) = \frac{e}{c} J^\mu(x) \\ \partial_{[\mu} F_{\nu\rho]} = 0 \end{array} \right. \quad (15.35)$$

representing a sum of microscopic contributions at each τ to the Maxwell fields at a given spacetime point.

The pre-Maxwell equations lead to the 5D wave equation

$$\partial_\beta \partial^\beta a^\alpha = (\partial_\mu \partial^\mu + \partial_\tau \partial^\tau) a^\alpha = (\partial_\mu \partial^\mu + \frac{\sigma}{c_5^2} \partial_\tau^2) a^\alpha = -\frac{e}{c} j_\Phi^\alpha(x, \tau) \quad (15.36)$$

with Green's function [15]

$$G_P(x, \tau) = -\frac{1}{2\pi} \delta(x^2) \delta(\tau) - \frac{c_5}{2\pi^2} \frac{\partial}{\partial x^2} \theta(-\sigma x^\alpha x_\alpha) \frac{1}{\sqrt{-\sigma x^\alpha x_\alpha}} = \quad (15.37)$$

$$= G_{\text{Maxwell}} + G_{\text{Correlation}} \quad (15.38)$$

where $G_{\text{Correlation}}$ is smaller than G_{Maxwell} by c_5/c and drops off faster with distance. Notice that $G_{\text{Correlation}}$ has spacelike support for $\sigma = -1$ and timelike support for $\sigma = +1$. Under concatenation $G_{\text{Maxwell}}(x, \tau)$ goes over to the standard Maxwell Green's function and $G_{\text{Correlation}}$ vanishes.

A "static" source event evolving along the x^0 -axis in its rest frame as $X(\tau) = (c\tau, 0, 0, 0)$ induces for an observer on the parallel trajectory $x(\tau) = (c\tau, \mathbf{x})$ a Yukawa-type potential [16]

$$a^0(x, \tau) = \frac{e}{4\pi|\mathbf{x}|} \frac{1}{2\xi} e^{-|\mathbf{x}|/\xi\lambda c} \quad (15.39)$$

with photon mass spectrum $m_\gamma c^2 \sim \hbar/\xi\lambda$. Using the accepted experimental error for photon mass $\Delta m_\gamma \sim 10^{-18}$ eV leads to $\lambda > 10^4$ seconds. The constant λ can be seen as a correlation time along the worldline, the width of the ensemble of events contributing to the pre-Maxwell current and potential [17]. In the limit $\lambda \rightarrow 0$ the kinetic term in the action (15.3) reduces to $f^{\alpha\beta}f_{\alpha\beta}$, the photon mass spectrum goes to infinity, and a^0 becomes a delta function. In the limit $\lambda \rightarrow \infty$ the photon mass spectrum vanishes and the pre-Maxwell system reduces to Maxwell electrodynamics. The Liénard-Wiechert potential for an arbitrary source event $X^\mu(\tau)$ at an observation point x^μ similarly leads to the Maxwell formula multiplied by the factor $\varphi(\tau - \tau_R)$ where τ_R is the retarded time found from $[x - X(\tau_R)]^2 = 0$. Comparing the Lorentz forces for e^-/e^+ and e^-/e^- scattering leads to an experimental bound on $c_5 \ll c$ [18].

15.4 Mass interactions and mass stability

A simple model of mass variation is a uniformly moving particle undergoing a stochastic perturbation $x = u\tau \rightarrow u\tau + X(\tau)$ when entering a dense distribution of charged particles [19]. If the typical short distance between charge centers is d then the particle will encounter charges periodically, with a short characteristic period $d/|u|$, leading to a high characteristic frequency $\omega_0 = 2\pi|u|/d$. Expanding the perturbation in a Fourier series

$$X(\tau) = \text{Re} \sum_n a_n e^{in\omega_0\tau} \quad a_n^\mu = \alpha d (s_n^0, \mathbf{s}_n) = \alpha d (cs_n^t, \mathbf{s}_n) \quad (15.40)$$

with normalized coefficients $s_n^\mu \sim 1$ and some macroscopic factor $\alpha \lesssim 1$. We obtain a small perturbation of position $|X^\mu(\tau)| \sim \alpha d$, but a velocity perturbation

$$\dot{x}^\mu(\tau) = u^\mu + \alpha|u| \text{Re} \sum_n 2\pi n s_n^\mu i e^{in\omega_0\tau} \quad (15.41)$$

of macroscopic scale $\alpha|u|$. Writing the particle mass as $m(\tau) = -M\dot{x}^2/c^2$ leads to a macroscopic mass perturbation

$$m \rightarrow m \left(1 + \frac{\Delta m}{m} \right) \quad \frac{\Delta m}{m} = 4\pi\alpha|u| \text{Re} \sum_n n s_n^t i e^{in\omega_0\tau} \quad (15.42)$$

which could persist when the particle leaves the charge distribution.

One possible reason that we do not see such mass perturbations more frequently is a self-interaction that tends to restore mass to its familiar on-shell value. We consider a particle with arbitrary $\dot{x}^0(\tau)$ in its rest frame, where $\ddot{x}^0 \neq 0$ entails mass variation through $-M\dot{x}^2 = Mc^2\dot{t}^2(\tau)$. Along the worldline, the particle may interact at time $\tau^* > \tau$ with the field it produces at τ , but of course G_{Maxwell} , the leading term in the Green's function, vanishes on $\Delta X(\tau^*, \tau) = X(\tau^*) - X(\tau) = c(t(\tau^*) - t(\tau), \mathbf{0})$, the timelike separation. Nevertheless, from (15.37) we see that $G_{\text{Correlation}}$ has support for $-\sigma x^\alpha x_\alpha > 0$, which in this case is the condition

$$-\left[\Delta X^2 + c_5^2(\tau^* - \tau)^2 \right] = c^2 \left([t(\tau^*) - t(\tau)]^2 - \frac{c_5^2}{c^2}(\tau^* - \tau)^2 \right) > 0 \quad (15.43)$$

when $\sigma = +1$. Expanding $t(\tau)$ in a Taylor series, one finds that condition (15.43) is satisfied if and only if $\ddot{t} \neq 0$, which in the rest frame implies mass variation. Now suppose that a particle evolves uniformly as $t = \tau$ until $\tau = 0$ when it makes a sudden jump to $t = (1 + \beta)\tau$. The field strength acting on the particle at $\tau^* > 0$ contains only the component

$$f^{50} \approx \frac{e}{4\pi^2} \frac{1}{c_5^2 (\beta\tau^*)^3} Q\left(\beta, \frac{c_5^2}{c^2}\right) \quad (15.44)$$

where $Q\left(\beta, \frac{c_5^2}{c^2}\right)$ is a positive function that vanishes for $\beta = 0$ or $c_5 = 0$. The Lorentz force is then

$$M\dot{x}^0 = -c_5 e f^{50} = \begin{cases} 0 & , \tau^* < 0 \\ -\frac{\lambda e^2}{4\pi^2} \frac{1}{c_5 (\beta\tau^*)^3} Q\left(\beta, \frac{c_5^2}{c^2}\right) & , \tau^* > 0 \end{cases} \quad (15.45)$$

$$M\dot{x}^i = -c_5 e f^{5i} \dot{x}_i = 0 \quad (15.46)$$

and

$$\frac{d}{d\tau} \left(-\frac{1}{2} M \dot{x}^2 \right) = e f^{5\mu} \dot{x}_\mu = -e c f^{50} \dot{t} = -\frac{\lambda e^2}{4\pi^2} \frac{c}{c_5^2 (\beta\tau^*)^3} Q\left(\beta, \frac{c_5^2}{c^2}\right) \dot{t} \quad (15.47)$$

which acts as a restoring force, damping the mass toward its on-shell value and vanishing on shell.

Another approach [20] describes the particle as a statistical ensemble with both an equilibrium energy and an equilibrium mass, controlled by temperatures and chemical potentials, assuring asymptotic states with the correct mass. The thermodynamic properties are found from the microcanonical ensemble, where both energy and mass are parameters of the distribution. A critical point in the free energy emerges from equilibrium requirements of the canonical ensemble (where total system mass is variable), and equilibrium requirements of the grand canonical ensemble (where a chemical potential arises for the particle number). Because particle mass is controlled by a chemical potential, asymptotic variations in the mass are restored to a given value by relaxation, satisfying the equilibrium conditions.

15.5 Off-Shell Quantum Electrodynamics

Transforming the classical Lagrangian (15.15) to Hamiltonian form, we are led to the Stueckelberg-Schrodinger equation

$$\left(i\hbar \partial_\tau + e \frac{c_5}{c} a_5 \right) \psi(x, \tau) = \frac{1}{2M} \left(p^\mu - \frac{e}{c} a^\mu \right) \left(p_\mu - \frac{e}{c} a_\mu \right) \psi(x, \tau) \quad (15.48)$$

with local 5D gauge invariance

$$\psi(x, \tau) \rightarrow e^{ie\Lambda(x, \tau)/\hbar c} \psi(x, \tau) \quad a_\alpha(x, \tau) \rightarrow a_\alpha(x, \tau) + \partial_\alpha \Lambda(x, \tau) \quad (15.49)$$

and global gauge invariance providing the conserved current $\partial_\alpha j^\alpha = 0$ with 4-vector part

$$j^\mu = -\frac{i\hbar}{2M} \left\{ \psi^* \left(\partial^\mu - \frac{ie}{c} a^\mu \right) \psi - \psi \left(\partial^\mu + \frac{ie}{c} a^\mu \right) \psi^* \right\} \quad (15.50)$$

and event density $j^5 = c_5 |\psi(x, \tau)|^2$ representing the probability of finding an event at a spacetime point x at time τ . The quantum Lagrangian is

$$\mathcal{L} = \psi^*(i\partial_\tau + ea_5)\psi - \frac{1}{2M}\psi^*(-i\partial_\mu - ea_\mu)(-i\partial^\mu - ea^\mu)\psi - \frac{\lambda}{4}f^{\alpha\beta}f_{\alpha\beta}^\Phi \quad (15.51)$$

where $f_{\alpha\beta}^\Phi(x, \tau)$ is defined in (15.32), which admits Jackiw first order constrained quantization [21] by introducing $\epsilon^\mu = f^{5\mu}$. Because a^5 does not appear in the Lagrangian, path integration over a^5 inserts the Gauss law constraint $\delta(\partial^\mu \epsilon_\mu^\Phi - e\psi^*\psi)$ which may be solved to eliminate longitudinal modes. Feynman rules may be read from the unconstrained Lagrangian

$$\mathcal{L} = i\psi^*\psi - \frac{1}{2M}\psi^*(-i\partial_\mu - ea_{\perp\mu})(-i\partial^\mu - ea_{\perp}^\mu)\psi + \frac{1}{2}a_{\perp\mu}(\square + \sigma\partial_\tau^2)a_{\perp}^\mu \quad (15.52)$$

as matter and photon propagators

$$\frac{1}{(2\pi)^5} \frac{-i}{\frac{1}{2M}p^2 - P - i\epsilon} \left[g^{\mu\nu} - \frac{k^\mu k^\nu}{k^2} \right] \frac{-i}{k^2 + \kappa^2 - i\epsilon} \frac{1}{1 + \lambda^2 \kappa^2} \quad (15.53)$$

along with three and four particle vertex factors

$$\frac{e}{2M} i(p+p')^\nu (2\pi)^5 \delta^4(p-p'-k) \delta(P-P'-\kappa) 12 \quad (15.54)$$

$$\frac{-ie^2}{M} (2\pi)^5 g_{\mu\nu} \delta^4(k-k'-p'+p) \delta(-\kappa + \kappa' + P' - P)$$

which conserve total energy-momentum and mass. The matter propagator

$$G(x, \tau) = \int \frac{d^4k d\kappa}{(2\pi)^5} \frac{e^{i(k \cdot x - \kappa\tau)}}{\frac{1}{2M}k^2 - \kappa - i\epsilon} = i\theta(\tau) \int \frac{d^4k}{(2\pi)^4} e^{i(k \cdot x - \frac{1}{2M}k^2 + i\epsilon)} \quad (15.55)$$

enforces retarded causality in τ , so that there are no matter loops, just as there are no grandfather paradoxes. This expression was previously found by Feynman [22] for the Klein-Gordon equation, leading to the Feynman propagator by extracting a stationary eigenstate of the mass operator $-i\hbar\partial_\tau$ as

$$\int_{-\infty}^{\infty} d\tau e^{-i(m^2/2M)\tau} G(x, \tau) = \int \frac{d^4k}{(2\pi)^4} \frac{e^{ik \cdot x}}{\frac{1}{2M}(k^2 + m^2) - i\epsilon} = 2M \Delta_F(x). \quad (15.56)$$

We see that the interaction kernel inherited from the classical electromagnetic term provides the natural mass cut-off $(1 + \lambda^2 K^2)^{-1}$ which renders the theory super-renormalizable. The cross-section for elastic scattering is nearly identical to the Klein-Gordon case, but the pole is slightly shifted away from 0° for non-zero mass exchange between the outgoing particles (expressed as an undetermined hyperangle, much as the scattering angle is undetermined in on-shell QED) [23].

15.6 General relativity with τ -evolution

As described in Section 15.2, the SHP framework poses a block universe $\mathcal{M}(\tau)$ that evolves to a block universe $\mathcal{M}(\tau + d\tau)$ under a Hamiltonian K . We thus expect that the spacetime metric $g_{\mu\nu}(x, \tau)$ should similarly evolve to $g_{\mu\nu}(x, \tau + d\tau)$. To find field equations that prescribe this evolution, we look for hints from the development of the pseudo-5D off-shell electromagnetic field equations, which differ from Maxwell equations written in five dimensions because excluding x^5 from the dynamical degrees of freedom breaks any 5D symmetry [13, 24]. Just as there is no Lorentz force for \ddot{x}^5 , there must be no geodesic equation for \ddot{x}^5 in curved spacetime.

In standard 4D general relativity (GR), the invariance of the squared interval $\delta x^2 = \gamma_{\mu\nu} \delta x^\mu \delta x^\nu = (x_2 - x_1)^2$ between neighboring events (an instantaneous displacement) is a geometrical statement, characterizing the manifold \mathcal{M} . For events $X_1 = (x_1, c_5 \tau_1)$ and $X_2 = (x_2, c_5 (\tau_1 + \delta\tau))$ belonging to $\mathcal{M}(\tau)$ and $\mathcal{M}(\tau + \delta\tau)$ the squared interval

$$dX^\alpha dX_\alpha = \left(\delta x + \frac{d x(\tau)}{d\tau} \delta\tau \right)^2 + \sigma c_5^2 \delta\tau^2 = g_{\alpha\beta}(x, \tau) \delta x^\alpha \delta x^\beta \quad (15.57)$$

suggests a pseudo-5D metric $g_{\alpha\beta}(x, \tau)$, analogous to the pseudo-5D electromagnetic field $f^{\alpha\beta}(x, \tau)$. The evolution of $g_{\alpha\beta}(x, \tau)$ differs from a standard metric defined in 5D, because it combines 4D geometrical symmetries of $\mathcal{M}(\tau)$ with the scalar dynamical symmetry of Hamiltonian K . To preserve the constraint $x^5 \equiv c_5 \tau$ we expand the classical Lagrangian as

$$L = \frac{1}{2} M g_{\alpha\beta}(x, \tau) \dot{x}^\alpha \dot{x}^\beta = \frac{1}{2} M g_{\mu\nu} \dot{x}^\mu \dot{x}^\nu + M c_5 g_{\mu 5} \dot{x}^\mu + \frac{1}{2} M c_5^2 g_{55} \quad (15.58)$$

to obtain four geodesic equations and an identity

$$0 = \ddot{x}^\alpha + \Gamma_{\beta\gamma}^\alpha \dot{x}^\beta \dot{x}^\gamma \longrightarrow \begin{cases} \ddot{x}^\mu + \Gamma_{\lambda\sigma}^\mu \dot{x}^\lambda \dot{x}^\sigma + 2c_5 \Gamma_{5\sigma}^\mu \dot{x}^\sigma + c_5^2 \Gamma_{55}^\mu = 0 \\ \ddot{x}^5 = \dot{c}_5 \equiv 0 \end{cases} \quad (15.59)$$

and the Hamiltonian

$$K = p_\mu \dot{x}^\mu - L = \frac{1}{2} M g_{\mu\nu} \dot{x}^\mu \dot{x}^\nu - \frac{1}{2} M c_5^2 g_{55} = L - M c_5^2 g_{55} \quad (15.60)$$

from which we find

$$\frac{dK}{d\tau} = -\frac{1}{2} M \dot{x}^\mu \dot{x}^\nu \frac{\partial g_{\mu\nu}}{\partial \tau} - \frac{1}{2} M c_5^2 \frac{\partial g_{55}}{\partial \tau} \quad (15.61)$$

showing that particle mass is not generally conserved along geodesics.

We define the event density in spacetime $n(x, \tau)$ and mass density $\rho(x, \tau) = M n(x, \tau)$, leading to the event current $j^\alpha(x, \tau) = \dot{x}^\alpha(\tau) \rho(x, \tau)$ and continuity equation $\nabla_\alpha j^\alpha = 0$ with covariant derivative ∇_μ defined in the standard manner and $\nabla_5 = \partial_5$. Current conservation leads to conservation of the analogously defined mass-energy-momentum tensor $T^{\alpha\beta} = \rho \dot{x}^\alpha \dot{x}^\beta$. If we write the standard

Einstein field equations in 5D and study the linearized form for weak gravitation $g_{\alpha\beta} \approx \eta_{\alpha\beta} + h_{\alpha\beta}$, we obtain a wave equation that can be solved using the Green's function (15.37). However, the metric perturbation found from a "static" source in its rest frame includes $h_{00} = 2h_{ij} = h_{55}$, which deviates from the expected structure, $h_{00} = h_{ij} \gg h_{55}$. To determine the correct modification of the field equations we choose a form that preserves the 5D symmetries of the Ricci tensor $R_{\alpha\beta}$, but breaks the apparent 5D symmetry in the relationship between $R_{\alpha\beta}$ and $T_{\alpha\beta}$. In trace-reversed form, we write [13]

$$R_{\alpha\beta} = \frac{8\pi G}{c^4} \left(T_{\alpha\beta} - \frac{1}{2} \bar{g}_{\alpha\beta} \bar{T} \right) \quad \bar{g}_{\mu\nu} = g_{\mu\nu} \quad \bar{g}_{5\alpha} = 0 \quad (15.62)$$

where $\bar{T} = \bar{g}^{\mu\nu} T_{\mu\nu}$, which for the "static" source in the weak field approximation leads to

$$g_{\mu\nu} = \left(- \left(1 - \frac{2Gm}{c^2 r} \right), \left(1 - \frac{2Gm}{c^2 r} \right)^{-1} \delta_{ij} \right) \quad g_{55} = \sigma + o \left(\frac{c_5^2}{c^2} \right) \quad (15.63)$$

consistent with a spherically symmetric Schwarzschild metric. A source in its rest frame with mass varying arbitrarily as $\dot{x}^0(\tau) = c[1 + \alpha(\tau)/2]$ leads to a τ -dependent perturbation. The geodesic equations for a test particle in this space undergoes a nonlinear x^0 acceleration, and satisfies a radial equation

$$\frac{d}{d\tau} \left\{ \frac{1}{2} \dot{R}^2 + \frac{1}{2} \frac{L^2}{M^2 R^2} - \frac{GM}{R} \left(1 + \frac{1}{2} \alpha(\tau) \right) \right\} = - \frac{GM}{2R} \frac{d}{d\tau} \alpha(\tau) \quad (15.64)$$

with conserved angular momentum $L = MR^2 \dot{\phi}$. The term in brackets on the LHS is the Hamiltonian in these coordinates, indicating that the mass of the test particle is not conserved when the mass of the source varies. This simple example suggests that a source particle of varying mass can transfer mass across spacetime to a test mass moving geodesically under the influence of the metric field induced by the source [24].

Decomposing these field equation (15.62) into 4+1 form [13], analogous to the 3+1 decomposition used in the ADM formalism [25], we find that the 20 spacetime components $R_{\mu\nu}$ are unconstrained second order evolution equations, while the five components $R_{\alpha 5}$ are constraints that propagate at first order in ∂_τ . Moreover, from $\bar{T} = T - g^{55} T_{55}$, the mass density T_{55} sourced by g_{55} and not necessarily constant, is seen to play the role of a small cosmological term Λ .

15.7 References

References

1. Thomson J J 1897 *Phil. Mag.* **44** 293–396
2. Millikan R A 1910 *Science* **32** 436–448
3. Zyla P A and et al (Particle Data Group) 2020 *Progress of Theoretical and Experimental Physics* **2020**

4. Shi Y 2021 Force, metric, or mass: Disambiguating causes of uniform gravity (*Preprint* 1908.02159)
5. Stueckelberg E 1941 *Helv. Phys. Acta* **14** 321–322 (In French) ;
Stueckelberg E 1941 *Helv. Phys. Acta* **14** 588–594 (In French)
6. Horwitz L and Piron C 1973 *Helv. Phys. Acta* **48** 316–326
7. Horwitz L and Lavie Y 1982 *Phys. Rev. D* **26** 819–838 ; Arshansky R and Horwitz L 1989 *J. Math. Phys.* **30** 213 ; Arshansky R and Horwitz L 1988 *Phys. Lett. A* **131** 222–226 ; Arshansky R and Horwitz L 1989 *J. Math. Phys.* **30** 66 ; Arshansky R and Horwitz L 1989 *J. Math. Phys.* **30** 380 ; Arshansky R 1986 The classical relativistic two-body problem and asymptotic mass conservation. Tel Aviv University preprint TAUP 1479-86
8. Land M, Arshansky R and Horwitz L 1994 *Found. Phys.* **24** 563–578 ; Land M and Horwitz L 1995 *J. Phys. A Math. Gen.* **28** 3289–3304 ; Land M and Horwitz L 2001 *Found. Phys.* **31** 967–991
9. Horwitz L and Arshansky R I 2018 *Physics Letters A* **382** 1701–1708 (*Preprint* 1707.03294)
10. Land M and Horwitz L P 2020 *Relativistic classical mechanics and electrodynamics* (Morgan and Claypool Publishers)
11. Horwitz L, Arshansky R and Elitzur A 1988 *Found. Phys.* **18** 1159
12. Saad D, Horwitz L and Arshansky R 1989 *Found. Phys.* **19** 1125–1149
13. Land M 2020 *Symmetry* **12** ; Land M 2021 *Journal of Physics: Conference Series* **1956** 012010
14. Land M and Horwitz L 1991 *Found. Phys. Lett.* **4** 61
15. Land M and Horwitz L 1991 *Found. Phys.* **21** 299–310
16. Land M 1996 *Found. of Phys.* **27** 19
17. Land M 2017 *Entropy* **19** 234 ISSN 1099-4300
18. Land M 2017 *Journal of Physics: Conference Series* **845** 012024
19. Land M 2017 *Journal of Physics: Conference Series* **845** 012025
20. Horwitz L P 2017 *Journal of Physics: Conference Series* **845** 012026
21. Jackiw R URL <https://arxiv.org/pdf/hep-th/9306075.pdf>
22. Feynman R 1950 *Phys. Rev.* **80** 440–457
23. Land M and Horwitz L 2013 *J. Phys. Conf. Ser.* **437** 012011
24. Land M 2019 *Astronomische Nachrichten* **340** 983–988
25. Arnowitt R L, Deser S and Misner C W 2004 *General Relativity and Gravitation* **40** 1997–2027



16 New way of second quantization of fermions and bosons

N.S. Mankoč Borštnik
email: norma.mankoc@fmf.uni-lj.si

Department of Physics, University of Ljubljana
SI-1000 Ljubljana, Slovenia

Abstract. This contribution presents properties of the second quantized not only fermion fields but also boson fields, if the second quantization of both kinds of fields origins in the description of the internal space of fields with the "basis vectors" which are the superposition of odd (when describing fermions) or even (when describing bosons) products of the Clifford algebra operators γ^a 's. The tensor products of the "basis vectors" with the basis in ordinary space forming the creation operators manifest the anticommutativity (of fermions) or commutativity (of bosons) of the "basis vectors", explaining the second quantization postulates of both kinds of fields. Creation operators of boson fields have all the properties of the gauge fields of the corresponding fermion fields, offering a new understanding of the fermion and boson fields.

Povzetek: Prispevek razloži drugo kvantizacijo ne le fermionskih ampak tudi bozonskih polj. Notranji prostor fermionov opišejo "osnovnimi vektorji", ki so superpozicija produktov lihega števila Cliffordovh operatorjev γ^a , bozonski "osnovnimi vektorji" pa so superpozicija produktov sodega števila Cliffordovih operatorjev γ^a . Kreacijski in anihilacijski operatorji, ki so tenzorski produkt končnega števila "osnovnih vektorjev" in zvezno neskončnega števila komutirajočih vektorjev v običajnem prostoru, "podedujejo" antikomutativnost ali komutativnost od "osnovnih vektorjev". Posledično fermionska stanja antikomutirajo in bozonska komutirajo, kar razloži postulate druge kvantizacije za fermionska in bozonska polja in ponudi nov pogled za lastnosti obeh vrst polj.

16.1 Introduction

In a long series of works [19,20,23,25,26,28,29,31] I have found, together with the collaborators ([1,26,32,34,35,37] and the references therein), with H.B. Nielsen and in long discussions with participants during the annual workshops "What comes beyond the standard models", the phenomenological success with the model named the *spin-charge-family* theory: The internal space of fermions are in this model described with the Clifford algebra objects of all linear superposition of odd products of γ^a 's in $d = (13 + 1)$. Fermions interact with only gravity — with the vielbeins and the two kinds of the spin connection fields (the gauge fields of $S^{ab} = \frac{i}{4}(\gamma^a\gamma^b - \gamma^b\gamma^a)$ and $\tilde{S}^{ab} = \frac{1}{4}(\tilde{\gamma}^a\tilde{\gamma}^b - \tilde{\gamma}^b\tilde{\gamma}^a)$ ¹). Spins from higher

¹ If there are no fermion present the two kinds of the spin connection fields are uniquely described by the vielbeins [36].

dimensions, $d > (3 + 1)$, described by γ^a 's, manifest in $d = (3 + 1)$ as charges of the *standard model* quarks and leptons and antiquarks and antileptons, appearing in (two times four) families, the quantum numbers of which are determined by the second kind of the Clifford algebra object \tilde{S}^{ab} 's. Gravity in higher dimensions manifests as the *standard model* vector gauge fields as well as the scalar Higgs and Yukawa couplings [1, 5, 23, 25, 26, 26–29, 31, 32, 34, 35, 37], predicting new scalar fields, which offer the explanation besides for higgs scalar and Yukawa couplings also for the asymmetry between matter and antimatter in our universe and for the dark matter (represented by the stable of the upper group of four families), predicting a new family — the fourth family to the observed three.

In this contribution I shortly repeat the description of the internal space of the second quantized fermion fields with the odd products of the Clifford operators γ^a 's, what leads to the creation operators for fermions without postulating the second quantization requirements of Dirac [7–9]. The creation operators for fermions, which are superposition of tensor products of the ordinary basis and the "basis vectors" describing the internal space of fermions, anticommute, explaining correspondingly the postulates of Dirac, offering also a new understanding of fermion fields ([1] and references therein). The creation operators of fermions appear in families, carrying either left or right handedness, their Hermitian conjugated partners belong to another set of Clifford odd "basis vectors" carrying the opposite handedness.

The main part of this contribution discusses properties of the second quantized boson fields, which are the gauge fields of the corresponding second quantized fermion fields. The internal space of bosons is described by the superposition of even products of γ^a 's. The boson fields correspondingly commute. The corresponding creation operators and their Hermitian conjugated partners belong to the same set of "basis vectors", carrying all the quantum numbers in adjoint representations. They interact among themselves and with the corresponding fermion fields.

In Sect. 16.2 the anticommuting Grassmann and Clifford algebras are presenting and the relations among them discussed. The "basis vectors" are defined as the eigeenvectors of the Cartan subalgebra of the Lorentz algebra for the Grassmann and the two Clifford algebras for odd and for even products of algebras members, and their anticommutation or commutation relations presented, Subsect. 16.2.1. The reduction of the two kinds of the Clifford algebras to only one makes the Clifford odd "basis vectors" anticommuting, giving to different irreducible representations of the Lorentz algebra the family quantum numbers, Subsect. 16.2.2. To make understanding of the properties of the Clifford odd and Clifford even "basis vectors" easier in Subsect. 16.2.3 the case of $d = (5 + 1)$ -dimensional space is chosen and the "basis vectors" of odd, 16.2.3, and even, 16.2.3, Clifford character are presented in details and then generalized to any even d , Subsect. 16.2.4.

In Sect. 16.3 the creation operators of the second quantized fermion and boson fields are discussed, as well as their Hermitian conjugated partners. In Subsect. 16.3.1 the simple action for fermion interacting with bosons and for corresponding bosons, as assumed in the *spin-charge-family* theory is presented.

Sect. 17.5 reviews shortly what one can learn in this contribution.

Both algebras, Grassmann and Clifford, offer "basis vectors" for the description of the internal space of fermions [1, 19, 20] and the corresponding bosons with which fermions interact. The oddness or evenness of "basis vectors", transferred to the creation operators, which are tensor products of the finite number of "basis vectors" and the (continuously) infinite number of momentum (or coordinate) basis, and to their Hermitian conjugated partners annihilation operators, offers the second quantization of fermions and bosons without postulating the second quantized conditions [7–9] for either the half integer spin fermions or integer spin bosons, enabling the explanation of the Dirac's postulates. Further investigations are needed in both case, for the boson case in particular, although promising, the time for this study was too short.

16.2 Grassmann and Clifford algebras

To describe the internal space of fermions and bosons one can use either the Grassmann or the Clifford algebras.

In Grassmann d -dimensional space there are d anticommuting operators θ^a , $\{\theta^a, \theta^b\}_+ = 0$, $a = (0, 1, 2, 3, 5, \dots, d)$, and d anticommuting derivatives with respect to θ^a , $\frac{\partial}{\partial \theta_a}$, $\{\frac{\partial}{\partial \theta_a}, \frac{\partial}{\partial \theta_b}\}_+ = 0$, offering together $2 \cdot 2^d$ operators, the half of which are superposition of products of θ^a and another half corresponding superposition of $\frac{\partial}{\partial \theta_a}$.

$$\begin{aligned} \{\theta^a, \theta^b\}_+ &= 0, & \{\frac{\partial}{\partial \theta_a}, \frac{\partial}{\partial \theta_b}\}_+ &= 0, \\ \{\theta_a, \frac{\partial}{\partial \theta_b}\}_+ &= \delta_{ab}, & (a, b) &= (0, 1, 2, 3, 5, \dots, d). \end{aligned} \quad (16.1)$$

Defining [32]

$$(\theta^a)^\dagger = \eta^{aa} \frac{\partial}{\partial \theta_a}, \quad \text{leads to} \quad (\frac{\partial}{\partial \theta_a})^\dagger = \eta^{aa} \theta^a. \quad (16.2)$$

θ^a and $\frac{\partial}{\partial \theta_a}$ are, up to the sign, Hermitian conjugated to each other. The identity is the self adjoint member of the algebra. We make a choice for the complex properties of θ^a , and correspondingly of $\frac{\partial}{\partial \theta_a}$, as follows

$$\begin{aligned} \{\theta^a\}^* &= (\theta^0, \theta^1, -\theta^2, \theta^3, -\theta^5, \theta^6, \dots, -\theta^{d-1}, \theta^d), \\ \{\frac{\partial}{\partial \theta_a}\}^* &= (\frac{\partial}{\partial \theta_0}, \frac{\partial}{\partial \theta_1}, -\frac{\partial}{\partial \theta_2}, \frac{\partial}{\partial \theta_3}, -\frac{\partial}{\partial \theta_5}, \frac{\partial}{\partial \theta_6}, \dots, -\frac{\partial}{\partial \theta_{d-1}}, \frac{\partial}{\partial \theta_d}). \end{aligned} \quad (16.3)$$

In d -dimensional space of anticommuting Grassmann coordinates and of their Hermitian conjugated partners derivatives, Eqs. (17.3, 16.2), there exist two kinds of the Clifford coordinates (operators) — γ^a and $\tilde{\gamma}^a$ — both expressible in terms of θ^a and their conjugate momenta $p^{\theta^a} = i \frac{\partial}{\partial \theta_a}$ [20].

$$\begin{aligned} \gamma^a &= (\theta^a + \frac{\partial}{\partial \theta_a}), & \tilde{\gamma}^a &= i(\theta^a - \frac{\partial}{\partial \theta_a}), \\ \theta^a &= \frac{1}{2}(\gamma^a - i\tilde{\gamma}^a), & \frac{\partial}{\partial \theta_a} &= \frac{1}{2}(\gamma^a + i\tilde{\gamma}^a), \end{aligned} \quad (16.4)$$

offering together $2 \cdot 2^d$ operators: 2^d of those which are products of γ^a and 2^d of those which are products of $\tilde{\gamma}^a$. Taking into account Eqs. (16.2, 16.4) it is easy to prove that they form two independent anticommuting Clifford algebras, Refs. ([1] and references therein)

$$\begin{aligned} \{\gamma^a, \gamma^b\}_+ &= 2\eta^{ab} = \{\tilde{\gamma}^a, \tilde{\gamma}^b\}_+, \\ \{\gamma^a, \tilde{\gamma}^b\}_+ &= 0, \quad (a, b) = (0, 1, 2, 3, 5, \dots, d), \\ (\gamma^a)^\dagger &= \eta^{aa} \gamma^a, \quad (\tilde{\gamma}^a)^\dagger = \eta^{aa} \tilde{\gamma}^a, \end{aligned} \tag{16.5}$$

with $\eta^{ab} = \text{diag}\{1, -1, -1, \dots, -1\}$.

While the Grassmann algebra can be used to describe the "anticommuting integer spin second quantized fields" and "commuting integer spin second quantized fields" [1, 25], the Clifford algebras describe the second quantized fermion fields, if the superposition of odd products of γ^a 's or $\tilde{\gamma}^a$'s are used. The superposition of even products of either γ^a 's or $\tilde{\gamma}^a$'s describe the commuting second quantized boson fields.

The reduction, Eq. (17.9) of Subsect. (16.2.2), of the two Clifford algebras — γ^a 's and $\tilde{\gamma}^a$'s — to only one is needed — γ^a 's are chosen — for the correct description of the internal space of fermions. After the decision that only γ^a 's are used to describe the internal space of fermions, the remaining ones, $\tilde{\gamma}^a$'s, are used to equip the irreducible representations of the Lorentz group (with the infinitesimal generators $S^{ab} = \frac{i}{4}\{\gamma^a, \gamma^b\}_-$) with the family quantum numbers in the case that the odd Clifford algebra describes the internal space of the second quantized fermions.

It then follows that the even Clifford algebra objects, the superposition of the even products of γ^a 's, offer the description of the second quantized boson fields, which are the gauge fields of the second quantized fermion fields, the internal space of which are described by the odd Clifford algebra objects. This will be demonstrated in this contribution.

16.2.1 "Basis vectors" determined by superposition of odd and even products of Clifford objects.

There are $\frac{d}{2}$ members of the Cartan subalgebra of the Lorentz algebra in even dimensional spaces. One can choose

$$\begin{aligned} \mathbf{S}^{03}, \mathbf{S}^{12}, \mathbf{S}^{56}, \dots, \mathbf{S}^{d-1 d}, \\ \tilde{\mathbf{S}}^{03}, \tilde{\mathbf{S}}^{12}, \tilde{\mathbf{S}}^{56}, \dots, \tilde{\mathbf{S}}^{d-1 d}, \\ \mathbf{S}^{ab} = \mathbf{S}^{ab} + \tilde{\mathbf{S}}^{ab}. \end{aligned} \tag{16.6}$$

Let us look for the "eigenstates" of each of the Cartan subalgebra members, Eq. (16.6), for each of the two kinds of the Clifford algebras separately,

$$\begin{aligned} \mathbf{S}^{ab} \frac{1}{2}(\gamma^a + \frac{\eta^{aa}}{ik} \gamma^b) &= \frac{k}{2} \frac{1}{2}(\gamma^a + \frac{\eta^{aa}}{ik} \gamma^b), & \mathbf{S}^{ab} \frac{1}{2}(1 + \frac{i}{k} \gamma^a \gamma^b) &= \frac{k}{2} \frac{1}{2}(1 + \frac{i}{k} \gamma^a \gamma^b), \\ \tilde{\mathbf{S}}^{ab} \frac{1}{2}(\tilde{\gamma}^a + \frac{\eta^{aa}}{ik} \tilde{\gamma}^b) &= \frac{k}{2} \frac{1}{2}(\tilde{\gamma}^a + \frac{\eta^{aa}}{ik} \tilde{\gamma}^b), & \tilde{\mathbf{S}}^{ab} \frac{1}{2}(1 + \frac{i}{k} \tilde{\gamma}^a \tilde{\gamma}^b) &= \frac{k}{2} \frac{1}{2}(1 + \frac{i}{k} \tilde{\gamma}^a \tilde{\gamma}^b) \end{aligned}$$

$k^2 = \eta^{aa}\eta^{bb}$. The proof of Eq. (17.7) is presented in Ref. [1], App. (I). Let us introduce for nilpotents $\frac{1}{2}(\gamma^a + \frac{\eta^{aa}}{ik}\gamma^b)$, $(\frac{1}{2}(\gamma^a + \frac{\eta^{aa}}{ik}\gamma^b))^2 = 0$ and projectors $\frac{1}{2}(1 + \frac{i}{k}\gamma^a\gamma^b)$, $(\frac{1}{2}(1 + \frac{i}{k}\gamma^a\gamma^b))^2 = \frac{1}{2}(1 + \frac{i}{k}\gamma^a\gamma^b)$ of both algebras the notation

$$\begin{aligned}
 {}^{ab}(k) &:= \frac{1}{2}(\gamma^a + \frac{\eta^{aa}}{ik}\gamma^b), & {}^{ab}\dagger(k) &= \eta^{aa}(-k), & ({}^{ab}(k))^2 &= 0, & {}^{ab}(k)(-k) &= \eta^{aa} [k] \\
 {}^{ab}[k] &:= \frac{1}{2}(1 + \frac{i}{k}\gamma^a\gamma^b), & {}^{ab}\dagger[k] &= [k], & ({}^{ab}[k])^2 &= [k], & {}^{ab}[k](-k) &= 0, \\
 {}^{ab}(\tilde{k}) &:= \frac{1}{2}(\tilde{\gamma}^a + \frac{\eta^{aa}}{ik}\tilde{\gamma}^b), & {}^{ab}\dagger(\tilde{k}) &= \eta^{aa}(-\tilde{k}), & ({}^{ab}(\tilde{k}))^2 &= 0, \\
 {}^{ab}[\tilde{k}] &:= \frac{1}{2}(1 + \frac{i}{k}\tilde{\gamma}^a\tilde{\gamma}^b), & {}^{ab}\dagger[\tilde{k}] &= [\tilde{k}], & ({}^{ab}[\tilde{k}])^2 &= [\tilde{k}], \\
 {}^{ab}(\tilde{k})[\tilde{k}] &= 0, & {}^{ab}\tilde{k} &= (\tilde{k}), & {}^{ab}(\tilde{k})[-\tilde{k}] &= (\tilde{k}), & {}^{ab}[\tilde{k}](-\tilde{k}) &= 0, \\
 {}^{ab}(\tilde{k})[k] &= 0, & {}^{ab}[k](\tilde{k}) &= (\tilde{k}), & {}^{ab}(\tilde{k})[-k] &= (\tilde{k}), & {}^{ab}[k](-\tilde{k}) &= 0, \\
 {}^{ab}(\tilde{k})[k] &= 0, & {}^{ab}[k](\tilde{k}) &= (\tilde{k}), & {}^{ab}(\tilde{k})[-k] &= (\tilde{k}), & {}^{ab}[k](-\tilde{k}) &= 0,
 \end{aligned} \tag{16.8}$$

Statement 1. *One can define "basis vectors" to be eigenvectors of all the members of the Cartan subalgebras as even or odd products of nilpotents and projectors in any even dimensional space.*

Due to the anticommuting properties of the Clifford algebra objects there are anticommuting and commuting "basis vectors". The anticommuting "basis vectors" contain an odd products of nilpotents, at least one nilpotent, the rest are then projectors. Let us denote the Clifford odd "basis vectors" of the Clifford γ^a kind as $\hat{b}_f^{m\dagger}$, where m and f determine the m^{th} member of the f^{th} irreducible representation. We shall denote by $\hat{b}_f^m = (\hat{b}_f^{m\dagger})^\dagger$ the Hermitian conjugated partner of the "basis vector" $\hat{b}_f^{m\dagger}$. The "basis vectors" of the Clifford $\tilde{\gamma}^a$ kind would correspondingly be denoted by $\hat{b}_f^{m\dagger}$ and \hat{b}_f^m .

It is not difficult to prove the anticommutation relations of the Clifford odd "basis vectors" and their Hermitian conjugated partners for both algebras ([1, 19] and references therein). Let us here present only the one of the Clifford algebras — γ^a 's.

$$\begin{aligned}
 \hat{b}_f^m *_{\mathcal{A}} |\psi_{oc} \rangle &= 0 |\psi_{oc} \rangle, \\
 \hat{b}_f^{m\dagger} *_{\mathcal{A}} |\psi_{oc} \rangle &= |\psi_f^m \rangle, \\
 \{\hat{b}_f^m, \hat{b}_{f'}^{m'}\} *_{\mathcal{A}} |\psi_{oc} \rangle &= 0 |\psi_{oc} \rangle, \\
 \{\hat{b}_f^{m\dagger}, \hat{b}_{f'}^{m'\dagger}\} *_{\mathcal{A}} |\psi_{oc} \rangle &= |\psi_{oc} \rangle,
 \end{aligned} \tag{16.9}$$

where $*_{\mathcal{A}}$ represents the algebraic multiplication of $\hat{b}_f^{m\dagger}$ and $\hat{b}_{f'}^{m'}$ among themselves and with the vacuum state $|\psi_{oc} \rangle$ of Eq.(17.10), which takes into account Eq. (17.5),

$$|\psi_{oc} \rangle = \sum_{f=1}^{2^{\frac{d}{2}-1}} \hat{b}_f^m *_{\mathcal{A}} \hat{b}_f^{m\dagger} |1 \rangle, \tag{16.10}$$

for one of the members m , anyone, of the odd irreducible representation f , with $|1\rangle$, which is the vacuum without any structure — the identity. It follows that $\hat{b}_f^m|\psi_{oc}\rangle = 0$. The relations are valid for both kinds of the odd Clifford algebras, we only have to replace $\hat{b}_f^{m\dagger}$ by $\hat{b}_f^{m\ddagger}$ and equivalently for the Hermitian conjugated partners.

The Clifford odd "basis vectors" almost fulfil the second quantization postulates for fermions. There is, namely, the property, which the second quantized fermions must fulfil in addition to the relations of Eq. (16.9). If the anticommutation relations of "basis vectors" and their Hermitian conjugated partners would fulfil the relation:

$$\{\hat{b}_f^m, \hat{b}_{f'}^{m'\ddagger}\}_{*A}|\psi_{oc}\rangle = \delta^{mm'}\delta_{ff'}|\psi_{oc}\rangle, \tag{16.11}$$

for either γ^a or $\tilde{\gamma}^a$, then the corresponding creation and annihilation operators would fulfil the anticommutation relations for the second quantized fermions, explaining the postulates of Dirac for the second quantized fermion fields. For any \hat{b}_f^m and any $\hat{b}_{f'}^{m'\ddagger}$ this is not the case. It turns out that besides $\hat{b}_{f=1}^{m=1} = (-)^{\overset{d-1}{56} \overset{d}{12} \overset{d}{03}} \dots (-)(-)(-i)$, for example, also $\hat{b}_{f'}^{m'\ddagger} = (-)^{\overset{d-1}{56} \overset{d}{12} \overset{d}{03}} \dots (-)[+][+i]$ and several others give, when applied on $\hat{b}_{f=1}^{m=1\dagger}$, nonzero contributions. There are namely $2^{\frac{d}{2}-1} - 1$ too many annihilation operators for each creation operator which give, applied on the creation operator, nonzero contribution.

The problem is solvable by the reduction of the two Clifford odd algebras to only one [1, 5, 36, 37] as it is presented in subsection 16.2.2: If γ^a 's are chosen to determine internal space of fermions, the remaining ones, $\tilde{\gamma}^a$'s, determine then quantum numbers of each family (described by the eigenvalues of \tilde{S}^{ab} of the Cartan subalgebra members). Correspondingly the creation and annihilation operators, expressible as tensor products, $*T$, of the "basis vectors" and the basis in ordinary (momentum or coordinate) space, fulfil the anticommutation relation for the second quantized fermions.

Let me point out that the Hermitian conjugated partners of the "basis vectors" belong to different irreducible representations of the corresponding Lorentz group than the "basis vectors". This can be understood, since the Clifford odd "basis vectors" have always odd numbers of nilpotents, so that an odd number of $(k)^{ab}$'s transforms under Hermitian conjugation into $(-k)^{ab}$'s, which can not be the member of the "basis vectors", since the even generators of the Lorentz transformations transform always even number of nilpotents, keeping the number of nilpotents always odd. It is different in the case of the Clifford even "basis vectors", since an even number of $(k)^{ab}$'s, transformed with the Hermitian conjugation into an even number of $(-k)^{ab}$'s belongs to the same group of the "basis vectors".

Statement 2. *The Clifford odd $2^{\frac{d}{2}-1}$ members of each of the $2^{\frac{d}{2}-1}$ irreducible representations of "basis vectors" have their Hermitian conjugated partners in another set of $2^{\frac{d}{2}-1} \cdot 2^{\frac{d}{2}-1}$ "basis vectors". Each of the two sets of the $2^{\frac{d}{2}-1} \times 2^{\frac{d}{2}-1}$ Clifford even "basis vectors" has their Hermitian conjugated partners within the same set.*

The Clifford even "basis vectors" commute. Let us denote the Clifford even "basis vectors", described by γ^{α} 's, by $\hat{A}_f^{m\dagger}$. There is no need to denote their Hermitian conjugated partners by \hat{A}_f^m , since in the even Clifford sector the "basis vectors" and their Hermitian conjugated partners appear within the same group. We shall manifest this in the toy model of $d = (5 + 1)$. In the Clifford even sector m and f are just two indexes: f denotes the subgroups within which the "basis vectors" do not have the Hermitian conjugated partners (Subsect. 16.2.3, Eq. (16.21)).

We shall need also the equivalent "basis vectors" in the Clifford even part of the kind $\tilde{\gamma}^{\alpha}$'s. Let these "basis vectors" be denoted by $\hat{\tilde{A}}_f^{m\dagger}$.

These commuting even Clifford algebra objects have interesting properties. I shall discuss the properties of even and odd "basis vectors" in Sects. 16.2.3, 16.2.4, first in $d = (5 + 1)$ -dimensional space, then in the general case.

16.2.2 Reduction of the Clifford space

The creation and annihilation operators of an odd Clifford algebra of both kinds, of either γ^{α} 's or $\tilde{\gamma}^{\alpha}$'s, turn out to obey the anticommutation relations for the second quantized fermions, postulated by Dirac [1], provided that each of the irreducible representations of the corresponding Lorentz group, describing the internal space of fermions, would carry a different quantum number.

But we know that a particular member m has for all the irreducible representations the same quantum numbers, that is the same "eigenvalues" of the Cartan subalgebra (for the vector space of either γ^{α} 's or $\tilde{\gamma}^{\alpha}$'s), Eq. (17.8).

Statement 3. *The only possibility to "dress" each irreducible representation of one kind of the two independent vector spaces with a new, let us say "family" quantum number, is that we "sacrifice" one of the two vector spaces.*

Let us "sacrifice" $\tilde{\gamma}^{\alpha}$'s, using $\tilde{\gamma}^{\alpha}$'s to define the "family" quantum numbers for each irreducible representation of the vector space of "basis vectors of an odd products of γ^{α} 's, while keeping the relations of Eq. (17.5) unchanged: $\{\gamma^a, \gamma^b\}_+ = 2\eta^{ab} = \{\tilde{\gamma}^a, \tilde{\gamma}^b\}_+$, $\{\gamma^a, \tilde{\gamma}^b\}_+ = 0$, $(\gamma^a)^\dagger = \eta^{aa} \gamma^a$, $(\tilde{\gamma}^a)^\dagger = \eta^{aa} \tilde{\gamma}^a$, $(a, b) = (0, 1, 2, 3, 5, \dots, d)$.

We therefore *postulate*:

Let $\tilde{\gamma}^{\alpha}$'s operate on γ^{α} 's as follows [20,29,31,32,35]

$$\{\tilde{\gamma}^a B = (-)^B i B \gamma^a\} |\psi_{oc} \rangle, \quad (16.12)$$

with $(-)^B = -1$, if B is (a function of) an odd products of γ^{α} 's, otherwise $(-)^B = 1$ [35], $|\psi_{oc} \rangle$ is defined in Eq. (17.10).

Statement 4. *After the postulate of Eq. (17.9) "basis vectors" which are superposition of an odd products of γ^{α} 's obey all the fermions second quantized postulates of Dirac, presented in Eqs. (16.11, 16.9).*

We shall see in Sect. 16.2.3 that the Clifford even "basis vectors" obey the bosons second quantized postulates.

After this postulate the vector space of $\tilde{\gamma}^a$'s is "frozen out". No vector space of $\tilde{\gamma}^a$'s needs to be taken into account any longer for the description of the internal space of fermions or bosons, in agreement with the observed properties of fermions. $\tilde{\gamma}^a$'s obtain the role of operators determining properties of fermion and boson "basis vectors".

Let me add that we shall still use \tilde{S}^{ab} for the description of the internal space of fermion and boson fields, Subsects. 16.2.3, 16.2.3, 16.2.3. \tilde{S}^{ab} 's remain as operators. One finds, using Eq. (17.9),

$$\begin{aligned} \overset{ab}{\tilde{k}}(\overset{ab}{k}) &= 0, & \overset{ab}{(-\tilde{k})}(\overset{ab}{k}) &= -i\eta^{aa} \overset{ab}{[k]}, & \overset{ab}{\tilde{k}}(\overset{ab}{[k]}) &= i(\overset{ab}{k}), & \overset{ab}{\tilde{k}}(-\overset{ab}{k}) &= 0, \\ \overset{ab}{[\tilde{k}]}(\overset{ab}{k}) &= \overset{ab}{(k)}, & \overset{ab}{[-\tilde{k}]}(\overset{ab}{k}) &= 0, & \overset{ab}{[\tilde{k}]}(\overset{ab}{[k]}) &= 0, & \overset{ab}{[-\tilde{k}]}(\overset{ab}{[k]}) &= \overset{ab}{[k]} \end{aligned} \quad (16.13)$$

Taking into account anticommuting properties of both Clifford algebras, γ^a 's and $\tilde{\gamma}^a$'s, it is not difficult to prove the relations in Eq. (16.13).

16.2.3 Properties of Clifford odd and even "basis vectors" in $d = (5 + 1)$

To make discussions easier let us first look for the properties of "basis vectors" in $d = (5 + 1)$ -dimensional space. Let us look at: **i.** internal space of fermions as the superposition of odd products of the Clifford objects γ^a 's, **ii.** internal space of the corresponding gauge fields as the superposition of even products of the Clifford objects γ^a 's.

Choosing the "basis vectors" to be eigenvectors of all the members of the Cartan subalgebra of the Lorentz algebra and correspondingly the products of nilpotents and projectors (Statement 1.) one finds the "basis vectors" presented in Table 16.1. The table presents the eigenvalues of the "basis vectors" for each member of the Cartan subalgebra for the group $SO(5, 1)$.

The *odd I* group (is chosen to) present the "basis vectors" describing the internal space of fermions. Their Hermitian conjugated partners are then the "basis vectors" presented in the group *odd II*.

The *even I* and *even II* represent commuting Clifford even "basis vectors", representing bosons, the gauge fields of fermions.

We shall analyse both kinds of "basis vectors" through the subgroups of the $SO(5, 1)$ group. The choices of $SU(2) \times SU(2) \times U(1)$ and $SU(3) \times U(1)$ subgroups of the $SO(5, 1)$ group will also be discussed just to see the differences in properties from the properties of the $SO(5, 1)$ group.

In Table 16.1 the properties of "basis vectors" are presented as products of nilpotents $\overset{ab}{(+i)}$ ($\overset{ab}{(+i)} = 0$) and projectors $\overset{ab}{[+]}$ ($\overset{ab}{[+]} = \overset{ab}{[+]}$). "Basis vectors" for fermions contain an odd number of nilpotents, "basis vectors" for bosons contain an even number of nilpotents. In both cases nilpotents $\overset{ab}{(+i)}$ and projectors $\overset{ab}{[+]}$ are chosen to be the "eigenvectors" of the Cartan subalgebra. Eq. (16.6), of the Lorentz algebra. The "basis vectors", determining the creation operators for fermions and their Hermitian conjugated partners, $\hat{b}_f^{m\dagger}$ and \hat{b}_f^m , respectively, as we shall see in Sub-

sect. 16.2.3 they are superposition of odd products of γ^a , algebraically anticommute, due to the properties of the Clifford algebra

$$\begin{aligned} \{\gamma^a, \gamma^b\}_+ &= 2\eta^{ab} = \{\tilde{\gamma}^a, \tilde{\gamma}^b\}_+, \\ \{\gamma^a, \tilde{\gamma}^b\}_+ &= 0, \quad (a, b) = (0, 1, 2, 3, 5, \dots, d), \\ (\gamma^a)^\dagger &= \eta^{aa} \gamma^a, \quad (\tilde{\gamma}^a)^\dagger = \eta^{aa} \tilde{\gamma}^a, \\ \gamma^a \gamma^a &= \eta^{aa}, \quad \gamma^a (\gamma^a)^\dagger = I, \quad \tilde{\gamma}^a \tilde{\gamma}^a = \eta^{aa}, \quad \tilde{\gamma}^a (\tilde{\gamma}^a)^\dagger = I, \end{aligned} \quad (16.14)$$

where I represents the unit operator.

“Basis vectors” of odd products of γ^a s in $d = (5 + 1)$. Let us see in more details properties of the Clifford odd “basis vectors”, analysing them also with respect to two kinds of the subgroups $SO(3, 1) \times U(1)$ and $SU(3) \times U(1)$ of the group $SO(5, 1)$, with the same number of Cartan subalgebra members in all three cases, $\frac{d}{2} = 3$. We use the expressions for the commuting operators for the subgroup $SO(3, 1) \times U(1)$

$$N_{\pm}^3 (= N_{(L,R)}^3) := \frac{1}{2}(S^{12} \pm iS^{03}), \quad \tilde{N}_{\pm}^3 (= \tilde{N}_{(L,R)}^3) := \frac{1}{2}(\tilde{S}^{12} \pm i\tilde{S}^{03}) \quad (16.15)$$

and for the commuting generators for the subgroup $SU(3)$ and $U(1)$

$$\begin{aligned} \tau^3 &:= \frac{1}{2}(-S^{12} - iS^{03}), \quad \tau^8 = \frac{1}{2\sqrt{3}}(-iS^{03} + S^{12} - 2S^{1314}), \\ \tau^4 &:= -\frac{1}{3}(-iS^{03} + S^{12} + S^{56}). \end{aligned} \quad (16.16)$$

The corresponding relations for $\tilde{\tau}^3, \tilde{\tau}^8$ and $\tilde{\tau}^4$ can be read from Eq. (16.16), if replacing S^{ab} by \tilde{S}^{ab} . Recognizing that $S^{ab} = S^{ab} + \tilde{S}^{ab}$ one reproduces all the relations for the corresponding $\tilde{\tau}$ and N_{\pm}^3 .

The rest of generators of both kinds of subgroups of the group $SO(5, 1)$ can be found in Eqs. (17.26, 17.28) of App. 16.7.

In Table 16.2 the properties of the odd “basis vectors” $\hat{b}_f^{m\dagger}$ are presented with respect to the generators of the group **i.** $SO(5, 1)$ (with 15 generators, 3 of them forming the corresponding Commuting among subalgebra), **ii.** $SO(4) \times U(1)$ (with 7 generators and 3 of the corresponding Cartan subalgebra members) and **iii.** $SU(3) \times U(1)$ (with 9 generators and 3 of the corresponding Cartan subalgebra members), together with the eigenvalues of the commuting generators. These “basis vectors” are already presented as a part of Table 16.1. They fulfil together with their Hermitian conjugated partners the anticommutation relations of Eqs. (16.9, 16.11).

The right handed, $\Gamma^{(5+1)} = 1$, fourthplet of the fourth family of Table 16.2 can be found in the first four lines of Table 16.5 if only the $d = (5 + 1)$ part is taken into account. The left handed fourthplet of the fourth family of Table 16.4 can be found in four lines from line 33 to line 36, again if only the $d = (5 + 1)$ part is taken into

Table 16.1: $2^d = 64$ "eigenvectors" of the Cartan subalgebra of the Clifford odd and even algebras in $d = (5 + 1)$ -dimensional space are presented, divided into four groups. The first group, odd I, is chosen to represent "basis vectors", named $\hat{b}_f^{m\dagger}$, appearing in $2^{\frac{d}{2}-1} = 4$ "families" ($f = 1, 2, 3, 4$), each "family" with $2^{\frac{d}{2}-1} = 4$ "family" members ($m = 1, 2, 3, 4$). The second group, odd II, contains Hermitian conjugated partners of the first group for each family separately, $\hat{b}_f^m = (\hat{b}_f^{m\dagger})^\dagger$. The "family" quantum numbers of $\hat{b}_f^{m\dagger}$, that is the eigenvalues of $(\xi^{03}, \xi^{12}, \xi^{56})$, are written above each "family". The properties of anticommuting "basis vectors" are discussed in Subsects. 16.2.3, 16.2.4. The two groups with the even number of γ^{α} 's, *even I* and *even II*, have their Hermitian conjugated partners within their own group each. The two groups which are products of even number of nilpotents and even or odd number of projectors represent the "basis vectors" for the corresponding boson gauge fields. Their properties are discussed in Subsecs. 16.2.3 and 16.2.4. $\Gamma^{(5+1)}$ and $\Gamma^{(3+1)}$ represent handedness in $d = (3 + 1)$ and $d = (5 + 1)$ space calculated as products of γ^{α} 's, App. 16.9.

"basis vectors"		m	f = 1 $(\frac{1}{2}, -\frac{1}{2}, -\frac{1}{2})$ 03 12 56	f = 2 $(-\frac{1}{2}, -\frac{1}{2}, \frac{1}{2})$ 03 12 56	f = 3 $(-\frac{1}{2}, \frac{1}{2}, -\frac{1}{2})$ 03 12 56	f = 4 $(\frac{1}{2}, \frac{1}{2}, \frac{1}{2})$ 03 12 56	s ⁰³	s ¹²	s ⁵⁶	$\Gamma^{(5+1)}$	$\Gamma^{(3+1)}$
odd I $\hat{b}_f^{m\dagger}$	1		03 12 56 [+][+][+]	03 12 56 [+][+][+]	03 12 56 [+][+][+]	03 12 56 [+][+][+]	$\frac{1}{2}$	$\frac{1}{2}$	$\frac{1}{2}$	1	1
	2		[−][−][+]	[−][−][+]	[−][−][+]	[−][−][+]	$-\frac{1}{2}$	$-\frac{1}{2}$	$\frac{1}{2}$	1	1
	3		[−][+][−]	[−][+][−]	[−][+][−]	[−][+][−]	$-\frac{1}{2}$	$\frac{1}{2}$	$-\frac{1}{2}$	1	−1
	4		[+][−][−]	[+][−][−]	[+][−][−]	[+][−][−]	$\frac{1}{2}$	$-\frac{1}{2}$	$-\frac{1}{2}$	1	−1
			03 12 56	03 12 56	03 12 56	03 12 56				$\Gamma^{(5+1)}$	
odd II \hat{b}_f^m	1		[−][+][+]	[+][+][−]	[+][−][+]	[−][−][−]				−1	
	2		[−][+][+]	[+][+][−]	[+][−][+]	[−][−][−]				−1	
	3		[−][+][+]	[+][+][−]	[+][−][+]	[−][−][−]				−1	
	4		[−][+][+]	[+][+][−]	[+][−][+]	[−][−][−]				−1	
even I	m		$(-\frac{1}{2}, \frac{1}{2}, \frac{1}{2})$ 03 12 56	$(\frac{1}{2}, -\frac{1}{2}, \frac{1}{2})$ 03 12 56	$(-\frac{1}{2}, -\frac{1}{2}, -\frac{1}{2})$ 03 12 56	$(\frac{1}{2}, \frac{1}{2}, -\frac{1}{2})$ 03 12 56	s ⁰³	s ¹²	s ⁵⁶	$\Gamma^{(5+1)}$	$\Gamma^{(3+1)}$
	1		[+][+][+]	[+][+][+]	[+][+][+]	[+][+][+]	$\frac{1}{2}$	$\frac{1}{2}$	$\frac{1}{2}$	1	1
	2		[−][−][+]	[−][−][+]	[−][−][+]	[−][−][+]	$-\frac{1}{2}$	$-\frac{1}{2}$	$\frac{1}{2}$	1	1
	3		[−][+][−]	[−][+][−]	[−][+][−]	[−][+][−]	$-\frac{1}{2}$	$\frac{1}{2}$	$-\frac{1}{2}$	1	−1
4		[+][−][−]	[+][−][−]	[+][−][−]	[+][−][−]	$\frac{1}{2}$	$-\frac{1}{2}$	$-\frac{1}{2}$	1	−1	
even II	m		$(\frac{1}{2}, \frac{1}{2}, \frac{1}{2})$ 03 12 56	$(-\frac{1}{2}, -\frac{1}{2}, \frac{1}{2})$ 03 12 56	$(\frac{1}{2}, -\frac{1}{2}, -\frac{1}{2})$ 03 12 56	$(-\frac{1}{2}, \frac{1}{2}, -\frac{1}{2})$ 03 12 56	s ⁰³	s ¹²	s ⁵⁶	$\Gamma^{(5+1)}$	$\Gamma^{(3+1)}$
	1		[−][+][+]	[−][+][+]	[−][+][+]	[−][+][+]	$-\frac{1}{2}$	$\frac{1}{2}$	$\frac{1}{2}$	−1	−1
	2		[+][−][+]	[+][−][+]	[+][−][+]	[+][−][+]	$\frac{1}{2}$	$-\frac{1}{2}$	$\frac{1}{2}$	−1	−1
	3		[+][+][−]	[+][+][−]	[+][+][−]	[+][+][−]	$\frac{1}{2}$	$\frac{1}{2}$	$-\frac{1}{2}$	−1	1
4		[−][−][−]	[−][−][−]	[−][−][−]	[−][−][−]	$-\frac{1}{2}$	$-\frac{1}{2}$	$-\frac{1}{2}$	−1	1	

account.

Statement 5. In a chosen d -dimensional space there is the choice that the "basis vectors" are right handed. Their Hermitian conjugated partners are correspondingly left handed. One could make the opposite choice, like in Table 16.4.

Then the "basis vectors" of Table 16.2 would be the Hermitian conjugated partners to the left handed "basis vectors" of Table 16.4. For the left handed "basis vectors" the vacuum state $|\psi_{oc} \rangle$, Eq. (17.10), chosen as the $\sum_f \hat{b}_f^m *_{\Lambda} \hat{b}_f^{m\dagger}$, has to be changed, since the vacuum state must have the property that $\hat{b}_f^m |\psi_{oc} \rangle = 0$

Table 16.2: The basic creation operators, "basis vectors" — $\hat{b}_f^{m=(ch,s)\dagger}$ (each is a product of projectors and an odd product of nilpotents, and is the "eigenvector" of all the Cartan subalgebra members, S^{03}, S^{12}, S^{56} and $\tilde{S}^{03}, \tilde{S}^{12}, \tilde{S}^{56}$, Eq. (16.6) (ch (charge), the eigenvalue of S^{56} , and s (spin), the eigenvalues of S^{03} and S^{12} , explain index m, f determines family quantum numbers, the eigenvalues of $(\tilde{S}^{03}, \tilde{S}^{12}, \tilde{S}^{56})$ — are presented for $d = (5 + 1)$ -dimensional case. This table represents also the eigenvalues of the three commuting operators $N_{L,R}^3$ and S^{56} of the subgroups $SU(2) \times SU(2) \times U(1)$ and the eigenvalues of the three commuting operators τ^3, τ^8 and τ^4 of the subgroups $SU(3) \times U(1)$, in these two last cases index m represents the eigenvalues of the corresponding commuting generators. $\Gamma^{(5+1)} = -\gamma^0\gamma^1\gamma^2\gamma^3\gamma^5\gamma^6$, $\Gamma^{(3+1)} = i\gamma^0\gamma^1\gamma^2\gamma^3$. Operators $\hat{b}_f^{m=(ch,s)\dagger}$ and $\hat{b}_f^{m=(ch,s)}$ fulfil the anticommutation relations of Eqs. (16.9, 16.11).

f	m	=(ch, s)	$\hat{b}_f^{m=(ch,s)\dagger}$	s^{03}	s^{12}	s^{56}	Γ^{3+1}	N_L^3	N_R^3	τ^3	τ^8	τ^4	\tilde{s}^{03}	\tilde{s}^{12}	\tilde{s}^{56}
I	1	$(\frac{1}{2}, \frac{1}{2})$	$\begin{matrix} 03 & 12 & 56 \\ (+i) & (+) & (+) \end{matrix}$	$\frac{1}{2}$	$\frac{1}{2}$	$\frac{1}{2}$	1	0	$\frac{1}{2}$	0	0	$-\frac{1}{2}$	$\frac{1}{2}$	$-\frac{1}{2}$	$-\frac{1}{2}$
	2	$(\frac{1}{2}, -\frac{1}{2})$	$\begin{matrix} 03 & 12 & 56 \\ (-i) & (-) & (+) \end{matrix}$	$-\frac{1}{2}$	$-\frac{1}{2}$	$\frac{1}{2}$	1	0	$-\frac{1}{2}$	0	$-\frac{1}{\sqrt{3}}$	$\frac{1}{6}$	$\frac{1}{2}$	$-\frac{1}{2}$	$-\frac{1}{2}$
	3	$(-\frac{1}{2}, \frac{1}{2})$	$\begin{matrix} 03 & 12 & 56 \\ (-i) & (+) & (-) \end{matrix}$	$-\frac{1}{2}$	$\frac{1}{2}$	$-\frac{1}{2}$	-1	$\frac{1}{2}$	0	$-\frac{1}{2}$	$\frac{1}{2\sqrt{3}}$	$\frac{1}{6}$	$\frac{1}{2}$	$-\frac{1}{2}$	$-\frac{1}{2}$
	4	$(-\frac{1}{2}, -\frac{1}{2})$	$\begin{matrix} 03 & 12 & 56 \\ (+i) & (-) & (-) \end{matrix}$	$\frac{1}{2}$	$-\frac{1}{2}$	$-\frac{1}{2}$	-1	$-\frac{1}{2}$	0	$\frac{1}{2}$	$\frac{1}{2\sqrt{3}}$	$\frac{1}{6}$	$\frac{1}{2}$	$-\frac{1}{2}$	$-\frac{1}{2}$
II	1	$(\frac{1}{2}, \frac{1}{2})$	$\begin{matrix} 03 & 12 & 56 \\ (+i) & (+) & (+) \end{matrix}$	$\frac{1}{2}$	$\frac{1}{2}$	$\frac{1}{2}$	1	0	$\frac{1}{2}$	0	0	$-\frac{1}{2}$	$-\frac{1}{2}$	$\frac{1}{2}$	$-\frac{1}{2}$
	2	$(\frac{1}{2}, -\frac{1}{2})$	$\begin{matrix} 03 & 12 & 56 \\ (-i) & (-) & (+) \end{matrix}$	$-\frac{1}{2}$	$-\frac{1}{2}$	$\frac{1}{2}$	1	0	$-\frac{1}{2}$	0	$-\frac{1}{\sqrt{3}}$	$\frac{1}{6}$	$-\frac{1}{2}$	$\frac{1}{2}$	$-\frac{1}{2}$
	3	$(-\frac{1}{2}, \frac{1}{2})$	$\begin{matrix} 03 & 12 & 56 \\ (-i) & (+) & (-) \end{matrix}$	$-\frac{1}{2}$	$\frac{1}{2}$	$-\frac{1}{2}$	-1	$\frac{1}{2}$	0	$-\frac{1}{2}$	$\frac{1}{2\sqrt{3}}$	$\frac{1}{6}$	$-\frac{1}{2}$	$\frac{1}{2}$	$-\frac{1}{2}$
	4	$(-\frac{1}{2}, -\frac{1}{2})$	$\begin{matrix} 03 & 12 & 56 \\ (+i) & (-) & (-) \end{matrix}$	$\frac{1}{2}$	$-\frac{1}{2}$	$-\frac{1}{2}$	-1	$-\frac{1}{2}$	0	$\frac{1}{2}$	$\frac{1}{2\sqrt{3}}$	$\frac{1}{6}$	$-\frac{1}{2}$	$\frac{1}{2}$	$-\frac{1}{2}$
III	1	$(\frac{1}{2}, \frac{1}{2})$	$\begin{matrix} 03 & 12 & 56 \\ (+i) & (+) & (+) \end{matrix}$	$\frac{1}{2}$	$\frac{1}{2}$	$\frac{1}{2}$	1	0	$\frac{1}{2}$	0	0	$-\frac{1}{2}$	$-\frac{1}{2}$	$-\frac{1}{2}$	$\frac{1}{2}$
	2	$(\frac{1}{2}, -\frac{1}{2})$	$\begin{matrix} 03 & 12 & 56 \\ (-i) & (-) & (+) \end{matrix}$	$-\frac{1}{2}$	$-\frac{1}{2}$	$\frac{1}{2}$	1	0	$-\frac{1}{2}$	0	$-\frac{1}{\sqrt{3}}$	$\frac{1}{6}$	$-\frac{1}{2}$	$-\frac{1}{2}$	$\frac{1}{2}$
	3	$(-\frac{1}{2}, \frac{1}{2})$	$\begin{matrix} 03 & 12 & 56 \\ (-i) & (+) & (-) \end{matrix}$	$-\frac{1}{2}$	$\frac{1}{2}$	$-\frac{1}{2}$	-1	$\frac{1}{2}$	0	$-\frac{1}{2}$	$\frac{1}{2\sqrt{3}}$	$\frac{1}{6}$	$-\frac{1}{2}$	$-\frac{1}{2}$	$\frac{1}{2}$
	4	$(-\frac{1}{2}, -\frac{1}{2})$	$\begin{matrix} 03 & 12 & 56 \\ (+i) & (-) & (-) \end{matrix}$	$\frac{1}{2}$	$-\frac{1}{2}$	$-\frac{1}{2}$	-1	$-\frac{1}{2}$	0	$\frac{1}{2}$	$\frac{1}{2\sqrt{3}}$	$\frac{1}{6}$	$-\frac{1}{2}$	$-\frac{1}{2}$	$\frac{1}{2}$
IV	1	$(\frac{1}{2}, \frac{1}{2})$	$\begin{matrix} 03 & 12 & 56 \\ (+i) & (+) & (+) \end{matrix}$	$\frac{1}{2}$	$\frac{1}{2}$	$\frac{1}{2}$	1	0	$\frac{1}{2}$	0	0	$-\frac{1}{2}$	$\frac{1}{2}$	$\frac{1}{2}$	$\frac{1}{2}$
	2	$(\frac{1}{2}, -\frac{1}{2})$	$\begin{matrix} 03 & 12 & 56 \\ (-i) & (-) & (+) \end{matrix}$	$-\frac{1}{2}$	$-\frac{1}{2}$	$\frac{1}{2}$	1	0	$-\frac{1}{2}$	0	$-\frac{1}{\sqrt{3}}$	$\frac{1}{6}$	$\frac{1}{2}$	$\frac{1}{2}$	$\frac{1}{2}$
	3	$(-\frac{1}{2}, \frac{1}{2})$	$\begin{matrix} 03 & 12 & 56 \\ (-i) & (+) & (-) \end{matrix}$	$-\frac{1}{2}$	$\frac{1}{2}$	$-\frac{1}{2}$	-1	$\frac{1}{2}$	0	$-\frac{1}{2}$	$\frac{1}{2\sqrt{3}}$	$\frac{1}{6}$	$\frac{1}{2}$	$\frac{1}{2}$	$\frac{1}{2}$
	4	$(-\frac{1}{2}, -\frac{1}{2})$	$\begin{matrix} 03 & 12 & 56 \\ (+i) & (-) & (-) \end{matrix}$	$\frac{1}{2}$	$-\frac{1}{2}$	$-\frac{1}{2}$	-1	$-\frac{1}{2}$	0	$\frac{1}{2}$	$\frac{1}{2\sqrt{3}}$	$\frac{1}{6}$	$\frac{1}{2}$	$\frac{1}{2}$	$\frac{1}{2}$

and $\hat{b}_f^{m\dagger} |\psi_{oc} \rangle = \hat{b}_f^{m\dagger}$.

One can notice that:

i. The family members of "basis vectors" have the same properties in all the families, independently whether one observes the group $SO(d - 1, 1)$ ($SO(5, 1)$ in the case of $d = (5 + 1)$) or of the subgroups with the same number of commuting operators ($SU(2) \times SU(2) \times U(1)$ or $\times SU(3) \times U(1)$ in $d = (5 + 1)$ case). The families carry different family quantum numbers. This is true for right, ($\Gamma^{(5+1)} = 1$), and for left ($\Gamma^{(5+1)} = -1$), representations.

ii. The sum of all the eigenvalues of all the commuting operators over the $2^{\frac{d}{2}-1}$ family members is equal to zero for each of $2^{\frac{d}{2}-1}$ families, separately for left and separately for right handed representations, independently whether the group $SO(d - 1, 1)$ ($SO(5, 1)$) or the subgroups ($SU(2) \times SU(2) \times U(1)$ or $\times SU(3) \times U(1)$)

are considered.

iii. The sum of the family quantum numbers over the four families is zero as well.
 iv. The properties of the left handed family members differ strongly from the right handed ones. It is easy to recognize this in our $d = (5 + 1)$ case when looking at $SU(3) \times U(1)$ quantum numbers since the right handed realization manifests the "colour" properties of "quarks" and "leptons" and the left handed the "colour" properties of "antiquarks" and "antileptons".

v. For a chosen even d there is a choice for either right or left handed family members. The choice of the handedness of the family members determine also the vacuum state for the chosen "basis vectors".

Let me add that the "basis vectors" and their Hermitian conjugated partners fulfil the anticommutation relations postulated by Dirac for the second quantized fermion fields. When forming tensor products, $*_{\top}$, of these "basis vectors" and the basis of ordinary, momentum or coordinate, space the single fermion creation and annihilation operators fulfil all the requirements of the Dirac's second quantized fermion fields, explaining therefore the postulates of Dirac, Sect. 16.3.

"Basis vectors" of even products of γ^{α} 's in $d = (5 + 1)$ The Clifford even "basis vectors", they are products of an even number of nilpotents, $(k)^{ab}$, and the rest up to $\frac{d}{2}$ of projectors, $[k]^{ab}$, commute since even products of (anticommuting) γ^{α} 's commute.

Let us see in more details several properties of the Clifford even "basis vectors":

A. The properties of the algebraic, $*_{\Lambda}$, application of the Clifford even "basis vectors" on the Clifford odd "basis vectors" $\hat{b}_f^{m\dagger}$, presented in Table 16.2, teaches us that the Clifford even "basis vectors" describe the internal space of the gauge fields of $\hat{b}_f^{m\dagger}$.

A.i.

Let $\hat{b}_f^{m\dagger}$ represents the m^{th} Clifford odd I "basis vector" (the part of the creation operators which determines the internal part of the fermion state) of the f^{th} family and let $\hat{A}_f^{m\dagger}$ denotes the m^{th} Clifford even II "basis vector" of the f^{th} irreducible representation with respect to S^{ab} — but not with respects to $S^{ab} = S^{ab} + \xi^{ab}$, which includes all $2^{\frac{d}{2}-1} \times 2^{\frac{d}{2}-1}$ members. Let us evaluate the algebraic products $\hat{A}_f^{m\dagger}$ on $\hat{b}_f^{m'\dagger}$ for any (m, m') and (f, f') .

Taking into account Eq. (17.8) and Tables (16.1, 16.2) one can easily evaluate the algebraic products $\hat{A}_f^{m\dagger}$ on $\hat{b}_f^{m'\dagger}$ for any (m, m') and (f, f') . Starting with $\hat{b}_1^{1\dagger}$ one

finds the non zero contributions only if applying $\hat{\mathcal{A}}_3^{m\dagger}$, $m = (1, 2, 3, 4)$ on $\hat{b}_1^{1\dagger}$

$$\begin{aligned}
 & \hat{\mathcal{A}}_3^{m\dagger} *_A \hat{b}_1^{1\dagger} (\equiv (+i)[+][+]) : \\
 & \hat{\mathcal{A}}_3^{1\dagger} (\equiv [+i][+][+]) *_A \hat{b}_1^{1\dagger} (\equiv (+i)[+][+]) \rightarrow \hat{b}_1^{1\dagger} , \\
 & \hat{\mathcal{A}}_3^{2\dagger} (\equiv (-i)(-)[+]) *_A \hat{b}_1^{1\dagger} \rightarrow \hat{b}_1^{2\dagger} (\equiv [-i](-)[+]) , \\
 & \hat{\mathcal{A}}_3^{3\dagger} (\equiv (-i)[+][+]) *_A \hat{b}_1^{1\dagger} \rightarrow \hat{b}_1^{3\dagger} (\equiv [-i][+][+]) , \\
 & \hat{\mathcal{A}}_3^{4\dagger} (\equiv [+i](-)(-)) *_A \hat{b}_1^{1\dagger} \rightarrow \hat{b}_1^{4\dagger} (\equiv (+i)(-)(-)) . \tag{16.17}
 \end{aligned}$$

The products of an even number of nilpotents and even or an odd number of projectors, represented by even products of γ^a 's, applying on family members of a particular family, obviously transform family members, representing fermions of one particular family, into the same or another family member of the same family. All the rest of $\hat{\mathcal{A}}_f^m$, $f \neq 3$, applying on $\hat{b}_1^{1\dagger}$, give zero for any family f .

Let us comment the above events, concerning only the internal space of fermions and, obviously, bosons: If the fermion, the internal space of which is described by Clifford odd "basis vector" $\hat{b}_1^{1\dagger}$, absorbs the boson $\hat{\mathcal{A}}_3^1$ (with $S^{03} = 0, S^{12} = 0, S^{56} = 0$), its "basis vector" $\hat{b}_1^{1\dagger}$ remains unchanged.

The fermion with the "basis vector" $\hat{b}_1^{1\dagger}$, if absorbing the boson with $\hat{\mathcal{A}}_3^2$ (with $S^{03} = -i, S^{12} = -1, S^{56} = 0$), changes its internal "basis vector" $\hat{b}_1^{1\dagger}$ into the "basis vector" $\hat{b}_1^{2\dagger}$ (which carries now $S^{03} = -\frac{i}{2}, S^{12} = -\frac{1}{2}$, and the same $S^{56} = \frac{1}{2}$ as before). The fermion with "basis vector" $\hat{b}_1^{1\dagger}$ absorbing the boson with the "basis vector" $\hat{\mathcal{A}}_3^3$ changes its "basis vector" to $\hat{b}_1^{3\dagger}$, while the fermion with the "basis vector" $\hat{b}_1^{1\dagger}$ absorbing the boson with the "basis vector" $\hat{\mathcal{A}}_3^4$ changes its "basis vector" to $\hat{b}_1^{4\dagger}$.

Let us see how do the rest of $\hat{\mathcal{A}}_f^m$, $m = (1, 2, 3, 4)$, $f = (1, 2, 3, 4)$ change the properties of $\hat{b}_1^{n\dagger}$, $n = 2, 3, 4$.

It is easy to evaluate if taking into account Eq. (17.8) that

$$\begin{aligned}
& \hat{\mathcal{A}}_4^{m\dagger} *_{\mathcal{A}} \hat{b}_1^{2\dagger} (\equiv [-i](-)[+]) : \\
& \hat{\mathcal{A}}_4^{1\dagger} (\equiv [+i](+)[+]) *_{\mathcal{A}} \hat{b}_1^{2\dagger} (\equiv [-i](-)[+]) \rightarrow \hat{b}_1^{1\dagger} , \\
& \hat{\mathcal{A}}_4^{2\dagger} (\equiv [-i](-)[+]) *_{\mathcal{A}} \hat{b}_1^{2\dagger} \rightarrow \hat{b}_1^{2\dagger} (\equiv [-i](-)[+]) , \\
& \hat{\mathcal{A}}_4^{3\dagger} (\equiv [-i](+)(-)) *_{\mathcal{A}} \hat{b}_1^{2\dagger} \rightarrow \hat{b}_1^{3\dagger} (\equiv [-i](+)(-)) , \\
& \hat{\mathcal{A}}_4^{4\dagger} (\equiv [+i](-)(-)) *_{\mathcal{A}} \hat{b}_1^{2\dagger} \rightarrow \hat{b}_1^{4\dagger} (\equiv [+i](-)(-)) , \\
& \hat{\mathcal{A}}_2^{m\dagger} *_{\mathcal{A}} \hat{b}_1^{3\dagger} (\equiv [-i](+)(-)) : \\
& \hat{\mathcal{A}}_2^{1\dagger} (\equiv [+i](+)(+)) *_{\mathcal{A}} \hat{b}_1^{3\dagger} (\equiv [-i](+)(-)) \rightarrow \hat{b}_1^{1\dagger} , \\
& \hat{\mathcal{A}}_2^{2\dagger} (\equiv [-i](-)(+)) *_{\mathcal{A}} \hat{b}_1^{3\dagger} \rightarrow \hat{b}_1^{2\dagger} (\equiv [-i](-)(+)) , \\
& \hat{\mathcal{A}}_2^{3\dagger} (\equiv [-i](+)(-)) *_{\mathcal{A}} \hat{b}_1^{3\dagger} \rightarrow \hat{b}_1^{3\dagger} (\equiv [-i](+)(-)) , \\
& \hat{\mathcal{A}}_2^{4\dagger} (\equiv [+i](-)(-)) *_{\mathcal{A}} \hat{b}_1^{3\dagger} \rightarrow \hat{b}_1^{4\dagger} (\equiv [+i](-)(-)) , \\
& \hat{\mathcal{A}}_1^{m\dagger} *_{\mathcal{A}} \hat{b}_1^{4\dagger} (\equiv [+i](-)(-)) : \\
& \hat{\mathcal{A}}_1^{1\dagger} (\equiv [+i](+)(+)) *_{\mathcal{A}} \hat{b}_1^{4\dagger} (\equiv [+i](-)(-)) \rightarrow \hat{b}_1^{1\dagger} , \\
& \hat{\mathcal{A}}_1^{2\dagger} (\equiv [-i](-)(+)) *_{\mathcal{A}} \hat{b}_1^{4\dagger} \rightarrow \hat{b}_1^{2\dagger} (\equiv [-i](-)(+)) , \\
& \hat{\mathcal{A}}_1^{3\dagger} (\equiv [-i](+)(-)) *_{\mathcal{A}} \hat{b}_1^{4\dagger} \rightarrow \hat{b}_1^{3\dagger} (\equiv [-i](+)(-)) , \\
& \hat{\mathcal{A}}_1^{4\dagger} (\equiv [+i](-)(-)) *_{\mathcal{A}} \hat{b}_1^{4\dagger} \rightarrow \hat{b}_1^{4\dagger} (\equiv [+i](-)(-)) . \tag{16.18}
\end{aligned}$$

All the rest of $\hat{\mathcal{A}}_f^m$, applying on $\hat{b}_1^{n\dagger}$, give zero for any other f except the one presented in Eqs. (16.17, 16.18).

We can repeat this calculation for all four family members $\hat{b}_f^{m\dagger}$ of any of families f' . concluding

$$\begin{aligned}
& \hat{\mathcal{A}}_3^{m\dagger} *_{\mathcal{A}} \hat{b}_f^{1\dagger} \rightarrow \hat{b}_f^{m\dagger} , \\
& \hat{\mathcal{A}}_4^{m\dagger} *_{\mathcal{A}} \hat{b}_f^{2\dagger} \rightarrow \hat{b}_f^{m\dagger} , \\
& \hat{\mathcal{A}}_2^{m\dagger} *_{\mathcal{A}} \hat{b}_f^{3\dagger} \rightarrow \hat{b}_f^{m\dagger} , \\
& \hat{\mathcal{A}}_1^{m\dagger} *_{\mathcal{A}} \hat{b}_f^{4\dagger} \rightarrow \hat{b}_f^{m\dagger} . \tag{16.19}
\end{aligned}$$

The recognition of this subsection concerns so far only internal space of fermions, not yet its dynamics in ordinary space. Let us interpret what is noticed:

Statement 6. A fermion with the "basis vector" $\hat{b}_f^{m\dagger}$, "absorbing" one of the commuting Clifford even objects, $\hat{\mathcal{A}}_f^{m\dagger}$, transforms into another family member of the same family, to $\hat{b}_f^{m\dagger}$, changing correspondingly the family member quantum numbers and keeping the same family quantum number or remains unchanged.

The application of the Clifford even "basis vector" $\hat{\mathcal{A}}_f^{m\dagger}$ on the Clifford odd "basis vector" does not cause the change of the family of the Clifford odd "basis vector".

A.ii.

We need to know the quantum numbers of the Clifford even "basis vectors", which obviously manifest properties of the boson fields since they bring to the Clifford odd "basis vectors" — representing the internal space of fermions — the quantum numbers which cause transformation into another fermion with a different Clifford odd "basis vectors" of the same family f . The Clifford even "basis vectors" do not cause the change of the family of fermions.

Let us point out that the Clifford odd "basis vectors" appear in $2^{\frac{d}{2}-1}$ families with $2^{\frac{d}{2}-1}$ family members in each family, four members in four families in the $d = (5 + 1)$ case, while the Hermitian conjugated partners belong to another group of $2^{\frac{d}{2}-1} \times 2^{\frac{d}{2}-1}$ Clifford odd "basis vectors", (to oddII in Table 16.1), while the Clifford even "basis vectors" have their Hermitian conjugated partners within the same group of $2^{\frac{d}{2}-1} \times 2^{\frac{d}{2}-1}$ members (appearing in our treating case in evenII in Table 16.1). Since we found in Eqs. (16.19, 16.17, 16.17) that the Clifford even "basis vector" transforms the Clifford odd "basis vector" into another member of the same family, changing the family members quantum numbers for an integer, they must carry the integer quantum numbers.

One can see in Table 16.1 that the members of the group evenII, for example, are Hermitian conjugated to one another in pairs and four of them are self adjoint. Correspondingly \dagger has no special meaning, it is only the decision that all the Clifford even "basis vector" are equipped with \dagger : $\hat{\mathcal{A}}_f^{m\dagger}$.

Let us therefore calculate the quantum numbers of $\hat{\mathcal{A}}_f^{m\dagger}$, where m and f distinguish among different Clifford even "basis vectors" (with f which does not really denote the family, since $\mathcal{S}^{ab} = S^{ab} + \tilde{\mathcal{S}}^{ab}$ defines the whole irreducible representation of $2^{\frac{d}{2}-1} \times 2^{\frac{d}{2}-1}$ "basis vectors") with the Cartan subalgebra operators $\mathcal{S}^{ab} = S^{ab} + \tilde{\mathcal{S}}^{ab}$, presented in Eqs. (16.6).

In Table 16.3 the eigenvalues of the Cartan subalgebra members of \mathcal{S}^{ab} are presented, as well as the eigenvalues of the commuting operators of subgroups $SU(2) \times SU(2) \times U(1)$, that is the eigenvalues of $(\mathcal{N}_L^3, \mathcal{N}_R^3, \mathcal{S}^{03})$, and of $SU(3) \times U(1)$, that is the eigenvalues of (τ^3, τ^8, τ^4) , expressions for which can be found in Eqs. (16.15, 16.16) if one takes into account that $\mathcal{S}^{ab} = S^{ab} + \tilde{\mathcal{S}}^{ab}$. The algebraic application of any member of a group f on the self adjoint operator (denoted in Table 16.3 by \bigcirc) of this group f , gives the same member back.

The vacuum state of the Clifford even "basis vectors" is correspondingly the normalized sum of all the self adjoint operators of these Clifford even group evenII. Each of $\mathcal{A}_f^{m\dagger}$ when applying on such a vacuum state gives the same $\hat{\mathcal{A}}_f^{m\dagger}$.

$$|\Phi_{\text{oc even}}\rangle = \frac{1}{2} ([+i] [-] [-] + [-i] [+] [-] + [+i] [+] [+] + [-i] [-] [+])\quad (16.20)$$

The pairs of "basis vectors" $\hat{\mathcal{A}}_f^{m\dagger}$, which are Hermitian conjugated to each other, are in Table 16.3 pointed out by the same symbols. This property is independent of the group or subgroups which we choose to observe properties of the "basis vectors". If treating the subgroup $SU(3) \times U(1)$ one finds the 8 members of $\mathcal{A}_f^{m\dagger}$, which belong to the group $SU(3)$ forming octet which has $\tau^4 = 0$, six of them appear in three pairs Hermitian conjugated to each other, two of them are self adjoint members of the octet, with eigenvalues of all the Cartan subalgebra members equal

to zero. There are also two singlets with eigenvalues of all the Cartan subalgebra members equal to zero. And there is the sextet, with three pairs which are mutually Hermitian conjugated. One can notice that the sum of all the eigenvalues of all the

Table 16.3: The "basis vectors" $\hat{\mathcal{A}}_f^{m\dagger}$, each is the product of projectors and an even number of nilpotents, and is the "eigenvector" of all the Cartan subalgebra members, S^{03} , S^{12} , S^{56} , Eq. (16.6), are presented for $d = (5 + 1)$ -dimensional case. Indexes m and f determine $2^{\frac{d}{2}-1} \times 2^{\frac{d}{2}-1}$ different members $\hat{\mathcal{A}}_f^{m\dagger}$. In the third column the "basis vectors" $\hat{\mathcal{A}}_f^{m\dagger}$ which are Hermitian conjugated partners to each other, and can therefore annihilate each other, are pointed out with the same symbol. For example with \star are equipped the first member with $m = 1$ and $f = 1$ and the last member with $m = 4$ and $f = 3$. The sign \bigcirc denotes the "basis vectors" which are self adjoint $(\hat{\mathcal{A}}_f^{m\dagger})^\dagger = \hat{\mathcal{A}}_f^{m\dagger}$. This table represents also the eigenvalues of the three commuting operators $\mathcal{N}_{L,R}^3$ and S^{56} of the subgroups $SU(2) \times SU(2) \times U(1)$ of the group $SO(5, 1)$ and the eigenvalues of the three commuting operators τ^3, τ^8 and τ^4 of the subgroups $SU(3) \times U(1)$.

f	m	*	$\hat{\mathcal{A}}_f^{m\dagger}$	S^{03}	S^{12}	S^{56}	\mathcal{N}_L^3	\mathcal{N}_R^3	τ^3	τ^8	τ^4
I	1	$\star\star$	$\begin{matrix} 03 & 12 & 56 \\ [+i] & (+) & (+) \end{matrix}$	0	1	1	$\frac{1}{2}$	$\frac{1}{2}$	$-\frac{1}{2}$	$-\frac{1}{2\sqrt{3}}$	$-\frac{2}{3}$
	2	\triangle	$\begin{matrix} 03 & 12 & 56 \\ (-i) & [-] & (+) \end{matrix}$	-i	0	1	$\frac{1}{2}$	$-\frac{1}{2}$	$-\frac{1}{2}$	$-\frac{3}{2\sqrt{3}}$	0
	3	\ddagger	$\begin{matrix} 03 & 12 & 56 \\ (-i) & (+) & [-] \end{matrix}$	-i	1	0	1	0	-1	0	0
	4	\bigcirc	$\begin{matrix} 03 & 12 & 56 \\ [+i] & [-] & [-] \end{matrix}$	0	0	0	0	0	0	0	0
II	1	\bullet	$\begin{matrix} 03 & 12 & 56 \\ (+i) & [+] & (+) \end{matrix}$	i	0	1	$-\frac{1}{2}$	$\frac{1}{2}$	$\frac{1}{2}$	$-\frac{1}{2\sqrt{3}}$	$-\frac{2}{3}$
	2	\otimes	$\begin{matrix} 03 & 12 & 56 \\ [-i] & (-) & (+) \end{matrix}$	0	-1	1	$-\frac{1}{2}$	$-\frac{1}{2}$	$\frac{1}{2}$	$-\frac{3}{2\sqrt{3}}$	0
	3	\bigcirc	$\begin{matrix} 03 & 12 & 56 \\ [-i] & [+] & [-] \end{matrix}$	0	0	0	0	0	0	0	0
	4	\ddagger	$\begin{matrix} 03 & 12 & 56 \\ (+i) & (-) & [-] \end{matrix}$	i	-1	0	-1	0	1	0	0
III	1	\bigcirc	$\begin{matrix} 03 & 12 & 56 \\ [+i] & [+] & [+] \end{matrix}$	0	0	0	0	0	0	0	0
	2	$\odot\odot$	$\begin{matrix} 03 & 12 & 56 \\ (-i) & (-) & [+] \end{matrix}$	-i	-1	0	0	-1	0	$-\frac{1}{\sqrt{3}}$	$\frac{2}{3}$
	3	\bullet	$\begin{matrix} 03 & 12 & 56 \\ (-i) & [+] & (-) \end{matrix}$	-i	0	-1	$\frac{1}{2}$	$-\frac{1}{2}$	$-\frac{1}{2}$	$\frac{1}{2\sqrt{3}}$	$\frac{2}{3}$
	4	$\star\star$	$\begin{matrix} 03 & 12 & 56 \\ [+i] & (-) & (-) \end{matrix}$	0	-1	-1	$-\frac{1}{2}$	$-\frac{1}{2}$	$\frac{1}{2}$	$\frac{1}{2\sqrt{3}}$	$\frac{2}{3}$
IV	1	$\odot\odot$	$\begin{matrix} 03 & 12 & 56 \\ (+i) & (+) & [+] \end{matrix}$	i	1	0	0	1	0	$\frac{1}{\sqrt{3}}$	$-\frac{2}{3}$
	2	\bigcirc	$\begin{matrix} 03 & 12 & 56 \\ [-i] & [-] & [+] \end{matrix}$	0	0	0	0	0	0	0	0
	3	\otimes	$\begin{matrix} 03 & 12 & 56 \\ [-i] & (+) & (-) \end{matrix}$	0	1	-1	$\frac{1}{2}$	$\frac{1}{2}$	$-\frac{1}{2}$	$\frac{3}{2\sqrt{3}}$	0
	4	\triangle	$\begin{matrix} 03 & 12 & 56 \\ (+i) & [-] & (-) \end{matrix}$	i	0	-1	$-\frac{1}{2}$	$\frac{1}{2}$	$\frac{1}{2}$	$\frac{3}{2\sqrt{3}}$	0

Cartan subalgebra members over the 16 members $\hat{\mathcal{A}}_f^{m\dagger}$ is equal to zero, independent of whether we treat the group $SO(5, 1)$, $SU(2) \times SU(2) \times U(1)$, or $SU(3) \times U(1)$.

A.iii.

In **A.i.** we saw that the application of $\hat{\mathcal{A}}_f^{m\dagger}$ on the fermion "basis vectors" $\hat{b}_f^{m\dagger}$ transforms the particular member $\hat{b}_f^{m\dagger}$ to one of the members of the same family f , changing eigenvalues of the Cartan subalgebra members for an integer. We found in **A.ii** the eigenvalues of the Cartan subalgebra members for each of $2^{\frac{d}{2}-1} \times 2^{\frac{d}{2}-1}$ (equal to 16 in $d = (5 + 1)$) $\hat{\mathcal{A}}_f^{m\dagger}$, recognizing that they do have properties of the boson fields.

It remains to look for the behaviour of these Clifford even "basis vector" when they apply on each other. Let us denote the self adjoint member in each group of "basis vectors" of particular f as $\hat{A}_f^{m_0\dagger}$. We easily see that

$$\begin{aligned} \{\hat{A}_f^{m\dagger}, \hat{A}_f^{m'\dagger}\}_- &= 0, \quad \text{if } (m, m') \neq m_0 \text{ or } m = m_0 = m', \forall f, \\ \hat{A}_f^{m\dagger} *_{\mathcal{A}} \hat{A}_f^{m_0\dagger} &= \hat{A}_f^{m\dagger}, \quad \forall m, \forall f. \end{aligned} \tag{16.21}$$

Two "basis vectors" $\hat{A}_f^{m\dagger}$ and $\hat{A}_f^{m'\dagger}$ of the same f and of $(m, m') \neq m_0$ are orthogonal.

The two "basis vectors" $\hat{A}_f^{m\dagger}$ and $\hat{A}_f^{m'\dagger}$, the algebraic product, $*_{\mathcal{A}}$, of which gives nonzero contribution, like $\hat{A}_1^{1\dagger} *_{\mathcal{A}} \hat{A}_2^{4\dagger} = \hat{A}_2^{1\dagger}$, "scatter" into the third one, or annihilate into vacuum $|\phi_{\text{oc_even}}\rangle$, Eq. (16.20), like $\hat{A}_2^{2\dagger} *_{\mathcal{A}} \hat{A}_4^{3\dagger} = \hat{A}_4^{2\dagger}$.² To generate creation and annihilation operators the tensor products, $*_{\mathcal{T}}$, of the "basis vectors" $\hat{A}_f^{m\dagger}$, as well as of the "basis vectors" $\hat{b}_f^{m\dagger}$, with the basis in ordinary, momentum or coordinate, space is needed.

Statement 7. *Two "basis vectors" $\hat{A}_f^{m\dagger}$ and $\hat{A}_f^{m_0\dagger}$ of the same f and of $(m, m') \neq m_0$ are orthogonal. The two "basis vectors" with nonzero algebraic product, $*_{\mathcal{A}}$, "scatter" into the third one, or annihilate into vacuum.*

B. Let us point out that the choice of the Clifford odd "basis vectors", odd I, describing the internal space of fermions, and consequently the choice of the Clifford even "basis vectors", even II, describing the internal space of their gauge fields, is ours. If we choose in Table 16.1 odd II to represent the "basis vectors" describing the internal space of fermions, then the corresponding "basis vectors" representing the internal space of bosonic partners are those of even I.

For a different choice of handedness of the Clifford odd "basis vectors" for describing fermions — making a choice of the left handedness instead of the right handedness — Table 16.2 should be replaced by Table 16.4 and correspondingly also **A.i.**, **A.ii.**, **A.iii.** should be rewritten.

For an even d there is a choice for either right or left handed family members. The choice of the handedness of the family members determine also the vacuum state for the chosen "basis vectors" for either — Clifford odd "basis vectors" of fermions or for the corresponding Clifford even "basis vectors" of the corresponding gauge boson fields.

C. The Clifford even "basis vectors" $\hat{A}_f^{m\dagger}$, representing the boson gauge fields to the corresponding Clifford odd "basis vectors" $\hat{b}_f^{m\dagger}$, have the properties that they transform Clifford odd "basis vectors" $\hat{b}_f^{m\dagger}$ of each family within the family members. There are the additional Clifford even "basis vectors" $\hat{A}_f^{m\dagger}$ which transform each family member of particular family into the same family member of some of the rest families.

² I use "scatter" in quotation marks since the "basis vectors" $\hat{A}_f^{m\dagger}$ determine only the internal space of bosons, as also the "basis vectors" $\hat{b}_f^{m\dagger}$ determine only the internal space of fermions.

These Clifford even "basis vectors" $\hat{\mathcal{A}}_f^{m\dagger}$ are products of an even number of nilpotents and of projectors, which are eigenvectors of the Cartan subalgebra operators $\tilde{S}^{03}, \tilde{S}^{12}, \tilde{S}^{56}, \dots, \tilde{S}^{d-1 d}$. The table like Table 16.3 should be prepared and their properties described as in the case of **A.i.**, **A.ii.**, **A.iii.**. A short illustration is to help understanding the role of these Clifford even "basis vectors" $\hat{\mathcal{A}}_f^{m\dagger}$.

Let us use for the Clifford even "basis vectors" $\hat{\mathcal{A}}_f^{m\dagger}$ the same arrangement with products of nilpotents and projectors as the one, chosen for the Clifford even "basis vectors" $\hat{\mathcal{A}}_f^{m\dagger}$ in the case of $d = (5 + 1)$ in Table 16.3, except that now nilpotents and projectors are eigenvectors of the Cartan subalgebra operators $\tilde{S}^{03}, \tilde{S}^{12}, \tilde{S}^{56}$, and are correspondingly written in terms of nilpotents $\overset{ab}{\tilde{k}}$ and projectors $\overset{ab}{[k]}$. The application of these nilpotents and projectors on nilpotents and projectors appearing in $\hat{b}_f^{m\dagger}$ are presented in Eq. (16.13). Making a choice of $\hat{\mathcal{A}}_1^{1\dagger} (\equiv [+i] \overset{03}{+} \overset{12}{+} \overset{56}{+})$, with quantum numbers $(S^{03} = 0, S^{12} = 1, S^{56} = 1)$, on $\hat{b}_1^{4\dagger} (\equiv (+i) \overset{03}{-} \overset{12}{-} \overset{56}{-})$ with the family members quantum numbers $(S^{03} = \frac{i}{2}, S^{12} = -\frac{1}{2}, S^{56} = -\frac{1}{2})$ and the family quantum numbers $(\tilde{S}^{03} = \frac{i}{2}, \tilde{S}^{12} = -\frac{1}{2}, \tilde{S}^{56} = -\frac{1}{2})$ it follows

$$\hat{\mathcal{A}}_1^{1\dagger} (\equiv [+i] \overset{03}{+} \overset{12}{+} \overset{56}{+}) *_A \hat{b}_1^{4\dagger} (\equiv (+i) \overset{03}{-} \overset{12}{-} \overset{56}{-}) \rightarrow \hat{b}_4^{4\dagger} (\equiv (+i) \overset{03}{-} \overset{12}{-} \overset{56}{-}). \quad (16.22)$$

$\hat{b}_4^{4\dagger} (\equiv (+i) \overset{03}{-} \overset{12}{-} \overset{56}{-})$ carry the same family members quantum numbers as $\hat{b}_1^{4\dagger} (S^{03} = \frac{i}{2}, S^{12} = -\frac{1}{2}, S^{56} = -\frac{1}{2})$ but belongs to the different family with the family quantum numbers $(\tilde{S}^{03} = \frac{i}{2}, \tilde{S}^{12} = \frac{1}{2}, \tilde{S}^{56} = \frac{1}{2})$.

The detailed analyse of these last two cases **B.** and **C.** will be studied after this Bled proceedings.

We can conclude that the Clifford even "basis vectors" $\hat{\mathcal{A}}_f^{m\dagger}$:

- a. Have the quantum numbers determined by the Cartan subalgebra members of the Lorentz group of $S^{ab} = S^{ab} + \tilde{S}^{ab}$. Applying algebraically, $*_A, \hat{\mathcal{A}}_f^{m\dagger}$ on the Clifford odd "basis vectors" $\hat{b}_f^{m\dagger}, \hat{\mathcal{A}}_3^{m\dagger}$ transform these "basis vectors" to another ones with the same family quantum numbers, $\hat{b}_f^{m\dagger}$.
- b. In any irreducibly representation of S^{ab} $\hat{\mathcal{A}}_f^{m\dagger}$ appear in pairs, which are Hermitian conjugated to each other or they are self adjoint.
- c. The self adjoint members $\hat{\mathcal{A}}_f^{m\dagger}$ define the vacuum state of the second quantized boson fields.
- d. Applying $\hat{\mathcal{A}}_f^{m\dagger}$ algebraically to each other these commuting Clifford even "basis vector" forming another Clifford even "basis vector" or annihilate into the vacuum.
- e. The choice of the left or the right handedness of the "basis vectors" of an odd Clifford character, describing the internal space of fermions, is ours. The left and the right handed "basis vectors" of an odd Clifford character are namely Hermitian conjugated to each other. With the choice of the handedness of the fermion "basis vectors" also the choice of boson Clifford even "basis vectors" — which are their corresponding gauge fields — are chosen.

f. There exist the Clifford even "basis vectors" $\hat{A}_f^{m\dagger}$ (like $\hat{A}_1^{1\dagger} (\equiv [+i] \binom{03}{+} \binom{12}{+} \binom{56}{\bar{1}})$) which transform the Clifford odd "basis vectors" $\hat{b}_f^{m\dagger}$, representing the internal space of fermions, into the Clifford odd "basis vectors" $\hat{b}_{f'}^{m\dagger}$ with the same family member m belonging to another family f' .

16.2.4 "Basis vectors" describing internal space of fermions and bosons in any even dimensional space

In Subsect. 16.2.3 the properties of the "basis vectors", describing internal space of fermions and bosons in a toy model with $d = (5 + 1)$ are presented in order to simplify (to make more illustrative) the discussions on the properties of the Clifford odd "basis vectors" describing the internal space of fermions and the Clifford even "basis vectors" describing the internal space of corresponding bosons, the gauge fields of fermions.

The generalization to any even d is straightforward. For the description of the internal space of fermions I follow here Ref. [1].

a. The "basis vectors" offering the description of the internal space of fermions, $\hat{b}_f^{m\dagger}$, must contain an odd product of nilpotents $\binom{ab}{k}$, $2n' + 1$, in $d = 2(2n + 1)$, $n' = (0, 1, 2, \dots, \frac{1}{2}(\frac{d}{2} - 1))$, and the rest is the product of n'' projectors $\binom{ab}{[k]}$, $n'' = \frac{d}{2} - (2n' + 1)$. Nilpotents and projectors are chosen to be "eigenvectors" of the $\frac{d}{2}$ members of the Cartan subalgebra.

After the reduction of the two kinds of the Clifford algebras to only one, γ^{α} 's, the generators S^{ab} of the Lorentz transformations in the internal space of fermions described by γ^{α} 's, determine the $2^{\frac{d}{2}-1}$ family members for each of $2^{\frac{d}{2}-1}$ families, while \tilde{S}^{ab} 's determine the $\frac{d}{2}$ numbers (the eigenvalues of the Cartan subalgebra members of the $2^{\frac{d}{2}-1}$ families).

The Clifford odd "basis vectors" $\hat{b}_f^{m\dagger}$ obey the postulates of Dirac for the second quantized fermion fields

$$\begin{aligned} \{\hat{b}_f^m, \hat{b}_{f'}^{m'\dagger}\}_{*_{\mathcal{A}}} |\psi_{oc}\rangle &= \delta^{mm'} \delta_{ff'} |\psi_{oc}\rangle, \\ \{\hat{b}_f^m, \hat{b}_{f'}^{m'}\}_{*_{\mathcal{A}}} |\psi_{oc}\rangle &= 0 \cdot |\psi_{oc}\rangle, \\ \{\hat{b}_f^{m\dagger}, \hat{b}_{f'}^{m'\dagger}\}_{*_{\mathcal{A}}} |\psi_{oc}\rangle &= 0 \cdot |\psi_{oc}\rangle, \\ \hat{b}_f^{m\dagger} *_{\mathcal{A}} |\psi_{oc}\rangle &= |\psi_f^m\rangle, \\ \hat{b}_f^m *_{\mathcal{A}} |\psi_{oc}\rangle &= 0 \cdot |\psi_{oc}\rangle, \end{aligned} \tag{16.23}$$

with (m, m') denoting the "family" members and (f, f') denoting "families", $*_{\mathcal{A}}$ represents the algebraic multiplication of $\hat{b}_f^{m\dagger}$ with their Hermitian conjugated objects \hat{b}_f^m , with the vacuum state $|\psi_{oc}\rangle$, Eq. (17.10), and $\hat{b}_f^{m\dagger}$ or $\hat{b}_{f'}^{m'}$ among themselves. It is not difficult to prove the above relations if taking into account Eq. (17.5).

The Clifford odd "basis vectors" $\hat{b}_f^{m\dagger}$'s and their Hermitian conjugated partners \hat{b}_f^m 's appear in two independent groups, each with $2^{\frac{d}{2}-1} \times 2^{\frac{d}{2}-1}$ members, Hermitian conjugated to each other.

It is our choice which one of these two groups with $2^{\frac{d}{2}-1} \times 2^{\frac{d}{2}-1}$ members to take as "basis vectors" $\hat{b}_f^{m\dagger}$'s. Making the opposite choice the "basis vectors" change handedness.

b. The "basis vectors" for bosons, $\hat{A}_f^{m\dagger}$, must contain an even number of nilpotents $\overset{ab}{(k)}$, $2n'$. In $d = 2(2n + 1)$, $n' = (0, 1, 2, \dots, \frac{1}{2}(\frac{d}{2} - 1))$, the rest, n'' , are projectors $\overset{ab}{[k]}$, $n'' = (\frac{d}{2} - (2n'))$.

The "basis vectors" are either self adjoint or have the Hermitian conjugated partners within the same group of $2^{\frac{d}{2}-1} \times 2^{\frac{d}{2}-1}$ members.

They do not form families, m and f only note a particular "basis vector". One of the members of particular f is self adjoint and participates to the vacuum state which has $2^{\frac{d}{2}-1}$ summands, Eq. (16.20).

The Clifford even "basis vectors" $\hat{A}_f^{m\dagger}$ commute, $\{\hat{A}_f^{m\dagger}, \hat{A}_f^{m'\dagger}\}_- = 0$, if both have the same index f and none of them or both of them are self adjoint operators.

$$\begin{aligned} \{\hat{A}_f^{m\dagger}, \hat{A}_f^{m'\dagger}\}_- &= 0, \quad \text{if } (m, m') \neq m_0 \text{ or } m = m_0 = m', \forall f, \\ \hat{A}_f^{m\dagger} *_{\mathcal{A}} \hat{A}_f^{m_0\dagger} &= \hat{A}_f^{m\dagger}, \quad \forall m, \forall f. \end{aligned} \tag{16.24}$$

The two "basis vectors", $\hat{A}_f^{m\dagger}$ and $\hat{A}_f^{m'\dagger}$, the algebraic product, $*_{\mathcal{A}}$, of which gives nonzero contribution, "scatter" into the third one, or annihilate into the vacuum $|\phi_{\text{oc even}}\rangle$.

Quantum numbers of $\hat{A}_f^{m\dagger}$ are determined by the Cartan subalgebra members of the Lorentz group $\mathcal{S}^{ab} = \mathcal{S}^{ab} + \tilde{\mathcal{S}}^{ab}$.

If a fermion with the "basis vector" $\hat{b}_f^{m\dagger}$ "absorbs" one of the commuting Clifford even objects, $\hat{A}_f^{m'\dagger}$, it transforms into another family member of the same family, to $\hat{b}_f^{m'\dagger}$, changing correspondingly the family member quantum numbers, keeping the family quantum number the same, or remains unchanged.

The remaining group of $2^{\frac{d}{2}-1} \times 2^{\frac{d}{2}-1}$ Clifford even "basis vectors", presented in Table 16.1 do not influence the chosen Clifford odd "basic vectors", but rather their Hermitian conjugated partners \hat{b}_f^m .

There are the even "basis vectors" $\hat{A}_f^{m\dagger}$, the nilpotents and projectors of which are $\overset{ab}{(\tilde{k})}$, $\overset{ab}{[\tilde{k}]}$, respectively. These "basis vectors" $\hat{A}_f^{m\dagger}$, if applying on the Clifford odd "basis vectors" $\hat{b}_f^{m\dagger}$, transform these "basis vectors" into "basis vectors" $\hat{b}_f^{m'\dagger}$ belonging to different family f , while the family member quantum number m remains unchanged.

Exchanging the role of the Clifford odd "basis vector" $\hat{b}_f^{m\dagger}$ and their Hermitian conjugated partners \hat{b}_f^m (what means in the case of $d = (5 + 1)$ the exchange of odd I, which is right handed, with odd II, which is lefthanded, in Table 16.1), not only causes the change of the handedness of the new $\hat{b}_f^{n\dagger}$, but also the change of the role of the Clifford even "basis vectors" (what means in the case of $d = (5 + 1)$ the exchange of even II with even I).

16.3 Second quantized fermion and boson fields with internal space described by Clifford algebra

After the **reduction** of the Clifford space to only the part determined by γ^a 's, the "basis vectors", which are superposition of odd products of γ^a 's, determine the internal space of fermions. The "basis vectors" are orthogonal and appear in even dimensional spaces in $2^{\frac{d}{2}-1}$ families, each with $2^{\frac{d}{2}-1}$ family members. Quantum numbers of family members are determined by S^{ab} , quantum numbers of families are determined by $\tilde{\gamma}^a$'s, or better by \tilde{S}^{ab} 's. $\tilde{\gamma}^a$'s anticommute among themselves and with γ^a 's, as they did before the reduction of the Clifford space, Eq. (17.11). "Basis vectors" $\hat{b}_f^{m\dagger}$, determining internal space of fermions, are in even dimensional spaces products of an odd number of nilpotents and an even number of projectors, chosen to be eigenvectors of the $\frac{d}{2}$ Cartan subalgebra members of the Lorentz algebra S^{ab} , Table 16.2. There are $2^{\frac{d}{2}-1} \times 2^{\frac{d}{2}-1}$ Hermitian conjugated partners of "basis vectors", denoted by $\hat{b}_f^m (= (\hat{b}_f^{m\dagger})^\dagger)$. It is our choice which one of these two groups of $2^{\frac{d}{2}-1} \times 2^{\frac{d}{2}-1}$ members are "basis vectors" and which one are their Hermitian conjugated partners. These two groups differ in handedness as can be seen in Table 16.1, if observing odd I and odd II, as well as if we compare Table 16.2 and Table 16.4.

The Clifford odd anticommuting "basis vectors", describing the internal space of fermions, obey together with their Hermitian conjugated partners the postulates of Dirac for the second quantized fermion fields, Eq. (17.11).

The Clifford even products of γ^a 's (with the even number of nilpotents) form twice $2^{\frac{d}{2}-1} \times 2^{\frac{d}{2}-1}$ "basis vectors", $\hat{A}_f^{m\dagger}$, describing properties of bosons, Table 16.3. Each of the two groups are commuting objects due to the fact that even number of γ^a 's commute.

Also the Clifford even "basis vectors" are chosen to be the eigenvectors of the Cartan subalgebra of the Lorentz group, this time determined by $\mathcal{S}^{ab} = S^{ab} + \tilde{S}^{ab}$, Eqs. (16.19, 16.21). While the Clifford odd "basis vectors" and their Hermitian conjugated partners form two independent groups, the Clifford even "basis vectors" have their Hermitian conjugated partners within each of the two groups.

The choice of the "basis vectors" among the two groups of the Clifford odd products of nilpotents and projectors for the description of the internal space of fermions, distinguishing also in handedness and other properties (Table 16.2 and Table 16.4) made as well the choice for the Clifford even "basis vectors" describing the corresponding boson fields. We notice in Table 16.1 that the choice of odd I for the description of the internal space of fermions makes even II to be the corresponding boson field.

The remaining group of the $2^{\frac{d}{2}-1} \times 2^{\frac{d}{2}-1}$ Clifford even "basis vectors", presented in Table 16.1 as even I are not the boson partners to the chosen Clifford odd odd I "basis vectors", but rather to their Hermitian conjugated partners \hat{b}_f^m , presented as odd II in the same Table 16.1.

The creation operators, either for creating fermions or for creating bosons, must have besides the "basis vectors" defining the internal space of fermions and bosons also the

basis in ordinary space in momentum or coordinate representation. I follow here shortly Ref. [1].

Let us briefly present the relations concerning the momentum or coordinate part of the single particle states. The longer version is presented in Ref. ([1] in Subsect. 3.3 and in App. J)

$$\begin{aligned}
 |\vec{p}\rangle &= \hat{b}_{\vec{p}}^\dagger |0_p\rangle, \quad \langle \vec{p}| = \langle 0_p | \hat{b}_{\vec{p}}, \\
 \langle \vec{p} | \vec{p}' \rangle &= \delta(\vec{p} - \vec{p}') = \langle 0_p | \hat{b}_{\vec{p}} \hat{b}_{\vec{p}'}^\dagger |0_p\rangle, \\
 &\text{leading to} \\
 \hat{b}_{\vec{p}'} \hat{b}_{\vec{p}}^\dagger &= \delta(\vec{p}' - \vec{p}), \tag{16.25}
 \end{aligned}$$

where the normalization $\langle 0_p | 0_p \rangle = 1$ to identity is assumed. While the quantized operators \hat{p} and \hat{x} commute $\{\hat{p}^i, \hat{p}^j\}_- = 0$ and $\{\hat{x}^k, \hat{x}^l\}_- = 0$, this is not the case for $\{\hat{p}^i, \hat{x}^j\}_- = i\eta^{ij}$. It therefore follows

$$\begin{aligned}
 \langle \vec{p} | \vec{x} \rangle &= \langle 0_{\vec{p}} | \hat{b}_{\vec{p}} \hat{b}_{\vec{x}}^\dagger |0_{\vec{x}}\rangle = (\langle 0_{\vec{x}} | \hat{b}_{\vec{x}} \hat{b}_{\vec{p}}^\dagger |0_{\vec{p}}\rangle)^\dagger \\
 \{\hat{b}_{\vec{p}}^\dagger, \hat{b}_{\vec{p}'}^\dagger\}_- &= 0, \quad \{\hat{b}_{\vec{p}}, \hat{b}_{\vec{p}'}\}_- = 0, \quad \{\hat{b}_{\vec{p}}, \hat{b}_{\vec{p}'}^\dagger\}_- = 0, \\
 \{\hat{b}_{\vec{x}}^\dagger, \hat{b}_{\vec{x}'}^\dagger\}_- &= 0, \quad \{\hat{b}_{\vec{x}}, \hat{b}_{\vec{x}'}\}_- = 0, \quad \{\hat{b}_{\vec{x}}, \hat{b}_{\vec{x}'}^\dagger\}_- = 0, \\
 &\text{while} \\
 \{\hat{b}_{\vec{p}}, \hat{b}_{\vec{x}}^\dagger\}_- &= e^{i\vec{p}\cdot\vec{x}} \frac{1}{\sqrt{(2\pi)^{d-1}}}, \quad \{\hat{b}_{\vec{x}}, \hat{b}_{\vec{p}}^\dagger\}_- = e^{-i\vec{p}\cdot\vec{x}} \frac{1}{\sqrt{(2\pi)^{d-1}}}, \tag{16.26}
 \end{aligned}$$

Statement 8. *While the internal space of either fermions or bosons has the finite degrees of freedom — $2^{\frac{d}{2}-1} \times 2^{\frac{d}{2}-1}$ — the momentum basis has obviously continuously infinite degrees of freedom.*

Let us use the common symbol \hat{a}_f^m for both “basis vectors” $\hat{b}_f^{m\dagger}$ and $\hat{A}_f^{m\dagger}$. And let be taken into account that either fermion or boson second quantized states are solving equations of motion, which relate p^0 and \vec{p} : $p^0 = |\vec{p}|$. Then the solution of the equations of motion can be written as the superposition of the tensor products, $*_{\text{T}}$, of a finite number of “basis vectors” describing the internal space of a second quantized single particle state, \hat{a}_f^m , and the continuously infinite momentum basis

$$\{\hat{a}_f^{s\dagger}(\vec{p})\} = \sum_m c^{sm}_f(\vec{p}) \hat{b}_{\vec{p}}^\dagger *_{\text{T}} \hat{a}_f^{m\dagger} |vac_c\rangle *_{\text{T}} |0_{\vec{p}}\rangle, \tag{16.27}$$

where \vec{p} determines the momentum in ordinary space and s determines all the rest of quantum numbers. The state written here as $|vac_o\rangle *_{\text{T}} |0_{\vec{p}}\rangle$ is considered as the vacuum for a starting single particle state from which one obtains the other single particle states by the operators, like $\hat{b}_{\vec{p}}^\dagger$, which pushes the momentum by an amount \vec{p} and the vacuum for either fermions $|\psi_{oc}\rangle$, Eq. (17.10), or bosons $|\phi_{oc\text{even}}\rangle$, Eq. (16.20).

The creation operators for fermions can be therefore written as

$$\{\hat{b}_f^{s\dagger}(\vec{p})\} = \sum_m c^{sm}_f(\vec{p}) \hat{b}_{\vec{p}}^\dagger *_{\text{T}} \hat{b}_f^{m\dagger} |\psi_{oc}\rangle *_{\text{T}} |0_{\vec{p}}\rangle, \tag{16.28}$$

while for the corresponding gauge bosons it follows

$$\{\hat{\mathcal{A}}_f^{s\dagger}(\vec{p}) = \sum_m c^{sm}_f(\vec{p}) \hat{b}_p^\dagger *_{\text{T}} \hat{\mathcal{A}}_f^{m\dagger}\} |\phi_{\text{oc even}} \rangle *_{\text{T}} |0_{\vec{p}} \rangle . \quad (16.29)$$

Since the "basis vectors" $\hat{b}_f^{m\dagger}$, describing the internal space of fermion, and their Hermitian conjugated partners do fulfil the anticommuting properties of Eq. (17.11), then also $\hat{b}_f^{s\dagger}(\vec{p})$ and $(\hat{b}_f^{s\dagger}(\vec{p}))^\dagger$, Eq. (17.12), fulfil the anticommutation relations of Eq. (17.11) due the commutativity of operators $\hat{b}_p^\dagger = (\hat{b}_{-\vec{p}}^\dagger)^\dagger = \hat{b}_{-\vec{p}}$ and anticommutativity of "basis vectors".

The "basis vectors" for fermions bring to the second quantized fermions, that is to the creation and correspondingly to the annihilation operators operating on the vacuum state, the *anticommutativity* and $2^{\frac{d}{2}-1} \times 2^{\frac{d}{2}-1}$ quantum numbers of family members and of families for each of continuously ∞ many \vec{p} . The fermion single particle states therefore already anticommute.

The $2^{\frac{d}{2}-1} \times 2^{\frac{d}{2}-1}$ Clifford even "basis vectors" $\hat{\mathcal{A}}_f^{m\dagger}$, appearing in pairs which are Hermitian conjugated to each other, fulfil the commuting properties of Eq. (16.21), transferring these commuting properties also to $2^{\frac{d}{2}-1} \times 2^{\frac{d}{2}-1}$ members of $\hat{\mathcal{A}}_f^{s\dagger}(\vec{p})$, Eq. (17.12), for any of continuously ∞ \vec{p} , so that $\hat{\mathcal{A}}_f^{s\dagger}(\vec{p})$ fulfil the commutation relations of Eq. (16.21) according to commutativity properties of operators $\hat{\mathcal{A}}_p^{m\dagger}$.

Statement 9. *The odd products of the Clifford objects γ^α 's offer the "basis vectors" to describe the internal space of the second quantized fermion fields. The even products of the Clifford objects γ^α 's offer the "basis vectors" to describe the internal space of the second quantized boson fields. They are the gauge fields of the fermion fields described by the odd Clifford objects.*

Statement 9.a *The description of the internal space of fermions with the odd Clifford algebra explains the second quantization postulates of Dirac. The quantized single fermion states anticommute.*

The $\hat{\mathcal{A}}_f^{s\dagger}(\vec{p})$ "basis vectors" bring to the second quantized bosons, that is to the creation operators and annihilation operators, appearing in pairs or as self adjoint operators, operating on the vacuum state, the *commutativity* properties and $2^{\frac{d}{2}-1} \times 2^{\frac{d}{2}-1}$ quantum numbers, explaining properties of boson particles. The ordinary basis, \hat{b}_p^\dagger , brings to the creation operators the continuously infinite degrees of freedom.

Statement 9.b *The description of the internal space of bosons with the even Clifford algebra explains the second quantization postulates for gauge fields. The quantized single boson states commute.*

Let us represent here the anticommutation relations for the creation and annihilation operators of the second quantized fermion fields $\hat{b}_f^{s\dagger}(\vec{p})$ and $\hat{b}_f^s(\vec{p})$ by taking

into account Eq. (17.11)

$$\begin{aligned}
\{\hat{\mathbf{b}}_f^{s'}(\vec{p}'), \hat{\mathbf{b}}_f^{s\dagger}(\vec{p})\}_+ |\psi_{oc} \rangle |0_{\vec{p}} \rangle &= \delta^{ss'} \delta_{ff'} \delta(\vec{p}' - \vec{p}) |\psi_{oc} \rangle |0_{\vec{p}} \rangle, \\
\{\hat{\mathbf{b}}_f^{s'}(\vec{p}'), \hat{\mathbf{b}}_f^s(\vec{p})\}_+ |\psi_{oc} \rangle |0_{\vec{p}} \rangle &= 0 |\psi_{oc} \rangle |0_{\vec{p}} \rangle, \\
\{\hat{\mathbf{b}}_f^{s'\dagger}(\vec{p}'), \hat{\mathbf{b}}_f^{s\dagger}(\vec{p})\}_+ |\psi_{oc} \rangle |0_{\vec{p}} \rangle &= 0 |\psi_{oc} \rangle |0_{\vec{p}} \rangle, \\
\hat{\mathbf{b}}_f^{s\dagger}(\vec{p}) |\psi_{oc} \rangle |0_{\vec{p}} \rangle &= |\psi_f^s(\vec{p}) \rangle \\
\hat{\mathbf{b}}_f^s(\vec{p}) |\psi_{oc} \rangle |0_{\vec{p}} \rangle &= 0 |\psi_{oc} \rangle |0_{\vec{p}} \rangle \\
|\mathbf{p}^0| &= |\vec{p}|.
\end{aligned} \tag{16.30}$$

The creation operators $\hat{\mathbf{b}}_f^{s\dagger}(\vec{p}, p^0)$ and their Hermitian conjugated partners annihilation operators $\hat{\mathbf{b}}_f^s(\vec{p}, p^0)$, creating and annihilating the single fermion state, respectively, fulfil when applying on the vacuum state, $|\psi_{oc} \rangle |0_{\vec{p}} \rangle$, the anti-commutation relations for the second quantized fermions, postulated by Dirac (Ref. [1], Subsect. 3.3.1, Sect. 5).

The anticommutation relations of Eq. (17.14) are valid also if we replace the vacuum state, $|\psi_{oc} \rangle |0_{\vec{p}} \rangle$, by the Hilbert space of Clifford fermions generated by the tensor product multiplication, $*_{\text{T}_H}$, of any number of the Clifford odd fermion states of all possible internal quantum numbers and all possible momenta (that is of any number of $\hat{\mathbf{b}}_f^{s\dagger}(\vec{p})$ of any (s, f, \vec{p})), Ref. ([1], Sect. 5).

The commutation relations among boson creation operators $\hat{\mathcal{A}}_f^{s\dagger}(\vec{p})$ can be written as

$$\{\hat{\mathcal{A}}_f^{s\dagger}(\vec{p}), \hat{\mathcal{A}}_f^{s'\dagger}(\vec{p}')\}_- = f^{ss's''ff'f''} \hat{\mathcal{A}}_f^{s''\dagger} \delta(\vec{p} - \vec{p}'). \tag{16.31}$$

Let us present an example with $\vec{p} = (0, 0, p^3, 0, 0)$ and the choice $\hat{\mathcal{A}}_1^{3\dagger}(\vec{p})$ and $\hat{\mathcal{A}}_2^{2\dagger}(\vec{p}')$, taken from Table 16.3, one finds

$$\{\hat{\mathcal{A}}_1^{3\dagger}(\vec{p}), \hat{\mathcal{A}}_2^{1\dagger}(\vec{p}')\}_- = -\delta(\vec{p} - \vec{p}') \hat{\mathcal{A}}_1^{2\dagger}(\vec{p}). \tag{16.32}$$

One can notice that the sums over each of the quantum numbers ($S^{03}, S^{12}, S^{56}, \mathcal{N}_L^3, \mathcal{N}_R^3, \tau^3, \tau^8$, of the left hand side are equal to the corresponding quantum numbers on the right hand side.

The study of properties of the second quantized bosons with the internal space of which is described by the Clifford even algebra has just started and needs further consideration.

Let us point out that when breaking symmetries, like in the case of $d = (5 + 1)$ into $SU(2) \times SU(2) \times U(1)$, one easily sees that the same, either the right or the left representations appear within the same, only the right, Table 16.2, or only the left, Table 16.4, representation, manifesting the right (left) hand fermions and the left (right) handed antifermions [24]. The same observation demonstrates also Table 16.5, in which in each octet of u-quarks and d-quarks of any colour and in the octet of colourless leptons the left and the right members of fermions and antifermions appear.

16.3.1 Simple action for fermion and boson fields

Let the space be $d = 2(2n + 1)$ -dimensional. The *spin-charge-family* theory proposes $d = (13 + 1)$ -dimensional space, or larger, so that the "basis vectors" describing the internal space of fermions and bosons, offers the properties of the observed quarks and leptons and their antiquarks and antileptons, as well as the corresponding boson fields, as we learn in this contribution.

The action for the second quantized massless fermion and antifermion fields, and the corresponding massless boson fields in $d = 2(2n + 1)$ -dimensional space is therefore

$$\begin{aligned}
 \mathcal{A} &= \int d^d x \, E \, \frac{1}{2} (\bar{\Psi} \gamma^\alpha p_{0a} \Psi) + \text{h.c.} + \\
 &\quad \int d^d x \, E \, (\alpha R + \tilde{\alpha} \tilde{R}), \\
 p_{0a} &= f^\alpha_a p_{0\alpha} + \frac{1}{2E} \{p_\alpha, E f^\alpha_a\}_-, \\
 p_{0\alpha} &= p_\alpha - \frac{1}{2} S^{ab} \omega_{ab\alpha} - \frac{1}{2} \tilde{S}^{ab} \tilde{\omega}_{ab\alpha}, \\
 R &= \frac{1}{2} \{f^{\alpha[a} f^{\beta b]}\} (\omega_{ab\alpha, \beta} - \omega_{c\alpha\alpha} \omega^c_{b\beta}) + \text{h.c.}, \\
 \tilde{R} &= \frac{1}{2} \{f^{\alpha[a} f^{\beta b]}\} (\tilde{\omega}_{ab\alpha, \beta} - \tilde{\omega}_{c\alpha\alpha} \tilde{\omega}^c_{b\beta}) + \text{h.c.} \quad (16.33)
 \end{aligned}$$

Here ${}^3 f^{\alpha[a} f^{\beta b]} = f^{\alpha a} f^{\beta b} - f^{\alpha b} f^{\beta a}$.

It is proven in Refs. [26, 38] that the spin connection gauge fields manifest in $d = (3 + 1)$ as the ordinary gravity, the known vector gauge fields and the scalar gauge fields, offering the (simple) explanation for the origin of higgs assumed by the *standard model*, explaining as well the Yukawa couplings.

16.4 Conclusions

In the *spin-charge-family* theory the Clifford algebra is used to describe the internal space of fermion fields, what brings new insights, new recognitions about properties of fermion and boson fields ([1] and references therein):

The use of the odd Clifford algebra elements γ^a 's to describe the internal space of fermions offers not only the explanation for all the assumptions of the *standard model*, with the appearance of the families of quarks and leptons and antiquarks and antileptons included, but also for the appearance of the dark matter in the universe, for the explanation of the second quantized postulates for fermions of

³ f^α_a are inverted vielbeins to e^a_α with the properties $e^a_\alpha f^\alpha_b = \delta^a_b$, $e^a_\alpha f^\beta_a = \delta^\beta_\alpha$, $E = \det(e^a_\alpha)$. Latin indices $a, b, \dots, m, n, \dots, s, t, \dots$ denote a tangent space (a flat index), while Greek indices $\alpha, \beta, \dots, \mu, \nu, \dots, \sigma, \tau, \dots$ denote an Einstein index (a curved index). Letters from the beginning of both the alphabets indicate a general index (a, b, c, \dots and $\alpha, \beta, \gamma, \dots$), from the middle of both the alphabets the observed dimensions $0, 1, 2, 3$ (m, n, \dots and μ, ν, \dots), indexes from the bottom of the alphabets indicate the compactified dimensions (s, t, \dots and σ, τ, \dots). We assume the signature $\eta^{ab} = \text{diag}\{1, -1, -1, \dots, -1\}$.

Dirac, for the matter/antimatter asymmetry in the universe, and for several other observed phenomena, making several predictions.

This article is the first trial to describe the internal space of bosons while using the even products of Clifford algebra objects $\gamma^{a's}$.

Although this study of the internal space of boson fields with the even Clifford algebra objects needs further considerations, yet the properties demonstrated in this paper are at least very promising.

Let me repeat briefly what I hope that we have learned.

i. There are two kinds of the anticommuting algebras, the Grassmann algebra, offering in d -dimensional space $2 \cdot 2^d$ operators, and the two Clifford algebras, each with 2^d operators. The Grassmann algebra operators are expressible with the operators of the two Clifford algebras and opposite, Eq. (16.4), and opposite. The two Clifford algebras are independent of each other, Eq. (16.5), forming two independent spaces.

ii. Either the Grassmann algebra or the two Clifford algebras can be used to describe the internal space of anticommuting objects, if the odd products of operators are used to describe the internal space of these objects, and of commuting objects, if the even products of operators are used to describe the internal space of these objects.

iii. The "basis vectors" can be found in each of these algebras, which are eigenvectors of the Cartan subalgebras, Eq. (16.6), of the corresponding Lorentz algebras S^{ab} , S^{ab} and \tilde{S}^{ab} , Eq. (17.7).

iv. After the reduction of the two Clifford algebras to only one — $\gamma^{ab's}$ — assuming how does $\tilde{\gamma}^a$ apply on γ^a : $\{\tilde{\gamma}^a B = (-)^B i B \gamma^a\} |\psi_{oc} \rangle$, with $(-)^B = -1$, if B is (a function of) an odd products of $\gamma^{a's}$, otherwise $(-)^B = 1$, there remain twice $2^{\frac{d}{2}-1}$ irreducible representations of S^{ab} , each with the $2^{\frac{d}{2}-1}$ members. $\tilde{\gamma}^{a's}$ operate on superposition of products of $\gamma^{a's}$.

v. The "basis vectors", which are superposition of odd products of $\gamma^{a's}$, can be arranged to fulfil the anticommutation relations, postulated by Dirac, explaining correspondingly the anticommutation postulates of Dirac, Eqs. (16.9, 16.11).

v.a. The Clifford odd $2^{\frac{d}{2}-1}$ members of each of the $2^{\frac{d}{2}-1}$ irreducible representations of "basis vectors" have their Hermitian conjugated partners in another set of $2^{\frac{d}{2}-1} \cdot 2^{\frac{d}{2}-1}$ "basis vectors", Tables (16.1, 16.2). The two sets of "basis vectors" differ in handedness, Tables (16.2, 16.4).

v.b. It is our choice which set we use to describe the creation operators and which one to describe the annihilation operators. Correspondingly we have either left or right handed creation operators.

v.c. The family members of "basis vectors" have the same properties in all the families. The sum of all the eigenvalues of all the commuting operators over the $2^{\frac{d}{2}-1}$ family members is equal to zero for each of $2^{\frac{d}{2}-1}$ families, separately for left and separately for right handed representations. The sum of the family quantum numbers over the four families is zero.

vi. The Clifford even "basis vectors", which are superposition of even products of $\gamma^{a's}$, commute.

vi.a. The Clifford even "basis vectors" have their Hermitian conjugated partners

within the same group of $2^{\frac{d}{2}-1} \times 2^{\frac{d}{2}-1}$ members, Table 16.3, or are self adjoint.

vi.b. Each of the two groups of the Clifford even $2^{\frac{d}{2}-1} \times 2^{\frac{d}{2}-1}$ "basis vectors" applies algebraically on only one of the two Clifford odd "basis vectors", (in Table 16.1 Clifford even II "basis vectors" apply on Clifford odd I "basis vectors"), conserving the quantum numbers of the internal space.

vi.c. The Clifford even "basis vectors", applying algebraically on the Clifford odd "basis vectors", transform the Clifford odd "basis vector" into another member of the same family, Eqs. (16.17, 16.18, 16.19).

vi.d. The Clifford even "basis vectors" have obviously the quantum numbers of the adjoint representations with respect to the fundamental representation of the Clifford odd partners of the Clifford even "basis vectors", Table 16.3.

vi.e. The sum of all the eigenvalues of all the Cartan subalgebra members over the members of Clifford even "basis vectors" is equal to zero, independent of the choice of the subgroups (with the same number of the Cartan subalgebra), Table 16.3.

vi.f. Two Clifford even "basis vectors" ($\hat{A}_f^{m\dagger}$ and $\hat{A}_f^{m'\dagger}$) of the same f and of $(m, m') \neq m_0$ are orthogonal. The two "basis vectors" with non zero algebraic product, $*_A$, "scatter" into the third one, or annihilate into the vacuum,.

vi.g. The superposition of products of even number of $\tilde{\gamma}^\alpha$'s transform the member of the Clifford odd "basis vector" of particular family into the same family member of another family.

vii. The creation and annihilation operators for either the Clifford odd or the Clifford even fields, contain besides the corresponding "basis vectors" also the basis in ordinary, coordinate or momentum, space, Eqs. (17.12, 16.28, 16.29).

vii.a. The tensor products, $*_T$, of the "basis vectors" describing the internal space of fermions or bosons and the basis in ordinary space have the properties of creation and annihilation operators for either fermion or boson fields, defining the states when applying on the corresponding vacuum states, Eqs. (17.10, 16.20).

vii.b. While the internal space of either fermions or bosons has the finite degrees of freedom — $2^{\frac{d}{2}-1} \times 2^{\frac{d}{2}-1}$ — the momentum basis has obviously continuously infinite degrees of freedom. Correspondingly the single particle states have continuously infinite degrees of freedom.

vii.c. There are the "basis vectors" describing the internal spaces of either fermions or bosons, which bring commutativity or anticommutativity to creation and annihilation operators.

vii.d. The single particle states described by applying the Clifford odd creation operators on the vacuum state, anticommute, while the single particle states described by applying the Clifford even creation operators on the vacuum state commute. The same rules are valid also when applying creation operators on the corresponding Hilbert spaces, Ref. (nh2021RPPNP), Sect. 5.

vii.e. Fermion fields described by using the Clifford odd creation operators interact with exchange of the corresponding boson fields described by the Clifford even creation operators, Eq. (16.19). Bosons fields interacts on both ways, with boson fields (if the corresponding two "basis vectors" have non zero algebraic product, $*_A$), as well as with fermions.

vii.f. The application of the creation operators with the Clifford even "basis vec-

tors", in which all the γ^a 's are replaced by $\tilde{\gamma}^a$'s, on the fermion creation operators, transform the fermion creation operator to another one, belonging to different family with the unchanged family members of the "basis vectors", Subsect. (16.2.4, part b.).

Let me conclude this contribution by saying that so far the description of the internal space of the second quantized fermions with the Clifford odd "basis vectors" offers a new insight into the Hilbert space of the second quantized fermions (although there are still open questions waiting to be discussed, like it is the appearance of the Dirac sea in the usual approaches), the equivalent description of the internal space of the second quantized boson fields with the Clifford even "basis vectors" needs, although to my opinion very promising, a lot of further study.

16.5 Eigenstates of Cartan subalgebra of Lorentz algebra

The eigenvectors of S^{ab} and \tilde{S}^{ab} in the space determined by γ^a 's is as follows

$$\begin{aligned} S^{ab} \frac{1}{2} (\gamma^a + \frac{\eta^{aa}}{ik} \gamma^b) &= \frac{k}{2} \frac{1}{2} (\gamma^a + \frac{\eta^{aa}}{ik} \gamma^b), \\ S^{ab} \frac{1}{2} (1 + \frac{i}{k} \gamma^a \gamma^b) &= \frac{k}{2} \frac{1}{2} (1 + \frac{i}{k} \gamma^a \gamma^b), \\ \tilde{S}^{ab} \frac{1}{2} (\tilde{\gamma}^a + \frac{\eta^{aa}}{ik} \tilde{\gamma}^b) &= \frac{k}{2} \frac{1}{2} (\tilde{\gamma}^a + \frac{\eta^{aa}}{ik} \tilde{\gamma}^b), \\ \tilde{S}^{ab} \frac{1}{2} (1 + \frac{i}{k} \tilde{\gamma}^a \tilde{\gamma}^b) &= -\frac{k}{2} \frac{1}{2} (1 + \frac{i}{k} \tilde{\gamma}^a \tilde{\gamma}^b). \end{aligned} \quad (16.34)$$

with $k^2 = \eta^{aa} \eta^{bb}$.

The proof of the first two equations of Eq.(16.34) goes as follows, $a \neq b$ is assumed:

$$\begin{aligned} \frac{i}{2} \gamma^a \gamma^b \frac{1}{2} (\gamma^a + \frac{\eta^{aa}}{ik} \gamma^b) &= \frac{i}{2} \frac{1}{2} (-\eta^{aa} \gamma^b + \frac{\eta^{aa} \eta^{bb}}{ik} \gamma^a) = \frac{k}{2} \frac{1}{2} (\gamma^a - \eta^{aa} \frac{i}{k} \gamma^b), \\ \frac{i}{2} \gamma^a \gamma^b \frac{1}{2} (1 + \frac{i}{k} \gamma^a \gamma^b) &= \frac{i}{2} \frac{1}{2} (\gamma^a \gamma^b - \frac{i}{k} \eta^{aa} \eta^{bb}) = \frac{k}{2} \frac{1}{2} (1 + \frac{i}{k} \gamma^a \gamma^b). \end{aligned}$$

For proving the second two equations it must be recognized that after the reduction of the Clifford space to only the part spent by γ^a 's, that is after requiring $\{\tilde{\gamma}^a B = (-)^B i B \gamma^a\} |\psi_{oc} \rangle$,

with $(-)^B = -1$, if B is (a function of) an odd product of γ^a 's, otherwise $(-)^B = 1$ [35], the relations of Eq. (16.5) remain unchanged.

One can see this as follows (I follow here Ref. [1], Statement 3a. of App.I)

$$\{\tilde{\gamma}^a, \tilde{\gamma}^b\}_+ = 2\eta^{ab} = \tilde{\gamma}^a \tilde{\gamma}^b + \tilde{\gamma}^b \tilde{\gamma}^a = \tilde{\gamma}^a i \gamma^b + \tilde{\gamma}^b i \gamma^a = i \gamma^b (-i) \gamma^a + i \gamma^a (-i) \gamma^b = 2\eta^{ab}.$$

$$\{\tilde{\gamma}^a, \gamma^b\}_+ = 0 = \tilde{\gamma}^a \gamma^b + \gamma^b \tilde{\gamma}^a = \gamma^b (-i) \gamma^a + \gamma^b i \gamma^a = 0.$$

Taking this into account it follows

$$\begin{aligned} \tilde{S}^{ab} \frac{1}{2} (\gamma^a + \frac{\eta^{aa}}{ik} \gamma^b) &= \frac{i}{2} \tilde{\gamma}^a \tilde{\gamma}^b \frac{1}{2} (\gamma^a + \frac{\eta^{aa}}{ik} \gamma^b) = \frac{i}{2} \frac{1}{2} (\gamma^a + \frac{\eta^{aa}}{ik} \gamma^b) \gamma^b \gamma^a = \frac{i}{2} \frac{1}{2} (-\eta^{aa} \gamma^b + \\ &\frac{\eta^{aa} \eta^{bb}}{ik} \gamma^a) = \frac{k}{2} \frac{1}{2} (\gamma^a + \frac{\eta^{aa}}{ik} \gamma^b), \\ \tilde{S}^{ab} \frac{1}{2} (1 + \frac{i}{k} \gamma^a \gamma^b) &= \frac{i}{2} \frac{1}{2} (1 + \frac{i}{k} \gamma^a \gamma^b) \gamma^b \gamma^a = \frac{i}{2} \frac{1}{2} (-\gamma^a \gamma^b + \frac{i}{k} \eta^{aa} \eta^{bb}) = -\frac{k}{2} \frac{1}{2} (1 + \\ &\frac{i}{k} \gamma^a \gamma^b), \end{aligned}$$

where it is taken into account that $k^2 = \eta^{aa} \eta^{bb}$.

16.6 Clifford odd and even "basis vectors" continue

In Table 16.2 the Clifford odd "basis vectors" of the right handedness were chosen for the description of the internal space of fermions in $d = (5 + 1)$ -dimensional space, noted in Table 16.1 as odd I.

If we make a choice of odd II for the Clifford odd "basis vectors" in Table 16.1, and take the odd I as their Hermitian conjugated partners, then these "basis vectors" are left (not right) handed and have properties presented in Table 16.4. We can compare their properties by the properties of the right handed "basis vectors" appearing in Table 16.2. The two groups odd I and odd II are Hermitian conjugated to each other. We clearly see if comparing both tables, Table 16.2 and

Table 16.4: The "basis vectors", this time left handed — $\hat{b}_f^{m=(ch,s)\dagger}$ (each is a product of projectors and an odd number of nilpotents, and is the "eigenstate" of all the Cartan subalgebra members, S^{03}, S^{12}, S^{56} and $\xi^{03}, \xi^{12}, \xi^{56}$, Eq. (16.6) (ch (charge), the eigenvalue of S^{56} , and s (spin), the eigenvalues of S^{03} and S^{12} , explain index m, f determines family quantum numbers, the eigenvalues of $(\xi^{03}, \xi^{12}, \xi^{56})$ — are presented for $d = (5 + 1)$ -dimensional case. Their Hermitian conjugated partners — $\hat{b}_f^{m=(ch,s)}$ — can be found in Table 16.2 as "basis vectors". This table represents also the eigenvalues of the three commuting operators $N_{L,R}^3$ and S^{56} of the subgroups $SU(2) \times SU(2) \times U(1)$ and the eigenvalues of the three commuting operators τ^3, τ^8 and τ^4 of the subgroups $SU(3) \times U(1)$, in these two last cases index m represents the eigenvalues of the corresponding commuting generators. $\Gamma^{(5+1)} = -\gamma^0\gamma^1\gamma^2\gamma^3\gamma^5\gamma^6 = -1$, $\Gamma^{(3+1)} = i\gamma^0\gamma^1\gamma^2\gamma^3$. Operators $\hat{b}_f^{m=(ch,s)\dagger}$ and $\hat{b}_f^{m=(ch,s)}$ fulfil the anticommutation relations of Eqs. (16.9, 16.11).

f	m	=(ch, s)	$\hat{b}_f^{m=(ch,s)\dagger}$	S^{03}	S^{12}	S^{56}	Γ^{3+1}	N_L^3	N_R^3	τ^3	τ^8	τ^4	ξ^{03}	ξ^{12}	ξ^{56}
I	1	$(\frac{1}{2}, \frac{1}{2})$	$\begin{matrix} 03 & 12 & 56 \\ (-i) & (+) & (+) \end{matrix}$	$-\frac{1}{2}$	$\frac{1}{2}$	$\frac{1}{2}$	-1	$\frac{1}{2}$	0	$-\frac{1}{2}$	$-\frac{1}{2\sqrt{3}}$	$-\frac{1}{6}$	$-\frac{1}{2}$	$\frac{1}{2}$	$\frac{1}{2}$
I	2	$(\frac{1}{2}, -\frac{1}{2})$	$\begin{matrix} 03 & 12 & 56 \\ (+i) & (-) & (+) \end{matrix}$	$\frac{1}{2}$	$-\frac{1}{2}$	$\frac{1}{2}$	-1	$-\frac{1}{2}$	0	$\frac{1}{2}$	$-\frac{1}{2\sqrt{3}}$	$-\frac{1}{6}$	$-\frac{1}{2}$	$\frac{1}{2}$	$\frac{1}{2}$
I	3	$(-\frac{1}{2}, \frac{1}{2})$	$\begin{matrix} 03 & 12 & 56 \\ (+i) & (+) & (-) \end{matrix}$	$\frac{1}{2}$	$\frac{1}{2}$	$-\frac{1}{2}$	1	0	$\frac{1}{2}$	0	$\frac{1}{\sqrt{3}}$	$-\frac{1}{6}$	$-\frac{1}{2}$	$\frac{1}{2}$	$\frac{1}{2}$
I	4	$(-\frac{1}{2}, -\frac{1}{2})$	$\begin{matrix} 03 & 12 & 56 \\ (-i) & (-) & (-) \end{matrix}$	$-\frac{1}{2}$	$-\frac{1}{2}$	$-\frac{1}{2}$	1	0	$-\frac{1}{2}$	0	0	$\frac{1}{6}$	$-\frac{1}{2}$	$\frac{1}{2}$	$\frac{1}{2}$
II	1	$(\frac{1}{2}, \frac{1}{2})$	$\begin{matrix} 03 & 12 & 56 \\ (-i) & (+) & (+) \end{matrix}$	$-\frac{1}{2}$	$\frac{1}{2}$	$\frac{1}{2}$	-1	$\frac{1}{2}$	0	$-\frac{1}{2}$	$-\frac{1}{2\sqrt{3}}$	$-\frac{1}{6}$	$\frac{1}{2}$	$-\frac{1}{2}$	$\frac{1}{2}$
II	2	$(\frac{1}{2}, -\frac{1}{2})$	$\begin{matrix} 03 & 12 & 56 \\ (+i) & (-) & (+) \end{matrix}$	$\frac{1}{2}$	$-\frac{1}{2}$	$\frac{1}{2}$	-1	$-\frac{1}{2}$	0	$\frac{1}{2}$	$-\frac{1}{2\sqrt{3}}$	$-\frac{1}{6}$	$\frac{1}{2}$	$-\frac{1}{2}$	$\frac{1}{2}$
II	3	$(-\frac{1}{2}, \frac{1}{2})$	$\begin{matrix} 03 & 12 & 56 \\ (+i) & (+) & (-) \end{matrix}$	$\frac{1}{2}$	$\frac{1}{2}$	$-\frac{1}{2}$	1	0	$\frac{1}{2}$	0	$\frac{1}{\sqrt{3}}$	$-\frac{1}{6}$	$\frac{1}{2}$	$-\frac{1}{2}$	$\frac{1}{2}$
II	4	$(-\frac{1}{2}, -\frac{1}{2})$	$\begin{matrix} 03 & 12 & 56 \\ (-i) & (-) & (-) \end{matrix}$	$-\frac{1}{2}$	$-\frac{1}{2}$	$-\frac{1}{2}$	1	0	$-\frac{1}{2}$	0	0	$\frac{1}{6}$	$\frac{1}{2}$	$-\frac{1}{2}$	$\frac{1}{2}$
III	1	$(\frac{1}{2}, \frac{1}{2})$	$\begin{matrix} 03 & 12 & 56 \\ (-i) & (+) & (+) \end{matrix}$	$-\frac{1}{2}$	$\frac{1}{2}$	$\frac{1}{2}$	-1	$\frac{1}{2}$	0	$-\frac{1}{2}$	$-\frac{1}{2\sqrt{3}}$	$-\frac{1}{6}$	$\frac{1}{2}$	$\frac{1}{2}$	$-\frac{1}{2}$
III	2	$(\frac{1}{2}, -\frac{1}{2})$	$\begin{matrix} 03 & 12 & 56 \\ (+i) & (-) & (+) \end{matrix}$	$\frac{1}{2}$	$-\frac{1}{2}$	$\frac{1}{2}$	-1	$-\frac{1}{2}$	0	$\frac{1}{2}$	$-\frac{1}{2\sqrt{3}}$	$-\frac{1}{6}$	$\frac{1}{2}$	$\frac{1}{2}$	$-\frac{1}{2}$
III	3	$(-\frac{1}{2}, \frac{1}{2})$	$\begin{matrix} 03 & 12 & 56 \\ (+i) & (+) & (-) \end{matrix}$	$\frac{1}{2}$	$\frac{1}{2}$	$-\frac{1}{2}$	1	0	$\frac{1}{2}$	0	$\frac{1}{\sqrt{3}}$	$-\frac{1}{6}$	$\frac{1}{2}$	$-\frac{1}{2}$	$-\frac{1}{2}$
III	4	$(-\frac{1}{2}, -\frac{1}{2})$	$\begin{matrix} 03 & 12 & 56 \\ (-i) & (-) & (-) \end{matrix}$	$-\frac{1}{2}$	$-\frac{1}{2}$	$-\frac{1}{2}$	1	0	$-\frac{1}{2}$	0	0	$\frac{1}{6}$	$\frac{1}{2}$	$-\frac{1}{2}$	$-\frac{1}{2}$
IV	1	$(\frac{1}{2}, \frac{1}{2})$	$\begin{matrix} 03 & 12 & 56 \\ (-i) & (+) & (+) \end{matrix}$	$-\frac{1}{2}$	$\frac{1}{2}$	$\frac{1}{2}$	-1	$\frac{1}{2}$	0	$-\frac{1}{2}$	$-\frac{1}{2\sqrt{3}}$	$-\frac{1}{6}$	$-\frac{1}{2}$	$-\frac{1}{2}$	$-\frac{1}{2}$
IV	2	$(\frac{1}{2}, -\frac{1}{2})$	$\begin{matrix} 03 & 12 & 56 \\ (+i) & (-) & (+) \end{matrix}$	$\frac{1}{2}$	$-\frac{1}{2}$	$\frac{1}{2}$	-1	$-\frac{1}{2}$	0	$\frac{1}{2}$	$-\frac{1}{2\sqrt{3}}$	$-\frac{1}{6}$	$-\frac{1}{2}$	$-\frac{1}{2}$	$-\frac{1}{2}$
IV	3	$(-\frac{1}{2}, \frac{1}{2})$	$\begin{matrix} 03 & 12 & 56 \\ (+i) & (+) & (-) \end{matrix}$	$\frac{1}{2}$	$\frac{1}{2}$	$-\frac{1}{2}$	1	0	$\frac{1}{2}$	0	$\frac{1}{\sqrt{3}}$	$-\frac{1}{6}$	$-\frac{1}{2}$	$-\frac{1}{2}$	$-\frac{1}{2}$
IV	4	$(-\frac{1}{2}, -\frac{1}{2})$	$\begin{matrix} 03 & 12 & 56 \\ (-i) & (-) & (-) \end{matrix}$	$-\frac{1}{2}$	$-\frac{1}{2}$	$-\frac{1}{2}$	1	0	$-\frac{1}{2}$	0	0	$\frac{1}{6}$	$-\frac{1}{2}$	$-\frac{1}{2}$	$-\frac{1}{2}$

Table 16.4, that they do differ in properties. In particular the difference among these two kinds of "basis vectors" is easily seen in the $SU(3) \times U(1)$ subgroup, that is in (τ^3, τ^8, τ^4) values.

In Table 16.5 one finds the left and the right handed content of one of the families, the fourth ones, presented in Ref. [1], Table 5, if $d = (5 + 1)$ is taken as the subspace of the space $d = (13 + 1)$.

16.7 Some useful relations in Grassmann and Clifford space, needed also in App. 16.8

The generator of the Lorentz transformation in Grassmann space is defined as follows [20]

$$\begin{aligned} \mathbf{S}^{ab} &= (\theta^a p^{\theta b} - \theta^b p^{\theta a}) \\ &= S^{ab} + \tilde{S}^{ab}, \quad \{S^{ab}, \tilde{S}^{cd}\}_- = 0, \end{aligned} \quad (16.35)$$

where S^{ab} and \tilde{S}^{ab} are the corresponding two generators of the Lorentz transformations in the Clifford space, forming orthogonal representations with respect to each other.

We make a choice of the Cartan subalgebra of the Lorentz algebra as follows

$$\begin{aligned} &\mathbf{S}^{03}, \mathbf{S}^{12}, \mathbf{S}^{56}, \dots, \mathbf{S}^{d-1 d}, \\ &S^{03}, S^{12}, S^{56}, \dots, S^{d-1 d}, \\ &\tilde{S}^{03}, \tilde{S}^{12}, \tilde{S}^{56}, \dots, \tilde{S}^{d-1 d}, \\ &\text{if } d = 2n. \end{aligned} \quad (16.36)$$

We find the infinitesimal generators of the Lorentz transformations in Clifford space

$$\begin{aligned} S^{ab} &= \frac{i}{4}(\gamma^a \gamma^b - \gamma^b \gamma^a), \quad S^{ab\dagger} = \eta^{aa} \eta^{bb} S^{ab}, \\ \tilde{S}^{ab} &= \frac{i}{4}(\tilde{\gamma}^a \tilde{\gamma}^b - \tilde{\gamma}^b \tilde{\gamma}^a), \quad \tilde{S}^{ab\dagger} = \eta^{aa} \eta^{bb} \tilde{S}^{ab}, \end{aligned} \quad (16.37)$$

where γ^a and $\tilde{\gamma}^a$ are defined in Eqs. (16.4, 16.5). The commutation relations for either \mathbf{S}^{ab} or S^{ab} or \tilde{S}^{ab} , $\mathbf{S}^{ab} = S^{ab} + \tilde{S}^{ab}$, are

$$\begin{aligned} &\{S^{ab}, \tilde{S}^{cd}\}_- = 0, \\ &\{S^{ab}, S^{cd}\}_- = i(\eta^{ad} S^{bc} + \eta^{bc} S^{ad} - \eta^{ac} S^{bd} - \eta^{bd} S^{ac}), \\ &\{\tilde{S}^{ab}, \tilde{S}^{cd}\}_- = i(\eta^{ad} \tilde{S}^{bc} + \eta^{bc} \tilde{S}^{ad} - \eta^{ac} \tilde{S}^{bd} - \eta^{bd} \tilde{S}^{ac}). \end{aligned} \quad (16.38)$$

The infinitesimal generators of the two invariant subgroups of the group $SO(3, 1)$ can be expressed as follows

$$\vec{N}_{\pm}(= \vec{N}_{(L,R)}) := \frac{1}{2}(S^{23} \pm iS^{01}, S^{31} \pm iS^{02}, S^{12} \pm iS^{03}). \quad (16.39)$$

The infinitesimal generators of the two invariant subgroups of the group $SO(4)$ are expressible with S^{ab} , $(a, b) = (5, 6, 7, 8)$ as follows

$$\begin{aligned}\bar{\tau}^1 &:= \frac{1}{2}(S^{58} - S^{67}, S^{57} + S^{68}, S^{56} - S^{78}), \\ \bar{\tau}^2 &:= \frac{1}{2}(S^{58} + S^{67}, S^{57} - S^{68}, S^{56} + S^{78}),\end{aligned}\quad (16.40)$$

while the generators of the $SU(3)$ and $U(1)$ subgroups of the group $SO(6)$ can be expressed by S^{ab} , $(a, b) = (9, 10, 11, 12, 13, 14)$

$$\begin{aligned}\bar{\tau}^3 &:= \frac{1}{2}\{S^{9\ 12} - S^{10\ 11}, S^{9\ 11} + S^{10\ 12}, S^{9\ 10} - S^{11\ 12}, \\ &S^{9\ 14} - S^{10\ 13}, S^{9\ 13} + S^{10\ 14}, S^{11\ 14} - S^{12\ 13}, \\ &S^{11\ 13} + S^{12\ 14}, \frac{1}{\sqrt{3}}(S^{9\ 10} + S^{11\ 12} - 2S^{13\ 14})\}, \\ \tau^4 &:= -\frac{1}{3}(S^{9\ 10} + S^{11\ 12} + S^{13\ 14}).\end{aligned}\quad (16.41)$$

The group $SO(6)$ has $\frac{d(d-1)}{2} = 15$ generators and $\frac{d}{2} = 3$ commuting operators. The subgroups $SU(3) \times U(1)$ have the same number of commuting operators, expressed with τ^{33} , τ^{38} and τ^4 , and 9 generators, 8 of $SU(3)$ and one of $U(1)$. The rest of 6 generators, not included in $SU(3) \times U(1)$, can be expressed as $\frac{1}{2}\{S^{9\ 12} + S^{10\ 11}, S^{9\ 11} - S^{10\ 12}, S^{9\ 14} + S^{10\ 13}, S^{9\ 13} - S^{10\ 14}, S^{11\ 14} + S^{12\ 13}, S^{11\ 13} - S^{12\ 14}\}$.

The hyper charge Y can be defined as $Y = \tau^{23} + \tau^4$.

The equivalent expressions for the "family" charges, expressed by \tilde{S}^{ab} , follow if in Eqs. (17.26 - 17.28) S^{ab} are replaced by \tilde{S}^{ab} .

Let us present some useful relations from Ref. [23].

$$\begin{aligned}{}^{ab}{}_{(k)}{}^{ab}{}_{(k)} &= 0, & {}^{ab}{}_{(k)}{}^{ab}{}_{(-k)} &= \eta^{aa} {}^{ab}{}_{[k]}, & {}^{ab}{}_{(-k)}{}^{ab}{}_{(k)} &= \eta^{aa} {}^{ab}{}_{[-k]}, & {}^{ab}{}_{(-k)}{}^{ab}{}_{(-k)} &= 0, \\ {}^{ab}{}_{[k]}{}^{ab}{}_{[k]} &= [k], & {}^{ab}{}_{[k]}{}^{ab}{}_{[-k]} &= 0, & {}^{ab}{}_{[-k]}{}^{ab}{}_{[k]} &= 0, & {}^{ab}{}_{[-k]}{}^{ab}{}_{[-k]} &= [-k], \\ {}^{ab}{}_{(k)}{}^{ab}{}_{[k]} &= 0, & {}^{ab}{}_{[k]}{}^{ab}{}_{(k)} &= (k), & {}^{ab}{}_{(-k)}{}^{ab}{}_{[k]} &= (-k), & {}^{ab}{}_{(-k)}{}^{ab}{}_{[-k]} &= 0, \\ {}^{ab}{}_{(k)}{}^{ab}{}_{[-k]} &= (k), & {}^{ab}{}_{[k]}{}^{ab}{}_{(-k)} &= 0, & {}^{ab}{}_{[-k]}{}^{ab}{}_{(k)} &= 0, & {}^{ab}{}_{[-k]}{}^{ab}{}_{(-k)} &= (-k).\end{aligned}\quad (16.42)$$

16.8 One family representation in $d = (13 + 1)$ -dimensional space with $2^{\frac{d}{2}-1}$ members representing quarks and leptons and antiquarks and antileptons in the *spin-charge-family* theory

In Table Table so13+1. the "basis vectors" of one irreducible representation, one family, of the Clifford odd basis vectors of left handedness, $\Gamma^{(13+1)}$, is presented, including all the quarks and the leptons and the antiquarks and the antileptons of

i	$ \alpha\psi_i\rangle$	$\Gamma(3,1)$	S^{12}	τ^{13}	τ^{23}	τ^{33}	τ^{38}	τ^4	Y	Q
	(Anti)octet, $\Gamma(7,1) = (-1)1, \Gamma(6) = (1) - 1$ of (anti)quarks and (anti)leptons									
42	\bar{d}_L^{-2} $\begin{matrix} 03 & 12 & 56 & 78 & 910 & 1112 & 1314 \\ (+i) & (-) & & (+) & & (-) & & (+) \end{matrix}$	-1	$-\frac{1}{2}$	0	$\frac{1}{2}$	$\frac{1}{2}$	$-\frac{1}{2\sqrt{3}}$	$-\frac{1}{6}$	$\frac{1}{3}$	$\frac{1}{3}$
43	\bar{u}_L^{-2} $\begin{matrix} 03 & 12 & 56 & 78 & 910 & 1112 & 1314 \\ - & [-i] & & (+) & & (-) & & (+) \end{matrix}$	-1	$\frac{1}{2}$	0	$-\frac{1}{2}$	$\frac{1}{2}$	$-\frac{1}{2\sqrt{3}}$	$-\frac{1}{6}$	$-\frac{2}{3}$	$-\frac{2}{3}$
44	\bar{e}_L^{-2} $\begin{matrix} 03 & 12 & 56 & 78 & 910 & 1112 & 1314 \\ - & (+i) & & (-) & & (-) & & (+) \end{matrix}$	-1	$-\frac{1}{2}$	0	$-\frac{1}{2}$	$\frac{1}{2}$	$-\frac{1}{2\sqrt{3}}$	$-\frac{1}{6}$	$-\frac{2}{3}$	$-\frac{2}{3}$
45	\bar{d}_R^{-2} $\begin{matrix} 03 & 12 & 56 & 78 & 910 & 1112 & 1314 \\ (+i) & & (+) & & (+) & & (-) & (+) \end{matrix}$	1	$\frac{1}{2}$	$\frac{1}{2}$	0	$\frac{1}{2}$	$-\frac{1}{2\sqrt{3}}$	$-\frac{1}{6}$	$-\frac{1}{6}$	$\frac{1}{3}$
46	\bar{u}_R^{-2} $\begin{matrix} 03 & 12 & 56 & 78 & 910 & 1112 & 1314 \\ - & [-i] & & (-) & & (+) & & (-) & (+) \end{matrix}$	1	$-\frac{1}{2}$	$\frac{1}{2}$	0	$\frac{1}{2}$	$-\frac{1}{2\sqrt{3}}$	$-\frac{1}{6}$	$-\frac{1}{6}$	$\frac{1}{3}$
47	\bar{e}_R^{-2} $\begin{matrix} 03 & 12 & 56 & 78 & 910 & 1112 & 1314 \\ (+i) & & (+) & & (-) & & (-) & (+) \end{matrix}$	1	$\frac{1}{2}$	$-\frac{1}{2}$	0	$\frac{1}{2}$	$-\frac{1}{2\sqrt{3}}$	$-\frac{1}{6}$	$-\frac{1}{6}$	$-\frac{2}{3}$
48	\bar{u}_R^{-2} $\begin{matrix} 03 & 12 & 56 & 78 & 910 & 1112 & 1314 \\ [-i] & & (-) & & (-) & & (+) & & (-) & (+) \end{matrix}$	1	$-\frac{1}{2}$	$-\frac{1}{2}$	0	$\frac{1}{2}$	$-\frac{1}{2\sqrt{3}}$	$-\frac{1}{6}$	$-\frac{1}{6}$	$-\frac{2}{3}$
49	\bar{d}_L^{-3} $\begin{matrix} 03 & 12 & 56 & 78 & 910 & 1112 & 1314 \\ [-i] & & (+) & & (+) & & (+) & & (-) \end{matrix}$	-1	$\frac{1}{2}$	0	$\frac{1}{2}$	0	$\frac{1}{\sqrt{3}}$	$-\frac{1}{6}$	$\frac{1}{3}$	$\frac{1}{3}$
50	\bar{d}_L^{-3} $\begin{matrix} 03 & 12 & 56 & 78 & 910 & 1112 & 1314 \\ (+i) & & (-) & & (+) & & (+) & & (-) \end{matrix}$	-1	$-\frac{1}{2}$	0	$\frac{1}{2}$	0	$\frac{1}{\sqrt{3}}$	$-\frac{1}{6}$	$\frac{1}{3}$	$\frac{1}{3}$
51	\bar{u}_L^{-3} $\begin{matrix} 03 & 12 & 56 & 78 & 910 & 1112 & 1314 \\ - & [-i] & & (+) & & (-) & & (+) & & (-) \end{matrix}$	-1	$\frac{1}{2}$	0	$-\frac{1}{2}$	0	$\frac{1}{\sqrt{3}}$	$-\frac{1}{6}$	$-\frac{2}{3}$	$-\frac{2}{3}$
52	\bar{u}_L^{-3} $\begin{matrix} 03 & 12 & 56 & 78 & 910 & 1112 & 1314 \\ - & (+i) & & (-) & & (-) & & (+) & & (-) \end{matrix}$	-1	$-\frac{1}{2}$	0	$-\frac{1}{2}$	0	$\frac{1}{\sqrt{3}}$	$-\frac{1}{6}$	$-\frac{2}{3}$	$-\frac{2}{3}$
53	\bar{d}_R^{-3} $\begin{matrix} 03 & 12 & 56 & 78 & 910 & 1112 & 1314 \\ (+i) & & (+) & & (-) & & (+) & & (-) \end{matrix}$	1	$\frac{1}{2}$	$\frac{1}{2}$	0	0	$\frac{1}{\sqrt{3}}$	$-\frac{1}{6}$	$-\frac{1}{6}$	$\frac{1}{3}$
54	\bar{d}_R^{-3} $\begin{matrix} 03 & 12 & 56 & 78 & 910 & 1112 & 1314 \\ - & [-i] & & (-) & & (+) & & (+) & & (-) \end{matrix}$	1	$-\frac{1}{2}$	$\frac{1}{2}$	0	0	$\frac{1}{\sqrt{3}}$	$-\frac{1}{6}$	$-\frac{1}{6}$	$\frac{1}{3}$
55	\bar{u}_R^{-3} $\begin{matrix} 03 & 12 & 56 & 78 & 910 & 1112 & 1314 \\ (+i) & & (+) & & (-) & & (+) & & (-) \end{matrix}$	1	$\frac{1}{2}$	$-\frac{1}{2}$	0	0	$\frac{1}{\sqrt{3}}$	$-\frac{1}{6}$	$-\frac{1}{6}$	$-\frac{2}{3}$
56	\bar{u}_R^{-3} $\begin{matrix} 03 & 12 & 56 & 78 & 910 & 1112 & 1314 \\ [-i] & & (-) & & (-) & & (+) & & (-) \end{matrix}$	1	$-\frac{1}{2}$	$-\frac{1}{2}$	0	0	$\frac{1}{\sqrt{3}}$	$-\frac{1}{6}$	$-\frac{1}{6}$	$-\frac{2}{3}$
57	\bar{e}_L $\begin{matrix} 03 & 12 & 56 & 78 & 910 & 1112 & 1314 \\ [-i] & & (+) & & (+) & & (+) & & (-) & & (-) \end{matrix}$	-1	$\frac{1}{2}$	0	$\frac{1}{2}$	0	0	$\frac{1}{2}$	1	1
58	\bar{e}_L $\begin{matrix} 03 & 12 & 56 & 78 & 910 & 1112 & 1314 \\ (+i) & & (-) & & (+) & & (+) & & (-) & & (-) \end{matrix}$	-1	$-\frac{1}{2}$	0	$\frac{1}{2}$	0	0	$\frac{1}{2}$	1	1
59	$\bar{\nu}_L$ $\begin{matrix} 03 & 12 & 56 & 78 & 910 & 1112 & 1314 \\ - & [-i] & & (+) & & (-) & & (-) & & (-) & & (-) \end{matrix}$	-1	$\frac{1}{2}$	0	$-\frac{1}{2}$	0	0	$\frac{1}{2}$	0	0
60	$\bar{\nu}_L$ $\begin{matrix} 03 & 12 & 56 & 78 & 910 & 1112 & 1314 \\ - & (+i) & & (-) & & (-) & & (-) & & (-) & & (-) \end{matrix}$	-1	$-\frac{1}{2}$	0	$-\frac{1}{2}$	0	0	$\frac{1}{2}$	0	0
61	$\bar{\nu}_R$ $\begin{matrix} 03 & 12 & 56 & 78 & 910 & 1112 & 1314 \\ (+i) & & (+) & & (-) & & (+) & & (-) & & (-) \end{matrix}$	1	$\frac{1}{2}$	$-\frac{1}{2}$	0	0	0	$\frac{1}{2}$	$\frac{1}{2}$	0
62	$\bar{\nu}_R$ $\begin{matrix} 03 & 12 & 56 & 78 & 910 & 1112 & 1314 \\ - & [-i] & & (-) & & (+) & & (-) & & (-) & & (-) \end{matrix}$	1	$-\frac{1}{2}$	$-\frac{1}{2}$	0	0	0	$\frac{1}{2}$	$\frac{1}{2}$	0
63	\bar{e}_R $\begin{matrix} 03 & 12 & 56 & 78 & 910 & 1112 & 1314 \\ (+i) & & (+) & & (+) & & (-) & & (-) & & (-) \end{matrix}$	1	$\frac{1}{2}$	$\frac{1}{2}$	0	0	0	$\frac{1}{2}$	$\frac{1}{2}$	1
64	\bar{e}_R $\begin{matrix} 03 & 12 & 56 & 78 & 910 & 1112 & 1314 \\ [-i] & & (-) & & (+) & & (-) & & (-) & & (-) \end{matrix}$	1	$-\frac{1}{2}$	$\frac{1}{2}$	0	0	0	$\frac{1}{2}$	$\frac{1}{2}$	1

Table 16.5: The left handed $(\Gamma(13,1) = -1 [23])$ multiplet of spinors — the members of the fundamental representation of the $SO(13, 1)$ group, manifesting the subgroup $SO(7, 1)$ of the colour charged quarks and antiquarks and the colourless leptons and antileptons — is presented in the massless basis using the technique presented in Refs. [23,31,34,35]. It contains the left handed $(\Gamma(3,1) = -1)$ weak $(SU(2)_I)$ charged $(\tau^{13} = \pm \frac{1}{2})$, Eq. (17.27), and $SU(2)_{II}$ chargeless $(\tau^{23} = 0)$, Eq. (17.27) quarks and leptons and the right handed $(\Gamma(3,1) = 1)$ weak $(SU(2)_I)$ chargeless and $SU(2)_{II}$ charged $(\tau^{23} = \pm \frac{1}{2})$ quarks and leptons, both with the spin S^{12} up and down $(\pm \frac{1}{2})$, respectively). Quarks distinguish from leptons only in the $SU(3) \times U(1)$ part: Quarks are triplets of three colours $(c^i = (\tau^{33}, \tau^{38}) = [(\frac{1}{2}, \frac{1}{2\sqrt{3}}), (-\frac{1}{2}, \frac{1}{2\sqrt{3}}), (0, -\frac{1}{\sqrt{3}})])$, Eq. (17.28) carrying the “fermion charge” $(\tau^4 = \frac{1}{6})$, Eq. (17.28). The colourless leptons carry the “fermion charge” $(\tau^4 = -\frac{1}{6})$. The same multiplet contains also the left handed weak $(SU(2)_I)$ chargeless and $SU(2)_{II}$ charged antiquarks and antileptons and the right handed weak $(SU(2)_I)$ charged and $SU(2)_{II}$ chargeless antiquarks and antileptons. Antiquarks distinguish from antileptons again only in the $SU(3) \times U(1)$ part: Antiquarks are antitriplets, carrying the “fermion charge” $(\tau^4 = -\frac{1}{6})$. The anticollourless antileptons carry the “fermion charge” $(\tau^4 = \frac{1}{6})$. $Y = (\tau^{23} + \tau^4)$ is the hyper charge, the electromagnetic charge is $Q = (\tau^{13} + Y)$. The vacuum state, on which the nilpotents and projectors operate, is presented in Eq. (17.10). The reader can find this Weyl representation also in Refs. [25], [26], [31] and the references therein.

the *standard model*. The needed definitions of the quantum numbers are presented in App. 16.7.

In Tables 16.1, 16.2, 16.3 a simple toy model for $d = (5 + 1)$ -dimensional space is discussed, and the properties of fermions (appearing in families) and their gauge boson fields (the vielbeins and the two kinds of the spin connection fields) analysed. The manifold $(5 + 1)$ was suggested to break either into $SU(2) \times SU(2) \times U(1)$ or to $SU(3) \times U(1)$ to study properties of the fermion and boson second quantized fields, with second quantization originating in the anticommutativity or commutativity of “basis vectors”.

Here only one family of “basis vectors” is presented to see that while the starting “basis vectors” can be either left or right handed, the subgroups of the starting

group contain left and right handed members, as it is $SU(2) \times SU(2) \times U(1)$ of $SO(5 + 1)$ in the toy model.

The breaks of the symmetries, manifesting in Eqs. (17.26, 17.27, 17.28), are in the *spin-charge-family* theory caused by the condensate and the nonzero vacuum expectation values (constant values) of the scalar fields carrying the space index (7, 8) (Refs. [23, 31] and the references therein), all originating in the vielbeins and the two kinds of the spin connection fields. The space breaks first to $SO(7, 1) \times SU(3) \times U(1)_{II}$ and then further to $SO(3, 1) \times SU(2)_I \times U(1)_I \times SU(3) \times U(1)_{II}$, what explains the connections between the weak and the hyper charges and the handedness of spinors.

16.9 Handedness in Grassmann and Clifford space

The handedness $\Gamma^{(d)}$ is one of the invariants of the group $SO(d)$, with the infinitesimal generators of the Lorentz group S^{ab} , defined as

$$\Gamma^{(d)} = \alpha \varepsilon_{a_1 a_2 \dots a_{d-1} a_d} S^{a_1 a_2} \cdot S^{a_3 a_4} \dots S^{a_{d-1} a_d} , \tag{16.43}$$

with α , which is chosen so that $\Gamma^{(d)} = \pm 1$.

In the Grassmann case S^{ab} is defined in Eq. (16.6), while in the Clifford case Eq. (16.43) simplifies, if we take into account that $S^{ab}|_{a \neq b} = \frac{i}{2} \gamma^a \gamma^b$ and $\tilde{S}^{ab}|_{a \neq b} = \frac{i}{2} \tilde{\gamma}^a \tilde{\gamma}^b$, as follows

$$\Gamma^{(d)} := (i)^{d/2} \prod_a (\sqrt{\eta^{aa}} \gamma^a), \quad \text{if } d = 2n . \tag{16.44}$$

Acknowledgment

The author N.S.M.B. thanks Department of Physics, FMF, University of Ljubljana, Society of Mathematicians, Physicists and Astronomers of Slovenia, for supporting the research on the *spin-charge-family* theory by offering the room and computer facilities and Matjaž Breskvar of Beyond Semiconductor for donations, in particular for the annual workshops entitled "What comes beyond the standard models".

References

1. N. Mankoč Borštnik, "Spin connection as a superpartner of a vielbein", *Phys. Lett.* **B 292** (1992) 25-29.
2. N. Mankoč Borštnik, "Spinor and vector representations in four dimensional Grassmann space", *J. of Math. Phys.* **34** (1993) 3731-3745.
3. N. Mankoč Borštnik, "Unification of spin and charges in Grassmann space?", hep-th 9408002, IJS.TP.94/22, Mod. Phys. Lett.**A** (10) No.7 (1995) 587-595.
4. N. S. Mankoč Borštnik, H. B. Nielsen, "How does Clifford algebra show the way to the second quantized fermions with unified spins, charges and families, and with vector and scalar gauge fields beyond the *standard model*", *Progress in Particle and Nuclear Physics*, <http://doi.org/10.1016/j.pnpnp.2021.103890> .

5. N.S. Mankoč Borštnik, H.B.F. Nielsen, "Understanding the second quantization of fermions in Clifford and in Grassmann space", *New way of second quantization of fermions — Part I and Part II*, in this proceedings [arXiv:2007.03517, arXiv:2007.03516].
6. N.S. Mankoč Borštnik, H.B.F. Nielsen, "Understanding the second quantization of fermions in Clifford and in Grassmann space" *New way of second quantization of fermions — Part I and Part II*, Proceedings to the 22nd Workshop "What comes beyond the standard models", 6 - 14 of July, 2019, Ed. N.S. Mankoč Borštnik, H.B. Nielsen, D. Lukman, DMFA Založništvo, Ljubljana, December 2019, [arXiv:1802.05554v4, arXiv:1902.10628].
7. P.A.M. Dirac *Proc. Roy. Soc. (London)*, **A 117** (1928) 610.
8. H.A. Bethe, R.W. Jackiw, "Intermediate quantum mechanics", New York : W.A. Benjamin, 1968.
9. S. Weinberg, "The quantum theory of fields", Cambridge, Cambridge University Press, 2015.
10. N.S. Mankoč Borštnik, H.B.F. Nielsen, "New way of second quantized theory of fermions with either Clifford or Grassmann coordinates and *spin-charge-family* theory " [arXiv:1802.05554v4, arXiv:1902.10628].
11. D. Lukman, N. S. Mankoč Borštnik, "Properties of fermions with integer spin described with Grassmann algebra", Proceedings to the 21st Workshop "What comes beyond the standard models", 23 of June - 1 of July, 2018, Ed. N.S. Mankoč Borštnik, H.B. Nielsen, D. Lukman, DMFA Založništvo, Ljubljana, December 2018 [arxiv:1805.06318, arXiv:1902.10628].
12. N.S. Mankoč Borštnik, H.B.F. Nielsen, *J. of Math. Phys.* **43**, 5782 (2002) [arXiv:hep-th/0111257].
13. N.S. Mankoč Borštnik, H.B.F. Nielsen, "How to generate families of spinors", *J. of Math. Phys.* **44** 4817 (2003) [arXiv:hep-th/0303224].
14. N.S. Mankoč Borštnik, "Spin-charge-family theory is offering next step in understanding elementary particles and fields and correspondingly universe", Proceedings to the Conference on Cosmology, Gravitational Waves and Particles, IARD conferences, Ljubljana, 6-9 June 2016, The 10th Biennial Conference on Classical and Quantum Relativistic Dynamics of Particles and Fields, *J. Phys.: Conf. Ser.* **845** 012017 [arXiv:1409.4981, arXiv:1607.01618v2].
15. N.S. Mankoč Borštnik, "The attributes of the Spin-Charge-Family theory giving hope that the theory offers the next step beyond the Standard Model", Proceedings to the 12th Bial Conference on Classical and Quantum Relativistic Dynamics of Particles and Fields IARD 2020, Prague, 1 – 4 June 2020 by ZOOM.
16. N.S. Mankoč Borštnik, "Matter-antimatter asymmetry in the *spin-charge-family* theory", *Phys. Rev. D* **91** (2015) 065004 [arXiv:1409.7791].
17. N. S. Mankoč Borštnik, "How far has so far the Spin-Charge-Family theory succeeded to explain the Standard Model assumptions, the matter-antimatter asymmetry, the appearance of the Dark Matter, the second quantized fermion fields..., making several predictions", Proceedings to the 23rd Workshop "What comes beyond the standard models", 4 - 12 of July, 2020 Ed. N.S. Mankoč Borštnik, H.B. Nielsen, D. Lukman, DMFA Založništvo, Ljubljana, December 2020, [arXiv:2012.09640]
18. N.S. Mankoč Borštnik, D. Lukman, "Vector and scalar gauge fields with respect to $d = (3 + 1)$ in Kaluza-Klein theories and in the *spin-charge-family* theory", *Eur. Phys. J. C* **77** (2017) 231.
19. N.S. Mankoč Borštnik, "The *spin-charge-family* theory explains why the scalar Higgs carries the weak charge $\pm \frac{1}{2}$ and the hyper charge $\mp \frac{1}{2}$ ", Proceedings to the 17th Workshop "What comes beyond the standard models", Bled, 20-28 of July, 2014, Ed. N.S. Mankoč Borštnik, H.B. Nielsen, D. Lukman, DMFA Založništvo, Ljubljana December 2014, p.163-82 [arXiv:1502.06786v1] [arXiv:1409.4981].

20. N.S. Mankoč Borštnik N S, "The spin-charge-family theory is explaining the origin of families, of the Higgs and the Yukawa couplings", *J. of Modern Phys.* **4** (2013) 823 [arXiv:1312.1542].
21. N.S. Mankoč Borštnik, H.B.F. Nielsen, "The spin-charge-family theory offers understanding of the triangle anomalies cancellation in the standard model", *Fortschritte der Physik, Progress of Physics* (2017) 1700046.
22. N.S. Mankoč Borštnik, "The explanation for the origin of the Higgs scalar and for the Yukawa couplings by the *spin-charge-family* theory", *J.of Mod. Physics* **6** (2015) 2244-2274, <http://dx.org./10.4236/jmp.2015.615230> [arXiv:1409.4981].
23. N.S. Mankoč Borštnik and H.B. Nielsen, "Why nature made a choice of Clifford and not Grassmann coordinates", Proceedings to the 20th Workshop "What comes beyond the standard models", Bled, 9-17 of July, 2017, Ed. N.S. Mankoč Borštnik, H.B. Nielsen, D. Lukman, DMFA Založništvo, Ljubljana, December 2017, p. 89-120 [arXiv:1802.05554v1v2].
24. N.S. Mankoč Borštnik and H.B.F. Nielsen, "Discrete symmetries in the Kaluza-Klein theories", *JHEP* 04:165, 2014 [arXiv:1212.2362].
25. N. S. Mankoč Borštnik, Second quantized "anticommuting integer spin fields", sent to Manuscript ID: symmetry-1300624 the third time 30.09. 2021, getting Manuscript ID: symmetry-1423760 as the answer, waiting for the response.
26. A. Borštnik, N.S. Mankoč Borštnik, "Left and right handedness of fermions and bosons", *J. of Phys. G: Nucl. Part. Phys.***24**(1998)963-977, hep-th/9707218.



17 The achievements of the *spin-charge-family* theory so far

N.S. Mankoč Borštnik

Department of Physics, University of Ljubljana, SI-1000 Ljubljana, Slovenia

Abstract. Fifty years ago, the *standard model* offered an elegant new step towards understanding elementary fermion and boson fields, making several assumptions, suggested by experiments. The assumptions are still waiting for an explanation. There are many proposals in the literature for the next step. The *spin-charge-family* theory, proposing a simple starting action in $d \geq (13 + 1)$ -dimensional space with fermions interacting with the gravity only (the vielbeins and the two kinds of the spin connection fields), is offering the explanation for not only all by the *standard model* assumed properties of quarks and leptons and antiquarks and antileptons, with the families included, of the vector gauge fields, of the Higgs's scalar and Yukawa couplings, of the appearance of the *dark matter*, of the *matter-antimatter asymmetry*, making several predictions, but explains as well the second quantization postulates for fermions and bosons by using the odd and the even Clifford algebra "basis vectors" to describe the internal space of fermions and bosons, respectively. Consequently the single fermion and single boson states already anticommute and commute, respectively. I present in this talk a very short overview of the achievement of the *spin-charge-family* theory so far, concluding with presenting not yet solved problems, for which the collaborators are very welcome.

Povzetek: Pred petdesetimi leti je *standardni model*, zgrajen na predpostavkah, porojenih iz rezultatov poskusov, ponudil eleganten nov korak k razumevanju osnovnih fermionskih in bozonskih polj. V literaturi je veliko predlogov, ki pojasnjujejo predpostavke in ponujajo nov korak. Teorija *spin-charge-family*, ki predlaga preprosto začetno akcijo v $d \geq (13 + 1)$ -razsežnem prostoru, v kateri si fermioni izmenjujejo samo gravitone (vektorske svežnje in dve vrsti spinskih povezav), ponuja razlago ne le za vse predpostavke *standardnega modela* — za vse lastnosti kvarkov in leptonov ter antikvarkov in antileptonov, ki se pojavljajo v družinah, za umeritvena vektorska polja, za Higgsove skalarje in Yukawe sklopitve — ampak tudi za pojave v vesolju kot so *temna snov*, nesimetrija med *snovjo in antisnovjo*, ponudi vrsto napovedi, ponudi pa tudi pojasnilo za postulate za drugo kvantizacijo za fermione in bozone. Opis notranjega prostora fermionov in bozonov z liho in sodo Cliffordovo algebro poskrbi, da fermionska stanja antikomutirajo, bozonska pa komutirajo. V predavanju ponudim kratek pregled dosedanjih dosežkov *spin-charge-family* teorije, v zaključku pa predstavim odprta vprašanja. Pri iskanju odgovorov nanje vabim k sodelovanju.

17.1 Introduction

The review article [1] presents a short overview of most of the achievements of the *spin-charge-family* theory so far. I shall make use of this article when presenting my talk.

Fifty years ago the *standard model* offered an elegant new step towards understanding elementary fermion and boson fields by postulating:

a. The existence of massless fermion family members with the spins and charges in the fundamental representation of the groups, **a.i.** the quarks as colour triplets and colourless leptons, **a.ii.** the left handed members as the weak doublets, the right handed weak chargeless members, **a.iii.** the left handed quarks differing from the left handed leptons in the hyper charge, **a.iv.** all the right handed members differing among themselves in hyper charges, **a.v.** antifermions carrying the corresponding anticharges of fermions and opposite handedness, **a.vi.** the families of massless fermions, suggested by experiments and required by the gauge invariance of the boson fields (there is no right handed neutrino postulated, since it would carry none of the so far observed charges, and correspondingly there is also no left handed antineutrino allowed in the *standard model*).

b. The existence of massless vector gauge fields to the observed charges of quarks and leptons, carrying charges in the adjoint representations of the corresponding charged groups and manifesting the gauge invariance.

c. The existence of the massive weak doublet scalar higgs, **c.i.** carrying the weak charge $\pm \frac{1}{2}$ and the hyper charge $\mp \frac{1}{2}$ (as it would be in the fundamental representation of the two groups), **c.ii.** gaining at some step of the expanding universe the nonzero vacuum expectation value, **c.iii.** breaking the weak and the hyper charge and correspondingly breaking the mass protection, **c.iv.** taking care of the properties of fermions and of the weak bosons masses, **c.v.** as well as the existence of the Yukawa couplings.

d. The presentation of fermions and bosons as second quantized fields.

e. The gravitational field in $d = (3 + 1)$ as independent gauge field. (The *standard model* is defined without gravity in order that it be renormalizable, but yet the standard model particles are "allowed" to couple to gravity in the "minimal" way.)

The *standard model* assumptions have been experimentally confirmed without raising any severe doubts so far, except for some few and possibly statistically caused anomalies ¹, but also by offering no explanations for the assumptions. The last among the fields postulated by the *standard model*, the scalar higgs, was detected in June 2012, the gravitational waves were detected in February 2016.

The *standard model* has in the literature several explanations, mostly with many new not explained assumptions. The most popular seem to be the grand unifying theories [2, 4–18, 59]. At least SO(10)-unifying theories offer the explanation for the postulates from **a.i.** to **a.iv.**, partly to **b.** by assuming that to all the "fermion" charges there exist the corresponding vector gauge fields — but does not explain the assumptions **a.v.** up to **a.vi.**, **c.** and **d.**, and does not connect gravity with gauge vector and scalar fields.

In a long series of works with collaborators ([19–23, 25, 26, 28–32, 38] and the references therein), we have found the phenomenological success with the model named the *spin-charge-family* theory, with fermions, the internal space of which is described with the Clifford algebra of all linear superposition of odd products of

¹ I think here on the improved *standard model*, in which neutrinos have non-zero masses, and the model has no ambition to explain severe cosmological problems.

γ^{α} 's in $d = (13 + 1)$, interacting with only gravity ([38] and references therein). The spins of fermions from higher dimensions, $d > (3 + 1)$, manifest in $d = (3 + 1)$ as charges of the *standard model*, gravity in higher dimensions manifest as the *standard model* gauge vector fields as well as the Higgs's scalar and Yukawa couplings [26,31].

Let be added that one irreducible representation of $SO(13, 1)$ contains, if looked from the point of view of $d = (3+1)$, all the quarks and leptons and antiquarks and antileptons and just with the properties, required by the *standard model*, including the relation between quarks and leptons and handedness and antiquarks and antileptons of the opposite handedness, as can be read in Table 5 of App. D, appearing in the contribution of the same author in this Proceedings [33].

All that in the *standard model* had to be assumed (extremely effective "read" from experiments and also from the theoretical investigations) in the *spin-charge-family* theory appear as a possibility from the starting simple action, Eq. (17.15), and from the assumption that the internal space of fermions are described by the odd Clifford algebra objects.

One can read in my second contribution to this Proceedings [33] that the description of the internal space of fermions with the odd Clifford algebra operators γ^{α} 's offers the explanation for the observed quantum numbers of quarks and leptons and antiquarks and antileptons while unifying spin, handedness, charges and families. The "basis vectors" which are superposition of odd products of operators γ^{α} 's, appear in irreducible representations which differ in the quantum numbers determined by $\tilde{\gamma}^{\alpha}$'s.

The simple starting action of the *spin-charge-family* theory offers the explanation for not only the properties of quarks and leptons and antiquarks and antileptons, but also for the vector gauge fields, scalar gauge fields, which represent higgs and explain the Yukawa couplings, and for the scalars, which cause matter/antimatter asymmetry, the proton decay, while the appearance of the dark matter is explained by the appearance of two groups of the decoupled families.

It appears, as it is explained in my second contribution to this Proceedings [33], that the description of the internal space of bosons fields (the gauge fields of the fermion fields described by the Clifford odd "basis vectors") with the Clifford even "basis vectors" explains the commutativity and the properties of the second quantized boson fields, as the description of the internal space of fermion fields with the Clifford odd "basis vectors" explains the anticommutativity and the properties of the second quantized fermion fields.

The description of fermions and bosons with the Clifford odd and Clifford even "basis vectors", respectively, makes fermions appearing in families, while bosons do not. Both kinds of "basis vectors" contribute finite number, $2^{\frac{d}{2}-1} \times 2^{\frac{d}{2}-1}$, degrees of freedom to the corresponding creation operators, while the basis of ordinary space contribute continuously infinite degrees of freedom.

Is the way proposed by the *spin-charge-family* theory the right way to the next step beyond the *standard model*? The theory certainly offers a different view of the properties of fermion and boson fields and a different view of the second quantization of both fields than that offered by group theory and the second quantization by postulates.

It has happened so many times in the history of science that the simpler model has shown up as a more "powerful" one.

My working hypotheses is that the laws of nature are simple and correspondingly elegant and that the many body systems around the phase transitions look to us complicated at least from the point of view of the elementary constituents of fermion and boson fields.

To this working hypotheses belong also the description of the internal space of fermions and bosons with the Clifford algebras and the simple starting action for the (second quantized) massless fermions interacting with the (second quantized)² massless bosons, representing gravity only — the vielbeins and the two kinds of the spin connection fields, the gauge fields of the two kinds of the generators of the Lorentz transformations $S^{ab} (= \frac{i}{2}(\gamma^a\gamma^b - \gamma^b\gamma^a))$ and $\tilde{S}^{ab} (= \frac{i}{2}(\tilde{\gamma}^a\tilde{\gamma}^b - \tilde{\gamma}^b\tilde{\gamma}^a))$. In Sect. 17.2 I shall very shortly overview the Clifford algebra description of the internal space of fermions, following Ref. [1], and bosons (explained in my additional contribution to this Proceedings [33]), after the reduction of the two independent groups of Clifford algebras to only one.

In Sect. 17.3 the definition of the creation and annihilation operators as tensor products of the "basis vectors" defined by the Clifford algebra objects and basis in ordinary space is presented.

In Sect. 17.4 the simple starting action of the *spin-charge-family* theory is presented and the achievements of the theory so far discussed.

In Sect. 17.5 the open problems of the *spin-charge-family* theory are presented, and the invitation to the reader to participate.

17.2 Clifford algebra and internal space of fermions and bosons

I follow here Ref. [1], Sect. 3 and also my second contribution to this Proceedings [33], Sect. 2.

Single fermion states are functions of external coordinates and of internal space of fermions. If M^{ab} denote infinitesimal generators of the Lorentz algebra in both spaces, $M^{ab} = L^{ab} + S^{ab}$, with $L^{ab} = x^a p^b - x^b p^a$, $p^a = i\frac{\partial}{\partial x_a}$, determining operators in ordinary space, while S^{ab} are equivalent operators in internal space of fermions, it follows

$$\begin{aligned} \{M^{ab}, M^{cd}\}_- &= i\{M^{ad}\eta^{bc} + M^{bc}\eta^{ad} - M^{ac}\eta^{bd} - M^{bd}\eta^{ac}\}, \\ \{M^{ab}, p^c\}_- &= -i\eta^{ac}p^b + i\eta^{cb}p^a, \\ \{M^{ab}, S^{cd}\}_- &= i\{S^{ad}\eta^{bc} + S^{ad} - S^{ac}\eta^{bd} - S^{bd}\eta^{ac}\}, \end{aligned} \quad (17.1)$$

while the Cartan subalgebra operators of the Lorentz algebra are chosen as

$$M^{03}, M^{12}, M^{56}, \dots, M^{d-1d}, \quad (17.2)$$

² Since the single fermion states, described by the Clifford odd "basis vectors", anticommute due to the anticommuting properties of the Clifford odd "basis vectors" and the single boson states, described by the Clifford even "basis vectors", correspondingly commute there are only the second quantized fermion and boson fields.

and will be used to define the basis in both spaces as eigenvectors of the Cartan subalgebra members. The metric tensor $\eta^{ab} = \text{diag}(1, -1, -1, \dots, -1, -1)$ for $a = (0, 1, 2, 3, 5, \dots, d)$ is used.

There are two kinds of anticommuting algebras, the Grassmann algebra θ^a 's and p^{θ^a} 's ($= \frac{\partial}{\partial \theta^a}$'s), in d -dimensional space with d anticommuting operators θ^a 's and with d anticommuting derivatives $\frac{\partial}{\partial \theta^a}$'s,

$$\begin{aligned} \{\theta^a, \theta^b\}_+ &= 0, & \left\{ \frac{\partial}{\partial \theta^a}, \frac{\partial}{\partial \theta^b} \right\}_+ &= 0, \\ \left\{ \theta^a, \frac{\partial}{\partial \theta^b} \right\}_+ &= \delta_{ab}, \quad (a, b) = (0, 1, 2, 3, 5, \dots, d), \\ (\theta^a)^\dagger &= \eta^{aa} \frac{\partial}{\partial \theta^a}, & \left(\frac{\partial}{\partial \theta^a} \right)^\dagger &= \eta^{aa} \theta^a, \end{aligned} \quad (17.3)$$

where the last line was our choice [32], and the two anticommuting kinds of the Clifford algebras γ^a 's and $\tilde{\gamma}^a$ 's³ are expressible with the Grassmann algebra operators and opposite

$$\begin{aligned} \gamma^a &= \left(\theta^a + \frac{\partial}{\partial \theta^a} \right), & \tilde{\gamma}^a &= i \left(\theta^a - \frac{\partial}{\partial \theta^a} \right), \\ \theta^a &= \frac{1}{2} (\gamma^a - i\tilde{\gamma}^a), & \frac{\partial}{\partial \theta^a} &= \frac{1}{2} (\gamma^a + i\tilde{\gamma}^a), \end{aligned} \quad (17.4)$$

offering together $2 \cdot 2^d$ operators: 2^d of those which are products of γ^a and 2^d of those which are products of $\tilde{\gamma}^a$, the same number of operators as of the Grassmann algebra operators. The two kinds of the Clifford algebras anticommute, fulfilling the anticommutation relations

$$\begin{aligned} \{\gamma^a, \gamma^b\}_+ &= 2\eta^{ab} = \{\tilde{\gamma}^a, \tilde{\gamma}^b\}_+, \\ \{\gamma^a, \tilde{\gamma}^b\}_+ &= 0, \quad (a, b) = (0, 1, 2, 3, 5, \dots, d), \\ (\gamma^a)^\dagger &= \eta^{aa} \gamma^a, & (\tilde{\gamma}^a)^\dagger &= \eta^{aa} \tilde{\gamma}^a, \\ \gamma^a \gamma^a &= \eta^{aa}, & \gamma^a (\gamma^a)^\dagger &= I, & \tilde{\gamma}^a \tilde{\gamma}^a &= \eta^{aa}, & \tilde{\gamma}^a (\tilde{\gamma}^a)^\dagger &= I, \end{aligned} \quad (17.5)$$

where I represents the unit operator. The two kinds of the Clifford algebra objects are obviously independent.

³ The existence of the two kinds of the Clifford algebras is discussed in [19,20,22,34,35].

The corresponding infinitesimal Lorentz generators are then \mathbf{S}^{ab} for the Grassmann algebra, and S^{ab} and \tilde{S}^{ab} for the two kinds of the Clifford algebras.

$$\begin{aligned}
 \mathbf{S}^{ab} &= \frac{i}{4}(\gamma^a \gamma^b - \gamma^b \gamma^a), \\
 \tilde{S}^{ab} &= \frac{i}{4}(\tilde{\gamma}^a \tilde{\gamma}^b - \tilde{\gamma}^b \tilde{\gamma}^a), \\
 \mathbf{S}^{ab} &= i(\theta^a \frac{\partial}{\partial \theta^b} - \theta^b \frac{\partial}{\partial \theta^a}), \\
 \{\mathbf{S}^{ab}, \tilde{S}^{ab}\}_- &= 0, \quad \mathbf{S}^{ab} = S^{ab} + \tilde{S}^{ab}, \\
 \{\mathbf{S}^{ab}, \theta^e\}_- &= -i(\eta^{ae} \theta^b - \eta^{be} \theta^a), \\
 \{\mathbf{S}^{ab}, p^{\theta^e}\}_- &= -i(\eta^{ae} p^{\theta^b} - \eta^{be} p^{\theta^a}), \\
 \{\mathbf{S}^{ab}, \gamma^c\}_- &= i(\eta^{bc} \gamma^a - \eta^{ac} \gamma^b), \\
 \{\tilde{S}^{ab}, \tilde{\gamma}^c\}_- &= i(\eta^{bc} \tilde{\gamma}^a - \eta^{ac} \tilde{\gamma}^b), \\
 \{\mathbf{S}^{ab}, \tilde{\gamma}^c\}_- &= 0, \quad \{\tilde{S}^{ab}, \gamma^c\}_- = 0.
 \end{aligned} \tag{17.6}$$

The reader can find a more detailed information in Ref. [1] in Sect. 3.

It is useful to choose the "basis vectors" in each of the two spaces to be products of eigenstates of the Cartan subalgebra members, Eq. (17.2), of the Lorentz algebras, ($S^{ab} = \frac{i}{4}(\gamma^a \gamma^b - \gamma^b \gamma^a)$, $\tilde{S}^{ab} = \frac{i}{4}(\tilde{\gamma}^a \tilde{\gamma}^b - \tilde{\gamma}^b \tilde{\gamma}^a)$). The "eigenstates" of each of the Cartan subalgebra members, Eqs. (17.4, 17.5), for each of the two kinds of the Clifford algebras separately can be found as follows,

$$\begin{aligned}
 S^{ab} \frac{1}{2}(\gamma^a + \frac{\eta^{aa}}{ik} \gamma^b) &= \frac{k}{2} \frac{1}{2}(\gamma^a + \frac{\eta^{aa}}{ik} \gamma^b), & S^{ab} \frac{1}{2}(1 + \frac{i}{k} \gamma^a \gamma^b) &= \frac{k}{2} \frac{1}{2}(1 + \frac{i}{k} \gamma^a \gamma^b), \\
 \tilde{S}^{ab} \frac{1}{2}(\tilde{\gamma}^a + \frac{\eta^{aa}}{ik} \tilde{\gamma}^b) &= \frac{k}{2} \frac{1}{2}(\tilde{\gamma}^a + \frac{\eta^{aa}}{ik} \tilde{\gamma}^b), & \tilde{S}^{ab} \frac{1}{2}(1 + \frac{i}{k} \tilde{\gamma}^a \tilde{\gamma}^b) &= \frac{k}{2} \frac{1}{2}(1 + \frac{i}{k} \tilde{\gamma}^a \tilde{\gamma}^b).
 \end{aligned} \tag{17.7}$$

$k^2 = \eta^{aa} \eta^{bb}$. The proof of Eq. (17.7) is presented in App. (I) of Ref. [1], Statement 2a. The Clifford "basis vectors" — nilpotents $\frac{1}{2}(\gamma^a + \frac{\eta^{aa}}{ik} \gamma^b)$, $(\frac{1}{2}(\gamma^a + \frac{\eta^{aa}}{ik} \gamma^b))^2 = 0$ and projectors $\frac{1}{2}(1 + \frac{i}{k} \tilde{\gamma}^a \tilde{\gamma}^b)$, $(\frac{1}{2}(1 + \frac{i}{k} \tilde{\gamma}^a \tilde{\gamma}^b))^2 = \frac{1}{2}(1 + \frac{i}{k} \tilde{\gamma}^a \tilde{\gamma}^b)$ — of both algebras are normalized, up to a phase, as described in the contribution of the same author in this Proceedings [33].

Both, nilpotents and projectors, have half integer spins.

It is useful to introduce the notation for the "eigenvectors" of the two Cartan subalgebras as follows, Ref. [34, 35],

$$\begin{aligned}
 \overset{ab}{(k)} &:= \frac{1}{2}(\gamma^a + \frac{\eta^{aa}}{ik} \gamma^b), & \overset{ab}{(k)}^\dagger &= \eta^{aa} \overset{ab}{(-k)}, & (\overset{ab}{(k)})^2 &= 0, & \overset{ab}{(k)} \overset{ab}{(-k)} &= \eta^{aa} \overset{ab}{[k]} \\
 \overset{ab}{[k]} &:= \frac{1}{2}(1 + \frac{i}{k} \gamma^a \gamma^b), & \overset{ab}{[k]}^\dagger &= \overset{ab}{[k]}, & (\overset{ab}{[k]})^2 &= \overset{ab}{[k]}, & \overset{ab}{[k]} \overset{ab}{[-k]} &= 0, \\
 \overset{ab}{(k)} \overset{ab}{[k]} &= 0, & \overset{ab}{[k]} \overset{ab}{(k)} &= \overset{ab}{(k)}, & \overset{ab}{(k)} \overset{ab}{[-k]} &= \overset{ab}{(k)}, & \overset{ab}{[k]} \overset{ab}{[-k]} &= 0.
 \end{aligned} \tag{17.8}$$

The corresponding expressions for nilpotents $\overset{ab}{(k)}$ and projectors $\overset{ab}{[k]}$ follows if we replace in Eq. (17.8) γ^a 's by $\tilde{\gamma}^a$'s, the same relation $k^2 = \eta^{aa} \eta^{bb}$ is valid for both algebras.

Let us notice that the "eigenvectors" of the Cartan subalgebras are equivalent and the eigenvalues are the same in both algebras: Both algebras have projectors and nilpotents: $(([\tilde{k}]^{\text{ab}})^2 = [\tilde{k}], ((k)^2 = 0), (([\tilde{k}]^{\text{ab}})^2 = [\tilde{k}], ((k)^2 = 0)$.

In each of the two independent algebras we have two groups of $2^{\frac{d}{2}-1}$ members which are eigenvectors of all the Cartan subalgebra members, Eq. (17.2), appearing in $2^{\frac{d}{2}-1}$ irreducible representations which have an odd Clifford character — they are products of an odd number of γ^{α} 's ($\tilde{\gamma}^{\alpha}$'s). These two groups are Hermitian conjugated to each other. We make a choice of one of the two groups of the Clifford odd "basis vectors" and name these "basis vectors" $\hat{b}_f^{m\dagger}$, m describing $2^{\frac{d}{2}-1}$ members of one irreducible representation, f describing one of $2^{\frac{d}{2}-1}$ irreducible representations. The $2^{\frac{d}{2}-1} \times 2^{\frac{d}{2}-1}$ members of the second group, Hermitian conjugated to $\hat{b}_f^{m\dagger}$, are named as $\hat{b}_f^m = (\hat{b}_f^{m\dagger})^\dagger$.

There are besides two Clifford odd groups in each of the two algebras γ^{α} 's and $\tilde{\gamma}^{\alpha}$'s, also two Clifford even groups. They are superposition of an even number of γ^{α} 's ($\tilde{\gamma}^{\alpha}$'s). I named these two $2^{\frac{d}{2}-1} \times 2^{\frac{d}{2}-1}$ Clifford even "basis vectors" $\hat{A}_f^{m\dagger}$ and $\hat{B}_f^{m\dagger}$, respectively. $\hat{A}_f^{m\dagger}$ represent gauge vectors of $\hat{b}_f^{m\dagger}$, on which they operate. $\hat{B}_f^{m\dagger}$ operate on \hat{b}_f^m . I discuss their properties in my second contribution of this Proceedings [33].

The "basis vectors" of an odd Clifford character, $\hat{b}_f^{m\dagger}$, and their Hermitian conjugated partners, \hat{b}_f^m , fulfil the postulates for second quantized fermions of Dirac, if we reduce both Clifford algebras to only one [?, 37, 38], while keeping all the relations, presented in Eq. (17.5), valid. Let us make a choice of γ^{α} 's and postulate the application of $\tilde{\gamma}^{\alpha}$'s on B which is a superposition of any products of γ^{α} 's as follows

$$\{\tilde{\gamma}^{\alpha B} = (-)^B i B \gamma^{\alpha}\} |\psi_{oc} \rangle, \tag{17.9}$$

with $(-)^B = -1$, if B is (a function of) an odd products of γ^{α} 's, otherwise $(-)^B = 1$ [35], $|\psi_{oc} \rangle$ is defined in Eq. (17.10). (Sects. (2.1, 2.2 in [33]) and Sects. (3.2.2, 3.2.3 in [1])).

The vacuum state $|\psi_{oc} \rangle$ is defined as follows

$$|\psi_{oc} \rangle = \sum_{f=1}^{2^{\frac{d}{2}-1}} \hat{b}_f^m *_{\mathcal{A}} \hat{b}_f^{m\dagger} |1 \rangle, \tag{17.10}$$

for one of the members m , anyone, of the odd irreducible representation f , with $|1 \rangle$, which is the vacuum without any structure, the identity, $*_{\mathcal{A}}$ means the algebraic product. It follows that $\hat{b}_f^m *_{\mathcal{A}} |\psi_{oc} \rangle = 0$ and $\hat{b}_f^{m\dagger} *_{\mathcal{A}} |\psi_{oc} \rangle = |\psi_{oc}^m \rangle$.

After the postulate of Eq. (17.9) "basis vectors" $\hat{b}_f^{m\dagger}$ which are superposition of an odd products of γ^{α} 's (represented by an odd number of nilpotents, the rest are projectors) obey all the fermions second quantization postulates of Dirac. There are \tilde{S}^{ab} which dress the irreducible representations with the family quantum numbers of the Cartan subalgebra members ($\tilde{S}^{03}, \tilde{S}^{12}, \tilde{S}^{56}, \dots, \tilde{S}^{d-1 d}$), Eq. (17.2).

$$\begin{aligned}
 \{\hat{b}_f^m, \hat{b}_{f'}^{m'\dagger}\}_{*_{\Lambda}} |\psi_{oc} \rangle &= \delta^{mm'} \delta_{ff'} |\psi_{oc} \rangle, \\
 \{\hat{b}_f^m, \hat{b}_{f'}^{m'}\}_{*_{\Lambda}} |\psi_{oc} \rangle &= 0 \cdot |\psi_{oc} \rangle, \\
 \{\hat{b}_f^{m\dagger}, \hat{b}_{f'}^{m'\dagger}\}_{*_{\Lambda}} |\psi_{oc} \rangle &= 0 \cdot |\psi_{oc} \rangle, \\
 \hat{b}_f^{m\dagger} *_{\Lambda} |\psi_{oc} \rangle &= |\psi_f^m \rangle, \\
 \hat{b}_f^m *_{\Lambda} |\psi_{oc} \rangle &= 0 \cdot |\psi_{oc} \rangle,
 \end{aligned} \tag{17.11}$$

with (m, m') denoting the "family" members and (f, f') denoting "families", $*_{\Lambda}$ represents the algebraic multiplication of $\hat{b}_f^{m\dagger}$ and \hat{b}_f^m with the vacuum state $|\psi_{oc} \rangle$ of Eq. (17.10) and among themselves, taking into account Eq. (17.5).

Ref. ([33], Sects. 2.4 and 3) presents the starting study of properties of the second quantized boson fields, the internal space of which is represented by the "basis vectors" $\hat{\mathcal{A}}_f^{m\dagger}$ which appear as the gauge fields of the second quantized fermion fields the internal space of which is described by the "basis vectors" $\hat{b}_f^{m\dagger}$.

We pay attention on even dimensional spaces, $d = 2(2n + 1)$ or $d = 4n$, $n \geq 0$, only.

17.3 Creation and annihilation operators

Here Sect. 3.3 of Ref. [1] is roughly followed.

Describing fermion fields as the creation $\hat{b}_f^{s\dagger}(\vec{p})$ and annihilation $\hat{b}_f^s(\vec{p})$ operators operating on the vacuum state we make tensor products, $*_{\tau}$, of $2^{\frac{d}{2}-1} \times 2^{\frac{d}{2}-1}$ Clifford odd "basis vectors" $\hat{b}_f^{m\dagger}$ and of continuously infinite basis in ordinary space determined by $\hat{b}_{\vec{p}}^{\dagger}$

$$\{\hat{b}_f^{s\dagger}(\vec{p}) = \sum_m c^{ms}_f(\vec{p}) \hat{b}_{\vec{p}}^{\dagger} *_{\tau} \hat{b}_f^{m\dagger}\} |\psi_{oc} \rangle *_{\tau} |0_{\vec{p}} \rangle, \tag{17.12}$$

where \vec{p} determines the momentum in ordinary space with $p^0 = |\vec{p}|$ and s determines all the rest of quantum numbers. The state $|\psi_{oc} \rangle *_{\tau} |0_{\vec{p}} \rangle$ is considered as the vacuum for a starting single particle state from which one obtains the other single particle state by the operators, $\hat{b}_{\vec{p}}$, which pushes the momentum by an amount \vec{p} , in a tensor product with $\hat{b}_f^{m\dagger}$. We have

$$\begin{aligned}
 |\vec{p} \rangle &= \hat{b}_{\vec{p}}^{\dagger} |0_p \rangle, \quad \langle \vec{p} | = \langle 0_p | \hat{b}_{\vec{p}}, \\
 \langle \vec{p} | \vec{p}' \rangle &= \delta(\vec{p} - \vec{p}') = \langle 0_p | \hat{b}_{\vec{p}} \hat{b}_{\vec{p}'}^{\dagger} |0_p \rangle, \\
 &\text{leading to} \\
 \hat{b}_{\vec{p}}, \hat{b}_{\vec{p}'}^{\dagger} &= \delta(\vec{p}' - \vec{p}),
 \end{aligned} \tag{17.13}$$

since we normalize $\langle 0_p | 0_p \rangle = 1$ to identity.

The "basis vectors" $\hat{b}_f^{m\dagger}$ which are products of an odd number of nilpotent, the rest to $\frac{d}{2}$ are then projectors, anticommute, transferring the anticommutativity to the creation operators $\hat{b}_f^{s\dagger}(\vec{p})$ and correspondingly also to their Hermitian conjugated partners annihilation operators $\hat{b}_f^s(\vec{p})$, Eq. (17.12). The creation and

annihilation operators then fulfil the anticommutation relations of the second quantized fermions explaining the postulates of Dirac

$$\begin{aligned}
 \{\hat{\mathbf{b}}_f^{s'}(\vec{p}'), \hat{\mathbf{b}}_f^{s\dagger}(\vec{p})\}_+ |\Psi_{oc} > |0_{\vec{p}} > &= \delta^{ss'} \delta_{ff'} \delta(\vec{p}' - \vec{p}) |\Psi_{oc} > |0_{\vec{p}} >, \\
 \{\hat{\mathbf{b}}_f^{s'}(\vec{p}'), \hat{\mathbf{b}}_f^s(\vec{p})\}_+ |\Psi_{oc} > |0_{\vec{p}} > &= 0 |\Psi_{oc} > |0_{\vec{p}} >, \\
 \{\hat{\mathbf{b}}_f^{s'\dagger}(\vec{p}'), \hat{\mathbf{b}}_f^{s\dagger}(\vec{p})\}_+ |\Psi_{oc} > |0_{\vec{p}} > &= 0 |\Psi_{oc} > |0_{\vec{p}} >, \\
 \hat{\mathbf{b}}_f^{s\dagger}(\vec{p}) |\Psi_{oc} > |0_{\vec{p}} > &= |\Psi_f^s(\vec{p}) > \\
 \hat{\mathbf{b}}_f^s(\vec{p}) |\Psi_{oc} > |0_{\vec{p}} > &= 0 |\Psi_{oc} > |0_{\vec{p}} > \\
 |p^0| &= |\vec{p}|.
 \end{aligned}
 \tag{17.14}$$

Statement *The description of the internal space of fermions with the superposition of odd products of γ^α 's, that is with the clifford odd "basis vectors", not only explains the Dirac's postulates of the second quantized fermions but also explains the appearance of families of fermions.*

Ref. [33] is offering the explanation for the second quantized commuting boson fields (described by the "basis vectors" of an even number of nilpotents, the rest are projectors), they are the gauge fields of the anticommuting fermion fields (described by the "basis vectors" of an odd number of nilpotents).

17.4 Achievements so far of spin-charge-family theory

Here Sects. (6, 7.2.2 and 7.3.1) of Ref. [1], which review shortly the achievements so far of the *spin-charge-family* theory, are followed.

The main new achievement of this theory in the last few years is the recognition that the description of the internal space of fermion fields with the Clifford algebra objects in $d > (3 + 1)$ not only offers the explanation for all the assumptions of the *standard model* for fermion and boson fields, with the appearance of families for fermion fields and the properties of the corresponding vector and scalar gauge fields included, but also get to know, that the anticommuting property of the internal space of fermions takes care of the second quantization properties of fermions, so that the second quantized postulates are not needed. The second quantized properties of fermions origin in their internal space and are transferred to creation and annihilation operators. This year contribution to Proceedings Ref. [33] offers the recognition that also commuting properties of the second quantized boson fields origin in the internal space of bosons.

Describing the internal space of bosons by the Clifford even "basis vectors", written in terms of the Clifford even number of γ^α 's, these Clifford even "basis vectors", $\hat{\mathcal{A}}_f^{m\dagger}$, applying on fermion states transform the "basis vectors" $\hat{\mathbf{b}}_f^{m\dagger}$ either into another "basis vectors" $\hat{\mathbf{b}}_f^{m'\dagger}$ with the same family quantum number f , or if written in terms of the Clifford even number of $\tilde{\gamma}^\alpha$'s, $\hat{\mathcal{A}}_f^{m\dagger}$, transform $\hat{\mathbf{b}}_f^{m'\dagger}$ to $\hat{\mathbf{b}}_{f'}^{m\dagger}$, keeping the family member quantum number m unchanged and changing the family quantum number to f' .⁴ This topic, started in Ref. [33], needs further study.

⁴ The first operation happens if the internal space of bosons is described by "basis vectors" which are even products of nilpotents of the kind $\hat{\mathcal{A}}_f^{m\dagger} = (-i)^{03} (-)^{12} (+)^{56} \dots (+)^{d-1} d$, in this

The *spin-charge-family* theory proposes a simple action for interacting second quantized massless fermions and the corresponding gauge fields in $d = (13 + 1)$ -dimensional space as

$$\begin{aligned}
 \mathcal{A} &= \int d^d x \ E \ \frac{1}{2} (\bar{\psi} \gamma^\alpha p_{0\alpha} \psi) + \text{h.c.} + \\
 &\int d^d x \ E (\alpha R + \tilde{\alpha} \tilde{R}), \\
 p_{0\alpha} &= f^\alpha_a p_{0\alpha} + \frac{1}{2E} \{p_\alpha, E f^\alpha_a\}_-, \\
 p_{0\alpha} &= p_\alpha - \frac{1}{2} S^{ab} \omega_{ab\alpha} - \frac{1}{2} \tilde{S}^{ab} \tilde{\omega}_{ab\alpha}, \\
 R &= \frac{1}{2} \{f^{\alpha[a} f^{\beta b]} (\omega_{ab\alpha, \beta} - \omega_{c\alpha\alpha} \omega^c_{b\beta})\} + \text{h.c.}, \\
 \tilde{R} &= \frac{1}{2} \{f^{\alpha[a} f^{\beta b]} (\tilde{\omega}_{ab\alpha, \beta} - \tilde{\omega}_{c\alpha\alpha} \tilde{\omega}^c_{b\beta})\} + \text{h.c.} \quad (17.15)
 \end{aligned}$$

Here $f^{\alpha[a} f^{\beta b]} = f^{\alpha a} f^{\beta b} - f^{\alpha b} f^{\beta a}$.

This simple action in $d = (13 + 1)$ -dimensional space,

- i. in which massless fermions interact with the massless gravitation fields only (with the vielbeins and the two kinds of the spin connection fields, the gauge fields of S^{ab} and \tilde{S}^{ab} , respectively),
- ii. together with the assumption that the internal space of the second quantized fermions are described by the Clifford odd "basis vectors" (what explains after the break of symmetries at low energies the appearance of quarks and leptons and antiquarks and antileptons of the *standard model* and the existence of families, predicting the number of families [46]),
- iii. and the internal space of the second quantized boson fields are described by the Clifford even "basis vectors", offers the explanations for
- iv. not only all the assumptions of the *standard model* — for properties of quarks and leptons and antiquarks and antileptons (explaining the relations among spins, handedness and charges of fermions and antifermions [23,44]) and for the appearance of families of quarks and leptons [34,35,42],
- v. for the second quantized postulates of Dirac [36,37],
- vi. for the appearance of the vector gauge fields to the corresponding fermion fields [26],

particular case two nilpotents form "basis vectors", the second operation happens if all the nilpotents $\overset{ab}{k}$ and projectors $\overset{cd}{[k]}$ are replaced by the corresponding $\overset{ab}{\tilde{k}}$ and $\overset{ab}{[\tilde{k}]}$, respectively.

⁵ f^α_a are inverted vielbeins to e^α_α with the properties $e^\alpha_\alpha f^\alpha_b = \delta^a_b$, $e^\alpha_\alpha f^\beta_a = \delta^\beta_\alpha$, $E = \det(e^\alpha_\alpha)$. Latin indices $a, b, \dots, m, n, \dots, s, t, \dots$ denote a tangent space (a flat index), while Greek indices $\alpha, \beta, \dots, \mu, \nu, \dots, \sigma, \tau, \dots$ denote an Einstein index (a curved index). Letters from the beginning of both the alphabets indicate a general index (a, b, c, \dots and $\alpha, \beta, \gamma, \dots$), from the middle of both the alphabets the observed dimensions 0, 1, 2, 3 (m, n, \dots and μ, ν, \dots), indexes from the bottom of the alphabets indicate the compactified dimensions (s, t, \dots and σ, τ, \dots). We assume the signature $\eta^{ab} = \text{diag}\{1, -1, -1, \dots, -1\}$.

- vii. for the appearance of gauge scalars explaining the interactions among fermions belonging to different families [26, 28, 29, 31, 39–41, 46], and correspondingly of the appearance of the higgs scalar and Yukawa couplings,
 - viii. predicting the number of families — the fourth one to the observed three [46],
 - ix. predicting the second group of four families the stable of which explains the appearance of the *dark matter* [23, 45],
 - x. predicting additional gauge fields,
 - xi. predicting additional scalar fields, which explain the existence of matter-antimatter asymmetry [25],
- and several others.

The manifold $M^{(13+1)}$ breaks at high scale $\propto 10^{16}$ GeV or higher first to $M^{(7+1)} \times M^{(6)}$ due to the appearance of the scalar condensate (so far just assumed, not yet proven that it appears spontaneously) of the two right handed neutrinos with the family quantum numbers of the group of four families, which does not include the observed three families bringing masses (of the scale of break $\propto 10^{16}$ GeV or higher) to all the gauge fields, which interact with the condensate [25].

Since the left handed spinors — fermions — couple differently (with respect to $M^{(7+1)}$) to scalar fields than the right handed ones, the break can leave massless and mass protected $2^{((7+1)/2-1)} (= 8)$ families [49]. The rest of families get heavy masses ⁶.

The manifold $M^{(7+1)} \times SU(3) \times U(1)$ breaks further by the scalar fields, presented in Sect. 17.4.2, to $M^{(3+1)} \times SU(3) \times U(1)$ at the electroweak break. This happens since the scalar fields with the space index (7, 8), Subsubsection. 17.4.2, they are a part of a simple starting action Eq.(17.15), gain the constant values (the nonzero vacuum expectation values independent of the coordinates in $d = (3 + 1)$). These scalar fields carry with respect to the space index the weak charge $\pm \frac{1}{2}$ and the hyper charge $\mp \frac{1}{2}$ [23, 25], Sect. 17.4.2, just as required by the *standard model*, manifesting with respect to \tilde{S}^{ab} and S^{ab} additional quantum numbers.

Let us point out that all the fermion fields (with the families of fermions and the neutrinos forming the condensate included), the vector and the scalar gauge fields, offering explanation for by the *standard model* postulated ones, origin in the simple starting action.

The starting action, Eq. (17.15), has only a few parameters. It is assumed that the coupling of fermions to ω^{ab}_c 's can differ from the coupling of fermions to $\tilde{\omega}^{ab}_c$'s, The reduction of the Clifford space, Eq. 17.9, causes this difference. The additional breaks of symmetries influence the coupling constants in addition.

The breaks of symmetries is under consideration for quite a long time and has not yet been finished.

⁶ A toy model [49, 52, 53] was studied in $d = (5 + 1)$ -dimensional space with the action presented in Eq. (17.15), The break from $d = (5 + 1)$ to $d = (3 + 1)$ × an almost S^2 was studied for a particular choice of vielbeins and for a class of spin connection fields. While the manifold $M^{(5+1)}$ breaks into $M^{(3+1)}$ times an almost S^2 the $2^{((3+1)/2-1)}$ families remain massless and mass protected. Equivalent assumption, although not yet proved how does it really work, is made also for the $d = (13 + 1)$ case. This study is in progress quite some time.

All the observed properties of fermions, of vector gauge fields and scalar gauge fields follow from the simple starting action, while the breaks of symmetries influence the properties of fermion and boson fields as well.

17.4.1 Properties of interacting massless fermions as manifesting in $d = (3 + 1)$ before electroweak break

One irreducible representation of $SO(13, 1)$ includes all the left handed and right handed quarks and leptons and antiquarks and antileptons as one can see in Table 5 of Ref. [33] in this Proceedings or in Table 7 of Ref. [1]. In both tables fermion "basis vectors" are represented by odd numbers of nilpotents and their properties analysed from the point of view of the *standard model* subgroups $SO(3, 1) \times SU(2) \times SU(2) \times SU(3) \times U(1)$ of the group $SO(13, 1)$. Quarks and leptons as well as antiquarks and antileptons appear with handedness as required by the *standard model*.

One easily notices that quarks and leptons have the same content of the subgroup $SO(7, 1)$, distinguishing only in $SU(3) \times U(1)$ content of $SO(6)$: all the quarks, left and right handed, have the "fermion" τ^4 equal to $\frac{1}{6}$ and appear in three colours, all the leptons, left and right handed, have τ^4 equal to $-\frac{1}{2}$ and are colourless. Also antiquarks and antileptons have the same content of the subgroup $SO(7, 1)$ (which is different from the one of quarks and leptons), and differ in $SU(3) \times U(1)$ content of $SO(6)$, all the antiquarks, left and right handed, have τ^4 equal to $-\frac{1}{6}$ and appear in three anticolours, all the antileptons have τ^4 equal to $\frac{1}{2}$ and are anticolourless.

Let us notice also that since there are two $SU(2)$ weak charges the right handed neutrinos and the left handed antineutrinos have non zero the second $SU(2)_{II}$ weak charge and interact with the $SU(2)_{II}$ weak field. Both have the *standard model* hyper charge $Y = \tau^4 + \tau^{23}$ equal to zero. Let me point out that this particular property are offered also by the $SO(10)$ unifying model [59], but with the manifold $M(3 + 1)$ decoupled from charges. (Comments can be found in Ref. [1], Sect. 7).

The expressions for the generators of the Lorentz transformations of subgroups $SO(3, 1) \times SU(2) \times SU(2) \times SU(3) \times U(1)$ of the group $SO(13, 1)$ can be found in App. 17.6 (also in Eqs. (39-41) of Ref. [33] or in Eqs. (85-89) of Ref. [1]).

The condensate, presented in Table 17.2 (Table 6 of Ref. [1]), makes one of the two weak $SU(2)$ fields massive and causes the break of symmetries from $M^{(13+1)}$ to $M^{(7+1)} \times SU(3) \times U(1)$ [49, 52, 53], leaving only two decoupled groups of four families massless, $2^{\frac{7+1}{2}-1} = 8$. The reader can find these two groups of families in Table 17.1 (from Table 5 of Ref. [1]).

Table 17.1 presents "basis vectors" ($\hat{b}_f^{m\dagger}$, Eq. (17.11)) for eight families of the right handed u-quark of the colour $(\frac{1}{2}, \frac{1}{2\sqrt{3}})$ and the right handed colourless ν -lepton. The $SO(7,1)$ content of the $SO(13, 1)$ group are in both cases identical, they distinguish only in the $SU(3)$ and $U(1)$ subgroups of $SO(6)$. All the members of any of these eight families of Table 17.1 follows from either the u-quark or the ν -lepton by the application of S^{ab} . Each family carries the family quantum numbers, determined by the Cartan subalgebra of \hat{S}^{ab} in Eq. (17.2) and presented in Table 17.1.

The two groups of families are after the break of symmetries decoupled since $\{\tilde{N}_L^i, \tilde{N}_R^j\}_- = 0, \forall(i, j), \{\tilde{\tau}^{1i}, \tilde{\tau}^{2j}\}_- = 0, \forall(i, j), \{\tilde{N}_{L,R}^i, \tilde{\tau}^{1,2j}\}_- = 0, \forall(i, j)$, while $\{S^{ab}, \tilde{S}^{cd}\}_- = 0$, since $\{\gamma^a, \tilde{\gamma}^a\}_- = 0$, Eq. (17.5).

Table 17.1: Eight families of the "basis vectors" $\hat{b}_f^{m\dagger}$, of $\hat{u}_R^{c1\dagger}$ — the right handed u-quark with spin $\frac{1}{2}$ and the colour charge ($\tau^{33} = 1/2, \tau^{38} = 1/(2\sqrt{3})$), appearing in the first line of Table 7 in Ref. [1], or Table 5 in Ref. [33] — and of the colourless right handed neutrino $\hat{\nu}_R^\dagger$ of spin $\frac{1}{2}$, appearing in the 25th line of Table 7 in Ref. [1], or Table 5 in Ref. [33] — are presented in the left and in the right part of this table, respectively. Table is taken from [31]. Families belong to two groups of four families, one (I) is a doublet with respect to $(\tilde{N}_L$ and $\tilde{\tau}^1)$ and a singlet with respect to $(\tilde{N}_R$ and $\tilde{\tau}^2)$, App. 17.6 (Eqs. (85-88) of Ref. [1]), the other group (II) is a singlet with respect to $(\tilde{N}_L$ and $\tilde{\tau}^1)$ and a doublet with respect to $(\tilde{N}_R$ and $\tilde{\tau}^2)$. All the families follow from the starting one by the application of the operators $(\tilde{N}_{R,L}^\pm, \tilde{\tau}^{(2,1)\pm})$. The generators $(N_{R,L}^\pm, \tau^{(2,1)\pm})$ transform \hat{u}_{1R}^\dagger to all the members of one family of the same colour charge. The same generators transform equivalently the right handed neutrino $\hat{\nu}_{1R}^\dagger$ to all the colourless members of the same family.

										$\tilde{\tau}^{13}$	$\tilde{\tau}^{23}$	\tilde{N}_L^3	\tilde{N}_R^3	$\tilde{\tau}^4$								
I	$\hat{u}_{R1}^{c1\dagger}$	03	12	56	78	910	1112	1314	$\hat{\nu}_{R1}^\dagger$	03	12	56	78	910	1112	1314	$-\frac{1}{2}$	0	$-\frac{1}{2}$	0	$-\frac{1}{2}$	
		(+i)	(+)		(+)	(+)		(+)		(+i)	(+)		(+)	(+)		(+)						
I	$\hat{u}_{R2}^{c1\dagger}$	03	12	56	78	910	1112	1314	$\hat{\nu}_{R2}^\dagger$	03	12	56	78	910	1112	1314	$-\frac{1}{2}$	0	$\frac{1}{2}$	0	$-\frac{1}{2}$	
		(+i)	(+)		(+)	(+)		(+)		(+i)	(+)		(+)	(+)		(+)						
I	$\hat{u}_{R3}^{c1\dagger}$	03	12	56	78	910	1112	1314	$\hat{\nu}_{R3}^\dagger$	03	12	56	78	910	1112	1314	$\frac{1}{2}$	0	$-\frac{1}{2}$	0	$-\frac{1}{2}$	
		(+i)	(+)		(+)	(+)		(+)		(+i)	(+)		(+)	(+)		(+)						
I	$\hat{u}_{R4}^{c1\dagger}$	03	12	56	78	910	1112	1314	$\hat{\nu}_{R4}^\dagger$	03	12	56	78	910	1112	1314	$\frac{1}{2}$	0	$\frac{1}{2}$	0	$-\frac{1}{2}$	
		(+i)	(+)		(+)	(+)		(+)		(+i)	(+)		(+)	(+)		(+)						
II	$\hat{u}_{R5}^{c1\dagger}$	03	12	56	78	910	1112	1314	$\hat{\nu}_{R5}^\dagger$	03	12	56	78	910	1112	1314	0	$-\frac{1}{2}$	0	$-\frac{1}{2}$	$-\frac{1}{2}$	
		(+i)	(+)		(+)	(+)		(+)		(+i)	(+)		(+)	(+)		(+)						
II	$\hat{u}_{R6}^{c1\dagger}$	03	12	56	78	910	1112	1314	$\hat{\nu}_{R6}^\dagger$	03	12	56	78	910	1112	1314	0	$-\frac{1}{2}$	0	$\frac{1}{2}$	$-\frac{1}{2}$	
		(+i)	(+)		(+)	(+)		(+)		(+i)	(+)		(+)	(+)		(+)						
II	$\hat{u}_{R7}^{c1\dagger}$	03	12	56	78	910	1112	1314	$\hat{\nu}_{R7}^\dagger$	03	12	56	78	910	1112	1314	0	$\frac{1}{2}$	0	$-\frac{1}{2}$	$-\frac{1}{2}$	
		(+i)	(+)		(+)	(+)		(+)		(+i)	(+)		(+)	(+)		(+)						
II	$\hat{u}_{R8}^{c1\dagger}$	03	12	56	78	910	1112	1314	$\hat{\nu}_{R8}^\dagger$	03	12	56	78	910	1112	1314	0	$\frac{1}{2}$	0	$\frac{1}{2}$	$-\frac{1}{2}$	
		(+i)	(+)		(+)	(+)		(+)		(+i)	(+)		(+)	(+)		(+)						

It is the assumption that the eight families from Table 17.1 remain massless after the break of symmetry from $SO(13, 1)$ to $SO(7, 1) \times SO(6)$, made after we proved for the toy model [49, 52] that the break of symmetry can leave some families of fermions massless, while the rest become massive. But we have not yet proven the masslessness of the $2^{\frac{7+1}{2}-1}$ families after the break from $SO(13, 1)$ to $SO(7, 1) \times SO(6)$.

The break from the starting symmetry $SO(13, 1)$ to $SO(7, 1) \times SU(3) \times U(1)$ is supposed to be caused by the appearance of the condensate of two right handed neutrinos with the family quantum numbers of the upper four families, that is of the four families, which do not contain the three so far observed families, at the energy of $\geq 10^{16}$ GeV. This condensate is presented in Table 17.2.

To see how do gravitational fields — vielbeins and the two spin connection fields, the gauge fields of S^{ab} and \tilde{S}^{ab} , respectively — contribute to dynamics of fermion fields and after the electroweak break also to the masses of twice four families and the vector gauge field let us rewrite the fermion part of the action, Eq. (17.15), in the way that the fermion action manifests in $d = (3 + 1)$, that is in the low energy regime before the electroweak break, by the *standard model* postulated

Table 17.2: The condensate of the two right handed neutrinos ν_R , with the quantum numbers of the VIIIth family, Table 17.1, coupled to spin zero and belonging to a triplet with respect to the generators τ^{2i} , is presented, together with its two partners. The condensate carries $\bar{\tau}^1 = 0$, $\tau^{23} = 1$, $\tau^4 = -1$ and $Q = 0 = Y$. The triplet carries $\bar{\tau}^4 = -1$, $\bar{\tau}^{23} = 1$ and $\tilde{N}_R^3 = 1$, $\tilde{N}_L^3 = 0$, $\tilde{Y} = 0$, $\tilde{Q} = 0$. The family quantum numbers of quarks and leptons are presented in Table 17.1. The definition of the operators $\bar{\tau}^1, \bar{\tau}^1, \bar{\tau}^2, \bar{\tau}^2, \tau^4, \tau^4, N_R^3, \tilde{N}_R^3, N_L^3, \tilde{N}_L^3, Q, Y, \tilde{Q}, \tilde{Y}$ can be found in App. 17.6 (and in Ref. [1], Eqs. (85-88) or in Eqs. (39-41) of Ref. [33]).

state	S^{03}	S^{12}	τ^{13}	τ^{23}	τ^4	Y	Q	$\bar{\tau}^{13}$	$\bar{\tau}^{23}$	$\bar{\tau}^4$	\tilde{Y}	\tilde{Q}	\tilde{N}_L^3	\tilde{N}_R^3
$(\nu_{1R}^{VIII} \rangle_1 \nu_{2R}^{VIII} \rangle_2)$	0	0	0	1	-1	0	0	0	1	-1	0	0	0	1
$(\nu_{1R}^{VIII} \rangle_1 e_{2R}^{VIII} \rangle_2)$	0	0	0	0	-1	-1	-1	0	1	-1	0	0	0	1
$(e_{1R}^{VIII} \rangle_1 e_{2R}^{VIII} \rangle_2)$	0	0	0	-1	-1	-2	-2	0	1	-1	0	0	0	1

properties, while manifesting the properties which make the *spin-charge-family* theory a candidate to go beyond the *standard model*:

i. The spins, handedness, charges and family quantum numbers of fermions are determined by the Cartan subalgebra of S^{ab} and \tilde{S}^{ab} , and the internal space of fermions is described by the Clifford "basis vectors" $\hat{b}_f^{m\ddagger}$.

ii. Couplings of fermions to the vector gauge fields, which are the superposition of gauge fields ω^{st}_m , Sect. 17.4.2, with the space index $m = (0, 1, 2, 3)$ and with charges determined by the Cartan subalgebra of S^{ab} and \tilde{S}^{ab} ($S^{ab}\omega^{cd}_e = i(\omega^{ad}_e\eta^{bc} - \omega^{bd}_e\eta^{ac})$ and equivalently for the other two indexes of ω^{cd}_e gauge fields, manifesting the symmetry of space $(d - 4)$), and couplings of fermions to the scalar gauge fields [19, 20, 23, 29, 31, 38, 41, 42, 45, 46] with the space index $s \geq 5$ and the charges determined by the Cartan subalgebra of S^{ab} and \tilde{S}^{ab} (as explained in the case of the vector gauge fields), and which are superposition of either ω^{st}_s or $\tilde{\omega}^{abt}_s$, Sect. 17.4.2

$$\begin{aligned} \mathcal{L}_f = & \bar{\Psi}\gamma^m(p_m - \sum_{\Lambda,i} g^{\Lambda i}\tau^{\Lambda i}\Lambda_m^{\Lambda i})\Psi + \\ & \{ \sum_{s=7,8} \bar{\Psi}\gamma^s p_{0s} \Psi \} + \\ & \{ \sum_{t=5,6,9,\dots,14} \bar{\Psi}\gamma^t p_{0t} \Psi \}, \end{aligned} \quad (17.16)$$

where $p_{0s} = p_s - \frac{1}{2}S^{s's''}\omega_{s's''s} - \frac{1}{2}\tilde{S}^{ab}\tilde{\omega}_{abs}$, $p_{0t} = p_t - \frac{1}{2}S^{t't''}\omega_{t't''t} - \frac{1}{2}\tilde{S}^{ab}\tilde{\omega}_{abt}$, with $m \in (0, 1, 2, 3)$, $s \in (7, 8)$, $(s', s'') \in (5, 6, 7, 8)$, (a, b) (appearing in \tilde{S}^{ab}) run within either $(0, 1, 2, 3)$ or $(5, 6, 7, 8)$, t runs $\in (5, \dots, 14)$, (t', t'') run either $\in (5, 6, 7, 8)$ or $\in (9, 10, \dots, 14)$. The spinor function ψ represents all family members of all the $2^{\frac{7+1}{2}-1} = 8$ families.

The first line of Eq. (17.16) determines in $d = (3+1)$ the kinematics and dynamics of fermion fields, coupled to the vector gauge fields [23, 26, 31]. The vector gauge fields are the superposition of the spin connection fields ω_{stm} , $m = (0, 1, 2, 3)$, $(s, t) = (5, 6, \dots, 13, 14)$, and are the gauge fields of S^{st} , Sect. 17.4.2.

The operators $\tau^{\Lambda i}$ ($\tau^{\Lambda i} = \sum_{a,b} c^{\Lambda i}_{ab} S^{ab}$, S^{ab} are the generators of the Lorentz transformations in the Clifford space of γ^a 's) are presented in Eqs. (17.27, 17.28) of App. 17.6. They represent the colour charge, $\vec{\tau}^3$, the weak charge, $\vec{\tau}^1$, and the hyper charge, $Y = \tau^4 + \tau^{23}$, τ^4 is the "fermion" charge, originating in $SO(6) \subset SO(13, 1)$, τ^{23} belongs together with $\vec{\tau}^1$ of $SU(2)_{\text{weak}}$ to $SO(4) (\subset SO(13 + 1))$.

One fermion irreducible representation of the Lorentz group contains, as seen in Table 7 of Ref. [1] or in Table 5 of Ref. [33], quarks and leptons and antiquarks and antileptons, belonging to the first family in Table 17.1.

Let us repeat again that the $SO(7, 1)$ subgroup content of the $SO(13, 1)$ group is the same for the quarks and leptons and the same for the antiquarks and antileptons. Quarks distinguish from leptons, and antiquarks from antileptons, only in the $SO(6) \subset SO(13, 1)$ part, that is in the colour (τ^{33}, τ^{38}) part and in the "fermion" quantum number τ^4 . The quarks distinguish from antiquarks, and leptons from antileptons, in the handedness, in the $SU(2)_I$ (weak), $SU(2)_{II}$, in the colour part and in the τ^4 part, explaining the relation between handedness and charges of fermions and antifermions, postulated in the *standard model*⁷.

All the vector gauge fields, which interact with the condensate, presented in Table 17.2, become massive, Sect. 17.4.2. The *vector gauge fields not interacting with the condensate* — the weak, colour, hyper charge and electromagnetic vector gauge fields — remain massless, in agreement with by the *standard model* assumed gauge fields before the electroweak break⁸.

After the electroweak break, caused by the scalar fields, the only conserved charges are the colour and the electromagnetic charge $Q = \tau^{13} + Y$ ($Y = \tau^4 + \tau^{23}$). All the rest interact with the scalar fields of the constant value.

The second line of Eq. (17.16) is the mass term, responsible in $d = (3 + 1)$ for the masses of fermions and of the weak gauge field (originating in spin connection fields ω^{st}_m). The interaction of fermions with the scalar fields with the space index $s = (7, 8)$ (to these scalar fields particular superposition of the spin connection fields ω^{ab}_s and all the superposition of $\tilde{\omega}^{ab}_s$ with the space index $s = (7, 8)$ and $(a, b) = (0, 1, 2, 3)$ or $(a, b) = (5, 6, 7, 8)$ contribute), which gain the constant values in $d = (3 + 1)$, makes fermions and antifermions massive.

The scalar fields, presented in the second line of Eq. (17.16), are in the *standard model* interpreted as the higgs and the Yukawa couplings, Sect. 17.4.2, predicting in the *spin-charge-family* theory that there must exist several scalar fields⁹.

These scalar gauge fields split into two groups of scalar fields. One group of two triplets and three singlets manifests the symmetry $\widetilde{SU}(2)_{(\widetilde{SO}(3,1),L)} \times \widetilde{SU}(2)_{(\widetilde{SO}(4),L)}$

⁷ Ref. [30] points out that the connection between handedness and charges for fermions and antifermions, both appearing in the same irreducible representation, explains the triangle anomalies in the *standard model* with no need to connect "by hand" the handedness and charges of fermions and antifermions.

⁸ The superposition of the scalar gauge fields $\tilde{\omega}^{st}_7$ and $\tilde{\omega}^{st}_8$, which at the electroweak break gain constant values in $d = (3 + 1)$, bring masses to all the vector gauge fields, which couple to these scalar fields.

⁹ The requirement of the *standard model* that there exist the Yukawa couplings, speaks by itself that there must exist several scalar fields explaining the Yukawa couplings.

$\times \text{U}(1)$. The other group of another two triplets and the same three singlets manifests the symmetry $\widetilde{\text{SU}}(2)_{(\widetilde{\text{SO}}(3,1),\text{R})} \times \widetilde{\text{SU}}(2)_{(\widetilde{\text{SO}}(4),\text{R})} \times \text{U}(1)$.

The three $\text{U}(1)$ singlet scalar gauge fields are superposition of $\omega_{s't's}$, $s = (7, 8)$, $(s', t') = (5, 6, \dots, 14)$, with the sums of $S^{s't'}$ arranged into superposition of τ^{13} , τ^{23} and τ^4 . The three triplets interact with both groups of quarks and leptons and antiquarks and antileptons [39–41, 45–48].

Families of fermions from Table 17.1, interacting with these scalar fields, split as well into two groups of four families, each of these two groups are coupled to one of the two groups of scalar triplets while all eight families couple to the same three singlets. The scalar gauge fields, manifesting $\widetilde{\text{SU}}(2)_{\text{L,R}} \times \widetilde{\text{SU}}(2)_{\text{L,R}}$, are the superposition of the gauge fields $\tilde{\omega}_{ab_s}$, $s = (7, 8)$, $(a, b) = \text{either } (0, 1, 2, 3) \text{ or } (5, 6, 7, 8)$, manifesting as twice two triplets.

17.4.2 Vector and scalar gauge fields before electroweak break

The second line of Eq. (17.15) represents the action for the gauge fields A_{gf}

$$\begin{aligned} A_{gf} &= \int d^d x \, E \, (\alpha R + \tilde{\alpha} \tilde{R}), \\ R &= \frac{1}{2} \{f^{\alpha[a} f^{\beta b]} (\omega_{ab\alpha, \beta} - \omega_{c\alpha\alpha} \omega^c_{\beta b})\} + \text{h.c.}, \\ \tilde{R} &= \frac{1}{2} \{f^{\alpha[a} f^{\beta b]} (\tilde{\omega}_{ab\alpha, \beta} - \tilde{\omega}_{c\alpha\alpha} \tilde{\omega}^c_{\beta b})\} + \text{h.c.} \end{aligned} \quad (17.17)$$

It is proven in Ref. [26] that the vector and the scalar gauge fields manifest in $d = (3 + 1)$, after the break of the starting symmetry, as the superposition of spin connection fields, when the space $(d - 4)$ manifest the assumed symmetry. f^β_a and e^α_α are vielbeins and inverted vielbeins respectively, $e^\alpha_\alpha f^\beta_a = \delta^\beta_\alpha$, $e^\alpha_\alpha f^\alpha_b = \delta^a_b$, $E = \det(e^\alpha_\alpha)$.

Varying the action of Eq. (17.17) with respect to the spin connection fields the expression for the spin connection fields ω_{ab}^e follows

$$\begin{aligned} \omega_{ab}^e &= \frac{1}{2E} \{e^e_\alpha \partial_\beta (E f^\alpha_{[a} f^\beta_{b]}) - e_{\alpha\alpha} \partial_\beta (E f^\alpha_{[b} f^{\beta e]}) - e_{b\alpha} \partial_\beta (E f^{\alpha[e} f^\beta_{a]})\} \\ &+ \frac{1}{4} \{\tilde{\Psi} (\gamma^e S_{ab} - \gamma_{[a} S_{b]}^e) \Psi\} \\ &- \frac{1}{d-2} \left\{ \delta_a^e \frac{1}{E} e^d_\alpha \partial_\beta (E f^\alpha_{[d} f^\beta_{b]}) + \tilde{\Psi} \gamma_d S^d_b \Psi \right\} \\ &- \delta_b^e \left\{ \frac{1}{E} e^d_\alpha \partial_\beta (E f^\alpha_{[d} f^\beta_{a]}) + \tilde{\Psi} \gamma_d S^d_a \Psi \right\}. \end{aligned} \quad (17.18)$$

Replacing S^{ab} in Eq. (17.18) with \tilde{S}^{ab} , the expression for the spin connection fields $\tilde{\omega}_{ab}^e$ follows.

If there are no spinors (fermions) present, $\Psi = 0$, then either ω_{ab}^e or $\tilde{\omega}_{ab}^e$ are uniquely expressed with the vielbeins.

Spin connection fields ω^{ab}_e represent vector gauge fields to the corresponding fermion fields if index e is $m = (0, 1, 2, 3)$. If $e \geq 5$ the spin connection fields manifest in $d = (3 + 1)$ as scalar gauge fields.

It is proven in Ref. [26]¹⁰ that in spaces with the desired symmetry the vielbein can be expressed with the gauge fields,

$$\begin{aligned}
 f^\sigma_m &= \sum_\Lambda \bar{\tau}^{\Lambda\sigma} \vec{A}_m^\Lambda, \\
 \tau^{\Lambda i\sigma} &= \sum_{st} c^{\Lambda i}_{st} (e_{s\tau} f^\sigma_t - e_{t\tau} f^\sigma_s) \chi^\tau, \\
 A_m^{\Lambda i} &= \sum_{st} c^{\Lambda i}_{st} \omega^{st}_m, \\
 \tau^{\Lambda i} &= \sum_{st} c^{\Lambda i}_{st} S^{st}, \\
 \{\tau^{\Lambda i}, \tau^{Bj}\}_- &= i\delta^{\Lambda B} f^{\Lambda ijk} \tau^{\Lambda k}.
 \end{aligned}
 \tag{17.19}$$

The vector gauge fields $A_m^{\Lambda i}$ of $\tau^{\Lambda i}$ represent in the *spin-charge-family* theory all the observed gauge fields, as well as the additional non observed vector gauge fields, which interacting with the condensate gain heavy masses.

The scalar (gauge) fields, carrying the space index $s = (5, 6, \dots, d)$, offer in the *spin-charge-family* for $s = (7, 8)$ the explanation for the origin of the Higgs’s scalar and the Yukawa couplings of the *standard model*, while scalars with the space index $s = (9, 10, \dots, 14)$ offer the explanation for the proton decay, as well as for the matter/antimatter asymmetry in the universe.

In the scalar gauge fields besides ω^{st}_s , also $\tilde{\omega}^{ab}_s$ contribute.

The explicit expressions for $c^{\Lambda i}_{ab}$, and correspondingly for $\tau^{\Lambda i}$, and $A_a^{\Lambda i}$, are written in Sects. 4.2.1. and 4.2.2 of Ref. [1].

2.a Vector gauge fields.

All the vector gauge fields are in the *spin-charge-family* theory expressible with the spin connection fields ω_{stm} as

$$A_m^{\Lambda i} = \sum_{s,t} c^{\Lambda i}_{st} \omega^{st}_m,
 \tag{17.20}$$

with $\sum_{\Lambda,i} \tau^{\Lambda i} A_m^{\Lambda i} = \sum_{a,b}^* S^{ab} \omega^{ab}_m$, * means that summation runs over (a, b) respecting the symmetry $SO(7, 1) \times SU(3) \times U(1)$, with $SO(7, 1)$ breaking further to $SO(3, 1) \times SU(2)_I \times SU(2)_{II}$.

The vector gauge fields are namely analysed from the point of view of the possibly observed fields in $d = (3 + 1)$ space: besides gravity, the colour $SU(3)$, the weak $SU(2)_I$, the second $SU(2)_{II}$ and the $U(1)_{\tau^4}$ - the vector gauge field of the "fermion" quantum number τ^4 .

¹⁰ We presented in Ref. [26] the proof, that the vielbeins f^σ_m (Einstein index $\sigma \geq 5, m = 0, 1, 2, 3$) lead in $d = (3 + 1)$ to the vector gauge fields, which are the superposition of the spin connection fields ω_{stm} : $f^\sigma_m = \sum_\Lambda \vec{A}_m^\Lambda \bar{\tau}^{\Lambda\sigma}_\tau \chi^\tau$, with $A_m^{\Lambda i} = \sum_{s,t} c^{\Lambda i}_{st} \omega^{st}_m$, when the metric in $(d - 4)$, $g_{\sigma\tau}$, is invariant under the coordinate transformations $\chi^{\sigma'} = \chi^\sigma + \sum_{\Lambda,i,s,t} \varepsilon^{\Lambda i}(\chi^m) c^{\Lambda i}_{st} E^{\sigma st}(\chi^\tau)$ and $\sum_{s,t} c^{\Lambda i}_{st} E^{\sigma st} = \tau^{\Lambda i\sigma}$, while $\tau^{\Lambda i\sigma}$ solves the Killing equation: $D_\sigma \tau_\tau^{\Lambda i} + D_\tau \tau_\sigma^{\Lambda i} = 0$ ($D_\sigma \tau_\tau^{\Lambda i} = \partial_\sigma \tau_\tau^{\Lambda i} - \Gamma_{\tau\sigma}^{\tau'} \tau_{\tau'}^{\Lambda i}$). And similarly also for the scalar gauge fields.

Due to the interaction with the condensate the second $SU(2)_{II}$ (one superposition of the third component of $SU(2)_{II}$ and of the $U(1)_{\tau^4}$ vector gauge fields and the rest two components of the $SU(2)_{II}$ vector gauge field) become massive, while the colour $SU(3)$, the weak $SU(2)_I$, the second superposition of the third component of $SU(2)_{II}$ and the $U(1)_{\tau^4}$, forming the hyper charge vector gauge field, remain massless. That is: All the vector gauge fields, as well as the scalar gauge fields of S^{ab} and of \tilde{S}^{ab} , which interact with the condensate, become massive.

The effective action for all the massless vector gauge fields, the gauge fields which do not interact with the condensate and remain therefore massless, before the electroweak break, equal to $\int d^4x \{-\frac{1}{4} F^{\Lambda i}_{mn} F^{\Lambda i mn}\}$, with the structure constants $f^{\Lambda ijk}$ concerning the colour $SU(3)$, weak $SU(2)$ and hyper charge $U(1)$ groups [26]. All these relations are valid as long as spinors and vector gauge fields are weak fields in comparison with the fields which force $(d-4)$ space to be (almost) curled, Ref. [50]. When all these fields, with the scalar gauge fields included, start to be comparable with the fields (spinors or scalars), which determine the symmetry of $(d-4)$ space, the symmetry of the whole space changes.

The electroweak break, caused by the constant (non zero vacuum expectation) values of the scalar gauge fields, carrying the space index $s = (7, 8)$, makes the weak and the hyper charge gauge fields massive. The only vector gauge fields which remain massless are, besides the gravity, the electromagnetic and the colour vector gauge fields — the observed three massless gauge fields.

2.b. Scalar gauge fields in $d = (3 + 1)$.

The starting action of the *spin-charge-family* theory offers scalar fields of two kinds:

- a. Scalar fields, taking care of the masses of quarks and leptons have the space index $s = (7, 8)$ and carry with respect to this space index the weak charge $\tau^{13} = \pm \frac{1}{2}$ and the hyper charge $Y = \mp \frac{1}{2}$, Table 17.3, Eq. (17.23). With respect to the index Ai , determined by the relation $\tau^{Ai} = \sum_{ab} c^{Ai}_{ab} S^{ab}$ and $\tilde{\tau}^{Ai} = \sum_{ab} c^{Ai}_{ab} \tilde{S}^{ab}$, that is with respect to S^{ab} and \tilde{S}^{ab} , they carry charges and family charges in adjoint representations.

- b. There are in the starting action of the *spin-charge-family* theory, Eq. (17.15), scalar fields, which transform antileptons and antiquarks into quarks and leptons and back. They carry space index $s = (9, 10, \dots, 14)$, They are with respect to the space index colour triplets and antitriplets, while they carry charges τ^{Ai} and $\tilde{\tau}^{Ai}$ in adjoint representations.

Following Refs. [1,31,38] I shall review both kinds of fields.¹¹

2.b.i Scalar gauge fields determining scalar higgs and Yukawa couplings

Making a choice of the scalar index equal to $s = (7, 8)$ (the choice of $(s = 5, 6)$ would also work) and allowing all superposition of $\tilde{\omega}_{\tilde{a}\tilde{b}s}$, while with respect to

¹¹ Let us demonstrate how do the infinitesimal generators S^{ab} apply on the spin connections fields $\omega_{bde} (= f^{\alpha}_e \omega_{bd\alpha})$ and $\tilde{\omega}_{\tilde{b}\tilde{d}\tilde{e}} (= f^{\alpha}_e \tilde{\omega}_{\tilde{b}\tilde{d}\alpha})$, on either the space index e or any of the indices $(b, d, \tilde{b}, \tilde{d})$ $S^{ab} \Lambda^{d\dots e\dots g} = i(\eta^{ae} \Lambda^{d\dots b\dots g} - \eta^{be} \Lambda^{d\dots a\dots g})$ (Section IV. and Appendix B in Ref. [31]).

ω_{abs} only the superposition representing the scalar gauge fields A_s^Q, A_s^Y and A_s^4 , $s = (7, 8)$ (or any three superposition of these three scalar fields) may contribute. Let us use the common notation A_s^{Ai} for all the scalar gauge fields with $s = (7, 8)$, independently of whether they originate in ω_{abs} — in this case $Ai = (Q, Y, \tau^4)$ — or in $\tilde{\omega}_{\text{abs}}$. All these gauge fields contribute to the masses of quarks and leptons and antiquarks and antileptons after gaining constant values (nonzero vacuum expectation values).

$$\begin{aligned} A_s^{Ai} \text{ represents } & (A_s^Q, A_s^Y, A_s^4, \vec{A}_s^{\tilde{1}}, \vec{A}_s^{\tilde{N}_L}, \vec{A}_s^{\tilde{2}}, \vec{A}_s^{\tilde{N}_R}), \\ \tau^{Ai} \text{ represents } & (Q, Y, \tau^4, \vec{\tau}^1, \vec{N}_L, \vec{\tau}^2, \vec{N}_R). \end{aligned} \tag{17.21}$$

Here τ^{Ai} represent all the operators which apply on fermions. These scalars with the space index $s = (7, 8)$, they are scalar gauge fields of the generators τ^{Ai} and $\tilde{\tau}^{Ai}$, are expressible in terms of the spin connection fields, App. 17.6 (Ref. [31], Eqs. (10, 22, A8, A9)).

All the scalar fields with the space index $(7, 8)$ carry with respect to this space index the weak and the hyper charge $(\mp \frac{1}{2}, \pm \frac{1}{2})$, respectively, all having therefore properties as required for the higgs in the *standard model*.

To make the scalar fields the eigenstates of $\tau^{13} = \frac{1}{2}(\mathcal{S}^{56} - \mathcal{S}^{78})$ and to check their properties with respect to $Y (= \tau^4 + \tau^{23} = (\frac{1}{2}(\mathcal{S}^{56} + \mathcal{S}^{78}) - \frac{1}{3}(\mathcal{S}^{9\ 10} + \mathcal{S}^{11\ 12} + \mathcal{S}^{13\ 14}))$ and $Q (= \tau^{13} + Y)$ we need to apply the operators τ^{13}, Y and Q on the scalar fields with the space index $s = (7, 8)$, taking into account the relation $\mathcal{S}^{ab} A^{d\dots e\dots g} = i(\eta^{ae} A^{d\dots b\dots g} - \eta^{be} A^{d\dots a\dots g})$.

Let us rewrite the second line of Eq. (17.16), paying no attention to the momentum $p_s, s \in (5, \dots, 8)$, when having in mind the lowest energy solutions manifesting at low energies.

$$\begin{aligned} & \sum_{s=(7,8), A, i} \bar{\psi} \gamma^s (-\tau^{Ai} A_s^{Ai}) \psi = \\ & - \sum_{A, i} \bar{\psi} \{ (+)^{78} \tau^{Ai} (A_7^{Ai} - i A_8^{Ai}) + (-)^{78} (\tau^{Ai} (A_7^{Ai} + i A_8^{Ai})) \} \psi, \\ & (\pm)^{78} = \frac{1}{2} (\gamma^7 \pm i \gamma^8), \quad A_{(\pm)}^{Ai} := (A_7^{Ai} \mp i A_8^{Ai}), \end{aligned} \tag{17.22}$$

with the summation over A and i performed, with A_s^{Ai} representing the scalar fields (A_s^Q, A_s^Y, A_s^4) determined by $\omega_{s', s'', s}$, as well as $(\vec{A}_s^{\tilde{4}}, \vec{A}_s^{\tilde{1}}, \vec{A}_s^{\tilde{2}}, \vec{A}_s^{\tilde{N}_R}$ and $\vec{A}_s^{\tilde{N}_L})$, determined by $\tilde{\omega}_{a, b, s}, s = (7, 8)$.

The application of the operators τ^{13}, Y and Q on the scalar fields $(A_7^{Ai} \mp i A_8^{Ai})$ with respect to the space index $s = (7, 8)$, gives

$$\begin{aligned} \tau^{13} (A_7^{Ai} \mp i A_8^{Ai}) &= \pm \frac{1}{2} (A_7^{Ai} \mp i A_8^{Ai}), \\ Y (A_7^{Ai} \mp i A_8^{Ai}) &= \mp \frac{1}{2} (A_7^{Ai} \mp i A_8^{Ai}), \\ Q (A_7^{Ai} \mp i A_8^{Ai}) &= 0. \end{aligned} \tag{17.23}$$

Since τ^4 , Y , τ^{13} and τ^{1+} , τ^{1-} give zero if applied on $(A_s^Q, A_s^Y$ and $A_s^4)$ (with respect to the quantum numbers (Q, Y, τ^4)), and since Y, Q, τ^4 and τ^{13} commute with the family quantum numbers, one sees that the scalar fields A_s^{Ai} ($= (A_s^Q, A_s^Y, A_s^{Y'}, \vec{A}_s^4, \vec{A}_s^Q, \vec{A}_s^1, \vec{A}_s^2, \vec{A}_s^{N_R}, \vec{A}_s^{N_L})$), $s = (7, 8)$, rewritten as $A_{78}^{Ai} = (A_7^{Ai} \mp i A_8^{Ai})$, are eigenstates of τ^{13} and Y , having the quantum numbers of the *standard model* Higgs's scalar.

These superposition of A_{78}^{Ai} are presented in Table 17.3 as two doublets with respect to the weak charge τ^{13} , with the eigenvalue of τ^{23} (the second $SU(2)_II$ charge) equal to either $-\frac{1}{2}$ or $+\frac{1}{2}$, respectively.

Table 17.3: The two scalar weak doublets, one with $\tau^{23} = -\frac{1}{2}$ and the other with $\tau^{23} = +\frac{1}{2}$, both with the "fermion" quantum number $\tau^4 = 0$, are presented. In this table all the scalar fields carry besides the quantum numbers determined by the space index also the quantum numbers A and i from Eq. (17.21). The table is taken from Ref. [31].

name	superposition	τ^{13}	τ^{23}	spin	τ^4	Q
A_{78}^{Ai} (-)	$A_7^{Ai} + iA_8^{Ai}$	$+\frac{1}{2}$	$-\frac{1}{2}$	0	0	0
A_{56}^{Ai} (-)	$A_5^{Ai} + iA_6^{Ai}$	$-\frac{1}{2}$	$-\frac{1}{2}$	0	0	-1
A_{78}^{Ai} (+)	$A_7^{Ai} - iA_8^{Ai}$	$-\frac{1}{2}$	$+\frac{1}{2}$	0	0	0
A_{56}^{Ai} (+)	$A_5^{Ai} - iA_6^{Ai}$	$+\frac{1}{2}$	$+\frac{1}{2}$	0	0	+1

It is not difficult to show that the scalar fields A_{78}^{Ai} are *triplets* as the gauge fields of the family quantum numbers $(\vec{N}_R, \vec{N}_L, \vec{\tau}^2, \vec{\tau}^1)$ or singlets as the gauge fields of $Q = \tau^{13} + Y$, $Q' = -\tan^2 \vartheta_1 Y + \tau^{13}$ and $Y' = -\tan^2 \vartheta_2 \tau^4 + \tau^{23}$.

Table 17.1 represents two groups of four families. It is not difficult to see that \vec{N}_L^\pm and $\vec{\tau}^{1\pm}$ transform the first four families among themselves, leaving the second group of four families untouched, while \vec{N}_R^\pm and $\vec{\tau}^{2\pm}$ do not influence the first four families and transform the second four families among themselves. All the scalar fields with $s = (7, 8)$ "dress" the right handed quarks and leptons with the hyper charge and the weak charge so that they manifest charges of the left handed partners.

The mass matrices 4×4 , representing the application of the scalar gauge fields on fermions of each of the two groups, have the symmetry $SU(2) \times SU(2) \times U(1)$ of the form as presented in Eq. (17.24)¹². The influence of scalar fields on the masses of quarks and leptons depends on the coupling constants and the masses of the

¹² The symmetry $SU(2) \times SU(2) \times U(1)$ of the mass matrices, Eq. (17.24), is expected to remain in all loop corrections [47].

scalar fields, determining parameters of the mass matrix

$$\mathcal{M}^\alpha = \begin{pmatrix} -a_1 - a & e & d & b \\ e^* & -a_2 - a & b & d \\ d^* & b^* & a_2 - a & e \\ b^* & d^* & e^* & a_1 - a \end{pmatrix}^\alpha, \tag{17.24}$$

with α representing family members — quarks and leptons [39–41, 46, 48]. In Subsect. 17.4.3 the predictions of the *spin-charge-family* theory following from the symmetry of mass matrices of Eq. (17.24) are discussed.

The *spin-charge-family* theory treats quarks and leptons in equivalent way. The differences among family members occur due to the scalar fields ($Q \cdot A_{78}^Q, Y \cdot A_{78}^Q, \tau^4 \cdot A_{78}^4$) [46, 48].

Twice four families of Table 17.1, with the two groups of two triplets applying each on one of the two groups of four families and one group of three singlets applying on all eight families, **i.** offer the explanation for the appearance of the Higgs’s scalar and Yukawa couplings of the observed three families, predicting the fourth family to the observed three families and several scalar fields, **ii.** predict that the stable of the additional four families with much higher masses that the lower four families contributes to the *dark matter*.

2.b.ii Scalar gauge fields causing transitions from antileptons and antiquarks into quarks and leptons [25]

Besides the scalar fields with the space index $s = (7, 8)$ which manifest in $d = (3 + 1)$ as scalar gauge fields with the weak and hyper charge $\pm \frac{1}{2}$ and $\mp \frac{1}{2}$, respectively, and which gaining at low energies constant values cause masses of families of quarks and leptons and of the weak gauge field, there are in the starting action, Eqs. (17.15, 17.16), additional scalar gauge fields with the space index $t = (9, 10, 11, 12, 13, 14)$. They are with respect to the space index t either triplets or antitriplets causing transitions from antileptons into quarks and from antiquarks into quarks and back. These scalar fields are in Eq. (17.16) presented in the third line.

These scalar fields are offering the explanation for the matter/antimatter asymmetry in the universe, and might be responsible for proton decay and lepton number nonconservation. The reader is kindly ask to read the article [25], for a short review one can see the Refs. [1, 23].

17.4.3 Predictions of *spin-charge-family* theory

Let me say that the fact that the simple starting action, Eq. (17.15) — in which fermions interact with gravity only (the vielbeins and the two kinds of the spin connection fields), while the internal spaces of fermions and bosons are describable by the “basis vectors” which are superposition of odd or even products of Clifford algebra operators $\gamma^{\alpha'}$ s, respectively — offers the explanation for all the assumptions of the *standard model* and for the second quantized postulates for fermions and bosons, while unifying all the so far known forces, with gravity

included, predicting new vector gauge fields, new scalar gauge fields and new families of fermions, gives a hope that the *spin-charge-family* theory is offering the right next step beyond the *standard model*.

i. The existence of the lower group of four families predicts the fourth family to the observed three, which should be seen in next experiments. The masses of quarks of these four families are determined by several scalar fields, all with the properties of the scalar higgs, some of them of which might also be observed. The symmetry [46,47], Eq. (17.24), and the values of mass matrices of the lower four families are determined with two triplet scalar fields, $\vec{\bar{A}}_{78}^{\bar{1}}_{(\pm)}$ and $\vec{\bar{A}}_{78}^{\bar{N}_L}_{(\pm)}$, and three singlet scalar fields, $A_{78}^Q_{(\pm)}$, $A_{78}^Y_{(\pm)}$, $A_{78}^4_{(\pm)}$, Eq. (17.21), explaining the Higgs's scalar and Yukawa couplings of the *standard model*, Refs. [23,27,31,46,48] and references therein.

Any accurate 3×3 submatrix of the 4×4 unitary matrix determines the 4×4 matrix uniquely. Since neither the quark and (in particular) nor the lepton 3×3 mixing matrix are measured accurately enough to be able to determine three complex phases of the 4×4 mixing matrix, we assume (what also simplifies the numerical procedure) [39–41,45,46] that the mass matrices are symmetric and real and correspondingly the mixing matrices are orthogonal. We fitted the 6 free parameters of each family member mass matrix, Eq. (17.24), to twice three measured masses (6) of each pair of either quarks or leptons and to the 6 (from the experimental data extracted) parameters of the corresponding 4×4 mixing matrix.

I present here the old results for quarks only, taken from Refs. [46]. The accuracy of the experimental data for leptons are not yet large enough that would allow any meaningful prediction¹³. It turns out that the experimental [54] inaccuracies are for the mixing matrices too large to tell trustworthy mass intervals for the quarks masses of the fourth family members¹⁴. Taking into account the calculations of Ref. [54] fitting the experimental data (and the meson decays evaluations in the literature as well as our own evaluations) the authors of the paper [46] very roughly estimate that the fourth family quarks masses might be pretty above 1 TeV.

Since the matrix elements of the 3×3 submatrix of the 4×4 mixing matrix depend weakly on the fourth family masses, the calculated mixing matrix offers the prediction to what values will more accurate measurements move the present ex-

¹³ The numerical procedure, explained in the paper [46], to fit free parameters of the mass matrices to the experimental data within the experimental inaccuracy of the mixing matrix elements of the so far observed quarks (the inaccuracy of masses do not influence the results very much) is tough.

¹⁴ We have not yet succeeded to repeat the calculations presented in Refs. [46] with the newest data from Ref. [55]. Let us say that the accuracy of the mixing matrix even for quarks remains in Ref. [55] far from needed to predict the masses of the fourth two quarks. For the chosen masses of the four family quarks the mixing matrix elements are expected to slightly change in the direction proposed by Eq. (17.25).

perimental data and also the fourth family mixing matrix elements in dependence of the fourth family masses, Eq. (17.25):

V_{ud} will stay the same or will very slightly decrease; V_{ub} and V_{cs} , will still lower; V_{td} will lower, and V_{tb} will lower; V_{us} will slightly increase; V_{cd} will (after decreasing) slightly rise; V_{cb} will still increase and V_{ts} will (after decreasing) increase.

In Eq. (17.25) the matrix elements of the 4×4 mixing matrix for quarks are presented, obtained when the 4×4 mass matrices respect the symmetry of Eq. (17.24) while the parameters of the mass matrices are fitted to the (exp) experimental data [54], Ref. [46]. The two choices of the fourth family quark masses are used in the calculations: $m_{u_4} = m_{d_4} = 700$ GeV (scf₁) and $m_{u_4} = m_{d_4} = 1\,200$ GeV (scf₂). In parentheses, () and [], the changes of the matrix elements are presented, which are due to the changes of the top mass within the experimental inaccuracies: with the $m_t = (172 + 3 \times 0.76)$ GeV and $m_t = (172 - 3 \times 0.76)$, respectively (if there are one, two or more numbers in parentheses the last one or more numbers are different, if there is no parentheses no numbers are different) [arxiv:1412.5866].

$$|V_{(ud)}| = \begin{pmatrix} \text{exp} & 0.97425 \pm 0.00022 & 0.2253 \pm 0.0008 & 0.00413 \pm 0.00049 & \\ \text{scf}_1 & 0.97423(4) & 0.22539(7) & 0.00299 & 0.00776(1) \\ \text{scf}_2 & 0.97423[5] & 0.22538[42] & 0.00299 & 0.00793[466] \\ \text{exp} & 0.225 \pm 0.008 & 0.986 \pm 0.016 & 0.0411 \pm 0.0013 & \\ \text{scf}_1 & 0.22534(3) & 0.97335 & 0.04245(6) & 0.00349(60) \\ \text{scf}_2 & 0.22531[5] & 0.97336[5] & 0.04248 & 0.00002[216] \\ \text{exp} & 0.0084 \pm 0.0006 & 0.0400 \pm 0.0027 & 1.021 \pm 0.032 & \\ \text{scf}_1 & 0.00667(6) & 0.04203(4) & 0.99909 & 0.00038 \\ \text{scf}_2 & 0.00667 & 0.04206[5] & 0.99909 & 0.00024[21] \\ \text{scf}_1 & 0.00677(60) & 0.00517(26) & 0.00020 & 0.99996 \\ \text{scf}_2 & 0.00773 & 0.00178 & 0.00022 & 0.99997[9] \end{pmatrix}. \tag{17.25}$$

Let me conclude that according to Ref. [46] the masses of the fourth family lie much above the known three. The larger are masses of the fourth family the larger are $V_{u_1 d_4}$ in comparison with $V_{u_1 d_3}$ and the more is valid that $V_{u_2 d_4} < V_{u_1 d_4}$, $V_{u_3 d_4} < V_{u_1 d_4}$. The flavour changing neutral currents are correspondingly weaker.

Let be noticed that the prediction of Ref. [56], $V_{u_1 d_4} > V_{u_1 d_3}$, $V_{u_2 d_4} < V_{u_1 d_4}$, $V_{u_3 d_4} < V_{u_1 d_4}$, agrees with the prediction of Refs. [46].

In Ref. [48] the authors discuss the question why the existence of the fourth family is not (at least yet) in contradiction with the experimental data.

ii. The theory predicts the existence of several scalar fields. To the lower four families two triplets and three singlets contribute, to the upper four families the same three singlets and different two triplets contribute, Eq. (17.21), Sects. 17.4.2, 17.4.2. Some superposition of the three singlets and two triplets contributing to masses and to mixing matrices of quarks and leptons of the lower four families will be observed, representing so far the observed scalar higgs and Yukawa couplings.

iii. The theory predicts the existence of besides the additional scalar fields also the additional vector gauge fields of very high mass, Sects. 17.4.2, 17.4.2.

iv. The theory predicts the existence of the upper four families of quarks and leptons and antiquarks and antileptons, Table 17.1, with the same family members charges, Table 7 of Ref [1], as are the charges of the lower four families, interacting correspondingly with the same vector gauge fields. At low energies the upper four families are decoupled from the lower four families.

The masses of the upper four families are determined by the two triplets $(\vec{A}_{78}^{\pm 2}, \vec{A}_{78}^{\pm \bar{N}_R})$

and three singlets $(A_{78}^{\pm Q}, A_{78}^{\pm Q'}, A_{78}^{\pm Y'})$, the same singlets contribute also to masses of the lower four families, Sect. 17.4.2.

The stable of the upper four families offers the explanation for the appearance of the *dark matter* in our universe.

Since the masses of the upper four families are much higher than the masses of the lower four families, the "nuclear" force among the baryons and mesons of these quarks and antiquarks differ a lot from the nuclear force of the baryons and fermions of the lower four families.

A rough estimation of properties of baryons of the stable fifth family members, of their behaviour during the evolution of the universe and when scattering on the ordinary matter, as well as a study of possible limitations on the family properties due to the cosmological and direct experimental evidences are done in Ref. [45].

In Ref. [57] the weak and "nuclear" scattering of such very heavy baryons by ordinary nucleons is studied, showing that the cross section for such scattering is very small and therefore consistent with the observation of experiments so far, provided that the quark mass of this baryon is about 100 TeV or above.

In Ref. [45] a simple hydrogen-like model is used to evaluate properties of baryons of these heavy quarks, with one gluon exchange determining the force among the constituents of the fifth family baryons¹⁵.

The authors of Ref. [45] study the freeze out procedure of the fifth family quarks and antiquarks and the formation of baryons and antibaryons up to the temperature $k_b T = 1$ GeV, when the colour phase transition starts which depletes almost all the fifth family quarks and antiquarks, while the colourless fifth family neutrons with very small scattering cross section decouples long before (at $k_b T = 100$ GeV).

The cosmological evolution suggests for the mass limits the range $10 \text{ TeV} < m_{q_5} < \text{a few} \cdot 10^2 \text{ TeV}$ and for the scattering cross sections $10^{-8} \text{ fm}^2 < \sigma_{c_5} < 10^{-6} \text{ fm}^2$. The measured density of the dark matter does not put much limitation on the properties of heavy enough clusters¹⁶.

¹⁵ The weak force and the electromagnetic force start to be at small distances due to heavy masses of quarks of the same order of magnitude as the colour force.

¹⁶ In the case that the weak interaction determines the cross section of the neutron n_5 , the interval for the fifth family quarks would be $10 \text{ TeV} < m_{q_5} c^2 < 10^5 \text{ TeV}$.

The DAMA/LIBRA experiments [60] limit, provided that they measure the heavy fifth family clusters, the quark mass in the interval: $200 \text{ TeV} < m_{q_5} < 10^5 \text{ TeV}$, Ref. [45].

Baryons of the fifth family are heavy, forming small enough clusters with small enough scattering amplitude among themselves and with the ordinary matter to be the candidate for the dark matter.

Masses of the stable fifth family of quarks and leptons are much above the fourth family members.

Although the upper four families carry the weak (of two kinds) and the colour charge, these group of four families are completely decoupled from the lower four families up to the $< 10^{16} \text{ GeV}$ when the breaks of symmetries are expected to recover.

17.5 Conclusions

The *spin-charge-family* theory [1, 20, 21, 23, 36, 37, 42, 44] assumes in $d = (13 + 1)$ -dimensional space a simple action, Eq. (17.15), for the massless fermions and for the massless vielbeins and the two kinds of spin connection fields, with which fermions interact. The description of the internal space of fermions with "basis vectors" which are superposition of an odd products of the Clifford algebra objects and of bosons with "basis vectors" which are superposition of an even products of the Clifford algebra objects offers the explanation for spins, charges and families of fermions and their vector and scalar gauge fields, as required by the *standard model*, while explaining as well the second quantization postulates for fermions and bosons.

Some of the predictions of the *spin-charge-family* theory can experiments soon confirm and correspondingly confirm (or reject) the theory. Because the theory offers meaningful answers to many open questions in physics of elementary fermion and boson fields and in cosmology and because the theory offers more and more answers the more effort and work is put into it, it might very well be that the theory does offer the right next step beyond the *standard model*.

The description of fermions and bosons, both second quantized, with the Clifford odd and the Clifford even "basis vectors", respectively, clarifies how strongly are all the properties of elementary fields determined by the internal space of fields, and that the internal space of fermions not only unifies spin, handedness, all the charges and families of fermions but manifests as well the strong connections with the corresponding boson vector and scalar gauge fields.

The theory obviously needs more collaborators as it is necessary to find answers to questions, like:

i. What is the dimension of space time? In any dimension $d = 2(2n + 1)$ there namely exist fermions of only one handedness, as discussed in Ref. [33], while in any subspace of this space there are fermions of both handedness. **i.a.** How can we look for anomalies of Kaluza-Klein theories in higher dimensions? **i.b.** As well as for the renormalizability?

ii. The spontaneous breaks of symmetries, from the starting one to the final ones, must carefully be done. **ii.a.** The breaks from any $d = 2(2n + 1)$ in steps to the

observable $d = (3 + 1)$ must be done, following the number of massless families of fermions and the appearance of the vector and scalar gauge fields in each step. So far we studied only the breaks of symmetry for the toy models [49, 51, 52], starting with $d = (5 + 1)$. **ii.b.** To learn more the electroweak break with the scalar fields defined in $d = 2(2n + 1)$, $n = 3$, with the space index $(7, 8)$ [49–52] needs additional treating.

iii. The second quantization of fermion and boson fields with the description of the internal space of fermions and bosons by the Clifford odd and even “basis vectors”, respectively, is opening a new insight in to quantum field theory. Ref. [33] presents only the first step to the second quantization of bosons by the Clifford even “basis vectors”. A further study is needed.

iv. One irreducible representation of the Lorentz group in the internal space of fermions, Table 7 in Ref. [1] and Table 5 in Ref. [33], includes all the quarks and leptons and antiquarks and antileptons observed so far (with not yet observed the right handed neutrinos and the left handed antineutrinos included). No Dirac sea is needed. **iv.a.** Additional studies of masses of fermions and antifermions in addition to those of Refs. [46, 58] are needed.

v. So far only three families of quarks and leptons have been observed. The *spin-charge-family* theory predicts the fourth family to the observed three, very weakly coupled to the observed three with masses a few TeV or higher. Although the accurately known 3×3 submatrix of the 4×4 unitary matrix determines the 4×4 matrix uniquely, even the quarks mixing matrix is known far non accurately enough to enable prediction of masses of the fourth family, Ref. [46]. **v.a.** A further study of the properties of the 4×4 mixing matrix as following from the mass matrices of quarks and leptons with the known symmetries (what reduces the number of free parameters to be fitted to the experimental data) is needed and the way of improving the experimental accuracy needs to be suggested. **v.b.** The proof that the symmetry of mass matrices $\widetilde{SU}(2) \times \widetilde{SU}(2) \times U(1)$ keeps in all orders of loop corrections, presented in Ref. [58], must be checked.

vi. There are scalar fields which are colour triplets and antitriplets, predicted by the *spin-charge-family* theory [25], which transform antileptons into quarks and antiquarks into quarks and back, causing in the expanding universe matter-antimatter asymmetry. The study is needed to see their influence on the lepton number non conservation.

vii. A study of the coupling constants of fermions to the corresponding gauge vector and scalar fields in comparison with those of $SO(10)$ and $SO(13 + 1)$ is needed.

viii. The masses of the upper four families after the electroweak break and the influence of the neutrino condensate on their masses must be studied. **viii.a.** The behaviour of the stable fifth family members, their “freezing” out and formation of neutral objects, interacting with the weak force, is needed and their contribution to the *dark matter*. **viii.b.** As well as the contribution of the heavy neutrinos to the *dark matter*.

ix. If the *spin-charge-family* theory is the right next step beyond the *standard model*, it is worthwhile to find out what it has in common with all the theories and models which seems to be promising.

x. And many more.

17.6 Infinitesimal generators of subgroups of $SO(13, 1)$ group

The relations are taken from Ref. [1].

The reader can calculate all the quantum numbers of Table 5 in Ref. [33] and of Table 17.1, if taking into account the generators of the two $SU(2)$ ($\subset SO(3, 1) \subset SO(7, 1) \subset SO(13, 1)$) groups, describing spins and handedness of fermions, their two kinds of the weak charges, the colour charges, the "fermion" charge, as well as the family quantum numbers.

One needs

$$\vec{N}_{\pm}(= \vec{N}_{(L,R)}) := \frac{1}{2}(S^{23} \pm iS^{01}, S^{31} \pm iS^{02}, S^{12} \pm iS^{03}), \quad \vec{\tilde{N}}_{\pm}(= \vec{\tilde{N}}_{(L,R)}) := \frac{1}{2}(\tilde{S}^{23} \pm i\tilde{S}^{01}, \quad (17.26)$$

the generators of the two $SU(2)$ ($SU(2) \subset SO(4) \subset SO(7, 1) \subset SO(13, 1)$) groups, describing the weak charge, $\vec{\tau}^1$, and the second kind of the weak charge, $\vec{\tau}^2$, of fermions and the corresponding family quantum numbers

$$\begin{aligned} \vec{\tau}^1 &:= \frac{1}{2}(S^{58} - S^{67}, S^{57} + S^{68}, S^{56} - S^{78}), & \vec{\tau}^2 &:= \frac{1}{2}(S^{58} + S^{67}, S^{57} - S^{68}, S^{56} + S^{78}), \\ \vec{\tilde{\tau}}^1 &:= \frac{1}{2}(\tilde{S}^{58} - \tilde{S}^{67}, \tilde{S}^{57} + \tilde{S}^{68}, \tilde{S}^{56} - \tilde{S}^{78}), & \vec{\tilde{\tau}}^2 &:= \frac{1}{2}(\tilde{S}^{58} + \tilde{S}^{67}, \tilde{S}^{57} - \tilde{S}^{68}, \tilde{S}^{56} + \tilde{S}^{78}), \end{aligned} \quad (17.27)$$

and the generators of $SU(3)$ and $U(1)$ subgroups of $SO(6) \subset SO(13, 1)$, describing the colour charge and the "fermion" charge of fermions as well as the corresponding family quantum number $\vec{\tau}^4$

$$\begin{aligned} \vec{\tau}^3 &:= \frac{1}{2}\{S^{9\ 12} - S^{10\ 11}, S^{9\ 11} + S^{10\ 12}, S^{9\ 10} - S^{11\ 12}, S^{9\ 14} - S^{10\ 13}, \\ &\quad S^{9\ 13} + S^{10\ 14}, S^{11\ 14} - S^{12\ 13}, S^{11\ 13} + S^{12\ 14}, \frac{1}{\sqrt{3}}(S^{9\ 10} + S^{11\ 12} - 2S^{13\ 14})\}, \\ \tau^4 &:= -\frac{1}{3}(S^{9\ 10} + S^{11\ 12} + S^{13\ 14}), \\ \tilde{\tau}^4 &:= -\frac{1}{3}(\tilde{S}^{9\ 10} + \tilde{S}^{11\ 12} + \tilde{S}^{13\ 14}). \end{aligned} \quad (17.28)$$

The (chosen) Cartan subalgebra operators, determining the commuting operators in the above equations, is presented in Eq. (17.2).

The hypercharge Y and the electromagnetic charge Q and the corresponding family quantum numbers then follows as

$$\begin{aligned} Y &:= \tau^4 + \tau^{23}, \quad Q := \tau^{13} + Y, \quad Y' := -\tau^4 \tan^2 \vartheta_2 + \tau^{23}, \quad Q' := -Y \tan^2 \vartheta_1 + \tau^{13}, \\ \tilde{Y} &:= \tilde{\tau}^4 + \tilde{\tau}^{23}, \quad \tilde{Q} := \tilde{Y} + \tilde{\tau}^{13}, \quad \tilde{Y}' := -\tilde{\tau}^4 \tan^2 \vartheta_2 + \tilde{\tau}^{23}, \quad \tilde{Q}' := -\tilde{Y} \tan^2 \vartheta_1 + \tilde{\tau}^{13}. \end{aligned} \quad (17.29)$$

Below are some of the above expressions written in terms of nilpotents and projectors

$$\begin{aligned}
 N_{\pm}^{\pm} &= N_{\pm}^1 \pm i N_{\pm}^2 = - \begin{pmatrix} 03 & 12 \\ \mp i & (\pm) \end{pmatrix}, & N_{\pm}^{\pm} &= N_{\pm}^1 \pm i N_{\pm}^2 = (\pm i)(\pm), \\
 \tilde{N}_{\pm}^{\pm} &= - \begin{pmatrix} 03 & 12 \\ \mp i & (\pm) \end{pmatrix}, & \tilde{N}_{\pm}^{\pm} &= (\pm i)(\pm), \\
 \tau^{1\pm} &= (\mp) \begin{pmatrix} 56 & 78 \\ (\pm) & (\mp) \end{pmatrix}, & \tau^{2\mp} &= (\mp) \begin{pmatrix} 56 & 78 \\ (\mp) & (\mp) \end{pmatrix}, \\
 \tilde{\tau}^{1\pm} &= (\mp) \begin{pmatrix} 56 & 78 \\ (\pm) & (\tilde{\mp}) \end{pmatrix}, & \tilde{\tau}^{2\mp} &= (\mp) \begin{pmatrix} 56 & 78 \\ (\tilde{\mp}) & (\mp) \end{pmatrix}.
 \end{aligned} \tag{17.30}$$

Acknowledgment

The author thanks Department of Physics, FMF, University of Ljubljana, Society of Mathematicians, Physicists and Astronomers of Slovenia, for supporting the research on the *spin-charge-family* theory by offering the room and computer facilities and Matjaž Breskvar of Beyond Semiconductor for donations, in particular for the annual workshops entitled "What comes beyond the standard models". Thanks also to all the participants of the Annual workshops "What comes beyond the standard models" for helpful discussions.

References

1. N. S. Mankoč Borštnik, H. B. Nielsen, "How does Clifford algebra show the way to the second quantized fermions with unified spins, charges and families, and with vector and scalar gauge fields beyond the *standard model*", *Progress in Particle and Nuclear Physics*, <http://doi.org/10.1016/j.pnpnp.2021.103890> [arxiv:2108/10.1016].
2. H. Georgi, in *Particles and Fields* (edited by C. E. Carlson), A.I.P., 1975; Google Scholar.
3. H. Fritzsch and P. Minkowski, *Ann. Phys.* **93** (1975) 193.
4. J. Pati and A. Salam, *Phys.Rev.* **D 8** (1973) 1240.
5. H. Georgy and S.L. Glashow, *Phys. Rev. Lett.* **32** (1974) 438.
6. Y. M. Cho, *J. Math. Phys.* **16** (1975) 2029.
7. Y. M. Cho, P. G. O. Freund, *Phys. Rev.* **D 12** (1975) 1711.
8. A. Zee, *Proceedings of the first Kyoto summer institute on grand unified theories and related topics*, Kyoto, Japan, June-July 1981, Ed. by M. Konuma, T. Kaskawa, World Scientific Singapore.
9. A. Salam, J. Strathdee, *Ann. Phys.* (N.Y.) **141** (1982) 316.
10. S. Randjbar-Daemi, A. Salam, J. Strathdee, *Nucl. Phys.* **B 242** (1984) 447.
11. W. Mecklenburg, *Fortschr. Phys.* **32** (1984) 207.
12. Z. Horvath, L. Palla, E. Crammer, J. Scherk, *Nucl. Phys.* **B 127** (1977) 57.
13. T. Asaka, W. Buchmuller, *Phys. Lett.* **B 523** (2001) 199.
14. G. Chapline, R. Slansky, *Nucl. Phys.* **B 209** (1982) 461.
15. R. Jackiw and K. Johnson, *Phys. Rev.* **D 8** (1973) 2386.
16. I. Antoniadis, *Phys. Lett.* **B 246** (1990) 377.
17. P. Ramond, *Field Theory, A Modern Primer*, Frontier in Physics, Addison-Wesley Pub., ISBN 0-201-54611-6.
18. P. Horawa, E. Witten, *Nucl. Phys.* **B 460** (1966) 506.
19. N. Mankoč Borštnik, "Spin connection as a superpartner of a vielbein", *Phys. Lett.* **B 292** (1992) 25-29.

20. N. Mankoč Borštnik, "Spinor and vector representations in four dimensional Grassmann space", *J. of Math. Phys.* **34** (1993) 3731-3745.
21. N. Mankoč Borštnik, "Unification of spin and charges in Grassmann space?", hep-th 9408002, IJS.TP.94/22, *Mod. Phys. Lett.A* (**10**) No.7 (1995) 587-595.
22. N. Mankoč Borštnik, "Unification of all interactions in Grassmann space, invited talk", Proceedings of the 7th Adriatic meeting on particle physics, Brioni, 13-20 Sept.1994, *Perspective in Particle Physics* 94, Ed. by D. Klabučar, I. Picek, D. Tadić, World Scientific(1995), Singapore, p. 291-303.
23. N.S. Mankoč Borštnik, "Spin-charge-family theory is offering next step in understanding elementary particles and fields and correspondingly universe", Proceedings to the Conference on Cosmology, Gravitational Waves and Particles, IARD conferences, Ljubljana, 6-9 June 2016, The 10th Biennial Conference on Classical and Quantum Relativistic Dynamics of Particles and Fields, *J. Phys.: Conf. Ser.* 845 012017 [arXiv:1409.4981, arXiv:1607.01618v2].
24. N.S. Mankoč Borštnik, "The attributes of the Spin-Charge-Family theory giving hope that the theory offers the next step beyond the Standard Model", Proceedings to the Conference on Cosmology, Gravitational Waves and Particles, IARD conferences, Prague, 1-4 June 2020, The 12th Biennial Conference on Classical and Quantum Relativistic Dynamics of Particles and Fields, sent to publisher.
25. N.S. Mankoč Borštnik, "Matter-antimatter asymmetry in the *spin-charge-family* theory", *Phys. Rev. D* **91** (2015) 065004 [arXiv:1409.7791].
26. N.S. Mankoč Borštnik, D. Lukman, "Vector and scalar gauge fields with respect to $d = (3 + 1)$ in Kaluza-Klein theories and in the *spin-charge-family* theory", *Eur. Phys. J. C* **77** (2017) 231.
27. N. S. Mankoč Borštnik, "How far has so far the Spin-Charge-Family theory succeeded to explain the Standard Model assumptions, the matter-antimatter asymmetry, the appearance of the Dark Matter, the second quantized fermion fields..., making several predictions", Proceedings to the 23rd Workshop "What comes beyond the standard models", 4 - 12 of July, 2020 Ed. N.S. Mankoč Borštnik, H.B. Nielsen, D. Lukman, DMFA Založništvo, Ljubljana, December 2020, [arXiv:2012.09640]
28. N.S. Mankoč Borštnik, "The *spin-charge-family* theory explains why the scalar Higgs carries the weak charge $\pm \frac{1}{2}$ and the hyper charge $\mp \frac{1}{2}$ ", Proceedings to the 17th Workshop "What comes beyond the standard models", Bled, 20-28 of July, 2014, Ed. N.S. Mankoč Borštnik, H.B. Nielsen, D. Lukman, DMFA Založništvo, Ljubljana December 2014, p.163-82 [arXiv:1502.06786v1] [arXiv:1409.4981].
29. N.S. Mankoč Borštnik N S, "The spin-charge-family theory is explaining the origin of families, of the Higgs and the Yukawa couplings", *J. of Modern Phys.* **4** (2013) 823 [arXiv:1312.1542].
30. N.S. Mankoč Borštnik, H.B.F. Nielsen, "The spin-charge-family theory offers understanding of the triangle anomalies cancellation in the standard model", *Fortschritte der Physik, Progress of Physics* (2017) 1700046.
31. N.S. Mankoč Borštnik, "The explanation for the origin of the Higgs scalar and for the Yukawa couplings by the *spin-charge-family* theory", *J.of Mod. Physics* **6** (2015) 2244-2274, <http://dx.org./10.4236/jmp.2015.615230> [arXiv:1409.4981].
32. N.S. Mankoč Borštnik and H.B. Nielsen, "Why nature made a choice of Clifford and not Grassmann coordinates", Proceedings to the 20th Workshop "What comes beyond the standard models", Bled, 9-17 of July, 2017, Ed. N.S. Mankoč Borštnik, H.B. Nielsen, D. Lukman, DMFA Založništvo, Ljubljana, December 2017, p. 89-120 [arXiv:1802.05554v1v2].
33. N. S. Mankoč Borštnik, "How do Clifford algebras show the way to the second quantized fermions with unified spins, charges and families, and to the corresponding second quantized vector and scalar gauge fields", Proceedings to 24th Bled Workshop "What

- Comes beyond the Standard Models”, 2021, Založništvo DMFA, Ljubljana, December 2021, [arxiv:].
34. N.S. Mankoč Borštnik, H.B.F. Nielsen, *J. of Math. Phys.* **43**, 5782 (2002) [arXiv:hep-th/0111257].
 35. N.S. Mankoč Borštnik, H.B.F. Nielsen, “How to generate families of spinors”, *J. of Math. Phys.* **44** 4817 (2003) [arXiv:hep-th/0303224].
 36. N.S. Mankoč Borštnik, H.B.F. Nielsen, “New way of second quantized theory of fermions with either Clifford or Grassmann coordinates and *spin-charge-family* theory ” [arXiv:1802.05554v4,arXiv:1902.10628].
 37. N.S. Mankoč Borštnik, H.B.F. Nielsen, “Understanding the second quantization of fermions in Clifford and in Grassmann space” *New way of second quantization of fermions — Part I and Part II*, Proceedings to the 22nd Workshop “What comes beyond the standard models”, 6 - 14 of July, 2019, Ed. N.S. Mankoč Borštnik, H.B. Nielsen, D. Lukman, DMFA Založništvo, Ljubljana, December 2019, [arXiv:1802.05554v4, arXiv:1902.10628].
 38. N.S. Mankoč Borštnik, “The attributes of the Spin-Charge-Family theory giving hope that the theory offers the next step beyond the Standard Model”, Proceedings to the 12th Bial Conference on Classical and Quantum Relativistic Dynamics of Particles and Fields IARD 2020, Prague, 1 – 4 June 2020 by ZOOM.
 39. M. Breskvar, D. Lukman, N. S. Mankoč Borštnik, “On the Origin of Families of Fermions and Their Mass Matrices — Approximate Analyses of Properties of Four Families Within Approach Unifying Spins and Charges”, Proceedings to the 9th Workshop “What Comes Beyond the Standard Models”, Bled, Sept. 16 - 26, 2006, Ed. by Norma Mankoč Borštnik, Holger Bech Nielsen, Colin Froggatt, Dragan Lukman, DMFA Založništvo, Ljubljana December 2006, p.25-50, hep-ph/0612250.
 40. G.regar, M. Breskvar, D. Lukman, N.S. Mankoč Borštnik, “Families of Quarks and Leptons and Their Mass Matrices”, Proceedings to the 10th international workshop “What Comes Beyond the Standard Model”, 17 -27 of July, 2007, Ed. Norma Mankoč Borštnik, Holger Bech Nielsen, Colin Froggatt, Dragan Lukman, DMFA Založništvo, Ljubljana December 2007, p.53-70, hep-ph/0711.4681.
 41. G.regar, M. Breskvar, D. Lukman, N.S. Mankoč Borštnik, “Predictions for four families by the Approach unifying spins and charges” *New J. of Phys.* **10** (2008) 093002, hep-ph/0606159, hep-ph/07082846.
 42. A. Borštnik Bračič, N. S. Mankoč Borštnik, “On the origin of families of fermions and their mass matrices”, hep-ph/0512062, *Phys. Rev. D* **74** 073013-28 (2006).
 43. G.regar, N.S. Mankoč Borštnik, “The new experimental data for the quarks mixing matrix are in better agreement with the *spin-charge-family* theory predictions”, Proceedings to the 17th Workshop “What comes beyond the standard models”, Bled, 20-28 of July, 2014, Ed. N.S. Mankoč Borštnik, H.B. Nielsen, D. Lukman, DMFA Založništvo, Ljubljana December 2014, p.20-45 [arXiv:1502.06786v1] [arxiv:1412.5866].
 44. N. Mankoč Borštnik, “Unification of spins and charges”, In. *J. of Theor. Phys.* **40** (2001) 315-338.
 45. G.regar, N.S. Mankoč Borštnik, “Does dark matter consist of baryons of new stable family quarks?”, *Phys. Rev. D* **80**, 083534 (2009), 1-16
 46. G.regar, N.S. Mankoč Borštnik, “The new experimental data for the quarks mixing matrix are in better agreement with the *spin-charge-family* theory predictions”,
 47. A. Hernandez-Galeana and N.S. Mankoč Borštnik, “The symmetry of 4×4 mass matrices predicted by the *spin-charge-family* theory — $SU(2) \times SU(2) \times U(1)$ — remains in all loop corrections”, Proceedings to the 21st Workshop “What comes beyond the standard models”, 23 of June - 1 of July, 2017, Ed. N.S. Mankoč Borštnik, H.B. Nielsen, D. Lukman, DMFA Založništvo, Ljubljana, December 2018 [arXiv:1902.02691, arXiv:1902.10628].

48. N.S. Mankoč Borštnik, H.B.F. Nielsen, "Do the present experiments exclude the existence of the fourth family members?", Proceedings to the 19th Workshop "What comes beyond the standard models", Bled, 11-19 of July, 2016, Ed. N.S. Mankoč Borštnik, H.B. Nielsen, D. Lukman, DMFA Založništvo, Ljubljana December 2016, p.128-146 [arXiv:1703.09699]. Proceedings to the 17th Workshop "What comes beyond the standard models", Bled, 20-28 of July, 2014, Ed. N.S. Mankoč Borštnik, H.B. Nielsen, D. Lukman, DMFA Založništvo, Ljubljana December 2014, p.20-45 [arXiv:1502.06786v1] [arxiv:1412.5866].
49. D. Lukman, N.S. Mankoč Borštnik and H.B. Nielsen, "An effective two dimensionality cases bring a new hope to the Kaluza-Klein-like theories", *New J. Phys.* 13:103027, 2011.
50. T.Troha, D. Lukman, N.S. Mankoč Borštnik, "Massless and massive representations in the *spinor technique*", *Int. J Mod. Phys. A* **29**, 1450124 (2014).
51. D. Lukman and N.S. Mankoč Borštnik, "Families of spinors in $d = (1 + 5)$ with a zweibein and two kinds of spin connection fields on an almost S^2 ", Proceedings to the 15th Workshop "What comes beyond the standard models", Bled, 9-19 of July, 2012, Ed. N.S. Mankoč Borštnik, H.B. Nielsen, D. Lukman, DMFA Založništvo, Ljubljana December 2012, 157-166, [arXiv:1302.4305, arXiv:1412.5826, arXiv:1502.06786].
52. D. Lukman and N.S. Mankoč Borštnik, "Spinor states on a curved infinite disc with non-zero spin-connection fields", *J. Phys. A: Math. Theor.* 45:465401, 2012 [arxiv:1205.1714, arxiv:1312.541, arXiv:hep-ph/0412208 p.64-84].
53. N.S. Mankoč Borštnik, H.B. Niesen, "Particular boundary condition ensures that a fermion in $d=1+5$, compactified on a finite disk, manifests in $d=1+3$ as massless spinor with a charge $1/2$, mass protected and chirally coupled to the gauge field", hep-th/0612126, arxiv:0710.1956, *Phys. Lett. B* **663**,265-269 [hep-th/0612126, arxiv:0710.1956].
54. A. Ceccucci (CERN), Z. Ligeti (LBNL), Y. Sakai (KEK), Particle Data Group, Aug. 29, 2014 [<http://pdg.lbl.gov/2014/reviews/rpp2014-rev-ckm-matrix.pdf>].
55. Review of Particle, Particle Data Group, P.A. Zyla, R.M. Barnett, J. Beringer, O. Dahl, D.A. Dwyer, D.E. Groom, C -J. Lin, K.S. Lugovsky, E. Pianori ..., Author Notes, Progress of Theoretical and Experimental Physics, Volume 2020, Issue 8, August 2020, 083C01, <https://doi.org/10.1093/ptep/ptaa104>, 14 August 2020.
56. B. Belfatto, R. Beradze, Z. Berezhiani, "The CKM unitarity problem: A trace of new physics at the TeV scale?", [arXiv:1906.02714].
57. N.S. Mankoč Borštnik, M. Rosina, "Are superheavy stable quark clusters viable candidates for the dark matter?", *International Journal of Modern Physics D (IJMPD)* **24** (No. 13) (2015) 1545003.
58. A. Hernandez-Galeana and N.S. Mankoč Borštnik, "The symmetry of 4×4 mass matrices predicted by the *spin-charge-family* theory — $SU(2) \times SU(2) \times U(1)$ — remains in all loop corrections", Proceedings to the 21st Workshop "What comes beyond the standard models", 23 of June - 1 of July, 2018, Ed. N.S. Mankoč Borštnik, H.B. Nielsen, D. Lukman, DMFA Založništvo, Ljubljana, December 2017 [arXiv:1902.02691, arXiv:1902.10628].
59. H. Fritzsch and P. Minkowski, *Ann. Phys.* **93** (1975) 193.
60. R. Bernabei et al, "First model independent results from DAMA/LIBRA-phase2" [arXiv:1805.10486v2].



18 Novel String Field Theory and Bound State, Projective Line, and sharply 3-transitive group

H.B. Nielsen^{1**}

e-mail: hbech@nbi.ku.dk

M. Ninomiya²

e-mail: msninomiya@gmail.com

¹ Niels Bohr Institute, University of Copenhagen, Blegdamsvej 17, 2100 Copenhagen, Denmark

² Yukawa Institute for Theoretical Physics, Kyoto University, Kyoto 606-0105, Japan; Yuji Sugawara Lab., Shiga-prefecture, Science and Engineering, Department of Physics Sciences, Ritumeikan university, Japan

Abstract. Using ideas from our long studied Novel String Field Theory we consider in this article a bound state of infinitely many constituents, something that at least very approximately could mean a hadron, since hadrons have typically very many constituents. Our main point, so far, is to speculate that there should be a very high degree of symmetry between the many constituents, since the constituents behave similarly at different places in the bound state. We assume speculatively that there is a group represented sharply 3-transitively as permutation of the constituents; one can namely only have *finite* number of elements sharply n -transitively permuted for n larger than 3. The scattering of such bound states will in the zero Bjorken x limit (which is suggested) only occur by exchange of parts of the system of constituents, quite like in our Novel String field Theory the “objects” are exchanged in bunches. The cyclically ordered chain of objects in this Novel String Field Theory are identified as a projective line structure. Also a p -adic field is a natural possibility.

Povzetek: Autorja postavljata novo teorijo strun, ki jo sestavljajo bodisi fermioni bodisi bozoni, ki ne interagirajo in se vendar sipajo. V tem prispevku želita posplošiti svoj prvotni predlog za struno iz neinteragirajočih delcev (polj) na splošnejše objekte, ki so vezana stanja velikega števila objektov, v struno strun. Primer takega sistema je vezano stanje velikega števila hadronov, ki imajo enake lastnosti v vseh delih vezanega stanja. Predpostavita 3-transitivnost, pri kateri se izmenjujejo sklopi delcev. Ciklično urejene verige hadronov imajo projektivno enodimenzionalno strukturo, dopušča pa ta nova teorija strun tudi p -adična polja.

PACS numbers: 11.25.-w, 11.27td, 11.10.-2, 03.70.tk, 11.25.

** Speaker: Talk presented in 24th Bled-Workshop “What comes beyond the Standard Models” Bled, July 3-11, 2021, Slovenia

18.1 Introduction

18.1.1 Bound State with Infinitely Many Constituents

For a bound state [1] of infinitely many constituents you would at first expect that the momentum of such a bound state would be shared evenly, so that each constituent would have a negligible part of the total momentum of the bound state. This is of course not safe, since a small part of the constituents might carry the bulk of the momentum, but then the majority of constituents would carry even less. One usually talks about a Bjorken- x [2] defined for each constituent and denoting the (average) fraction of the bound state momentum carried by that constituent.

Scattering of Constituent on Constituent Not Important for Many Constituents

If the single constituents carry only infinitesimally small fraction of the momentum of the bound state, the scattering of one constituent in one bound state with one in another bound state would not be much connected to the scattering of the two bound states.

Rather **scattering of bound states on each other would be dominated by one bound state exchanging a bunch of constituents with the other bound state.**

Scattering by Exchange of Constituents

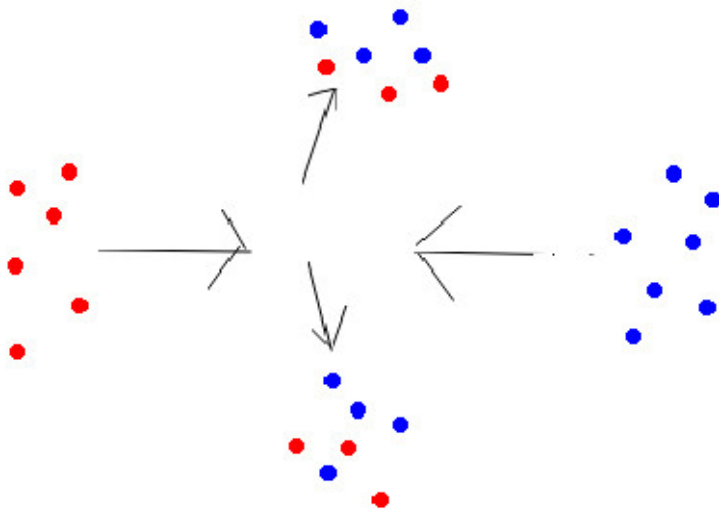


Fig. 18.1: **Scattering by Exchange of Constituents** This figure illustrates the scattering of two bound states with (infinitely) many constituents marked in the one as blue and in the other bound state as red. After the scattering there appears again two bound states, but now notice that both of them have partly blue-marked and red-marked constituents. This we may call an “exchange of parts of the constituents”-scattering.

A Motivation for People Interested in making Higher Dimensional Theories: It is wellknown: You do not have genuine renormalizable quantum field theories in higher than 3+1 dimensions.
 However Exception: A very bad scalar theory with ϕ^3 -interaction in up to 5+1, and **completely free theories**.

18.1.2 Novel String Field Theory of Ours

According to the Novel String Field Theory of ours [3,6], which we shall go a bit into later, (super)string theory can be considered a **completely free theory!**
“exchange of parts of constituents”-scattering known from our Novel String Field Theory

In our novel string field theory, on which we worked much earlier, the strings are - somewhat similarly, but differently, to/from C. Thorn's [5] string bit resolution of the string into “bits” (constituents) - described by means of “objects”. After scattering of a couple of strings (almost, except for a null-set) all the objects from the initial strings are either refound in the final state strings or recognized as having been annihilated. Although we can consider the “objects” constituents, they do not scatter on each other, but rather do not interact at all.

18.2 Motivation

18.2.1 Motivation and Plan

- Interpret the great feature of string theory to be that it is indeed - in our Novel String field theory - a basically free and therefore solvable theory, so that even no divergence problems appear.
- Ask if we can generalize such a string theory, still clinging the idea that the “constituents” (identified with our “objects”) do not interact under the scattering of the strings (identified as “bound states”).
- Thereby getting e.g. meaningfull (renormalizable) theories in higher than 3+1 dimensions.

18.2.2 This work especially: Generalize Möbius Transformations

Our series of objects making up so to say an open string in our novel string field theory are organized in what we call a cyclically ordered chain, which is topologically a circle. It has in fact a “natural” symmetry under a Möbius group, as we shall explain, and can also be considered a projective line (meaning a line as in projective geometry, in which one adds to the lines an extra “point at infinity”, so that the line topologically becomes a circle rather than a usual line).

As a major part of the presentation we like to seek to go back from a very general group being analogous to the Möbius group to see to what extend we can reconstruct projective line for some field (in the sense of the algebraic structure with unit element and invertibility for both a multiplication and an addition).

Reminder of: Möbius transformations in Veneziano model and string theory [4]

From very early times in string theory and Veneziano model theory the Möbius transformations has shown up. In fact physicists [7] were so kind as to call the variable in the formulation of the Veneziano model with some extra variables so that the formulation became precisely invariant under Möbius transformations Koba-Nielsen variables.

What is Möbius transformations ? A priori the Möbius transformations are defined as transformations of the extended complex number set $\mathbf{C} \cup \{\infty\}$ of the complex numbers with a number ∞ added, a set equivalent to the complex projective line \mathbf{CP}^1 given by the transformation function

$$z \rightarrow f(z) = \frac{az + b}{cz + d}, \quad (18.1)$$

but shall in the present article be more interested just in the real number version transforming only $\mathbf{R} \cup \{\infty\}$, and with the constants a, b, c, d being real numbers.

18.3 Novel SFT

How we thought in our Novel String Field Theory in the present Articles: We used the splitting of the position variable field on the string into left and right-moving parts

$$X^\mu(\sigma, \tau) = X_R^\mu(\tau - \sigma) + X_L^\mu(\tau + \sigma), \quad (18.2)$$

where σ is the "spatial" coordinate enumerating the points along the string and τ a "time" for the single string, both arranged in the conformal gauge, meaning they have been partially gauge chosen so that the Lagrangian simplified to a usual 1+1 dimensional massless scalar for each value of the external index μ enumerating the imbedding space dimensions 25+1. .

18.3.1 Crucial Feature of Our Novel String Field Theory, Use X_R and X_L .

Our approach was to discretize into small pieces - analogous to the string bits by Charles Thorn, who used the full X - in the variables on which these X_R and X_L only depends, namely $\tau - \sigma$ and $\tau + \sigma$ respectively. This means that **we** contrary to C. Thorn discretize into pieces variables which are not a priori physically enumerating the material of which the string consists, but a priori could be just formal parameters enumerating some degrees of freedom of the system(=the string). Therefore a priori we could not be sure if the "objects" corresponding to the small pieces in variables $\tau - \sigma$ or $\tau + \sigma$ can be considered "constituents".

By Changing The Physical Interpretation a bit, the "Objects" may be however be perceived as Constituents. A priori the "objects" are associated only with half the degrees of freedom of a string bit - namely only the right or the left moving d.o.f. - are **not** genuine constituents. If you speculate that **the string is just a smart way of looking at it, but not necessarily the only way**, then we may speculate physically to split up a string bit (as by C. Thorn) into two physically separate

objects, a right and a left. Since the two, when interpreted as the “objects” do not interact, are not really needed to be considered the same constituent, we can then make the physical speculation, or interpretation rather, that the two “objects” for same string bit are two quite independent **constituents**.

So we are allowed to **take it that the “objects” are constituents**.

18.3.2 Objects describing strings

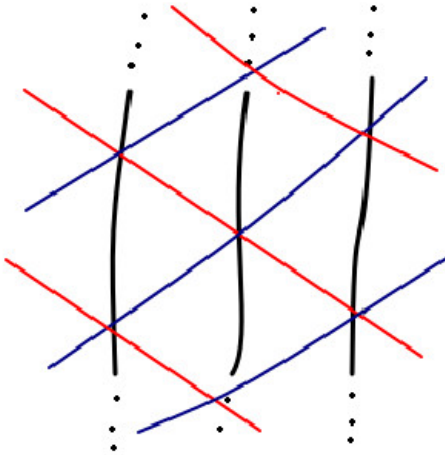


Fig. 18.2: How strings are seen as crossing places of the objects being Constituents Representing Strings Locally.

The figure shall illustrate how two kinds of “objects” denoted by red and blue colored lines telling their path through space (respectively R and L), when flowing through space in long series - infinitesimally close to the neighbors -can represent/look like a string moving with lower velocity.

The “objects” move with velocity of light - actually they are free so they never change even direction -, but the string seemingly there move typically slower. The string at one moment is just where the objects meet at that moment.

The strings are just some way of seeing the objects.

18.3.3 Philosophy of Looking at String Theory in this Talk:

String Theory is a successful theory in higher dimensions because it is actually - according to our Novel String Field Theory - **a free theory**, so that it is, one can say, renomalizable even in higher dimensions. The “ objects” are free massless particles.

String Versus Novel Object Chains? Is there a truth? We claim that there seemingly are **two different ways** of imagining the strings in string theory:

- 1. The **strings** are the true physical objects.
- 2. The **chains of "objects"** are the true physical objects.

You may of course claim, that if we are right that the two ways of looking at it are equivalent, then both are right!

But you could also begin to find argument, that one viewpoint is better or more true than the other one:

In a moment we shall give a couple of weak arguments, that the **chains of objects are more true!**

Mysterious in String Theory: Cross sections for End and String crossing are same order of magnitude?

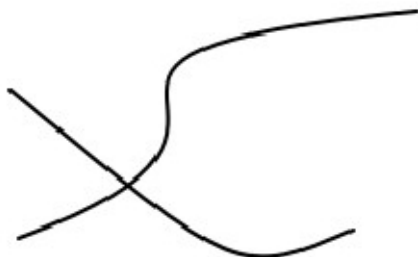


Fig. 18.3: On this figure you should imagine that the two strings truly cross each other in the sense of going through the same point. This type of hitting each other of two strings is more likely than that they should just hit each other just with the end points

You expect End hitting much more unlikely than hitting of proper string bulk

- For two sticks or strings you expect the cross section for that they hit to be of the order of the product of their length.
- But two genuine point particles will have in principle zero cross section for hitting each other.

Thus we are forced to make a **Conclusion:**

Something wrong with string interpretation!

Can Vacuum Extensions of String Tails Solve Mystery by one string having an end common with another without knowing Scattering of two circular chains (of "objects") always goes with two local interactions of the chains

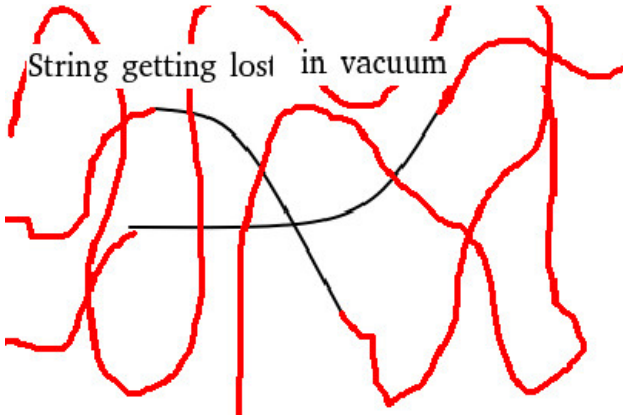


Fig. 18.4: This figure illustrates how one may think, that all the strings continue into being virtually present in the vacuum, so that although we at first think of strings being like particles located to a place and moving around, then in fact these phenomenological strings have indeed tails continuing out as virtual present string-material present virtually in the vacuum (which is of course in all quantum (field) theories a very complicated state). We call this possible phenomenon of virtual string pieces in vacuum “Strings lost in vacuum”.

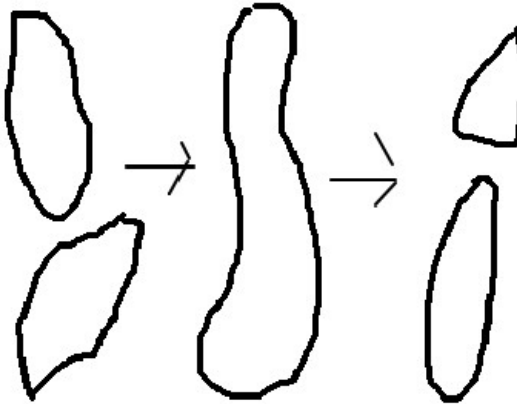


Fig. 18.5: Here we illustrate how two cyclically ordered chains of objects (to the left) becomes two other cyclically ordered objects (to the right) via two steps of local modification. First - illustrated by the left-most of the two arrows - the two cyclically ordered chains on the left side by a single local combination becomes the single cyclically ordered chain illustrated in the middle. Next this single cyclically ordered chain touches itself and thereby split into the two cyclically ordered chains illustrated on the right-most.

18.4 Generalizing

It Would be Wonderful to Generalize String Theory, Now we say it is Free

Basically as soon as you calculate scatterings by approximating that all constituents continue without interacting, you are in our present sense generalizing string theory.

So bound states of very many constituents so as each of them having very little momentum share are scattering as a generalization of the strings seen as composed from objects.

18.5 Symmetry

Symmetry

If a bound state or an almost bound state consists of infinitely many constituents, then one will, unless there are infinitely many types of particles, expect that most of the constituents are in many ways very similar in their way of sitting in the bound state.

One thus expects a large amount of symmetry between the constituents.

An idea to implement this expectation is to postulate a group of transformations of the constituents into each other, under which the "structure" of the bound state is invariant.

Much Transformations / Much Symmetry High n Transitivity

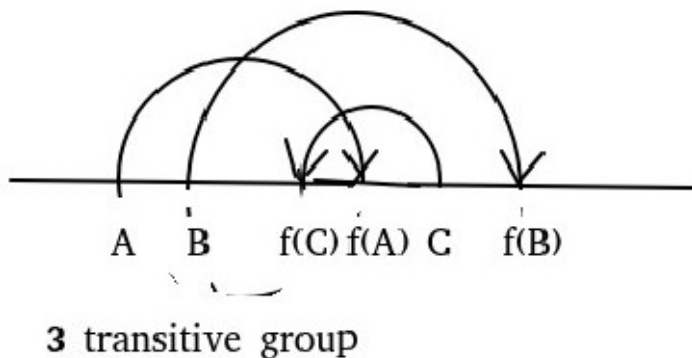


Fig. 18.6: The horizontal line here illustrates the set on which a group G acts sharply 3-transitively meaning that there is a unique (that is what "sharply" means) group element f mapping the three points A , B , and C into three given points $f(A)$, $f(B)$, and $f(C)$ (that is what means it is 3-transitive).

18.5.1 3-transitive group action

We say the group G acts on the space S n -transitively, when you for every n points A, \dots, K can find a group element $f \in G$ transforming these n into n prescribed image points [11, 12]. We call it “sharply”, when the group element achieving that is unique.

$$\text{Any } f \in G \tag{18.3}$$

$$\text{acts } f : S \rightarrow S \tag{18.4}$$

$$\text{For any } n \text{ points } A, \dots, K \tag{18.5}$$

$$\text{and another set of } n \text{ points } A', \dots, K' \quad \text{there exists } f \tag{18.6}$$

$$\text{so that } f(A) = A' \tag{18.7}$$

$$\vdots \tag{18.8}$$

$$f(K) = K' \tag{18.9}$$

18.5.2 Zassenhaus theorem, that is a not quite true theorem on 3-transitive transformations

A mathematical article by Katrin Tent, Advances in Mathematics Volume 286, 2 January 2016, Pages 722-728, begins:

“The finite sharply 2- and 3-transitive groups were classified by Zassenhaus in [17] in the 1930’s and were shown to arise from so-called near-fields. They essentially look like the groups of affine linear transformations $x \rightarrow ax + b$ or Moebius transformations $x \rightarrow \frac{ax+b}{cx+d}$, respectively.”

18.5.3 Our own Zassenhaus-like theorem:

Thinking instead Zassenhaus finite groups on infinite ones:

A set on which transforms a group in a sharply 3-transitive way will be a projective line corresponding to some field F and the transformations under the group will be Möbius transformations $x \rightarrow \frac{ax+b}{cx+d}$ with the variable enumerating the points on the “projective line” x as well as the constants a, b, c, d of the transformation (group element) belong to the field F .

Planning to “derive” this our own theorem, like Zassenhaus

We should at least reconstruct the field of real numbers \mathbf{R} in the case we consider the Möbius transformations of the real projective line $\mathbf{R} \cup \infty$ as the sharply 3-transitive group of transformations.

First step in Reconstructing the Field F from the Group of sharply 3-transitive transformations

Choose a point in the set S being transformed sharply 3-transitive under the group G and call it ∞ . Then look for the subgroup G_1 of the group G consisting of the

elements in G with only one fixed point in S , being ∞ , (and of course also the unit element in G)

The idea is to identify the subgroup G_1 having ∞ as the only fix point with the additive group of the field F to be found. The group multiplication in G_1 inherited from G of course shall be written with $+$.

(Say $y, z \in (G_1, *)$, then $y * x = y + z$).

(Here $*$ is the group multiplication in G .)

Second Step in Derivation, Identify Scalngs from Two Fix-point Transformations

Next we notice that by requiring just one more fixed point than the ∞ we get (at least in the true Möbius case) a group of scalings of the “numbers” (the elements in G_1) around a certain number. We might call the second fix-point 0 and a similarity transformation of G_1 (the subgroup with one fix-point) by one m in the group leaving 0 and ∞ say G_2 , (so $m \in G_2$) say the similarity transformation

$$y \in G_1 \rightarrow m * y * m^{-1} \in G_1 \tag{18.10}$$

$$\text{would be called } y \rightarrow m \cdot y. \tag{18.11}$$

This would first be a multiplication with an $m \in G_2$.

Third step, Get Identification of G_2 with G_1 by Selecting Point in S to call 1

A priori the subgroup G_1 leaving ∞ and no other points in S invariant, is of course different from the subgroup G_2 of elements in the 3-transitive transformation group of S , which we called G having only two invariant points ∞ and $0 \in S$.

We may, however, choose a third point $1 \in S$ (just in a few lines we call it explicitly $1_{in S}$, because we want to use the notation 1 also for an element in G_1 , which we must then call $1_{in G_1}$ to distinguish) different from the two points ∞ and $0 \in S$ and define a correspondence:

$$y \in G_1 \sim m_y = m \text{ so that } y = m \cdot 1 = m * 1 * m^{-1} \tag{18.12}$$

(here we needed a $1 \in G_1$, but we can make a corresponding 1 in S as $1_{in S} = 1_{in G_1}(0)$. Remember that $1_{in G_1}$ is indeed an element in subgroup G_1 of G and thus a map $1_{in G_1} : S \rightarrow S$ so that it makes sence to take the image of an element in S , namely $0 \in S$).

18.6 Why just sharply 3-transitive? A good question.

Above we went to consider just sharply 3-transitively acting symmetries as the symmetry required for the system of constituents of the bound state with very many consituents and very much symmetry. It was done in the spirit that 3 was a high number, when we talk about sharp transitivity. But is it a high number, and why just 3?

The answer is that this 3 is indeed the highest transitivity one can have, if one wants the set on which the group acts to be infinite.

Jordan [11] classified, that finite quadruply transitive group in which only the identity fixes four letters must be one of the following groups: the symmetric group of four or five letters, the alternating group of six letters or the Mathieu

group [13] on eleven letters. In a work by Marshall Hall [12] we find this work slightly extended and especially implying that **there is no infinite set on which a group acts sharply 4-transitively.**

Thus in our search for a bound state consisting of infinitely many or at least more than 11 constituents (the Mathieu group case; we shall not here tell exactly what a Mathieu group is) we simply cannot find any sharply 4-transitive group acting on it. We must be satisfied at most with a 3-transitive.

18.7 Wavefunction?

No Interaction: What determines the Wavefunction?

If we either assume or approximate away the interaction between the constituents, then what can determine the wave function?

Usually the wave function of a bound state in non-relativistic physics is given as an eigenfunction of a Hamiltonian

$$H\psi(\text{“constituent-positions”}) = E\psi(\text{“constituent-positions”}) \quad (18.13)$$

But relativistically one has to use the Nambu-Bethe-Salpeter equation [1], which is analogous to this eigenvalue equation for a bound state, where E is the energy of the bound state. **But if there is no interaction the Hamiltonian H is just trivial (essentially 0) and of no help!**

Nambu-Bethe-Salpeter-equation

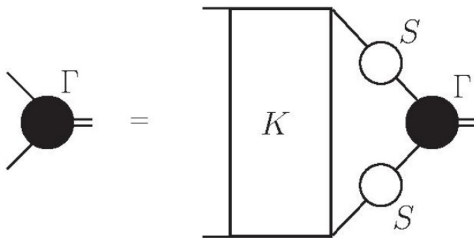


Fig. 18.7: Formal graphic writing of the Bethe-Salpeter equation with two constituents. The propagators with S are the propagators for the constituents, the black sphere Γ is the wave function for the bound state, and the block K symbolizes the interaction between the constituents. You may consider the Bethe-Salpeter-equation as analogous to the eigenvalue equation in the case of non-relativistic constituents. It is worth calling attention to, that while we for non-relativistic binding are accustomed to only describing the constituents by say their momenta (and the energy is only a consequence of that and it is positive energy for the constituent,) then here in the Nambu-Bethe-Salpeter equation the energy (or equivalently its conjugate x^0) is also formally a degree of freedom for the constituent. And the energy of the constituents can also be negative.

Alternatives to make Wavefunction (meaningful)

- Postulate a new law of nature on initial and even final conditions specifying the nature of allowed wave functions (to have e.g. the smooth chain character giving the string topologically)
- Say that you do not take non-interaction 100% serious but allow very short scale or high energy interactions.

This would be very realistic in higher dimensions than 3+1.

In fact couplings of a certain energy scale order of magnitude are very weak in higher dimensions (at low energy). So one might at low energy in higher dimensions only see the interactions as left over influence on the wave functions, but that would be negligible in the scatterings (at low energy).

Speculation of mainly Short Distance Interacting Particles in High Dimensions

- From dimensional arguments the interaction between particles in an effective quantum field theory in high dimension goes to zero for small energy scales. So the particles have only short range interactions.
- It is very easy that bound states can exist bound by the short range forces; but they will typically have interactions only at short distances too and high masses unless mass protected.
- If some bound states or “fundamental” particle, e.g. from being chiral fermions, are mass protected they will of course be massless until their symmetry protection somehow gets spoiled.

Speculation of mainly Short Distance Interacting Particles in High Dimensions (continued)

- But if they are of small extension - like fundamental scale - they will effectively not interact from a low energy scale point of view.
- Only if we have spatially largely extended bound states, can there be appreciable interactions at low energy scales.

18.8 Hamiltonian ?

There is a little not quite acceptable point in our “novel string field theory” consisting in, that we stress that there is no development or at least that “objects” behave freely - in fact the position moves in a trivial way if we identify a conjugate variable to what is essentially the momentum (called in our papers J) - but nevertheless we had also a paper [18] in which a Hamiltonian appeared, which gave the usual string spectrum. That of course cannot both be right: Either we have trivial or no development at all or we have the not completely trivial Hamiltonian formulated in our variables for the “objects”.

Here we must remind of an a bit technical detail in our novel string field theory:



Fig. 18.8: Here we have drawn a presumably very realistic picture of a bound state of many particles. Analysing perturbative quantum field theory you will typically find that each dressed particle consists of at first two constituents - so that the dressed particles are really bound states - but since when even further analysed, these will again turn out to consist of more constituents each, even the dressed particles come to consist of more and more constituents. So a picture with pairs forming again pairs and so on is very realistic for such perturbatively treated states. Such a picture with pairs forming pairs etc. is also very similar to what gets when the field we arrive at happens to be the 2-adic field.

Because variables the X_R and X_L which we used to take out the degrees of freedom for the "objects" do not commute with themselves taken at neighboring points of the variable such as $\tau - \sigma$ we had to after having divided the variable $\tau - \sigma$ into small pieces to include in the true representing objects only every second one of the pieces. That we formulated by saying we only take as the true objects the small pieces with an *even* number in the series along in the variable $\tau - \sigma$. Then the idea was to instead represent the odd numbered pieces as being proportional to the difference of the conjugate momenta to the variables on the even places.

Without going too much in detail with this problem of only using every second of the bits into which we cut the variable $\tau - \sigma$ we may tell that we obtained a Hamiltonian H which gives the energy of the string in say infinite momentum frame expressed by means of the momentum variable (which we called $J^\mu(I)$ and defined only for even values of the piece enumerating integer I) and the conjugate position variable (which we called $\Pi^\mu(I)$ again using only even I).

The crux of this writing down the Hamiltonian, that could give the string energy is that not only does it contain the for a free theory expected terms going with the square of the momenta, but it had also, namely corresponding to the odd pieces in

the chain which were of the form

$$(\Pi^i(I+1) - \Pi^i(I-1))^2 = (X_R^i(I+1) - X_R^i(I-1))^2 \text{ (for } I \text{ odd)} \quad (18.14)$$

Such terms look like interaction terms between the neighboring even numbered “objects” and should not be allowed if we want to think of the model for the string as being a construction / a bound state made out of *non-interacting constituents*! Infact the Hamiltonian giving the usual energy of the string takes the form, for the Mass square M^2 :

$$M^2 = 2P^+P^- - \sum_{i=1}^{24} (P^i)^2 \quad (18.15)$$

$$= 2 \left(\sum_{I=0}^{N-1} J^+(I) \right) \left(\sum_{I=0}^{N-1} J^-(I) \right) \left(\frac{1}{2\pi\alpha'} \right)^2 \quad (18.16)$$

$$- \sum_{i=1}^{24} \left(\sum_{I=0}^{N-1} J^i(I) \right)^2 \frac{1}{(2\pi\alpha')^2} \quad (18.17)$$

in infnite momentum frame, where the summation I runs over the objects as sitting along the cyclically ordered chain (identified with the projective line discretized) and i over the transverse dimenisions, while the infinite momentum frame co-ordinates denoted with index $+$ and the index $-$ take care of the longitudinal momentum and of the energy.

In our works on the novel string field theory we make in order to not have too many degrees of freedom in the description with the “objects” the trick of replacing the odd I objects present at first by an expression in terms of the conjugate momenta for the even I variables $J^\mu(I)$, (for the transverse coordinates i say)

$$J^i(I) = -\pi\alpha' (\Pi^i(I+1) - \Pi^i(I-1)). \quad (18.18)$$

In this notation with only the even objects being taken as physical, while the odd ones are replaced by the conjugate of the neighbors the mass square may be rather written

$$M^2 = \frac{1}{(2\pi\alpha')^2} \sum_{i=1}^{24} \left(N \sum_{I=0}^{N-2} i_{\text{even}} (J^i(I))^2 - \sum_{K=0}^{N-2} k_{\text{even}} \sum_{I=0}^{N-2} i_{\text{even}} J^i(I) J^i(K) \right) + \frac{N}{4} \sum_{i=1}^{24} \sum_{I=1}^{N-1} i_{\text{odd}} (\Pi^i(I+1) - \Pi^i(I-1))^2 \quad (18.19)$$

For details on this kind of Hamiltonian expressions we refer to our work [18]. This kind of Hamiltonian expressions obviously has the problem of having the seeming interaction between the neighboring even numbered objects.

But then how can we keep up our claim of free constituents?

The idea to overcome this seeming contradiction in our description of our novel string field theory previously has to do with yet a technical point to which we must allude:

We had to impose a condition that the state of the cyclical chain of objects to make up the description of an open string should obey

$$J^i(I+1) \approx -\alpha' (\Pi^i(I+1) - \Pi^i(I-1)) \approx J^i(I-1) \text{ (here } i \text{ odd)} \quad (18.20)$$

where in our a bit stupid notation the momentum of an even object is denoted by $J^i(I)$ for I even and the corresponding position variable in our old notation is $\Pi^i(I)$ correspondingly, since the Π and the J are conjugate.

But now the way this approximate relation has to be implemented is by the *state* of the chain of objects has to be so as to full fill it.

So this relation relating the vector from one even object to the next in position space to the momenta of the two neighboring objects is a restriction on the state, one could say an intial state condition.

18.8.1 Rewritting the Hamiltonian

The crux of the matter of the idea to solve the just above explained seeming contradiction is to say:

As long as we are only interested in states of the system of “ objects” obeying the equation (18.20), we should at least approximately be allowed to use this condition (18.20) to substitute parts of the Hamiltonian as using it as an equation, and then one can easily compute that we can rewrite the wanted hamitonian to totally free one!

This then means that indeed we can claim that if we have series of infinitely many genuine particles (scalars in the simple case of the bosonic string) which are free - they do not interact - but are in such a states that they form a chain and further obey our constraint (18.20), then the free Hamiltonian can for such special states be replaced by the usual string Hamiltonian. So for the states of relevance we indeed get the usual energy spectrum well known for the strings, in spite of the fact that we take the cnstituent particles to be genuine particles that do not interact.

18.9 An Idea of a Picture

Let us here present the idea, that we should apply the present infinite constituent bound state picutre in a world in which the genuine physics theory is **higher dimensional** - as e.g. the model by Norma Mankoc Borstnik [15] - and that we in practice only see bound states of very many *mass protected particles* such as chiral fermions or gauge particles. For example in 4 dimensions a chiral fermion is described by spinor field $\psi(x)$ imposed the restriction

$$(\Gamma - 1)\psi(x) = 0 \tag{18.21}$$

$$\text{where } \Gamma \text{ is the chirality, the analogue of } \gamma_5. \tag{18.22}$$

Then at low energies there will be effectively no interactions, because the dimensionality of the coupling constants, κ say, would be of dimensions mass to negative powers. E.g. an intraction could be of the four fermion type

$$\mathcal{L}(x) = \kappa \bar{\psi}(x) \gamma_\mu \psi(x) * \bar{\psi}(x) \gamma^\mu \psi(x) + ... \tag{18.23}$$

$$[\kappa] = \left[\text{GeV}^{\text{“negative”}} \right] \tag{18.24}$$

$$\text{so } \kappa \approx 0 \text{ at low energies.} \tag{18.25}$$

So bound states of many such mass protected particles would have in the effective low energy scattering limit [14] no interactions, just as we discussed in the present article.

However, the initial - and even final - conditions for the bound states, which in the no interaction approximation need an extra explanation, could now be understood as **a left over from the high energy time, when the bound states were formed**. That is to say: Once upon a time in the time just after Big Bang, say, the coming constituents interacted because at high energies, the couplings - like κ - with negative power of mass dimensions would not be quite negligible. This interaction at high energy would bring the mass protected particles into bound state structures - once cooling takes place - , which would then survive into the colder times, when only the low energy approximation would be relevant, and the constituents would effective no longer interact.

If it happens that the surviving bound states are of the many constituent types, and they would obtain the symmetry properties speculated in the present article, they would, if the symmetry becomes the Møbius group with *real* numbers as the field, become real field projective lines, meaning circles topologically. That is to say, we would get the cyclically ordered chains of objects described in our earlier Novel String Field Theory [6]. If one would instead take the p-adic field, one (presumably) would obtain instead the p-adic Veneziano model scheme [8]. In any case in the here now suggested background model for our infinitely many constituent bound states, there would be a usual quantum field theory picture in higher dimensions behind, and the model should inherit the good physical properties from such a quantum field theory, although it would not be a renormalizable one. Only the low energy limit with only exchange of constituents interactions would be what one might call "renormalizable". Really it would in the most important case be string theory and that we would rather call "finite" than renormalizable, but the "finite" theories are, one could say, included in the renormalizable ones. By taking such an at high energy interacting scheme as the model behind our bound states one would get a more solid physical picture and could from this picture better understand how to treat e.g. the Nambu-Bethe-Salpeter-equation technique. In such a philosophy of the high dimensional theory behind one should have a good chance using Weinbergs effective field theory [14] thinking to see that the bound state scattering based on the Nambu-Bethe-Salpeter formalism [1] would lead to amplitudes acceptable from say axiomatic field theory [16] point of view. It thus looks as an outlook that we are close to having a scheme for making models for scattering amplitudes, that are physically acceptable.

18.9.1 Scale Symmetry

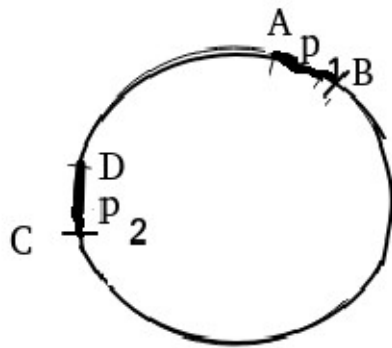
Let us note, that when we in the low energy limit have just the free mass protected, say chiral fermions or free "photons", then the theory is **scale invariant**. There are no dimensionized parameters left. So if it is as suggested string theory the dimensionized parameter α' in string theory cannot be in the low energy approximation proper, but can only come in via initial and final state conditions. That is to say here, that the Regge trajectory slope parameter α' can only come in by

having been inherited from the era, when it was hot and cooled down so that the dimensionized parameters such as κ were relevant.

18.9.2 Momentum Fluctuation in “Unexcited cyclically ordered system of objects/constituents”

At least for the unexcited bound state, but approximately for all in practice occurring bound states in the model, we should have that the momentum distribution for the constituents should be invariant under the Møbius transformations.

In the figure we see a drawing of the cyclically ordered chain equivalent to the



$$\langle p_1 p_2 \rangle = \text{coef.} \frac{AB * CD}{CB * AD} = \text{coef.} \cdot (A, C; B, D)$$

Fig. 18.9: Illustrated are the two small pieces AC and BD with respectively momenta p_2 and p_1 on the projective line drawn as a circle. We use the symbol $(A, C; B, D)$ for the anharmonic ratio, which in terms of e.g. distances counted with sign on the circle would be $(A, C; B, D) = \frac{AB * CD}{CB * AD} = \frac{AB}{CB} : \frac{AD}{CD}$.

real number projective line. The “four” (really we should call it d-momentum, because we consider here more than four dimensions in order to have the effective disappearance of the couplings) momentum p_1 and p_2 of the collection of the constituents sitting in the projective line in the two small (infinitesimally small) pieces AB and CD respectively have in the “ground state” of the bound state the

correlation

$$\langle p_1 p_2 \rangle = \text{coef.} * (A, C; B, D) \quad (18.26)$$

$$\text{where } (A, C; B, D) = \text{“anharmonic raatio”} \quad (18.27)$$

$$= \frac{AB * CD}{CB * AD} = \frac{AB}{CB} : \frac{AD}{CD}. \quad (18.28)$$

$$\text{or more precisely: } \langle p_1^\mu p_2^\nu \rangle = g^{\mu\nu} \cdot \text{coef.} * (A, C; B, D). \quad (18.29)$$

The form given by the anharmonic ratio is specified by the Möbius invariance under real numbers, because only the anharmonic ratios are invariant for four points. Here the pairs of letters like AB means the difference of the field F coordinate for B minus that for A. However, the coefficient coef. is an a priori unspecified constant. What the value shall be is only specified by the initial and final state information on the bound states we had to impose. In the picture of there being a short distance or high energy interaction underneath the coef. would inherit from such a short distance interaction. In the string theory with the open strings identified with our bound states this coefficient would be given by the Regge-slope α' ,

$$\text{coef.} \propto \frac{1}{\alpha'}. \quad (18.30)$$

It should be in mind that the scale symmetry is only broken by these initial and final state informations.

So the α' energy scale in the Veneziano model in our picture comes in via the initial and final state information, only.

18.10 The Cyclic ordering partly violates the full Möbius symmetry

We have to mention what formally looks like a little problem:

In our novel string field theory we had to impose the condition (18.20), which is **not invariant under shift of orientation along the cyclically ordered chain**. Formally such a condition would break the symmetry under half of the Möbius transformations. To have this condition consistent with the symmetry we should only keep those Möbius transformations, which leave the orientation along the chain or in the words of the present article along the projective line intact. This means that formally the group does not act 3-transitively, but only 3-transitively modulo the cyclic orientation.

But from what we could call an estetic point of view this only orientation keeping subgroup is quite nice in as far as it indeed lies inside the full Möbius group as a topologically seprate part, a component.

It might be needed in our building of the bound states from a high energy theory to let this one have sufficient breaking of its symmetries so as to deliver such bound states that the orientation gets fixed.

18.11 Conclusion

Conclusion

We have proposed an approximation applicable hopefully to some bound states: that they have so many constituents with so equally divided momenta - or better Bjorken x 's ≈ 0 [2] - that we can ignore the scattering of the constituents, when the bound states scatter.

(This means the constituents are in the approximation free, and thus the bound state not truly bound)

Conclusion Details

- Requiring High Symmetry in form of 3-transitive symmetry operation we expected - like Zassenhaus - the constituents to form a structure like a projective line $F \cup \{\infty\}$ for a field F . The string is the case $F = \mathbf{R}$ i.e. the field is the real number field. (Topologically the projective line is a circle.)
- We suggest that such string theory might be used when the approximation of many constituents with little momentum each becomes good. (of course string theory historically started as attempt to describe hadron physics [19])
- The p-adic theory [8] of Veneziano model is suggestively incorporated.

Acknowledgement

One of us (H.B.N.) acknowledges the Niels Bohr Institute for allowing him to work as emeritus and for partial economic support. Also thanks food etc. support from the Corfu conference and to Norma Mankoc Borstnik for asking for a way to get meaningful quantum field theories in higher than 4 dimensions. The thinking on hadronic like bound states could namely be looked upon as an attempt to find such a scheme using bound states as the theory behind the particles for which to make the convergent theory.

M. Ninomiya acknowledges Yukawa Institute of Theoretical Physics, Kyoto University, and also the Niels Bohr Institute and Niels Bohr International Academy for giving him very good hospitality during his stay. M.N. also acknowledges at Yuji Sugawara Lab. Science and Engineering, Department of physics sciences Ritsumeikan University, Kusatsu Campus for allowing him as a visiting Researcher.

References

1. Yichiro Nambu for earlier work Prog.Theoretical Phys. 5[4] 614 (1950) July-August. H. Bethe and E. Salpeter, "A relativistic Equation for bound state problem", Phys. Rev. 84, 1232 (1951)
2. J. Bjorken "Inelastic Electron-Proton and γ -Proton Scattering and the Structure of Nucleon, Phys.Rev.185 (1969)
3. H. B. Nielsen and M. Ninomiya, A New Type of String Field Theory, in Proceedings of the 10th Tohwa International Symposium in String Theory, July 3-7, 2001 Fukuoka Japan AIP conference Proc vol. 607 p. 185-201; arXiv: hep-th 0111240.v1, Nov.2001
H. B. Nielsen and M. Ninomiya, An idea of New String Field Theory - Liberating Right and Left movers, in Proceedings of the 14th Workshop, "What Comes Beyond the Standard Models" Bled July 11-21, 2011, eds. N. M. Borstnik, H. B. Nielsen and D. Luckman arXiv 1112. 542 [hep-th]
H. B. Nielsen and M. Ninomiya, "A Novel String Field Theory Solving String Theory by Liberating Left and Right Movers", JHEP_202P_05131.v2 (2013)'

4. As for bosonic string field theory in the light-cone gauge:
 M. Kaku and K. Kikkawa, Phys. Rev. D10(1974)110;
 M. Kaku and K. Kikkawa, Phys. Rev. D10(1974)1110;
 M. Kaku and K. Kikkawa, Phys. Rev. D10(1974) 1823;
 S. Mandelstam, Nucl. Phys. B64 (1973)205;
 E. Cremmer and Gervais, Nucl. Phys., B90 (1975) 410
 Witten type mid-point interaction of covariant string field theory for open string:
 E. Witten, Nucl. Phys. B268 (1986) 253.
5. R. Giles and C. B. Thorn, A lattice Approach to String Theory, Phys. Rev. D16 (1977) 366
 C.B. Thorn, On the Derivation of Dual Model from Field theory, Phys. Lett. 70B (1977) 85
 C. B. Thorn, On the Derivation of Dual Models from Field Theory 2, Phys. Rev. D17 (1978) 1073
 C. B. Thorn, Reformulating string theory with $1/N$ expansion, In Moscow 1991. Proceedings, Sakharov Memorial Lecture in Physics, Vol 1* 447 hep-th/9405069
 O. Bergman, C. B. Thorn, String Bit Model for Superstring, Phys. Rev. D52 (1995) 5980
 C. B. Thorn, Space from String Bits, JHEP11 (2014) 110
6. H. B. Nielsen (Bohr Inst.) and M. Ninomiya (Ritsumeikan U.) (2019) Contribution paper to 22nd Workshop on What comes Beyond the Standard Models p. 232-236
 H. B. Nielsen (Bohr Inst.) and M. Ninomiya (Ocami, Osaka City U.), "Novel String Field theory with also Negative Energy Constituents/Objects gives Veneziano Amplitude", JHEP 02(2018) 097, e-print: 1705.01739[hep-th]
 H. B. Nielsen and M. Ninomiya, "An Object Model of String Field Theory and Derivation of Veneziano Amplitude, published in Proc. of Corfu 2016 (2017) 134, arXiv 1705.01739.
 H. B. Nielsen and M. Ninomiya, "Instructive Review of Novel SFT with non-interacting constituents objects and the generalization to p-adic theory", Corfu Summer Institute 2019 "School and Workshops on Elementary Particle Physics and Gravity" (Corf 2019) 31. August - 25. September Corfu Greece, arXiv 2006.09546.
7. E.g.: J.L. Gervais "Operator Expression for the Koba-Nielsen Multi-Veneziano Formula and Gauge Identities" Nuclear Physics B21 (1970) 192-204.
 Masatsugu Minami "Modular Group and Non-cyclic Symmetry of the Veneziano Formula", Progress of Theoretical Physics, Vol.53,No.1,January 1975
8. Peter Freund and M Olson, "Non-archimedian strings", Physics Letters B 1992 (1987)
 I. Volovich, "p-adic space-time and string theory", Math. Phys. 71 574 -576 (1987)
 P. Freund and E. Witten, "Adelic string Amplitudes", Phys. Letter B 199 191 (1987)
9. "p-Adic, Adelic and Zeta Strings" Branko Dragovich, Institute of Physics, P.O. Box 57, 11001 Belgrade, SERBIA
10. Holger B. Nielsen, Masao Ninomiya, "Dirac Sea for Bosons. I: - Formulation of Negative Energy Sea for Bosons" Progress of Theoretical Physics, Volume 113, Issue 3, March 2005, Pages 603-624, <https://doi.org/10.1143/PTP.113.603>
 Holger B. Nielsen, Masao Ninomiya, "Dirac Sea for Bosons. II: - Study of the Naive Vacuum Theory for the Toy Model World Prior to Filling the Negative Energy Sea" — Progress of Theoretical Physics, Volume 113, Issue 3, March 2005, Pages 625-643, <https://doi.org/10.1143/PTP.113.625>
11. C. Jordan, Recherches sur les substitutions, J. Math. Pures Appl. (2) 17 (1872), 351-363
12. Marshall Hall "On a theorem of Jordan", <https://projecteuclid.org/download/pdf.1/euclid.pjm/1103044881>
13. C. Jordan, Journal de Mathématiques Pures et Appliquées (1872), Volume: 17, page 351-367, ISSN: 0021-7874

14. S. Weinberg, *Physica A*96, 327 (1979), Steven Weinberg, PoS(Proceedings of Science) (CD09)001 "Effective Field Theory, Past and Future".
15. Norma Mankoc Borstnik, See e.g. (other) contribution(s) in the present Proceedings to the 24th workshop on "What comes beyaond the Standard Models" in Bled.
16. Streater, R. F.; Wightman, A. S. (1964). "PCT, Spin and Statistics, and All That." New York: W. A. Benjamin. OCLC 930068;
Bogoliubov, N.; Logunov, A.; Todorov, I. (1975). "Introduction to Axiomatic Quantum Field Theory." Reading, Massachusetts: W. A. Benjamin. OCLC 1527225.
Araki, H. (1999). "Mathematical Theory of Quantum Fields". Oxford University Press. ISBN 0-19-851773-4.
17. Cambridge Togets in Mathematics Book 24 (English Edition);they are the five sporadic simple groups called M11, M12, M23, and M24, which multiple transitive groups on 11, 12, 22, 23 arzt objects
18. Holger B. Nielsen, Masao Ninomiya,arXiv:1211.1454v3 [hep-th] 28 May 2013 OIQP-12-10 "A Novel String Field Theory Solving String Theory by Liberating Left and Right Movers"
19. Nambu, Y. (1970). "Quark model and the factorization of the Veneziano amplitude." In R. Chand (ed.), *Symmetries and Quark Models: Proceedings of the International Conference held at Wayne State University, Detroit, Michigan, June 18–20, 1969* (pp. 269–277). Singapore: World Scientific.
Nielsen, H. B. "An almost physical interpretation of the dual N point function." Nordita preprint (1969); unpublished. Mentioned in: XVth INTERNATIONAL CONFERENCE ON HIGH ENERGY PHYSICS, KIEV, 1970.
Susskind, L (1969). "Harmonic oscillator analogy for the Veneziano amplitude". *Physical Review Letters*. 23 (10): 545–547. Bibcode:1969PhRvL..23..545S. doi:10.1103/physrevlett.23.545.
Susskind, L (1970). "Structure of hadrons implied by duality". *Physical Review D*. 1 (4): 1182–1186. Bibcode:1970PhRvD...1.1182S. doi:10.1103/physrevd.1.1182.



19 Atomic Size Dark Matter Pearls, Electron Signal

H.B. Nielsen^{1**}

email: hbech@nbi.dk

C.D.Froggatt²

email: Colin.froggatt@glasgow.ac.uk

¹ Niels Bohr Institute, Copenhagen, Denmark

² Glasgow University, Glasgow, UK

Abstract. We seek to explain both the seeming observation of dark matter by the seasonal variation of the DAMA-LIBRA data and the observation of “electron recoil” events at Xenon1T in which the liquid-Xe-scintillator was excited by electrons - in excess to the expected background - by the *same* dark matter model. In our model the dark matter consists of bubbles of a new type of vacuum containing ordinary atomic matter, say diamond, under high pressure ensured by the surface tension of the separation surface (domain wall). This atomic matter is surrounded by a cloud of electrons extending almost out to atomic size. We also seek to explain the self interactions of dark matter suggested by astronomical studies of dwarf galaxies and the central structure of galaxy clusters. At the same time we consider the interaction with matter in the shielding responsible for slowing the dark matter down to a low terminal velocity, so that collisions with nuclei in the underground detectors have insufficient energy to be detected. Further we explain the “mysterious” X-ray line of 3.5 keV from our dark matter particles colliding with each other so that the surfaces/skins unite. Even the 3.5 keV X-ray radiation from the Tycho supernova remnant is explained as our pearls hitting cosmic rays in the remnant.

What the DAMA-LIBRA and Xenon1T experiments see is supposed to be our dark matter pearls excited during their stopping in the shielding or the air. The most remarkable support for our type of model is that both these underground experiments see events with about 3.5 keV energy, just the energy of the X-ray line.

We get a good numerical understanding of the fitted cross section over mass ratio of self interacting dark matter observed in the study of dwarf galaxies. Also the total energy of the dark matter pearls stopped in the shield is reasonably matching order of magnitudewise with the absolute observation rates of DAMA-LIBRA and Xenon1T, although the proposed explanation of their ratio requires further development.

It should be stressed that accepting that the different phases of the vacuum could be realized inside the Standard Model, our whole scheme could be realized inside the Standard Model. So then no new physics is needed for dark matter!

Povzetek: Avtorja predlagata novo vrsto vakuuma, ki bi lahko pojasnila neujemanje med meritvama poskusov DAMA-LIBRA in Xenon1T. V njunem modelu imajo lastnosti *temne snovi* mehurčki v vakuumu, ki vsebuje običajno snov, recimo diamant, pod visokim tlakom, ki je posledica površinske napetosti med običajno snovjo in oblakom elektronov, velikosti atoma. S tem modelom razložita, zakaj je interakcija med konstituenti *temne snovi* tako

** Speaker at the Work Shop “What comes beyond the Standard Models” in Bled.

majhna, kako se *temna snov* upočasni pri interakciji z običajno snovjo v ščitu galaksije. Posledično ima temna snov majhno hitrost pri trkih z jedri v podzemskih detektorjih v soglasju z rezultati obeh poskusov. Podporo svojemu predlogu vidita avtorja tudi v tem, da pojasni hkrati rentgensko črto z energijo 3,5 keV v sevanju supernove Tycho in da experimenta DAMA/LIBRA in Xenon1T izmerita trke temne snovi prav pri energiji 3,5 KeV. Sipalna amplituda in gostota njune temne snovi se ujemata z izmerjenima, pri tem pa njun model ostaja znotraj *standardnega modela*.

19.1 Introduction

For a long time we have worked on a dark matter model [1–8], in which the dark matter consisted of cm-size pearls which were in fact bubbles of a new vacuum type surrounded by a skin caused by the surface tension of this new vacuum. This skin kept a piece of usual atomic matter highly compressed inside the bubble. In fitting data with this model the most and almost only successful fit consisted in that we fitted, with a common parameter, both the overall rate and the very 3.5 keV energy of the X ray line originally observed in several galaxy clusters, Andromeda and the Milky Way Center [9–14] and supposedly coming from dark matter. But now it turned out that this successful fitting relation between the 3.5 keV energy and the overall rate of the X-ray radiation only depends on the density of the pearls or equivalently the fermi momentum or energy of the electrons kept inside the pearls, but not on the absolute size of the pearls. Thus we could change the model to make the pearl sizes much smaller, as we shall do in this article, so that they are e.g. now rather of atomic size. Really we shall let the pearls be of radius $r_{\text{cloud } 3.3\text{MeV}} = 5 * 10^{-12}\text{m}$. But even such small pearls get stopped to some extent by the shielding into which they must penetrate to reach the underground experiments like the DAMA-LIBRA and Xenon experiments looking for dark matter. Using an astronomical observation based model by Correa [15] especially, we shall construct a rather definite picture of our pearls from which we estimate that the pearls hitting the earth actually get stopped presumably in the atmosphere, but if not there then at least in the earth shielding. The pearls thereby lose so much speed that it becomes quite understandable that the Xenon-experiments, looking for nuclei being hit by them and causing scintillation in fluid xenon, will not see any such events. However the DAMA-LIBRA experiment [16, 17] would not distinguish if it is a nucleus that is hit or some energy is released which causes the scintillator to luminesce. So only the DAMA-LIBRA experiment would be able to get a signal if the dark matter, e.g. our pearls, could be somehow excited and emit their excitation energy when they pass through the detector. In our model we shall indeed suggest that the pearls get excited and emit their energy by electron emission. That would not be easy to distinguish for DAMA-LIBRA but would still of course come with seasonal variation¹ so that it would be observed as dark matter by DAMA-LIBRA. Whether the emission is via electrons or nuclei would not matter. But for the xenon-experiments such electron emission was effectively

¹ We note however that the ANAIS experiment has failed to see an annual modulation with NAI(Tl) scintillators and their results [18] are incompatible with the DAMA-LIBRA results at 3.3σ .

not counted for a long time, but now rather recently the Xenon1T experiment has actually observed an excess of "electron recoil events". So they have now in fact seen an electron emission somehow.

We shall see in section 19.7 that both the excess of electron recoil events in Xenon1T [19] and the events seen by DAMA-LIBRA [16, 17] have the energy of each event remarkably enough centering about the energy value 3.5 keV of the mysterious X-ray line found astronomically!

This coincidence of course strongly suggests that these events from DAMA-LIBRA and Xenon1T are related to dark matter particles that can be excited precisely by this energy 3.5 keV.

In our earlier papers [5–7] we have already connected the excitability of our pearls by just this energy 3.5 keV and especially the emission of photons (or here in the present work also electrons) with just this energy with a gap in the single particle electron spectrum of the pearls caused by what we call the homolumo-gap effect. A very serious warning, which needs an explanation in order to rescue our model, is delivered by the fact that if as we now suggest the Xenon1T electron recoil event excess is coming from just the same decay of dark matter excitations as the DAMA-Libra observation, then these two experiments ought a priori to see equally many events, say per kg. However, DAMA-LIBRA sees 250 times as many events as Xenon1T sees excess events.

We shall postpone this question to a later article in detail, but the hope for now is that the Xenon1T experiment has the observed decaying pearls falling through a fluid, namely the fluid xenon, while the scintillator in DAMA-LIBRA is a solid made from NaI(Tl). The pearls are likely to form a little Xe-fluid bubble around them and flow or fall through the xenon-fluid, while they will much more easily get caught so as to almost sit still or only move much slower through the NaI scintillator. If so the pearls with their supposed excitations would spend much more time in the DAMA-LIBRA NaI than in a corresponding volume of xenon-liquid.

In the following section 19.2 we describe how the particles making up the dark matter in our model are imagined to be bubbles of the size $R = r_{\text{cloud } 3.3\text{MeV}} = 5 * 10^{-12}\text{m}$ with heavy atomic matter inside, which is surrounded out to a radius $r_{\text{cloud } 3.5\text{keV}} = 5 * 10^{-11}\text{m}$ by electrons. Here the quantities 3.3 MeV and 3.5 keV in the subscripts are the numerical electric potentials felt by an electron at the distances mentioned. A special point to note in this section already present in the earlier articles about the big pearls is the homolumo-gap effect, causing a band or gap in the energy levels without any single particle electron eigenstates. The width of this gap is fitted to the 3.5 keV line in the observed X-ray spectrum from galaxy clusters, the Milky Way Center etc. [9–11].

Next in section 19.3 we briefly review astronomical observations and modelling of the dark matter, which suggests the idea that dark matter interacts with itself (strongly interacting dark matter SIDM). It is only when the corresponding cross section σ is divided by the particle mass M do we have a combination that has any chance of being observed by its effects on the atomic matter. In fact this ratio $\frac{\sigma}{M}$ matches well with the atomic physics structure of our pearls including the cloud of electrons outside the bubble itself.

In section 19.4 we list a series of numerical successes of our model for the dark matter, hopefully making the reader see that there is really some reason for it being at least in some respects correct.

In section 19.5 we restate that our dark matter pearls get stopped and at the same time excited, mainly to emit quanta of energy 3.5 keV, in the air and/or in the shielding above the experiments. According to our best estimates they get stopped already about 53 km up in the air. It is the braking energy from this slowing down that is supposed to feed the excitations.

A special estimation, based on energy considerations, of whether the number of events seen by DAMA-LIBRA and by the Xenon1T electron recoil excess are of a reasonable order of magnitude is put forward in section 19.6. The success of such an estimation has to be rather limited in as far as the rates of the two observations - that should have been the same if we do not include the possibility of faster or slower motion through the detectors - deviate by a factor of 250.

In section 19.7 we call attention to the perhaps most remarkable fact supporting a major aspect of our model: That the energy per event for both DAMA-LIBRA and the Xenon1T-electron recoil excess centers around 3.5 keV, just the energy of the photons in the mysterious X-ray line seen in galactic clusters mentioned above! So all three effects should correspond to the emission of an electron or photon due to the same energy transition inside dark matter.

Finally in section 19.8 we conclude and provide a short outlook.

19.2 Pearl

Dark Matter Atomic Size Pearls, Electronic 3.5 keV Signal

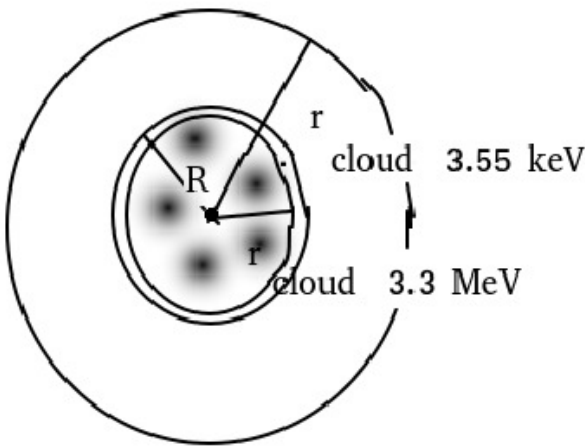


Fig.19.1: The figure illustrates the bit smaller than atom-size complicated/macrosopic dark matter particle in our model, a pearl.

We sketch the structure of our small dark matter pearls in Figure 1.

- In the middle is a spherical bubble of radius

$$R \approx r_{\text{cloud } 3.3\text{MeV}} \approx 5 * 10^{-12}\text{m}. \tag{19.1}$$

Here $r_{\text{cloud } 3.3\text{MeV}}$ denotes the radius where the electron potential is 3.3 MeV, which is identified with the Fermi energy E_f of the electrons in the bulk of the pearl - i.e. inside the radius R . We estimated the value $E_f = 3.3$ MeV in previous papers [6–8] by fitting the overall rate of the intensity of the 3.5 keV line emitted by galactic clusters and the very frequency 3.5 keV of the radiation in our model.

- The outer radius

$$r_{\text{cloud } 3.5\text{keV}} \approx 5 * 10^{-11}\text{m} \tag{19.2}$$

is where the electron potential is 3.5 keV. By our story of the “homolumo gap”: the electron density crudely goes to zero at this radius. (It gradually falls in the range between $r_{\text{cloud } 3.3\text{MeV}}$ and $r_{\text{cloud } 3.5\text{keV}}$).

The electron density and potential in the pearls

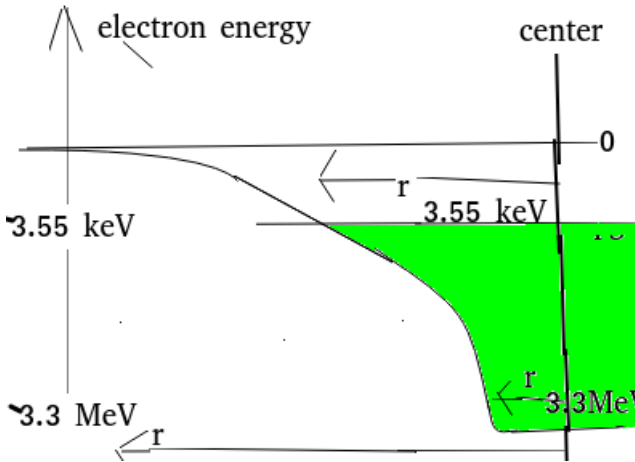


Fig. 19.2: Explaining the electron density and electric potential in the Pearl

- Due to an effect, we call the *homolumo-gap effect* [5,20], the nuclei in the bubble region and the electrons themselves become arranged in such a way as to prevent there from being any levels in an interval of width 3.5 keV. So, as illustrated in Figure 19.2, outside the distance $r_{3.5\text{keV}} = r_{\text{cloud } 3.5\text{keV}}$ from the center of the pearl at which the Coulomb potential is ~ 3.5 keV deep there are essentially (\sim in the Thomas-Fermi approximation) no more electrons in the pearl-object.

- The radius $r_{3.3\text{MeV}} = r_{\text{cloud } 3.3\text{MeV}}$ at which the potential felt by an electron is 3.3 MeV deep, is supposed to be just the radius to which the many nuclei inside the pearl (which replace the single nucleus in ordinary atoms) reach out. So inside the bubble the potential is much more flat.
- The energy difference between the zero energy line and the effective Fermi surface, above which there are no more electrons, is of order 3.5 keV, the energy so crucial in our work.
- Since in the Thomas-Fermi approximation there are no electrons outside roughly the radius $r_{3.5\text{keV}} = r_{\text{cloud } 3.5\text{keV}}$, this radius will give the maximal cross section, even for very low velocity $\sigma_{v \rightarrow 0}$.

The homolumo gap effect.

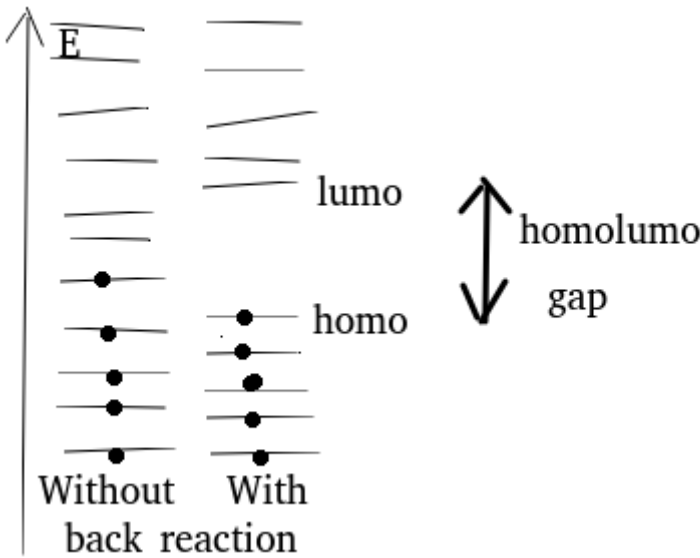


Fig. 19.3: Explanation of Homolumo-gap effect

Let us consider the spectrum of energy levels for the electrons in a piece of material, e.g. one of our pearls, and at first assume that the positions or distributions of the charged particles in the material are fixed.

Then the ground state is just a state built e.g. as a Slater determinant for the electrons being in the lowest single electron states, so many as are needed to have the right number of electrons.

But now, if the charged particles can be moved due to their interactions, the ground state energy could be lowered by moving them so that the filled electron state levels get lowered.

So we expect introducing such a "back reaction" will lower the filled states.

When the filled levels get moved downwards, then the homo = “highest occupied molecular orbit” level will be lowered and its distance to the next level, the lomo (= lowest unoccupied molecular orbit), will appear extended on the energy axis. *We believe that we can estimate the homolomo-gap E_H .*

Using the Thomas-Fermi approximation - or crudely just some dimensional argument where the fine structure constant has the dimension of velocity - we calculated the homolomo gap in highly compressed ordinary matter for relativistic electrons:

$$E_H \sim \left(\frac{\alpha}{c}\right)^{3/2} \sqrt{2} p_f \quad (19.3)$$

$$\text{where } p_f = \text{Fermi momentum} \quad (19.4)$$

$$\frac{\alpha}{c} = \frac{1}{137.03\dots} \quad (19.5)$$

(the $\sqrt{2}$ comes from our Thomas-Fermi calculation).

It is by requiring this homolomo-gap to be the 3.5 keV energy of the X-ray line mysteriously observed by satellites from clusters of galaxies, Andromeda and the Milky Way Center that we estimate the Fermi-energy to be $E_f \approx p_f = 3.3$ MeV in the interior bulk of the pearl.

Brief summary of theoretical ideas underlying our dark matter pearls

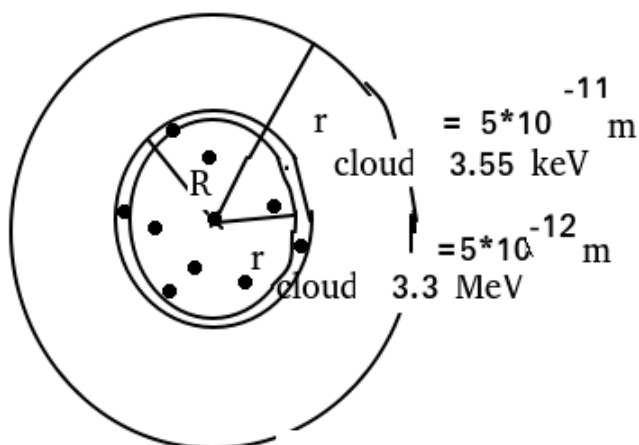


Fig. 19.4: Our Picture of Dark Matter Pearls.

- **Principle** Nothing but Standard Model! (Seriously it would mean not in a BSM-workshop.)
- **New Assumption** Several Phases of Vacuum with Same Energy Density; this is the so-called Multiple Point Principle [5,6,21–26].

- **Central Part** Bubble of New Phase of Vacuum with e.g. carbon under very high pressure, surrounded by a surface with tension S (= domain wall) providing the pressure.
- **Outer part** Cloud of Electrons much like an ordinary atom having a nucleus with a charge of order ten to a hundred thousand ($Z \approx 5 * 10^4$ effectively).

19.3 Non-gravitational Interactions

The collisionless cold dark matter model provides a good description of the large scale structure of the Universe. However there are various problems at small scales [27,28] for the hypothesis that dark matter only has gravitational interactions. Originally Spergel et al [29] suggested that the lack of a peak or cusp in the center of galaxy clusters, as expected for cold dark matter with purely gravitational interactions, required self interacting dark matter with a relatively large cross section. The relevant parameter is in fact the cross section per mass $\frac{\sigma}{M}$ and for the cores in galaxy clusters, where the collision velocity is $v \sim 1000$ km/s, a value $\frac{\sigma}{M} \sim 0.1$ cm²/g is needed. The self interaction can of course be velocity dependent and the cores in spiral galaxies where $v \sim 100$ km/s require $\frac{\sigma}{M} \sim 1$ cm²/g. In dwarf galaxies around our Milky Way, where dark matter moves more slowly $v \sim 30$ km/s, larger cross section to mass ratios $\frac{\sigma}{M} \sim 50$ cm²/g are needed.

Recently Correa [15] made a study of the velocity dependence of self interacting dark matter. In particular she analysed the Milky Way dwarf galaxies and her results are displayed in Figure 19.5. The extrapolation of Correa’s fit to the data towards zero velocity points to the ratio $\frac{\sigma}{M} \rightarrow 150$ cm²/g. This ratio can be taken as an experimental estimate of the impact area over the mass as seen for very soft collisions. In our model the cross section in this low velocity limit is given by the extent out to which the electrons surrounding our pearls reach. This range of extension of electrons is supposed to be given by the requirement that the electron binding energy is of the order of the homolumo gap value 3.5 keV. So we denote this radius by $r_{\text{cloud } 3.5\text{keV}}$. Similarly the radius of the bubble containing the nucleons inside our dark matter pearl corresponds to a radius $r_{\text{cloud } 3.3\text{MeV}}$ at which the potential for the electron is -3.3 MeV (= Fermi energy of the electrons). The high velocity hard collisions of our pearls, supposed to result in the unification of two pearls into a single pearl, correspond to interactions between the bubble skins with a cross section of order $\pi r_{\text{cloud } 3.3\text{MeV}}^2$.

We will now consider the electric potential for our pearl using the Thomas-Fermi approximation for a heavy atom [30–32]. In this approximation the Coulomb potential of the “nuclear” charge Z is multiplied by the Thomas-Fermi screening function $\chi(r/b)$ where

$$b = 0.88 \frac{a_0}{Z^{1/3}} \tag{19.6}$$

and a_0 is the Bohr radius. The skin of the bubble or “nucleus” of the pearl mainly acts on the nucleons or rather nuclei. So the electrons spread out and an appreciable part, say half of them, are outside the central part of the pearl inside the skin. Therefore the effective charge Z of the central part of the pearl or bubble of the new phase is e.g. one half of the number of protons inside the skin. Assuming also

7 dark matter and Milky Way dwarf galaxies 9

Name	Final profile			Preferred cross section
	M_{200} [$10^9 M_\odot$]	c_{200}	r_{core} [pc]	σ/m_χ [cm^2g^{-1}]
UM	0.13	34.2	180.8	40 – 50
Draco	1.17	26.8	472.9	20 – 30
Carina	1.09	19.1	648.4	40 – 50
Sextans	0.32	20.8	395.5	70 – 120
CVnI	0.46	25.7	356.8	50 – 80
Sculptor	1.65	25.8	553.2	30 – 40
Fornax	2.29	15.3	1036.7	30 – 50
LeoII	0.05	30.6	148.8	90 – 150
LeoI	1.17	31.1	410.8	50 – 70

Table 2. From left to right: name of the dSph galaxy, present-time virial mass, concentration parameter and core size of the subhalo hosting the dSph and range of preferred cross section values that reproduce the observed DM central densities.

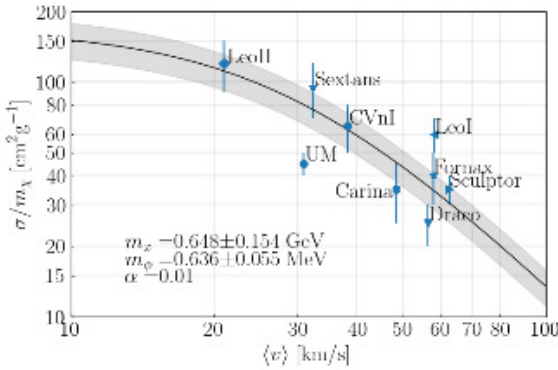


Figure 6. Cross section per unit mass, σ/m_χ , as a function of the average collision velocity, $\langle v \rangle$, of DM particles within each subhalo’s core. Symbols show the range of σ/m_χ needed for the SIDM model to reproduce the central DM densities reported by Kaplinghat et al. (2019). The solid line corresponds to the best-fit relation given by eq. (15) to the MW dSph data.

Fig. 19.5: Cross section per mass $\frac{\sigma}{M}$ of self interacting dark matter particles as a function of the collision velocity v in dwarf galaxies from reference [15].

that there are about equally many neutrons and protons inside the central part, the mass of the pearl is then given order of magnitudewise by $M = 4m_N * Z$, where m_N is the nucleon mass.

In the Thomas-Fermi approach we are then led to the following equations for $r_{\text{cloud } 3.5\text{keV}}$ and $r_{\text{cloud } 3.3\text{MeV}}$:

$$\frac{\alpha * Z}{r_{\text{cloud } 3.5\text{keV}}} * \chi(r_{\text{cloud } 3.5\text{keV}}/b) = 3.5 \text{ keV} \tag{19.7}$$

$$\frac{\alpha * Z}{r_{\text{cloud } 3.3\text{MeV}}} * \chi(r_{\text{cloud } 3.3\text{MeV}}/b) = 3.3 \text{ MeV} \tag{19.8}$$

$$b = 0.88 * \frac{\alpha_0}{Z^{1/3}} \tag{19.9}$$

$$\tag{19.10}$$

We identify $r_{\text{cloud } 3.5\text{keV}}$ with the radius of the electron cloud and $r_{\text{cloud } 3.3\text{MeV}}$ with the skin radius R of the pearl.

It is going to be an important success of our model that we get a similar value for $R \approx r_{\text{cloud } 3.3\text{MeV}}$ using another method to calculate it. We shall use

$$\frac{\sigma}{M}|_{v \rightarrow 0} = 150 \text{ cm}^2/\text{g} \tag{19.11}$$

and

$$\sigma = \pi * r_{\text{cloud } 3.5\text{keV}}^2 \tag{19.12}$$

to determine the mass M . Then using the formula for the mass of a pearl in terms of the radius R and the Fermi momentum [7,8]

$$\frac{M}{m_N} = \frac{8}{9\pi} * (R * p_f)^3, \tag{19.13}$$

we can calculate another value for R .

In our updated contribution to the Bled Proceedings from last year [8] we estimated a pearl mass of $M \sim 10^5 \text{ GeV}$. So we take here $Z = 5.3 * 10^4$ as a typical charge in the central part of the pearl, for which then $b = 1.24 * 10^{-12} \text{ m}$. Using numerical values for the Thomas-Fermi screening function in the paper [33], we obtain from (19.7) the radius of the electron cloud to be

$$r_{\text{cloud } 3.5\text{keV}} = 4.96 * 10^{-11} \text{ m} \tag{19.14}$$

Then assuming the low velocity ratio $\frac{\sigma}{M} = 150 \text{ cm}^2/\text{g}$ we obtain

$$M = \frac{\pi * (4.96 * 10^{-11} \text{ m})^2}{150 \text{ cm}^2/\text{g}} \tag{19.15}$$

$$= 5.2 * 10^{-19} \text{ g} \tag{19.16}$$

$$= 3.1 * 10^5 \text{ m}_N \tag{19.17}$$

As a side remark notice that, using our proposed rule of taking Z to be a quarter of the number M/m_N , we would get $Z = 8 * 10^4$ to be compared with our input here $5.3 * 10^4$, which is very well consistent within a factor 2.

Next using (19.13) with $p_f = 3.3 \text{ MeV} = 1.6 * 10^{13} \text{ m}^{-1}$

$$(R * p_f)^3 = 3.1 * 10^5 * \frac{9\pi}{8} \quad (19.18)$$

$$= 10.9 * 10^5 \quad (19.19)$$

$$R * 1.6 * 10^{13} \text{ m}^{-1} = \sqrt[3]{10.9 * 10^5} = 102 \quad (19.20)$$

giving

$$R = \frac{102}{1.6 * 10^{13} \text{ m}^{-1}} \quad (19.21)$$

$$= 6.4 * 10^{-12} \text{ m}. \quad (19.22)$$

This is to be compared with the Thomas-Fermi value obtained from (19.8) using the numerical values for $\chi(r/b)$ in [33]

$$R = r_{\text{cloud } 3.3\text{MeV}} = 3.66 * 10^{-12} \text{ m}. \quad (19.23)$$

These two different estimates of the radius $r_{\text{cloud } 3.3\text{MeV}}$ at which the potential is 3.3 MeV essentially coincide to the accuracy of our calculation; they deviate by a factor of order unity $6.4/3.7=1.7$. So we could claim that formally our model is able to predict the low velocity limit $\frac{\sigma}{M}|_{v \rightarrow 0}$ in agreement with the value $150 \text{ cm}^2/\text{g}$ estimated from the study of dwarf galaxies around the Milky Way.

We shall take the average of the two values (19.22) and (19.23) as our best estimate of the bubble skin radius:

$$r_{\text{cloud } 3.3\text{MeV}} = 5.0 * 10^{-12} \text{ m} \quad (19.24)$$

and from (19.14) we have the radius of the electron cloud

$$r_{\text{cloud } 3.5\text{keV}} = 5.0 * 10^{-11} \text{ m}. \quad (19.25)$$

We note that these two radii differ by an order of magnitude, which means that the quantity $\frac{\sigma}{M}$ for our pearls should differ by two orders of magnitude between low velocities and high velocities, as astronomical observations indicate is the case for self interacting dark matter [15].

19.4 Achievements

- **Low velocity $\frac{\sigma}{M}|_{v \rightarrow 0}$ cross section to mass ratio.** The a priori story, that dark matter has only gravitational interactions seems not to work perfectly: Especially in dwarf galaxies (around our Milky Way) where dark matter moves relatively slowly an appreciable self interaction cross section to mass ratio $\frac{\sigma}{M}$ is needed. According to the fits in [15] this ratio has the low velocity limit $\frac{\sigma}{M}|_{v \rightarrow 0} = 150 \text{ cm}^2/\text{g}$. We may say our pearl-model “predicts” this ratio in order of magnitude.

- **Can make the Dark Matter Underground Searches get Electron Recoil Events**
Most underground experiments are designed to look for dark matter particles hitting the nuclei in the experimental apparatus, which is then scintillating so that such hits presumed to be on nuclei can be seen. But our pearls are excited in such a way that they send out energetic *electrons* (rather than nuclei) and this does not match with what is looked for, except in the DAMA-LIBRA experiment. In this experiment the only signal for events coming from dark matter is a seasonal variation due to the Earth running towards or away from the dark matter flow.
- **The Intensity of 3.5 keV X-rays from Clusters etc.** We fit the very photon-energy 3.5 keV and the overall intensity from a series of clusters, a galaxy, and the Milky Way Center [8] with one parameter $\frac{\xi_{fS}^{1/4}}{\Delta V} = 0.6 \text{ MeV}^{-1}$.
- **3.5 keV Radiation from the Tycho Supernova Remnant.** Jeltema and Profumo [34] discovered the 3.5 KeV X-ray radiation coming from the remnant of Tycho Brahe’s supernova, which was unexpected for such a small source. We have a scenario giving the correct order of magnitude for the observed intensity in our pearl model: supposedly our pearls are getting excited by the high intensity of cosmic rays in the supernova remnant [8].
Even though we can use only the one parameter $\frac{\xi_{fS}^{1/4}}{\Delta V} = \frac{2}{p_f}$, it is nice to know the notation:

$$\begin{aligned} \Delta V &= \text{“ difference in potential for a nucleon between the} \\ &\quad \text{inside and the outside of the central part of the pearl”} \\ &\approx 2.5 \text{ MeV} \end{aligned} \tag{19.26}$$

$$\xi_{fS} = \frac{R}{R_{\text{crit}}} \quad \text{estimated to be } \approx 5 \tag{19.27}$$

$$\begin{aligned} \text{where } R &= \text{“actual radius of the new vacuum part”} \\ &\approx r_{\text{cloud } 3.3\text{MeV}} \end{aligned} \tag{19.28}$$

$$\begin{aligned} \text{and } R_{\text{crit}} &= \text{“ Radius when pressure is so high} \\ &\quad \text{that nucleons are just about being spit out”} \end{aligned} \tag{19.29}$$

The subscript fS on the parameter ξ_{fS} indicates that the surface tension S is fixed independent of the radius R.

- **DAMA-rate** Estimating observation rate of DAMA-LIBRA from kinetic energy of the incoming dark matter as known from astronomy.
- **Xenon1T Electron recoil rate** Same for the *electron recoil excess* observed by the Xenon1T experiment.

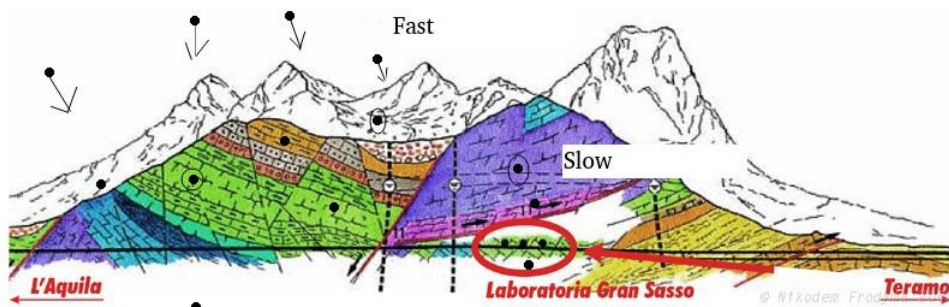
In order to explain these last calculational estimates it is necessary to know how we imagine the dark matter to interact and get slowed down in the air and the earth shielding; also how the dark matter particles get excited and emit 3.5 keV radiation or electrons.

About the Xenon1T and DAMA-rates:

- **Absolute rates very crudely** Our estimate of the absolute rates for the two experiments are very very crude, because we assume that the dark matter particles - in our model small macroscopic systems with ten thousands of nuclei inside them - can have an exceedingly smooth distribution of lifetimes on a logarithmic scale. These calculations are discussed in section 19.6.
- **The ratio of rates** The ratio of the rates in the two experiments - Xenon1T electron recoil excess and DAMA - should in principle be very accurately predicted in our model, because they are supposed to see exactly the same effect just in two different detectors in the same underground laboratory below the Gran Sasso mountain! One would therefore expect the rates to be the same, but the Xenon1T rate is 250 times smaller than the DAMA rate. We briefly refer to a possible resolution of this problem, which needs further study, in section 19.6.

19.5 Impact

Illustration of Interacting and Excitable Dark Matter Pearls



The dark matter pearls come in with high speed (galactic velocity), but get stopped down to much lower speed by interaction with the air and the shielding mountains, whereby they also get excited to emit 3.5 keV X-rays or *electrons*.

Pearls Stopping and getting Excited in Earth Shield

What happens when the dark matter pearls in our model of less than atomic size hit the earth shielding above the experimental halls of e.g. DAMA?

- **Stopping** Taking it that the pearls stop in the earth: The pearls are stopped in about $5 * 10^{-6}$ s from their galactic speed of about 300 km/s down to a speed 49 km/s below which collisions with nuclei can no longer excite the 3.5 keV excitations. The stopping length, modulo a logarithmic factor, is $\frac{1}{4}$ m. But taking it that they stop in the air, which is more likely: They are stopped over a range of about 7 km - as the atmosphere density goes up with a factor $e = 2.71..$ over such a range in about $2 * 10^{-2}$ s.
- **Excitation** As long as the velocity is still over the ca. 49 km/s collisions with nuclei in the shielding can excite the electrons inside the pearl by 3.5 keV or more and make pairs of quasi electrons and holes say. We expect that often the creation of (as well as the decay of) such excitations require electrons to pass

through a (quantum) tunnel and that consequently there will be decay half lives of very different sizes. We hope even up to many hours or days...

- **Slowly sinking:** After being stopped in of the order of $\frac{1}{4}$ m of the shielding, the pearls continue with a much lower velocity driven by the gravitational attraction of the Earth. After say about 26 hours a pearl reaches the 1400 m down to the laboratories. Most of the pearls have returned to their ground states, but some exceptionally long living excitations survive.

Note that the slowly sinking velocity is so low that collisions with nuclei cannot give such nuclei enough speed to excite the scintillation counters neither in DAMA nor in Xenon-experiments.

- **Electron or γ emission** Typically the decay of an excitation could be that a hole in the Fermi sea of the electron cloud of the pearl gets filled by an outside electron under emission of another electron by an Auger-effect. The electron must tunnel into the pearl center. This can make the decay lifetime become very long and very different from case to case.

Emission as electrons or photons makes Xenon-experiments not see events, except...

That the decay energy is released most often as electron energy means that such events are discarded by most of the Xenon-experiments, which only expect the nucleus recoils to be dark matter events. This would explain the long standing controversy consisting in DAMA seeing dark matter with a much bigger rate than the upper limits from the other experiments.

Rather recently though Xenon1T looked for potential excess events among the *electron recoil events* and found 16 events/year/tonne/keV in the lowest keV-bands over a background of the order of (76 ± 2) events/year/tonne/keV.

In our model this rate should be compatible with the DAMA event rate. However they deviate by a factor of 250. It therefore appears that we need the pearls to run much faster through the xenon-apparatus than through the DAMA one.

19.6 Numerical Rates for DAMA and Xenon1T-electron-recoil-excess

19.6.1 The Kinetic Energy Flux from Dark Matter

The dark matter density D_{sol} in our part of the Milky Way and its velocity v are of the orders of magnitude

$$D_{\text{sol}} = 0.3 \text{ GeV/cm}^3 \quad (19.30)$$

$$= 5.34 * 10^{-22} \text{ kg/m}^3 \quad (19.31)$$

$$v = 300 \text{ km/s} \quad (\text{relative to solar system}) \quad (19.32)$$

This gives a kinetic energy density

$$D_{\text{kin energy}} = \frac{1}{2}v^2 D_{\text{sol}} \quad (19.33)$$

$$= 0.5 * (10^{-3})^2 c^2 * 5.34 * 10^{-22} \text{kg/m}^3 \quad (19.34)$$

$$= 2.40 * 10^{-11} \text{J/m}^3 \quad (19.35)$$

meaning an influx of kinetic energy

$$\text{“power per m}^2\text{”} = v D_{\text{kin energy}} \quad (19.36)$$

$$= \frac{1}{2}v^3 D_{\text{sol}} \quad (19.37)$$

$$= 3 * 10^5 \text{m/s} * 2.40 * 10^{-11} \text{J/m}^3 \quad (19.38)$$

$$= 7.2 * 10^{-6} \text{W/m}^2 \quad (19.39)$$

Distributing this energy rate over the amount of matter down to the depth 1400 m with density 3000 kg/m^3 we obtain the energy rate per kg

$$\text{“ power to deposit”} = \frac{7.2 * 10^{-6} \text{W/m}^2}{1400 \text{ m} * 3000 \text{ kg/m}^3} \quad (19.40)$$

$$= 1.7 * 10^{-12} \text{W/kg}. \quad (19.41)$$

However, assuming that all the events from the dark matter - as given by the modulated part of the signal found by DAMA-LIBRA - are just due to decays with the decay energy 3.5 keV, the rate of energy deposition per kg observed by DAMA-LIBRA [17] is

$$\text{“deposited rate”} = 0.0412 \text{cpd/kg} * 3.5 \text{keV} \quad (19.42)$$

$$= \frac{0.0412 \text{cpd/kg} * 3.5 * 1.6 * 10^{-16} \text{J}}{86400 \text{s/day}} \quad (19.43)$$

$$= 2.7 * 10^{-22} \text{W/kg}, \quad (19.44)$$

which is

$$\frac{2.7 * 10^{-22} \text{W/m}^2}{1.7 * 10^{-12} \text{W/m}^2} = 1.6 * 10^{-10} \text{ times as much}. \quad (19.45)$$

We can express this by saying that there is a need for a suppression factor suppression being $1.6 * 10^{-10}$ for the DAMA-LIBRA rate. For the excess of the electronic recoil events found by Xenon1T the corresponding suppression factor must be the 250 times smaller number. This is because the event rate of these excess electron recoil events is 250 times smaller than that of the modulation part of the DAMA rate and the depth of the experiment under the earth is the same 1400 m. Thus we summarize the *experimentally* determined suppression factors:

$$\text{suppression}_{\text{DAMA}} = 1.6 * 10^{-10} \quad (19.46)$$

$$\text{suppression}_{\text{Xenon1T}} = \frac{1.6 * 10^{-10}}{250} = 6.4 * 10^{-13}. \quad (19.47)$$

19.6.2 Estimating “suppression” theoretically

The idea for obtaining theoretical estimates of these suppression factors is to say that the observed events come from excitations of our pearls with a lifetime of the order of the time it takes for the pearl, after its excitation under its stopping in the air or in the stone above the experiments, to reach down to the experimental detectors. We here assume the scattering cross section of dark matter on ordinary matter to be similar to that on dark matter. So we estimate the passage time of the pearl down to the detectors as being of the order of 26 hours, by using the low velocity value for the cross section over mass ratio

$$\text{To be used for passage velocity: } \frac{\sigma}{M} = 150 \text{ cm}^2/\text{g} \quad (19.48)$$

Once the pearl has been stopped so much that its velocity is only upheld by the gravitational field with the acceleration $g = 9.8 \text{ m/s}^2$, the terminal velocity will be obtained formally from the drag-equation²

$$\text{Drag force } D = gM = 0.5 * C_d * \sigma * \rho v^2. \quad (19.49)$$

Here ρ is the density of the material passed through and the drag coefficient C_d is of order unity (so the 0.5 is hardly relevant). That is to say the terminal velocity becomes:

$$v_{\text{terminal}} \approx \sqrt{\frac{g}{\frac{\sigma}{M} * \rho}} \quad (19.50)$$

$$\approx \sqrt{\frac{9.8 \text{ m/s}^2}{150 \text{ cm}^2/\text{g} * 3 \text{ g/cm}^3}} \quad (19.51)$$

$$= \sqrt{2.2 \text{ cm}^2/\text{s}^2} = 1.5 \text{ cm/s}, \quad (19.52)$$

which allows a pearl to pass though 1400 m in

$$\text{“passage time”} = \frac{140000 \text{ cm}}{1.5 \text{ cm/s}} \quad (19.53)$$

$$= 93000 \text{ s} = 26 \text{ hours}. \quad (19.54)$$

19.6.3 Equally hard to excite and to de-excite

In order that there can be any de-excitations of the pearls after such 26 hours it is of course needed that an appreciable part of the possible 3.5 keV excitations of our pearls have lifetimes of this order of magnitude. A priori these excitations are excitons for which the electron and hole can be close by and decay rapidly or it is possible that one of the partners is outside in the electron cloud and long lived. By arguing that some tunnelling of electrons in or out or around in the pearl may be needed for some (de-)excitations, we can claim that the lifetimes for

² Strictly speaking this equation is only valid if the pearl velocity is greater than the thermal velocity of the nuclei in the shielding and so needs further study.

the various excitation possibilities are smoothly distributed over a wide range in the logarithm of the lifetime; then there will be some pearl-excitations with the appropriate lifetime, although somewhat suppressed by a factor of the order of $1/\text{width}$ where the width here is the width of the logarithmic distribution. We shall take this width to be of order $\ln \text{suppression}_{\text{DAMA}} \sim 23$. But more importantly: If a certain excitation is long-lived, it is also hard to produce. So we shall talk about an effective “stopping” or “filling time” for a pearl passing into the Earth, and imagine that during this “stopping” or “filling time” the excitations of the pearls have to be created. So the probability for excitation or suppression would be expected to be

$$\text{suppression} \approx \frac{\text{“filling time”}}{\text{“lifetime”}}. \tag{19.55}$$

If the excitation happens to be of sufficiently long lifetime - say of order 26 hours - then we can expect it to have a sensible chance of de-exciting just in the experimental detectors in Gran Sasso, DAMA or Xenon1T say.

But what shall we take for this “stopping” or “filling time”? A relatively simple idea, which is presumably right, is to say that the stopping takes place high in the atmosphere because a pearl entering the Earth’s atmosphere with galactic speed will be slowed down in the high air with a $\frac{\sigma}{M} \sim 2 \text{ cm}^2/\text{g}$. Now the density of the atmosphere rises by a factor $e = 2.718\dots$ per about 7 km. So as the slowing down begins it will, because of this rising density, essentially stop again after 7 km. Thus the time during which the pearl is truly slowing down in speed and forming 3.5 keV excitations is of the order of the time it takes for it to run 7 km. With the pearl velocity of about 300 km/s (essentially the escape velocity for the galaxy) we then have

$$\text{“stopping time”} \approx \frac{7 \text{ km}}{300 \text{ km/s}} \tag{19.56}$$

$$= 0.023 \text{ s} \tag{19.57}$$

The crucial factor, which we believe to be most important, is that in order to excite an excitation with a lifetime of the order 93000 s it would a priori need 93000 s so that, if we only have 0.023 s, then there will be a suppression:

$$\text{suppression} = \frac{\text{“stopping time”}}{\text{“lifetime”}} \tag{19.58}$$

$$\approx \frac{\text{“stopping time”}}{\text{“passage time”}} \tag{19.59}$$

$$\approx \frac{0.023 \text{ s}}{93000 \text{ s}} \tag{19.60}$$

$$= 2.5 * 10^{-7}. \tag{19.61}$$

This crudest estimate has to be compared with the experimental suppressions given above

$$\text{suppression}_{\text{DAMA}} = 1.6 * 10^{-10} \tag{19.62}$$

$$\Rightarrow \frac{\text{suppression}_{\text{theory}}}{\text{suppression}_{\text{DAMA}}} = \frac{2.5 * 10^{-7}}{1.6 * 10^{-10}} \tag{19.63}$$

$$= 1.6 * 10^3 \tag{19.64}$$

$$\text{suppression}_{\text{Xenon1T}} = \frac{1.6 * 10^{-10}}{250} = 6.4 * 10^{-13} \tag{19.65}$$

$$\Rightarrow \frac{\text{suppression}_{\text{theory}}}{\text{suppression}_{\text{Xenon1T}}} = \frac{2.5 * 10^{-7}}{6.4 * 10^{-13}} \tag{19.66}$$

$$= 3.9 * 10^5. \tag{19.67}$$

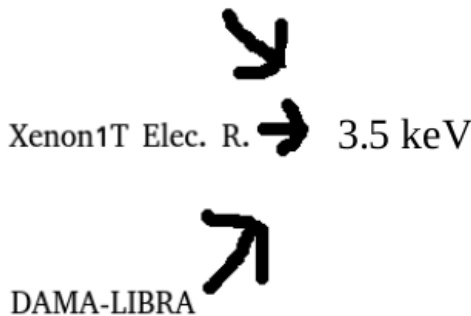
But here can be several corrections to $\text{suppression}_{\text{theory}}$, at least we should correct by the width in logarithm of the supposed distribution of the lifetimes among the different excitations. Above we suggested a factor 23, which would bring the DAMA rate to only deviate by about a factor 100. Our estimate is of course extremely uncertain.

We can never get the DAMA rate and the electron recoil excess rate from Xenon1T agree with the same estimate in as far as they deviate by a factor 250. Our only chance is in a later paper to justify say the story that, because the scintillator in which the Xenon1T events are observed is *fluid* while the NaI in the Dama experiment is solid, the pearls pass much faster through the Xenon1T apparatus than they pass through the DAMA instrument. Imagine say that the pearls partly hang and get stuck in the DAMA experiment, but that they cannot avoid flowing down all the time while they are in the fluid Xe in the Xenon1T scintillator.

19.7 3.5keV

Order of magnitudewise we see 3.5 keV in 3 different places.

X-ray galaxy cl.



The energy level difference of about 3.5 keV occurring in 3 different places is important evidence motivating our model of dark matter particles being excitable by 3.5 keV:

- **The line** From places in outer space with a lot of dark matter, galaxy clusters, Andromeda and the Milky Way Center, an unexpected X-ray line with photon energies of 3.5 keV (to be corrected for Hubble expansion...) was seen.
- **Xenon1T** The Dark matter experiment Xenon1T did not find the standard nuclei-recoil dark matter, but found an excess of *electron-recoil* events with energies concentrated crudely around 3.5 keV.
- **DAMA** The seasonally varying component of their events lie in energy between 2 keV and 6 keV, not far from centering around 3.5 keV.

We take it seriously and not as an accident that both DAMA and Xenon1T see events with energies of the order of the controversial astronomical 3.5 keV X-ray line. We are thereby driven towards the hypothesis that the energies for the events in these underground experiments are determined from a decay of an excited particle, rather than from a collision with a particle in the scintillator material. It would namely be a pure accident, if a collision energy should just coincide with the dark matter excitation energy observed astronomically.

So we ought to have decays rather than collisions! How then can the dark matter particles get excited ?

You can think of the dark matter pearls in our model hitting electrons and/or nuclei on their way into the shielding:

- **Electrons** Electrons moving with the speed of the dark matter of the order of 300 km/s toward the pearls in the pearl frame will have kinetic energy of the order

$$E_e \approx \frac{1}{2} * 0.5 \text{ MeV} * \left(\frac{300 \text{ km/s}}{3 * 10^5 \text{ km/s}}\right)^2 = 0.25 \text{ eV.} \quad (19.68)$$

- **Nuclei** If the nuclei are say Si, the energy in the collision will be $28 * 1900$ times larger $\sim 5 * 10^4 * 0.25 \text{ eV} \approx 10 \text{ keV}$. That would allow a 3.5 keV excitation. To deliver such $\approx 10 \text{ keV}$ energy the nucleus should hit something harder than just an electron inside the pearls. It should preferably hit a nucleus, e.g. C, inside the pearl.

19.8 Conclusion

- We have described a seemingly viable model for dark matter consisting of atomic size but macroscopic pearls. These pearls consist of a bubble of a new speculated type of vacuum containing some normal material - presumably carbon - under the high pressure of the skin (surface tension). They each contain about a hundred thousand nucleons in the bubble of radius about $5 * 10^{-12} \text{ m}$.
 - The electrons in a pearl have partly been pushed out of the genuine bubble of the new vacuum phase, out to a distance of about $5 * 10^{-11} \text{ m}$.
- We have compared the model or attempted to fit:

- Astronomical suggestions for the self interaction of dark matter in addition to pure gravity.
- The astronomical 3.5 keV X-ray emission line found by satellites, supposedly from dark matter.
- The underground dark matter searches.

We list below the quantities we have crudely estimated:

1. The low velocity cross section divided by mass.
2. That the signal from Xenon1T and Dama should agree except that the pearls may run with different velocities through the scintillator materials, because the xenon-instruments use *fluid* xenon, while the DAMA-LIBRA experiment uses the solid NaI.
3. The absolute rate of the two underground experiments. (But unfortunately unless we explain the ratio of the rates for the two experiments as say due to the different velocities through the scintillator materials, we can of course never predict the absolute rate to be better than deviating by about a factor of 250 with at least one of them.)
4. The rate of emission of the 3.5 keV X-ray line from the Tycho supernova remnant due to the excitation of our pearls by cosmic rays [8].
5. Relation between the frequency 3.5 keV and the overall emission rate of this X-ray line observed from galaxy clusters etc.
6. We also previously predicted the ratio of dark matter to atomic matter (=“usual” matter) in the Universe to be of order 5 by consideration of the binding energies per nucleon in helium and heavier nuclei, assuming that the atomic matter at some time about 1 s after the Big Bang was spit out from the pearls under a fusion explosion from He fusing into say C [1].

19.8.1 Outlook

At the end we want to mention a few ideas which we hope will be developed as a continuation of the present model:

- **Speculative Phase from QCD.** QCD and even more QCD with Nambu-Jona-Lasinio type spontaneous symmetry breaking is sufficiently complicated, that possibly a new phase appropriate for our pearls could be hiding there. There is already an extremely interesting observation [35].
- **Relative Rates of DAMA and Xenon1T.** A crucial test for our model is to reproduce the relative event rates in DAMA and in the excess of electron recoils in Xenon1T. This requires a careful study of the viscosity of fluid xenon and the properties of our pearls.
- **Walls in the Cosmos.** With the usual expectations for the density per area or equivalently tension S , cosmology would be so severely changed by such domain walls that models with say $S^{1/3} \geq 10$ MeV are phenomenologically not tenable. However, with our fit to a surprisingly small tension with $S^{1/3} \approx 2.2$ MeV it just barely becomes possible to have astronomically extended domain walls, e.g. walls around the large voids between the bands of galaxies; so that

these voids could be say formally huge dark matter pearls, though with much smaller density. In fact a series of domain walls with our fitted $S = 2.2^3 \text{ MeV}^3$ with distances between them of the order of 13 milliard light years would have a density not much different for that of the universe we know.

- **New Experiments?** According to our estimates the observed rate of decays of our dark matter pearls should be larger the less shielding they pass through. So an obvious test of our model would be to make a DAMA-like experiment closer to the earth surface where we would expect a larger absolute rate than in DAMA, although there might of course be more background. Actually such an experiment is already being performed by the ANAIS group [18], but they have so far failed to see an annual modulation in their event rate.

Acknowledgement

HBN thanks the Niels Bohr Institute for his stay there as emeritus. CDF thanks Glasgow University and the Niels Bohr Institute for hospitality and support. Also we want to thank many colleagues for discussions and for organizing conferences, where we have discussed previous versions of the present model, especially the Bled and Corfu meetings.

References

1. C. D. Froggatt and H. B. Nielsen, Phys. Rev. Lett. **95** 231301 (2005) [arXiv:astro-ph/0508513].
2. C.D. Froggatt and H.B. Nielsen, Proceedings of Conference: C05-07-19.3 (Bled 2005); arXiv:astro-ph/0512454.
3. C. D. Froggatt and H. B. Nielsen, Int. J. Mod. Phys. A **30** no.13, 1550066 (2015) [arXiv:1403.7177].
4. C. D. Froggatt and H. B. Nielsen, Mod. Phys. Lett. **A30** no.36, 1550195 (2015) [arXiv:1503.01089].
5. H.B. Nielsen, C.D. Froggatt and D. Jurman, PoS(CORFU2017)075.
6. H.B. Nielsen and C.D. Froggatt, PoS(CORFU2019)049.
7. C. D. Froggatt, H. B. Nielsen, "The 3.5 keV line from non-perturbative Standard Model dark matter balls", arXiv:2003.05018.
8. H. B. Nielsen (speaker) and C.D. Froggatt, "Dark Matter Macroscopic Pearls, 3.5 keV -ray Line, How Big?", arXiv:2012.00445.
9. E. Bulbul, M. Markevitch, A. Foster et al., ApJ. **789**, 13 (2014) [arXiv:1402.2301].
10. A. Boyarsky, O. Ruchayskiy, D. Iakubovskiy and J. Franse, Phys. Rev. Lett. **113**, 251301 (2014) [arXiv:1402.4119].
11. A. Boyarsky, J. Franse, D. Iakubovskiy and O. Ruchayskiy, Phys. Rev. Lett. **115**, 161301 (2015) [arXiv:1408.2503].
12. S. Bhargava et al, MNRAS **497** 656 (2020) [arXiv:2006.13955].
13. D. Sicilian et al, ApJ. **905** 146 (2020) [arXiv:2008.02283]
14. J. W. Foster et al, Phys. Rev. Lett. **127** 051101 (2021) [2102.02207].
15. Camila A. Correa, MNRAS **503**, 920 (2021) [arXiv:2007.02958].
16. R. Bernabei et al., Eur. Phys. J. **C73**, 2648 (2013). [arXiv:1308.5109].

17. R. Bernabei et al, *Prog. Part. Nucl. Phys.* **114**, 103810 (2020).
18. J. Amaré et al, *Phys. Rev.* **D103**, 102005 (2021) [arXiv:2103.01175].
19. E. Aprile et al, *Phys. Rev.* **D102**, 072004 (2020) [arXiv:2006.09721].
20. H. A. Jahn and E. Teller, *Proc. Roy. Soc. London* **A161** 220 (1937)
21. D. L. Bennett, C. D. Froggatt and H. B. Nielsen, NBI-HE-94-44, GUTPA-94-09-3, Presented at Conference: C94-07-20 (ICHEP 1994), p.0557-560.
22. D. L. Bennett, C. D. Froggatt and H. B. Nielsen, NBI-95-15, GUTPA-95-04-1, Presented at Conference: C94-09-13 (Adriatic Meeting 1994), p.0255-279 [arXiv:hep-ph/9504294].
23. D. L. Bennett and H. B. Nielsen, *Int. J. Mod. Phys.* **A9** 5155 (1994).
24. D. L. Bennett, C. D. Froggatt and H. B. Nielsen, NBI-HE-95-07, Presented at Conference: C94-08-30 (Wendisch-Rietz) p.394-412.
25. C. D. Froggatt and H. B. Nielsen, *Phys. Lett.* **B368** 96 (1996) [arXiv:hep-ph/9511371].
26. H.B. Nielsen (Speaker) and C.D. Froggatt, Presented at Conference: C95-09-03.1 (Corfu 1995); arXiv:hep-ph/9607375.
27. D.H. Weinberg et al, *PNAS* **112**, 12249 (2015) [arXiv:1306.0913].
28. Sean Tulin and Hai-Bo Yu, *Phys. Rep.* **730**, 1 (2018) [arXiv:1705.02358]
29. D. N. Spergel, and P. J. Steinhardt, *Phys. Rev. Lett.* **84**, 3760 (2000) [arXiv:astro-ph/9909386]
30. L.H. Thomas, *Proc. Cambridge Philos. Soc.* **23**, 542 (1927).
31. E. Fermi, *Rend. Accad. Naz. Lincei* **6**, 602 (1927).
32. L. Spruch, *Rev. Mod. Phys.* **63**, 153 (1991).
33. K Parand et al *Electronic Journal of Differential Equations*, Vol. 2016(2016), No. 331, pp. 1-18.
34. T. Jeltema and S. Profumo, *MNRAS* **450**, 2143 (2015) [arXiv:1408.1699]
35. Andrei Kryjevski, David B. Kaplan, Thomas Schaefer, *Phys. Rev.* **D71**, 034004 (2005) [arXiv:hep-ph/0404290]



20 Galactic model with a phase transition from dark matter to dark energy

I. Nikitin

email: igor.nikitin@scai.fraunhofer.de

Fraunhofer Institute for Algorithms and Scientific Computing, Schloss Birlinghoven, 53757 Sankt Augustin, Germany

Abstract. This work continues the construction of a recently proposed model of dark matter stars. In this model, dark matter quanta are sterile massless particles that are emitted from the central regions of the galaxy in the radial direction. As a result, at large distances r from the center of the galaxy, the mass density of dark matter has the form $\rho \sim r^{-2}$, in contrast to the homogeneous model $\rho = \text{Const}$. In the cosmological context, the homogeneous model with massless particles corresponds to the radiation epoch of the expansion of the universe, while the proposed inhomogeneous model turns out to be equivalent to Λ CDM. In this paper, scenarios will be considered in which the radial emission of dark matter is brought into hydrostatic equilibrium with a uniform background. It is shown that solutions exist if the uniform background has an equation of state typical for dark energy. Thus, this model describes a phase transition from dark matter inside the galaxy to dark energy outside of it. The specific mechanism for such a transition could be Bose-Einstein condensation. In addition, the question of what happens if dark matter particles are not sterile, for example, are photons of the Standard Model, is considered.

Povzetek: To delo je nov korak v predlaganem modelu zvezd iz temne snovi. V tem modelu so kvanti temne snovi sterilni brezmasni delci, ki jih seva center galaksije v radialni smeri. Zato ima v velikih oddaljenostih r od središča galaksije masna gostota temne snovi obliko $\rho \sim r^{-2}$, za razliko od homogenega modela, kjer je $\rho = \text{Const}$. Homogeni model z brezmasnimi delci opiše temno snov v obdobju širjenja vesolja, v katerem prevladuje sevanje, predlagani nehomogeni model pa se je izkazal enakovreden modelu Λ CDM. V tem prispevku obravnava avtor razmere, v katerih je radialna emisija temne snovi v hidrostatičnem ravnovesju z enakomernim ozadjem. Pokaže, da taka rešitev obstaja, če velja za enakomerno ozadje enačba stanja za temno energijo. Tedaj opisuje ta model fazni prehod iz temne snovi znotraj galaksije v temno energijo izven nje. Specifičen mehanizem za tak prehod bi lahko bila Bose-Einsteinova kondezacija. Pri tem se pojavi vprašanje, kaj se zgodi, če delci temne snovi niso sterilni, kot na primer niso sterilni fotoni Standardnega modela.

20.1 Introduction

This work continues the construction of the model [1] presented at Bled 2020 Workshop “What Comes Beyond the Standard Models?”. In this model, the sources

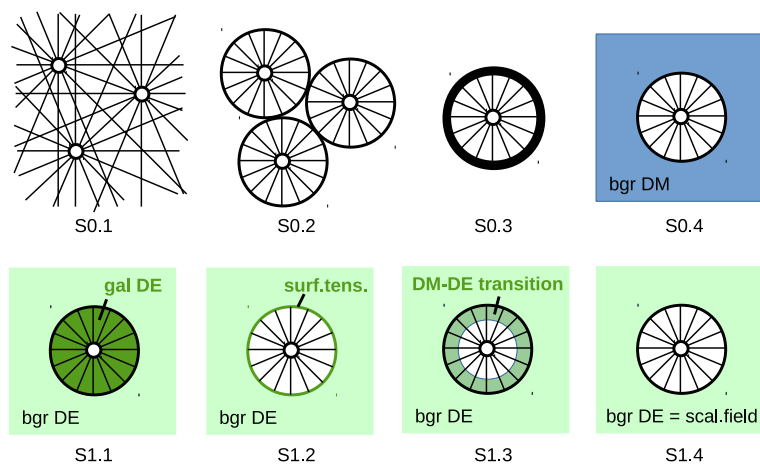


Fig. 20.1: The considered scenarios for a connection of galactic dark matter halo with uniform background, at the top – rejected, at the bottom – accepted ones.

of dark matter are Planck cores, Planck density objects located inside black holes. These objects are permanently emitting particles of dark matter, of originally Planck energy and Planck flux density. In this work, massless particles will be considered as quanta of dark matter, that are also sterile, which means that they do not enter into any interactions except gravitational. Radiation occurs in a T-symmetric way, into the future and into the past, so no energy is spent during the radiation, and such objects retain their mass. The radiation occurs in the radial direction; therefore, the considered flows have no transverse pressure. We denote this type of matter as null radial dark matter (NRDM).

The solution of Einstein's field equations with such matter term has a structure different from the Schwarzschild's one. This explains the designation of such compact massive objects as quasi-black holes, dark stars, Planck stars [2–5]. These solutions do not have an event horizon; instead, a deep gravitational well is formed at the gravitational radius. In our model, calculations for realistic astrophysical scenarios show the redshift value $z \sim 10^{49}$, which leads to a shift of the emitted dark matter from the Planck's $\lambda_{in} \sim 10^{-35} \text{m}$ to the ultrahigh wavelengths $\lambda_{out} \sim 10^{14} \text{m}$, respectively, ultralow energies $E_{out} \sim 10^{-20} \text{eV}$. Such extreme values complicate direct detection of isolated dark matter particles. Nevertheless, the total number of emitted quanta corresponds to the initially high Planck values. The energy density and radial pressure of such radiation creates a hidden mass distribution corresponding to the observed rotation curves of galaxies. The total mass contained in such radiation, due to its extension, significantly exceeds the mass of the emitting object within its gravitational radius. The geometric mass density profile $\rho \sim r^{-2}$ typical for the radial radiation creates a linearly growing mass profile $M \sim r$ and flat rotation curves $v^2 = GM/r = \text{Const}$. Taking into account the contributions of all black holes in the galaxy, supermassive and stellar mass ones, the distributions are modulated, and the observed nonflat rotation curves

of galaxies are reproduced with good accuracy. In addition, consideration of the astrophysical scenario with the fall of an asteroid onto the Planck core leads to electromagnetic radiation with the characteristics of Fast Radio Bursts.

In this work, the main attention will be paid to the following question. If we count the massless dark matter as homogeneous (hot dark matter, HDM), then the solution of the Friedmann equations will correspond to the radiation epoch and will not coincide with the current evolution, which in the standard model corresponds to a mixture of contributions from uniform cold dark matter (CDM) and dark energy (DE). However, in the model under consideration, the distribution of matter is inhomogeneous, and, as we will see, it allows the construction of models that are in agreement with the experiment. Thus, within the framework of this model, NRDM mimics CDM at the cosmological level. The CDM macro-particles are galaxies with massive halos surrounding them.

In more detail, we will consider several scenarios for the connection of galaxies in NRDM configuration with a uniform background. The backgrounds considered are vacuum, CDM and matter with DE equation of state. In the first two cases, totally uniform DE contribution can be also added. The hydrostatic equilibrium of the system and the correspondence of the densities to the observed Ω -parameters will be used as selection criteria. As a result of the analysis, it turned out that of the considered scenarios, only NRDM-DE connections meet the selection criteria. Such scenarios can be interpreted as a phase transition of dark matter from the NRDM state inside galaxies to the DE state outside. The specific mechanism for such a transition can be Bose-Einstein condensation (BEC).

In addition, we will consider the question of what happens if the dark matter particles are not exactly sterile, for example, are photons of the Standard Model. Phase transitions between dark matter and dark energy have been addressed in a number of recent works. In [6], a phase transition in a system of two scalar fields was considered, with a massive phase of dark matter condensing around galaxies, while outside one of the fields was absent, and the other turned into an exponentially rolling mode corresponding to dark energy. Conceptually, this model expands the cosmons theory [7], in which there is only one scalar field representing dark energy in the exponentially rolling mode, while its fluctuations represent dark matter. In the works [8, 9], a phase transition similar to the Ising model of ferromagnetism was considered, effectively generating two cosmological constants during the evolution of the universe. In the works [10–13] various scenarios of phase transitions at an early stage of the evolution of the universe, with the formation of bubbles of a new vacuum – dark energy were considered. In these scenarios, there was a transfer and filtration of dark matter through the walls of the bubbles, which in specific calculations reproduces its present abundance. In earlier works [14, 15], bubbles of a different vacuum after the phase transition were stabilized and led to the formation of massive compact objects – dark energy stars.

More general scenarios of the interaction of dark energy and dark matter were considered in a number of works [16–19], in the framework of the so-called Q-phenomenology. In this approach, the components of the dark sector are considered as two massive fluids, in which, in the absence of interaction, the energies are

conserved separately. When interaction is enabled between components, energy exchange occurs, parameterized by a single scalar function Q . For this function, one chooses linear dependencies of elementary densities, products of their degrees – by analogy with the kinetics of chemical reactions, and various other model forms. The calculation results were then compared with the cosmological observables. In works [20–33] the interaction of dark matter and dark energy was considered in relation to cosmological tensions. These are the discrepancies between the Hubble parameter and other cosmological properties, found in different types of observations, in particular, for the early and late stages of the evolution of the universe. The direct relation of the dark matter – dark energy interaction models with cosmological tensions can be explained. In the absence of the interaction, the components of the dark sector evolve independently, being bound only by the common gravitational field. From here it is easy to obtain the individual dependences of the component densities on the scale factor of the universe. This makes directly observable variables (such as distribution of CMB inhomogeneities, luminosity-distance-redshift dependence, etc.) related with model parameters (such as Hubble parameter today, linear fluctuation of the matter density field, etc.). When the interaction is turned on, the components begin to pump into each other; as a result, the relationship of the model parameters with the observed variables is modified. A similar approach is used in the models of dynamical dark energy [34–36], where the equation of state or the density of dark energy are modified directly. The resulting changes manifest themselves as tensions between the values of the Hubble parameter, deduced from different types of measurements without model modification. Within this framework, with the right model modification, the cosmological tensions should disappear.

The idea that dark matter and/or energy are associated with Bose-Einstein condensation, are represented by a superfluid liquid, was considered in a number of works [37–43]. In particular, [43] considered a complex scalar field with a potential equivalent to Chaplygin gas. While the specific form of the potential is not important, the presence of a minimum in it is significant. In this model, the dark energy is the state of Bose-Einstein condensate, asymptotically attained by the scalar field at this minimum. Dark matter was viewed as an excited state described by a gas of quasiparticles. In our work, a similar model will be considered, in which the outer zone of the galactic halo will also be occupied by Bose-Einstein condensate, while the distribution of dark matter in the inner part of the halo will be associated with the emission of particles from RDM stars.

First, in Section 20.2, we will recall the structure of the RDM model, then consider a number of scenarios for its connection with a uniform background. Not all of the scenarios will be successful, but we will describe all in detail to rule out unsuccessful options. Section 20.3 considers separately the photon case. The details of the constructions are given in the Appendix.

20.2 Estimations for various scenarios

The model [1] considers three cases: massive, null or tachyon radial dark matter (M/N/T-RDM). The tachyon case is too exotic and will not be considered here. On

the other hand, the massive case is similar to the commonly considered uniform cold dark matter (CDM). In this paper, we focus on the intermediate case, null or light-like dark matter. The quanta of such dark matter are massless sterile particles of an unspecified type.

The main formulas that determine the distribution of masses and pressures of dark matter in the model under consideration are

$$\rho = p_r = \epsilon/(8\pi r^2), \quad p_t = 0, \quad \rho_{\text{grav}} = \rho + p_r + 2p_t, \quad (20.1)$$

where ρ is the mass density, p_r is the radial pressure, p_t is the transverse pressure, ρ_{grav} is the gravitating mass density, r is the radius, ϵ is constant scaling parameter, in the geometric system of units $G = c = 1$. Such dependence's are established at large distances from the center of the galaxy, when all sources of dark matter (RDM stars), distributed over the galaxy in proportion to the density of the luminous matter, can be considered as concentrated in one center. The integrated gravitating mass for such a distribution is linear in the radius: $M_{\text{grav}} = \epsilon r$, and the square of the orbital velocity is constant and equal to $v^2 = M_{\text{grav}}/r = \epsilon$.

In relation to the ϵ -parameter for the Milky Way (MW) galaxy, [1] provides several estimates. The simplest, if one places a single RDM star in the center of the galaxy and completely neglect the contribution of the luminous matter, leads to a flat rotation curve with an orbital velocity $v \sim 200\text{km/s}$, $\epsilon = (v/c)^2 \sim 4 \cdot 10^{-7}$. A more accurate estimate is obtained from the fit of the MW rotation curve, the so-called Grand Rotation Curve (GRC, [44–48]). From this fit it can be seen, [1] Fig.2, that on an approximately flat portion of the rotation curve at the position of the Sun $r \sim 8\text{kpc}$ there is a significant contribution of luminous matter, as a result of which the contribution of dark matter to v^2 is less than the trivial estimate. Further, with increasing radius, the contribution of luminous matter decreases, while the contribution of dark matter remains constant up to $R_{\text{cut}} \sim 50\text{kpc}$. This contribution corresponds to the galactic $\epsilon = M_{\text{dm}}(R_{\text{cut}})/R_{\text{cut}}$, in geometric units, being averaged over the scenarios considered in [1]: $M_{\text{dm}}(R_{\text{cut}}) \sim 2.6 \cdot 10^{11} M_{\odot}$, $\epsilon \sim 2.5 \cdot 10^{-7}$. In this work, we will carry out estimates in order of magnitude, so it is not so important which definition of the galactic ϵ will be chosen. We prefer the latter, more precise definition and the corresponding value $M_{\text{dm}}(R_{\text{cut}})$.

When the contribution of individual black holes (identified with RDM stars) is considered, [1] Fig.5 gives estimates for the central supermassive and peripheral stellar black holes: $\epsilon_{\text{smbh}} \sim 10^{-10} - 10^{-7}$, $r_{\text{s,smbh}} \sim 1.2 \cdot 10^{10}\text{m}$; $\epsilon_{\text{sbbh}} \sim 10^{-16} - 10^{-12}$, $r_{\text{s,sbbh}} \sim 3 \cdot 10^4\text{m}$. This gives a floating estimate for the external wavelength of DM particles: $\lambda_{\text{out}} = r_s(8\pi/\epsilon)^{1/2}$, $\lambda_{\text{out,smbh}} \sim 10^{14} - 10^{16}\text{m}$, $\lambda_{\text{out,sbbh}} \sim 10^{11} - 10^{13}\text{m}$. This wavelength is highly dependent on the model used to describe the internal structure of RDM stars. In this work, for estimations, we prefer to use the value of the external wavelength λ_{out} and the corresponding redshift factor $A_{\text{QG}}^{1/2} = l_p/\lambda_{\text{out}}$ as phenomenological parameters.

The considered scenarios for the connection of galaxies in the NRDM configuration with a uniform background are schematically shown in Fig.20.1.

20.2.1 Rejected scenarios

Scenario S0.1: superposition of galactic halos without cutting. In this scenario, the dark matter halo of each galaxy extends to the radius of the visible universe $R_{\text{uni}} \sim 14\text{Gpc}$, dark matter from different halos does not interact and gives an additive contribution to the total mass density. If this scenario was valid, then it would be different from the radiation epoch, due to the following reasons. For the radiation epoch, the Big Bang (more precisely, the moment of recombination) is the initial flash, after which the homogeneous photon gas cools down as the universe expands. The energy of the photons changes with the scale factor as a^{-1} , and their numerical density as a^{-3} , which gives the dependence a^{-4} for the mass density. For the RDM model, despite the expansion of the universe and the separation of RDM stars from each other, the energy of DM particles near RDM stars is fixed, related to the above-mentioned parameter λ_{out} . It is important that this energy does not fall over time. The number density of RDM stars falls as a^{-3} , and as a result the average mass density also falls as a^{-3} , just like for CDM.

The scenario is prohibited due to the following evaluation. According to calculations for the Milky Way galaxy [1], the cutoff radius and halo mass are $R_{\text{cut}} \sim 50\text{kpc}$, $M_{\text{dm}}(R_{\text{cut}}) \sim 2.6 \cdot 10^{11} M_{\odot}$, and the mass of the disk and other emitting structures can be neglected in the order estimate. If one does not use the cutoff and continues the halo to the border of the universe, $M_{\text{dm}}(R_{\text{uni}}) = M_{\text{dm}}(R_{\text{cut}})R_{\text{uni}}/R_{\text{cut}} \sim 7.3 \cdot 10^{16} M_{\odot}$. If the result is multiplied by the estimated number of galaxies in the universe $N_{\text{gal}} \sim 2 \cdot 10^{12}$, we get $M_{\text{dm}} \sim 1.5 \cdot 10^{29} M_{\odot}$. Compared to the estimated mass of dark matter in the universe $M_{\text{dm,uni}} \sim 4.5 \cdot 10^{23} M_{\odot}$, this value is overestimated by the factor $\sim 3.2 \cdot 10^5$. The mass density averaged over the volume of the universe for the obtained value of M_{dm} will be $\rho_{\text{dm}} \sim 8.6 \cdot 10^{-22} \text{kg/m}^3$, which is $\sim 3.2 \cdot 10^5$ more than the estimate from the critical density $\Omega_{\text{dm}}\rho_{\text{crit}} = 2.7 \cdot 10^{-27} \text{kg/m}^3$.

The following corrections can be made to this calculation. The geometric cutoff by R_{uni} for the galaxies located far from the center (which we locate in the MW) can reduce the halo mass, but the factor is small, at most 2. The mass density is everywhere understood as the gravitating mass density, which also includes the pressure $\rho_{\text{grav}} = \rho + p_r$. At cosmological distances, the energy of DM particles is redshifted, but considering distances up to $0.03R_{\text{uni}} \sim 420\text{Mpc}$, the mass density decrease factor will not exceed 20% (for the Hubble parameter $H_0 = 72\text{km/s/Mpc}$ such distances correspond to $z \sim 0.1$, 10% decrease in energy and 10% slowdown in time, affecting 20% decrease in flux density). This can be used to estimate the mass from below, as a result the $> 7.6 \cdot 10^3$ discrepancy will remain unexplained. Further, the estimate is based on the assumption that all galaxies have masses of the order of the MW. This, of course, is not the case, there is a distribution of galaxies by masses. An accurate account of the distribution of galaxies will be given in the Appendix, and a similar result will be obtained, within the accuracy of modeling the distribution of galaxies.

Now we assume that all galaxies are copies of the MW, the halo of each galaxy is extended to the radius R_{gal} and the relation $N_{\text{gal}}M_{\text{dm}}(R_{\text{cut}})/R_{\text{cut}} \cdot R_{\text{gal}} = M_{\text{dm,uni}}$ holds, at which all the necessary mass relations are joined. Substituting the known data, we get $R_{\text{gal}} = 44\text{kpc}$, which almost coincides with the value

of $R_{\text{cut},MW}$. An exact match of $R_{\text{gal}} = R_{\text{cut},MW}$ can be achieved by slightly adjusting the estimated number of galaxies to $N'_{\text{gal}} = 1.7 \cdot 10^{12}$. Thus, according to this estimate, if we imagine that the universe consists of copies of the MW galaxy, the halo of which is cut off by $R_{\text{cut}} \sim 50\text{kpc}$, then the total mass of dark matter in the universe will coincide in order of magnitude with its cosmological estimate. With this configuration, dark matter is entirely concentrated in galaxies and is absent in the intergalactic environment.

Let's find out what happens if the R_{cut} parameter is increased to 1Mpc. This is possible when the estimated number of galaxies is reduced to $N'_{\text{gal}} \sim 8.7 \cdot 10^{10}$. It is known that the mass-to-light ratio of galaxies stops changing at distances of this order of magnitude, see [49] Fig.2.5. Moreover, this value is of the order of intergalactic distances. Thus, a scenario is theoretically possible in which galaxies touch each other in the outer zones of their halos, although it may require tensions of the N_{gal} parameter.

Finally, for the original scenario in which the halos overlap and reach the size of the universe, it would be $N'_{\text{gal}} \sim 6.2 \cdot 10^6$, a too strong deviation from the observed value. Therefore, this scenario can be considered as excluded.

Scenario S0.2: touching halos in dynamic equilibrium. The above variant with halos touching each other in the outer region, with the refinement that galaxies can exchange dark matter. Null dark matter leaking from one galaxy is absorbed by neighboring galaxies, and vice versa. In fact, the world lines of dark matter form a network connecting the galaxies, and the concept of a spherical halo is only an approximation.

The problem here is as follows. As a result of the expansion of galaxies, DM particles coming from neighboring galaxies are subject to a small redshift z and decrease their energy and flux density by the corresponding factor. We consider RDM stars in a stationary T-symmetric scenario. The parameters of dark matter, in particular, its energy and flux density, coincide for the incoming and outgoing flows. Therefore, the exiting particles also have a reduced energy and flux density. With multiple reflections between galaxies, the redshift of DM particles accumulates, exactly as it would in a homogeneous environment. RDM stars act as spherical mirrors, changing the direction of the DM particles, but not their energy characteristics. Such an environment turns out to be equivalent to HDM, its evolution coincides with the era of radiation, which is different from the observed evolution of the universe today.

In fact, the stationary state of RDM stars requires T-symmetry only for the energy flux density ϵ , the individual energies of incoming and outgoing DM particles can be different, compensated by different number flux densities. This will not help, since it is energy density that governs cosmological evolution. Note also that in the equation $\rho_P = \epsilon / (8\pi r_s^2 A_{QG})$, which determines conditions on the surface of the Planck core, in the considered scenario the factors ϵ and A_{QG} are scaled equally so that the gravitational radius r_s can remain unchanged. Strictly speaking, changing ϵ and A_{QG} in stationary scenarios is also unacceptable, but we consider this change as performed rather slowly, quasi-statically. What happens in fast scenarios, as well as with T-asymmetric ϵ and variable r_s , can be found out only

after solving the dynamic RDM problem, which goes beyond the scope of this work.

Scenario S0.3: a halo surrounded by a massive thin shell. We now look at a few scenarios from the *termination shock* type. This phenomenon occurs at the edge of the solar system when the radially directed solar wind meets the isotropic interstellar medium. Similar phenomena can occur with dark matter at the edge of the galaxy when the radial flow of dark matter meets the intergalactic environment. First, we will consider a scenario in which an NRDM galaxy at radius R_{cut} is surrounded by a thin CDM layer, and there is a vacuum outside. The CDM layer is held in equilibrium by the NRDM pressure force and the force of gravity. If such a scenario was possible, the galaxies would be isolated from each other and would be massive balls floating in a vacuum. On a cosmological level, such matter is equivalent to CDM.

The equilibrium condition of forces can be written as $\epsilon/(8\pi r^2) \cdot 4\pi r^2 = \epsilon/r \cdot m$ for $r = R_{\text{cut}}$, whence the mass of the CDM layer $m = R_{\text{cut}}/2$, in geometric units. This is a huge mass, exceeding the mass of the galaxy $M_{\text{dm}}(R_{\text{cut}}) = \epsilon R_{\text{cut}}$, where $\epsilon \ll 1$, for MW $\epsilon = 2.5 \cdot 10^{-7}$. Formally, with such a mass, the galaxy is covered by its event horizon, becoming a black hole. More precisely, the calculation uses Newtonian equations and only shows that there is no solution in weak fields. The interpretation of this result is that the relativistic pressure at the boundary of the NRDM galaxy can be compensated only by relativistic gravitational forces.

The distribution of matter in the CDM layer obeys the Tolman-Oppenheimer-Volkoff (TOV) equation, the solution of which in weak fields and for a thin layer is described by the one-dimensional hydrostatic equation $\rho = \rho_0 \exp(-gh/w)$, where w - parameter of the equation of state (EOS) $p = w\rho$, for CDM $w = kT/m \ll 1$, all equations are written in geometric units. The pressure equilibrium at the boundary of the layer leads to $\epsilon/(8\pi R_{\text{cut}}^2) = w\rho_0$, also $g = \epsilon/R_{\text{cut}}$, whence $\rho = \epsilon/(8\pi R_{\text{cut}}^2 w) \cdot \exp(-\epsilon h/(wR_{\text{cut}}))$. Integrating this value, we get $m = 4\pi R_{\text{cut}}^2 \int \rho dh = R_{\text{cut}}/2$. The result is independent of w and coincides with the estimate above.

Scenario S0.4: halo surrounded by homogeneous dark matter. A variation of the previous scenario, where instead of vacuum there is a homogeneous dark matter with isotropic EOS outside: $p_{\text{bgr}} = w\rho_{\text{bgr}}$. Here we will consider two options: CDM $w \ll 1$, HDM $w = 1/3$. Pressure equilibrium at the halo boundary: $\epsilon/(8\pi R_{\text{cut}}^2) = w\rho_{\text{bgr}}$, gravitating masses: $M_{\text{dm,gal}} = N_{\text{gal}}\epsilon R_{\text{cut}}$, $M_{\text{dm,bgr}} = (1 + 3w)\rho_{\text{bgr}} \cdot (4\pi/3)(R_{\text{uni}}^3 - N_{\text{gal}}R_{\text{cut}}^3)$, an estimate of the total mass of dark matter in the universe: $M_{\text{dm,uni}} = M_{\text{dm,gal}} + M_{\text{dm,bgr}} = N_{\text{gal}}\epsilon R_{\text{cut}} + \epsilon(1 + 3w)/(6wR_{\text{cut}}^2)(R_{\text{uni}}^3 - N_{\text{gal}}R_{\text{cut}}^3)$. Note that, according to earlier calculations, the first term already corresponds in order to the cosmological estimate for the mass of dark matter. Only if the second term is small, this correspondence could be preserved. However, if we assume that the intergalactic distances significantly exceed the size of the halo, and the estimate $R_{\text{uni}}^3 \gg N_{\text{gal}}R_{\text{cut}}^3$ holds, then the second term $M_{\text{dm,uni}} \sim \epsilon R_{\text{uni}}^3/R_{\text{cut}}^2 \cdot (1+3w)/(6w)$, which for $\epsilon = 2.5 \cdot 10^{-7}$, $R_{\text{uni}} \sim 14\text{Gpc}$ and $R_{\text{cut}} \sim 50\text{kpc}$ matches $M_{\text{dm,uni}}/M_{\odot} \sim 5.7 \cdot 10^{27} (1 + 3w)/(6w)$. It can be seen that

already for $w = 1/3$ and even more so for $w \ll 1$ the result significantly exceeds the value $M_{\text{dm,uni}}/M_{\odot} \sim 4.5 \cdot 10^{23}$, obtained from cosmological estimates. Also for the above option with tension, $R_{\text{cut}} = 1\text{Mpc}$, $N'_{\text{gal}} = 8.7 \cdot 10^{10}$ the resulting formula is $M_{\text{dm,uni}}/M_{\odot} = 4.5 \cdot 10^{23} + 1.4 \cdot 10^{25}(1 + 3w)/(6w)$ does not allow CDM/HDM as background matter, for continuous matching with NRDM pressure at halo boundaries.

20.2.2 Accepted scenarios

Next, we'll look at scenarios involving dark energy. We will represent dark energy as a kind of matter, perhaps a kind of dark matter or its other phase state, which has an isotropic EOS $p_{\text{de}} = -\rho_{\text{de}}$, that is, $w = -1$, with positive ρ_{de} , constant within each phase. The density of the gravitating mass for such matter is negative and is equal to $\rho_{\text{de,grav}} = \rho_{\text{de}} + 3p_{\text{de}} = -2\rho_{\text{de}}$. The negativity of this density, provided that it prevails over other components, is the driving mechanism for the accelerated expansion of the universe.

Scenario S1.1: jump in the dark energy density at the halo boundary. Let there be two different dark energy densities, outside the halo $\rho_{\text{de,bgr}}$, inside the halo $\rho_{\text{de,gal}}$, with a jump at R_{cut} . Equilibrium pressure condition $\epsilon/(8\pi R_{\text{cut}}^2) = p_{\text{de,bgr}} - p_{\text{de,gal}} = \rho_{\text{de,gal}} - \rho_{\text{de,bgr}}$, gravitating masses: $M_{\text{dm,gal}} = N_{\text{gal}}\epsilon R_{\text{cut}}$, $M_{\text{de,gal}} = -2\rho_{\text{de,gal}}N_{\text{gal}} \cdot (4\pi/3)R_{\text{cut}}^3$, $M_{\text{de,bgr}} = -2\rho_{\text{de,bgr}} \cdot (4\pi/3)(R_{\text{uni}}^3 - N_{\text{gal}}R_{\text{cut}}^3)$, an estimate of the total mass of dark matter and dark energy in the universe: $M_{\text{dm+de,uni}} = M_{\text{dm,gal}} + M_{\text{de,gal}} + M_{\text{de,bgr}} = (2/3)\epsilon N_{\text{gal}}R_{\text{cut}} - (8\pi/3)\rho_{\text{de,bgr}}R_{\text{uni}}^3$. The second term here describes the total gravitating mass of dark energy, as if it uniformly filled the entire universe, including galactic halos. The first term is the gravitating mass of the galactic halo reduced by the factor $(2/3)$. In general, the model behaves like a mixture of uniform cold dark matter and uniform dark energy, like Λ CDM. In order of magnitude, for $R_{\text{cut}} = 50\text{kpc}$, the CDM mass corresponds to cosmological estimates. Fine tuning is also possible similar to scenario S0.1, the factor $(2/3)$ can be compensated for by a small increase in the estimated number of galaxies $N'_{\text{gal}} = 2.6 \cdot 10^{12}$.

Let us also analyze the expression for the gravitating mass of one galaxy: $M(r) = \epsilon r - 2\rho_{\text{de,gal}}(4\pi/3)r^3$. In the expression for the internal dark energy density $\rho_{\text{de,gal}} = \epsilon/(8\pi R_{\text{cut}}^2) + \rho_{\text{de,bgr}}$ for the selected value $R_{\text{cut}} = 50\text{kpc}$, after conversion to natural units, the first term is $5.6 \cdot 10^{-24}\text{kg/m}^3$, the second $\rho_{\text{de,bgr}} = \Omega_{\text{de}}\rho_{\text{crit}} = 6.8 \cdot 10^{-27}\text{kg/m}^3$, the first term dominates. Thus, continuous matching of pressures at the galactic boundary requires a jump in the dark energy density by a factor of $\sim 10^3$. Note that this jump can be reduced by adjusting the R_{cut} parameter.

Further, the expression for the mass function at the selected parameters becomes $M(r)/M_{\odot} = 2.6 \cdot 10^{11}(r/R_{\text{cut}}) - 8.7 \cdot 10^{10}(r/R_{\text{cut}})^3$. In the inner part of the rotation curve, for example, up to the position of the Sun $r \sim 8\text{kpc}$, the first term dominates. Thus, the interior of the rotation curve is unaffected by the dark energy introduced into the model. In the outer part of the curve, the contribution of the enhanced internal dark energy density becomes noticeable, finally, it is this contribution

that leads to the factor $(2/3)$ in the mass formulas. The term proportional to the external dark energy density for the chosen parameters of the model makes a negligible contribution within the galaxy. It begins to dominate in the formula $M(r > R_{\text{cut}}) = (2/3)\epsilon R_{\text{cut}} - (8\pi/3)\rho_{\text{de,bgr}}r^3$ at distances $r > 0.6\text{Mpc}$, at which the effects of cosmological expansion become noticeable.

It becomes clear that in the considered scenario the rotation curve undergoes a change only in its outer part, where it decreases by $\sqrt{2/3}$ factor, about 18%. As we will see later, the measurement errors in this range significantly exceed this variation, which makes it impossible to distinguish this solution from the reference profile.

Thus, we have obtained the first scenario, which connects null matter in galactic halos with a cosmological background of dark energy and turns out to be equivalent to the uniform ΛCDM model. A calculation based on a simple equilibrium of pressures does not provide any indication for the possible nature of the increased density of dark energy within the galaxy. Phenomenologically, dark energy can be described as a medium in which its constituent particles experience mutual attraction. This attraction corresponds to negative pressure, while the work of external forces $-pdV$ is used to increase the internal energy ρdV , in accordance with EOS $-p = \rho$. The presence of two phases with different pressures suggests two varieties for such media. An analogy can be drawn here with the string model. The energy of a string is proportional to its length, just like the total mass for dark energy is proportional to its volume. The strings have a fixed tension, which is a constant in the model. One can consider strings with different tensions as separate varieties of the same model. The considered scenario demonstrates a fundamental possibility; further possible alternatives will be considered.

Scenario S1.2: surface tension at the boundary between the halo and the background from dark energy. Let inside R_{cut} be NRDM, outside – dark energy with density $\rho_{\text{de,bgr}}$, and surface tension with coefficient σ acts on the boundary. Equilibrium pressure condition $\epsilon/(8\pi R_{\text{cut}}^2) = 2\sigma/R_{\text{cut}} + p_{\text{de,bgr}} = 2\sigma/R_{\text{cut}} - \rho_{\text{de,bgr}}$, gravitating masses: $M_{\text{dm,gal}} = N_{\text{gal}}\epsilon R_{\text{cut}}$, $M_{\text{de,surf}} = -N_{\text{gal}}\sigma \cdot 4\pi R_{\text{cut}}^2$, $M_{\text{de,bgr}} = -2\rho_{\text{de,bgr}} \cdot (4\pi/3)(R_{\text{uni}}^3 - N_{\text{gal}}R_{\text{cut}}^3)$, an estimate of the total mass of dark matter and dark energy in the universe: $M_{\text{dm+de,uni}} = M_{\text{dm,gal}} + M_{\text{de,surf}} + M_{\text{de,bgr}} = (3/4)\epsilon N_{\text{gal}}R_{\text{cut}} + (2\pi/3) \cdot N_{\text{gal}}R_{\text{cut}}^3\rho_{\text{de,bgr}} - (8\pi/3)\rho_{\text{de,bgr}}R_{\text{uni}}^3$. Here the third term corresponds to the cosmological contribution of dark energy, it grows in the negative direction in proportion to the volume of the expanding universe. The first and second terms are preserved in the expansion and represent CDM. At $R_{\text{cut}} = 50\text{kpc}$, the first term significantly exceeds the second, and, as in the previous scenario, allows fine tuning of the parameters to the cosmological value of CDM density.

In the above formulas, the gravitating mass corresponding to the boundary layer is calculated as follows. Surface tension is related to negative transverse pressure and positive energy density as $-p_t = \rho = \sigma/dr$, where dr is the layer thickness. The gravitating mass of the spherical layer is $M = (\rho + 2p_t)Sdr = -\sigma \cdot 4\pi R_{\text{cut}}^2$. There is also a radial pressure p_r inside the layer, which continuously interpolates

the boundary values, remains bounded, and makes a vanishing contribution at $dr \rightarrow 0$.

When choosing $R_{\text{cut}} = 50\text{kpc}$, the density jump between external dark matter and NRDM is still $\sim 10^3$ times, but here it is compensated by surface tension. As in the previous scenario, the pressure jump can be reduced by adjusting the R_{cut} parameter. The mass function for $r < R_{\text{cut}}$ coincides with the NRDM dependence $M(r < R_{\text{cut}}) = \epsilon r$, thus the inner rotation curve does not change. When passing through R_{cut} , the mass function undergoes a jump $M(R_{\text{cut}} + 0) = (3/4)\epsilon R_{\text{cut}} - 2\pi R_{\text{cut}}^3 \rho_{\text{de,bgr}}$, the coefficient $(3/4)$ appears in the first term, and the second term also appears. With the chosen parameters, the first term is $1.9 \cdot 10^{11} M_{\odot}$, the second $-7.9 \cdot 10^7 M_{\odot}$, the first term dominates. Further, the mass function includes the cosmological term $M(r > R_{\text{cut}}) = (3/4)\epsilon R_{\text{cut}} + (2\pi/3)R_{\text{cut}}^3 \rho_{\text{de,bgr}} - (8\pi/3)\rho_{\text{de,bgr}} r^3$, which dominates for $r > 0.6\text{Mpc}$.

The resulting scenario is very close to the previous one, only a different mechanism is used to compensate for the pressure jump at the edge of the galaxy. Phenomenologically, if we consider dark energy as a medium consisting of interacting particles, the presence of a boundary can lead to the appearance of a surface term in the equations, as for classical media. The jump in the mass function that appears in this scenario corresponds to a jump in the rotation curve by the factor $\sqrt{3/4}$, about 13%. This jump also occurs in the outer region, where the scatter of experimental data is large, so that it can be unnoticed. Also, this jump can be an idealization of a more complex scenario in which the transition layer has a finite thickness. The possibility of a gradual change of EOS will be explored in the following scenario.

Scenario S1.3: phase transition of dark matter to dark energy. In this scenario, we assume that dark energy is a form of dark matter, and with the increasing radius, there is a continuous transition between the corresponding EOS: $p_r = w_r \rho$, $p_t = w_t \rho$, (w_r, w_t) change from $(1, 0)$ for $r = R_{\text{cut}1}$ to $(-1, -1)$ for $r = R_{\text{cut}2} > R_{\text{cut}1}$. The result depends on the transition path, which we fix from physical considerations as follows. Initially, from $r = R_{\text{cut}1}$ to the intermediate point $r = R_{\text{cut}1b}$, only w_t changes, from 0 to -1 . The inclusion of transverse attraction between flows of dark matter leads to the Joule-Thomson effect known in gas dynamics, cooling of flows, which in our case manifests itself in a rapid decrease in the mass density ρ . Further, from $r = R_{\text{cut}1b}$ to $r = R_{\text{cut}2}$ only w_r changes, from 1 to -1 . In this range, the contributions of dark matter from different sources are mixed, the matter becomes isotropic. Further, the matter obeys isotropic EOS for dark energy, and its density and pressure become constant.

It is convenient to solve the problem in logarithmic variables $\chi = \log r$, $\xi = \log \rho$, with the restriction $\rho > 0$. To interpolate $w_{t,r}$ in the corresponding intervals, we choose functions linear in χ , and the positions of the endpoints $\{x_1, x_{1b}, x_2\} = \log\{R_{\text{cut}1}, R_{\text{cut}1b}, R_{\text{cut}2}\}$ will be chosen from the correspondence of the model to the cosmological parameters.

The stationary spherically symmetric solutions considered here satisfy the hydrostatic equation for anisotropic medium, see Appendix for details: $r(p_r + \rho)\mathcal{A}'_r + 2A(r(p_r)'_r + 2p_r - 2p_t) = 0$. The first term describes the gravitational interac-

tion, which in our problems can be neglected. The reason for this is that in the weak field limit $A \sim 1 + 2\phi$, $A'_r \sim 2g$, where ϕ is the gravitational potential, $g = \phi'_r = M_{\text{grav}}(r)/r^2$ is gravitational field in the used system of units, $|\phi| \ll 1$, $rg \ll 1$. In our models, the density and pressure are controlled by a small common factor ϵ , and the first term turns out to be of the next smallness order compared to the second one. This property of the weak-field regime can also be verified on the exact solutions of the hydrostatic equation, given in Appendix.

Thus, we can concentrate on the second term: $\tau(p_r)'_r + 2p_r - 2p_t = 0$. Let's go to logarithmic variables and substitute EOS: $w_r \xi'_x + (w_r)'_x + 2(w_r - w_t) = 0$. The solution is: $\xi = -\int dx((w_r)'_x + 2(w_r - w_t))/w_r$. In the following, we will consider regular solutions in which the denominator and the numerator in the integrand vanish simultaneously: $w_r = 0$, $(w_r)'_x = 2w_t$. Note that, with our choice of the interpolation order, the condition $w_r = 0$ can be satisfied only at the second stage, in the interval $[x_{1b}, x_2]$, while, due to the linearity of the interpolation, the condition $(w_r)'_x = 2w_t = -2$ holds on this entire interval.

At the first stage $[x_1, x_{1b}]$, $(w_r, w_t) = (1, -q)$, $q = (x - x_1)/(x_{1b} - x_1)$, calculating the integral, we get $\xi_{1b} - \xi_1 = -3(x_{1b} - x_1)$. At the second stage $[x_{1b}, x_2]$, $(w_r, w_t) = (1 - 2q, -1)$, $q = (x - x_{1b})/(x_2 - x_{1b})$, from the condition $(w_r)'_x = -2$ we get $q'_x = 1$, that is, $x_2 = x_{1b} + 1$. Calculating the integral, we get $\xi_2 - \xi_{1b} = -2$. Hence $\log(\rho_1/\rho_2) = \xi_1 - \xi_2 = 3(x_{1b} - x_1) + 2$. Choosing $\rho_1 = \epsilon/(8\pi R_{\text{cut}1}^2)$, $R_{\text{cut}1} = R_{\text{cut}} = 50\text{kpc}$, $\epsilon = 2.5 \cdot 10^{-7}$, $\rho_2 = \rho_{\text{de,bgr}} = \Omega_{\text{de}} \rho_{\text{crit}} = 6.8 \cdot 10^{-27} \text{kg/m}^3$, and also converting all values into the natural system of units, we get: $\rho_1/\rho_2 = 824$, $R_{\text{cut}1b} = 0.24\text{Mpc}$, $R_{\text{cut}2} = 0.65\text{Mpc}$. Thus, the required density variation from NRDM to the background dark energy in the considered scenario fixes the halo cutoff parameters to reasonable values.

Next, consider the contribution of the galaxy to the cosmological mass density. The gravitating mass density is $\rho_{\text{grav}} = (1 + w_r + 2w_t)\rho$, and the gravitating mass of the spherical layer is $\Delta M_{\text{grav}} = 4\pi \int \rho_{\text{grav}} r^2 dr$. After the transition to logarithmic variables, the integrals over two interpolation intervals can be taken analytically. Omitting cumbersome expressions, we will immediately give the numerical answer $\{M_1, \Delta M_1, \Delta M_2, M_{\text{vac}}\} = \{2.60, 2.67, -2.60, 2.35\} \cdot 10^{11} M_\odot$. Here $M_1 = \epsilon R_{\text{cut}}$ is the mass of the NRDM halo, $\Delta M_{1,2}$ are the masses of the spherical layers for two interpolation intervals, $M_{\text{vac}} = (8\pi/3)\rho_{\text{de,bgr}} R_{\text{cut}2}^3$ is the compensation mass of the vacuole arising from the rearrangement of the terms $M_{\text{dm+de,uni}} = N_{\text{gal}} M_{\text{dm+de,gall}} - (8\pi/3)\rho_{\text{de,bgr}}(R_{\text{uni}}^3 - N_{\text{gal}} R_{\text{cut}2}^3) = N_{\text{gal}}(M_{\text{dm+de,gall}} + M_{\text{vac}}) - (8\pi/3)\rho_{\text{de,bgr}} R_{\text{uni}}^3$. The M_{vac} term should be taken into account in cosmological calculations, when reducing to the parameters of a homogeneous medium, while when calculating the rotation curves only the actually present masses should be taken, and M_{vac} should be omitted. Interestingly, there is an identity $M_1 + \Delta M_2 = 0$, which holds exactly, at the analytical level, but is probably a coincidence due to a special choice of interpolating functions. Also of interest is the approximate equality of all mass contributions in their absolute value. The cosmological mass per galaxy is the sum of all these contributions and is equal to $M_{\text{dm+de,gall}} + M_{\text{vac}} = 5 \cdot 10^{11} M_\odot$. This gives a coincidence with the cosmological CDM mass $M_{\text{dm,uni}} = 4.5 \cdot 10^{23} M_\odot$ in order of magnitude, for exact coincidence the estimated number of galaxies should be reduced to $N'_{\text{gal}} = 9 \cdot 10^{11}$,

2.2 times less than the nominal value. One can also adjust the ϵ parameter, but since our estimates of the halo cutoff parameters were tied to MW values, these estimates must be repeated when ϵ changes.

The constructed scenario, obviously, contains wide arbitrariness in the choice of interpolating functions and is rather a proof of the existence of a solution satisfying cosmological estimates. This existence in itself is non-trivial. Recall that in standard cosmology, null, hot dark matter leads to a different rate of cosmological expansion today and is forbidden. The possibility of joining hot dark matter with dark energy within the galactic halo, at a cosmological level equivalent to Λ CDM, is the main result of this work. The specific way of joining may be different, in the Appendix we will discuss the possibility of narrowing this arbitrariness.

For now, note that the interpolation order selected in the model is significant. The reverse order when (w_r, w_t) changes from $(1, 0)$ to $(-1, 0)$ for $r \in [R_{\text{cut}1}, R_{\text{cut}1b}]$ leads to the condition $(w_r)'_x = 2w_t = 0$, not feasible for linear functions. If we interpolate both terms at the same time, $(w_r, w_t) = (1 - 2q, -q)$, $q = (x - x_1)/(x_{2b} - x_1)$, from the conditions $w_r = 0$, $(w_r)'_x = 2w_t$ we get $q = 1/2$, $q'_x = 1/2$, that is, $x_{2b} = x_1 + 2$. Moreover, $\xi_{2b} = \xi_1 - 2$, which for $R_{\text{cut}1} = 50\text{kpc}$ gives $R_{\text{cut}2b} = e^2 R_{\text{cut}1} = 0.37\text{Mpc}$, $\rho_1/\rho_{2b} = e^2 \sim 7.4$, far from the experimental value of $\rho_1/\rho_2 \sim 824$. The physical rationale with the initial cooling of dark matter due to the Joule-Thomson effect and the subsequent transition to the isotropic phase for the cooled gas was important for obtaining the strong density drop observed in real galaxies.

Here are some graphs showing the behavior of the main physical profiles in the considered scenario. Fig.20.2 left shows the dependence of $\xi = \log \rho$ on $x = \log r$. Initially, the graph contains an NRDM line with a slope of -2 , which corresponds to the $\rho \sim r^{-2}$ dependence. Further, at point 1, the transverse interaction between the flows turns on, and the Joule-Thomson effect is superimposed on the continuing radial drop in density. Here, the slope of the graph $d\xi/dx$ is continuously changing from -2 to -4 . Further, in the interval from 1b to 2, a transition to the isotropic phase follows, the slope in this case being equal to -2 . After point 2, there is isotropic dark energy with constant density, slope 0. The resulting density variation between points 1 and 2 corresponds to the experimentally observed factor of $\rho_1/\rho_2 \sim 824$.

For comparison, the option shown in gray when (w_r, w_t) are linearly interpolated at the same time. The slope between points 1 and 2b is -1 . After 2b, there is an isotropic phase with a slope of 0. Due to these changes, the graph goes much higher than the previous one, the density variation does not correspond to the observed value.

Fig.20.2 right shows the dependence of $M_{\text{grav}}(r)$. Initially, there is an NRDM part with a characteristic linear dependence, then at point 1b, the dependence passes through a maximum and, after point 2, is described by a negative cubic term corresponding to the contribution of dark energy.

Scenario S1.4: Bose-Einstein condensation. In this scenario, two phases are also considered: the internal NRDM phase, described by the classical particle model, and the external phase, described by a complex scalar field. This field theory is

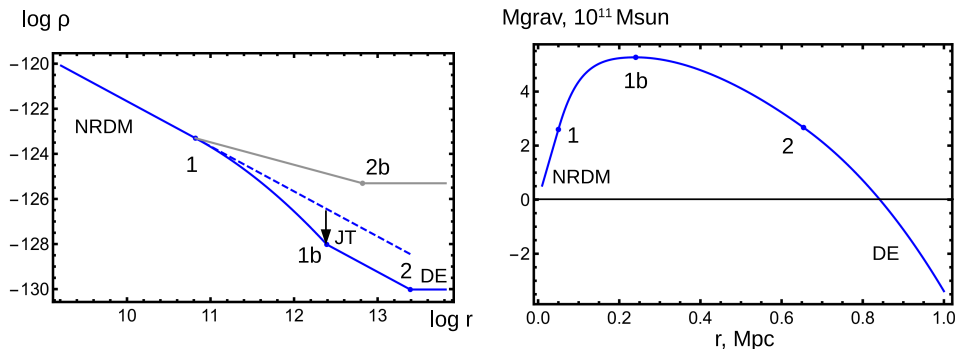


Fig. 20.2: Physical profiles for scenario S1.3.

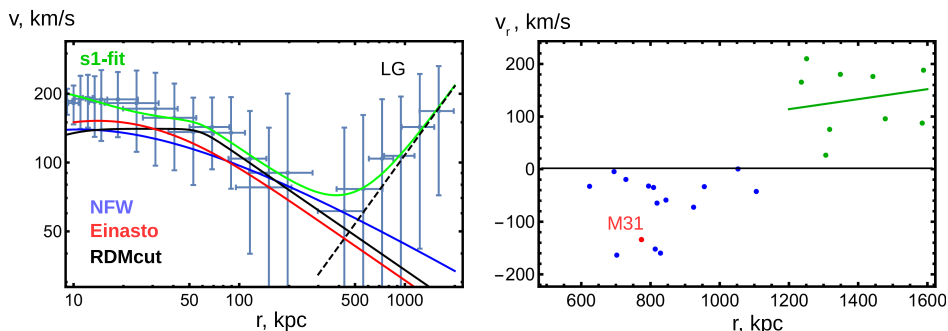


Fig. 20.3: Left: an external part of the Milky Way rotation curve, according to [48]. A variety of profiles are shown, including the RDMcut scenario from [1]. Right: outer part of the dependence of radial velocity on the distance, according to [46]. The position of the galaxy M31 is marked, the outer part of the graph is fitted with a Hubble-alike dependence.

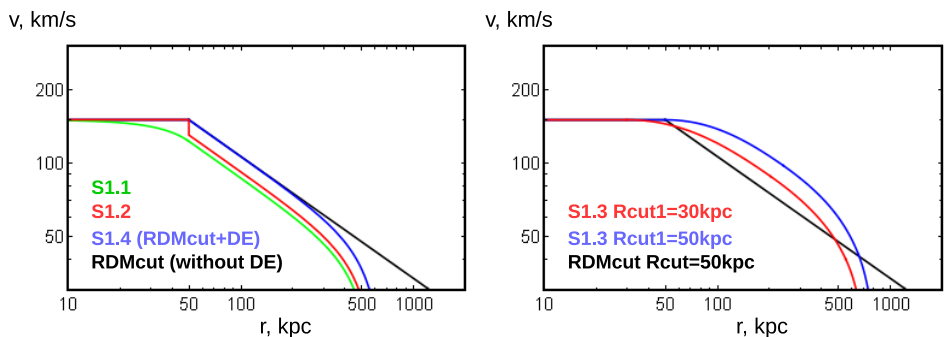


Fig. 20.4: Profiles built in the scenarios of this work, compared with the RDMcut profile.

used in phenomenological models of Bose-Einstein condensation, as well as in cosmological models of quintessence and its variants (k-essence, quartessence, Chaplygin gas), see [43] and references therein. Therefore, this scenario assumes that dark matter particles are emitted by RDM stars in the galaxy and undergo Bose-Einstein condensation at large distances. Alternatively, these can be particles of different types that are in contact equilibrium at the edge of the galactic halo. In the field theory under consideration, the Lagrangian, the energy-momentum tensor, and the equations of motion have the form [50] Chap.6.3,7.5:

$$L = -(\partial_\mu \phi^* \partial^\mu \phi)/2 - V(|\phi|^2), \quad (20.2)$$

$$T_{\mu\nu} = (\partial_\mu \phi^* \partial_\nu \phi + \partial_\nu \phi^* \partial_\mu \phi)/2 + g_{\mu\nu} L, \quad (20.3)$$

$$(-\partial^2/\partial t^2 + \Delta)\phi = 2V'(|\phi|^2)\phi. \quad (20.4)$$

Here the equations of motion are written in a flat background, and the rest of the expressions are valid for an arbitrary metric. We also remind that for a scalar field the covariant and coordinate derivatives are equal: $\nabla_\mu \phi = \partial_\mu \phi$. The field equations belong to the well-known nonlinear Klein-Gordon type with the potential. For $V(|\phi|^2) = \text{Const} + m^2|\phi|^2/2$ the equations become linear and describe the behavior of a free massive scalar field. We neglect the influence of gravity on the scalar field, assuming that the gravitational fields are weak and the corresponding solutions are relativistic.

We will use a smooth potential $V(s^2)$, which has a minimum for a nonzero value of the argument $V(s_1^2) = V_{\min}$, $s_1^2 > 0$. For this minimum, the constant function $\phi = s_1$ is the exact solution to the problem. For such a function, using a spherical coordinate system and a metric of signature $(-+++)$, we write out the mixed components of the energy-momentum tensor:

$$T_\mu^\nu = \text{diag}(-\rho, p_r, p_t, p_t) = -V_{\min} \cdot \text{diag}(1, 1, 1, 1), \quad (20.5)$$

$$\rho = V_{\min}, \quad p_r = p_t = -V_{\min}, \quad (20.6)$$

$$\rho_{\text{grav}} = \rho + p_r + 2p_t = -2V_{\min}. \quad (20.7)$$

The result coincides with the standard EOS of dark energy, which explains the interest to this model in the cosmological context. We will fix $V_{\min} > 0$, and for simplicity we will assume $V > 0$ everywhere.

In this paper, we consider stationary spherically symmetric problems for which there are particular solutions of the form $\phi = e^{iEt} s(r)$, with real $E, s(r)$. With this substitution, the dimension is reduced $(E^2 + \Delta)s = 2V'(s^2)s$. Next, we will consider stationary solutions $E = 0$, $\phi = s(r)$. The uniqueness of solutions with stationary boundary conditions is demonstrated in the Appendix. Thus, all solutions that can be attached to the constant $\phi = s_1$ are globally stationary and have the form $\phi = s(r)$.

Calculating EOS for stationary solutions

$$T_\mu^\nu = \text{diag}(0, s'^2, 0, 0) - \text{diag}(1, 1, 1, 1) \cdot (s'^2/2 + V(s^2)), \quad (20.8)$$

$$\rho = -p_t = s'^2/2 + V(s^2) > 0, \quad p_r = s'^2/2 - V(s^2), \quad (20.9)$$

$$\rho_{\text{grav}} = \rho + p_r + 2p_t = -2V(s^2). \quad (20.10)$$

If the potential is shallow, then $\rho_{\text{grav}} \sim -2V_{\text{min}}$, as for DE. This result is quite remarkable. As a consequence, the scenario can be configured in such a way that the gravitating density profile immediately after the NRDM phase $\rho_{\text{grav}} = \epsilon/(4\pi r^2) > 0$ drops sharply to the DE phase $\rho_{\text{grav}} \sim -2V_{\text{min}}$. This reproduces the phenomenological RDMcut scenario discussed in [1], with a sharp cutoff of the density to almost zero at the R_{cut} radius. The DE contribution begins to be felt at much larger distances and reproduces the observed effect of accelerated cosmological expansion there.

Technically, the condition of connection for the radial pressure component at the boundary between the phases must still be met. This condition can be satisfied if the model has enough degrees of freedom to ensure that in p_r , the first term $s'^2/2$ dominates over the second $-V(s^2)$. In this case, it is possible to ensure the continuous connection with the positive p_r from the NRDM phase, no matter how large this value may be. Physical manifestations are defined only by ρ_{grav} and do not depend on the details of this connection.

We will make such a connection for a particular choice of the potential. First of all, we write the right-hand side of the equations of motion in the form $2V'(s^2)s = V(s^2)'_s$. Next, using the reparametrization of the argument $V(s^2) = V_1(s)$, we choose the potential as given below. The remarkable properties of such a potential are the linearity of the equation of motion, the existence of an analytical solution, and also the fact that any potential in the vicinity of the minimum can be written as follows:

$$V_1(s) = V_{\text{min}} + \alpha/2 (s - s_1)^2, \quad \alpha > 0, \quad s_1 > 0, \quad (20.11)$$

$$s'' + 2s'/r = \alpha(s - s_1), \quad (20.12)$$

$$s = s_1 + (e^{-\sqrt{\alpha}r} C_1)/r + (e^{\sqrt{\alpha}r} C_2)/(2\sqrt{\alpha}r). \quad (20.13)$$

Selecting a branch with finite $s \rightarrow s_1$ at $r \rightarrow \infty$, we get $C_2 = 0$. We also impose the condition $C_1 > 0$ in order to ensure $s > s_1$ on the solutions. For $s > s_1$, the ascending branch of $V_1(s)$ corresponds to the positive square of the mass, normal particles. At that time, for $s < s_1$, the descending branch of $V_1(s)$ formally corresponds to the negative square of the mass, the tachyon case, but this branch is not used in the solutions we have considered. Calculating the components

$$p_r = e^{-2\sqrt{\alpha}r} C_1^2 (1 + 2\sqrt{\alpha}r)/(2r^4) - V_{\text{min}}, \quad (20.14)$$

$$\rho_{\text{grav}} = -\alpha C_1^2 e^{-2\sqrt{\alpha}r}/r^2 - 2V_{\text{min}}, \quad (20.15)$$

we see that by choosing C_1 it is always possible to achieve a connection with positive p_r from the NRDM phase. At the same time, choosing small α , one can reach $\rho_{\text{grav}} \sim -2V_{\text{min}}$. With such a choice of parameters, the solution comes arbitrarily close to the RDMcut+DE profile shown in Fig.20.3, thereby providing a deeper physical foundation for it.

As before, exact matching with cosmological estimates can be achieved by comparing $N'_{\text{gal}}(M_{\text{dm,gal}} + M_{\text{vac}})$, $M_{\text{dm,gal}} = \epsilon R_{\text{cut}} c^2/G$, $M_{\text{vac}} = (8\pi/3)\rho_{\text{de,bgr}} R_{\text{cut}}^3$, with known $M_{\text{dm,uni}} \sim 4.5 \cdot 10^{23} M_{\odot}$. Exact matching is ensured, in particular, when choosing $R_{\text{cut}} = 50\text{kpc}$, $N'_{\text{gal}} = 1.7 \cdot 10^{12}$, or $R_{\text{cut}} = 44\text{kpc}$, $N'_{\text{gal}} = 2 \cdot 10^{12}$, or $R_{\text{cut}} = 0.6\text{Mpc}$, $N'_{\text{gal}} = 1.4 \cdot 10^{11}$.

20.3 Addition: photon case

Since the photons of the Standard Model are not sterile, corrections are required to use them in the described scenarios. Specifically, an analysis of three questions is required:

- generation of longwave photons by compact massive objects;
- the passage of such photons through the interstellar medium;
- Bose-Einstein condensation of photons.

In this article, we will only consider in detail the question of photon generation. The main difference from the sterile case is the interaction of photons at high energies, leading to the production of e^+e^- pairs and other particles. We will assume that these particles are localized in the ultrarelativistic plasma layer between the NRDM phase and the Planck core. Fortunately, the EOS of ultrarelativistic plasma is independent of its actual composition and even its temperature. Such a plasma is described by the universal TOV equation with a factor $w = 1/3$, as if the plasma consisted entirely of radiation. In this case, it is only important that the kinetic energies of plasma particles significantly exceed their rest masses, and also that the EOS is isotropic and has equal components of radial and transverse pressure. The second question, about the possible passage of photons through the ISM, imposes a limitation on their frequency. Electromagnetic waves can propagate in the ISM only if their frequency exceeds Langmuir's value, which varies from a few kHz in the central regions of the galaxy to some Hz in the outer regions. On the other hand, if the wavelength becomes comparable to the size of galactic structures, then, presumably, waves can penetrate them without absorption, similar to long radio waves penetrating the walls of buildings and other structures. That is, it can be expected that the ISM transparency window, which closes at Langmuir's frequency, reopens at ultra-low frequencies.

Finally, the third question, about the possibility of Bose-Einstein condensation of photons, has been intensively discussed recently. In a complete vacuum, photons cannot condense, because they are massless, and the state of minimum energy for them coincides with the vacuum. At the same time, in [51] and references therein it was noted that in ISM/IGM photons have a dispersion relation equivalent to the presence of a nonzero mass of a photon. As a result, there is a theoretical possibility that the photons in medium can undergo Bose-Einstein condensation.

Now we will consider the question of photon generation by the NRDM|TOV system. The required equations are listed in the Appendix. The equations are formulated for the metric profiles A and B, in the logarithmic representation: $x = \log r$, $a = \log A$, $b = \log B$. Hereinafter, $A = -g_{tt}$ and $B = g_{rr}$ denote the temporal and radial components of the metric tensor, which completely describe the structure of the gravitational field for stationary spherically symmetric problems. We numerically solve these equations using *Mathematica* NDSolve algorithm. As noted in [1], TOV systems are characterized by critical phenomena, abrupt changes in the solution with continuous change in parameters. As a result, the NRDM|TOV system has a richer solution structure than a pure NRDM.

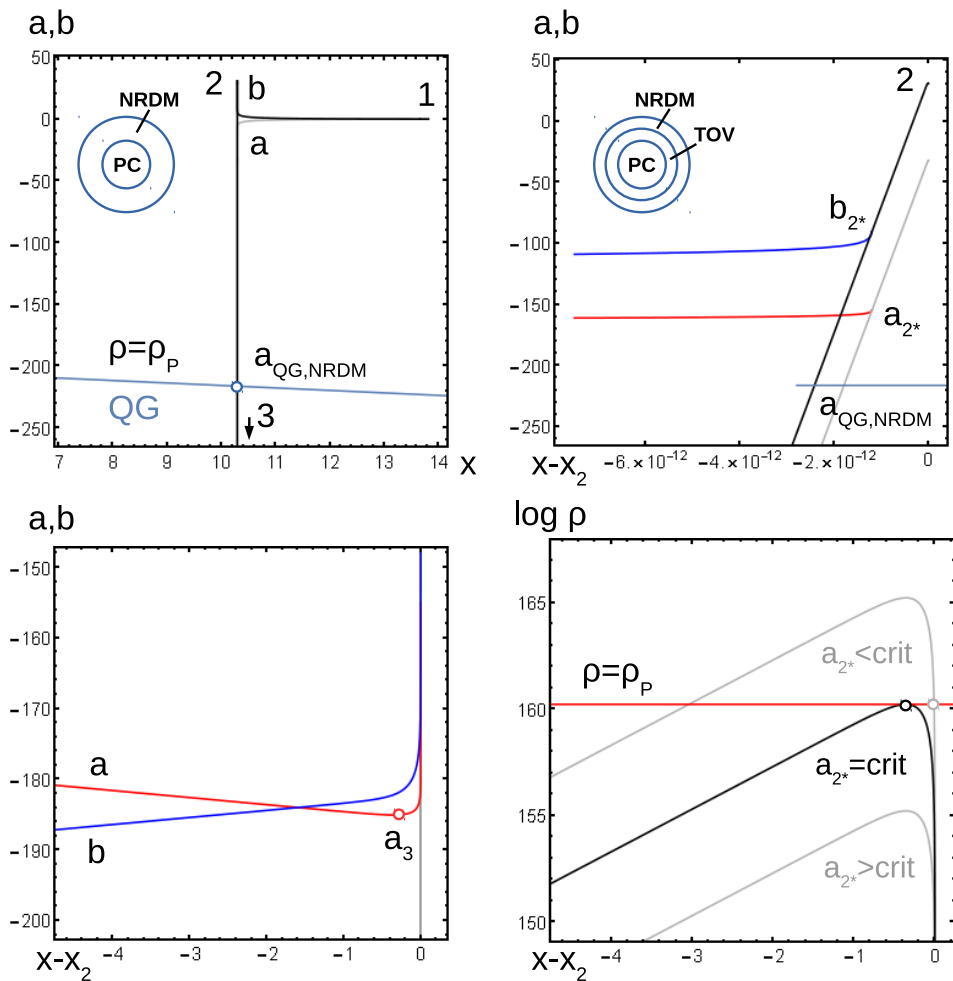


Fig. 20.5: Solutions with NRDM, TOV and PC (Planck core) phases. See text for details.

Fig.20.5 shows the solution for a compact object of stellar mass $M = 10M_{\odot}$. At the same time, as the study of the rotation curves [1] shows, the parameter ϵ for the external NRDM phase can be chosen in the interval $10^{-12} \dots -16$, and here we choose it in the center of this interval : $\epsilon = 10^{-14}$.

The top left image shows the behavior of a pure NRDM solution, similar to the graphs from [1] for a supermassive solution. The solution starts at point 1, located at a large distance from the object, in the weak field region. Then, near the gravitational radius, the solution tries to enter the Schwarzschild mode with symmetrically diverging a and b profiles. The b profile reaches its maximum at point 2, which is very close to the Schwarzschild radius r_s . After passing point 2, the solution goes into the supershift or mass inflation mode [52]. In a thin layer

Table 20.2: NRDM—TOV-star, stellar mass, critical case

model parameters	$M = 10M_{\odot}, r_s = 29532.4\text{m}, \epsilon = 10^{-14}$
starting point of integration	$a_1 = 0, b_1 = 0.0299773,$ $r_1 = 10^6\text{m}, L_1 = 1.05738 \cdot 10^6\text{m}$
supershift begins	$a_2 = -32.2362, b_2 = 30.8799,$ $r_2/r_s - 1 = 5.26127 \cdot 10^{-7}, L_2 = 5.819 \cdot 10^{-3}\text{m}$
NRDM—TOV transition	$a_{2*} = -154.936, b_{2*} = -90.434,$ $r_{2*}/r_2 - 1 = -1.2 \cdot 10^{-12}, L_{2*} = 1.32074 \cdot 10^{-29}\text{m}$
supershift ends	$a_3 = -185.052, b_3 = -182.216,$ $r_3 = 20638\text{m}, L_3 = 3.01835 \cdot 10^{-36}\text{m}$
minimal radius, end of integration	$a_4 = -95.1895, b_4 = -272.808,$ $r_4 = l_p = 1.62 \cdot 10^{-35}\text{m}, L_4 = 0$

Table 20.4: various scenarios, global parameters

NRDM, $E_{in} = E_p, \lambda_{in} = l_p$	
$M = 10M_{\odot}, \epsilon = 10^{-12}$	$A_{QG} = 1.2 \cdot 10^{-92}, \lambda_{out} = 4.8 \cdot 10^{-6}\text{pc}$
$M = 10M_{\odot}, \epsilon = 10^{-16}$	$A_{QG} = 1.2 \cdot 10^{-96}, \lambda_{out} = 4.8 \cdot 10^{-4}\text{pc}$
$M = 4.06 \cdot 10^6 M_{\odot}, \epsilon = 10^{-7}$	$A_{QG} = 7.2 \cdot 10^{-99}, \lambda_{out} = 6.2 \cdot 10^{-3}\text{pc}$
$M = 4.06 \cdot 10^6 M_{\odot}, \epsilon = 10^{-10}$	$A_{QG} = 7.2 \cdot 10^{-102}, \lambda_{out} = 0.2\text{pc}$
NRDM—TOV critical, $E_{in} = 0.512\text{MeV}, \lambda_{in} = 2.42 \cdot 10^{-12}\text{m}$	
$M = 10M_{\odot}, \epsilon = 10^{-12}$	$A_{2*} = 5.15 \cdot 10^{-70}, \lambda_{out} = 3.46\text{Mpc}$
$M = 10M_{\odot}, \epsilon = 10^{-14}$	$A_{2*} = 5.15 \cdot 10^{-68}, \lambda_{out} = 0.346\text{Mpc}$
$M = 10M_{\odot}, \epsilon = 10^{-16}$	$A_{2*} = 5.15 \cdot 10^{-66}, \lambda_{out} = 0.0346\text{Mpc}$
$M = 4.06 \cdot 10^6 M_{\odot}, \epsilon = 10^{-7}$	$A_{2*} = 2.97 \cdot 10^{-86}, \lambda_{out} = 4.56 \cdot 10^5\text{Gpc} \gg R_{uni}$
$M = 4.06 \cdot 10^6 M_{\odot}, \epsilon = 10^{-10}$	$A_{2*} = 2.94 \cdot 10^{-83}, \lambda_{out} = 1.45 \cdot 10^4\text{Gpc} \gg R_{uni}$

near this point, the a and b profiles rapidly decrease with decreasing x , while the mass density rapidly increases. At the point a_{QG} , the mass density reaches the Planck value. At this point, the NRDM phase joins the Planck core (PC). We recall that in the models under consideration, the Planck core has a large effectively negative mass due to quantum effects. This mass produces a force of gravitational repulsion, which maintains in equilibrium a coat of large positive mass located in the supershift region. These two masses almost cancel each other out, so that the object as a whole has an initial stellar mass.

The top right image shows the modification of the solution when it is connected with the TOV phase. The a and b profiles rapidly falling in a thin x -layer of the NRDM phase, before passing the Planck boundary and after crossing the 2_* phase boundary, are replaced by more slowly falling TOV phase profiles. In the figure at the bottom left, the TOV solution is continued into a wider x -layer. At point 3, the solution passes through the minimum of the a profile. Further, the profiles a and b diverge symmetrically in the region of large negative values, which is typical for the Schwarzschild singularity of negative mass [50] Sec.28.5. Unlike

other known solutions, this singularity is not naked, it is covered with a massive coat and remains in the superstrong redshift zone until the integration stops at the Planck radius.

The figure at the bottom right shows the behavior of the mass density of the solution in the TOV phase. The maximum density is reached at the minimum point α_3 . The *critical solution*, which touches the Planck density line, is specially highlighted. For this solution, all the other TOV graphs in this figure are shown. The key parameters for this solution are also listed in Table 20.2.

Upon reaching the Planck density, the solution joins the Planck core. *In supercritical mode*, that is, when the point of joining of the phases α_{2*} is selected below the critical position, the density reaches the Planck value earlier, the boundary of the Planck core shifts accordingly.

In subcritical mode, the Planck density is not reached at all, and the solution continues until the central singularity. This singularity is quite similar to the Planck core, since it also has a large negative mass, and its repulsive force keeps the system in equilibrium. The singularity can be smeared over the $r \sim l_p$ neighborhood to obtain a regular core. One can also expand the core to larger radius values. We will call such solutions the Planck core of type II, in contrast to the previously considered solutions, to which we assign the type I. Their difference is that core I arises when the NRDM or TOV matter reaches the Planck density, while for core II the density of this matter remains sub-Planckian, and the core consists of other matter exceeding the Planck density. NRDM solutions for the physically relevant selection of parameters necessarily exceed the Planck density, so a type I core is formed there. For the TOV phase, both types of solutions are possible.

Wavelengths of photons in the resulting gravitational field are easy to calculate. The initial wavelength, which was equal to $\lambda_{in} = l_p$ on the surface of the Planck core for the NRDM solution, is replaced by $E_{in} = 0.512\text{MeV}$, $\lambda_{in} = 2.42 \cdot 10^{-12}\text{m}$ at the interface for the NRDM|TOV solution. This choice corresponds to the threshold for the production of e^+e^- pairs in the collision of incoming and outgoing photon fluxes. An ultrarelativistic TOV plasma is composed of these pairs and other higher-energy particles. Applying the redshift to this wavelength for the critical case $A_{2*} = 5.15 \cdot 10^{-68}$ from Table 20.2, we get $\lambda_{out} = \lambda_{in}/\sqrt{A_{2*}} = 1.07 \cdot 10^{22}\text{m} = 0.346\text{Mpc}$. In the supercritical mode, longer wavelengths are obtained, in the subcritical mode, shorter ones. Note the coincidence of the obtained wavelength with the characteristic size of the MW galaxy. This coincidence is even more surprising if we note that the metric coefficients appearing in the intermediate calculations vary in the considered solutions by a hundred orders of magnitude.

L-integral. Table 20.2 also lists the values of the invariant length integral measured in the radial direction: $L = \int dr\sqrt{B}$. Integration starts from the minimum radius $r = l_p$. The integral up to point 3 turns out to be less than the Planck length, which does not pose a problem, since this region contains a Planck core with unknown properties, and the integration over this region should not be carried out at all. The integral up to point 2^* represents the thickness of the TOV layer. It is noteworthy that in the r -coordinate this thickness is about 9km, while in the

L-coordinate this thickness is microscopic: $L_{2*} = 8 \cdot 10^5 l_p$. This difference is an indicator of a strong deformation of the radial direction in the solution, which manifests itself in an extremely small B-factor. Note that the “aerial” r-coordinate is related to the area of the corresponding sphere (always equal to $4\pi r^2$), while the L-coordinate is the more appropriate local thickness characteristic. The resulting thin layer corresponds to a superdense TOV plasma sandwiched between the Planck core and NRDM coat under tremendous pressure. We remind that in our calculations we consider all the media to be continuous, disregarding their microscopic structure. Apparently, a quantum calculation should be carried out in this region, after which the results obtained here should be revised. In this work, we restrict ourselves to classical calculations. Further, up to point 2, the coordinate r changes microscopically by $\sim 3.5 \cdot 10^{-8} \text{m}$, while the change in L is about 6mm. In this region, the deformation becomes inverse, due to the large B-factor near point 2. Finally, in the outer region, an L-integral is accumulated, comparable to the change in r, since the region of weak fields prevails here, and the space becomes flat.

The picture obtained in the analysis of the L-integral coincides with the structure of compact massive objects and the presence of a “shrinking volume” [3] inside them. In the region shallow in the L-coordinate, thin superdense layers of matter are localized, creating strong deformations of space, strong gravitational fields that determine the structure of the solution as a whole.

Sensitivity to model parameters. Table 20.4 shows the calculation results for different scenarios. For a pure NRDM model, the value of λ_{out} varies in the range of $10^{11} \dots 10^{16} \text{m}$ or $10^{-6} \dots 10^{-1} \text{pc}$. If the DM particles in this scenario were photons, their propagation in the ISM would be prohibited, since their frequency is significantly less than Langmuir’s value and the wavelength is significantly less than the size of the galaxy. However, this scenario is limited to the sterile case and does not consider photons as DM particles. The photon case assumes an NRDM|TOV combination, and here, for compact objects of stellar mass, wavelengths are obtained in the range of 34.6kpc-3.46Mpc, that is, comparable to galactic sizes. We assume that such waves can propagate in ISM and condense in BEC, thereby providing a logical closure for the considered model. For the supermassive case, typical for central black holes in galaxies, λ_{out} values are obtained that are much larger than the size of the universe $R_{\text{uni}} \sim 14 \text{Gpc}$. This means that either supermassive black holes in this scenario do not participate in the formation of dark matter, or cosmological processes must be taken into account for their analysis. Note also that in the case of a pure NRDM for the described parameters there are exact formulas: $A_{\text{QG}} = \epsilon (l_p/r_s)^2 / (8\pi)$, $\lambda_{\text{out}} = r_s (8\pi/\epsilon)^{1/2}$. For the NRDM|TOV combination, we currently have only empirical relationships. Namely, for the data in Table 20.4, with fixed r_s and variable ϵ , the relations hold $A_{2*} \sim \epsilon^{-1}$, $B_{2*} \sim \epsilon^{-3}$, $\lambda_{\text{out}} \sim \epsilon^{1/2}$, which are the sign of hidden symmetries in the considered system.

Qualitative analysis. At the first glance, the presented results are relevant only to the model of NRDM|TOV stars studied here. Now we will show that many features of the described solution are typical for a wider class of models, possibly for all compact massive objects [2–5]. First of all, *erasure of the event horizon* is associated

with the T-symmetry of solutions, which results in a grid of the intersecting flows of incoming and outgoing particles. For true black holes, there are only incoming flows, and for T-conjugated white holes, only outgoing flows. In the solutions under consideration, there can be no horizons that could prevent the entry or exit of the particles. Another explanation for the horizon erasure effect arises when observing the mass function $M(r)$. The region below the horizon corresponds to $2M(r)/r > 1$. In the presence of distributed positive mass density, the function $M(r)$ decreases with decreasing r (one can imagine how positive mass layers are removed from the solution). If the density is high enough, then $2M(r)$ decreases faster than r , so no horizon is formed. High density arises from the phenomenon of *mass inflation* [52]. This phenomenon occurs due to the positive feedback between pressure and gravity. In strong gravitational fields, in equilibrium systems, the pressure increases rapidly with decreasing radius, due to the hydrostatic equation. At high pressure, it begins to contribute to gravity on the same basis as mass density, which also increases due to EOS. As a result, the gravitational field is strengthened, which leads to a further increase in pressure and density. As a result, a thin layer is formed in the solution, in which pressure, density and gravitational field increase very rapidly. Further, the rapid decrease in the mass function $M(r)$ does not stop at zero crossing, *the mass becomes negative*. While the local density is still positive, the value of the central mass located under a certain radius r is negative. A successful closure of the model is the concept of the *Planck core*, according to which, when the Planck density is exceeded, the quantum corrections make the mass effectively negative [4, 5]. We described another possibility in this work, when a central singularity or a superdense core, consisting of matter other than the surrounding massive coat, has a negative mass. Next, we observe the behavior of the *metric profiles* A and B , where the first describes the time dilation and redshift, and the second describes the deformation of the radial coordinate. The mass function is directly related to the B -profile by the formula $B = (1 - 2M/r)^{-1}$. Large negative masses correspond to a small positive B . As a result, the integral of length $L = \int dr \sqrt{B}$ in this region becomes small, the region becomes *shallow* in L , although in r it can occupy an essential part of the solution. Together with the coefficient B , A also becomes small in the region of mass inflation, which is typical for strong gravitational fields. This leads to a *strong time dilation and redshift*, as a result, from the point of view of an external observer, the object is dark, almost like a black hole. At the same time, high energies inside the object can result in high density radiation. The redshift does not affect the flux density in the transverse direction and shifts the radiation to the low-energy region. In the models under consideration, the superstrong redshift stretches photons into ultra-long wave packets that can reach the size of a galaxy, while a large number of such photons, after taking into account all sources, leads to a significant contribution to the mass of the galaxy. Thus, microscopically thin high-energetic layers inside compact objects appear to be conjugated with galactic-scale structures. At large distances from the center, the radiation density decreases as $\rho \sim r^{-2}$, which leads to flat rotation curves of galaxies. The distribution of black holes in the galaxy modulates these dependencies and allows to describe *the observed rotation curves* with their deviations from the flat shape [1]. These calculations do not depend on

the nature of the emitting objects, only on the assumption that their distribution is proportional to the luminous matter. Thus, radiation from compact massive objects, be they photons or other particles, may be directly unobservable due to long wavelengths. However, it can determine the rotation curves of galaxies and produce other gravitational effects that are usually associated with *dark matter*. If this type of radiation can pass the interstellar medium and become Bose-Einstein condensate outside the galaxy, one will simultaneously obtain the description of *dark energy*.

20.4 Conclusion

This work continued the construction of a recently proposed model of NRDM-stars. In this model, the quanta dark of matter are sterile massless particles that are emitted from quasi-black holes located mainly in the central regions of the galaxy. At large distances from the center of the galaxy, the emission is directed radially and the mass density has the form $\rho \sim r^{-2}$, in contrast to the homogeneous model $\rho = \text{Const}$. In the cosmological context, the homogeneous model with massless particles corresponds to the radiation epoch of the expansion of the universe, while the proposed inhomogeneous model turns out to be equivalent to Λ CDM.

Specifically, several scenarios were considered in which the radial emission of dark matter is brought into hydrostatic equilibrium with a uniform background:

- S1.1: a jump in the dark energy density at the edge of the galactic halo;
- S1.2: a surface tension at the boundary between the halo and the dark energy background;
- S1.3: a phase transition of dark matter into dark energy, accompanied by the Joule-Thomson effect;
- S1.4: Bose-Einstein condensation of dark matter inside the galaxy into dark energy outside of it.

From the junction conditions, the density correspondence to the observed Ω -parameters and mass functions typical for Λ CDM model were obtained. In these scenarios, CDM macro-particles are galaxies with massive halos surrounding them, floating in a homogeneous medium with the dark energy equation of state. Additionally, the question of what happens if dark matter particles are not sterile, for example, are photons of the Standard Model, is considered. When high-energy photons collide inside NRDM stars, as a result of the production of e^+e^- pairs and other particles, a thin layer of ultrarelativistic plasma appears. The performed classical calculation shows that the photons emitted from this layer, after applying the gravitational redshift, acquire a wavelength comparable to the galactic sizes. For the logical closure of the photon scenario in this model, it is also necessary to study the questions of the passage of such longwave photons through the interstellar medium and Bose-Einstein condensation of the photons in the intergalactic medium. The study of these questions will be continued.

Acknowledgements

The author thanks the organizers and participants of the Bled 2021 Workshop “What comes beyond the Standard models?” for fruitful discussions. The author also thanks Kira Konich for proofreading the paper.

Appendix: Details of constructions

Modeling the outer part of the rotation curve. Fig.20.3 on the left shows the outer part of the MW rotation curve, overlaid with various model profiles. RDMcut represents the simplest radial dark matter halo model introduced in [1], which is cut off at the R_{cut} radius, so that the velocity on the outer portion of the curve is $v = (GM_{\text{dm}}(R_{\text{cut}})/r)^{1/2}$. The graph also shows the standard galactic profiles of Navarro-Frenk-White (NFW) and Einasto, with parameters adjusted to the experimental points. The source of experimental data is the work [48]. It can be seen that all the profiles pass approximately the same way in the corridor of experimental scatter. Since the scatter in the outer region of the rotation curve is extremely large, it is not possible to select any particular profile based on this data.

Fig.20.4 shows the profiles obtained in the accepted scenarios of this work, compared with the RDMcut profile, with the parameters $\epsilon = 2.5 \cdot 10^{-7}$, $R_{\text{cut}} = 50\text{kpc}$. The profiles are related to the gravitating mass by the relation $v = (GM_{\text{grav}}(r)/r)^{1/2}$. The characteristic downward bend of all new profiles at large distances corresponds to the negative contribution of dark energy growing under the root. With a large value of the radius, the gravitating mass becomes negative, and the corresponding radial acceleration also changes sign. In this zone, v is not defined, circular orbital motion is impossible, here the accelerated cosmological expansion of the universe begins to dominate.

All new profiles pass close to RDMcut and with it fit into the corridor of errors. The S1.4 profile is effectively the same as RDMcut if DE contribution is included in it. Profile S1.3 for the parameters selected above is shown in Fig.20.4 right in blue. It can be pulled closer to RDMcut by setting $R_{\text{cut}1} = 30\text{kpc}$, as a result, the key parameters of the model will slightly change: $\epsilon = 2.5 \cdot 10^{-7}$, $\{R_{\text{cut}1}, R_{\text{cut}1b}, R_{\text{cut}2}\} = \{0.03, 0.20, 0.55\}\text{Mpc}$, $\{M_1, \Delta M_1, \Delta M_2, M_{\text{vac}}\} = \{1.56, 2.07, -1.56, 1.41\} \cdot 10^{11} M_{\odot}$, $M_{\text{dm+de,gal}} + M_{\text{vac}} = 3.5 \cdot 10^{11} M_{\odot}$, while the cosmological estimates are performed with new values $\rho_1/\rho_2 = 2288$, $N'_{\text{gal}} = 1.3 \cdot 10^{12}$.

Let's pay attention again to Fig.20.3 left. Noteworthy is the presence of a rise in the experimental curve at the exterior of this graph. It is responsible for the Local Group (LG) structures outside of the MW. Recall that the galaxy M31/Andromeda closest to the MW is located at a distance of $r_{\text{M31}} \sim 0.8\text{Mpc}$. Therefore, at the exterior of the curve, the radius begins to capture M31 and other LG structures, increasing the total gravitating mass. Note that spherical symmetry is lost in this case, and the formula $v = (GM_{\text{grav}}(r)/r)^{1/2}$ should no longer be used for the velocity, except as a rough approximation. In the fit [1], shown in green on the graph, the RDMcut contribution of dark matter was taken into account, as well as the contribution of luminous matter, which is active at small radii, and the region increasing at large LG radii was described empirically as an additive homogeneous background. The density value obtained at the fit was $\rho_{\text{bgr}} \sim 4.4 \cdot 10^{-26} \text{kg/m}^3$, which is 4.4 times higher than the critical cosmological density. In this interpretation, this contribution has nothing to do with the cosmological background, it only describes the overdensity averaged by the Local Group, limited in space.

For a more detailed analysis, Fig.20.3 right shows the raw data from [46], on the basis of which the experimental rotation curve [48] was built. Strictly speaking, Fig.20.3 right shows not the rotation curve, but the dependence of the experimentally measured radial velocity

component on the distance. The outer part of this dependence is taken from [46], Table 1, SF sample, r_{GC} and v_{GC} columns. The radial velocities Fig.20.3 right have a sign, in contrast to Fig.20.3 left, where the absolute value of the velocity is given. The pattern is striking: on the outer part of the curve $v_r > 0$, which corresponds to expansion, on the inner part of $v_r < 0$, there is a contraction. The outer part can be approximated by the Hubble law $v = Hr$ with the value $H = 95 \pm 16 \text{ km/s/Mpc}$. Compared to recent cosmological estimates $H_0 = 68 - 77 \text{ km/s/Mpc}$, the average value is somewhat overestimated, but fits within 1.7 standard deviations. Thus, the outer part of the curve is consistent with the Hubble flow. It was noted in [53] that Hubble's law begins to operate directly outside of LG, here we see that it also operates on the outer border of LG. The inner part of the graph Fig.20.3 on the right corresponds to the collapse of matter under the influence of gravitation towards massive galaxies that are part of LG. Recall that LG consists of two large galaxies, MW and M31, and many globular clusters and satellite galaxies. For these satellites, the radial velocities were measured relative to the MW, which are used to construct the outer part of the rotation curve [48].

In the work [54], a model of the outer region of LG is described, which reproduces just such a picture, Hubble flow at the outer boundary of the region and the collapse of matter to the center of mass of LG at the inner boundary. In [54], Fig.10 qualitatively coincides with our Fig.20.3 right. The details show differences caused by using a different coordinate system and a different dataset for analysis. The work [54] also gives estimates of the total masses of MW and M31: $M_{MW} = (0.8^{+0.4}_{-0.3}) \cdot 10^{12} M_\odot$ and $M_{M31} = (1.5^{+0.5}_{-0.4}) \cdot 10^{12} M_\odot$. Since [54] uses an additive homogeneous contribution of dark energy, for comparison with our scenario, we need to take into account the M_{vac} term, which in the above scenarios gives the value $M_{MW} = (0.3 - 0.5) \cdot 10^{12} M_\odot$, within 1-1.7 standard deviations from the value [54]. As for Andromeda, [46] assumed that the masses of MW and M31 were equal, and LG required additional mass that is not part of these galaxies. Whereas in [54] scenarios with M31 mass 2 times the MW mass are preferred, and additional LG mass is not required.

In our work, we concentrate on describing internal orbits closely bound to the MW, for which the masses of external structures are not important. The exact solution to the spherically asymmetric problem of the interaction of nearby galaxies with overlapping halos is rather nontrivial. The resulting halo shape can deviate from the sphere. The gravitational field is not described by a simple rotation curve depending only on the radius. The result depends on a variety of model assumptions such as dark matter EOS and initial conditions. Therefore, in this work, we prefer to restrict ourselves to cosmological estimates for spherically symmetric halos of separately standing galaxies and will not consider the cases of nearby galaxies overlapping by the outer parts of their halos. In practice, this means that in the MW rotation curve we will consider only the descending part, cutting off its LG tail.

Model independent reconstruction of EOS. Let us describe another algorithm that, for spherically symmetric halos, in principle, can reconstruct EOS directly from the rotation curve, without the assumptions about the phase transition path made in scenario S1.3. Let us know the rotation curve for an average-mass galaxy, approximated by some empirical profile. The mass function $M_{grav}(r)$ and the density $\rho_{grav}(r)$ are trivially recovered from it. On the outside of the rotation curve, these two functions are matched with cosmological estimates: $M_{grav}(R_{max}) + M_{vac}(R_{max}) = M_{dm,uni}/N_{gal}$, $M_{vac}(r) = (8\pi/3)\rho_{de,bgr}r^3$ and $\rho_{grav}(R_{max}) = -2\rho_{de,bgr}$. Note that these conditions are imposed directly on the experimental curves and not on the EOS components. We use the relations $\rho_{grav} = \rho + p_r + 2p_t$ and $r(p_r)' + 2p_r - 2p_t = 0$, these are two relations for three profiles (ρ, p_r, p_t) . As a result, one functional degree of freedom remains. One can set an arbitrary function p_r , then (ρ, p_t) will be reconstructed by linear formulas, even without solving differential equations.

Boundary conditions on the outer radius are of the form $p_r = p_t = -\rho$, in this case, due to the conditions imposed above, it will automatically satisfy $\rho = \rho_{de,bgr}$, $p_r = p_t = -\rho_{de,bgr}$, $p'_r = 0$. Using these constraints on (p_r, p'_r) as boundary conditions, we can construct EOS in parametric form $(\rho, p_r, p_t)(r)$. This construction can be supplemented with boundary conditions for NRDM at the inner radius $\rho = p_r, p_t = 0$, by introducing the gravitational term into the hydrostatic equation, and other model corrections.

A similar algorithm for recovering EOS from rotation curves was used in the work [55]. In this case, EOS was assumed to be isotropic $p_r = p_t$, as a result, the solution did not contain functional ambiguities, but the NRDM-type solution was missed. The main obstacle to the implementation of such algorithms is the extremely large scatter in the outer region of the rotation curves, which allows different empirical profiles and leads to an inaccurate reconstruction of EOS in this region.

Taking into account the mass distribution of galaxies. The above calculations use the estimated value of the number of galaxies $N_{gal} = 2 \cdot 10^{12}$ from [56]. This value takes into account the evolution of the universe over time and represents an estimate of the number of observed galaxies up to redshift values $z < 8$. In fact, to compare with the density of dark matter today, we need the number of galaxies in a simultaneous slice in a ball of radius $R_{uni} \sim 14\text{Gpc}$. This radius is purely nominal, the final formulas include the ratio $M_{dm,uni}/N_{gal}$, from which this radius drops out. In fact, we need an estimate of the density of galaxies dN_{gal}/dV near our position, for small z . The mentioned ratio is expressed through this density: $M_{dm,uni}/N_{gal} = \rho_{dm}/(dN_{gal}/dV)$.

In [56], the density of galaxies is modeled using the Schechter function:

$$dN_{gal}/dV/dM = \phi^* \log(10) 10^{(M-M^*)(1+\alpha)} \exp(-10^{(M-M^*)}), \quad (20.16)$$

where $M = \log_{10}(M_{lm,gal}/M_{\odot})$, $M_{lm,gal}$ is the stellar mass of the galaxy. For the rest of the parameters, the values from the second row of Table 1 in [56] were selected, representing the most accurate fit for the galaxies closest to us: $\alpha = -1.29$, $M^* = 11.44$, $\phi^* = 12.2 \cdot 10^{-4} \text{Mpc}^{-3}$. Integrating this expression over the interval $6 \leq M \leq 12$ shown in Fig.1 in [56], we obtain $dN_{gal}/dV = 0.154 \text{Mpc}^{-3}$, multiplying by $(4\pi/3)R_{uni}^3$, we get $N_{gal} = 1.766 \cdot 10^{12}$. It is noteworthy that the obtained value is close to the number $2 \cdot 10^{12}$, which was found in [56] for the same mass interval and took into account the evolution of the universe.

Next, we need the mean $\langle v^2 \rangle$ for the square of the outer orbital velocity, on the same distribution. To find it, we use the Tully-Fisher relation $v \sim (M_{lm})^p$ with exponent $p = 1/4$. Let us introduce a normalization to the value of MW and denote $\eta_p = \langle (M_{lm}/M_{lm,MW})^p \rangle$, so that $\langle v^2 \rangle / v_{MW}^2 = \eta_{1/2}$. Using the value $M_{lm,MW} = 6.08 \cdot 10^{10} M_{\odot}$ from [57] and calculating the average, we get $\eta_{1/2} = 0.0455$, $N_{gal}\eta_{1/2} = 1.196 \cdot 10^{11}$. This estimate is based only on experimental data in the form of Schechter and Tully-Fisher relations. It needs to be compared with the corrected N'_{gal} parameter in our scenarios.

Before proceeding to the comparison, note that for the integration we have chosen the lower limit $M_{min} = 6$, as in [56]. This limit is slightly below the experimental data collection limit $M_{min} = 8$, that is, extrapolation is used in the calculations. Note that the number of galaxies strongly depends on this limit. If we take $M_{min} = 8$, we get $N_{gal} = 4.189 \cdot 10^{11}$. At the same time, the value of $\eta_{1/2}$ will increase by approximately the same factor and the value of $N_{gal}\eta_{1/2}$ will practically not change. The same effect is observed for all $p > 0.3$. The reason for this is that the cumulative value of $N_{gal}\eta_p$ is expressed by an integral dominated by large masses.

Also note that the modeling width for Schechter function Fig.1 [56] is 0.4-1dex, and the scatter width of Tully-Fisher relation [58] for v^2 is about 0.8dex. Therefore, deviations of $< 1.8\text{dex}$ in comparison of model and experiment can be tolerated.

Most of our scenarios have a clear algebraic structure, producing an analytical answer of the form $M_{\text{dm,uni}} = N_{\text{gal}}(M_{\text{dm,gal}} + M_{\text{vac}})$, $M_{\text{dm,gal}} = k_1 \epsilon R_{\text{cut}} c^2 / G$, $M_{\text{vac}} = k_2 (8\pi/3) \rho_{\text{de,bgr}} R_{\text{cut}}^3$. The constants $k_{1,2}$ for scenarios {S1.1, S1.2, S1.4} are of the form $k_1 = \{2/3, 3/4, 1\}$, $k_2 = \{0, 1/4, 1\}$. In calculations in order of magnitude, for fixed $N_{\text{gal}} = 2 \cdot 10^{12}$, $M_{\text{dm,uni}} \sim 4.5 \cdot 10^{23} M_{\odot}$, and for $R_{\text{cut}} < 0.6 \text{Mpc}$, the contribution of M_{vac} can be neglected. Also, in order of magnitude, we can consider $k_1 \sim 1$. As a result, we get the only relation $M_{\text{dm,uni}} \sim N_{\text{gal}} \epsilon R_{\text{cut}} c^2 / G$ for these three scenarios, which we must check with the experiment.

Next, we will make two estimates. In the first, for scenarios {S1.1, S1.2, S1.4}, we will assume that R_{cut} is fixed, and ϵ is distributed over galaxies. In this case, the relation has the form $M_{\text{dm,uni}} \sim N_{\text{gal}} \langle \epsilon \rangle R_{\text{cut}} c^2 / G$. The same relationship is obtained if we assume that R_{cut} is distributed, but uncorrelated with ϵ , in this case it will be $M_{\text{dm,uni}} \sim N_{\text{gal}} \langle \epsilon \rangle \langle R_{\text{cut}} \rangle c^2 / G$. Further, taking into account $\epsilon = (v/c)^2$ and using the value $\eta_{1/2}$ introduced above, we get $M_{\text{dm,uni}} \sim N_{\text{gal}} \eta_{1/2} M_{\text{dm,MW}}$, $M_{\text{dm,MW}} = \epsilon_{\text{MW}} R_{\text{cut}} c^2 / G$. It is convenient to rewrite this relation as $N'_{\text{gal}} \sim N_{\text{gal}} \eta_{1/2}$, where $N'_{\text{gal}} = M_{\text{dm,uni}} / M_{\text{dm,MW}}$ is the corrected number of galaxies introduced above in scenarios with MW copies. Substituting here $\epsilon_{\text{MW}} = 2.5 \cdot 10^{-7}$, with R_{cut} varying within 50kpc-0.6Mpc we get $N'_{\text{gal}} = 1.7 \cdot 10^{12} - 1.4 \cdot 10^{11}$, which coincides with the experimental estimate $N_{\text{gal}} \eta_{1/2} = 1.196 \cdot 10^{11}$ within 1.2-0.1dex, with preference for large values of R_{cut} .

Next, let's make the estimation for the S1.3 scenario. In it, the adjustment of the ϵ and R_{cut} parameters is not as easy as in other scenarios, unless additional assumptions are made about the scaling of galaxies. As a working hypothesis, suppose the mass density is scaled as $\rho(r) \rightarrow \rho(r/a)$, that is, in Fig.20.2 left, the graph simply shifts horizontally when looking at different galaxies. It is easy to verify that all structural elements that define the position of key points in the scenario withstand this scaling. The mass function shown in Fig.20.2 right scales as $M_{\text{grav}}(R) \rightarrow 4\pi \int_0^R dr r^2 \rho_{\text{grav}}(r/a) = a^3 M_{\text{grav}}(R/a)$, the $M_{\text{vac}}(R)$ contribution is also scaled, which must be added here in cosmological estimates. Thus, the total mass of dark matter in the galaxy under the taken assumptions is scaled as $M_{\text{dm,gal}} \rightarrow M_{\text{dm,gal}} a^3$. At the same time, the square of the orbital velocity $v^2 = GM/R$ is scaled as $v^2 \rightarrow v^2 a^2$, the velocity is scaled as $v \rightarrow va$. Due to the Tully-Fisher relation, the luminous mass scales as $M_{\text{lm}} \rightarrow M_{\text{lm}} a^4$. Thus, $M_{\text{dm}} \sim (M_{\text{lm}})^{3/4}$ proportionality holds along the sequence under consideration, the required correction factor is $N_{\text{gal}} \eta_{3/4} = 8.302 \cdot 10^{10}$.

Note that the function $N_{\text{gal}} \eta_p$ has a minimum at $p \sim 0.9$ and changes little in the range $p = 0.3 \dots 2$, so other dependencies $M_{\text{dm}} \sim (M_{\text{lm}})^p$ lead to a similar result for p in this interval. Also note that in other works, other values of p were obtained, [59] $p = 0.3$, [60] $p = 1.34$, [61] Eq. (7) $p = 0.3 - 1.1$ for spiral galaxies, [62] Eq. (21) $p = 1.05 - 1.24$ for dwarf disc galaxies. This result strongly depends on the choice of the mass profile and the halo cutoff radius. In our scenario S1.3, the cutoff is applied at the outer radius $R_{\text{cut}2}$, where the phase transition of dark matter into dark energy is completed, outside of which the density of dark matter vanishes.

Compared with the value obtained in S1.3 required for joining the relations $N_{\text{gal}} \eta_{3/4} = \sum M_{\text{dm,gal}} / M_{\text{dm,MW}} \sim 8 \cdot 10^{10}$ and $M_{\text{dm,uni}} / M_{\text{dm,MW}} \sim 9 \cdot 10^{11}$, there is a discrepancy of 1.1dex. If we change the modeling of S1.3 a little and achieve an exact fit to the experimental estimate [54] $M_{\text{MW}} \sim 8 \cdot 10^{11} M_{\odot}$, we get a discrepancy of 0.8dex. Thus, our assumption about the scale invariance of scenario S1.3 fits into the existing scatter of experimental data. At the same time, it becomes clear that the remaining discrepancy, in fact, is not related to the details of our modeling, but is the result of direct comparison of different experimental estimates. Using relations of the form $M_{\text{dm}} \sim (M_{\text{lm}})^p$ from the experimental works cited above, a similar result will be obtained.

A similar result will also be obtained in our other scenarios if we accept the same scaling assumptions in them, that is, $R_{\text{cut}} \sim a$ and $\epsilon \sim a^2$. In this case, the contributions $M_{\text{dm,gal}}$ and M_{vac} are scaled in the same way $\sim a^3$, and if for the initially taken MW galaxy the contribution M_{vac} can be neglected, then it can be neglected along the entire sequence. The relation $N'_{\text{gal}} \sim N_{\text{gal}}\eta_{3/4}$ is subject to verification, where $N'_{\text{gal}} = 1.7 \cdot 10^{12} - 1.4 \cdot 10^{11}$ for $R_{\text{cut}} = 50\text{kpc} - 0.6\text{Mpc}$. The deviation from $N_{\text{gal}}\eta_{3/4} = 8.302 \cdot 10^{10}$ here is 1.3dex-0.2dex, with a preference for larger values of R_{cut} .

Structure of solutions of the nonlinear Klein-Gordon equation. In general, solutions of this equation for stationary spherically symmetric problems do not admit separation of variables and cannot be represented in the form $\phi(t, r) = e^{iEt}s(r)$ or their linear combinations. However, in the special case of harmonic boundary conditions $\phi(t, r_1) = e^{iEt}s_1$, $\phi'_r(t, r_1) = e^{iEt}d_1$, the following consideration can be used. Let's perform the numerical integration of this equation using the finite difference scheme

$$\partial^2 \phi / \partial t^2 = (\phi(t + dt, r) + \phi(t - dt, r) - 2\phi(t, r)) / dt^2, \tag{20.17}$$

$$\partial^2 \phi / \partial r^2 = (\phi(t, r + dr) + \phi(t, r - dr) - 2\phi(t, r)) / dr^2, \tag{20.18}$$

$$\partial \phi / \partial r = (\phi(t, r + dr) - \phi(t, r - dr)) / (2dr). \tag{20.19}$$

This is not the scheme that is used in practice to solve such equations, but here, for the purpose of proof, it can be applied with a sufficiently small choice of integration steps. When integrating the solution by layers of constant r , starting from $r = r_1$ and then recurrently into the region $r < r_1$, it is easy to check that the equation solved with respect to the leading layer $\phi(t, r - dr)$ will always carry the phase factor e^{iEt} and the amplitude $s(r)$ depending only on r . Thus, the solution will globally have the form $\phi(t, r) = e^{iEt}s(r)$. In the particular case $E = 0$, the solution will be globally stationary $\phi(t, r) = s(r)$.

A slight subtlety is that this reasoning is valid for finite r_1 , while for the considered solutions the boundary condition is imposed for $r \rightarrow \infty$, asymptotically. This problem can be solved as follows. Let's approximate the potential near the minimum by an analytically solvable form (20.11). The solutions will be (20.13) with $C_2 = 0$. For a finite value of r_1 , when the solution is still in the considered vicinity of the minimum, calculate $s(r_1)$ and $s'(r_1)$ on the solution and use them as boundary conditions in the above numerical integration scheme. As a result, a global solution of the required form will be obtained.

Note also that as long as the consideration concerns stationary solutions, there is no difference between the theories of complex and real scalar field. The difference appears for $E \neq 0$, the real harmonic solutions have the form $\phi = \cos(Et)s(r)$. In this case, the time dependence penetrates into the argument of the potential function, and there is no reduction in the dimension. In the nonlinear theory of real scalar field, single-frequency harmonic functions can only be approximate solutions [42].

NRDM—TOV system. Stationary spherically symmetric gravitational fields are described by the metric tensor and the energy-momentum tensor

$$g_{\mu\nu} = \text{diag}(-A(r), B(r), r^2, (r \sin \theta)^2), \quad T_{\nu}^{\mu} = \text{diag}(-\rho(r), p_r(r), p_t(r), p_t(r)), \tag{20.20}$$

in the coordinate system composed of the time of distant observer and the standard spherical coordinate system $x^{\mu} = (t, r, \theta, \phi)$. Einstein's equations for such problems are:

$$\rho = (-B + B^2 + rB'_r) / (8\pi r^2 B^2), \quad p_r = (A - AB + rA'_r) / (8\pi r^2 AB), \tag{20.21}$$

$$p_t = (-rB(A'_r)^2 - 2A^2 B'_r + A(-rA'_r B'_r + 2B(A'_r + rA''_{rr}))) / (32\pi r A^2 B^2). \tag{20.22}$$

This system can be taken from [63] (11.36-38) and converted to our notations or derived from the first principles using Mathematica code [64]. It is easy to check that this system satisfies the relation

$$r(p_r + \rho)A'_r + 2A(r(p_r)'_r + 2p_r - 2p_t) = 0. \quad (20.23)$$

This equation has a profound meaning, as a consistency condition for the Einstein equations, Bianchi identity. It is equivalent to conservation of energy-momentum $\nabla_\mu T^\mu_\nu = 0$. It also has a physical meaning of hydrostatic equation, since it describes a distribution of pressure and density in a stationary spherically symmetric gravitational field.

Now let's consider EOS for two phases

$$\text{NRDM: } p_r = \rho, \quad p_t = 0, \quad \text{TOV: } p_r = p_t = w\rho, \quad w = 1/3 \quad (20.24)$$

and join the corresponding solutions of the Einstein equations. First of all, the analysis of the matching conditions for the hydrostatic equation shows that at the phase boundary p_r must be C^0 -continuous, while ρ and p_t undergo a jump, repeating the jump of EOS. Further, analyzing the behavior of the metric profiles in the Einstein equations, we see that A must be C^1 -continuous, and B - C^0 -continuous.

The hydrostatic equation for such EOS can be solved analytically:

$$\text{NRDM: } p_r = \epsilon/(8\pi r^2 A), \quad \text{TOV: } p_r = k/(4\pi A^2), \quad (20.25)$$

where ϵ and k are integration constants. Further, the Einstein equations for our combined model are:

$$\text{NRDM: } a'_x = -1 + e^b + \epsilon e^{b-a}, \quad b'_x = 1 - e^b + \epsilon e^{b-a}, \quad (20.26)$$

$$\text{TOV: } a'_x = -1 + e^b + 2ke^{2x-2a+b}, \quad b'_x = 1 - e^b + 6ke^{2x-2a+b}, \quad (20.27)$$

in logarithmic variables $x = \log r$, $a = \log A$, $b = \log B$. Integration starts in the NRDM phase from a point distant from the center, where the initial conditions are selected $a_1 = 0$, $b_1 = -\log(1 - 2M_1/r_1)$, $2M_1 = \epsilon r_1 + r_s$. In this case, C^0 -continuous matching of p_r at the phase boundary $r = r_{2*}$ leads to the condition $k = \epsilon A_{2*}/(2r_{2*}^2)$, whereby the equation (20.27) can be rewritten as

$$\text{TOV: } a'_x = -1 + e^b + \epsilon e^{2(x-x_{2*})-2a+b+a_{2*}}, \quad (20.28)$$

$$b'_x = 1 - e^b + 3\epsilon e^{2(x-x_{2*})-2a+b+a_{2*}}. \quad (20.29)$$

From this it is clear that C^0 -continuous matching of (a, b) at the phase boundary enables C^0 -continuous matching also for the derivative a'_x , while b'_x undergoes a jump by a factor 3. This provides the continuity mode C^1 for a , C^0 for b , in accordance with the above theoretical analysis.

References

1. I. Nikitin: On dark stars, Planck cores and the nature of dark matter, Bled Workshops in Physics **21**, 221-246 (2020); arXiv:2102.07769.
2. M. Visser, C. Barceló, S. Liberati, S. Sonego: Small, dark, and heavy: But is it a black hole?, Proc. of Science **075**, Black Holes in General Relativity and String Theory, 010 (2008); arXiv:0902.0346.
3. B. Holdom, J. Ren: Not quite a black hole, Phys. Rev. **D95**, 084034 (2017); arXiv:1612.04889.

4. C. Rovelli, F. Vidotto: Planck stars, *Int. J. Mod. Phys. D* **23**, 1442026 (2014); arXiv:1401.6562.
5. C. Barceló, R. Carballo-Rubio, L. J. Garay, G. Jannes: The lifetime problem of evaporating black holes: mutiny or resignation, *Class. Quantum Grav.* **32**, 035012 (2015); arXiv:1409.1501.
6. R. Brandenberger, J. Fröhlich, R. Namba: Unified dark matter, dark energy and baryogenesis via a “cosmological wetting transition”, *J. of Cosmology and Astroparticle Phys.* **2019**, 069 (2019); arXiv:1907.06353.
7. C. Wetterich: Cosmon dark matter?, *Phys. Rev. D* **65**, 123512 (2002); arXiv:hep-ph/0108266.
8. A. Banihashemi, N. Khosravi, A. H. Shirazi: Ups and downs in dark energy: phase transition in dark sector as a proposal to lessen cosmological tensions, *Phys. Rev. D* **101**, 123521 (2020); arXiv:1808.02472.
9. A. Banihashemi, N. Khosravi, A. Shafieloo: Dark energy as a critical phenomenon: a hint from Hubble tension, *J. of Cosmology and Astroparticle Phys.* **2021**, 003 (2021); arXiv:2012.01407.
10. J.-P. Hong, S. Jung, K.-P. Xie: Fermi-ball dark matter from a first-order phase transition, *Phys. Rev. D* **102**, 075028 (2020); arXiv:2008.04430.
11. M. J. Baker, J. Kopp, A. J. Long: Filtered dark matter at a first order phase transition, *Phys. Rev. Lett.* **125**, 151102 (2020); arXiv:1912.02830.
12. E. Hall, T. Konstandin, R. McGehee, H. Murayama: Asymmetric matters from a dark first-order phase transition, Report IPMU19-0171, DESY19-209; arXiv:1911.12342.
13. K. Ghorbani, P. H. Ghorbani: A simultaneous study of dark matter and phase transition: two-scalar scenario, *J. of High Energy Phys.* **2019**, 77 (2019); arXiv:1906.01823.
14. G. Chapline: Dark energy stars, Proc. of the Texas Conference on Relativistic Astrophysics, Stanford, CA, December, 2004; arXiv:astro-ph/0503200.
15. G. Chapline, E. Hohlfeld, R. B. Laughlin, D. I. Santiago: Quantum phase transitions and the breakdown of classical general relativity, *Int. J. Mod. Phys. A* **18**, 3587-3590 (2003); arXiv:gr-qc/0012094.
16. A. B. Balakin, A. S. Ilin: Dark energy and dark matter interaction: kernels of Volterra type and coincidence problem, *Symmetry* **10**, 411 (2018); arXiv:1809.05678.
17. W. Yang, N. Banerjee, A. Paliathanasis, S. Pan: Reconstructing the dark matter and dark energy interaction scenarios from observations, *Phys. Dark Univ.* **26**, 100383 (2019); arXiv:1812.06854.
18. G. Cheng, Y.-Z. Ma, F. Wu, J. Zhang, X. Chen: Testing interacting dark matter and dark energy model with cosmological data, *Phys. Rev. D* **102**, 043517 (2020); arXiv:1911.04520.
19. A. Paliathanasis, S. Pan, W. Yang: Dynamics of nonlinear interacting dark energy models, *Int. J. Mod. Phys. D* **28**, 1950161 (2019); arXiv:1903.02370.
20. Z. Rezaei: Dark matter – dark energy interaction and the shape of cosmic voids, *The Astrophys. J.* **902**, 102 (2020); arXiv:2010.10823.
21. M. Lucca, D. C. Hooper: Tensions in the dark: shedding light on dark matter – dark energy interactions, *Phys. Rev. D* **102**, 123502 (2020); arXiv:2002.06127.
22. W. Yang, S. Pan, A. Paliathanasis: Cosmological constraints on an exponential interaction in the dark sector, *Mon. Not. Roy. Astron. Soc.* **482**, 1007-1016 (2019); arXiv:1804.08558.
23. V. H. Cárdenas, D. Grandón, S. Lepe: Dark energy and dark matter interaction in light of the second law of thermodynamics, *The European Phys. J. C* **79**, 357 (2019); arXiv:1812.03540.
24. S. Pan, W. Yang, E. Di Valentino, A. Shafieloo, S. Chakraborty: Reconciling H_0 tension in a six parameter space?, *J. of Cosmology and Astroparticle Phys.* **2020**, 062 (2020); arXiv:1907.12551.

25. X. Li, A. Shafieloo: Evidence for emergent dark energy, *The Astrophys. J.* **902**, 58 (2020); arXiv:2001.05103.
26. E. Di Valentino, A. Melchiorri, O. Mena, S. Vagnozzi: Interacting dark energy in the early 2020s: a promising solution to the H_0 and cosmic shear tensions, *Phys. Dark Univ.* **30**, 100666 (2020); arXiv:1908.04281.
27. E. Di Valentino, A. Melchiorri, O. Mena, S. Vagnozzi: Non-minimal dark sector physics and cosmological tensions, *Phys. Rev.* **D101**, 063502 (2020); arXiv:1910.09853.
28. E. Di Valentino, O. Mena: A fake interacting dark energy detection?, *Mon. Not. Roy. Astron. Soc. Lett.* **500**, L22-L26 (2021); arXiv:2009.12620.
29. K. L. Pandey, T. Karwal, S. Das: Alleviating the H_0 and σ_8 anomalies with a decaying dark matter model, *J. of Cosmology and Astroparticle Phys.* **2020**, 026 (2020); arXiv:1902.10636.
30. S. Ghosh, R. Khatri, T. S. Roy: Dark neutrino interactions phase out the Hubble tension, *Phys. Rev.* **D102**, 123544 (2020); arXiv:1908.09843.
31. S. Pan, W. Yang, A. Paliathanasis: Nonlinear interacting cosmological models after Planck 2018 legacy release and the H_0 tension, *Mon. Not. Roy. Astron. Soc.* **493**, 3114-3131 (2020); arXiv:2002.03408.
32. S. Panpanich, P. Burikham, S. Ponglertsakul, L. Tannukij: Resolving Hubble tension with quintom dark energy model, *Chin. Phys.* **C45** (2021) 015108; arXiv:1908.03324.
33. M. Archidiacono, D. C. Hooper, R. Murgia, S. Bohr, J. Lesgourgues, M. Viel: Constraining dark matter – dark radiation interactions with CMB, BAO, and Lyman- α , *J. of Cosmology and Astroparticle Phys.* **2019**, 055 (2019); arXiv:1907.01496.
34. M. Martinelli, I. Tutusaus: CMB Tensions with low-redshift H_0 and S_8 measurements: impact of a redshift-dependent type-Ia supernovae intrinsic luminosity, *Symmetry* **11**, 986 (2019); arXiv:1906.09189.
35. G.-B. Zhao et al.: Dynamical dark energy in light of the latest observations, *Nature Astronomy* **1**, 627-632 (2017); arXiv:1701.08165.
36. Y. Wang, L. Pogosian, G.-B. Zhao, A. Zucca: Evolution of dark energy reconstructed from the latest observations, *The Astrophys. J. Lett.* **869**, L8 (2018); arXiv:1807.03772.
37. E. Castellanos, C. Escamilla-Rivera: Dark energy as generalised superfluid excitations; arXiv:2006.06129.
38. E. G. M. Ferreira: Unified superfluid dark sector, in: *Quantum Theory and Symmetries*, CRM Series in Mathematical Physics, Springer 2021; arXiv:1911.07371.
39. K. Huang: Dark energy and dark matter in a superfluid universe, *Int. J. Mod. Phys.* **A28**, 1330049 (2013); arXiv:1309.5707.
40. J.-W. Lee, I.-G. Koh: Galactic halos as boson stars, *Phys. Rev.* **D53**, 2236-2239 (1996); arXiv:hep-ph/9507385.
41. E. Braaten, A. Mohapatra, H. Zhang: Dense axion stars; *Phys. Rev. Lett.* **117**, 121801 (2016); arXiv:1512.00108.
42. L. Visinelli, S. Baum, J. Redondo, K. Freese, F. Wilczek: Dilute and dense axion stars, *Phys. Lett.* **B777**, 64-72 (2018); arXiv:1710.08910.
43. V. A. Popov: Dark energy and dark matter unification via superfluid Chaplygin gas, *Phys. Lett.* **B686**, 211-215 (2010); arXiv:0912.1609.
44. Y. Sofue, V. C. Rubin: Rotation curves of spiral galaxies, *Ann. Rev. Astron. Astrophys.* **39**, 137-174 (2001); arXiv:astro-ph/0010594.
45. Y. Sofue, M. Honma, T. Omodaka: Unified rotation curve of the Galaxy – decomposition into de Vaucouleurs bulge, disk, dark halo, and the 9-kpc rotation dip, *Publications of the Astronomical Society of Japan* **61**, 227-236 (2009); arXiv:0811.0859.
46. Y. Sofue: Pseudo rotation curve connecting the Galaxy, dark halo, and Local Group, *Publications of the Astronomical Society of Japan* **61**, 153-161 (2009); arXiv:0811.0860.

47. Y. Sofue: A grand rotation curve and dark matter halo in the Milky Way galaxy, *Publications of the Astronomical Society of Japan* **64**, 75 (2012); arXiv:1110.4431.
48. Y. Sofue: Rotation curve and mass distribution in the Galactic Center – from black hole to entire Galaxy, *Publications of the Astronomical Society of Japan* **65**, 118 (2013); arXiv:1307.8241.
49. S. Dodelson: *Modern Cosmology*, Elsevier, 2003.
50. M. Blau: *Lecture Notes on General Relativity*, University of Bern, 2021, www.blau.itp.unibe.ch/newlecturesGR.pdf
51. A. Kruchkov, Yu. Slyusarenko: Bose-Einstein condensation of photons in an ideal atomic gas, *Phys. Rev.* **A88**, 013615 (2013); arXiv:1305.1210.
52. A. J. S. Hamilton, S. E. Pollack: Inside charged black holes: II. Baryons plus dark matter, *Phys. Rev.* **D71**, 084032 (2005), arXiv:gr-qc/0411062.
53. F. Sylos Labini, M. Montuori, L. Pietronero: Scale-invariance of galaxy clustering, *Phys. Rep.* **293**, 61-226 (1998); arXiv:astro-ph/9711073.
54. J. Peñarrubia, Yin-Zhe Ma, M. G. Walker, A. McConnachie: A dynamical model of the local cosmic expansion, *Mon. Not. Roy. Astron. Soc.* **443**, 2204-2222 (2014); arXiv:1405.0306.
55. J. Barranco, A. Bernal, D. Nunez: Dark matter equation of state from rotational curves of galaxies, *Mon. Not. Roy. Astron. Soc.* **449**, 403 (2015), arXiv:1301.6785.
56. C. J. Conselice, A. Wilkinson, K. Duncan, A. Mortlock: The evolution of galaxy number density at $z < 8$ and its implications, *The Astrophys. J.* **830**, 83 (2016); arXiv:1607.03909.
57. T. C. Licquia, J. A. Newman: Improved estimates of the Milky Way's stellar mass and star formation rate from hierarchical Bayesian meta-analysis, *The Astrophys. J.* **806**, 96 (2015); arXiv:1407.1078.
58. A. G. Bedregal, A. Aragón-Salamanca, M. R. Merrifield: The Tully-Fisher relation for S0 galaxies, *Mon. Not. Roy. Astron. Soc.* **373**, 1125-1140 (2006); arXiv:astro-ph/0609076.
59. R. Schaeffer, S. Maurogordato, A. Cappi, F. Bernardeau: The fundamental plane of galaxy clusters, *Mon. Not. Roy. Astron. Soc.* **263**, L21-L26 (1993); arXiv:astro-ph/9304018.
60. M. Girardi, P. Manzato, M. Mezzetti, G. Giuricin, F. Limboz: Observational mass-to-light ratio of galaxy systems from poor groups to rich clusters, *The Astrophys. J.* **569**, 720 (2002).
61. P. Salucci et al.: The universal rotation curve of spiral galaxies. II. The dark matter distribution out to the virial radius, *Mon. Not. Roy. Astron. Soc.* **378**, 41-47 (2007); arXiv:astro-ph/0703115.
62. E. V. Karukes, P. Salucci: The universal rotation curve of dwarf disk galaxies, *Mon. Not. Roy. Astron. Soc.* **465**, 4703-4722 (2017); arXiv:1609.06903.
63. M. Visser: *Lorentzian Wormholes: from Einstein to Hawking*, Springer, 1996.
64. J. B. Hartle: *Gravity: An Introduction to Einstein's General Relativity*, Addison-Wesley, 2003.



21 Ultraviolet divergences in supersymmetric theories regularized by higher derivatives

K.V. Stepanyantz

email: stepan@m9com.ru

Moscow State University, Faculty of Physics, Department of Theoretical Physics, 119991 Moscow, Russia

Abstract. Structure of quantum corrections in $\mathcal{N} = 1$ supersymmetric gauge theories is investigated in the case of using the regularization by higher covariant derivatives. It is demonstrated that this regularization allows revealing some interesting features which lead to the exact relations between the renormalization group functions. In particular, the NSVZ equation, which relates the β -function to the anomalous dimension of the matter superfields, naturally appears in this case. We briefly review the all-loop derivation of this equation and the construction of a simple renormalization prescription under which it is valid.

Povzetek: Avtor razišče strukturo kvantnih popravkov v $\mathcal{N} = 1$ super-simetričnih umeritvenih teorijah z regularizacijo z višjimi kovariantnimi odvodi. Pokaže, da ta način regularizacije omogoča razkritje natančnih razmerij med funkcijami renormalizacijskih skupin. Denimo, enačba NSVZ, ki povezuje funkcijo β z anomalno dimenzijo superpolj snovi, postane očitna. Avtor na kratko predstavi izpeljavo popravkov te enačbe v vseh redih ter ponudi preprosto navodilo za renormalizacijo, ko ta enačba velja.

21.1 Introduction

The investigation of quantum corrections in supersymmetric theories is very important for both theory and phenomenological applications. As well known, ultraviolet (UV) divergences in these theories are restricted by some nonrenormalization theorems. The most known of them are the following:

1. $\mathcal{N} = 1$ superpotential is not renormalized [1],
2. $\mathcal{N} = 2$ theories are finite beyond the first loop [2–4],
3. $\mathcal{N} = 4$ supersymmetric Yang–Mills theory is all-loop finite [2, 3, 5–7].

Due to the nonrenormalization theorems it is even possible to construct finite theories with $\mathcal{N} < 4$ supersymmetry. For $\mathcal{N} = 2$ supersymmetric theories this can be done by a special choice of a gauge group and representations for the hypermultiplets [8]. For $\mathcal{N} = 1$ supersymmetric theories [9–13] and theories with softly broken supersymmetry [14–16] it is also necessary to make a special tuning of a renormalization scheme.

However, the above list of the nonrenormalization theorems is not complete. For instance, it is reasonable to include into this list the exact Novikov, Shifman,

Vainshtein, and Zakharov (NSVZ) β -function [17–20]. This is an equation which in general relates the β -function and the anomalous dimension of the matter superfields in $\mathcal{N} = 1$ supersymmetric gauge theories,

$$\beta(\alpha, \lambda) = -\frac{\alpha^2 \left(3C_2 - T(\mathbf{R}) + C(\mathbf{R})_i^j (\gamma_\phi)_j^i(\alpha, \lambda)/r \right)}{2\pi(1 - C_2\alpha/2\pi)}, \quad (21.1)$$

where α and λ denote the gauge and Yukawa coupling constants, respectively, and we do not specify the definitions of the renormalization group functions (RGFs). The numerical factors in the equation (21.1) are defined as

$$\begin{aligned} \text{tr}(T^A T^B) &\equiv T(\mathbf{R}) \delta^{AB}; & (T^A)_i^k (T^A)_k^j &\equiv C(\mathbf{R})_i^j; \\ f^{ACD} f^{BCD} &\equiv C_2 \delta^{AB}; & r &\equiv \delta_{\Lambda\Lambda} = \dim G. \end{aligned} \quad (21.2)$$

However, there is an important problem, for which renormalization prescriptions the nonrenormalization theorems do hold. Really, the explicit calculations in $\mathcal{N} = 1$ supersymmetric theories made in the $\overline{\text{DR}}$ -scheme in [21–24] revealed that the NSVZ relation in this scheme is valid only in the one- and two-loop approximations, where this relation does not depend on a renormalization prescription. However, it turned out that with the help of a specially tuned finite renormalization of the gauge coupling constant one can restore the NSVZ equation, at least, in the three- and four-loop approximations [22–26]. This (very nontrivial) fact implies that the NSVZ relation holds, but only in some special renormalization schemes usually called “the NSVZ schemes”. Evidently, the $\overline{\text{DR}}$ -scheme does not belong to them.

In this paper we briefly review the recent progress in constructing the all-loop prescription giving some NSVZ schemes based on the perturbative derivation of the NSVZ β -function made in [27–29]. The main ingredient needed for this is the regularization by higher covariant derivatives proposed by A.A.Slavnov [30, 31] rather long ago. Note that, by construction, it also includes the Pauli–Villars regularization for removing residual one-loop divergencies [32]. In the supersymmetric case this regularization can be self-consistently formulated in terms of $\mathcal{N} = 1$ superfields [33, 34] and, therefore, does not break supersymmetry.

21.2 The NSVZ equation for $\mathcal{N} = 1$ SQED

21.2.1 Regularization, quantization, and RGFs

As the simplest example illustrating how to derive the NSVZ equation and how to construct NSVZ schemes we consider the (massless) $\mathcal{N} = 1$ supersymmetric electrodynamics (SQED) with N_f flavors. Manifest supersymmetry at all steps of calculating quantum corrections is achieved by formulating the theory in terms of $\mathcal{N} = 1$ superfields,

$$S = \frac{1}{4e_0^2} \text{Re} \int d^4x d^2\theta W^\alpha W_\alpha + \sum_{\alpha=1}^{N_f} \frac{1}{4} \int d^4x d^4\theta \left(\phi_\alpha^* e^{2V} \phi_\alpha + \tilde{\phi}_\alpha^* e^{-2V} \tilde{\phi}_\alpha \right). \quad (21.3)$$

In the action (21.3) the (real) gauge superfield is denoted by V , while ϕ_α and $\tilde{\phi}_\alpha$ are chiral matter superfields with opposite $U(1)$ charges. In the Abelian case the strength of the superfield V is defined as $W_\alpha = \bar{D}^2 D_\alpha V/4$.

Setting $C_2 = 0$, $C(R) = I$ (where I is the $2N_f \times 2N_f$ identity matrix), $T(R) = 2N_f$, and $r = 1$ in the equation (21.1) we see that in this case the NSVZ β -function takes the form [35,36]¹

$$\beta(\alpha) = \frac{\alpha^2 N_f}{\pi} (1 - \gamma(\alpha)) \tag{21.4}$$

and relates the L -loop β -function to the $(L - 1)$ -loop anomalous dimension of the matter superfields $\gamma(\alpha)$.

The considered theory will be regularized by higher covariant derivatives in two steps. First, we add a term with higher derivatives to the action (21.3) and regularize divergences beyond the one-loop approximation. Then the resulting regularized action can be written as

$$S_{\text{reg}} = \frac{1}{4e_0^2} \text{Re} \int d^4x d^2\theta W^a R(\partial^2/\Lambda^2) W_a + \sum_{\alpha=1}^{N_f} \frac{1}{4} \int d^4x d^4\theta \left(\phi_\alpha^* e^{2V} \phi_\alpha + \tilde{\phi}_\alpha^* e^{-2V} \tilde{\phi}_\alpha \right), \tag{21.5}$$

where $R(\partial^2/\Lambda^2)$ is a regulator function, e.g., $R = 1 + \partial^{2n}/\Lambda^{2n}$. Next, for removing one-loop divergences and subdivergences that will be still present, the Pauli-Villars determinants are inserted into the generating functional,

$$Z[J, j, \tilde{j}] = \int D\mu \left(\det PV(V, M) \right)^{N_f} \exp \left\{ iS_{\text{reg}} + iS_{\text{gf}} + S_{\text{sources}} \right\}. \tag{21.6}$$

The masses of the corresponding (Pauli-Villars) superfields should satisfy the important condition $M = a\Lambda$ with $a \neq a(e_0)$.

Calculating RGFs it is important to distinguish between the ones defined in terms of the bare coupling constant α_0 ,

$$\beta(\alpha_0) \equiv \frac{d\alpha_0(\alpha, \Lambda/\mu)}{d \ln \Lambda} \Big|_{\alpha=\text{const}}; \quad \gamma(\alpha_0) \equiv -\frac{d \ln Z(\alpha, \Lambda/\mu)}{d \ln \Lambda} \Big|_{\alpha=\text{const}}, \tag{21.7}$$

and the ones (standardly) defined in terms of the renormalized coupling constant α [37],

$$\tilde{\beta}(\alpha) \equiv \frac{d\alpha(\alpha_0, \Lambda/\mu)}{d \ln \mu} \Big|_{\alpha_0=\text{const}}; \quad \tilde{\gamma}(\alpha) \equiv \frac{d \ln Z(\alpha_0, \Lambda/\mu)}{d \ln \mu} \Big|_{\alpha_0=\text{const}}. \tag{21.8}$$

The former RGFs are independent of a renormalization prescription if a regularization is fixed, although they certainly depend on a regularization. The latter

¹ So far we again do not specify the definitions of RGFs.

(standard) RGFs depend both on a regularization and on a renormalization prescription. However, both definitions of RGFs up to a formal replacement of the argument coincide in the so-called HD+MSL renormalization scheme [38,39],

$$\tilde{\beta}(\alpha)\Big|_{\text{HD+MSL}} = \beta(\alpha_0 \rightarrow \alpha); \quad \tilde{\gamma}(\alpha)\Big|_{\text{HD+MSL}} = \gamma(\alpha_0 \rightarrow \alpha). \quad (21.9)$$

This implies that a theory is regularized by higher derivatives and only powers of $\ln \Lambda/\mu$ are included into the renormalization constants. (Because this way of removing divergences is very similar to minimal subtraction in the case of using the dimensional technique, it is called minimal subtractions of logarithms.)

21.2.2 The three-loop β -function with the higher derivative regularization

The first calculations of the lowest quantum corrections for $\mathcal{N} = 1$ SQED regularized by higher derivatives revealed that with this regularization the integrals giving the β -function defined in terms of the bare coupling constant are integrals of total derivatives [40] and even double total derivatives [41] with respect to the momentum of the matter loop. The result for the three-loop β -function in this form can be found, e.g., in [42,43]. Note that such integrals do not vanish due to singularities of the integrands,

$$\int \frac{d^4 Q}{(2\pi)^4} \frac{\partial}{\partial Q^\mu} \frac{\partial}{\partial Q_\mu} \left(\frac{f(Q^2)}{Q^2} \right) = \frac{1}{4\pi^2} f(0) \neq 0, \quad (21.10)$$

where we assume that $f(Q^2)$ is a non-singular function rapidly decreasing at infinity. Using equations similar to (21.10) it is possible to reduce a number of loop integrations by 1. A detailed analyses revealed that this leads to the following simple graphical interpretation of the Abelian NSVZ equation [41]. If one considers a vacuum supergraph, then a certain set of superdiagrams contributing to the β -function is produced by attaching two external gauge lines in all possible ways. From the other side, cuts of matter lines in the original vacuum supergraph give a set of two-point superdiagrams contributing to the anomalous dimension of the matter superfields, in which a number of loops is less by 1. The equation (21.4) relates these two contributions. At the three-loop level a detailed check of this graphical interpretation has been done in [44]. In particular, it turned out that for theories regularized by higher derivatives the NSVZ equation holds even at the level of loop integrals provided RGFs are defined in terms of the bare coupling constant. The explicit expressions for these RGFs found in [45] for an arbitrary function $R(x)$ are written as

$$\begin{aligned} \frac{\beta(\alpha_0)}{\alpha_0^2} &= \frac{N_f}{\pi} + \frac{\alpha_0 N_f}{\pi^2} - \frac{\alpha_0^2 N_f}{\pi^3} \left(N_f \ln a + N_f + \frac{N_f A}{2} + \frac{1}{2} \right) + O(\alpha_0^3); \\ \gamma(\alpha_0) &= -\frac{\alpha_0}{\pi} + \frac{\alpha_0^2}{\pi^2} \left(N_f \ln a + N_f + \frac{N_f A}{2} + \frac{1}{2} \right) + O(\alpha_0^3), \end{aligned} \quad (21.11)$$

where

$$\Lambda \equiv \int_0^\infty dx \ln x \frac{d}{dx} \frac{1}{R(x)}; \quad a = \frac{M}{\Lambda}. \quad (21.12)$$

We see that they do not depend on the parameters fixing a subtraction scheme, but depend on the regularization parameters Λ and a . However, for all their values the NSVZ equation is valid.

RGFs defined in terms of the renormalized coupling constant do not in general satisfy the NSVZ equation,

$$\begin{aligned} \tilde{\beta}(\alpha) &= \frac{N_f}{\pi} + \frac{\alpha N_f}{\pi^2} - \frac{\alpha^2 N_f}{2\pi^3} - \frac{\alpha^2 N_f^2}{\pi^3} \left(\ln a + 1 + \frac{\Lambda}{2} + b_2 - b_1 \right) + O(\alpha^3) \\ \tilde{\gamma}(\alpha) &= -\frac{\alpha}{\pi} + \frac{\alpha^2}{2\pi^2} + \frac{\alpha^2 N_f}{\pi^2} \left(\ln a + 1 + \frac{\Lambda}{2} - b_1 + g_1 \right) + O(\alpha^3), \end{aligned} \quad (21.13)$$

and depend on the finite constants b_i and g_i fixing the renormalization prescription. These constants are defined by the equations

$$\begin{aligned} \frac{1}{\alpha_0} &= \frac{1}{\alpha} - \frac{N_f}{\pi} \left(\ln \frac{\Lambda}{\mu} + b_1 \right) - \frac{\alpha N_f}{\pi^2} \left(\ln \frac{\Lambda}{\mu} + b_2 \right) + O(\alpha^2). \\ Z &= 1 + \frac{\alpha}{\pi} \left(\ln \frac{\Lambda}{\mu} + g_1 \right) + O(\alpha^2). \end{aligned} \quad (21.14)$$

In the HD+MSL scheme they vanish

$$g_1 = b_1 = b_2 = 0, \quad (21.15)$$

and both definition of RGFs give the same functions up to the formal replacement of arguments. Evidently, in this case the NSVZ equation holds, although the scheme dependence is already essential.

The three-loop β -function and the two-loop anomalous dimension of the matter superfields in the $\overline{\text{DR}}$ and MOM schemes can be found in [22, 46, 47]. In these schemes the NSVZ equation relating these RGFs does not hold.

21.2.3 The all-loop results

In [42] the all-loop expression for the β -function of $\mathcal{N} = 1$ SQED (defined in terms of the bare coupling constant in the case of using the higher derivative regularization) was presented in the form of a functional integral over the gauge superfield V , which is an integral of double total derivatives in the momentum space. Certainly, this integral of double total derivatives is reduced to the sum of singular contributions with the help of equations similar to (21.10). The all-loop sum of the singularities which has also been calculated in [42] gives the exact NSVZ β -functions for RGFs defined in terms of the bare couplings,

$$\frac{\beta(\alpha_0)}{\alpha_0^2} = \frac{N_f}{\pi} \left(1 - \gamma(\alpha_0) \right). \quad (21.16)$$

Thus, if $\mathcal{N} = 1$ SQED is regularized by higher derivatives, then RGFs defined in terms of the bare coupling constant satisfy the NSVZ equation in all orders for an arbitrary renormalization prescription. (Note that both sides of this equation do not depend on the parameter ξ_0 in the gauge fixing term, so that this result is valid for an arbitrary ξ -gauge.) Analogous result has been obtained in [48] with the help of a different method.

Consequently, some NSVZ schemes for RGFs defined in terms of the renormalized coupling constant are given by the HD+MSL prescription. Note that they constitute a certain subclass in the continuous set of the NSVZ schemes described in [49]. Really, minimal subtractions of logarithms can supplement various versions of the higher derivative regularization, which can differ in the form of the higher derivative regulator $R(x)$ and the constant a defined by the equation (21.12). Note that the class of NSVZ schemes also includes the on-shell scheme, which is another all-loop NSVZ renormalization prescription [50].

21.3 Non-Abelian supersymmetric gauge theories regularized by higher derivatives

Below we will describe the derivation of the NSVZ equation and NSVZ schemes for renormalizable non-Abelian $\mathcal{N} = 1$ supersymmetric gauge theories. In the massless limit they are described by the classical action

$$S = \frac{1}{2e_0^2} \text{Re tr} \int d^4x d^2\theta W^\alpha W_\alpha + \frac{1}{4} \int d^4x d^4\theta \phi^{*i} (e^{2V})_i{}^j \phi_j + \left(\frac{1}{6} \lambda_0^{ijk} \int d^4x d^2\theta \phi_i \phi_j \phi_k + \text{c.c.} \right), \quad (21.17)$$

which is written in a manifestly supersymmetric form with the help of $\mathcal{N} = 1$ superspace. Below we will assume that the gauge group G is simple, and the chiral matter superfields ϕ_i transform under its representation R . The classical non-Abelian expression for the supersymmetric gauge superfield strength is $W_\alpha = \bar{D}^2 (e^{-2V} D_\alpha e^{2V}) / 8$. Also the bare Yukawa couplings λ_0^{ijk} should satisfy the condition

$$\lambda_0^{ijm} (T^A)_m{}^k + \lambda_0^{imk} (T^A)_m{}^j + \lambda_0^{mjk} (T^A)_m{}^i = 0, \quad (21.18)$$

which provides the gauge invariance of the cubic interaction term.

Quantizing the theory we use the background field method realized by the replacement $e^{2V} \rightarrow e^{2\mathcal{F}(V)} e^{2V}$, where in the right hand side \mathbf{V} and V are the background and quantum gauge superfields, respectively. The function $\mathcal{F}(V)$ is needed for describing the nonlinear renormalization of the quantum gauge superfield [51–53] and includes an infinite set of parameters analogous to the parameter in the gauge fixing term. Explicit calculations [54, 55] demonstrated that this function is really different from V . Moreover, the renormalization group equations cannot be satisfied without taking the nonlinear terms into account [56].

Following [57, 58], to introduce the regularization, we modify the action by adding terms with higher powers of the covariant derivatives

$$\nabla_\alpha = D_\alpha; \quad \bar{\nabla}_{\dot{\alpha}} = e^{2\mathcal{F}(V)} e^{2V} \bar{D}_{\dot{\alpha}} e^{-2V} e^{-2\mathcal{F}(V)}, \quad (21.19)$$

after which the regularized action takes the form

$$\begin{aligned} S_{\text{reg}} = & \frac{1}{2e_0^2} \text{Re tr} \int d^4x d^2\theta W^\alpha \left(e^{-2V} e^{-2\mathcal{F}(V)} \right)_{\text{Adj}} R\left(-\frac{\bar{\nabla}^2 \nabla^2}{16\Lambda^2}\right)_{\text{Adj}} \\ & \times \left(e^{2\mathcal{F}(V)} e^{2V} \right)_{\text{Adj}} W_\alpha + \frac{1}{4} \int d^4x d^4\theta \phi^{*i} \left[F\left(-\frac{\bar{\nabla}^2 \nabla^2}{16\Lambda^2}\right) e^{2\mathcal{F}(V)} e^{2V} \right]_i^j \phi_j \\ & + \left(\frac{1}{6} \lambda_0^{ijk} \int d^4x d^2\theta \phi_i \phi_j \phi_k \right) + \text{c.c.} \end{aligned} \quad (21.20)$$

and will contain the regulator functions $R(x)$ and $F(x)$. It is reasonable to choose the gauge fixing term which does not break the background gauge invariance and is analogous to the ξ -gauge fixing term in the usual Yang–Mills theory, although now it should contain one more regulator function $K(x)$. Certainly, the Faddeev–Popov and Nielsen–Kalosh ghosts must also be introduced according to the standard procedure.

The residual one-loop divergences are removed by inserting into the generating functional the Pauli–Villars determinants [32]. In the considered supersymmetric case one needs two such determinants [57, 58],

$$\begin{aligned} Z = & \int D\mu \text{Det}(PV, M_\varphi)^{-1} \text{Det}(PV, M)^{T(R)/T(R_{PV})} \\ & \times \exp \left\{ i \left(S_{\text{reg}} + S_{\text{gf}} + S_{\text{FP}} + S_{\text{NK}} + S_{\text{sources}} \right) \right\}, \end{aligned} \quad (21.21)$$

where the masses of the Pauli–Villars superfields $\varphi_{1,2,3}$ in the adjoint representation and Φ_i in a representation R_{PV} are $M_\varphi = a_\varphi \Lambda$ and $M = a\Lambda$, respectively, and the coefficients a_φ and a do not depend on couplings.

21.4 The all-loop derivation of the NSVZ equation: the main steps

21.4.1 The ultraviolet finiteness of the triple gauge-ghost vertices

The first step needed for proving the non-Abelian NSVZ relation is the nonrenormalization theorem for the three-point vertices with two external lines of the Faddeev–Popov ghosts and one external line of the quantum gauge superfield [27] (see also [59] for the generalization to the case of theories with multiple gauge couplings). According to this nonrenormalization theorem the triple gauge-ghost vertices are finite in all orders.² The all-loop proof of this statement in the general ξ -gauge is based on the superfield Feynman rules and the Slavnov–Taylor

² Similar statements in the Landau gauge were also proved for some theories formulated in terms of usual fields [60, 61].

identities. The one- and two-loop checks of it have been done in [27] and [62,63], respectively.

There are 4 vertices of the considered structure with the external lines corresponding to the superfields $\bar{c} Vc$, $\bar{c}^+ Vc$, $\bar{c} Vc^+$, and $\bar{c}^+ Vc^+$, where \bar{c} and c are the Faddeev–Popov antighost and ghost, respectively. The renormalization constants for all these vertices coincide and are equal to $Z_\alpha^{-1/2} Z_c Z_V$, where

$$\frac{1}{\alpha_0} = \frac{Z_\alpha}{\alpha}; \quad V = Z_V Z_\alpha^{-1/2} V_R; \quad \bar{c}c = Z_c Z_\alpha^{-1} \bar{c}_R c_R, \quad (21.22)$$

so that the nonrenormalization theorem can be expressed by the equation

$$\frac{d}{d \ln \Lambda} (Z_\alpha^{-1/2} Z_c Z_V) = 0. \quad (21.23)$$

21.4.2 An equivalent form of the NSVZ equation

The next step of the derivation is to rewrite the NSVZ relation in an equivalent form [27]. For this purpose the non-Abelian NSVZ equation for RGFs defined in terms of the bare couplings is presented as

$$\frac{\beta(\alpha_0, \lambda_0)}{\alpha_0^2} = -\frac{3C_2 - T(R) + C(R)_i^j (\gamma_\phi)_j^i(\alpha_0, \lambda_0)/r}{2\pi} + \frac{C_2}{2\pi} \cdot \frac{\beta(\alpha_0, \lambda_0)}{\alpha_0}. \quad (21.24)$$

The β -function in the right hand side is expressed in terms of the anomalous dimensions $\gamma_c(\alpha_0, \lambda_0)$ and $\gamma_V(\alpha_0, \lambda_0)$ (of the ghosts and of the quantum gauge superfield, respectively) with the help of the equation (21.23),

$$\begin{aligned} \beta(\alpha_0, \lambda_0) &= \left. \frac{d\alpha_0(\alpha, \lambda, \Lambda/\mu)}{d \ln \Lambda} \right|_{\alpha, \lambda = \text{const}} = -\alpha_0 \left. \frac{d \ln Z_\alpha}{d \ln \Lambda} \right|_{\alpha, \lambda = \text{const}} \\ &= -2\alpha_0 \left. \frac{d \ln(Z_c Z_V)}{d \ln \Lambda} \right|_{\alpha, \lambda = \text{const}} = 2\alpha_0 \left(\gamma_c(\alpha_0, \lambda_0) + \gamma_V(\alpha_0, \lambda_0) \right). \end{aligned} \quad (21.25)$$

Substituting this expression into the the right hand side of (21.24) we obtain the equation

$$\begin{aligned} \frac{\beta(\alpha_0, \lambda_0)}{\alpha_0^2} &= -\frac{1}{2\pi} \left(3C_2 - T(R) - 2C_2 \gamma_c(\alpha_0, \lambda_0) \right. \\ &\quad \left. - 2C_2 \gamma_V(\alpha_0, \lambda_0) + C(R)_i^j (\gamma_\phi)_j^i(\alpha_0, \lambda_0)/r \right) \end{aligned} \quad (21.26)$$

relating the β -function to the anomalous dimensions of the quantum superfields. Note that the β -function in a certain loop is now expressed in terms of the anomalous dimensions only in the previous loop, while the original NSVZ equation relates the β -function only to the anomalous dimension of the matter superfields, but in all previous loops. That is why the NSVZ equation in the form (21.26) has a graphical interpretation analogous to the Abelian case. Namely, if one considers a supergraph without external lines, then attaching two legs of the background

gauge superfield in all possible ways gives a contribution to $\beta(\alpha_0, \lambda_0)$, while various cuts of internal lines in the original vacuum supergraphs give contributions to the anomalous dimensions of the quantum superfields. The equation (21.26) relates all these contributions.

21.4.3 The β -function and integrals of double total derivatives

Next, it is necessary to prove that in supersymmetric theories regularized by higher covariant derivatives the β -function defined in terms of the bare couplings is given by integrals of double total derivatives with respect to the loop momenta.³ This fact was observed in a large number of explicit calculations, see, e.g., [65–68]. Its all-loop proof in the non-Abelian case has been done in [28]. With the help of a rather complicated technique it was demonstrated that the β -function is determined by an expression which formally vanishes due to the Slavnov–Taylor identity corresponding to the background gauge invariance. Analyzing the Feynman rules it was demonstrated that this expression is a sum of integrals of double total derivatives which are in fact nontrivial due to singularities of the integrands. Moreover, considering this formally vanishing expression as a starting point, one can construct a method for obtaining the β -function in $\mathcal{N} = 1$ supersymmetric theories regularized by higher covariant derivatives in $\mathcal{N} = 1$ superspace [28, 69, 70]. This method requires to calculate only (specially modified) vacuum supergraphs and produces the result for a contribution to the β -function which comes from all superdiagrams obtained from them by attaching two external lines of the background gauge superfield. Note that this result is automatically obtained in the form of an integral of double total derivatives with respect to loop momenta.

The correctness of the method for calculating the β -function has been confirmed by a certain number of (very nontrivial) explicit calculations. For instance, using this method the two-loop β -function of $\mathcal{N} = 1$ supersymmetric Yang–Mills theory with matter superfields in an arbitrary ξ -gauge has been reproduced in [69]. In particular, it turned out that the NSVZ equations (21.1) and (21.26) are satisfied even at the level of loop integrals. However, in this approximation the NSVZ relations are scheme independent, so that it is desirable to consider the next order of the perturbation theory.

The explicit three-loop calculation is very complicated and (with the higher covariant derivative regularization) has not yet completely been done. However, a part of the three-loop β -function depending on the Yukawa couplings was found in [67, 68] with the help of the standard technique. Subsequently the same part of the β -function was obtained in [28] with the help of the new technique which requires calculating only specially modified vacuum supergraphs. The results produced by both methods coincided. This means that the new method really works correctly.

³ This is not true for theories regularized by dimensional reduction due to a different structure of loop integrals [64].

21.4.4 Summation of singular contributions

The method for constructing integrals of double total derivatives described above can be used for deriving the exact NSVZ β -function in all orders of the perturbation theory. The main idea is that the integrals of double total derivatives can be taken with the help of equations similar to (21.10). Then they are reduced to the sums of singularities which correspond to various cuts of internal lines in vacuum supergraphs. These sums were calculated in all orders in [29] (see also [71]). The result can be presented in the following form:

$$\frac{\beta(\alpha_0, \lambda_0)}{\alpha_0^2} - \frac{\beta_{1\text{-loop}}(\alpha_0)}{\alpha_0^2} \tag{21.27}$$

$$= \frac{1}{\pi} C_2 \gamma_V(\alpha_0, \lambda_0) + \frac{1}{\pi} C_2 \gamma_c(\alpha_0, \lambda_0) - \frac{1}{2\pi r} C(R)_i^j (\gamma_\phi)_j^i(\alpha_0, \lambda_0).$$

\uparrow
 gauge propagators

\uparrow
 Faddeev–Popov ghost propagators

\uparrow
 matter propagators

We see that the sums of singularities corresponding to cuts of the gauge, ghost, and matter propagators produce the corresponding anomalous dimensions in the NSVZ equation written in the form (21.26). Substituting the one-loop expression for the β -function⁴ we obtain the NSVZ equation for RGFs defined in terms of the bare couplings. Note that a renormalization prescription in this case is not fixed, but using of the higher covariant derivative regularization is highly essential. Thus, we obtain the main result: the NSVZ relations (21.1) and (21.26) for RGFs defined in terms of the bare couplings are valid in all orders of the perturbation theory for RGFs defined in terms of the bare couplings if a theory is regularized by higher covariant derivatives. Note that these RGFs are scheme-independent for a fixed regularization, so that this result holds for any subtraction scheme supplementing the higher covariant derivative regularization.

21.4.5 HD+MSL as an all-loop prescription giving some NSVZ schemes

In the HD+MSL scheme RGFs defined in terms of the renormalized couplings coincide with the ones defined in terms of the bare couplings. Therefore, from the above statement we obtain that the NSVZ equation (in both forms) for RGFs defined in terms of the renormalized couplings holds under the HD+MSL renormalization prescription in all orders of the perturbation theory. Note that this prescription gives a certain class of the NSVZ schemes,⁵ because minimal subtractions of logarithms can supplement various versions of the higher covariant derivative regularization.

⁴ With the higher covariant derivative regularization it has been calculated in [57].

⁵ A continuous set of NSVZ schemes was described in [59, 72, 73].

21.5 Three-loop β -function for theories regularized by higher derivatives

Now we know a renormalization prescription under which the NSVZ equation holds. This allows to obtain a β -function in a certain loop by calculating the anomalous dimension of the matter superfields in the previous loops. For instance, the three-loop β -function for a general renormalizable $\mathcal{N} = 1$ supersymmetric theory has been constructed in [45] with the help of the NSVZ equation and the expression for the two-loop anomalous dimension obtained with this regularization. Note that the NSVZ equation was used for RGFs defined in terms of the bare couplings, while the standard RGFs (also obtained in [45]) do not in general satisfy it. However, there is a certain particular case, for which the NSVZ equation in this order holds for an arbitrary renormalization prescription. This is theories finite in the one-loop approximation [9] (see also [74] for a recent review), which satisfy the conditions

$$T(R) = 3C_2; \quad \lambda_{i\bar{m}n}^* \lambda^{j\bar{m}n} = 4\pi\alpha C(R)_i^j. \quad (21.28)$$

Really, according to [45], in this case the two-loop anomalous dimension of the matter superfields and the three-loop β -function defined in terms of the renormalized couplings have the form

$$\begin{aligned} (\tilde{\gamma}_{\Phi,2\text{-loop}})_i^j(\alpha, \lambda) = & -\frac{3\alpha^2}{2\pi^2} C_2 C(R)_i^j \left(\ln \frac{\alpha_\varphi}{\alpha} - b_{11} + b_{12} \right) - \frac{\alpha}{4\pi^2} \left(\frac{1}{\pi} \lambda_{i\bar{m}n}^* \right. \\ & \left. \times \lambda^{j\bar{m}l} C(R)_l^n + 2\alpha [C(R)^2]_i^j \right) (A - B - 2g_{12} + 2g_{11}); \end{aligned} \quad (21.29)$$

$$\begin{aligned} \frac{\tilde{\beta}_{3\text{-loop}}(\alpha, \lambda)}{\alpha^2} = & \frac{3\alpha^2}{4\pi^3 r} C_2 \text{tr} [C(R)^2] \left(\ln \frac{\alpha_\varphi}{\alpha} - b_{11} + b_{12} \right) + \frac{\alpha}{8\pi^3 r} \left(\frac{1}{\pi} C(R)_j^i \right. \\ & \left. \times C(R)_l^n \lambda_{i\bar{m}n}^* \lambda^{j\bar{m}l} + 2\alpha \text{tr} [C(R)^3] \right) (A - B - 2g_{12} + 2g_{11}), \end{aligned} \quad (21.30)$$

where

$$A = \int_0^\infty dx \ln x \frac{d}{dx} \frac{1}{R(x)}; \quad B = \int_0^\infty dx \ln x \frac{d}{dx} \frac{1}{F^2(x)} \quad a = \frac{M}{\Lambda}; \quad \alpha_\varphi = \frac{M_\varphi}{\Lambda}, \quad (21.31)$$

and b_i and g_i are finite constants which fix a subtraction scheme in the lowest approximations. From the equations (21.29) and (21.30) we see that for one-loop finite theories the NSVZ equation is satisfied in the lowest nontrivial approximation for an arbitrary renormalization prescription,

$$\frac{\beta_{3\text{-loop}}(\alpha, \lambda)}{\alpha^2} = -\frac{1}{2\pi r} C(R)_i^j (\gamma_{\Phi,2\text{-loop}})_j^i(\alpha, \lambda). \quad (21.32)$$

This result can be generalized. It is known that for $\mathcal{N} = 1$ supersymmetric theories finite in the one-loop approximation one can tune a subtraction scheme so that the theory will be all-loop finite [10–13]. If a subtraction scheme is tuned in such a way

that the β -function vanishes in the first L loops and the anomalous dimension of the matter superfields vanishes in the first $(L - 1)$ loops, then [75] for an arbitrary renormalization prescription the $(L + 1)$ -loop gauge β -function satisfies the relation

$$\frac{\beta_{L+1}(\alpha, \lambda)}{\alpha^2} = -\frac{1}{2\pi r} C(R)_i^j (\gamma_{\phi, L})_j^i(\alpha, \lambda). \quad (21.33)$$

This implies that if a theory is finite in a certain approximation, then its β -function vanishes in the next order in exact agreement with the earlier known result of [76, 77].

21.6 Conclusion

Using the regularization by higher covariant derivatives, it is possible to reveal a number of interesting quantum features in supersymmetric theories. In particular, it is possible to construct an all-loop perturbative proof of the NSVZ equation and formulate simple renormalization prescriptions under which it is valid. Namely, it is valid for RGFs defined in terms of the bare couplings for any subtraction scheme supplementing this regularization. This fact has a simple graphical interpretation and follows from the factorization of loop integrals giving the β -function into integrals of double total derivatives, which takes place with the higher covariant derivative regularization. (Also the proof involves the nonrenormalization of triple gauge-ghost vertices, which is another interesting feature of quantum corrections in supersymmetric theories.) The usual RGFs (defined in terms of the renormalized couplings) satisfy the NSVZ equation in the HD+MSL scheme, when in theories regularized by higher covariant derivatives minimal subtractions of logarithms are used for removing divergences. This statement sheds light on the question of how one should calculate quantum corrections to obtain some exact result in various supersymmetric theories.

Acknowledgements

This work has been supported by Foundation for Advancement of Theoretical Physics and Mathematics "BASIS", grant No. 19-1-1-45-1.

References

1. M. T. Grisaru, W. Siegel, M. Rocek: Improved Methods for Supergraphs, Nucl. Phys. B **159**, 429 (1979).
2. M. T. Grisaru, W. Siegel: Supergraphity. 2. Manifestly Covariant Rules and Higher Loop Finiteness, Nucl. Phys. B **201**, 292 (1982). Erratum: [Nucl. Phys. B **206**, 496 (1982)].
3. P. S. Howe, K. S. Stelle, P. K. Townsend: Miraculous Ultraviolet Cancellations in Supersymmetry Made Manifest, Nucl. Phys. B **236**, 125 (1984).
4. I. L. Buchbinder, S. M. Kuzenko, B. A. Ovrut: On the $D = 4$, $N=2$ nonrenormalization theorem, Phys. Lett. B **433**, 335 (1998).
5. M. F. Sohnius, P. C. West: Conformal Invariance in $N=4$ Supersymmetric Yang-Mills Theory, Phys. Lett. B **100**, 245 (1981).

6. S. Mandelstam: Light Cone Superspace and the Ultraviolet Finiteness of the $N=4$ Model, *Nucl. Phys. B* **213**, 149 (1983).
7. L. Brink, O. Lindgren, B. E. W. Nilsson: $N=4$ Yang-Mills Theory on the Light Cone, *Nucl. Phys. B* **212**, 401 (1983).
8. P. S. Howe, K. S. Stelle, P. C. West: A Class of Finite Four-Dimensional Supersymmetric Field Theories, *Phys. Lett. B* **124**, 55 (1983).
9. A. Parkes, P. C. West: Finiteness in Rigid Supersymmetric Theories, *Phys. Lett. B* **138**, 99 (1984).
10. D. I. Kazakov: Finite $N = 1$ SUSY Field Theories and Dimensional Regularization, *Phys. Lett. B* **179**, 352 (1986).
11. A. V. Ermushev, D. I. Kazakov, O. V. Tarasov: Finite $N=1$ Supersymmetric Grand Unified Theories, *Nucl. Phys. B* **281**, 72 (1987).
12. C. Lucchesi, O. Piguet, K. Sibold: Vanishing Beta Functions in $N = 1$ Supersymmetric Gauge Theories, *Helv. Phys. Acta* **61**, 321 (1988).
13. C. Lucchesi, O. Piguet, K. Sibold: Necessary and Sufficient Conditions for All Order Vanishing Beta Functions in Supersymmetric Yang-Mills Theories, *Phys. Lett. B* **201**, 241 (1988).
14. I. Jack, D. R. T. Jones, A. Pickering: Renormalization invariance and the soft Beta functions, *Phys. Lett. B* **426**, 73 (1998).
15. D. I. Kazakov: Finiteness of soft terms in finite $N=1$ SUSY gauge theories, *Phys. Lett. B* **421**, 211 (1998).
16. D. I. Kazakov, M. Y. Kalmykov, I. N. Kondrashuk, A. V. Gladyshev: Softly broken finite supersymmetric grand unified theory, *Nucl. Phys. B* **471**, 389 (1996).
17. V. A. Novikov, M. A. Shifman, A. I. Vainshtein, V. I. Zakharov: Exact Gell-Mann-Low Function of Supersymmetric Yang-Mills Theories from Instanton Calculus, *Nucl. Phys. B* **229**, 381 (1983).
18. D. R. T. Jones: More on the Axial Anomaly in Supersymmetric Yang-Mills Theory, *Phys. Lett. B* **123**, 45 (1983).
19. V. A. Novikov, M. A. Shifman, A. I. Vainshtein, V. I. Zakharov: Beta Function in Supersymmetric Gauge Theories: Instantons Versus Traditional Approach, *Phys. Lett. B* **166**, 329 (1986).
20. M. A. Shifman, A. I. Vainshtein: Solution of the Anomaly Puzzle in SUSY Gauge Theories and the Wilson Operator Expansion, *Nucl. Phys. B* **277**, 456 (1986).
21. L. V. Avdeev, O. V. Tarasov: The Three Loop Beta Function In The $N=1$, $N=2$, $N=4$ Supersymmetric Yang-mills Theories, *Phys. Lett. B* **112**, 356 (1982).
22. I. Jack, D. R. T. Jones, C. G. North: $N=1$ supersymmetry and the three loop gauge Beta function, *Phys. Lett. B* **386**, 138 (1996).
23. I. Jack, D. R. T. Jones, C. G. North: Scheme dependence and the NSVZ Beta function, *Nucl. Phys. B* **486**, 479 (1997).
24. R. V. Harlander, D. R. T. Jones, P. Kant, L. Mihaila, M. Steinhauser: Four-loop beta function and mass anomalous dimension in dimensional reduction, *JHEP* **0612**, 024 (2006).
25. I. Jack, D. R. T. Jones, A. Pickering: The Connection between DRED and NSVZ, *Phys. Lett. B* **435**, 61 (1998).
26. L. Mihaila: Precision Calculations in Supersymmetric Theories, *Adv. High Energy Phys.* **2013**, 607807 (2013).
27. K. V. Stepanyantz: Non-renormalization of the $V\bar{c}c$ -vertices in $\mathcal{N} = 1$ supersymmetric theories, *Nucl. Phys. B* **909**, 316 (2016).
28. K. V. Stepanyantz: The β -function of $\mathcal{N} = 1$ supersymmetric gauge theories regularized by higher covariant derivatives as an integral of double total derivatives, *JHEP* **1910**, 011 (2019).

29. K. Stepanyantz: The all-loop perturbative derivation of the NSVZ β -function and the NSVZ scheme in the non-Abelian case by summing singular contributions, *Eur. Phys. J. C* **80**, no. 10, 911 (2020).
30. A. A. Slavnov: Invariant regularization of nonlinear chiral theories, *Nucl. Phys. B* **31**, 301 (1971).
31. A. A. Slavnov: Invariant regularization of gauge theories, *Theor.Math.Phys.* **13**, 1064 (1972).
32. A. A. Slavnov: The Pauli-Villars Regularization for Nonabelian Gauge Theories, *Theor. Math. Phys.* **33**, 977 (1977).
33. V. K. Krivoshchekov: Invariant Regularizations for Supersymmetric Gauge Theories, *Theor. Math. Phys.* **36**, 745 (1978).
34. P. C. West: Higher Derivative Regulation of Supersymmetric Theories, *Nucl. Phys. B* **268**, 113 (1986).
35. A. I. Vainshtein, V. I. Zakharov, M. A. Shifman: Gell-mann-low Function In Supersymmetric Electrodynamics, *JETP Lett.* **42**, 224 (1985).
36. M. A. Shifman, A. I. Vainshtein, V. I. Zakharov: Exact Gell-mann-low Function In Supersymmetric Electrodynamics, *Phys. Lett. B* **166**, 334 (1986).
37. A. L. Kataev, K. V. Stepanyantz: NSVZ scheme with the higher derivative regularization for $\mathcal{N} = 1$ SQED, *Nucl. Phys. B* **875**, 459 (2013).
38. V. Y. Shakhmanov, K. V. Stepanyantz: New form of the NSVZ relation at the two-loop level, *Phys. Lett. B* **776**, 417 (2018).
39. K. V. Stepanyantz: Structure of Quantum Corrections in $\mathcal{N} = 1$ Supersymmetric Gauge Theories, *Bled Workshops Phys.* **18**, no.2, 197 (2017).
40. A. A. Soloshenko, K. V. Stepanyantz: Three loop beta function for $N=1$ supersymmetric electrodynamics, regularized by higher derivatives, *Theor. Math. Phys.* **140**, 1264 (2004).
41. A. V. Smilga, A. Vainshtein: Background field calculations and nonrenormalization theorems in 4-D supersymmetric gauge theories and their low-dimensional descendants, *Nucl. Phys. B* **704**, 445 (2005).
42. K. V. Stepanyantz: Derivation of the exact NSVZ β -function in $N=1$ SQED, regularized by higher derivatives, by direct summation of Feynman diagrams, *Nucl. Phys. B* **852**, 71 (2011).
43. S. S. Aleshin *et al.*: Three-loop verification of a new algorithm for the calculation of a β -function in supersymmetric theories regularized by higher derivatives for the case of $\mathcal{N} = 1$ SQED, *Nucl. Phys. B* **956**, 115020 (2020).
44. A. E. Kazantsev, K. V. Stepanyantz: Relation between two-point Green's functions of $\mathcal{N} = 1$ SQED with N_f flavors, regularized by higher derivatives, in the three-loop approximation, *J. Exp. Theor. Phys.* **120**, no.4, 618 (2015).
45. A. Kazantsev, K. Stepanyantz: Two-loop renormalization of the matter superfields and finiteness of $\mathcal{N} = 1$ supersymmetric gauge theories regularized by higher derivatives, *JHEP* **2006**, 108 (2020).
46. A. L. Kataev, K. V. Stepanyantz: Scheme independent consequence of the NSVZ relation for $\mathcal{N} = 1$ SQED with N_f flavors, *Phys. Lett. B* **730**, 184 (2014).
47. A. L. Kataev, K. V. Stepanyantz: The NSVZ beta-function in supersymmetric theories with different regularizations and renormalization prescriptions, *Theor. Math. Phys.* **181**, 1531 (2014).
48. K. V. Stepanyantz: The NSVZ β -function and the Schwinger-Dyson equations for $\mathcal{N} = 1$ SQED with N_f flavors, regularized by higher derivatives, *JHEP* **1408**, 096 (2014).
49. I. O. Goriachuk, A. L. Kataev, K. V. Stepanyantz: A class of the NSVZ renormalization schemes for $\mathcal{N} = 1$ SQED, *Phys. Lett. B* **785**, 561 (2018).
50. A. L. Kataev, A. E. Kazantsev, K. V. Stepanyantz: On-shell renormalization scheme for $\mathcal{N} = 1$ SQED and the NSVZ relation, *Eur. Phys. J. C* **79**, no.6, 477 (2019).

51. O. Piguet, K. Sibold: Renormalization of $N = 1$ Supersymmetrical Yang-Mills Theories. 1. The Classical Theory, Nucl. Phys. B **197**, 257 (1982).
52. O. Piguet, K. Sibold: Renormalization of $N = 1$ Supersymmetrical Yang-Mills Theories. 2. The Radiative Corrections, Nucl. Phys. B **197**, 272 (1982).
53. I. V. Tyutin: Renormalization Of Supergauge Theories With Nonextended Supersymmetry (in Russian), Yad. Fiz. **37**, 761 (1983).
54. J. W. Juer, D. Storey: Nonlinear Renormalization in Superfield Gauge Theories, Phys. Lett. B **119**, 125 (1982).
55. J. W. Juer, D. Storey: One Loop Renormalization of Superfield Yang-Mills Theories, Nucl. Phys. B **216**, 185 (1983).
56. A. E. Kazantsev, M. D. Kuzmichev, N. P. Meshcheriakov, S. V. Novgorodtsev, I. E. Shirokov, M. B. Skoptsov, K. V. Stepanyantz: Two-loop renormalization of the Faddeev-Popov ghosts in $\mathcal{N} = 1$ supersymmetric gauge theories regularized by higher derivatives, JHEP **1806**, 020 (2018).
57. S. S. Aleshin, A. E. Kazantsev, M. B. Skoptsov, K. V. Stepanyantz: One-loop divergences in non-Abelian supersymmetric theories regularized by BRST-invariant version of the higher derivative regularization, JHEP **1605**, 014 (2016).
58. A. E. Kazantsev, M. B. Skoptsov, K. V. Stepanyantz: One-loop polarization operator of the quantum gauge superfield for $\mathcal{N} = 1$ SYM regularized by higher derivatives, Mod. Phys. Lett. A **32**, no.36, 1750194 (2017).
59. D. Korneev, D. Plotnikov, K. Stepanyantz, N. Tereshina: The NSVZ relations for $\mathcal{N} = 1$ supersymmetric theories with multiple gauge couplings, JHEP **10**, 046 (2021).
60. M. A. L. Capri, D. R. Granado, M. S. Guimaraes, I. F. Justo, L. Mihaila, S. P. Sorella, D. Vercauteren: Renormalization aspects of $N=1$ Super Yang-Mills theory in the Wess-Zumino gauge, Eur. Phys. J. C **74**, no.4, 2844 (2014).
61. D. Dudal, H. Verschelde, S. P. Sorella: The Anomalous dimension of the composite operator A^{*2} in the Landau gauge, Phys. Lett. B **555**, 126 (2003).
62. M. Kuzmichev, N. Meshcheriakov, S. Novgorodtsev, I. Shirokov, K. Stepanyantz: Finiteness of the two-loop matter contribution to the triple gauge-ghost vertices in $N=1$ supersymmetric gauge theories regularized by higher derivatives, Phys. Rev. D **104**, no.2, 025008, (2021).
63. M. Kuzmichev, N. Meshcheriakov, S. Novgorodtsev, V. Shatalova, I. Shirokov and K. Stepanyantz: Finiteness of the triple gauge-ghost vertices in $\mathcal{N} = 1$ supersymmetric gauge theories: the two-loop verification, [arXiv:2111.04031 [hep-th]].
64. S. S. Aleshin, A. L. Kataev, K. V. Stepanyantz: Structure of three-loop contributions to the β -function of $\mathcal{N} = 1$ supersymmetric QED with N_f flavors regularized by the dimensional reduction, JETP Lett. **103**, no.2, 77 (2016).
65. A. B. Pimenov, E. S. Shevtsova, K. V. Stepanyantz: Calculation of two-loop beta-function for general $N=1$ supersymmetric Yang-Mills theory with the higher covariant derivative regularization, Phys. Lett. B **686**, 293 (2010).
66. K. V. Stepanyantz: Factorization of integrals defining the two-loop β -function for the general renormalizable $N=1$ SYM theory, regularized by the higher covariant derivatives, into integrals of double total derivatives, arXiv:1108.1491 [hep-th].
67. V. Y. Shakhmanov, K. V. Stepanyantz: Three-loop NSVZ relation for terms quartic in the Yukawa couplings with the higher covariant derivative regularization, Nucl. Phys. B **920**, 345 (2017).
68. A. E. Kazantsev, V. Y. Shakhmanov, K. V. Stepanyantz: New form of the exact NSVZ β -function: the three-loop verification for terms containing Yukawa couplings, JHEP **1804**, 130 (2018).
69. K. Stepanyantz: The higher covariant derivative regularization as a tool for revealing the structure of quantum corrections in supersymmetric gauge theories, Proceedings of the Steklov Institute of Mathematics, **309**, 284 (2020).

70. M. D. Kuzmichev, N. P. Meshcheriakov, S. V. Novgorodtsev, I. E. Shirokov, K. V. Stepanyantz: Three-loop contribution of the Faddeev–Popov ghosts to the β -function of $\mathcal{N} = 1$ supersymmetric gauge theories and the NSVZ relation, *Eur. Phys. J. C* **79**, no.9, 809 (2019).
71. K. V. Stepanyantz: The NSVZ β -function for theories regularized by higher covariant derivatives: the all-loop sum of matter and ghost singularities, *JHEP* **2001**, 192 (2020).
72. I. O. Goriachuk: A class of the NSVZ schemes in supersymmetric gauge theories, Proceedings of XXVI International conference of students, graduate students, and young scientists on fundamental sciences “Lomonosov–2019”, section “Physics”, Moscow, (2019).
73. I. O. Goriachuk, A. L. Kataev: Exact β -Function in Abelian and non-Abelian $\mathcal{N} = 1$ Supersymmetric Gauge Models and Its Analogy with the QCD β -Function in the C-scheme, *JETP Lett.* **111**, no.12, 663 (2020).
74. S. Heinemeyer, M. Mondragón, N. Tracas, G. Zoupanos: Reduction of Couplings and its application in Particle Physics, *Phys. Rept.* **814**, 1 (2019).
75. K. Stepanyantz: Exact β -functions for $\mathcal{N} = 1$ supersymmetric theories finite in the lowest loops, *Eur. Phys. J. C* **81**, 571 (2021).
76. A. J. Parkes, P. C. West: Three Loop Results in Two Loop Finite Supersymmetric Gauge Theories, *Nucl. Phys. B* **256**, 340 (1985).
77. M. T. Grisaru, B. Milewski, D. Zanon: The Structure of UV Divergences in Ssym Theories, *Phys. Lett. B* **155**, 357 (1985).

Institute of Astroparticle Physics (CosmoVia)

The Virtual Institute of Astroparticle Physics (VIA) which operates on website <http://viavca.in2p3.fr/site.html>, has provided the platform for our online virtual meetings.

Since 2014 VIA online lectures combined with individual work on Forum acquired the form of Open Online Courses. Aimed to individual work with students the Course is not Massive, but the account for the number of visits to VIA site converts VIA in a specific tool for MOOC activity.

VIA sessions, being a traditional part of Bled Workshops' program, have converted at XXIV Bled Workshop "What comes beyond the Standard models?" into the only format, challenging to preserve the creative nonformal atmosphere of meetings in Bled, Slovenia. We openly discuss the state of art of VIA platform: <http://bsm.fmf.uni-lj.si/bled2021bsm/presentations.html>
<https://bit.ly/bled2021bsm>.



22 Challenging BSM physics and cosmology on the online platform of Virtual Institute of Astroparticle physics

M. Yu. Khlopov^{1,2,3}

e-mail: khlopov@apc.univ-paris7.fr

¹ Centre for Cosmoparticle Physics “Cosmion”, National Research Nuclear University MEPhI”, 115409 Moscow, Russia

² Université de Paris, CNRS, Astroparticule et Cosmologie, France; F-75013 Paris, France

³ Institute of Physics, Southern Federal University, Russia, Stachki 194, Rostov on Don 344090, Russia

Abstract. Under the conditions of pandemia the unique multi-functional complex of Virtual Institute of Astroparticle Physics (VIA) operating on website <http://viavca.in2p3.fr/site.html>, has provided the platform for online virtual meetings. We review VIA experience in presentation online for the most interesting theoretical and experimental results, participation online in conferences and meetings, various forms of collaborative scientific work as well as programs of education at distance, combining online videoconferences with extensive library of records of previous meetings and Discussions on Forum. Since 2014 VIA online lectures combined with individual work on Forum acquired the form of Open Online Courses. Aimed to individual work with students the Course is not Massive, but the account for the number of visits to VIA site converts VIA in a specific tool for MOOC activity. VIA sessions, being a traditional part of Bled Workshops’ program, have converted at XXIV Bled Workshop “What comes beyond the Standard models?” into the only format, challenging to preserve the creative nonformal atmosphere of meetings in Bled, Slovenia. We openly discuss the state of art of VIA platform.

Povzetek: V času pandemije je večnamenski kompleks Virtualnega inštituta za fiziko astrodelcev (VIA), ki je dostopen na spletnem naslovu <http://viavca.in2p3.fr/site.html>, zagotovil platformo za spletna virtualna srečanja. V prispevku predstavlja avtor izkušnje VIA na področjih spletnih predstavitev najbolj zanimivih teoretičnih in eksperimentalnih rezultatov, na področju spletnih konferenc in srečanj, pri različnih oblikah znanstvenega sodelovanja ter pri izobraževanjih na daljavo. VIA združuje spletne videokonference z obsežno knjižnico zapisov prejšnjih srečanj in razprav na forumu.

Od leta 2014 so VIA spletna predavanja v kombinaciji z individualnim delom na Forumu pridobila obliko odprtih spletnih tečajev. Ker je VIA v osnovi namenjena individualnemu delu s študenti, ni prilagojena velikemu številu sodelujočih. Pri večjem številu sodelujočih deluje VIA kot posebno orodje za dejavnost množičnih odprtih spletnih tečajev (MOOC - massive open online courses). Seje VIA so tradicionalni del delavnic z naslovom “What comes beyond the Standard models?”, ki potekajo vsako leto na Bledu. Na že XXIV delavnici se je VIA preoblikovala v edinstven format, ki omogoča ustvarjalno neformalno vzdušje srečanj na Bledu v Sloveniji. V prispevku predstavljamo razpravo o stanju tehnologije platforme VIA.

22.1 Introduction

Studies in astroparticle physics link astrophysics, cosmology, particle and nuclear physics and involve hundreds of scientific groups linked by regional networks (like ASPERA/ ApPEC [1,2]) and national centers. The exciting progress in these studies will have impact on the knowledge on the structure of microworld and Universe in their fundamental relationship and on the basic, still unknown, physical laws of Nature (see e.g. [3,4] for review). The progress of precision cosmology and experimental probes of the new physics at the LHC and in nonaccelerator experiments, as well as the extension of various indirect studies of physics beyond the Standard model involve with necessity their nontrivial links. Virtual Institute of Astroparticle Physics (VIA) [5] was organized with the aim to play the role of an unifying and coordinating platform for such studies.

Starting from the January of 2008 the activity of the Institute took place on its website [6] in a form of regular weekly videoconferences with VIA lectures, covering all the theoretical and experimental activities in astroparticle physics and related topics. The library of records of these lectures, talks and their presentations was accomplished by multi-lingual Forum. Since 2008 there were **220 VIA online lectures**, VIA has supported distant presentations of **192 speakers at 32 Conferences** and provided transmission of talks at **78 APC Colloquiums**.

In 2008 VIA complex was effectively used for the first time for participation at distance in XI Bled Workshop [7]. Since then VIA videoconferences became a natural part of Bled Workshops' programs, opening the virtual room of discussions to the world-wide audience. Its progress was presented in [8–19].

Here the current state-of-art of VIA complex, integrated since 2009 in the structure of APC Laboratory, is presented in order to clarify the way in which discussion of open questions beyond the standard models of both particle physics and cosmology were presented at the virtual XXIV Bled Workshop on the platform of VIA facility. In the conditions of pandemia, when all the offline meetings were forbidden, VIA videoconferencing became the only possibility to continue in 2021 traditions of open discussions at Bled meetings.

22.2 VIA structure and activity

22.2.1 The problem of VIA site

The structure of the VIA site was based on Flash and is virtually ruined now in the lack of Flash support. This original structure is illustrated by the Fig. 22.1. The home page, presented on this figure, contained the information on the coming and records of the latest VIA events. The upper line of menu included links to directories (from left to right): with general information on VIA (About VIA); entrance to VIA virtual rooms (Rooms); the library of records and presentations (Previous), which contained records of VIA Lectures (Previous → Lectures), records of online transmissions of Conferences (Previous → Conferences), APC Colloquiums (Previous → APC Colloquiums), APC Seminars (Previous → APC Seminars) and Events (Previous → Events); Calendar of the past and future VIA events (All events) and

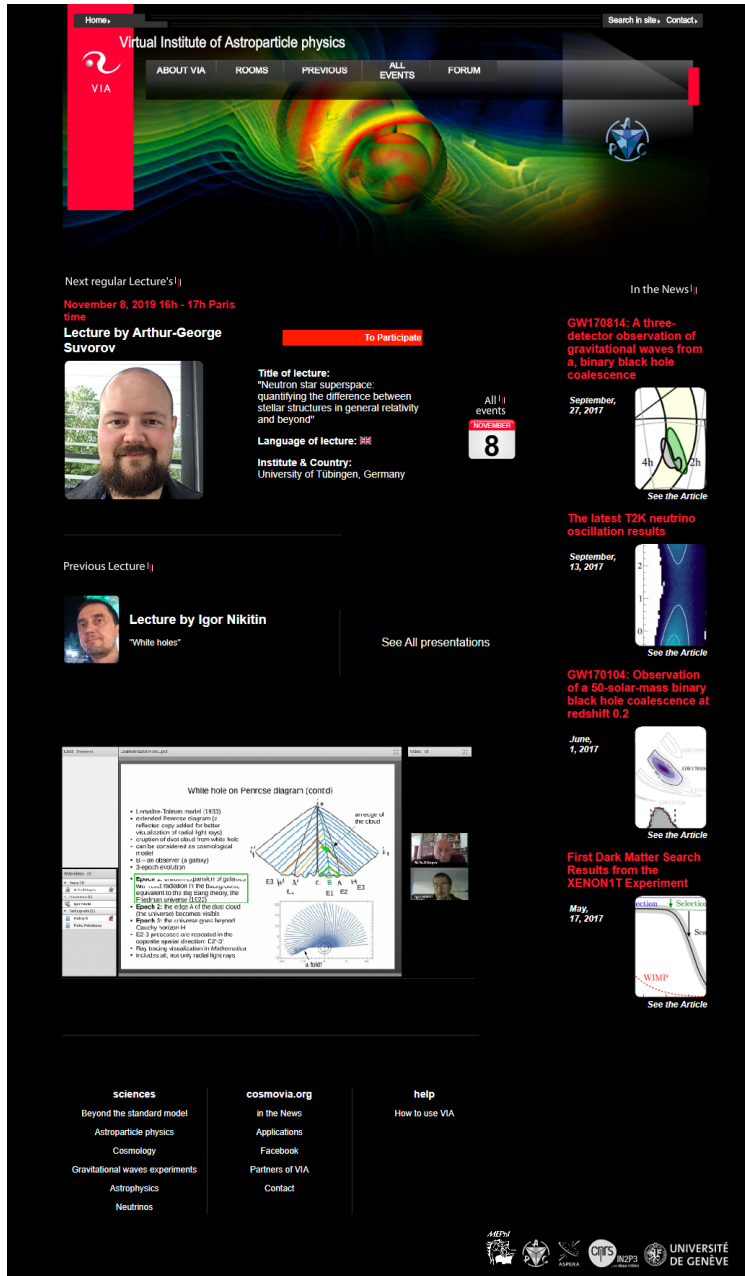


Fig. 22.1: The original home page of VIA site

VIA Forum (Forum). In the upper right angle there were links to Google search engine (Search in site) and to contact information (Contacts). The announcement of the next VIA lecture and VIA online transmission of APC Colloquium occupied the main part of the homepage with the record of the most recent VIA events below. In the announced time of the event (VIA lecture or transmitted APC Colloquium) it was sufficient to click on "to participate" on the announcement and to Enter as Guest (printing your name) in the corresponding Virtual room. The Calendar showed the program of future VIA lectures and events. The right column on the VIA homepage listed the announcements of the regularly up-dated hot news of Astroparticle physics and related areas.

In the lack of Flash support this system of links is ruined, but fortunately, they continue to operate separately and it makes possible to use VIA Forum, by direct link to it, as well as direct links to virtual room of adobeConnect used for regular Laboratory meetings and Seminar and to Zoom (see Fig 22.2). The necessity to restore all the links within VIA complex is a very important task to revive the full scale of VIA activity. Another problem is the necessity to convert .flv files of records in mp4 format.

22.2.2 VIA activity

In 2010 special COSMOVIA tours were undertaken in Switzerland (Geneva), Belgium (Brussels, Liege) and Italy (Turin, Pisa, Bari, Lecce) in order to test stability of VIA online transmissions from different parts of Europe. Positive results of these tests have proved the stability of VIA system and stimulated this practice at XIII Bled Workshop. The records of the videoconferences at the XIII Bled Workshop were put on VIA site [20].

Since 2011 VIA facility was used for the tasks of the Paris Center of Cosmological Physics (PCCP), chaired by G. Smoot, for the public program "The two infinities" conveyed by J.L.Robert and for effective support a participation at distance at meetings of the Double Chooz collaboration. In the latter case, the experimentalists, being at shift, took part in the collaboration meeting in such a virtual way.

The simplicity of VIA facility for ordinary users was demonstrated at XIV Bled Workshop in 2011. Videoconferences at this Workshop had no special technical support except for WiFi Internet connection and ordinary laptops with their internal webcams and microphones. This test has proved the ability to use VIA facility at any place with at least decent Internet connection. Of course the quality of records is not as good in this case as with the use of special equipment, but still it is sufficient to support fruitful scientific discussion as can be illustrated by the record of VIA presentation "New physics and its experimental probes" given by John Ellis from his office in CERN (see the records in [21]).

In 2012 VIA facility, regularly used for programs of VIA lectures and transmission of APC Colloquiums, has extended its applications to support M.Khlopov's talk at distance at Astrophysics seminar in Moscow, videoconference in PCCP, participation at distance in APC-Hamburg-Oxford network meeting as well as to provide online transmissions from the lectures at Science Festival 2012 in University Paris7. VIA communication has effectively resolved the problem of referee's attendance

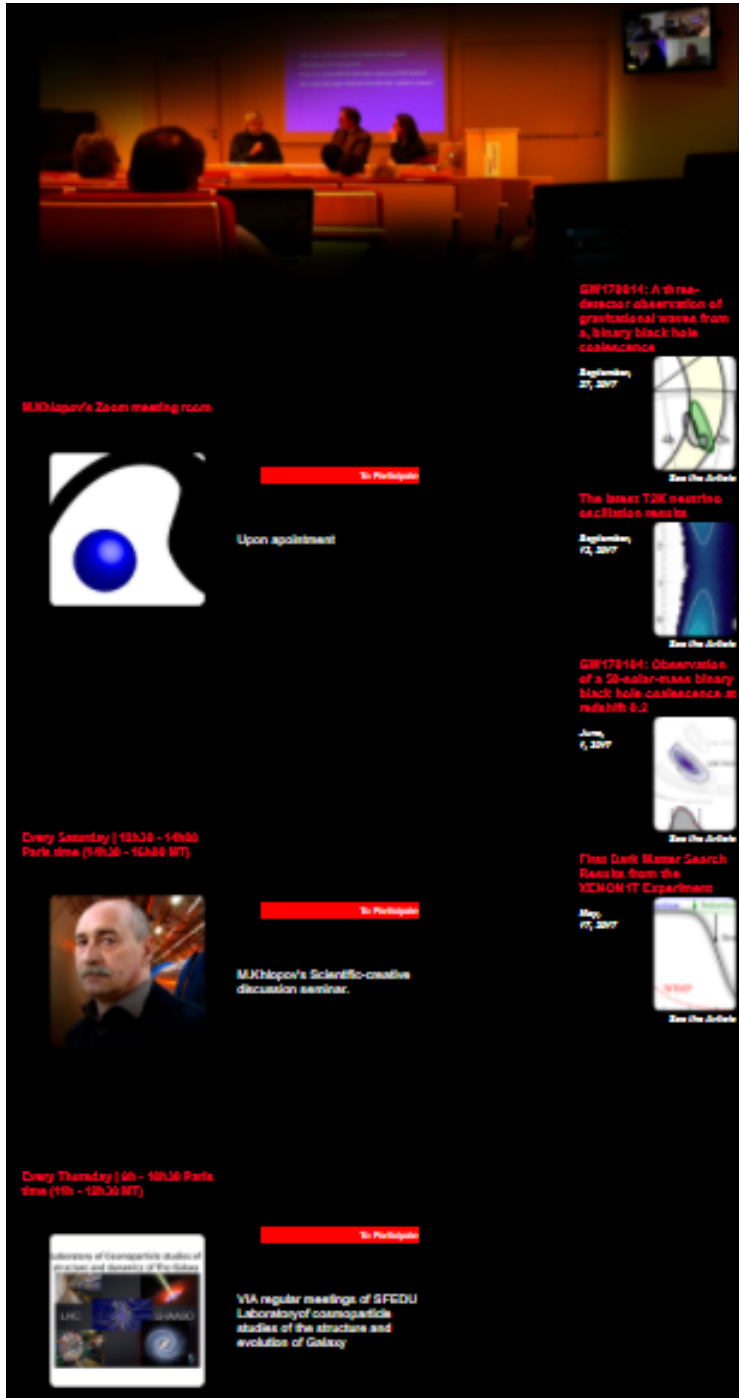


Fig. 22.2: The current home page of VIA site

at the defence of PhD thesis by Mariana Vargas in APC. The referees made their reports and participated in discussion in the regime of VIA videoconference. In 2012 VIA facility was first used for online transmissions from the Science Festival in the University Paris 7. This tradition was continued in 2013, when the transmissions of meetings at Journées nationales du Développement Logiciel (JDEV2013) at Ecole Polytechnique (Paris) were organized [23].

In 2013 VIA lecture by Prof. Martin Pohl was one of the first places at which the first hand information on the first results of AMS02 experiment was presented [22]. In 2014 the 100th anniversary of one of the founders of Cosmoparticle physics, Ya. B. Zeldovich, was celebrated. With the use of VIA M.Khlopov could contribute the programme of the "Subatomic particles, Nucleons, Atoms, Universe: Processes and Structure International conference in honor of Ya. B. Zeldovich 100th Anniversary" (Minsk, Belarus) by his talk "Cosmoparticle physics: the Universe as a laboratory of elementary particles" [24] and the programme of "Conference YaB-100, dedicated to 100 Anniversary of Yakov Borisovich Zeldovich" (Moscow, Russia) by his talk "Cosmology and particle physics".

In 2015 VIA facility supported the talk at distance at All Moscow Astrophysical seminar "Cosmoparticle physics of dark matter and structures in the Universe" by Maxim Yu. Khlopov and the work of the Section "Dark matter" of the International Conference on Particle Physics and Astrophysics (Moscow, 5-10 October 2015). Though the conference room was situated in Milan Hotel in Moscow all the presentations at this Section were given at distance (by Rita Bernabei from Rome, Italy; by Juan Jose Gomez-Cadenas, Paterna, University of Valencia, Spain and by Dmitri Semikoz, Martin Bucher and Maxim Khlopov from Paris) and its proceeding was chaired by M.Khlopov from Paris. In the end of 2015 M. Khlopov gave his distant talk "Dark atoms of dark matter" at the Conference "Progress of Russian Astronomy in 2015", held in Sternberg Astronomical Institute of Moscow State University.

In 2016 distant online talks at St. Petersburg Workshop "Dark Ages and White Nights (Spectroscopy of the CMB)" by Khatri Rishi (TIFR, India) "The information hidden in the CMB spectral distortions in Planck data and beyond", E. Kholupenko (Ioffe Institute, Russia) "On recombination dynamics of hydrogen and helium", Jens Chluba (Jodrell Bank Centre for Astrophysics, UK) "Primordial recombination lines of hydrogen and helium", M. Yu. Khlopov (APC and MEPHI, France and Russia) "Nonstandard cosmological scenarios" and P. de Bernardis (La Sapienza University, Italy) "Balloon techniques for CMB spectrum research" were given with the use of VIA system. At the defense of PhD thesis by F. Gregis VIA facility made possible for his referee in California not only to attend at distance at the presentation of the thesis but also to take part in its successive jury evaluation.

Since 2018 VIA facility is used for collaborative work on studies of various forms of dark matter in the framework of the project of Russian Science Foundation based on Southern Federal University, Russia (Rostov on Don). In September 2018 VIA supported online transmission of **17 presentations** at the Commemoration day for Patrick Fleury, held in APC.

The discussion of questions that were put forward in the interactive VIA events is continued and extended on VIA Forum. Presently activated in English, French

and Russian with trivial extension to other languages, the Forum represents a first step on the way to multi-lingual character of VIA complex and its activity. Discussions in English on Forum are arranged along the following directions: beyond the standard model, astroparticle physics, cosmology, gravitational wave experiments, astrophysics, neutrinos. After each VIA lecture its pdf presentation together with link to its record and information on the discussion during it are put in the corresponding post, which offers a platform to continue discussion in replies to this post.

22.2.3 VIA e-learning, OOC and MOOC

One of the interesting forms of VIA activity is the educational work at distance. For the last eleven years M.Khlopov's course "Introduction to cosmoparticle physics" is given in the form of VIA videoconferences and the records of these lectures and their ppt presentations are put in the corresponding directory of the Forum [25]. Having attended the VIA course of lectures in order to be admitted to exam students should put on Forum a post with their small thesis. In this thesis students are proposed to chose some BSM model and to study the cosmological scenario based on this chosen model. The list of possible topics for such thesis is proposed to students, but they are also invited to chose themselves any topic of their own on possible links between cosmology and particle physics. Professor's comments and proposed corrections are put in a Post reply so that students should continuously present on Forum improved versions of work until it is accepted as admission for student to pass exam. The record of videoconference with the oral exam is also put in the corresponding directory of Forum. Such procedure provides completely transparent way of evaluation of students' knowledge at distance.

In 2018 the test has started for possible application of VIA facility to remote supervision of student's scientific practice. The formulation of task and discussion of progress on work are recorded and put in the corresponding directory on Forum together with the versions of student's report on the work progress.

Since 2014 the second semester of the course on Cosmoparticle physics is given in English and converted in an Open Online Course. It was aimed to develop VIA system as a possible accomplishment for Massive Online Open Courses (MOOC) activity [26]. In 2016 not only students from Moscow, but also from France and Sri Lanka attended this course. In 2017 students from Moscow were accompanied by participants from France, Italy, Sri Lanka and India [27]. The students pretending to evaluation of their knowledge must write their small thesis, present it and, being admitted to exam, pass it in English. The restricted number of online connections to videoconferences with VIA lectures is compensated by the wide-world access to their records on VIA Forum and in the context of MOOC VIA Forum and videoconferencing system can be used for individual online work with advanced participants. Indeed Google Analytics shows that since 2008 VIA site was visited by more than **250 thousand** visitors from **155** countries, covering all the continents by its geography (Fig. 22.3). According to this statistics more than half of these visitors continued to enter VIA site after the first visit. Still the form of individual educational work makes VIA facility most appropriate for PhD courses and it



Fig. 22.3: Geography of VIA site visits according to Google Analytics

could be involved in the International PhD program on Fundamental Physics, which was planned to be started on the basis of Russian-French collaborative agreement. In 2017 the test for the ability of VIA to support fully distant education and evaluation of students (as well as for work on PhD thesis and its distant defense) was undertaken. Steve Branchu from France, who attended the Open Online Course and presented on Forum his small thesis has passed exam at distance. The whole procedure, starting from a stochastic choice of number of examination ticket, answers to ticket questions, discussion by professors in the absence of student and announcement of result of exam to him was recorded and put on VIA Forum [28].

In 2019 in addition to individual supervisory work with students the regular scientific and creative VIA seminar is in operation aimed to discuss the progress and strategy of students scientific work in the field of cosmoparticle physics.

In 2020 the regular course now for M2 students continued, but the problems of adobe Connect, related with the lack of its support for Flash in 2021 made necessary to use the platform of Zoom, This platform is rather easy to use and provides records, as well as whiteboard tools for discussions online can be solved by accomplishments of laptops by graphic tabloids.

22.2.4 Organisation of VIA events and meetings

First tests of VIA system, described in [5,7–9], involved various systems of video-conferencing. They included skype, VRVS, EVO, WEBEX, marratech and adobe Connect. In the result of these tests the adobe Connect system was chosen and properly acquired. Its advantages were: relatively easy use for participants, a possibility to make presentation in a video contact between presenter and audience, a possibility to make high quality records, to use a whiteboard tools for discussions, the option to open desktop and to work online with texts in any format. This choice however should be reconsidered in future or at least accomplished by Zoom in view of the lack of support for Flash on which VIA site is based.

Initially the amount of connections to the virtual room at VIA lectures and discussions usually didn't exceed 20. However, the sensational character of the exciting news on superluminal propagation of neutrinos acquired the number of participants, exceeding this allowed upper limit at the talk "OPERA versus Maxwell and Einstein" given by John Ellis from CERN. The complete record of this talk and is available on VIA website [29]. For the first time the problem of necessity in extension of this limit was put forward and it was resolved by creation of a virtual "infinity room", which can host any reasonable amount of participants. Starting from 2013 this room became the only main virtual VIA room, but for specific events, like Collaboration meetings or transmissions from science festivals, special virtual rooms can be created. This solution strongly reduced the price of the licence for the use of the adobeConnect videoconferencing, retaining a possibility for creation of new rooms with the only limit to one administrating Host for all of them.

The ppt or pdf file of presentation is uploaded in the system in advance and then demonstrated in the central window. Video images of presenter and participants appear in the right window, while in the lower left window the list of all the attendees is given. To protect the quality of sound and record, the participants are required to switch out their microphones during presentation and to use the upper left Chat window for immediate comments and urgent questions. The Chat window can be also used by participants, having no microphone, for questions and comments during Discussion. The interactive form of VIA lectures provides oral discussion, comments and questions during the lecture. Participant should use in this case a "raise hand" option, so that presenter gets signal to switch out his microphone and let the participant to speak. In the end of presentation the central window can be used for a whiteboard utility as well as the whole structure of windows can be changed, e.g. by making full screen the window with the images of participants of discussion.

Regular activity of VIA as a part of APC included online transmissions of all the APC Colloquiums and of some topical APC Seminars, which may be of interest for a wide audience. Online transmissions were arranged in the manner, most convenient for presenters, prepared to give their talk in the conference room in a normal way, projecting slides from their laptop on the screen. Having uploaded in advance these slides in the VIA system, VIA operator, sitting in the conference room, changed them following presenter, directing simultaneously webcam on the presenter and the audience. If the advanced uploading was not possible, VIA streaming was used - external webcam and microphone are directed to presenter and screen and support online streaming. This experience will find proper place, when, hopefully, pandemia ends and regular meetings in real can become possible.

22.2.5 VIA activity in the conditions of pandemia

The lack of usual offline connections and meetings in the conditions of pandemia made the use of VIA facility especially timely and important. This facility supports regular weekly meetings of the Laboratory of cosmoparticle studies of the structure and dynamics of Galaxy in Institute of Physics of Southern Federal University,

Russia (Rostov on Don, Russia) and M.Khlopov's scientific - creative seminar and their announcements occupied their permanent position on VIA homepage (Fig. 22.2), while their records were put in respective place of VIA forum, like [30] for Laboratory meetings.

The platform of VIA facility was used for regular Khlopov's course "Introduction to Cosmoparticle physics" for M2 students of MEPHI (in Russian) and in 2020 supported regular seminars of Theory group of APC.

The programme of VIA lectures continued to present hot news of astroparticle physics and cosmology, like talk by Zhen Cao from China on the progress of LHAASO experiment or lecture by Sunny Vagnozzi from UK on the problem of consistency of different measurements of the Hubble constant.

The results of this activity inspired the decision to hold in 2020 XXIII Bled Workshop online on the platform of VIA [19].

The conditions of pandemia continued in 2021 and VIA facility was successfully used to provide the platform for various online meetings. 2021 was announced by UNESCO as A.D.Sakharov year in the occasion of his 100th anniversary VIA offered its platform for various events commemorating A.D.Sakharov's legacy in cosmoparticle physics. In the framework of 1 Electronic Conference on Universe ECU2021), organized by the MDPI journal "Universe" VIA provided the platform for online satellite Workshop "Developing A.D.Sakharov legacy in cosmoparticle physics" [31].

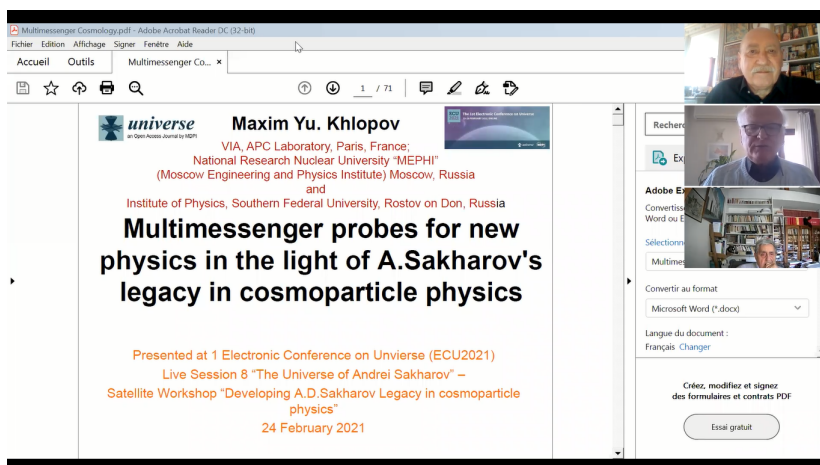


Fig. 22.4: M.Khlopov's talk "Multimessenger probes for new physics in the light of A.D.Sakharov legacy in cosmoparticle physics" at the satellite Workshop "Developing A.D.Sakharov legacy in cosmoparticle physics" of ECU2021.

22.3 VIA platform for virtual XXIV Bled Workshop

VIA sessions at Bled Workshops continued the tradition coming back to the first experience at XI Bled Workshop [7] and developed at XII, XIII, XIV, XV, XVI, XVII, XVIII, XIX, XX, XXI and XXII Bled Workshops [8–18]. They became a regular but supplementary part of the Bled Workshop's program. In the conditions of pandemia it became the only form of Workshop activity in 2020 [19] and continued to be so in 2021.

During the XXIV Bled Workshop the announcement of VIA sessions was put on VIA home page, giving an open access to the videoconferences at the Workshop sessions. The preliminary program as well as the corrected program for each day were continuously put on Forum [32] with the slides and records of all the talks and discussions [32].

VIA facility tried to preserve the creative atmosphere of Bled discussions. All the talks in the program of XXIV Bled Workshop were given in the format videoconferences as the talks "How far has so far the Spin-Charge-Family theory succeeded to offer the explanation for the observed phenomena:..." by Norma Mankoc-Borštnik from Ljubljana, Slovenia (Fig. 22.5) or "Mirror dark matter in laboratory and sky" by A. Addazi, (Fig. 22.6), from Sichuan University, China (see records in [32]).

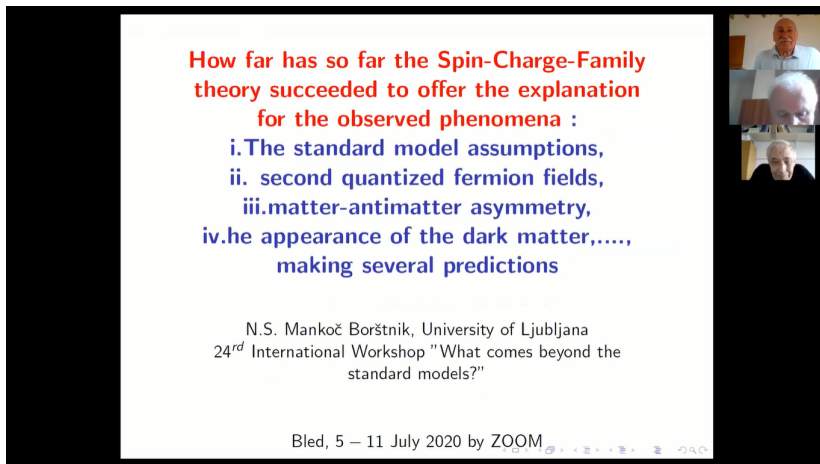


Fig. 22.5: The talk "How far has so far the Spin-Charge-Family theory succeeded to offer the explanation for the observed phenomena:..." by Norma Mankoc-Borštnik at XXIV Bled Workshop

During the Workshop the VIA virtual room was open, inviting distant participants to join the discussion and extending the creative atmosphere of these discussions to the world-wide audience. The participants joined these discussions from different parts of world: L. Bonora from Italy (Fig. 22.7), R. Mohapatra (Fig. 22.8) and Q. Shafi (Fig. 22.9) from US, E. Kiritsis (Fig. 22.10) from Crete and I. Antoniadis (Fig. 22.11) from Paris.



Fig. 22.6: VIA talk “Mirror dark matter in laboratory and sky” by A. Addazi from Chengdu, China at XXIV Bled Workshop

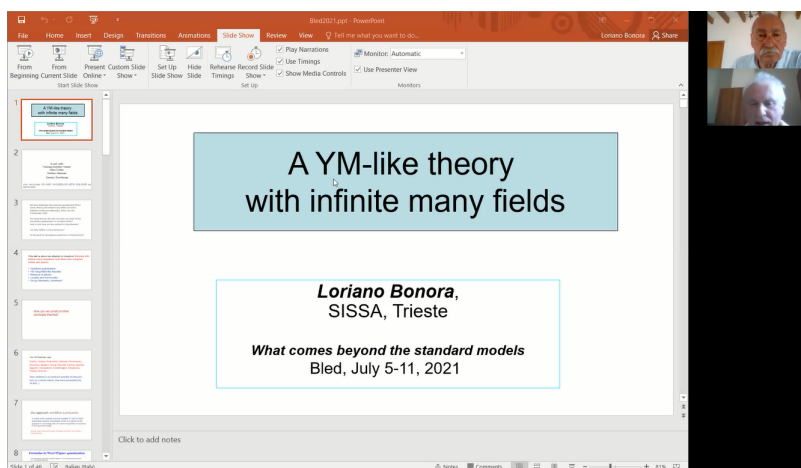


Fig. 22.7: VIA talk “A YM-like theory with infinite many fields” by Loriano Bonora at XXIV Bled Workshop

These talks highly enriched the program and their records, as well as records of all the talks and discussions can be found on VIA Forum [32]. The online format of Workshop provided remote presentation of students’ scientific debuts in BSM physics and cosmology.

Though the technical conditions didn’t make possible nonformal private discussions of participants, still VIA facility has managed to join scientists from Mexico, USA, France, Italy, Russia, Slovenia, Denmark, India, China and many other countries in discussion of open problems of physics and cosmology beyond the Standard models.

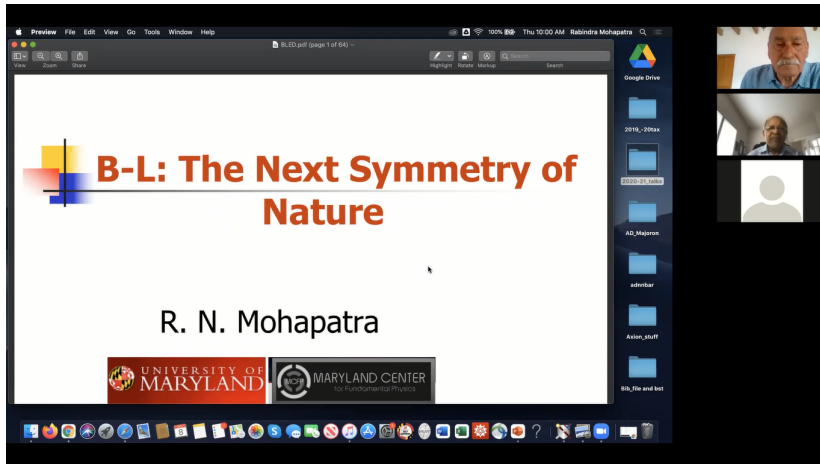


Fig. 22.8: VIA talk "B-L: the next symmetry of Nature" by Rabindra Mohapatra at XXIV Bled Workshop

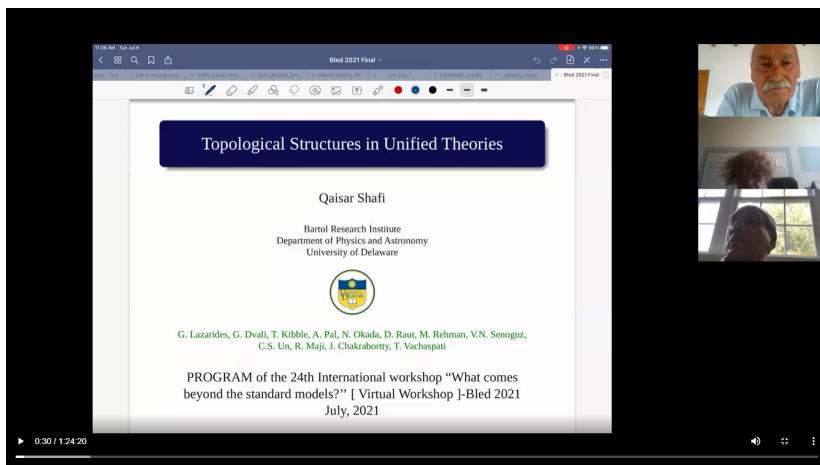


Fig. 22.9: VIA talk "Topological structures in the Unified Theory" by Qaisar Shafi at XXIV Bled Workshop

22.4 Conclusions

The Scientific-Educational complex of Virtual Institute of Astroparticle physics provides regular communication between different groups and scientists, working in different scientific fields and parts of the world, the first-hand information on the newest scientific results, as well as support for various educational programs at distance. This activity would easily allow finding mutual interest and organizing task forces for different scientific topics of cosmology, particle physics, astroparticle physics and related topics. It can help in the elaboration of strategy of

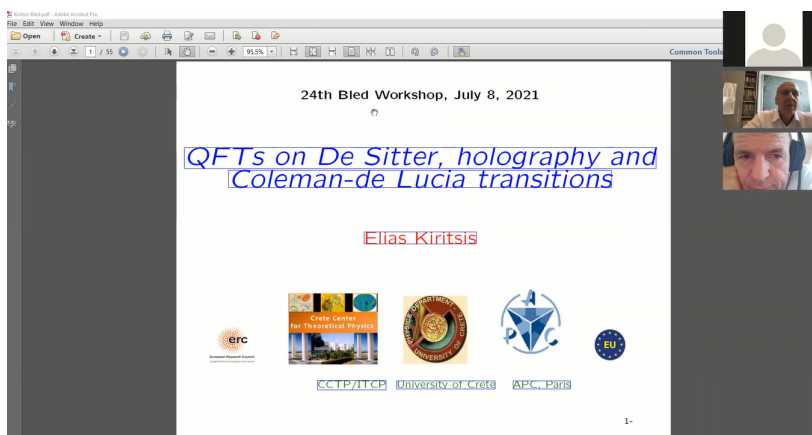


Fig. 22.10: VIA talk “QFTs on De Sitter, holography and Coleman - de Lucia transitions ” by Elias Kiritsis at XXIV Bled Workshop

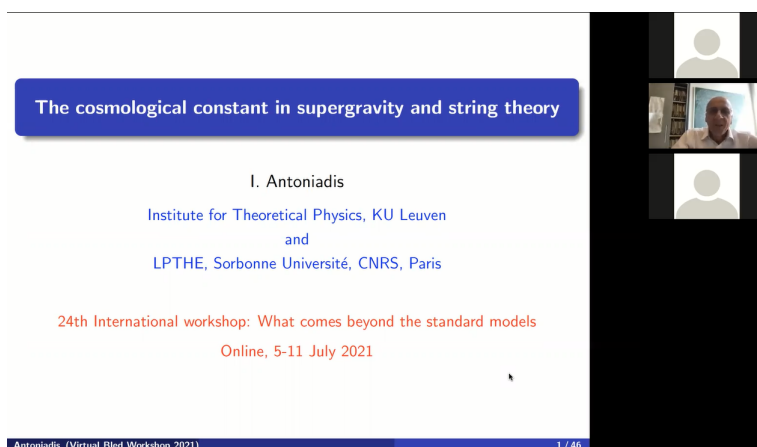


Fig. 22.11: VIA talk “The cosmological constant in supergravity and string theory” by Ignatios Antoniadis at XXIV Bled Workshop

experimental particle, nuclear, astrophysical and cosmological studies as well as in proper analysis of experimental data. It can provide young talented people from all over the world to get the highest level education, come in direct interactive contact with the world known scientists and to find their place in the fundamental research. These educational aspects of VIA activity can evolve in a specific tool for International PhD program for Fundamental physics. Involvement of young scientists in creative discussions was an important aspect of VIA activity at XXIII Bled Workshop. VIA applications can go far beyond the particular tasks of astroparticle physics and give rise to an interactive system of mass media communications.

VIA sessions, which became a natural part of a program of Bled Workshops, maintained in 2020 the platform for online discussions of physics beyond the Standard Model for distant participants from all the world in the lack of possibility of offline meetings. This discussion can continue in posts and post replies on VIA Forum. The experience of VIA applications at Bled Workshops plays important role in the development of VIA facility as an effective tool of e-science and e-learning. One can summarize the advantages and flaws of online format of Bled Workshop. It makes possible to involve in the discussions scientists from all the world (young scientists, especially) free of the expenses related with meetings in real (voyage, accommodation, ...), but loses the advantage of nonformal discussions at walks along the beautiful surrounding of the Bled lake and other places of interest. The improvement of VIA technical support by involvement of Zoom provided better platform for nonformal online discussions, but in no case can be the substitute for Bled meetings and its creative atmosphere in real. One can summarize that VIA sessions should remain a useful but still supplementary tool of Bled Workshop meetings in real, provided that such real meetings are possible.

Acknowledgements

The initial step of creation of VIA was supported by ASPERA. I express my tribute to memory of P.Binetruy and express my gratitude to J.Ellis and S.Katsanevas for permanent stimulating support, to J.C. Hamilton for support in VIA integration in the structure of APC laboratory, to K.Belotsky, A.Kirillov, M.Laletin and K.Shibaev for assistance in educational VIA program, to A.Mayorov, A.Romaniouk and E.Soldatov for fruitful collaboration, to K.Ganga, J.Errard, A.Kouchner and D.Semikoz for collaboration in development of VIA activity in APC, to M.Pohl, C.Kouvaris, J.-R.Cudell, C. Giunti, G. Cella, G. Fogli and F. DePaolis for cooperation in the tests of VIA online transmissions in Switzerland, Belgium and Italy and to D.Rouable for help in technical realization and support of VIA complex. The work was supported by grant of Russian Science Foundation (Project No-18-12-00213-P). I express my gratitude to the Organizers of Bled Workshop N.S. Mankoč Borštnik, H.Nielsen and my tribute to memory of D. Lukman for cooperation in the organization of VIA online Sessions at XXIV Bled Workshop. I am grateful to T.E.Bikbaev for technical assistance and help. I am grateful to Sandi Ogrizek for creation of compact links to VIA Forum.

References

1. <http://www.aspera-eu.org/>
2. <http://www.appec.org/>
3. M.Yu. Khlopov: *Cosmoparticle physics*, World Scientific, New York -London-Hong Kong - Singapore, 1999.
4. M.Yu. Khlopov: *Fundamentals of Cosmic Particle Physics*, CISP-Springer, Cambridge, 2012.
5. M. Y. Khlopov, Project of Virtual Institute of Astroparticle Physics, arXiv:0801.0376 [astro-ph].

6. <http://viavca.in2p3.fr/site.html>
7. M. Y. Khlopov, Scientific-educational complex - virtual institute of astroparticle physics, 981–862008.
8. M. Y. Khlopov, Virtual Institute of Astroparticle Physics at Bled Workshop, 10177–1812009.
9. M. Y. Khlopov, VIA Presentation, 11225–2322010.
10. M. Y. Khlopov, VIA Discussions at XIV Bled Workshop, 12233–2392011.
11. M. Y. .Khlopov, Virtual Institute of astroparticle physics: Science and education online, 13183–1892012.
12. M. Y. .Khlopov, Virtual Institute of Astroparticle physics in online discussion of physics beyond the Standard model, 14223–2312013.
13. M. Y. .Khlopov, Virtual Institute of Astroparticle physics and “What comes beyond the Standard model?” in Bled, 15285-2932014.
14. M. Y. .Khlopov, Virtual Institute of Astroparticle physics and discussions at XVIII Bled Workshop, 16177-1882015.
15. M. Y. .Khlopov, Virtual Institute of Astroparticle Physics — Scientific-Educational Platform for Physics Beyond the Standard Model, 17221-2312016.
16. M. Y. .Khlopov: Scientific-Educational Platform of Virtual Institute of Astroparticle Physics and Studies of Physics Beyond the Standard Model, 18273-2832017.
17. M. Y. .Khlopov: The platform of Virtual Institute of Astroparticle physics in studies of physics beyond the Standard model, 19383-3942018.
18. M. Y. .Khlopov: The Platform of Virtual Institute of Astroparticle Physics for Studies of BSM Physics and Cosmology, Journal20249-2612019.
19. M. Y. .Khlopov: Virtual Institute of Astroparticle Physics as the Online Platform for Studies of BSM Physics and Cosmology, Journal21249-2632020.
20. http://viavca.in2p3.fr/what_comes_beyond_the_standard_models_xiii.html
21. http://viavca.in2p3.fr/what_comes_beyond_the_standard_models_xiv.html
22. http://viavca.in2p3.fr/pohl_martin.html
23. In <http://viavca.in2p3.fr/> Previous - Events - JDEV 2013
24. http://viavca.in2p3.fr/zeldovich_100_meeting.html
25. In <https://bit.ly/bled2021bsm> Forum- Discussion in Russian - Courses on Cosmoparticle physics
26. In <https://bit.ly/bled2021bsm> Forum - Education - From VIA to MOOC
27. In <https://bit.ly/bled2021bsm> Forum - Education - Lectures of Open Online VIA Course 2017
28. In <https://bit.ly/bled2021bsm> Forum - Education - Small thesis and exam of Steve Branchu
29. <http://viavca.in2p3.fr/johnellis.html>
30. In <https://bit.ly/bled2021bsm> Forum - LABORATORY OF COSMOPARTICLE STUDIES OF STRUCTURE AND EVOLUTION OF GALAXY
31. In <https://bit.ly/bled2021bsm> Forum - CONFERENCES - CONFERENCES ASTROPARTICLE PHYSICS - The Universe of A.D. Sakharov at ECU2021
32. In <https://bit.ly/bled2021bsm> Forum - CONFERENCES BEYOND THE STANDARD MODEL - XXIV Bled Workshop “What comes beyond the Standard model?”

Postscriptum

In Memory of Mag. Dragan Lukman, 11 March 1962 - 19 July 2021

Words do not obey thoughts and feelings when writing in memory of someone who has been a collaborator for many years, a friend I talked to over short coffees about all open questions of our world: in physics, cosmology, mathematics, about society, human life, about values; we just never talked about personal life.

Dragan Lukman joined us in Koper on my Project on elementary fermion and boson fields (the project at the Department of Physics, Faculty of Mathematics and Physics, University of Ljubljana), when I managed to establish the Institute of Technical and Natural Sciences in Koper (PINT). He also was involved in common projects with industry.

At that time, the Bled workshop was held for the second year. Dragan took over the technical side of editing workshops and proceedings of the workshops up to this year 2021, the 24th workshop. He was all the time an excellent helper and a good friend to all.

The first research in the field of physics of elementary fermionic and bosonic fields, in which Dragan participated, were at first published in the proceedings of the workshops "What comes beyond the standard models". They belong to a project entitled *spin-charge-family* theory, which I am developing since 1992, also together with colleagues and students. There are still some articles that are not yet prepared for publication in international journals in which Dragan participated.

An overview of all proceedings can be found on the home page of the Bled Workshops

[http: // bsm.fmf.uni-lj.si/bled2021bsm/presentations.html](http://bsm.fmf.uni-lj.si/bled2021bsm/presentations.html),

after 2008 also on the Cosmovia forum: <https://bit.ly/bled2021bsm>.

Proceedings are cited in articles published also in international journals in this field, among them those coauthored with Dragan.

A song can say a lot and Astri Kleppe on behalf of all of us, who appreciated Dragan and liked him, wrote the poem, appearing in this Proceedings.

Norma Susana Mankoč Borštnik
norma.mankoc@fmf.uni-lj.si

Dragan Lukman was introduced into the research work in the middle of eighties of previous century when Slovenia started with the "1000 Young Researchers Project". After finishing his diploma work at the Department of Physics Dragan decided to expand his field of interest to the field of mathematics. He enrolled the postgraduate course at the Department of Mathematics and simultaneously he participated in the research work at the National Institute of Chemistry as a member of the Laboratory for Molecular Modelling. In due course he accomplished all the necessary steps to attain the degree of master of mathematical sciences. His participation in the scientific work resulted in ten publications in international scientific journals. Dragan was able to cope with the research work in quite diverse fields such as strict statistical mechanics, the application of molecular dynamics simulation of biological systems and even technologically oriented studies of mechanical properties of fullerenes.

Prof. dr. Branko Borštnik,

The head of The Laboratory for Molecular Modelling at the National Institute for Chemistry Ljubljana, Slovenia in the period when Dragan Lukman was member of the group

Mag. Dragan Lukman, holding Master of Science degree in Mathematics and Bachelor degree in Physics, both degrees received from University of Ljubljana, has approached me, after important recommendations from Prof.dr. Norma Mankoč Borštnik, in May 2019 with an interest to apply for a research position in my research project Quantum Localization in Chaotic Systems being carried out at CAMTP - Center for Applied Mathematics and Theoretical Physics of the University of Maribor, funded by the Slovenian Research Agency ARRS. In our first interview with him it was immediately obvious that he has quite wide experience in working with various research groups in Slovenia, predominantly with Norma Mankoč and her coworkers, but also with others, with broad knowledge in physics and mathematics, and in computational physics. Therefore my decision to offer him the job was easy. Thus he has joined my core research group, a part of CAMTP, whose members also are dr. Qian Wang, dr. Črt Lozej (my PhD student at the time) and dr. Benjamin Batistič (also my former PhD student, 2015, now postdoc). We started to work together with Dragan on 1 June 2019. Our main object of study was the phenomenon of quantum or dynamical localization in classically chaotic systems, one of the central issues in the domain of quantum chaos. More precisely, we have been studying very extensively and deeply the localization phenomena in the so called lemon billiards, a special family of two dimensional billiards with extremely rich behaviour both classically and quantumly. They are important paradigmatic model systems. The selection of billiards was made possible only thanks to the extensive calculations by Črt Lozej in the course

of his PhD thesis. Dragan started his work quite enthusiastically, and was using mainly the software codes developed over the many years by Benjamin Batistić and recently very drastically improved and expanded by Črt Lozej. In doing so we were discovering very many exciting results which emerged by our heavy computations, and Dragan was always very careful, fast, responsive and reliable, with good physical insight, presenting the results in a shortest possible time, working every day from early morning until the late afternoon, and even on weekends at home. Based on the results under his cooperation four important papers have been produced, 3 of them already published in excellent journals (Physical Review E, Physics MDPI, Nonlinear Phenomena in Complex Systems), the fourth one just in the progress of writing. Therefore Dragan's contribution to our results is quite essential and appreciated.

Dragan was a very pleasant personality, highly modest and quiet person, always helpful, never complaining, and deeply dedicated to his work, not only at our institute, but also in other groups. We did not know much about his personal life, as he was a very shy person and did not show emotions, but this does not mean that he was not sensible and empathic. The tragic news about his sudden death on his way to work in the early morning on Monday 19 July 2021 was a great shock for all of us. We shall remember him as a wonderful fellow and a very good researcher. Our papers with him are a long lasting remembrance of him.

Prof.dr. Marko Robnik, member of EASA

Founder and Director of CAMTP - Center for Applied Mathematics and Theoretical Physics, University of Maribor

Robnik@uni-mb.si

Draganu Lukmanu v spomin in zahvalo, 11. marec 1962 - 19. julij 2021

Prave besede kar ne stečejo v zapis v spomin nekomu, ki je bil dolga leta sodelavec, prijatelj in s katerim sva ob kratkih kavicah prediskutirala vsa odprta vprašanja tega sveta, v fiziki, v kozmologiji, v matematiki, v družbi, v človekovem življenju, o vrednotah, le o osebnem življenju nisva govorila nikoli.

Dragan Lukman se mi je pridružil v Kopru na projektu Fizike osnovnih delcev in polj, Oddelka za fiziko Fakultete za matematiko in fiziko Univerze v Ljubljani, ko mi je uspelo ustanoviti Primorski inštitut za naravoslovne in tehnične vede Koper. Sodeloval je tudi na projektih, ki smo jih razvili z gospodarstvom.

Tedaj je Blejska delavnica tekla že drugo leto. Prevzel je tehnično plat urejanja delavnice in zbornika delavnice vse do letošnje 24. delavnice. Bil je vseskozi izvrsten pomočnik in dober prijatelj vsem.

Prve raziskave na področju fizike osnovnih fermionskih in bozonskih polj, pri katerih je Dragan sodeloval, so bile najprej objavljene v zbornikih delavnic "What comes beyond the standard models". Sodiijo v projekt z naslovom *spin-charge-family theory*, ki ga razvijam, tudi skupaj s sodelavci in študenti, že od leta 1992. Je še nekaj prispevkov, ki še niso dozoreli za objavo v mednarodnih revijah, pri katerih je Dragan sodeloval.

Pregled vseh zbornikov je najti na domači strani Blejskih delavnic

<http://bsm.fmf.uni-lj.si/bled2021bsm/presentations.html>,

po letu 2008 pa tudi na Cosmovia forum: <https://bit.ly/bled2021bsm>.

V prispevkih zbornikov so citirani članki, ki so, potem ko so dozoreli, objavljeni v mednarodnih revijah s tega področja, tudi tisti v soavtorstvu z Draganom.

Pesem pove lahko zelo veliko in Astri Kleppe je v imenu vseh nas, ki smo Dragana cenili in imeli radi, napisala pesem, ki jo objavljamo v tem zborniku.

Norma Susana Mankoč Borštnik

norma.mankoc@fmf.uni-lj.si

Dragan Lukman se je pridružil moji raziskovalni skupini v Laboratoriju za molekularno modeliranje na Nacionalnem kemijskem inštitu sredi osemdesetih let prejšnjega stoletja, ko je Slovenija odprla projekt "1000 mladih raziskovalcev", ki je omogočil vključitev podiplomskih študentov v raziskovalno delo. Po diplomu na Oddelku za fiziko, Fakultete za matematiko in fiziko, Univerze v Ljubljani se je Dragan odločil za magistrski študij na Oddelku za matematiko, raziskovalno delo pa je nadaljeval

na Kemijskem inštitutu v moji skupini. Pravočasno je opravil vse potrebno za pridobitev stopnje magistra matematičnih znanosti. Sodeloval je pri znanstvenem delu, ki je bilo objavljeno v desetih člankih v mednarodnih znanstvenih revijah. Dragan je sodeloval pri raziskavah na precej raznolikih področjih, kot so stroga statistična mehanika, uporaba molekularne dinamike za simulacijo bioloških sistemov in celo pri tehnološko usmerjenem študiju mehanskih lastnosti fulerenov.

prof. dr. Branko Borštnik,
dolgoletni vodja laboratorija za molekularno modeliranje na Kemijskem inštitutu
v Ljubljani
branko.borstnik@ki.si

Mag. Dragan Lukman, ki je imel magisterij iz matematike ter diplomu iz fizike z Univerze v Ljubljani, me je kontaktiral, na osnovi pomembnih priporočil Prof.dr. Norme Mankoč Borštnik, v maju 2019, z zanimanjem za delovno mesto raziskovalca na mojem raziskovalnem projektu Kvantna lokalizacija v kaotičnih sistemih, ki je bil izvajan na CAMTP - Centru za uporabno matematiko in teoretično fiziko Univerze v Mariboru, in je bil financiran s strani ARRS. Že ob prvem intervjuju je postalo nemudoma jasno, da ima kar široke izkušnje v sodelovanju z različnimi raziskovalnimi skupinami v Sloveniji, predvsem z Normo Mankoč Borštnik in njenimi sodelavci, a tudi z drugimi, s širokim znanjem v fiziki in matematiki ter v računski teoretični fiziki. Zato je bila lahka moja odločitev, da mu ponudim zaposlitev. Tako se je pridružil moji jedrni raziskovalni skupini, ki je del CAMTP in katere člani so tudi dr. Qian Wang, dr. Črt Lozej (moj tedanji doktorand) in dr. Benjamin Batistić (tudi moj nekdanji doktorand, 2015, sedaj podoktorski sodelavec). Naše sodelovanje z Draganom se je pričelo 1. junija 2019. Naš glavni predmet raziskav je bil pojav kvantne ali dinamične lokalizacije v klasičnih kaotičnih sistemih, ena glavnih tem na področju kvantnega kaosa. Natančneje, obširno in poglobljeno smo proučevali lokalizacijske pojave v tako imenovanih limonastih biljardih, ki so posebna družina dvo-dimenzionalnih biljardov z izjemno bogatim vedenjem tako klasično kot kvantno. Le-ti so pomembni paradigmatični modelski sistemi. Izbor teh biljardov je bil omogočen zahvaljujoč obširnim računom Črta Lozeja v teku njegove doktorske disertacije. Dragan je pričel z delom dokaj navdušeno, in je uporabljal v glavnem softverske programe, ki jih je v dolgih letih razvijal in razvil Benjamin Batistić, in ki jih je v zadnjem času zelo korenito izboljšal in razširil Črt Lozej. Na tej poti smo odkrili veliko novih vznemirljivih rezultatov, ki so izšli iz naših masivnih računov, in Dragan je bil vselej zelo skrben, hiter, odziven in zanesljiv, z dobrim fizikalnim vpogledom. Rezultate je predstavil v kar najkrajšem možnem času, pri čemer je delal vsak dan od zgodnjega jutra do poznega popoldneva, pa tudi čez vikend od doma. Na osnovi rezultatov v okviru sodelovanja z njim smo pripravili štiri pomembne članke, trije od njih

so že objavljeni v odličnih revijah (Physical Review E, Physics MDPI, Nonlinear Phenomena in Complex Systems), četrti pa je v procesu pisanja. Zato je Draganov prispevek k našim rezultatom bistven in cenjen.

Dragan je bil prijazna osebnost, zelo skromen in tih, zmerom v pomoč, nikoli se ni pritoževal, ter predan svojemu delu, ne samo na našem inštitutu, temveč tudi v drugih skupinah. O njegovem zasebnem življenju nismo vedeli veliko, saj je bil zelo plah, in ni kazal čustev, kar pa ne pomeni, da ni bil senzibilen in empatičen. Tragična novica o njegovi nenadni smrti na njegovi poti na delo zgodaj zjutraj v ponedeljek 19. julija 2021 je bila velik šok za vse nas. Spominjali se ga bomo kot čudovitega kolega in zelo dobrega raziskovalca. Naši skupni članki z njim so trajen spomin nanj.

Prof. dr. Marko Robnik, član EASA

Ustanovitelj in direktor CAMTP - Centra za uporabno matematiko in teoretično fiziko Univerze v Mariboru

Robnik@uni-mb.si

To Dragan, in grateful memory

A man of great integrity
A private man,
who shyly would inform you
about things misunderstood, and facts
about cosmology, computers
or Slovenia.
His land.

He was a helper, much too humble,
and so gentle
that we sometimes did not see him.
And suddenly he's gone.
A summer day, the brightest day
in early afternoon,
the coffee cup half full, and children
laughing in the park nearby
When suddenly a wind
as light
as butterfly
came by
and brought him
to the other side,

and left us here
in our confusion, our never ending
search for understanding
All our reasoning, our turning
every stone
in this chaotic pain
and beauty
where our lives take place.

BLEJSKE DELAVNICE IZ FIZIKE, LETNIK 22, ŠT. 1, ISSN 1580-4992

BLED WORKSHOPS IN PHYSICS, VOL. 22, NO. 1

Zbornik 24. delavnice 'What Comes Beyond the Standard Models', Bled, 5. – 11. julij 2021 [Virtualna delavnica 5.–11. julin 2021]

Proceedings to the 24rd workshop 'What Comes Beyond the Standard Models', Bled, July 5.–11., 2021 [Virtual Workshop, July 5.–11., 2021]

Uredili Norma Susana Mankoč Borštnik, Holger Bech Nielsen, Dragan Lukman and Astri Kleppe

Izid publikacije je finančno podprla Javna agencija za raziskovalno dejavnost RS iz sredstev državnega proračuna iz naslova razpisa za sofinanciranje domačih znanstvenih periodičnih publikacij

Brezplačni izvod za udeležence

Tehnični urednik Matjaž Zaveršnik

Založilo: DMFA – založništvo, Jadranska 19, 1000 Ljubljana, Slovenija

Natisnila tiskarna Itagraf v nakladi 130 izvodov

Publikacija DMFA številka 2146
